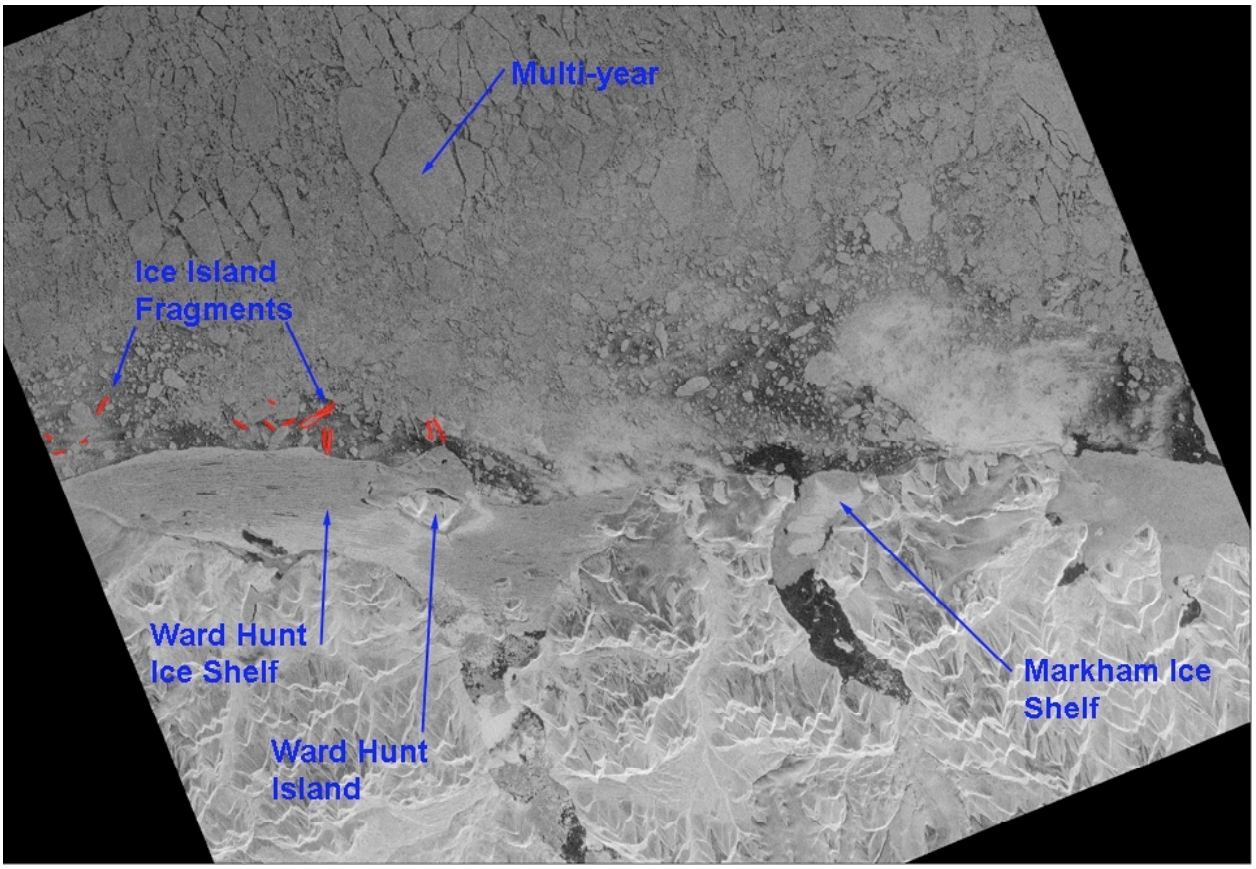

BEAUFORT AND CHUKCHI SEAS ICE DESIGN CRITERIA

EXTREME ICE FEATURES AND MULTI-YEAR FLOE/RIDGE STATISTICS

by

Canatec Associates International Ltd
Suite 122, 3553 – 31st Street NW
Calgary, Alberta, Canada T2L 2K7

for the JIP Partners

Shell International Exploration and Production Inc.,
ConocoPhillips Canada Resources Corp.,
Chevron Canada Ltd,
Exxon-Mobil Upstream Research Company,
BP Exploration Operating Company Ltd and
U.S. Dept of the Interior Minerals Management Service

November 2010

Abstract

Objectives

The objectives of this project were to acquire and analyze recent data on extreme ice features, multi-year floe sizes, multi-year floe and ridge thickness and ice drift velocity, and to compare results with previous ice design statistics where possible.

Extreme Ice Features

An extreme ice feature, or EIF, is defined as an ice feature that would cause an extreme design load on an offshore production platform. It is at least 20 m thick and 500 m in diameter and is often frozen into a large multi-year floe. EIFs include ice islands, ice island fragments, multi-year hummock fields and areas of multi-year land fast sea ice. Ice islands originate from the ice shelves of northern Ellesmere Island. Multi-year hummock fields, or MYHF, are very rough multi-year floes containing a series of densely packed parallel ridges. Multi-year land fast sea ice, while not 20 m in thickness can contain other EIFs embedded within. All these features are known to form along the western shores of the Arctic Islands and to occasionally break free and enter the Beaufort Gyre, which in turn drifts south and west into proximity with the lease areas for offshore drilling.

New radar satellite imagery of the coastal pack ice was acquired in a 100 km wide swath from Ellesmere Island to Prince Patrick Island. The satellite data was acquired on July 31st and August 1st, 2008, just days after a major event in which scores of ice islands and fragments were calved from the ice shelves on Ellesmere Island. The planning for data acquisition is described in Chapter 3.

All features were mapped in a GIS program and precisely located. Major and minor axes, diameter or maximum length, perimeter and area, were measured and a data base established. Equivalent diameter and several other derived parameters were calculated. The data and results are described in Chapter 4.

Some 200 EIFs were identified consisting of 40 ice islands 93 ice island fragments (<1 km long) and 67 multi-year hummock fields. All of these were detected in the radar imagery coverage of 183,980 km^2. Though this was the largest number of EIFs counted in such a survey to date, the average size was smaller than previously measured. The majority of the ice island fragments were smaller than 500 m in equivalent diameter. The population of EIFs greater than 500 m in equivalent diameter was only 99. This results in an areal density of 5.4 x 10^{-4} EIFs per km^2. This is lower than the areal density of 8.4 x 10^{-4} EIFs per km^2 based on Pilkington et.al. 1992.

In the 2008 data there were 44 ice islands and 55 multi-year hummock fields greater than 500 m in equivalent diameter. The areal density for ice islands was 2.4 x 10^{-4} in 2008 - up from the 1992 estimate of 1.6 x 10^{-4}. The areal density of MYHFs dropped from 4.8 x 10^{-4} to 3 x 10^{-4} since 1992. It is known that other ice islands were formed one week after the main survey of 2008 when the Markham ice shelf drifted out of its inlet and broke into several large ice islands, but the total number of fragments was not known. This would

have raised the areal density of EIFs in 2008, but by an unknown amount. For comparison, the total area of all ice islands and fragments on August 1st was 123 km^2. The total area lost from the ice shelves in the summer of 2008 was 227 km^2.

In terms of size the median equivalent diameter for all EIFs larger than 500m was 1.2 km, and the mean was 1.8 km, as compared with a 1.4 km median and 1.9 km mean for the previous survey. Ice islands and fragments, though more numerous than before, are smaller on average. Median and mean diameter were 1.05 km and 1.5 km respectively, compared to 1.4 km and 1.9 km in Pilkington (1992). MYHFs are a little less numerous than in the previous survey, with more in the smaller sizes. Median was 1.1 km and mean was 2.0 km. The mean MYHF diameter was large because of a few very large features, the largest being 13.8 km in equivalent diameter.

In the absence of direct measurements after calving, thickness of ice island EIFs can be estimated from the thickness of the parent ice shelf. For example, the Ward Hunt shelf was estimated at 40-50 m thick and this was later confirmed by a measurement of 42 m on the Hobson's Choice ice island. Recent (April 2008) GPR field data on the thickness of the Milne, Petersen and Serson ice shelves was analyzed. Analysis of this GPR data is discussed in Chapter 5.

The Milne shelf ranged from 50 to 94 m thick. The central Petersen ranged from 40 to 65 m thick. Neither of these lost any mass to calving in 2008. The Serson ice shelf ranged from about 16 to 63 m in thickness with a mean of 38 m. Seventeen ice islands and fragments were identified as a result of the collapse of this ice shelf in late July 2008. In addition, data from four areas of multi-year land fast sea ice, or MLSI, were processed and analyzed. While not considered an extreme ice feature, a piece of MLSI many km long and 6-10 m thick is still a significant feature. A remnant MLSI from Yelverton Bay was found to have an average thickness of 6 m over a distance of more than 10 km.

Multi-Year Floe Sizes

Radar satellite images of multi-year floes at the edge of the polar pack ice of the Beaufort and Chukchi Seas were obtained from two of the project sponsors. The images covered three lease areas - the Canadian Beaufort, the Alaskan Beaufort and the Chukchi Sea - and two seasons - winter and summer. Several thousand floes were mapped in a GIS program, measurements were made of major and minor axes, diameter, area and perimeter, and a data base was established. The data were analyzed and compared by region, by season and with previous studies. The summary that follows will refer to statistics for all floes greater than 500 m in diameter. There is more detail in Chapter 6.

There is a trend to smaller multi-year floe sizes from East to West in the winter. In late winter (early June) the median floe diameter was 2.1 km in the Canadian Beaufort, 2.0 km in the Alaskan Beaufort and 1.9 km in the Chukchi Sea. Mean diameter was 3.3 km in the east versus 2.7 km in the west. Maximums were 44 km in the east and 21 km in the west.

No such trend can be noted in summer (August). Median floe size in the east was smaller than in the west: 1.5 km compared to 1.8 km. Yet the larger floes were bigger in the east.

The greater number of large floes in the east augmented the average floe diameter to 3.5 km compared with 2.3 km in the Chukchi Sea. In the Canadian Beaufort summer large floes continue to enter the lease areas from the polar pack to the north. At the same time, warmer water and wave action deteriorate most of the floes to produce many small floes and a small median value. In the Chukchi Sea there is no replenishment of large floes.

The well-known trend from large floes at the end of winter to small and deteriorated floes by late summer is documented for the Canadian Beaufort Sea. Median diameter decreases from 6 km in midwinter to 2 km in late winter, 1.5 km in early summer and 0.8 km in late summer.

One image covered a late-September multi-year ice incursion over lease areas in the Canadian Beaufort. This can be compared with a similar event in late September 1981, (see Arsenault 1981) which was used as a basis for part of the 1982 design statistics. Median and mean diameter for the present study were 0.8 km and 1.4 km, - considerably smaller than the 1.5 km and 2.1 km obtained in the 1981 study. However there was more similarity at the large end of the scale. The 99 percentile diameter was 9 km in 1981 and 8 km in 2008.

In addition, data on average multi-year ice concentrations over the past 10 years was mapped for the winter and summer periods across the region. A comparison with Canadian Beaufort Sea records from 30 years before indicates that the average multi-year ice concentration in the lease area has decreased. The 5% mean multi-year concentration contour in the 1970s corresponds to the 2% contour in the decade since 1999. Chapter 7 summarizes this data.

Multi-year Floe and Ridge Thickness from ULS and IPS

Upward looking sonar records from the October 2000a submarine cruise from near Point Barrow to the North Pole were analyzed. The transect was divided into 6 Areas. For each floe or ridge keel a set of geometrical parameters was calculated. Some 33,000 floes and 14,000 ridges were profiled and analyzed. This geometric data for each Area was analyzed statistically and exceedance distribution functions were fit. In the report a detailed analysis is given for Area D - the Chukchi Sea and the western Alaskan Beaufort. Data analysis and exceedance distributions for all areas were written to a data base that is described in Chapter 8

Some of the many results for Area D are: average draft of "old" ice was 2.26 m; Maximum and mean keel draft were 15 m and 6.5 m. Maximum and mean ridge width were 260 m and 16 m. Mean distance from a floe edge to a ridge was 156 m.

The most severe conditions were near the Pole. Average thickness of the old ice was 2.5 m. The deepest keel was 23.9 m.

Data from 3 ice profiling sonar (IPS) moorings deployed west of Banks Island were analyzed in the same way as the submarine data. This area is subject to multi-year ice most of the time. Some 32,000 floes and 25,000 ridges drifted over site 5 alone. Analysis showed that conditions were similar to conditions near the North Pole as determined from the submarine data. Maximum keel draft was 36 m. Average draft was 2.8 m.

At the 10^{-2} probability level, keel depth was 14 m. This compares with 14-19 m cited in Marcellus et.al.1982.

Another aspect of the sonar data, IPS and ULS, was the infrequent detection of multi-year hummock fields, defined as an ice floe of greater than 10 m in average draft and wider than 500m. Only one MYHF was detected in the ULS data and two in the IPS data. This is markedly different from the 1982 analysis of ULS which found 64 MYHFs.

Ice Drift Velocity

Ice drift speed and direction data from selected ADCP deployments in the Canadian Beaufort Sea were analyzed. Since there was no ADCP ice drift data in the public domain for the Alaskan Beaufort and Chukchi Seas, ice velocity statistics in those areas were obtained from drift tracks from the International Arctic Buoy Program (IABP).

A detailed statistical analysis was conducted of 13 years of ADCP data from 1990 to 2003 at Site 1, near 70.5^{o} N 135° W in the Canadian Beaufort Sea. Results are in Chapter 10. Mean winter speed was 10.7 cm/sec. Mean summer speed was 15 cm/sec. The maximum speed of 100.7 cm/sec (almost 2 knots) occurred in the winter. Ice drift can be in any direction but is predominantly to the West in winter. In summer it is more evenly distributed with a greater tendency to drift towards the WNW and ESE.

Drift velocity statistics presented in Marcellus (1982) were based on radar tracking from drill ships in the summer or from drift buoy data in the winter. The summer mean speed from drill ships was 17.7 cm/sec - similar to ADCP data from the 1990s. The drift buoy data was much less accurate and at longer measurement intervals than the ADCP data. Winter mean speed was 5 cm/sec - less than half the estimate from ADCP data.

Several ADCPs have been deployed in the Alaskan Beaufort and Chukchi lease areas, but the data are not in the public domain. Data from 10 drift buoys that traversed the lease areas was obtained from the IABP and analyzed. Results are in Chapter 11. Mean summer and winter speeds for the Chukchi Sea were 14.6 cm/sec and 10 cm/sec. Maximum speed was 73 cm/sec. in summer and 105 cm/sec in winter. Offshore Alaska the mean winter speed was 13 cm/sec and the maximum was 65 cm/sec. Mean and maximum for summer, based on very sparse data, were 32 cm/sec and 63 cm/sec.

Detection of multi-year ridges from sonar data

One problem with sonar data is that when a ridge is passing overhead one cannot be sure if it is first-year or multi-year. Conversely if a satellite image shows the presence of a multi-year floe with ridges, it is not possible to know the thickness profile, or even the average thickness of the floe.

Chapter 9 describes an investigation into the sonar records west of Banks Island at a time when multi-year ice was known to be present. The sonar data was compared with simultaneous, high resolution radar satellite imagery and a correlation was sought. The task was made difficult by the deformation within the drifting pack ice, and correlations between ice surface and keel were not definitive. There were indicators within the sonar profiles to suggest a way to differentiate first year ice from second-year and multi-year ice.

Filtering techniques may yield better results but this was beyond the scope of the present project.

In a sample of radar imagery over the polar pack many of the ridges identified had recently been formed of multi-year ice but were not yet fully consolidated. This is described in Section 8-11. If a substantial number of ridge keels in the sonar records are actually composed of unconsolidated multi-year ice blocks, then it would be of interest to be able to isolate the truly consolidated ridge keels. It is possible that the thickness of multi-year keels has been over-estimated. This is an issue that requires further investigation.

Conclusion

Changes have occurred in the ice shelves of northern Canada and in the ice regime of the Beaufort and Chukchi Seas over the past several decades that warranted an update of the statistics on which design criteria are based. This study documents the recent statistics of key ice parameters relevant to the design of structures. The results may be used to update estimates of impact probability of an ice feature with a structure in the lease areas, and to refine models of ice-structure interaction for the calculation of ice forces.

Acknowledgements

The planning, analysis and writing for this report were executed by the principals, employees and associates of Canatec, with assistance from university researchers. Report authors were D.McGonigal, D.Hagen, R.Marcellus, Dr.R.Pilkington, Dr.S.Tiffin, L.Guzman and Dr.D.Mueller.

The authors would like to thank the JIP partner organizations who funded the project and their representatives for their active participation through the steering committee. The JIP partners were ConocoPhillips Canada Resources Corp., Chevron Canada Ltd, Shell International Exploration and Production Inc., Exxon-Mobil Upstream Research Company, BP Exploration Operating Company Ltd and the U.S. Dept of the Interior Minerals Management Service (MMS).

Special appreciation goes to Dr. W.Spring and Mr. G.Thomas for in-depth review and commentary on the draft report. Thanks also to Mr. B.D.Wright for his support and guidance at all stages of the project.

Definitions

APOA	Arctic Petroleum Operators Association
ADCP	Acoustic Doppler Current Profiler – A current meter that uses the Doppler technique to measure water currents at different water depths.
AOGA	Alaska Oil and Gas Association
Beaufort Gyre	The long term drift current in the Arctic Ocean that causes the Polar Pack to rotate slowly in a clockwise direction.
CIS	Canadian Ice Service
EIF	Extreme Ice Feature.
EIS	Environmental Impact Statement - for the Canadian Beaufort Sea in 1982
FYI	First Year Ice - Ice that has formed during the current winter season, it has a relatively high salinity and low strength compared to older ice.
IABP	International Arctic Buoy Program
Ice Floe	A large piece of ice that has separated from the main ice pack.
II	Ice Islands – Massive Tabular Ice Features with constant thickness of 20-60m (depending on age) originating from the ice shelves of the western Canadian Arctic Islands.
IOS	Institute of Ocean Sciences
IPS	Ice Profiling Sonar – upward looking sonar deployed on the seabed recording the depth and movement of the ice features drifting over them.
Ice Rafting	A process in which a section of ice sheet rides over an adjacent section, resulting in increased thickness. This is usually caused by wind effects acting on relatively thin first year ice.
Ice Ridging	A process in which initially level ice is deformed due to impact, pressure or other events to form a linear feature of rafted ice and blocks comprising a sail above water and a keel under water.
Ice Rubble	An accumulation of ice blocks as a result of continuous action of ice moving and deforming against a previously grounded ice feature or structure.
ISOPE	International Society of Offshore and Polar Engineers
LFI	Land fast ice - Ice that is frozen in place by contact with the coastline and also held in place by grounded features in the shallow water environment.

MLSI	Multi-Year Land-Fast Sea Ice
MYF	Multi-Year Floe
MYI	Multi Year Ice that has survived at least one summer season, it usually has lower salinity and higher strength than first year ice.
MYHF	Multi Year Hummock Field – A massive feature formed from an area of dense ridging that has become multi-year, with a contiguous thickness greater than 10 m.
NIC	National Ice Centre (US)
NSIDC	National Snow and Ice Data Centre
OTC	Offshore Technology Conference
PERD	Program for Energy Research and Development
Polar Pack	The area of multi year ice floes that perennially covers the Arctic Basin.
SBS	Southern Beaufort Sea – the southern region of the Beaufort encompassing the land fast ice and shear zone (see below). This is the region where most of the oil and gas activities are expected.
Shear Zone	A section of pack ice at the edge of the land fast ice, which is active and mobile, resulting in potentially large movements as a result of winds and currents. The ice is a mix of first year and multi year ice. A shearing action between the drifting pack ice and the stationary LFI can form large shear ridges at the edge of the LFI
ULS	Upward Looking Sonar, usually attached to a submarine, to profile the underside of the ice cover during voyages .

Table of Contents

Abstract…… i
Acknowledgements…… vi
Definitions…… vii
Table of Contents…… ix
List of Figures…… xiii
List of Tables…… xix

1 INTRODUCTION 1-1
1.1 Extreme Ice Parameters Affecting Design 1-1
1.2 Possible Effects of Changing Climate 1-1
1.3 Project Goals 1-2
2 LITERATURE REVIEW 2-1
2.1 Background 2-1
2.1.1 The State of Arctic Ice Research 2-1
2.1.2 The Study Zone 2-3
2.1.3 Scope of Literature Search 2-6
2.2 Ice Islands, Ice Shelves and Multi-year Land Fast Sea Ice 2-6
2.2.1 Origin 2-6
2.2.2 Areal Extent and Recent Changes 2-6
2.2.3 Thickness of Ice Shelves 2-8
2.2.4 Ice Islands 2-8
2.2.5 Drift of Ice Islands 2-10
2.2.6 Glacial Ice from Ellesmere 2-10
2.2.7 Glacial Ice from North Greenland 2-11
2.3 Multi-Year Land Fast Ice 2-14
2.4 Occurrence of Multi-Year Floes, Ridges and Hummock Fields 2-15
2.4.1 Occurrence and Trends 2-15
2.4.2 Multi Year Ice Thickness 2-17
2.4.3 Multi-Year Ridge Geometry 2-18
2.5 Sonar as a Tool for Identifying Multi-year Keels 2-19
2.6 Correlation of Sonar with Satellite Images 2-23
2.7 Impact Probability on Structures 2-24
3 SATELLITE DATA ACQUISITION 3-1
3.1 Satellite Platforms Used 3-1
3.2 Planning and Execution of the Satellite Acquisition 3-1
3.2.1 Planned Swaths 3-1
3.2.2 Break Up 2008 and Changes in Plan 3-3
3.3 Satellite Imagery Coverage 3-4
3.3.1 EIF Sampling Area - High Arctic 3-4
3.3.2 Multi Year Floe Sampling Areas - Beaufort and Chukchi 3-6
3.3.3 Sonar Satellite Correlation Areas - Canadian Beaufort 3-7
4 EXTREME ICE FEATURES 4-1
4.1 Quality of Satellite Data 4-1
4.1.1 Envisat Data 4-1

4.1.2 MODIS Data ... 4-2
4.1.3 Radarsat 2 Data ... 4-3
4.1.4 Landsat Data ... 4-3
4.2 EIF Count Methodology ... 4-4
4.2.1 Software Tools ... 4-4
4.2.2 Ice Islands and Ice Island Fragments ... 4-5
4.2.3 Multi Year Hummock Fields ... 4-6
4.3 EIF Count Results and Areal Density ... 4-6
4.4 EIF Data Base ... 4-8
4.4.1 Data Compilation and Derived Parameters ... 4-8
4.4.2 Database Description ... 4-10
4.5 Statistical Analysis of EIF parameters ... 4-11
4.5.1 Database Subsets Analyzed ... 4-11
4.5.2 EIF Statistics By Zone ... 4-13
4.5.3 EIF Statistics By Type ... 4-15
4.5.4 Equivalent Diameter Statistics ... 4-17
4.6 Comparison with Previous Surveys ... 4-19
4.7 Glacial Ice Advance on Ellesmere Island ... 4-21
5 ICE SHELVES AND MULTI-YEAR LANDFAST SEA ICE ... 5-1
5.1 Introduction ... 5-1
5.2 Methods ... 5-1
5.3 Ice Shelf Thickness Data ... 5-2
5.4 Changes in Ice Shelf Extent 1998 - 2008 ... 5-9
5.5 Multi-Year Land Fast Sea Ice Thickness ... 5-12
5.6 Changes to Multi-year Land Fast Sea Ice Extent 1998 - 2008 ... 5-20
6 MULTI YEAR FLOE SIZES ... 6-1
6.1 Overview ... 6-1
6.2 Methodology for Analysis and Interpretation ... 6-2
6.2.1 Procedure ... 6-2
6.2.2 Variations in Image Resolution ... 6-2
6.2.3 Conglomerate and Continuous Floes ... 6-2
6.3 Multi – Year Floe Data Base ... 6-3
6.3.1 Data Sets ... 6-3
6.3.2 Multi-Year Floe Parameters ... 6-3
6.3.3 Spatial and Temporal Coverage ... 6-4
6.4 Interpretation and Analysis of Multi-Year Floe Size ... 6-8
6.4.1 Late Winter Floe Sizes using RadarSat 2 June 4 & 9, 2008 ... 6-8
6.4.2 Summer Floe Sizes Radarsat 2 Wide Aug – Sept, 2008 ... 6-15
6.4.3 Summer Floe Sizes High Arctic Envisat August, 2, 2008 ... 6-21
6.4.4 Winter Floe Sizes MODIS March 7, 2008 ... 6-23
6.4.5 Statistics of Shape Indicators ... 6-25
6.5 Discussion of Results ... 6-26
6.5.1 Regional Variations in Late Winter ... 6-26
6.5.2 Regional Variations in Summer ... 6-28
6.5.3 Seasonal Variations ... 6-29
6.5.4 Comparison with Previous Data ... 6-31
7 OLD ICE CONCENTRATION ... 7-1

7.1 Ice Concentration statistics. ... 7-1
7.2 Changes in Old Ice Concentration ... 7-3
8 OLD ICE THICKNESS FROM ULS and IPS ... 8-1
8.1 ULS Data Source and Initial Processing ... 8-1
8.2 ULS Data Grouping and Gaps in the Data ... 8-1
8.3 ULS Data Analysis and Parameter Definitions ... 8-4
8.3.1 Data Analysis Procedure and Disposition of Data Plots ... 8-4
8.3.2 Alternative Ridge and Floe Definitions ... 8-4
8.3.3 Standard Deviation of 5m Cutoff and Rayleigh Ridges ... 8-5
8.3.4 Data Base Parameters ... 8-7
8.4 Summary Plots for Area D, Alaskan Beaufort Sea ... 8-9
8.5 Comparison of Ridge Statistics by Area ... 8-24
8.5.1 Keel Maximum Draft and Standard Deviation ... 8-24
8.5.2 Ridge Widths ... 8-25
8.5.3 Mean Floe Draft Excluding Ridges ... 8-25
8.5.4 Spatial Distance between Ridge Keel Peaks ... 8-26
8.5.5 Width of Floes Containing Ridges ... 8-27
8.5.6 Summary of 2000a Submarine Cruise Data Area Comparison ... 8-28
8.6 IPS Data Analyzed and Selected Results ... 8-28
8.7 Discussion on Ice Types Contained in the IPS Data ... 8-30
8.8 Comparison of Submarine and IPS data ... 8-32
8.9 Hummock Fields ... 8-34
8.9.1 Hummock Fields in the ULS Data - Western Arctic Ocean ... 8-34
8.9.2 Hummock Fields in the IPS Data West of Banks Island ... 8-36
8.10 Data on the HD ... 8-36
8.11 Ridge Count from Satellite Imagery ... 8-37
9 CORRELATING SURFACE IMAGERY WITH KEEL PROFILES ... 9-1
9.1 Introduction ... 9-1
9.2 Comparison of IPS and Satellite data ... 9-1
9.3 Detailed Look at IPS Data ... 9-7
9.4 Conclusions ... 9-9
10 ICE VELOCITY FROM MOORED ADCP – CANADIAN BEAUFORT SEA ... 10-1
10.1 Data Source ... 10-1
10.2 Ice Velocity Statistics – Southern Canadian Beaufort Sea ... 10-2
10.2.1 Data Description ... 10-2
10.2.2 Ice Velocity Analysis Site 1 – All Years ... 10-3
10.2.3 Ice Velocity Analysis for Calendar Year 2002 ... 10-8
10.3 Ice Velocity Statistics - North-East Canadian Beaufort ... 10-13
10.3.1 Data Description ... 10-13
10.3.2 Ice Velocity Analysis for Site 5 – 1996-1998 ... 10-14
11 ICE VELOCITY FROM DRIFT BUOY DATA – CHUKCHI AND ALASKAN BEAUFORT SEAS ... 11-1
11.1 Data Source ... 11-1
11.2 Alaskan Beaufort Sea Drift Buoy Data ... 11-3
11.3 Chukchi Sea Drift Buoy Data ... 11-6
12 CONCLUSIONS AND RECOMMENDATIONS ... 12-1
12.1 Overview ... 12-1

12.2 Literature Review 12-1
12.3 Satellite Data Acquisition 12-2
12.4 Extreme Ice Features EIFs 12-2
12.4.1 General 12-2
12.4.2 Ice Islands and Ice Island Fragment Occurrence 12-2
12.4.3 Multi-Year Hummock Field Occurrence 12-3
12.5 Thickness of Ice Shelves and Multi-Year Land Fast Sea Ice (MLSI) 12-3
12.6 Multi-Year Floe Size and Concentration 12-4
12.7 Old Ice Thickness from Submarine ULS Data 12-5
12.8 Old Ice Thickness from IPS Data West of Banks Island 12-5
12.9 Correlation of Satellite Images of Surface with Keel Profiles 12-6
12.10 Ice Drift in the Southern Canadian Beaufort Sea 12-6
12.11 Ice Drift in the Chukchi and Alaskan Beaufort Seas 12-6
12.12 Implications for EIF Impact Probability 12-7
13 REFERENCES 13-1
14 APPENDIX A - SATELLITE IMAGERY AND EIF ANALYSIS 14-1
14.1 A-1 Radarsat 2 Data 14-1
14.2 A-2 Landsat Data 14-9
14.3 A-3 MODIS Data 14-14
14.4 A-4 Envisat Imagery 14-16
15 APPENDIX B Calculated Parameters for EIF and M–Y Floe Data Bases 15-1
16 APPENDIX C - EXTREME ICE FEATURES DATA BASE 16-1

List of Figures

Figure 2-1 General Current Circulation of the Arctic Seas..... 2-3
Figure 2-2 General Ice Drift in the Arctic Basin (from NSIDC) 2-4
Figure 2-3 Ice Drift from IABP 2008 (International Arctic Buoy Program)..... 2-5
Figure 2-4 Ice Shelves and Multi-year Land fast Ice - Ellesmere Island before 2006 2-7
Figure 2-5 Ice Shelves - Ellesmere Island 2007 Conditions 2-7
Figure 2-6 Ice Shelves - Ellesmere Island 2008 Conditions 2-7
Figure 2-7 Makeup of Hobson's Choice Ice Island..... 2-9
Figure 2-8 Recent Drift of Ayles Ice Island..... 2-10
Figure 2-9 Potential sources of EIFs from N Greenland 2-11
Figure 2-10 Petermann Glacier Calving of 2008 2-12
Figure 2-11 Sources of Glacial Ice 2-13
Figure 2-12 Suspected Main Land-fast Multi-year Sea Ice Shelves 1991..... 2-14
Figure 2-13 Changes in Age and Thickness of Sea Ice 2-16
Figure 2-14 Changes in Old Sea Ice Occurrence 2-16
Figure 2-15 Beaufort Sea Extreme Ice Draft Occurrence..... 2-18
Figure 2-16 Keel Draft Probability from submarine tracks 1960s 2-18
Figure 2-17 Deployment of Upward Looking Moored Sonar..... 2-20
Figure 2-18 Woods Hole Instrument Locations 2003-2004 2-21
Figure 2-19 US Scientific Submarine Cruises 2-22
Figure 2-20 First Year Ridge Cross Sections from Bowen and Topham (1996)..... 2-23
Figure 3-1 Radarsat orbits for EIF sample..... 3-2
Figure 3-2 Envisat orbits for EIF sample..... 3-2
Figure 3-3 Multi-Year ice edge 2008-06-30 and planned Envisat acquisitions..... 3-3
Figure 3-4 Progression of Break Up 2008 and Retreat of Multi-Year Pack Ice Edge 3-4
Figure 3-5 Coverage by Envisat, Radarsat, Landsat and MODIS July-August 2008 3-5
Figure 3-6 Envisat data in the Southern Beaufort Sea July-August 2008 3-6
Figure 3-7 ERS coverage 1996 at IPS Site 5 west of Banks Island 3-7
Figure 4-1 Sample of ENVISAT imagery 4-1
Figure 4-2 Sample of MODIS imagery 4-2
Figure 4-3 Sample of Radarsat 2 Imagery 4-3
Figure 4-4 Sample of Landsat Imagery, SW of Meighen Island..... 4-4
Figure 4-5 EIF Distribution in North Section (II - red, IIF - pink, MYHF - brown)..... 4-7
Figure 4-6 EIF Distribution in South Section (II - red, IIF - pink, MYHF - brown)..... 4-8
Figure 4-7 Zones Used in the EIF Analysis 4-10
Figure 4-8 Box Plots of EIF Area and Diameter by Zone 4-13
Figure 4-9 Exceedence Probability for Area..... 4-14
Figure 4-10 Exceedence Probability for Diameter..... 4-14
Figure 4-11 Exceedence Probability for Area for features > 500m diam..... 4-16
Figure 4-12 Exceedence Probability for Diameter for features > 500m diam..... 4-16
Figure 4-13 Box plots of area by EIF Type for features > 500m diam. 4-17
Figure 4-14 Exceedence Plot of Equivalent Diameter All EIFs >500m diameter 4-18
Figure 4-15 Exceedence Plot of Equivalent Diameter for Ice Islands >500m..... 4-18
Figure 4-16 Exceedence Plot of Equivalent Diameter Multi-Year Hummock Fields..... 4-19
Figure 4-17 Floating Glacier behind the Milne Ice Shelf..... 4-22

Figure 5-1 Milne Ice Shelf GPR transect and thickness 5-3
Figure 5-2 Milne Ice Shelf Thickness Histogram and Profile 5-4
Figure 5-3 Petersen Ice Shelf GPR transect and thickness 5-5
Figure 5-4 Petersen Ice Shelf Thickness Histogram and Profile..... 5-6
Figure 5-5 Serson ice shelf GPR transect and thickness..... 5-7
Figure 5-6 Serson Ice Shelf Thickness Histogram and Profile 5-8
Figure 5-7 Ice shelf extent from Radarsat-1 imagery acquired Jan - April 1998..... 5-9
Figure 5-8 Ice shelf extent from Radarsat-1 imagery acquired Jan-Feb 2003 5-10
Figure 5-9 Ice shelf extent from Radarsat-1 imagery acquired Jan/April 2006..... 5-10
Figure 5-10 Ice shelf extent from Radarsat-1 imagery acquired in February 2008. 5-11
Figure 5-11 Ice shelf extent from MODIS and Formosat-2 imagery late August 2008.. 5-11
Figure 5-12 Yelverton Bay multi-year sea ice GPR transect and thickness 5-13
Figure 5-13 Yelverton Bay ice thickness histogram and profile..... 5-14
Figure 5-14 M'Clintock Inlet multiyear sea ice GPR transect and thickness 5-15
Figure 5-15 M'Clintock Inlet ice thickness histogram and profile 5-16
Figure 5-16 Bromley Island, Cape Richards and Taconite Inlet MLSI GPR transect 5-17
Figure 5-17 Bromley Island, Cape Richards ice thickness histogram and profile..... 5-18
Figure 5-18 Taconite Inlet ice thickness histogram and profile..... 5-19
Figure 5-19 Ice shelf (red) and MLSI (grey) extent from Radarsat-1 Jan-April 1998... 5-20
Figure 5-20 Ice shelf (red) and MLSI (grey) extent from Radarsat-1 Jan/April 2006 ... 5-21
Figure 6-1 Three General Areas for Floe Size Analysis..... 6-1
Figure 6-2 Map of All M-Y Floes Analyzed for Chukchi and Beaufort Seas 2008..... 6-4
Figure 6-3 Map of Convex Hull Polygons Enclosing M-Y Floe Data Sets..... 6-5
Figure 6-4 Convex Hull Polygons of M-Y Floes for 3 Areas in Late Winter..... 6-6
Figure 6-5 Convex Hull Polygons of M-Y Floes for 4 areas in Summer 6-7
Figure 6-6 Convex Hull Polygon of M-Y Foes in Mid Winter..... 6-8
Figure 6-7 M-Y Floes Chukchi Sea June 9, 2008 (Radarsat2 100m res) 6-9
Figure 6-8 Exceedence Probability - multi-year floe area - Chukchi late winter..... 6-10
Figure 6-9 Exceedence Probability - multi-year floe diameter - Chukchi late winter... 6-10
Figure 6-10 M-Y Floes Alaskan Beaufort June 4, 2008. Radarsat2..... 6-11
Figure 6-11 Exceedence Probability - M-Y Floe Area - Alaskan Beaufort late winter .. 6-12
Figure 6-12 Exceedence Probability - M-Y Floe Diam. - Alaskan Beaufort late winter 6-12
Figure 6-13 M-Y Floes Canadian Beaufort June 9, 2008. Radarsat2..... 6-13
Figure 6-14 Exceedence Probability - M-Y Floe Area - Canadian Beaufort late winter 6-14
Figure 6-15 Exceedence Probability - M-Y Floe Diam - Canadian Beaufort late winter 6-14
Figure 6-16 M-Y Floes Chukchi Sea August 2nd, 2008 Radarsat2 6-15
Figure 6-17 Exceedence Probability - M-Y Floe Area - Chukchi summer 6-16
Figure 6-18 Exceedence Probability - M-Y Floe Diameter - Chukchi summer 6-16
Figure 6-19 M-Y Floes Canadian Beaufort August 12th 2008 Radarsat2..... 6-17
Figure 6-20 Exceedence Probability - M-Y Floe Area - Canadian Beaufort summer 6-18
Figure 6-21 Exceedence Probability - M-Y Floe Diam - Canadian Beaufort summer ... 6-18
Figure 6-22 M-Y floe sizes Sept 27th, 2008 Canadian Beaufort 6-19
Figure 6-23 Exceedence Probability - M-Y Floe Area - Canadian Beaufort Sept 27..... 6-20
Figure 6-24 Exceedence Probability - M-Y Floe Diam - Canadian Beaufort Sept 27.... 6-20
Figure 6-25 M-Y Floes SW Prince Patrick I. Aug 2nd, 2008 Envisat..... 6-21
Figure 6-26 Exceedence Probability - M-Y Floe Area - N. Canadian Beaufort summer 6-22
Figure 6-27 Exceedence Probability - M-Y Floe Diam - N.Canadian Beaufort summer 6-22

Figure 6-28 March 7, 2008. MODIS 240m resolution 6-23
Figure 6-29 Exceedence Probability - M-Y Floe Area - Beaufort winter 6-24
Figure 6-30 Exceedence Probability - M-Y Floe Diameter - Beaufort winter 6-24
Figure 6-31 Histograms of circularity Indicators for all datasets..... 6-25
Figure 6-32 Circularity Indicator for the different datasets. 6-25
Figure 6-33 M-Y floe diameter (in km.) for three regions in late winter 6-26
Figure 6-34 M-Y floe area (in sq.km.) for three regions in late winter..... 6-27
Figure 6-35 M-Y Floe Diameter for two areas in early summer..... 6-28
Figure 6-36 M-Y Floe Area for two areas in early summer 6-29
Figure 6-37 M-Y Floe Diameter progression from winter to summer 2008 6-30
Figure 7-1 Annual Old Ice Concentration Contours from 1999 to 2008..... 7-1
Figure 7-2 Winter Old Ice Concentration Contours from 1999 to 2008..... 7-2
Figure 7-3 Summer Old Ice Concentration Contours from 1999 to 2008. 7-3
Figure 7-4 Summer Multi-Year Ice Concentration 1970s and 2000s Canadian Beaufort7-4
Figure 8-1 Upward looking sonar Submarine Cruise October,2000 8-1
Figure 8-2 Areas Analyzed for the 2000a Submarine Data 8-2
Figure 8-3 Gap in the 2000a Dataset at 88.25 N and 150.1 E..... 8-3
Figure 8-4 Typical Data Gap in the 2000a sonar data. 8-3
Figure 8-5 A Typical Floe Plot (contained on the HD) 8-4
Figure 8-6 Plot of a 5 m Cutoff Ridge and a Rayleigh Ridge..... 8-5
Figure 8-7 Comparison of the Standard Deviation of Ridge Draft for Cutoff (upper graph) and Rayleigh Ridges (lower graph) 8-6
Figure 8-8 Definition sketch of key multi-year floe and ridge parameters..... 8-7
Figure 8-9 Area D Exceedance Plot of Ridge Maximum Draft..... 8-10
Figure 8-10 Area D Exceedance Plot of Ridge Maximum Draft less 5 m with best Fit . 8-10
Figure 8-11 Area D Exceedance Plot of Ridge Draft Std. Dev..... 8-11
Figure 8-12 Area D Exceedance Plot of Ridge Width..... 8-11
Figure 8-13 Area D Ridge Apex Angle Statistics (mean apex angle of 159 degrees) 8-12
Figure 8-14 Area D Exceedance Plot of Ridge Keel Angle..... 8-12
Figure 8-15 Area D Exceedance Plot of Distance ($x10^4$ m) between Ridge Crests (a spatial representation of frequency of ridges along a line in an Area including thin ice).... 8-13
Figure 8-16 Exceedance Plot of Distance between Ridge Peaks on Same Floe..... 8-13
Figure 8-17 Area D Exceedance Plot Distance from Floe Edge to Ridge Starting Point8-14
Figure 8-18 Area D Exceedance Plot of Ridge Area..... 8-14
Figure 8-19 Ridge Width vs. Keel Maximum Draft..... 8-15
Figure 8-20 Ridge Width vs. Keel Average Draft..... 8-15
Figure 8-21 Ridge Width x Max. Draft vs. Ridge Area. 8-16
Figure 8-22 Area D Correlation Lag 1, Lag 2, and Lag 3 Analyses 8-16
Figure 8-23 Exceedance Plot of Mean Floe Draft Including Ridges less 1 m..... 8-17
Figure 8-24 Exceedance Plot of Floe Draft Std. Dev including ridges 8-18
Figure 8-25 Exceedance Plot of Floe Draft Std. Dev./Mean Including Ridges. 8-18
Figure 8-26 Exceedance Plot of Mean Floe Draft Excluding Ridges 8-19
Figure 8-27 Exceedance Plot of Floe Draft Std. Dev. Excluding Ridges..... 8-19
Figure 8-28 Exceedance Plot of Floe Draft Std. Dev./Mean Excluding Ridges..... 8-20
Figure 8-29 Exceedance Plot of Floe Width 8-20
Figure 8-30 Exceedance Plot of Width of Floes Containing Ridges..... 8-21
Figure 8-31 Exceedance Plot of Lead in distance from Floe Edge to Closest Ridge..... 8-21

Figure 8-32 Exceedance Plot of Width of Thin Ice Sections 8-22
Figure 8-33 Mean Thin Ice Draft Statistics..... 8-22
Figure 8-34 Thin Ice Draft Standard Deviation Statistics 8-23
Figure 8-35 Exceedance Plot of Keel Maximum Draft for Different Areas..... 8-24
Figure 8-36 Exceedance Plot of Ridge Draft Standard Deviation for Different Areas... 8-24
Figure 8-37 Exceedance Plot of Ridge Widths for Different Areas..... 8-25
Figure 8-38 Exceedance Plot Mean Floe Draft Excluding Ridges for Different Areas . 8-26
Figure 8-39 Exceedance Plot Distance between Ridge Peaks for Different Areas..... 8-26
Figure 8-40 Exceedance Plot of Width of Floes Containing Ridges for Different Areas 8-27
Figure 8-41 Exceedance Plot of Width of Floes Containing Ridges for a 1 m and 2 m Floe Cutoff for Areas A and B 8-28
Figure 8-42 Stationary Upward Looking Sonar Data Sites west Banks Island 8-29
Figure 8-43 All Draft Data at Site 6 NE Coast of Banks Island 8-30
Figure 8-44 All Draft Data at Site 5 West Coast of Banks Island..... 8-31
Figure 8-45 Comparison of Maximum Keel Draft Statistics for IPS Sites 5 and 6 and the results of the 2000a Submarine Cruse..... 8-32
Figure 8-46 Comparison of Ridge Draft Standard Deviation Statistics for IPS Sites 5 and 6 and the results of the 2000a Submarine Cruse 8-33
Figure 8-47 Comparison of Ridge Width Statistics for IPS Sites 5 and 6 and the results of the 2000a Submarine Cruse..... 8-33
Figure 8-48 Comparison of Floe Width (containing ridges) Statistics for IPS Sites 5 and 6 and the results for Areas A and B of the 2000a Submarine Cruse 8-34
Figure 8-49 Ridge Width vs. Average Thickness from the 5 m Cutoff Ridge Analysis 8-35
Figure 8-50 Big Hummock Field at 89.5N and 222E..... 8-35
Figure 8-51 Hummock Field found in the 1996-1997 data for Site 5. 8-36
Figure 8-52 Hummock Field found in the 1996-1997 data for Site 5. 8-36
Figure 8-53 Location of Imagery used in the Ridge Count Analysis. 8-37
Figure 8-54 Ridges and Ridged Areas Identified on the Envisat Image 8-38
Figure 8-55 Enlargement of the left side of Figure 6.54..... 8-38
Figure 9-1 Overlay of IPS data on ERS-2 SAR image for 1996/08/30..... 9-3
Figure 9-2 Overlay of IPS data on ERS-2 SAR image for 1996/09/18..... 9-4
Figure 9-3 Overlay of IPS data on ERS-2 SAR image for 1996/10/24..... 9-5
Figure 9-4 Overlay of IPS data on Radarsat image for 1996/11/10 9-6
Figure 9-5 Example of first year ice in IPS data 9-7
Figure 9-6 Example of old and first year ice in the IPS data (author interpretation)..... 9-8
Figure 9-7 Example of mainly second year ice in IPS data 9-9
Figure 10-1 Map of IPS/ADCP Deployment Locations by IOS 10-1
Figure 10-2 Frequency histograms for Ice Speed for all years at Site 1..... 10-3
Figure 10-3 Exceedance Probability for Ice Speed at Site 1 - Annual 10-4
Figure 10-4 Exceedance Probability for Ice Speed at Site 1 - Summer..... 10-4
Figure 10-5 Exceedance Probability for Ice Speed at Site 1 - Winter..... 10-5
Figure 10-6 Box Plot of Ice Speed Statistics for Site 1: Annual, Winter, Summer 10-6
Figure 10-7 Ice Drift Roses and Scatter Plots for Site 1: Annual, Summer, Winter... 10-7
Figure 10-8 Frequency histograms for Ice Speed for 2002 at Site 1 10-8
Figure 10-9 Exceedance probability for ice speed 2002 at Site 1 - annual..... 10-9
Figure 10-10 Exceedance probability for ice speed 2002 at Site 1 - summer..... 10-9
Figure 10-11 Exceedance probability for ice speed 2002 at Site 1 - winter 10-10

Figure 10-12 Box plot of drift speed statistics for Site 1 2002 10-11
Figure 10-13 Ice Drift Roses and scatter plots for Site 1 - 2002.....10-12
Figure 10-14 IPS/ADCP Locations West of Banks Island NE Canadian Beaufort.....10-13
Figure 10-15 Frequency histograms of Ice Speed at Site 5 1996-1998.....10-14
Figure 10-16 Exceedance probability of speed at Site 5 – All data 10-14
Figure 10-17 Exceedance probability of speed at Site 5 - Winter.....10-15
Figure 10-18 Exceedance probability of Speed at Site 5 – Summer.....10-15
Figure 10-19 Box Plot of Drift speed statistics for Site 5.....10-16
Figure 10-20 Ice Drift Roses and Scatter Plots of ice drift at Site 5 10-17
Figure 11-1 Ice Drift over a 60 day period to April 23, 2009 from IABP website..... 11-1
Figure 11-2 Arctic Buoy Drift Tracks 1999-2008 (left image)..... 11-2
Figure 11-3 IABP Drift Tracks in Alaskan Beaufort Sea 1987-2008..... 11-3
Figure 11-4 Speed histograms for summer and winter – Alaskan Beaufort Sea 11-3
Figure 11-5 Exceedance Plots for summer and winter – Alaskan Beaufort Sea..... 11-4
Figure 11-6 Drift Roses for IABP Buoys – Alaskan Beaufort Sea 1987-2008..... 11-5
Figure 11-7 IABP Drift Tracks in the Chukchi Sea 1987 - 2008..... 11-6
Figure 11-8 Drift Speed histograms for summer and winter - Chukchi Sea..... 11-7
Figure 11-9 Drift Speed exceedance plots for summer and winter - Chukchi Sea 11-7
Figure 11-10 Drift Roses for IABP Buoys – Chukchi Sea 1987 - 2008..... 11-9
Figure 14-1 Radarsat 2 August 2, 2008 50km swath, 8m resolution. – PPI 1 14-1
Figure 14-2 Radarsat 2 August 2, 2008 50km swath, 8m resolution. – PPI 2 14-2
Figure 14-3 Radarsat 2 August 2, 2008 50km swath, 8m resolution. – PPI 3 14-3
Figure 14-4 Radarsat 2 August 2, 2008 50km swath, 8m resolution. – PPI 4 14-4
Figure 14-5 Radarsat 2 July 30, 2008 50km swath, 8m resolution. – Meighen #1 14-5
Figure 14-6 Radarsat 2 July 30, 2008 50km swath, 8m resolution. – Meighen #2 14-6
Figure 14-7 Radarsat 2 July 30, 2008 50km swath, 8m resolution. – Meighen #3 14-7
Figure 14-8 Radarsat 2 July 30, 2008 50km swath, 8m resolution. – Meighen #4 14-8
Figure 14-9 LANDSAT July 29, 2008 100km swath, 30m resolution. Meighen I. 14-9
Figure 14-10 LANDSAT July 29, 2008 100km swath, 30m resolution. Axel Heiberg Island 14-11
Figure 14-11 LANDSAT – July 27, 2008 12.5m resolution.....14-12
Figure 14-12 LANDSA July 27, 2008 100km swath, 30m resolution. Prince Patrick Island 14-13
Figure 14-13 Aug. 1, 2008. MODIS of Ellesmere Island at 240m Resolution.....14-14
Figure 14-14 Aug 1, 2008 MODIS Pack Ice off Borden Island.....14-15
Figure 14-15 (1 of 22) Envisat July 31, 2000 100km swath, 30m res. (Ward Hunt Island) 14-16
Figure 14-16 (2 of 22) Envisat August 1, 2008 100km swath, 30m res (Ayles-Milne Shelves) 14-17
Figure 14-17 (3 of 22) Envisat August 1, 2008 100km swath, 30m res (Petersen -Serson Shelves) 14-18
Figure 14-18 (4 of 22) Envisat August 1, 2008 100km swath, 30m res (Nansen Sound and North) 14-19
Figure 14-19 (5 of 22) Envisat – August 1, 2008 100km swath, 30m res (Nansen Sound and South).....14-20
Figure 14-20 (6 of 22) Envisat August 1, 2008 100km swath, 30m res (Offshore Axel Heiberg Island) 14-21

Figure 14-21 (7 of 22) Envisat August 1, 2008 100km swath, 30m res (Meighen Island) 14-22
Figure 14-22 (8 of 22) Envisat August 1, 2008 100km swath, 30m res. (NW of Meighen Island).....14-23
Figure 14-23 (9 of 22) Envisat August 1, 2008 100km swath, 30m res. (NW of Ellef Ringnes Island) 14-24
Figure 14-24 (10 of 22) Envisat August 1, 2008 100km swath, 30m res. (Borden Island) 14-25
Figure 14-25 (11 of 22) Envisat August 1, 2008 100km swath, 30m res. (NW of Prince Patrick Island).....14-26
Figure 14-26 (12 of 22) Envisat August 1, 2008 100km swath, 30m res. (WSW of Prince Patrick Island).....14-27
Figure 14-27 (13 of 22) Envisat August 1, 2008 100km swath, 30m res. (SSW of Prince Patrick Island).....14-28
Figure 14-28 (14 of 22) Envisat August 1, 2008 100km swath, 30m res. (W of Prince Patrick Island).....14-29
Figure 14-29 (15 of 22) Envisat July 31, 2008 100km swath, 30m res. (W of Ellef Ringnes Island) 14-30
Figure 14-30 (16 of 22) Envisat July 31, 2008 100km swath, 30m res. (100kms W of Meighen Island) 14-31
Figure 14-31 (17 of 22) Envisat Aug 1, 2008 100km swath, 30m res. (Arctic Ocean 83N 83W).....14-32
Figure 14-32 (18 of 22) Envisat Jul 31, 2008 100km swath, 30m res. (W Coast Prince Patrick Isl.) 14-33
Figure 14-33 (19 of 22) Envisat Aug 1, 2008 100km swath, 30m res. (Along Ellesmere Island coast).....14-34
Figure 14-34 (20 of 22) Envisat Aug 1, 2008 100km swath, 30m res. (Along Ellesmere Island coast).....14-35
Figure 14-35 (21 of 22) Envisat Aug 1, 2008 100km swath, 30m res. (100km W of Prince Patrick Island – Arctic Ocean).....14-36
Figure 14-36 (22 of 22) Envisat Aug 1, 2008 100km swath, 30m res. (50km W of Brock Island).....14-37
Figure 15-1 Example of Major and Minor Axes and Diameter 15-1
Figure 15-2 Example of shape with Ellipsoid Roundness of nearly 1 15-2

List of Tables

Table 2-1 Key Arctic Research Institutions 2-2
Table 2-2 Summary of Recent Calving 2-8
Table 4-1 Observed Areal Densities of EIFs >500m in equivalent diameter 4-7
Table 4-2 EIFs 2008 Divided by Zone 4-12
Table 4-3 EIFs 2008 Divided by Type 4-12
Table 4-4 Basic Parameters for all EIF data by Type 4-15
Table 4-5 Basic Parameters for EIFs> 500m in diameter by Type 4-15
Table 4-6 Comparison of EIF Populations 4-20
Table 4-7 Comparison of EIF Areal Densities 4-20
Table 4-8 Comparison of EIF Sizes (Equivalent Diameter > 500m) 4-21
Table 5-1 GPR measurements versus direct observations of snow and ice thickness..... 5-2
Table 5-2 Ice Shelf Thickness Data 5-2
Table 5-3 Ice Shelf Extent 1998-2008 5-9
Table 5-4 Multi-Year Land Fast Sea Ice Thickness (MLSI) data 5-12
Table 5-5 Multi-Year Land Fast Sea Ice Extent 1998-2008 5-20
Table 6-1 Data sets developed from analysis of satellite imagery 6-3
Table 6-2 Basic M-Y Floe statistics for late winter Chukchi Sea 6-9
Table 6-3 Basic M-Y Floe statistics late winter Alaskan Beaufort 6-11
Table 6-4 Basic M-Y Floe statistics for late winter Canadian Beaufort Sea 6-13
Table 6-5 Basic M-Y Floe statistics for Summer Chukchi Sea 6-15
Table 6-6 Basic M-Y Floe statistics for Summer Canadian Beaufort Sea..... 6-17
Table 6-7 Basic M-Y Floe statistics for late Summer Canadian Beaufort Sea 6-19
Table 6-8 Basic M-Y Floe statistics for Summer Prince Patrick I. 6-21
Table 6-9 Basic M-Y Floe statistics for mid-winter Alaskan Beaufort Sea 6-23
Table 6-10 M-Y Floe Diameter in late September - Comparison 1980 and 2008 6-31
Table 6-11 M-Y Floe Diameter in mid-Winter – comparison 1990 and 2008 6-32
Table 8-1 Draft data for Different Areas of the 2000a Submarine Transect 8-2
Table 8-2 Thin Ice Statistics contained in the Database files (..... 8-7
Table 8-3 Ridge Statistics contained in the Database files 8-8
Table 8-4 Extra Ridge Statistics contained in the Database files 8-8
Table 8-5 Floe Statistics contained in the Database files..... 8-9
Table 8-6 Number of floes and Ridges Found 8-9
Table 8-7 IPS Data Analyzed 8-29
Table 8-8 Populations of floes and ridges from the IPS analysis. 8-30
Table 8-9 Ice Type Concentrations at Site 5 – 96/97 8-31
Table 8-10 Ice Type Concentrations at Site 6 – 97/98 8-31
Table 10-1 Summary of IPS Deployment Locations 10-2
Table 10-2 Break-up and freeze-up dates at the IPS Locations 10-2
Table 10-3 Number of Records for Summer and Winter 10-3
Table 10-4 Gaps in the IPS Data 10-3
Table 10-5 Ice Speed Statistics for Site 1 10-6
Table 10-6 Summary Drift Speed Statistics for Site 1 2002 10-11
Table 10-7 Break-up and Freeze-up Dates at Site 5 1996 - 1998 10-13
Table 10-8 Total and useful number of records for Site 5 10-13

Table 10-9 Summary of drift speed statistics for Site 5.....10-16
Table 11-1 IABP Buoys traversing Alaskan Beaufort and Chukchi Sea Lease Areas.... 11-2
Table 11-2 Speed Statistics for IABP Buoys - Alaskan Beaufort 1987-2008 11-4
Table 11-3 Speed Statistics for IABP Buoys - Chukchi Sea 1987 - 2008..... 11-8

This page was deliberately left blank

1 INTRODUCTION

1.1 Extreme Ice Parameters Affecting Design

The design of offshore structures for the western Arctic of North America is likely to be governed by their interactions with very large and thick ice features which include ice islands, multi-year hummock fields and large multi-year floes with embedded ridges. These features are referred to as Extreme Ice Features, or EIFs - a term coined during the time of exploration drilling in the Canadian Beaufort Sea in the early 1980s. An EIF is not the same as the "extreme" ice event, or the 1 in 100-year ice event, which would be derived from probabilistic analysis. However the statistics of EIFs and other ice parameters would be used to define the extreme ice event. EIFs are transported from the High Arctic via the Beaufort Gyre and enter the southern Canadian and Alaskan Beaufort Seas and the US Chukchi Sea.

To evaluate ice loading at a structure, the statistical distributions of ice parameters are required as inputs to a probabilistic model. The key parameters are ice strength, thickness, interaction geometry, velocity and feature size. Limit driving forces in the pack ice surrounding an EIF also play an important role. Thickness includes both the average thickness and the local thickness (of a ridge or embedded hummock field). Ridge orientation and floe edge geometry up to the ridge are also factors (Morrison and Marcellus, 1991). Winter and summer concentrations of multi-year ice are important to assess impact probabilities. Pilkington et.al., 1992, estimated return periods of 50 to 125 years for such an event.

In this project, the type and size of features were obtained from new satellite imagery obtained in 2008 and statistics were calculated. Multi year ice thickness was obtained from both stationary seabed installations and submarine sonar data collected within the past 10 years. Ice velocity statistics were derived from ice drift buoy data and from bottom mounted ice profiling sonar. Ice concentrations were derived from historical ice charts.

1.2 Possible Effects of Changing Climate

In recent years the effects of climate change on the arctic climate and ice cover have received increasing attention. Satellite photos showed that the pack ice edge retreated to unprecedented limits, during the summers of 2001-2005, and also in 2007 and 2008, as documented by the National Snow and Ice Data Centre (NSIDC). In the Southern Beaufort Sea (SBS) the open water seasons have become slightly longer on average, and the open water area more extensive than was the case in the 1980s. However, the pack ice may still return to shallow water areas (20-60 meters depth) on occasion. For example, 2006 was a "bad" summer from an ice point of view because multi-year ice (MY) floes had drifted close to shore the previous winter, remained in the region and caused a short open water season with many potential ice hazards.

A 1-metre reduction in average multi-year ice thickness was detected during the 1990s in the Central Arctic (Rothrock et al., 1999) as compared with earlier decades. This is not reflected in the pack ice that borders the Canadian Arctic Islands and Beaufort Sea. Ice Profiling Sonars (IPS) deployed under the pack ice since 1990 by the Institute of Ocean Sciences (IOS), have generated an extensive data base of ice movements, depth of the

bottom surface of the ice and ocean current profiles. These data do not show significant thinning of the pack ice in that area, (Melling, 2005). Nevertheless, in the longer term, the trend appears to be toward a milder ice climate in the Arctic.

With renewed interest in offshore drilling on the Beaufort shelf it is pertinent to investigate whether the ice conditions that determine criteria for design of structures and marine operations have changed significantly in the past 2 decades.

1.3 Project Goals

The goals of this project were:

- to quantify the statistics of key ice parameters including II, MYHF and MY floes using recent data, and
- to evaluate any changes to design criteria since the most recent studies.

In particular, the project was intended to:

- Indicate changes in the edge of the Ice shelves and in the population of Ice Islands off the north shore of Ellesmere Island over the past decade.
- Indicate the locations of IIs and MYHFs in the region up-drift of the SBS (i.e. from North Banks Island to Ellesmere Island, along the western edge of the Arctic Islands).
- Tabulate in a database the locations, sizes and geometrical properties of IIs and MYHFs in the region up-drift of the SBS and present statistics of their size.
- Estimate the total numbers of IIs and MYHFs currently in the perimeter of the Beaufort Gyre, based on the samples obtained, and the possible future movements of these features.
- Determine the size and statistics of MY floes and in particular, the size of MY ice attached to MYHFs.
- Determine floe thickness and keel thickness ranges for MY ice floes from Upward Looking Sonar and Ice Profilers and calculate the statistics.
- Compile recent ice velocity statistics from drift buoys and IPS deployments,
- Assess changes in the occurrence of MY ice in the areas of interest,

The intention is that statistical data produced in the study may be used to update estimates of the risk of impact of EIFs against offshore structures in the areas of interest, and may further the development of models of ice-structure interaction.

2 LITERATURE REVIEW

2.1 Background

2.1.1 The State of Arctic Ice Research

The first comprehensive effort to synthesize state-of-art research into the design statistics for Beaufort Sea structures design was the 1982 EIS, or Environmental Impact Statement. This was produced by the 3 main operators in the Canadian sector of the Beaufort Sea, Esso, Gulf and Dome Petroleum. By the late 1980s, offshore petroleum activity was winding down throughout the Canadian arctic. US oil company interest in American Beaufort Sea operations offshore was also declining by the late '80s. Research and data gathering on ice conditions related to oil and gas activity more or less drew to a close around the same time. The study by Pilkington et al. (1992) on extreme ice features in the Beaufort Sea summarized the state of the art up to that time.

Attention shifted away from the small and regional scale feature aspects important to structural design and operations, to the issue of climate change. Ice issues important to climate change are things like albedo, snow accumulation, broad circulatory patterns, growth and disintegration, and measurements of thinning, across the entire arctic basin (Symon et al. 2005). However, even in this new orientation, there has been relatively little original data gathering and few researchers active in this area over the past 16 years, despite the public attention given to the topic.

The abrupt decline of research on the engineering-operations aspects was paralleled by the scattering of the ice experts themselves and the disbanding of most labs, consulting companies and university courses. In Canada, only Memorial University and the NRC have continued operations at any scale, sustained by the East Coast offshore and other sea-ice related activities such as the Confederation Bridge. In the USA, the University of Alaska at Fairbanks and the University of Washington in Seattle remained as the most active research groups, but Arctic ice projects related to engineering and operations also declined. The National Research Council of Canada has attempted to keep this area alive, archiving data, periodically reviewing the state of R&D in the arctic offshore and promoting the scientific and engineering issues involved (Timco 1996, Timco et al. 2005, Wright 1995) and studying mechanical properties of ice (Johnston 2004).

Table 2-1 summarizes the main research or data-related institutions where knowledge about arctic ice is being produced. For most of the research groups, the main focus is on climate change and the attendant thinning of ice cover and its related environmental impacts. With a few exceptions, the groups are small, sometimes involving only 1 key person.

Despite this general situation of limited knowledge advancement relating to EIF for the Beaufort and Chukchi Seas, these people and groups have continued to advance in 3 broad groupings. First are engineering and operational aspects, found typically in conference proceedings such as POAC (Port and Ocean Engineering under Arctic Conditions), IAHR (International Association for Hydraulics Research), ISOPE (International Society of Offshore and Polar Engineers), Cold Regions Science and Technology, and ICETECH.

Table 2-1 Key Arctic Research Institutions

Country	Performing Sector	Institutes	Comments
Canada	National labs	National Research Council, Institute for Ocean Sciences	Mostly physical and engineering properties
	Data and mapping	Canadian Ice Service	
	University research and teaching	Memorial, Manitoba, Alberta Trent, Ottawa, Calgary	Mainly the first 3 schools
USA	National labs	Jet Propulsion Lab, Cold Regions Research and Engineering Laboratory,	World wide coverage
	Data and Mapping	NASA, National Ice Center, National Snow and Ice Data Center (NSIDC, Boulder)	World wide coverage
	University research and teaching	Alaska (Fairbanks), Washington (Seattle), Dartmouth College, Colorado (Denver)	Mainly the first 2 schools
UK	University research	Cambridge	No PhD student production
Finland	University research and teaching	Helsinki U of Technology	Occasional production of PhD theses on arctic ice, but main focus is on naval architecture, ship-ice interaction, Baltic
Norway	University research and teaching	Norwegian University of Science and Technology (Trondheim)	Active in support of offshore petroleum, but in areas that have limited ice cover, very little multi-year ice and no ice islands
Denmark	Data and Mapping	Danish Meteorological Institute (Copenhagen)	Mapping (focus is on East and West Greenland)
Germany	National lab	Alfred Wegener Institute (Hamburg)	Little presence related to EIFs. Main focus is climate change.
Russia	National labs, data and mapping	Arctic and Antarctic Research Institute (St. Petersburg)	Institute has declined by about 10x in professional staff since 1991. Not involved with Arctic work outside Russian zones.
	University research and teaching	St. Petersburg, Moscow, St. Petersburg Hydrometeorological Institute, Latvik (plus a few more in the rest of the country),	Publication in international scientific journals is very limited
Japan	corporate	Ship & Ocean Foundation, Japan Industries Association (Kitagawa 2001)	Scientific focus is regional, on Sea of Okhotsk. Most effort is on arctic tanker design and Beaufort Sea production structures
China	National lab.	Chinese Arctic and Antarctic Administration	Has recently opened an arctic research station, in Spitsbergen
	University research and teaching	Dalian	
Korea and Singapore	Corporate	Various shipyards with research institutes and model tanks	Involvement is in building ships and structures for Arctic; recent significant increase in learning and investment in this field

Second are scientific studies, which tend to focus on aspects of sea ice, glaciology and geography. The scientific output relating to our topic seems to be published most frequently

in Geophysical Research Letters and Journal of Geophysical Research, with another 2 dozen or so journals relating to oceanography, meteorology, remote sensing, polar regions, environment and climate change taking up the rest.

Third, there have been developments in instrumentation and measurement techniques of importance, a few relevant data gathering studies and several other research advances that, while not directly on our topic, do provide important insights. The remainder of this chapter examines them.

2.1.2 The Study Zone

Some EIFs in the Beaufort/Chukchi areas are formed locally and others are swept in by general current circulation in the Arctic Ocean. This current pattern defines where we need to review literature and collect new data. General currents are portrayed by Figure 2-1 (http://www.amap.no/ Figure 2 - 20)

Figure 2-1 General Current Circulation of the Arctic Seas

The main features affecting our study regions are the Beaufort Gyre and the Transpolar Drift Stream. The former sweeps ice clockwise along the Canadian Arctic Archipelago

through the Beaufort Sea. There is a constant entrainment of ice islands, growth of ice, formation of multi-year features balanced with periodic melting and losses through the channels of the archipelago and via the Transpolar Drift Stream.

More detailed data on ice drift show the same average pattern, in Figure 2-2 (http://nsidc.org/seaice/processes/circulation.html) averaged from 1978 to 2003.

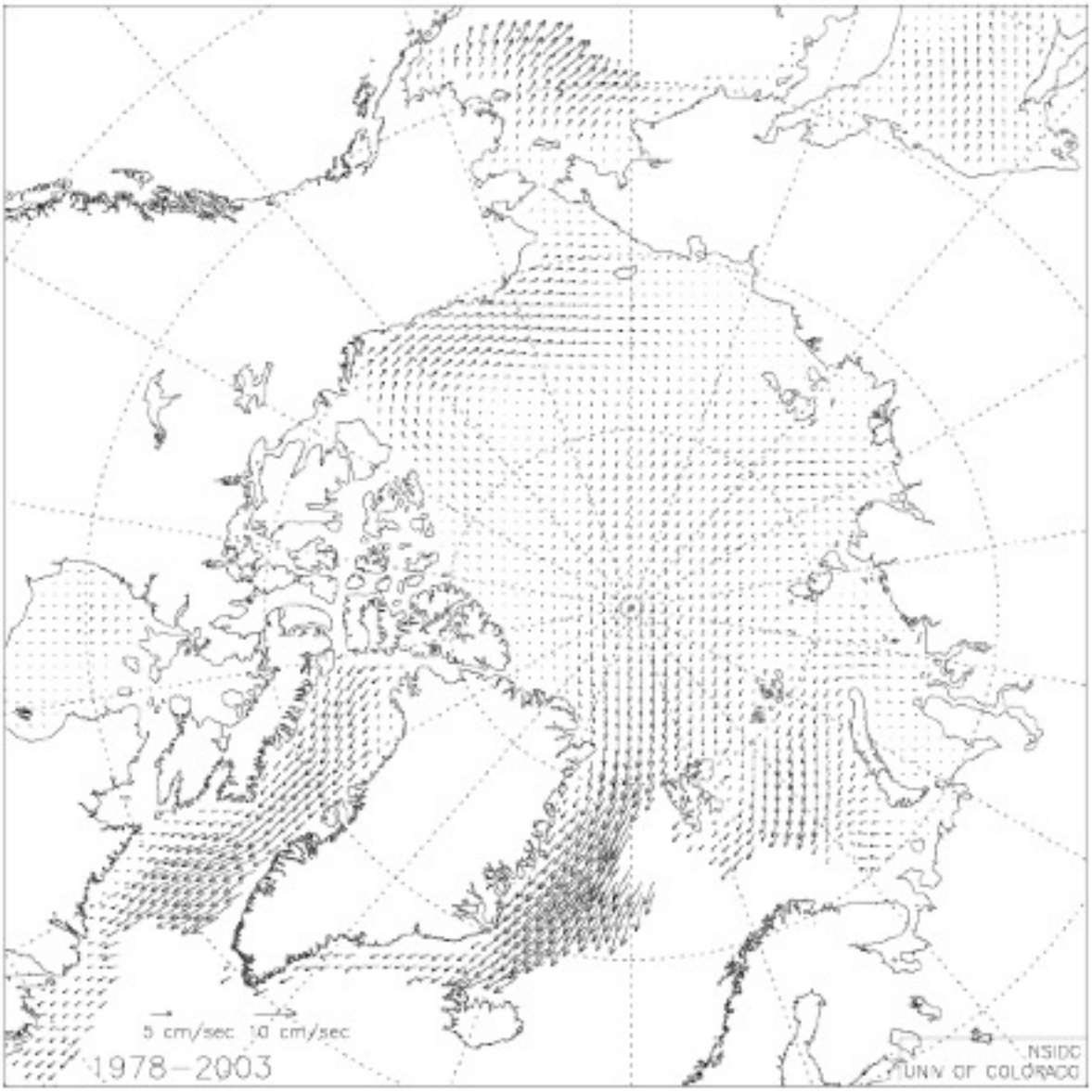

Figure 2-2 General Ice Drift in the Arctic Basin (from NSIDC)

It is important to note that this general pattern is highly variable, on small scales from localized wind pressure and on large scales from severe, long lasting meteorological events. The entire Beaufort Gyre grows during extreme cyclonic events and shrinks during anticylonic events (Darby and Bischof 2004). Ice drift follows these current shifts

(Lukovich and Barber 2006). The Beaufort Gyre can even disappear entirely or reverse direction (http://nsidc.org/seaice/processes/circulation.html). Tucker et al. (2001) measured a decrease in ridge size and average thinning of Beaufort Sea ice by 1.5 metres in the mid 1980s to early 1990s during an extended period of weakening of the Beaufort Gyre. Rigor et al. (2002) and Dumas et al. (2003) found the same general reduction of ridging in the Beaufort. These events can also cause surges of ice export through the Fram Strait, rapidly reducing the volume of ice in the Arctic, which then begins to build up again (Pfirman et al. 2004). Symon et al. (2005, p.458) present data that show the Beaufort Gyre sweeps more closely to the northern coast of Greenland during strong cylonic events. This shift in current could conceivably entrain ice islands created from land fast multi-year ice shelves and glaciers in Greenland as well. This possibility is shown by Figure 2-3, which maps International Arctic Buoy Program data from late summer 2008 (http://iabp.apl.washington.edu/maps_daily_arcticbasin.html) .

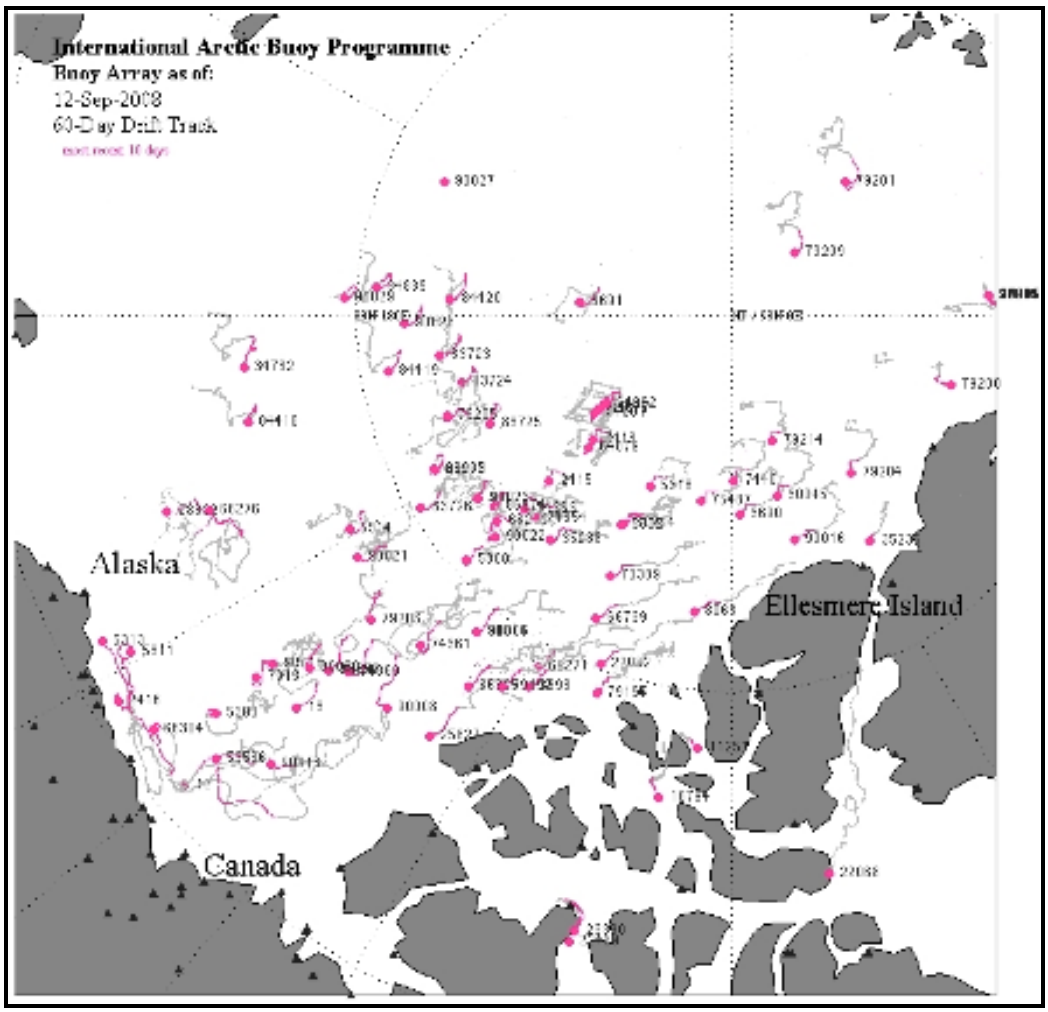

Figure 2-3 Ice Drift from IABP 2008 (International Arctic Buoy Program)

In summary, while we have good representations of average conditions, Symon et al. (2005) state the dynamic of Arctic currents is still "largely unexplored".

2.1.3 Scope of Literature Search

Given the general lack of recent research and professional practice in this area, we retain the definitions of extreme ice features as developed in the Pilkington et al. (1992) report. The literature search focused on:

1. Ice islands and ice shelves- origin, dimensions, current locations, quantity
2. Multi-year ice hummock fields (ridges, floes) - dimensions, current locations, drift patterns, quantity
3. Multi-year land fast ice – changes from calving, calving rates and predictions
4. Identifying multi-year ridges through sonar scanning of keel profiles
5. Correlation of satellite images to sonar measurements of EIFs
6. Long-range forecasts of ice conditions, implications of climate change
7. Impact prediction of extreme ice features on platforms.

The time period for this literature search was 1992 to the present. Published journal literature, conference proceedings and thesis outputs were searched, as well as industry reports. Telephone or personal conversations were held with senior experts in all areas and countries mentioned above to review these findings and to uncover any ongoing projects that may not yet have produced published output.

2.2 Ice Islands, Ice Shelves and Multi-year Land Fast Sea Ice

2.2.1 Origin

Ice shelves are formed by a complex process of seawater freezing and remelt, snow accretion and freshwater flow over and under the sheets that freezes. These shelves form in deep embayments and tend to be very stable and old, up to 4,000 years (Jeffries 1992). They are often fronted by a thinner, much newer kind of shelf, known as multi-year land-fast sea ice. While apparently quite stable for millennia, it seems that the ice shelves off Ellesmere Island have undergone a dramatic retreat in the last century. Vincent et al. (2001) estimate there has been a 90% decline in this last century, occurring in several discontinuous steps.

2.2.2 Areal Extent and Recent Changes

Figure 2-4 shows multi-year land fast ice in gray and ice shelves in black for part of Ellesmere Island in 2005 (Copland et al. 2007). Figure 2-5 shows the Ellesmere Island ice shelves (from left to right: Serson, Petersen, Milne, Ward Hunt and Markham, outlined in black) at the end of August 2007, when the multi-year land fast sea ice in Yelverton Bay appears to have fractured. Figure 2-6 shows the same area at the end of August 2008 after the Markham ice shelf broke up and drifted away, and the Serson ice shelf substantially broke up. (See http://www.people.trentu.ca/~dmueller/iceshelfloss2008/)

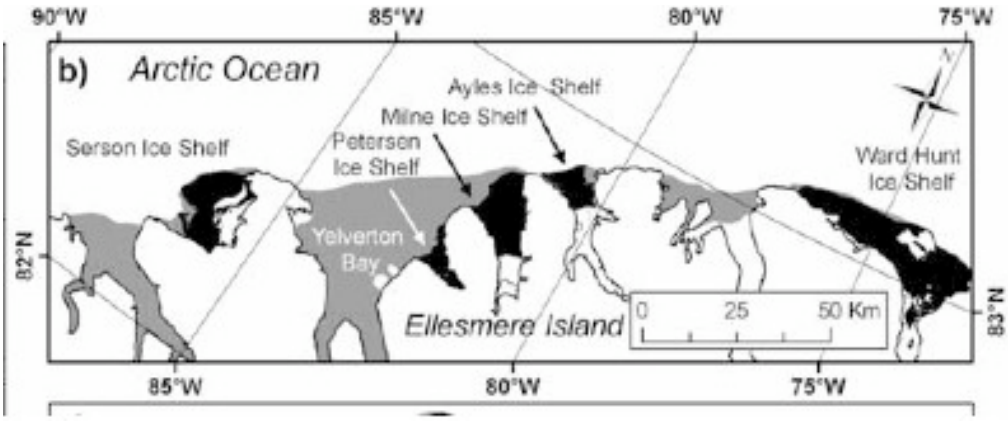

Figure 2-4 Ice Shelves and Multi-year Land fast Ice - Ellesmere Island before 2006

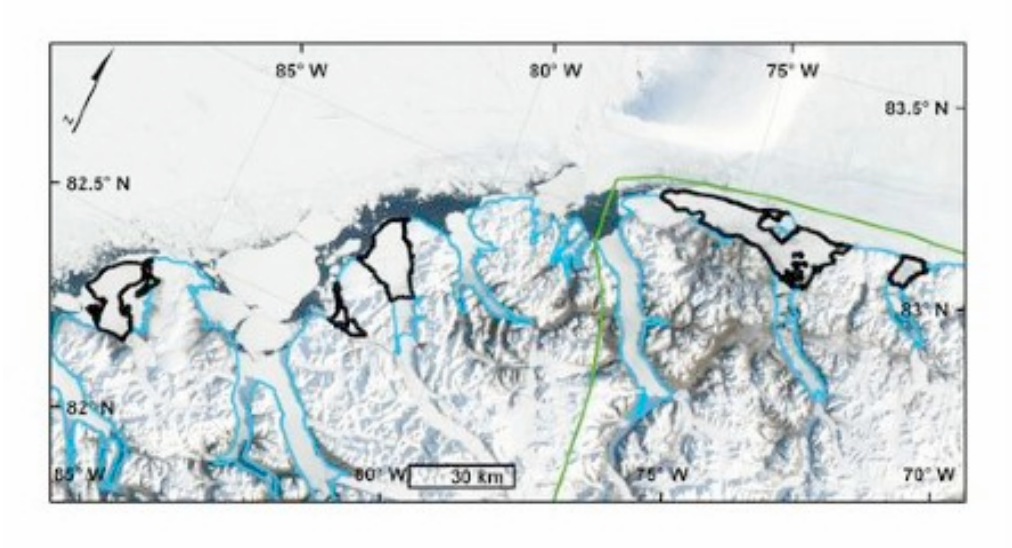

Figure 2-5 Ice Shelves - Ellesmere Island 2007 Conditions

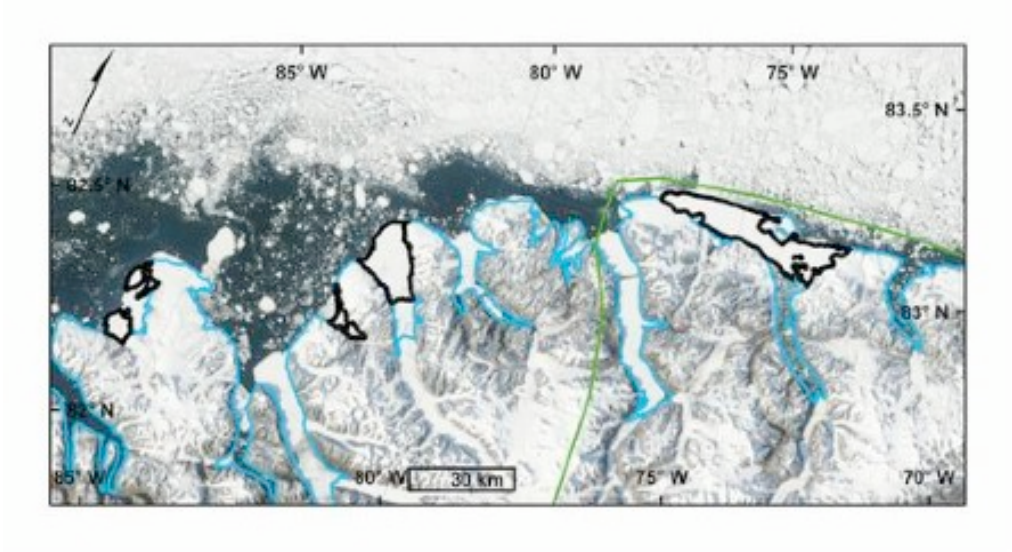

Figure 2-6 Ice Shelves - Ellesmere Island 2008 Conditions

Table 2-2 indicates about the extent of recent (1992-2008) calving from Ellesmere Island ice shelves into the Arctic Ocean. Other shelves calve into different bodies of water and it is assumed (based on sketchy current data) that they do not enter the Beaufort Gyre.

Table 2-2 Summary of Recent Calving

Year	Amount	Location	Reference
1992-2002	<30 km^2	Ellesmere Island	Mueller, personal communication
2002	6 km^2	Ward Hunt shelf	Mueller and Jeffries 2003
2005	84 km^2	Ayles shelf	Copland et al. 2007
2005	12 km^2	Peterson Shelf	Copland et al. 2007
2007	7.5 km^2	Peterson Shelf	Mueller, personal communication
2008	214 km^2	Principally Markham, Serson, Ward Hunt	Mueller et al. 2008

Mueller (personal communication) estimates there remains about 720 km^2 of ice left on these shelves after the summer 2008 losses.

2.2.3 Thickness of Ice Shelves

Ward Hunt ice shelf thickness was estimated at 43-54 m from seismic surveys in the 1950s and 40-50 m from airborne radio echo soundings in 1981 by Narod et. al. A thickness measurement of 42 m taken on Hobson's Choice Ice Island which calved from eastern Ward Hunt, confirmed this (Jeffries 1992). Water column profiling behind the Ward Hunt shelf by Vincent et al in 1999 suggested a thickness of 35m: a 22% decrease since 1983. Narod et al (1987) measured the Milne ice shelf varying from 70 to 100 m. Their measurements were described as having significant variation and error. Recent GPR (ground penetrating radar) data by Mueller and Copland were analyzed as part of this study; see Chapter 5. Much of the Milne ice shelf was found to be 45-90m thick with a maximum measured thickness of 94.4m.

2.2.4 Ice Islands

The patterns of calving of ice islands from ice shelves are poorly documented. Fragments that calved a few years ago seemed to be very large, but those from the summer of 2008 seemed to break almost immediately into much smaller pieces, sometimes as small as 75 metres in diameter (Dr. Derek Mueller, Trent U, personal communication). Fragments from the Peterson glacier seemed to break off following the water pooling and ridging patterns, one ridge at a time, leaving very long, narrow pieces. Copland et al. (2007) noted that the Ayles shelf initially produced an island 66.4 km2, with approximate dimensions of

15km x 6 km. Other pieces breaking off at the same time were up to 4km long and totaled 20.7 km2 in area.

It is also thought that the increased seasonal melting of land-fast ice may liberate ice islands that were previously immobile, although there are currently no data to support or confirm this hypothesis (personal communication, Dr. Derek Mueller, Trent U).

How the situation of accelerated calving may evolve in the future cannot be well predicted. Jeffers et al. (2001) maintain that the loss of "sea ice plugs" blocking the entrances to these fjords was a major factor in the following shelf breakup. Braun (2006) reviews literature that suggests floating ice shelves may only have a few stable configurations and that large losses may be expected over a relatively short time frame when conditions change.

Location, geometry and disintegration of ice islands are entirely unstudied in the period after 1992. Sackinger et al. (1991) suggest that during multiple circuits in the Beaufort Gyre, ice islands may lose thickness, with fragments of multi-year land-fast sea ice thinning down to more common multi-year floes. The opposite can happen as well; the Hobson's Choice ice island that was studied in great detail was actually made up of the original ice shelf material, multi-year land-fast sea ice (MLSI) and multi-year sea (pack) ice (MYPI), as Figure 2-7 illustrates (Jeffries 1992).

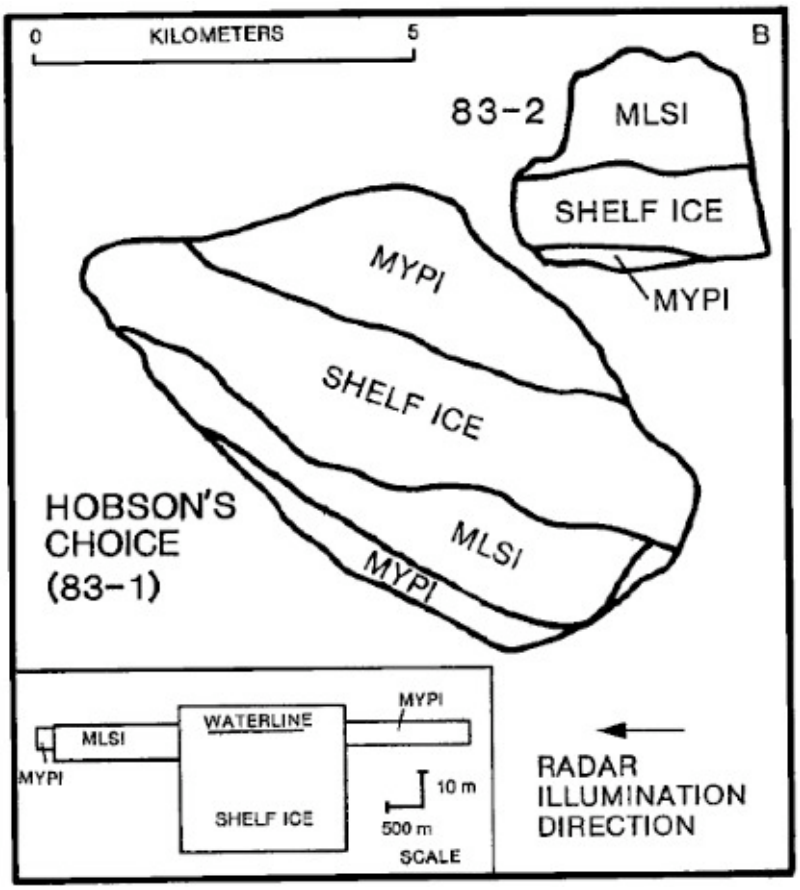

Figure 2-7 Makeup of Hobson's Choice Ice Island

2.2.5 Drift of Ice Islands

The ice islands that break off from ice shelves are generally entrained by the Beaufort Gyre and tend to drift southwards into the southern Beaufort. We can therefore expect a significant increase in ice islands passing through the southern Beaufort and Chukchi Seas for several years given the recent losses from the ice shelves.

Some ice islands exit the Arctic Ocean through channels between the Arctic Islands before reaching the southern Beaufort. Drift of Ayles ice island has been monitored by the Canadian Ice Service using satellite reporting beacons (http://www.sailwx.info/shiptrack/shipposition.phtml?call=47551). Both main fragments of the ice island have moved into the channels of the archipelago and are drifting erratically southwards away from the Beaufort. The Canadian Ice Service is also charting the ice islands that were produced in 2008. Analysis of this movement is the subject of a different study. The drift of one of the Ayles ice islands is shown in Figure 2-8 below.

Figure 2-8 Recent Drift of Ayles Ice Island

In addition, the Canadian Ice Service is monitoring the drift of recently calved fragments from the Ward Hunt breakup using the satellite imagery, and indicating their location on ice charts.

2.2.6 Glacial Ice from Ellesmere

Some land-fast ice sheets off Ellesmere Island contain small quantities of glacial ice (Jeffries, 1992), the amounts and characteristics of which are little known (personal communication Dr. Martin Sharp, U of Alberta). In northern Greenland, they may include significantly more glacial ice. A partial measure of calving into the Arctic from Nansen Sound can be calculated from Williamson et al. (2008) who measured glacial volumetric flow rates from the Agassiz ice cap. This cap feeds tidewater glaciers on the Arctic and Baffin sides of Ellesmere Island. Four of these glaciers (Otto, Antoinette, Lake Tuborg and

d'Ibreville) flow into Nansen Sound which in turn discharges into the Arctic Ocean, and seem to constitute the glacial discharge into this sound. Using results presented in their Table 1, one can estimate an average volumetric discharge rate of 0.21 km^3/year from 1999 to 2003. The authors do not link this study with any of the ice sheet calving literature, so it is not clear exactly how much of this glacial ice will eventually reach the Arctic Ocean. New radar imagery obtained in the present study identified changes to the glacial ice that is currently trapped by the Milne ice shelf but which may eventually discharge into the Arctic Ocean if the Milne ice shelf breaks up. See Section 4.7.

2.2.7 Glacial Ice from North Greenland

Higgins, 1989, identified four North Greenland sources capable of producing large tabular icebergs that could be drawn into the Beaufort Gyre if the land fast sea ice were to break up and allow such bergs to drift offshore. These are the Petermann, Ryder and C.H. Ostenfeld glaciers and the Kap Kane ice shelves, shown in Figure 2-9 (based on a MODIS image from June 2002, from the NASA website visibleearth). The first three glaciers have a potentially high production rate of icebergs, with annual movement of 500-900 m. Movement of the Kap Kane glaciers is an order of magnitude smaller at 8-23 m/year.

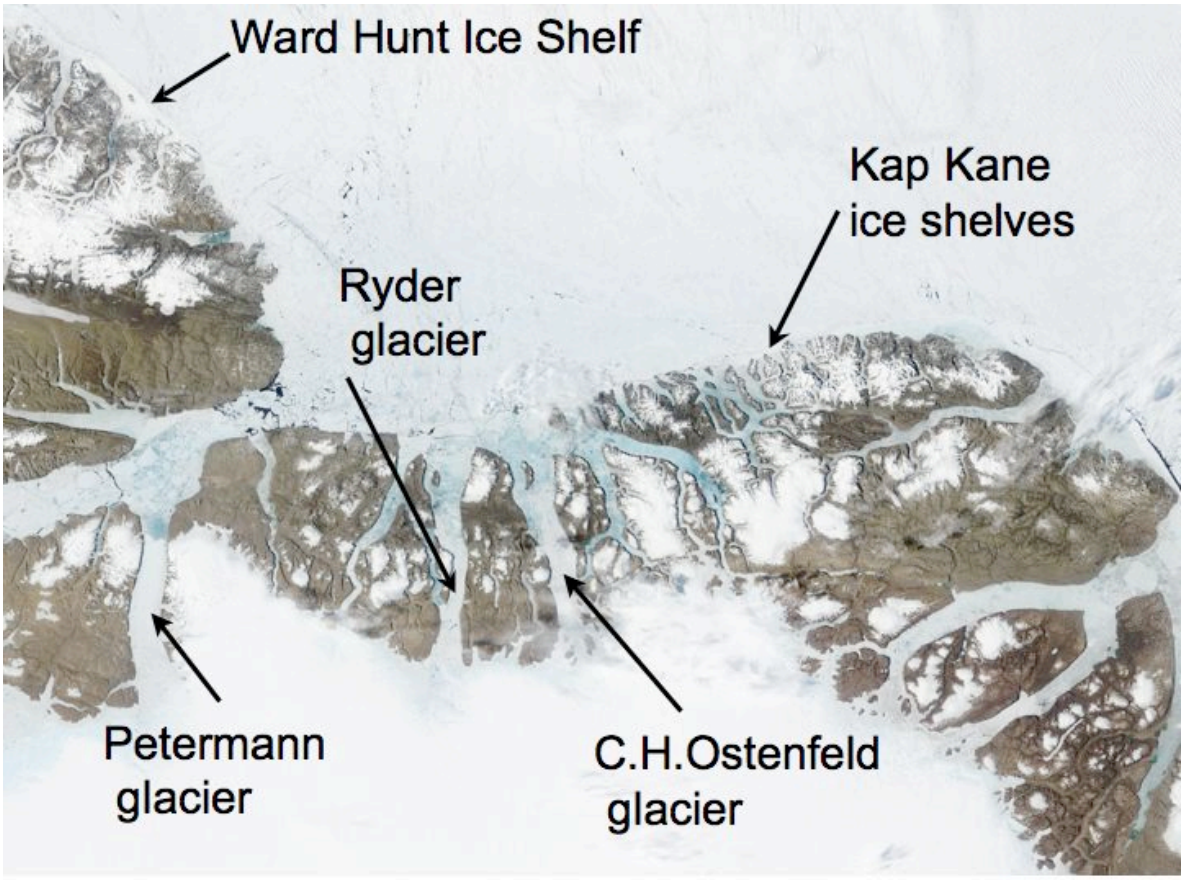

Figure 2-9 Potential sources of EIFs from N Greenland

Icebergs from the Ryder and C.H.Osterfeld glaciers are generally trapped for decades behind the land fast sea ice, however Higgins notes that in exceptional summers the sea ice retreats and allows large tabular bergs to escape the fiords. One such summer is thought to

have occurred between 1953 and 1961, according to aerial photographic evidence. K.Hansen of DMI (personal communication) indicates that in 2002-2003 the shore-fast ice in this region underwent an unusual melt, and this condition was repeated in 2008, so it is possible that glacial ice in the form of tabular icebergs was liberated.

Icebergs released from the Petermann glacier are more likely to drift into Kennedy Channel, between Ellesmere Island and Greenland and continue south into the Davis Strait rather than drift north into the Arctic Ocean. Higgins,1989, cites a 1978 paper by Dunbar that reported a large berg offshore Newfoundland in May 1976 thought to have originated from the Petermann glacier in September 1974. In the past decade the Petermann glacier has undergone significant calving. In 2000-2001, 86 km2 was lost, and most recently in 2008 29 km2 calved (Figure 2-10, from, http://researchnews.osu.edu/archive/boxicepix.htm).

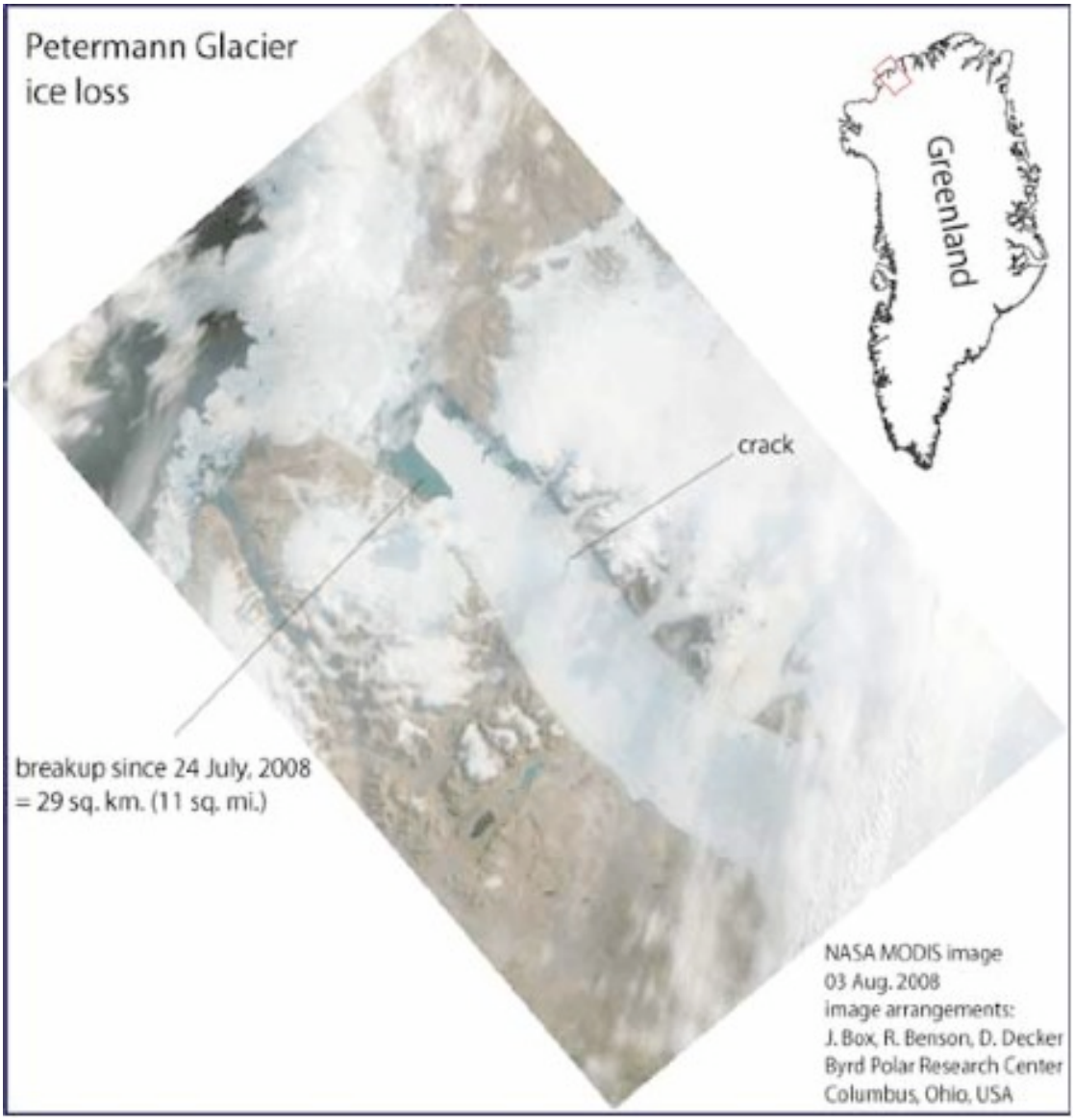

Figure 2-10 Petermann Glacier Calving of 2008

If the Petermann glacier continues to break up to the crack shown in Figure 2-10, this would liberate about 160 km2, or about 1/3 of the remaining ice tongue. This glacier ice thins from 600 m thickness at the grounding line to 70 m at the terminus.

Sugden (1982), mentions 3 main glacial sources in this area. Figure 2-11 shows these along with the other main sources known in 1982, presented by AMAP (http://www.amap.no/). Most are outside the Beaufort Gyre and indeed outside the Arctic Ocean.

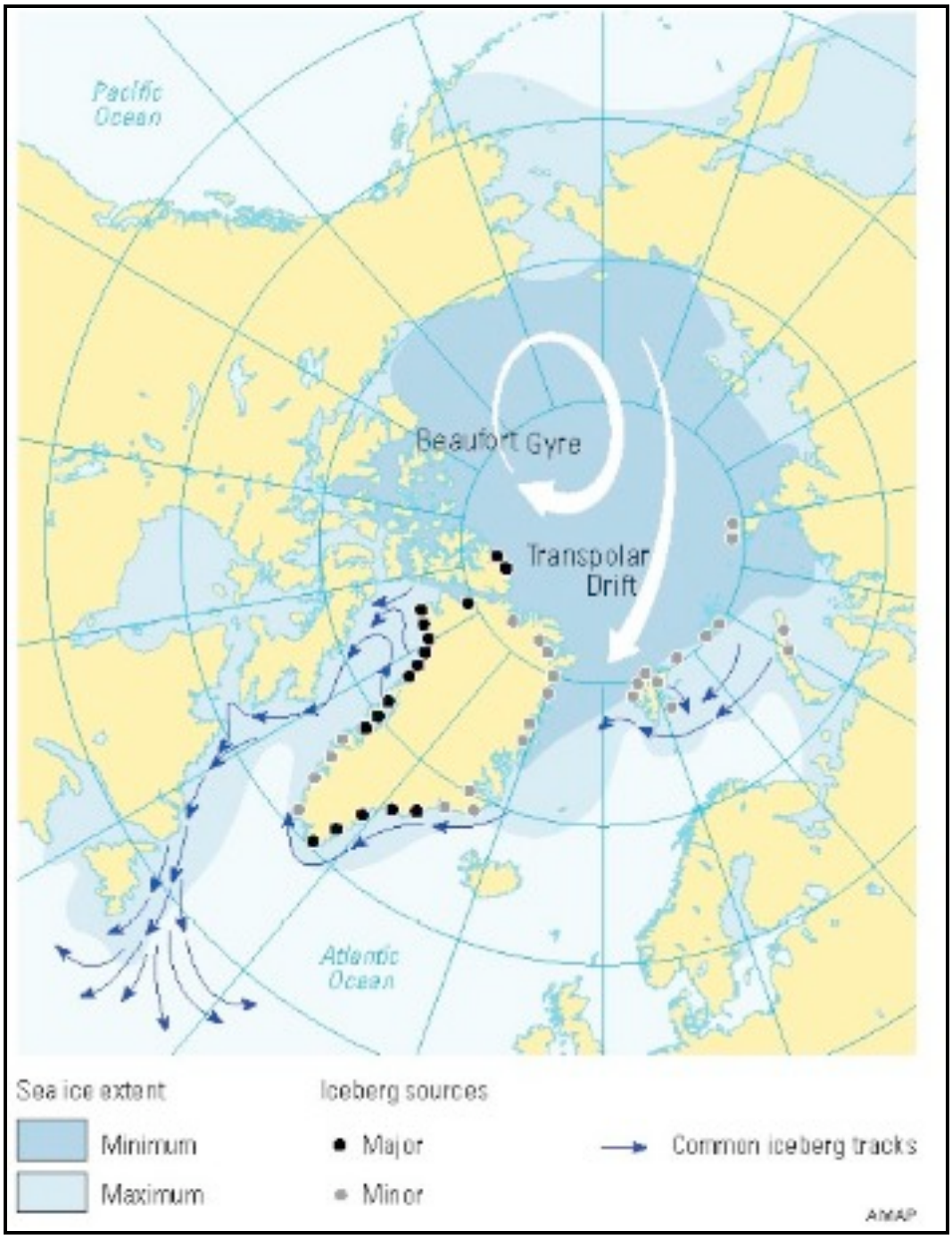

Figure 2-11 Sources of Glacial Ice

It may even be possible for some ice islands to originate in the Laptev Sea and drift into the Beaufort Gyre, as suggested by the Arctic Monitoring and Assessment Program, AMAP (http://www.amap.no/ Figure 3 - 26) and Dowdeswell et al. (1994). The probabilities are low, but there are no measurements on the topic.

2.3 Multi-Year Land Fast Ice

When ice shelves break up, they seem to be partially at least, replaced by multi-year land-fast sea ice (MLSI) which gradually thickens (Jeffries 1992). Some of this MLSI that fills in the ice shelf losses results from new freezing and some from entry of previously formed fragments (Jeffries and Sackinger 2000). Figure 2-4 shows the main area of MLSI ice along the coast of Ellesmere Island, most of which appears to have been lost since 2006.

Multi-year land-fast sea ice may also be found on many other coasts of the Queen Elizabeth Islands, without the occurrence of ice shelves. The terminology is somewhat confusing as some authors refer to ice shelves for all of the above and others call them tabular icebergs. Land-fast multi-year sea ice shelves in other parts of the Queen Elizabeth Islands were an area of concern in the Pilkington et al. (1992) report. The shelves shown in Figure 2-12 were found in a 1980 SLAR survey by Arsenault. This ice has broken up and drifted away.

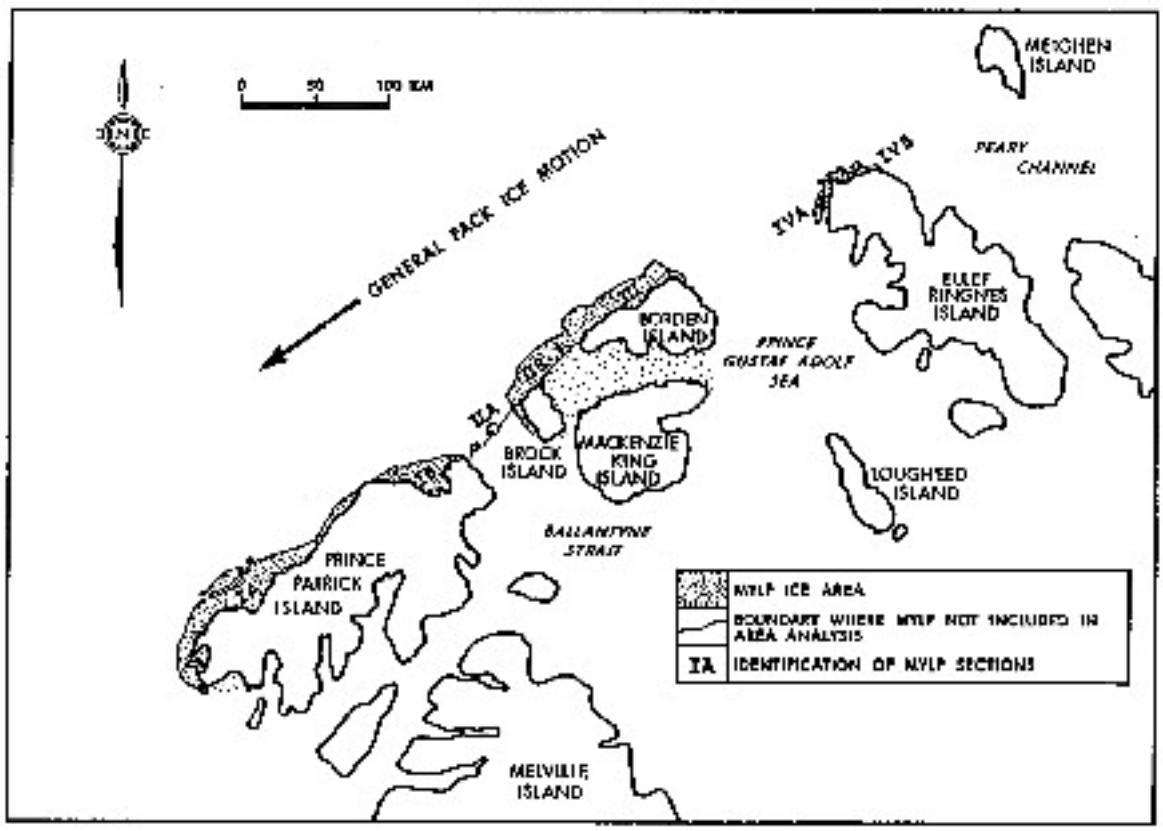

Figure 4.13: Areas of Multi-year landfast ice, Queen Elizabeth Islands

Figure 2-12 Suspected Main Land-fast Multi-year Sea Ice Shelves 1991

In the literature search, we have not been able to identify any recent study that deals with land-fast ice at these locations. Flato and Brown (1996) present a thermodynamic model of annual land-fast ice formation using comparative data from Alert and in the Arctic Archipelago, but do not deal with other dynamics. Konig (2007) studies land-fast sea ice, but is only concerned with first year instances.

2.4 Occurrence of Multi-Year Floes, Ridges and Hummock Fields

2.4.1 Occurrence and Trends

The second main type of extreme ice feature is multi-year ice, which occurs in isolated floes or entrained in first year ice floes, and takes the form of ridges and large fields of deep-draft hummocks. The importance to structures of such multi-year features is their size and thickness. They are also considered by Arctic ship captains as by far the most important feature of concern for navigation (Timco et al. 2005 p.52).

Widespread reports of thinning Arctic ice and global warming could give the impression that multi-year features are diminishing. Traditional knowledge of the Inuit notes significant changes in ice. Enoch Sheidt from Kotzebue, Alaska states that the ice is "not freezing up as thick. When we go hunt seal by snow machine - used to be late October now it's getting to December." J. Wongittilin Sr. reports "solid ice has disappeared and there are no longer huge icebergs during fall and winter. The ice now comes later and goes out earlier and it is getting thinner." http://www.iser.uaa.alaska.edu/projects/contam/ResourceGuide/ice_cover.htm). There is a great deal of consistent scientific evidence to indicate the Arctic is rapidly warming and that Arctic sea ice has undergone a general dramatic thinning. Symon et al. (2005, p.54) state that although the region has undergone great cyclical variations in climate over millennia, "the observed warming in the Arctic in the latter half of the 20th century appears to be without precedent since the early Holocene".

However, there are four critical caveats to observe. First, the eastern Beaufort, along with the Canadian Arctic Archipelago, are among the areas that retain the most severe ice coverage (http://nsidc.org/arcticseaicenews/). Symon et al. (2005, p. 194) summarize five sea ice cover prediction models and show that there could be solid ice cover throughout the Canadian/US arctic in winter even by 2100 and that significant ice cover near the coast in the Beaufort will remain into the third decade of this century. Figure 2-13 shows their estimate of the changes in multi-year ice coverage in the Arctic from 1987 to 2005, using ice drift buoy data (http://iabp.apl.washington.edu/research_seaiceageextent.html).

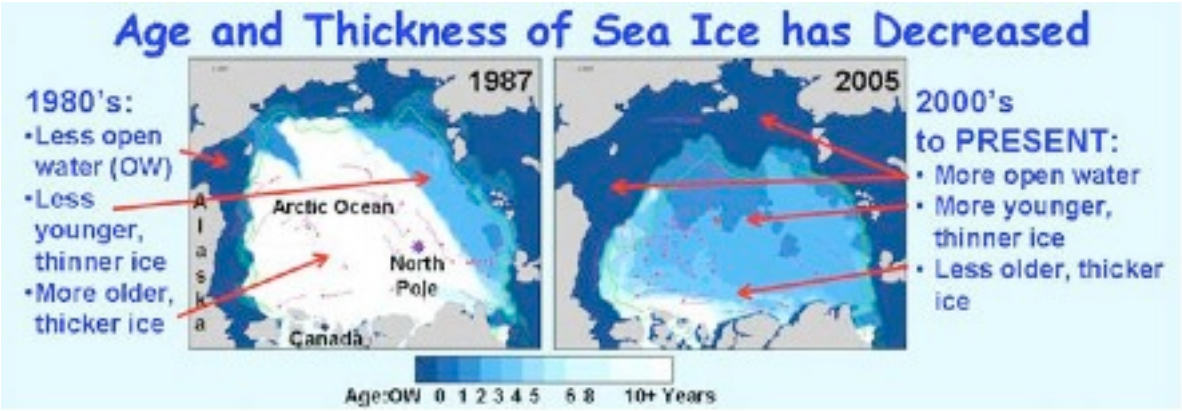

Figure 2-13 Changes in Age and Thickness of Sea Ice

These data are quite similar to what Figure 2-14 presents, which is an analysis of trends in summer total accumulated coverage for old ice (>2 years) based on Canadian Ice Service archives from 1966 to 2007. The dark blue areas show a percent increase per decade of from 20 to 50% in the eastern Beaufort. The area closer to the Chukchi, however, shows a reduction of 11 to 20% (Tivy et al. in preparation). Galley et al. (2008), focusing on the southern Beaufort and Amundsen Gulf, show the same trends, but in much more detail.

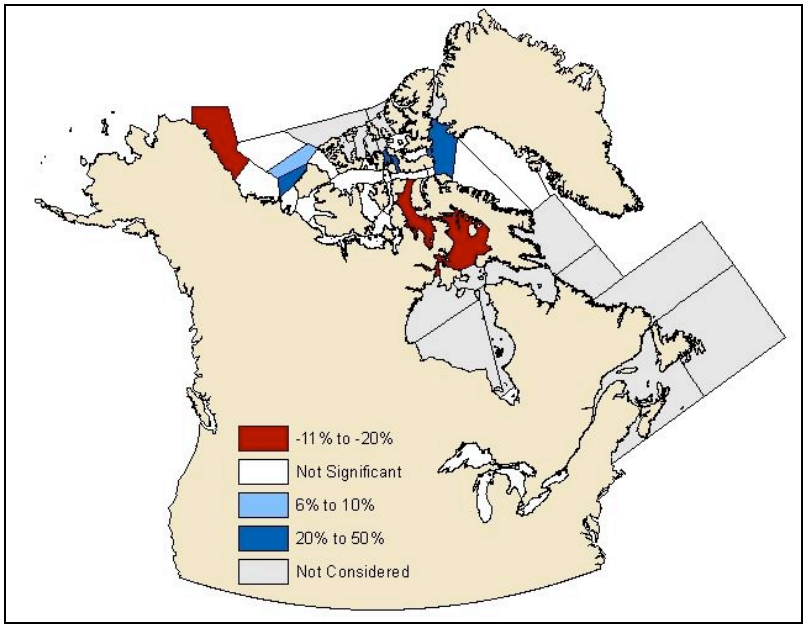

Figure 2-14 Changes in Old Sea Ice Occurrence

Second, it must be noted that the projections of thinning ice cover relate to average conditions. Departures from average and local, small-scale phenomena may be very significant for engineering and operations purposes. Howell and Yackel (2004) calculate that ice conditions in the Arctic Archipelago over 34 years show "extreme inter-annual

variability", a conclusion that Falkingham et al. (2002) reach as well for the entire Canadian Arctic. Howell and Yackel (2004) state that "multi-year ice invasions into Northwest Passage shipping lanes appear to be a major pitfall of future navigation routing in the face of climate warming". Falkingham et al. (2002) posit that "choke points" for shipping will develop at certain points as multi-year features are swept into them and concentrate. Most of these choke points are in the channels of the Arctic Archipelago, but a major one is off Point Barrow, Alaska. Rigor and Wallace (2004) maintain that cyclical events like the Arctic Oscillation can account for significant reductions of ice thickness, and the amount of multi-year ice and multi-year ridges. During times when the Beaufort Gyre diminishes, the Transpolar Drift sweeps more multi-year ice out. At the same time, younger, thinner ice re-circulates back to the Alaskan/Chukchi coast more quickly, decreasing the time that new ice has to ridge and thicken before returning for another melt season. Pfirman et al. (2004) maintain that this phenomenon has been largely the cause of the recent observed thinning. By implication, a prolonged period of the opposite strengthening in the Arctic Oscillation should cause more multi-year ice to form and become thicker (Rigor and Wallace 2004, Belchansky et al. 2005). An animation of conditions from 1979 to 2007 at http://iabp.apl.washington.edu/animations/Rigor&Wallace2004_AgeOfIce1979to2007.mpg clearly shows this high degree of annual variability within the overall trend.

Third, the evidence for such complex phenomena is not always consistent. For example, Fissel et al. (2008), reporting on analysis presented in Melling and Riedel (2005), show that extreme ice features as measured by ice keel draft occurrence have not statistically changed in the Beaufort Sea from 1991 to 2003 and Kwok (2005) suggests that the current diminishing of multi-year ice is likely to continue, not reverse.

Fourth, Mahoney (2006) has found, in his study of land-fast ice in Alaska that the significant diminishing of this annual cover allows for pack ice to incur into coastal waters.

2.4.2 Multi Year Ice Thickness

Despite the media attention to these northern ice shelves' breakup and the common use of dramatic adjectives like "catastrophic", it must be kept in mind that ice showing extreme features is a rare occurrence in the Beaufort. Figure 2-15 shows a histogram sonar measurements of ice drafts in the Beaufort Sea (72 32N, 143 34 W) for August 1991 and graphically illustrates the rare nature of these events (Lipscomb 1998, p.9). While encounters with such features by a structure must be factored into design criteria and operational procedures, they will rarely occur.

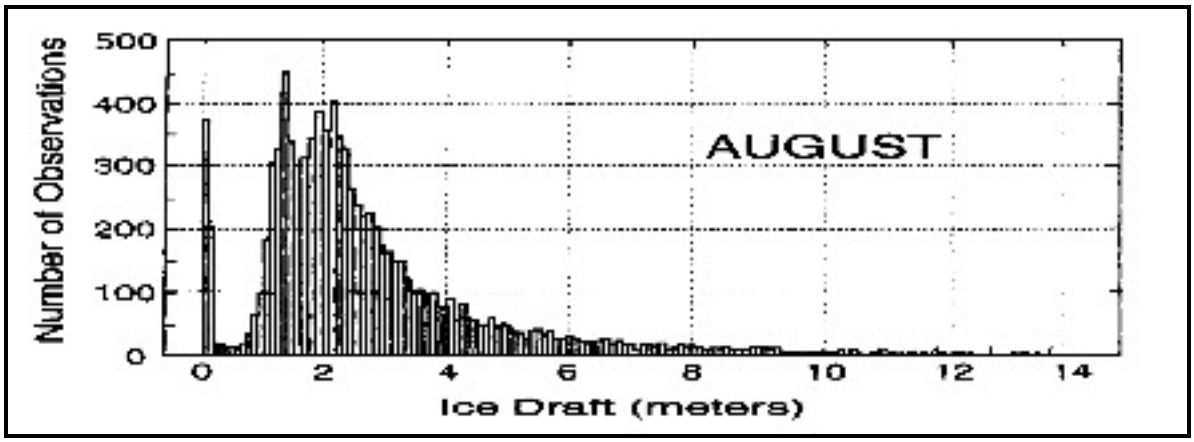

Figure 2-15 Beaufort Sea Extreme Ice Draft Occurrence

2.4.3 Multi-Year Ridge Geometry

McLaren et al. (1984) analyzed keel data from submarine tracks, one of which passed from the M'Clure Strait out into the Beaufort Sea up to the 3,500 m isobath in 1960. Figure 2-16 shows the recurrence probability for keel depths for this run, along with several of the other tracks. An extreme keel depth of 29 m was found on one track near Prince Patrick Island.

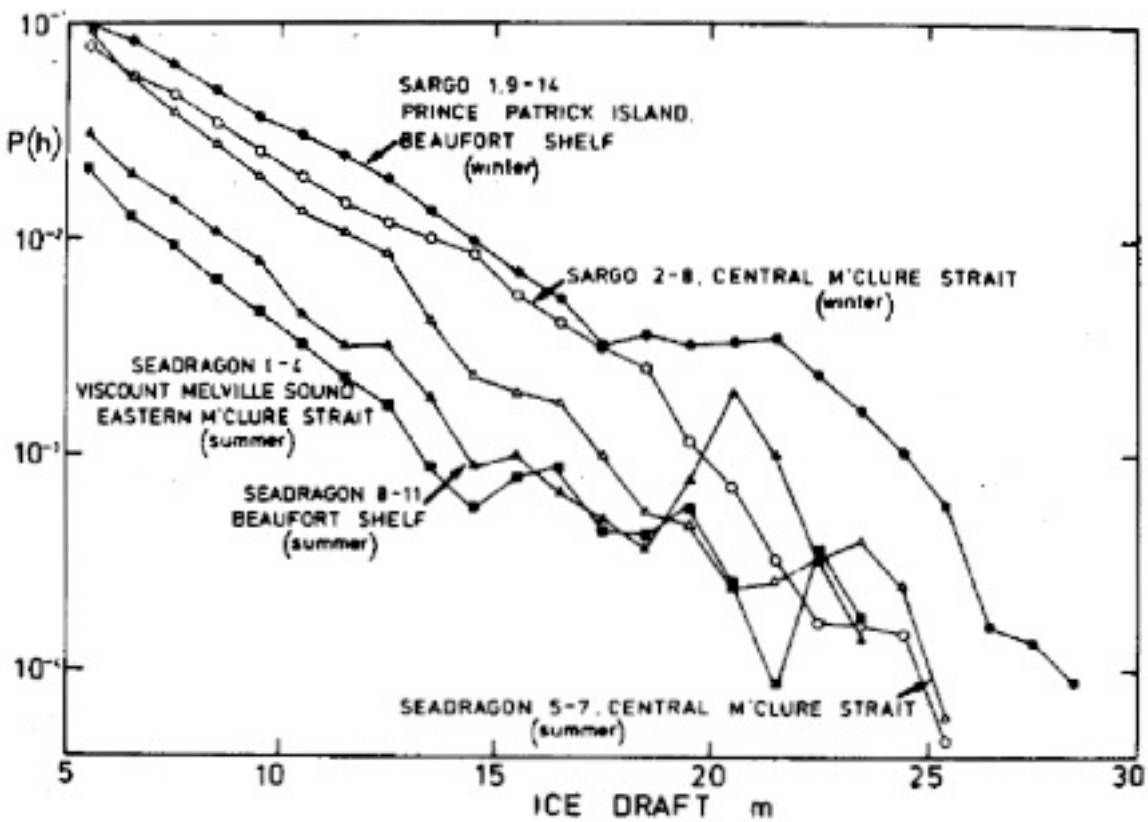

Figure 2-16 Keel Draft Probability from submarine tracks 1960s

The keel depth has been generally related to the sail height and width by Timco and Burden (1997). Their work shows Beaufort first-year ridges to have an average ratio of keel depth to sail height of 4.5 with a standard deviation of 1.9. Johannessen et al. (2001), in their paper on modeling of ridges in the Pechora Sea state that the Timco and Burden research is the best available representation of ridge geometry in their initial formation. However, continued ridging and multi-year development will generally increase the keel's width but not its draft (Hopkins 1998). Wright et.al. (1981) have estimated an average keel to sail ratio of 3.2:1 for multi-year ridges based on field profiles. Modeling of more complex multi-year features seems not to have been done. There was no research found on the important, complex feature of multi-year hummock fields, only a passing reference to this phenomenon by Fissel et al. (2008). Davis and Wadhams' (1995) review of literature on multi-year ridges shows great variability in measured and modeled slopes for keels and sails, and for ridge widths, lengths and orientations. In addition, most multi-year ridges form systems of ridges, not long isolated features. This suggests no easy way to identify from sonar which ice is multi-year, except the tendency for extreme features to take several years to build up. There seems to have been no research on this particular topic. Further insight on this topic is presented in Chapter 6.

It seems that all the recent research on ridging relates to formation processes, first year ridges, volume accretion and melting. The literature search in the doctoral thesis by Amundrud (2004) does not contain any references to ridge geometry more recent than 1998. The only other doctoral thesis on ridges found was by Heinonen (2004), focusing on mechanical properties of first year structures. The most recent work on ridges is reported by Hoyland (2007), and Shafrova and Hoyland (2007) on first year ice in the Barents Sea, focusing on morphology and small scale strength. Kharitonov (2007) reviews internal structure of ridges in Russian Arctic zones, with minor reference to multi-year ice. There seems to be no discussion in the literature about distinguishing multi-year from first year ice by underwater sonar, except to a passing reference by Wadhams et al. (2008) that undeformed first year ice sheets are smooth with cracks, and multi-year ice has an undulating surface with crater like depressions derived from top surface melt. This is further discussed in Chapter 6.

2.5 Sonar as a Tool for Identifying Multi-year Keels

Amundrud et al. (2004) review the technique of measuring under-ice profiles by bottom-moored sonar, which the Canadian Institute of Ocean Sciences has conducted in the Beaufort since 1990. The upward-looking single-beam sonar measures vertical distance and a separate, acoustic Doppler current profiler instrument measures ice drift velocity. Fissel et al. (2008) have compiled a list of Arctic sites using this technique, mapped in Figure 2-17.

The red dots refer to public scientific data sets, the orange to long term profiles taken by the Institute of Ocean Sciences which have been acquired for use by petroleum companies and the yellow dots to sites put in place explicitly by petroleum companies for environmental monitoring for planned exploration activities. The exact location of these sites moves slightly from year to year as the instruments are recovered to collect the data, replace power supplies and then redeployed.

The 4 red dots in the centre of the Beaufort Sea represent approximate locations of data taken by Woods Hole Oceanographic Institute, as part of their Beaufort Gyre Exploration Project (http://www.whoi.edu/beaufortgyre/deployment2004/index.html).

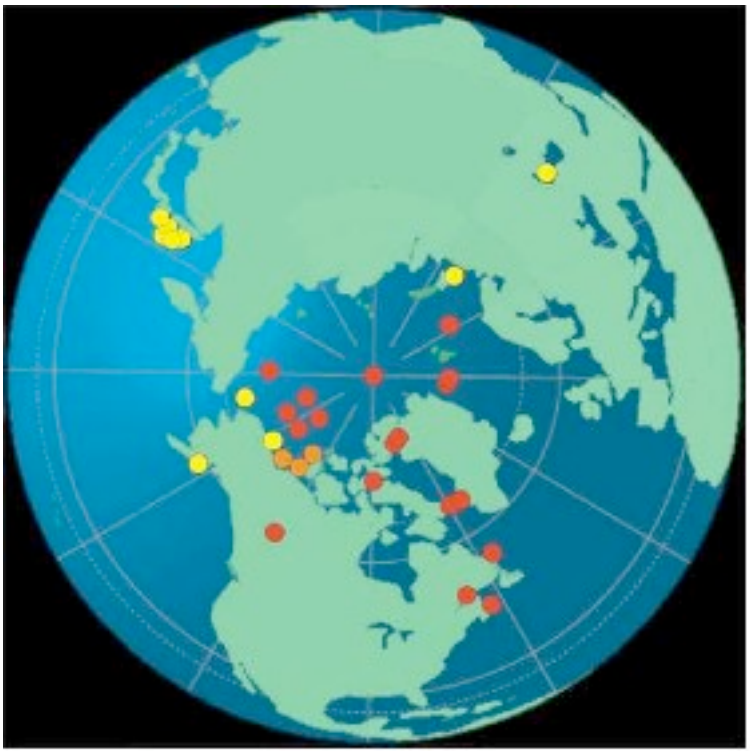

Figure 2-17 Deployment of Upward Looking Moored Sonar

A more accurate location of the Woods Hole 2003 and 2004 survey sites is shown by the stars in Figure 2-18.

The Woods Hole sampling rate is similar to that employed by Fissel et al. (2008), which gives a horizontal resolution from 50 metres distance of 0.8 metres and a vertical resolution of +- 0.05 metres. Their project seems to have carried satellite measurement of ice thickness to correlate to the sonar profiles (http://www.whoi.edu/beaufortgyre/methods.html), but it does not appear the analyses have been published at this time. Given the circulation patterns in the Beaufort, extreme ice features at these locations may have passed through the Beaufort and Chukchi lease areas and/or could pass through them again. The dot at the North Pole in Figure 2-17, above represents data from the University of Washington's Applied Physics Laboratory, which uses a much slower sampling rate and does not generate high enough resolution for measuring geometry of keel profiles (Melling, personal communication). The dot for the Barents Sea area probably refers to work by Abrahamsen et al. (2006), which used a sampling rate of from 4 to 5 minutes, to produce daily averages of draft, insufficient for profiling. The Sea of Okhotsk data are probably those reported by Fukamachi et al. (2006). The Fram Strait data are taken by Vinje et al. (1998), with a sampling rate suitable only for averages.

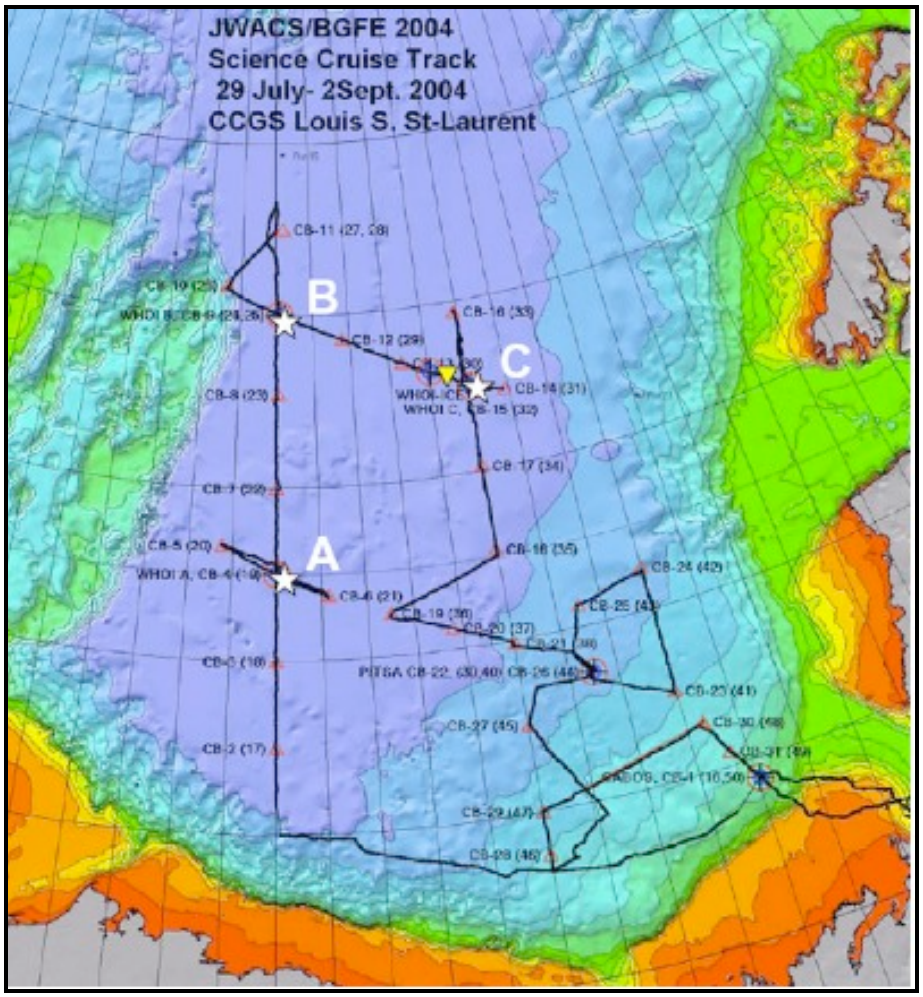

Figure 2-18 Woods Hole Instrument Locations 2003-2004

A second source of sonar data for under ice profiling comes from submersibles. Wadhams et al. (2008) report on the very recent development of autonomous submersibles that need to be launched from vessels into open water and smaller tethered devices that can be launched from holes in the ice cover.

Submarine sonar measurements are a third source of data. As discussed by Shy (1999), selected records of sonar ice drafts from US Navy submarine tracks in the Arctic Ocean were declassified, mostly in 1992. They were recorded electromechanically on strip charts in the 1970s and then digitally on floppy disks. However, the exact location of each track was not declassified, except to indicate the data were collected from within a 150 km radius of the North Pole. (Note that tracks used by McLaren et al. (1984) seem to be fairly exactly located.) The data have been digitized and analyzed by various authors, for purposes of computing average ice thickness changes. Since beam angle is consistently 2 degrees and the data have a horizontal resolution of 10cm, with an maximum estimated error of 12% over mean draft (Wadhams 1997), these data should be still useful for further analysis of multi-year keels.

Scientific observations of Arctic oceanography from US Naval submarines were made in the period from 1993 to 1997, in the SCICEX project. Among them were under-ice profiles from sonar. Figure 2-19 below displays the routes and dates of these submarine surveys (http://www.ldeo.columbia.edu/res/pi/SCICEX/Media/scicextracks.jpg).

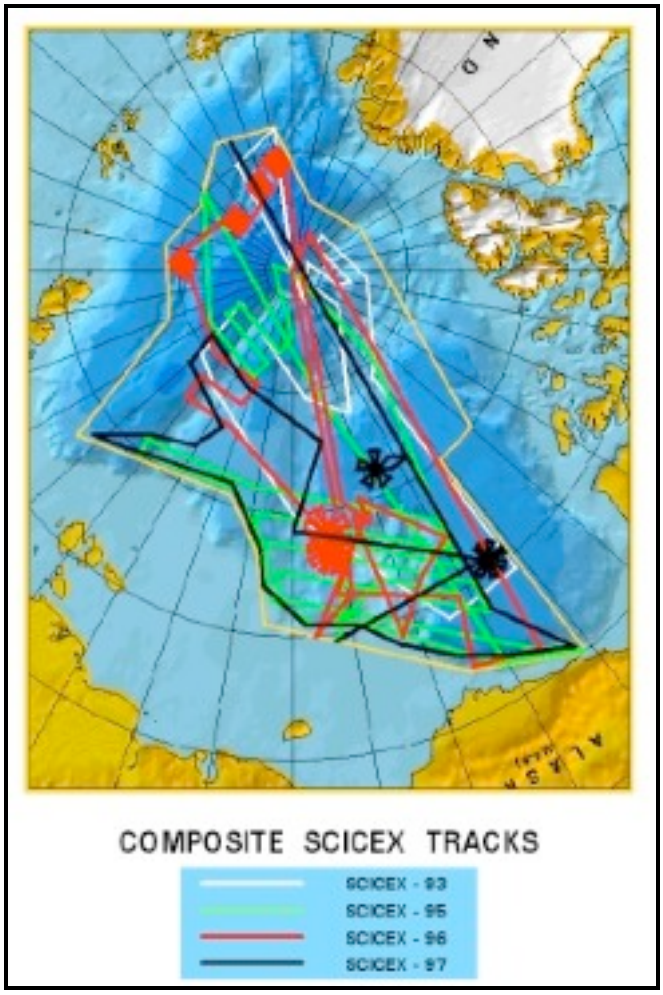

Figure 2-19 US Scientific Submarine Cruises

Rothrock et al. (1999) state that more data were collected outside this area of international waters, which could imply that there are data sets that have not been declassified running closer to the lease areas of the JIP partners. The sonar ice data are available at the National Snow and Ice Centre website. No publication has indicated the resolution of these scans and the only analysis of the data is in terms of average thicknesses (Rothrock et al. 1999, Rothrock et al. 2003). The SCICEX website states that the 1997 cruise was correlated with satellite imagery but gives no further information. ULS data from the 2000a Submarine Cruise are presented in Chapter 6.

It is suspected that there are also similar data tracks made by Russian submarine cruises, but these have not been declassified. Brovin (personal communication) states that there have been attempts to acquire them for public research and attempts by the navy to release them but conditions of sale could never be agreed upon.

The only other source of submarine sonar data is from British navy cruises. Davis and Wadhams (1995) for the first time were able to combine sidescan sonar with upward looking sonar, enabling them to measure keel geometry by correcting for the transect angle, and obtain 3 dimensional displays.

2.6 Correlation of Sonar with Satellite Images

Haas (2004) states that measuring thickness of sea ice from radar satellite imagery is very problematic, useful only for large extents of uniform surfaces. In order to utilize satellite images to predict extreme ice features, it would be useful to have research that correlated detailed sonar images for the underside, of the kind reported by Wadhams et al. (2006, 2008), with high resolution surface images from the topside. Only 2 research projects were located that relate to this issue. First, Bowen and Topham (1996) correlating stereographic aerial photos and sonar show the correlations between various cross sections of sails and keels for a first year ridge. While they found great variability in shapes and relationships, the average keel to sail ratio is 4.05 +/- 1.69, close to Timco and Burden's (1997) estimate of 4.5. Figure 2-20 below shows some ridge cross sections.

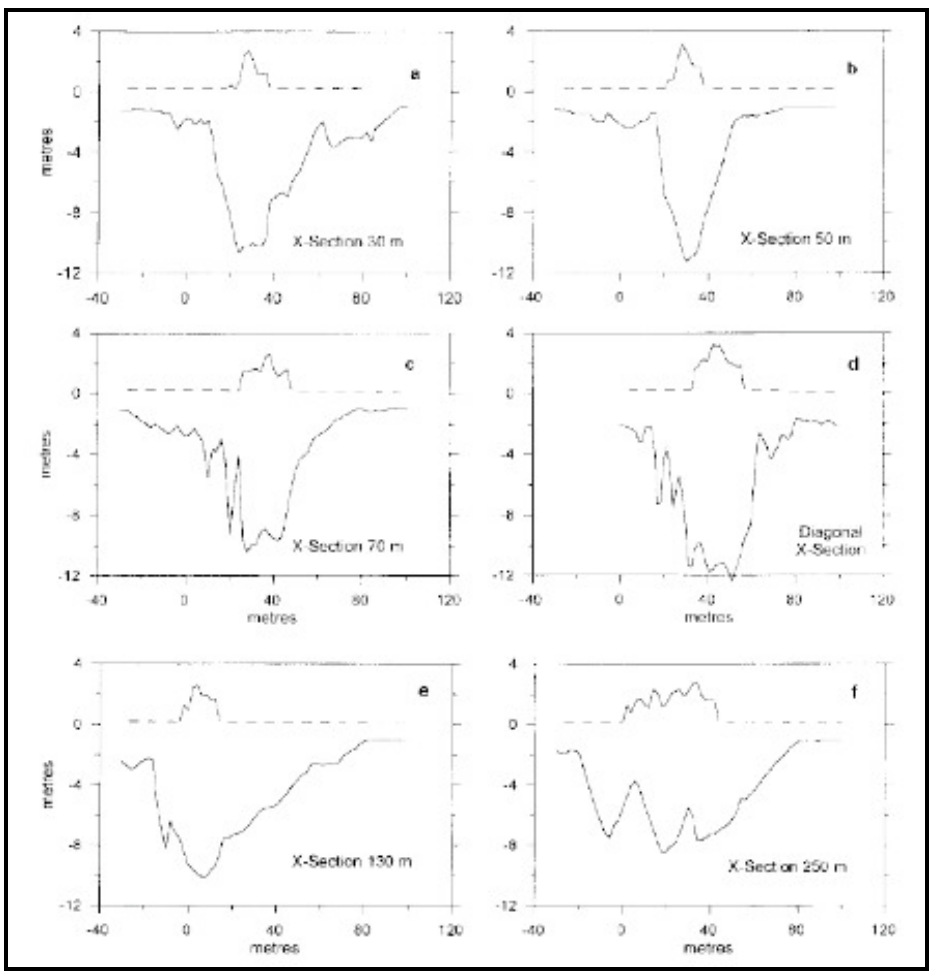

Figure 2-20 First Year Ridge Cross Sections from Bowen and Topham (1996)

The second paper is by Melling (1998) who reports on 1991 first year ice ridge measurement in the Beaufort Sea. He stresses several factors limiting the accuracy of such correlations: fixing the common location reference point; different fields of view; identifying leads as ridges; different positioning of sail and keel (as can be seen in the previous figure). He finds a strong linear correlation between the keel draft and peak backscatter, as well as between the frequency of ridges and the mean draft of the ice field. The former correlation is due to the fact that sail height is related to ridge width, which accounts for radar brightness. Unfortunately, Melling states that for multi-year ice, there is less contrast in backscatter between ridges and floes, and less likelihood that topside topography mirrors under-ice topography.

Wadhams et al. (2008) indicate this is a topic ripe for future research, now made feasible by advances in portable sonar instrumentation capable of 3D measurement.

2.7 Impact Probability on Structures

Impact probability methods were developed for the Canadian Beaufort Sea in de Paoli et.al (1982) and estimates updated in Pilkington et.al. (1992). Lu (1992) studied aspects of extreme ice features impacting offshore structures, but not probabilities of impact. Johannessen et al. (2001) report on modeling ice ridge drift into an impact alert zone in the Pechora Sea. Li (1991) developed Monte Carlo simulations for ice island drift in the Arctic Ocean and concluded that the two areas of most frequent recurrence would be the Canadian Beaufort Sea and the Chukchi Sea. Smith and Lee (2001) report on the development of an Alaska Sea Ice Atlas, which will have risk analysis features, but it appears from the literature search that this project is not yet complete. Fuglem and Jordaan discuss ice island/structure impact probability for the Beaufort Sea in a chapter in a book on Ice Islands by Mueller et al (2009 in preparation).

The level of sophistication of impact probability models varies from simple formulae using average values up to full scale Monte Carlo simulations. The simpler models usually consider the structure diameter, the average diameter of the EIFs, the average speed of the pack ice, and the average density of EIFs in #/km^2. One or more reduction factor is usually included to account for loss of EIFs between the source (usually the Ellesmere Island ice shelves) and the area of operational interest. Losses can occur through the channels of the Arctic Islands and through deviation of the drift direction away from the operational areas. Water depth should also be included in such models because the thicker features will ground out before reaching drilling prospects in shallower water. For summer impacts by multi-year floes the average floe diameter would be used. Typical return periods have ranged from tens to thousands of years depending on the assumptions made.

3 SATELLITE DATA ACQUISITION

3.1 Satellite Platforms Used

Satellite data were collected for this project using four different platforms. In order of coverage amounts, these were:

- Envisat 100 km swath, HH polarization, 30m resolution
- Radarsat 2 50 km swath, HH polarization, 8m resolution
- Landsat 100 km swath, 15m resolution
- MODIS 2300 km swath, 240m resolution

Envisat was used as the principle imaging platform, and most of the area of interest was imaged using it. Radarsat2 hi-resolution data was collected in two small areas to be used primarily for verification/calibration of the lower resolution Envisat imagery. Landsat data was collected due to low cost, its ability to provide a visible-light presentation of the ice scenes, and to validate the Envisat data. The MODIS data was collected in order to provide a broad-scale snapshot of the entire area of interest, at minimal cost. Coverage and utilization of these image types is discussed in the following section.

3.2 Planning and Execution of the Satellite Acquisition

3.2.1 Planned Swaths

In the planning stages, satellite orbits for Radarsat and Envisat were investigated that would sample a large swath of the Arctic Ocean adjacent to the Arctic Islands from Ellesmere to Banks Islands, where extreme ice features were known to originate. It was important to sample the multi-year pack ice, so late-winter charts from the CIS, Canadian Ice Service, were used to judge the extent of coverage. Figures 3-1 and 3-2 show possible orbits that would have given good coverage. In the end the most cost-effective solution was to use Envisat for most of the coverage, supplemented by Radarsat, Landsat and MODIS.

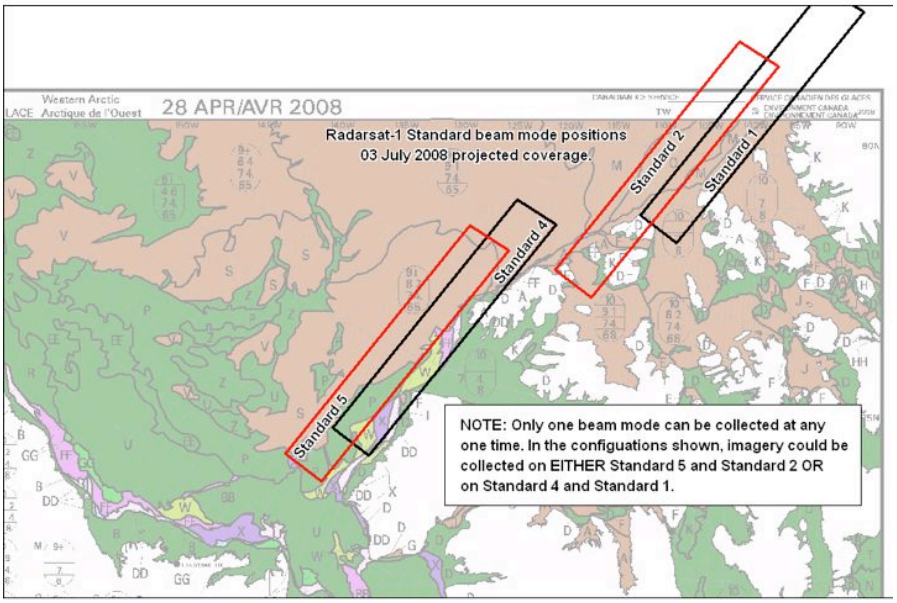

Figure 3-1 Radarsat orbits for EIF sample

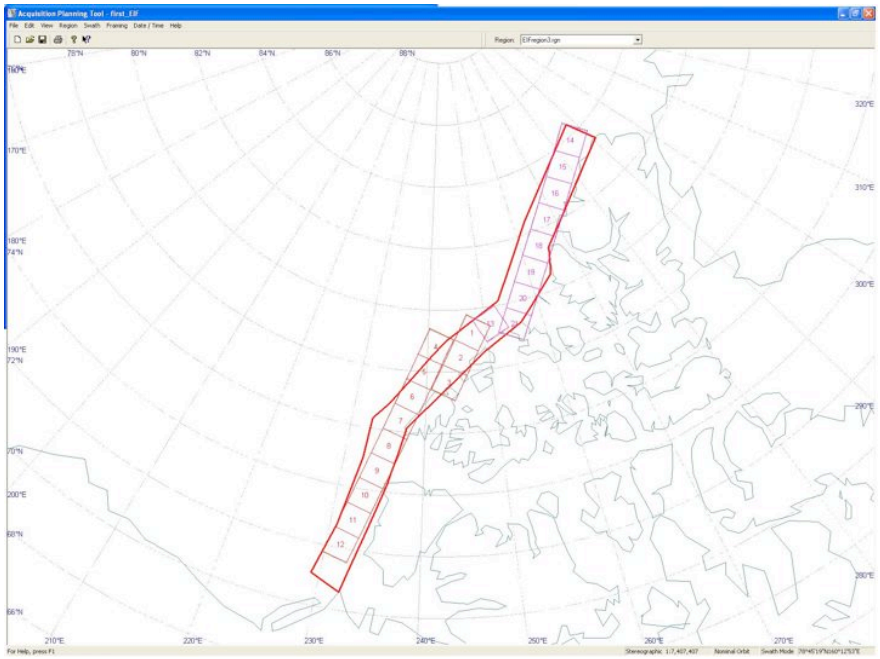

Figure 3-2 Envisat orbits for EIF sample

In a similar way, Envisat orbits were planned to sample multi-year floes close to 3 areas for potential drilling in the Canadian Beaufort, the Alaskan Beaufort and the Chukchi Seas. The position of the multi-year pack ice was monitored starting late in the winter of 2007-2008. Since Envisat image acquisition must be booked 3 weeks in advance, sample swaths

were chosen to account for expected movement of the multi-year ice edge. Figure 3-3 shows a composite of the Multi-year ice edge for 30th June 2008 and planned Envisat acquisitions.

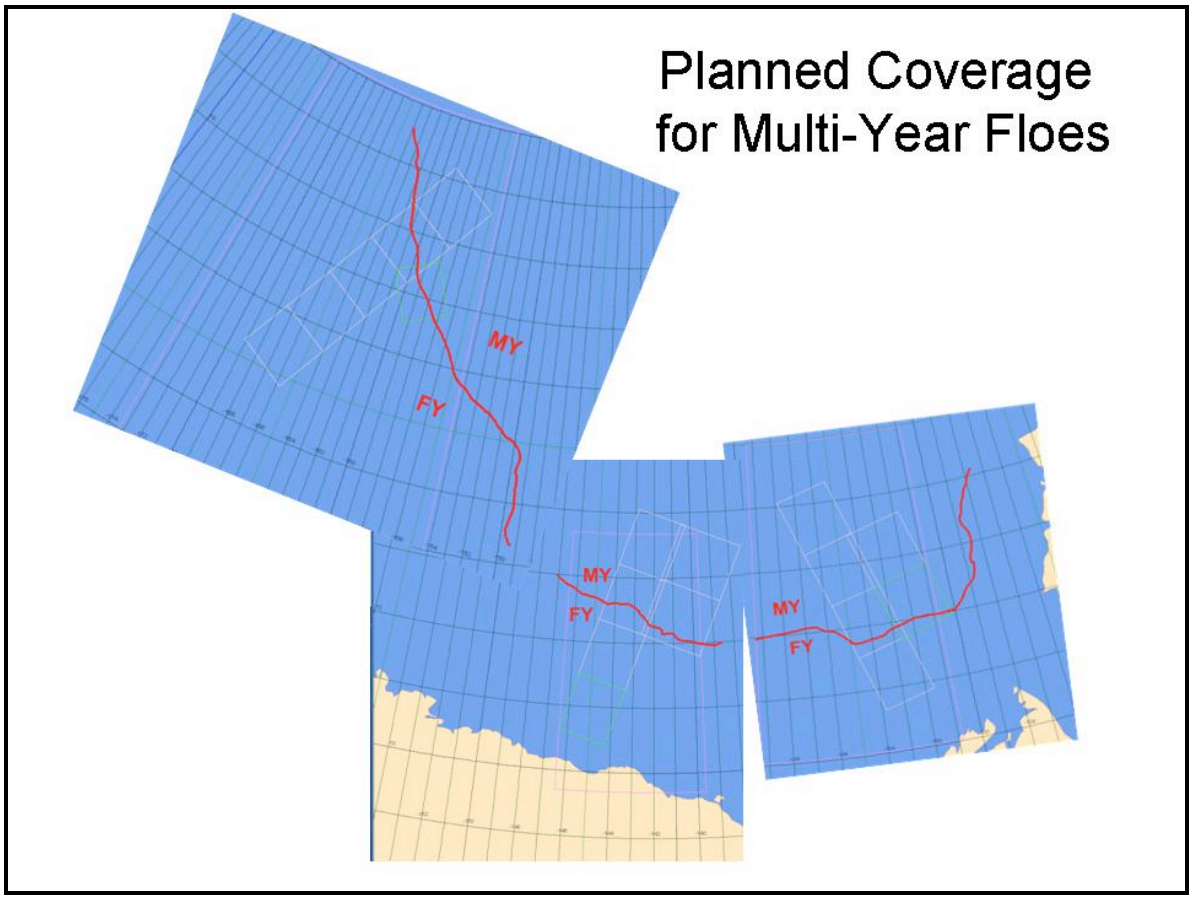

Figure 3-3 Multi-Year ice edge 2008-06-30 and planned Envisat acquisitions

3.2.2 Break Up 2008 and Changes in Plan

As the break-up progressed in the succeeding weeks, the first year ice melted rapidly and the edge of the multi-year pack ice retreated far to the north leaving mostly open water in the southern areas of interest. The programmed images for the Chukchi Sea were cancelled as it was obvious early on that there was a risk of obtaining no multi-year floe data. In addition, any multi-year floes imaged would have been very far away from the areas of interest. For the Alaskan and Canadian Beaufort Seas, the images were programmed around 10-11th July, for acquisition on 31st July- 01st August. In the intervening period, the ice retreated rapidly as shown in the sequence of CIS images in Figure 3-4, leaving one of the largest open water expanses ever recorded in the Beaufort and Chukchi Seas. In the Figure, the area of predominantly multi-year ice is indicated by the brown colour. Most of the images obtained for the Multi-Year floe part of the project yielded no useful data. Fortunately, images were made available by Shell and Exxon as detailed in Section 3.3.2.2 and these are analyzed and discussed in Chapter 5.

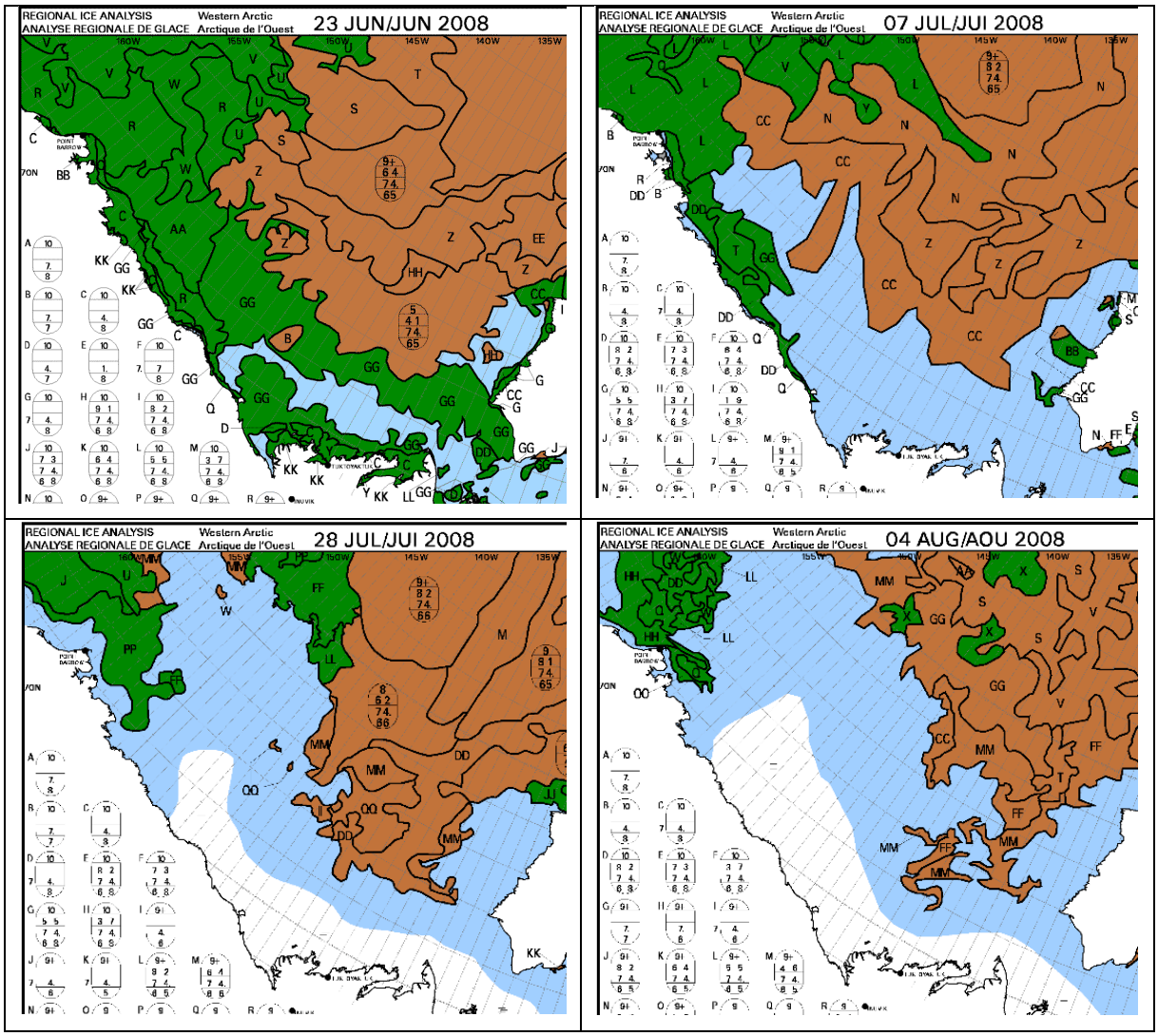

Figure 3-4 Progression of Break Up 2008 and Retreat of Multi-Year Pack Ice Edge

For the EIF sample area it was decided not to gather data offshore Banks Island as the ice was already drifting west leaving considerable open water. Imagery of dense pack ice was sampled from Prince Patrick Island north to Ellesmere Island. The data yield for the EIF part of the project was high as discussed in the next section.

3.3 Satellite Imagery Coverage

3.3.1 EIF Sampling Area - High Arctic

The area of coverage was established with three principle objectives:

- Repeat coverage of the area covered in the 1992 study
- Complete coverage of all Ice Shelves on Ellesmere Island, and

- Coverage of the off-shore/near-shore area from Prince Patrick Island to just east of the Ward Hunt Ice Shelf

A map showing the area covered by Envisat (as imagery), Radarsat 2 (in green), Landsat (in yellow) and MODIS (in red) is shown in Figure 3-5.

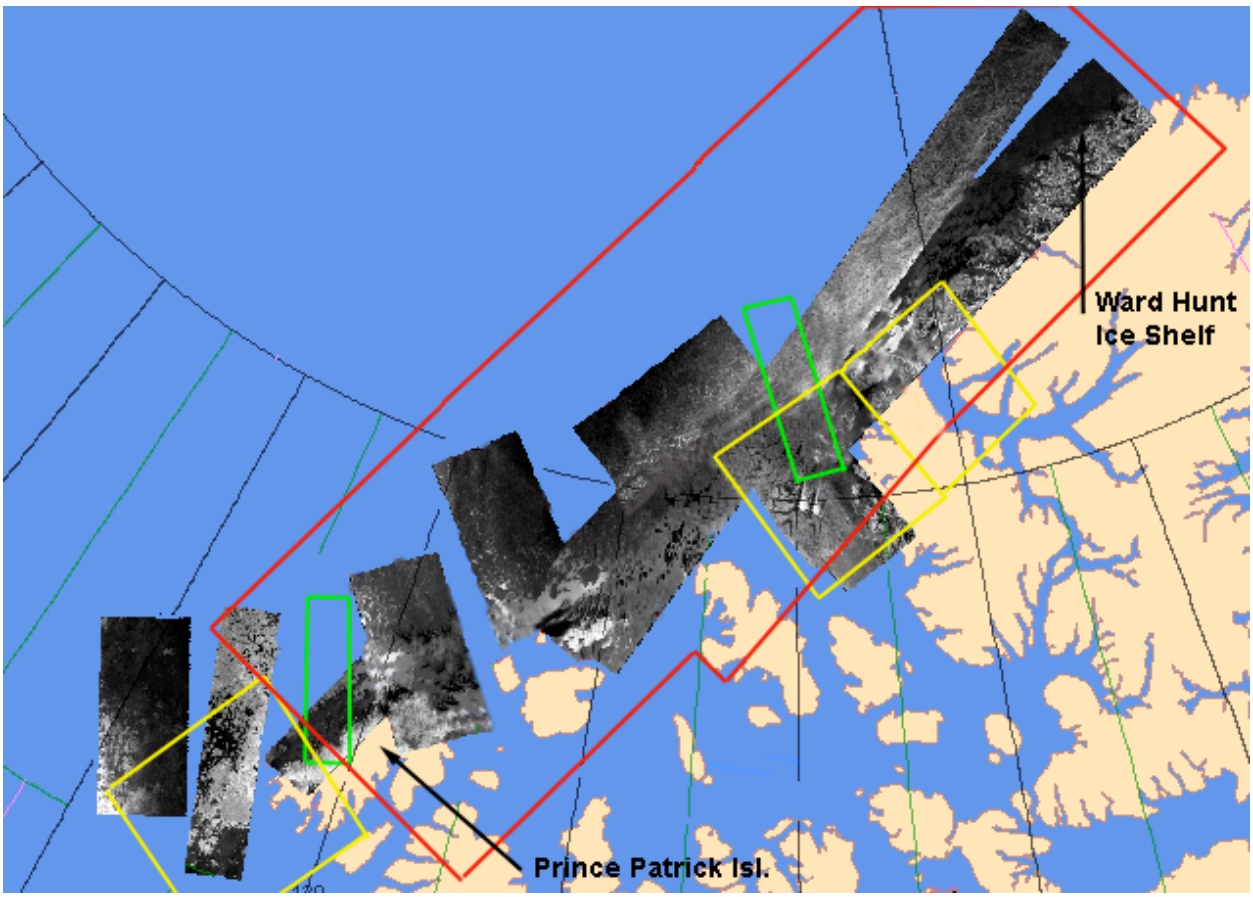

Figure 3-5 Coverage by Envisat, Radarsat, Landsat and MODIS July-August 2008

The Envisat data was intended to provide the primary coverage (30m res.), and the Radarsat2 data (8m resolution) was intended to be used to "calibrate" the interpretation of the Envisat data. The Landsat data was used as a validation point of visible-light data to verify the Envisat and Radarsat data, while the MODIS imagery was used as an overview to put hi-resolution images into the context of the region.

Although the report Pilkington et.al. 1992, identified 12-15m data as ideal for locating EIFs, resolution requirements of that dataset were partially related to the use of photographic imagery. Minimum EIF size was established at 500m as that was a 2mm. feature on a 1:250,000 print of imagery – as small as one could realistically physically measure. In this investigation, through the use of all digital imagery, predominantly 30m, resolution data was deemed adequate for EIFs down to 180m in their smallest dimension (6 pixels). Recent experience with pixel-level analysis of radar data has identified 6 pixels as the smallest target that can be consistently classified. In addition, the 1992 report had as one of its conclusions: "*EIFs less than 500m in diameter when north of Prince Patrick*

Island are typically broken into much smaller pieces by the time they reach the southern Beaufort". Thus the use of predominantly 30m resolution data resulting in a minimum detectable EIF size of 180 m was deemed appropriate for this project. However, all EIFs smaller than 180m were recorded whenever they were identified on the Radarsat (8m) or on the Landsat (15m). Ice Island fragments as small as 30 m x 70 m were recorded.

3.3.2 Multi Year Floe Sampling Areas - Beaufort and Chukchi

3.3.2.1 New Envisat Imagery

Figure 3-6 shows the locations of Envisat images obtained in the Alaskan and Canadian Beaufort Seas. Much of the area imaged was open water. Some ice was detected in the northern images of the Canadian Beaufort set, but not sufficient for a meaningful analysis.

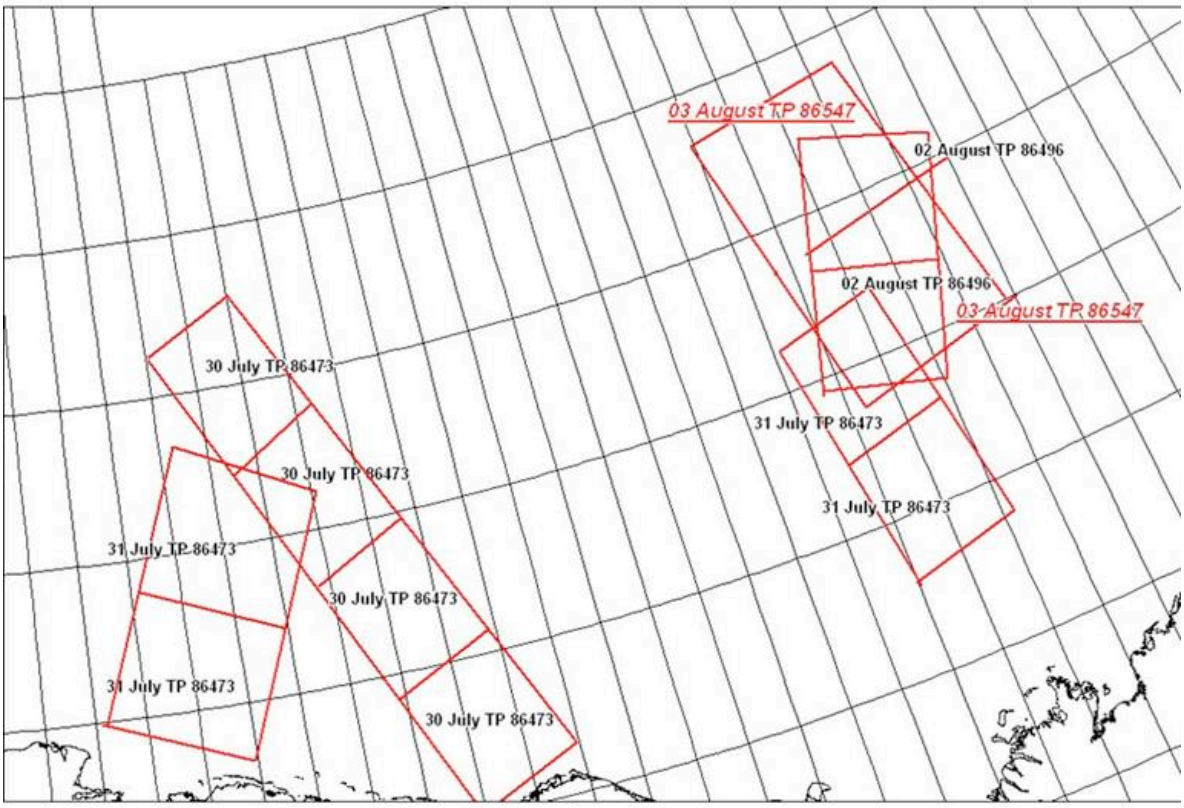

Figure 3-6 Envisat data in the Southern Beaufort Sea July-August 2008

3.3.2.2 Radarsat Imagery

In order to make up for the poor data return in the drilling areas due to the unusual extent of open water at the time the Envisat images were obtained, a request was made to the industry JIP partners for access to imagery taken before the full break-up and in the same year, 2008. Shell had gathered Radarsat data spanning the area from the Chukchi to the Canadian Beaufort continuously from June to November 2008. Three scenes from early

June, prior to the retreat of the polar pack, were chosen for analysis. Exxon, through its Canadian subsidiary Imperial Oil Resource Ventures Ltd had access to Radarsat coverage of multi-year ice incursions that took place in the mid-to-late summer of 2008 in the Canadian Beaufort, and at Point Barrow in early August. These data sets provided coverage of all the operational areas of interest and allow comparison of late winter and summer conditions for the year 2008. The generosity of Shell and Exxon/Esso is gratefully acknowledged. Without their help this part of the project would not have been possible.

3.3.3 Sonar Satellite Correlation Areas - Canadian Beaufort

Historical records of MODIS, Radarsat,, ERS and SPOT imagery were examined for images obtained when multi-year ice was known to have been in the vicinity of the IPS (Ice Profiling Sonar) deployments to the West of Banks Island.

Radarsat was available but even archived data more than 10 years old would have cost the full price, so it was not considered cost-effective. In the end, 4 ERS images from August to November 1996 were purchased and analyzed in conjunction with 1 of the 3 IPS sites– Site 5. This work is discussed in Chapter 8. Figure 3-7 illustrates the scope of ERS coverage west of Banks Island.

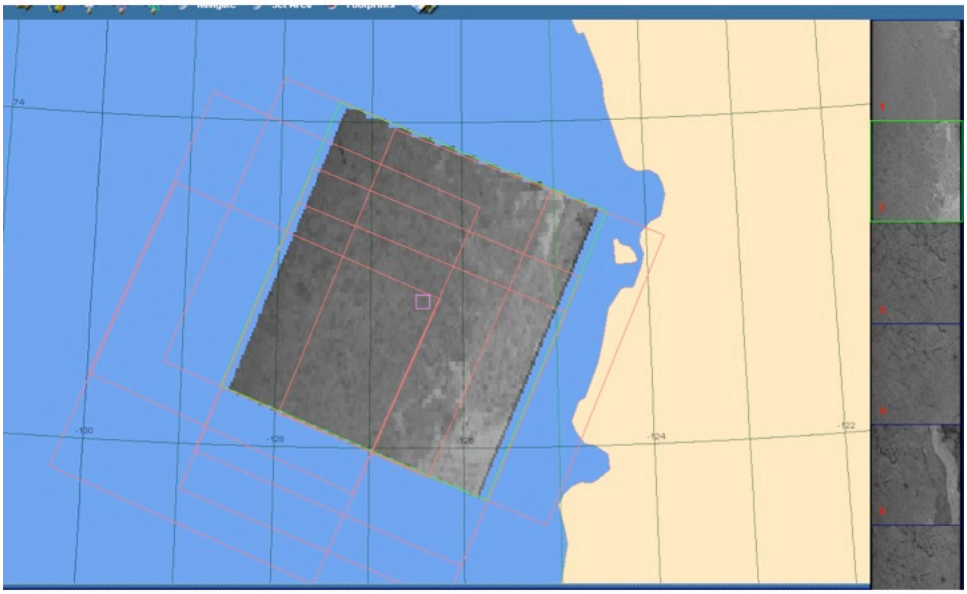

Figure 3-7 ERS coverage 1996 at IPS Site 5 west of Banks Island

4 EXTREME ICE FEATURES

4.1 Quality of Satellite Data

4.1.1 Envisat Data

Envisat imagery was acquired covering the entire area-of-interest. The imagery was of high quality, with no missing or degraded data. As the principle data source, Envisat was used as the "base" where all EIFs were ultimately located and logged. Although some targets that were at or near the sensor's resolution had to be verified by the high-resolution Radarsat data (8m), or the hi-resolution Landsat data (15m), overall target detection was very good. A sample of the imagery is shown below in Figure 4-1. All Envisat images appear in Appendix A.

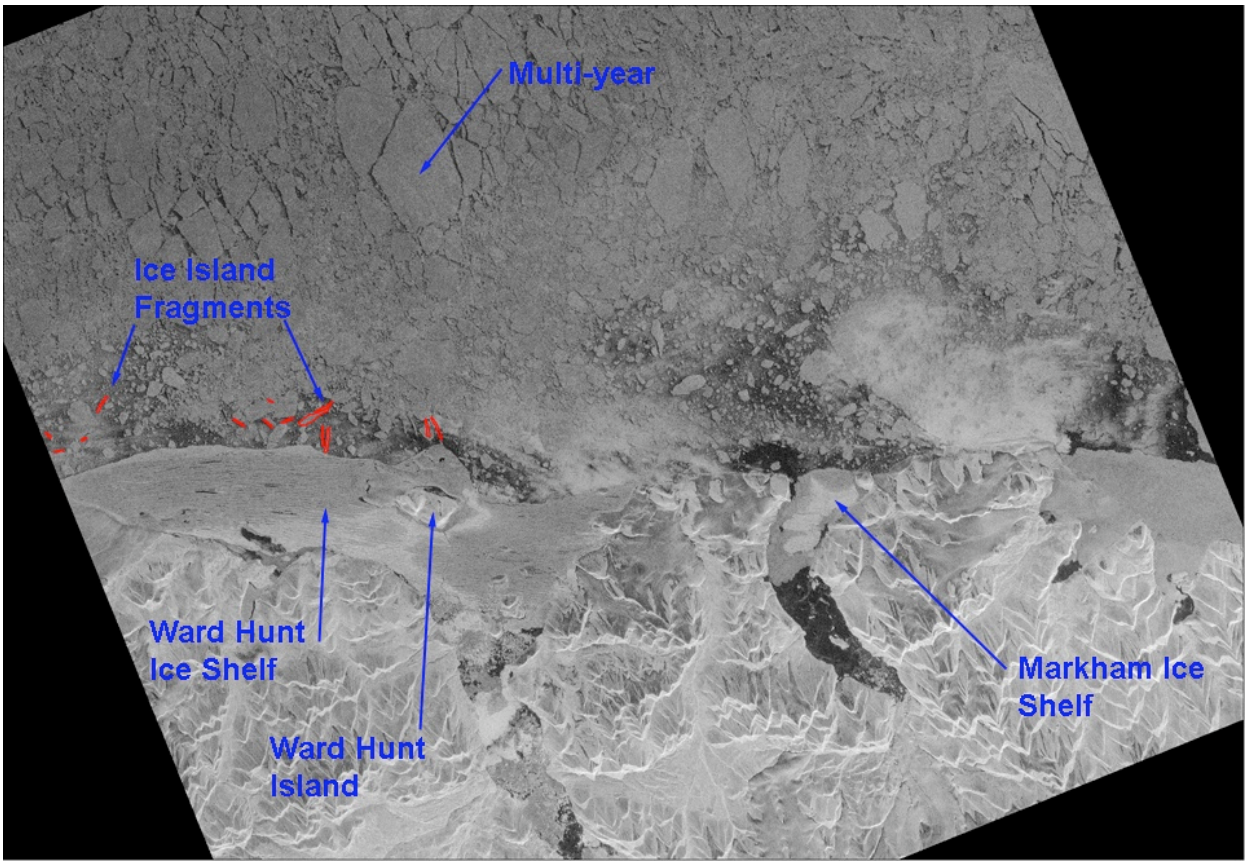

Figure 4-1 Sample of ENVISAT imagery

In the above example from the north coast of Ellesmere Island, the Ward Hunt and Markham ice shelves are indicated. A calving event had occurred earlier and many small ice island fragments were in the area. A slightly offshore ice drift had created low ice concentrations adjacent to the coast, and fracturing on the seaward side of the ice shelf was apparent in several areas.

Use of Envisat (or Radarsat) imagery during mid-summer can sometimes create difficulties in determining ice type due to the layer of surface melt water on all ice types. In the case of

EIF detection in the summer however, the principle target characteristics are shape, fracture type, and texture. Although texture is somewhat affected by surface melt water, the extreme freeboard of EIFs generally allows drainage of melt water, thus texture is affected very little. Due to the high mobility of the area in summer, most ice floes become somewhat rounded. EIFs on the other hand do not become rounded but remain very angular thus assisting in their detection at this time of year.

4.1.2 MODIS Data

Terra-MODIS imagery of the region was acquired at the same time as the main data collection – July 30th to Aug 2nd. Although the relatively low resolution of this imagery limited its utility in locating EIFs, it did provide a good overview, and clearly identified the larger features. A sample of the MODIS imagery is shown below in Figure 4-2.

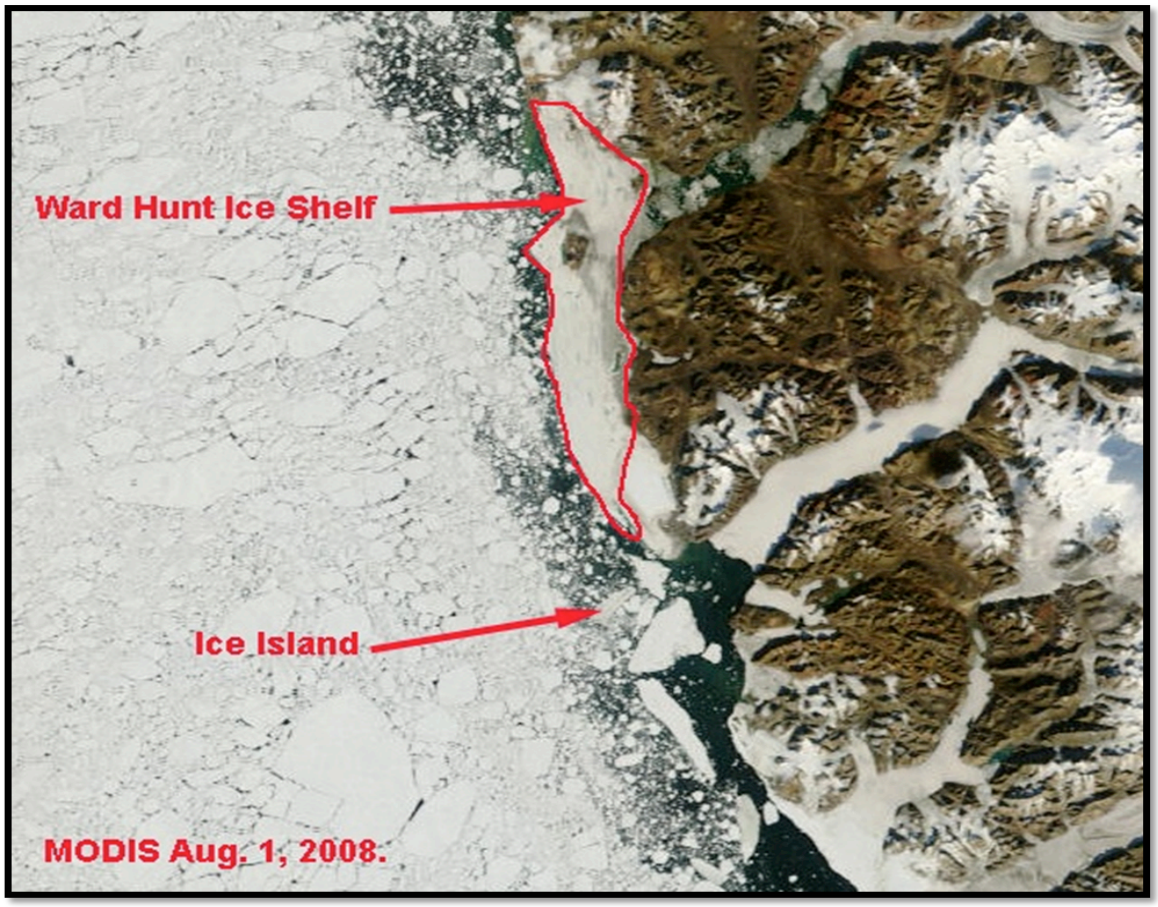

Figure 4-2 Sample of MODIS imagery

In the previous example the "banding" characteristic of Ice Islands is quite apparent. By having these broad-area-coverage MODIS images it was easier to understand what the regional ice conditions were at the time of the high-resolution image acquisition. The MODIS imagery was also used to track the larger floes over the data collection period to assess overlap. The full swath of MODIS covering the area-of-interest is contained in APPENDIX A.

4.1.3 Radarsat 2 Data

The first imagery to be analyzed was the two swaths of fine beam (8m resolution) Radarsat 2 data – the locations of which were shown in Figure 3-5 as green boxes (collected July 30th and August 2nd). This hi-resolution data was intended to *calibrate* the interpreter's eye, and verify how many really small (below Envisat resolution) EIFs were in each of these two areas. A sample of the imagery is shown below in Figure 4-3

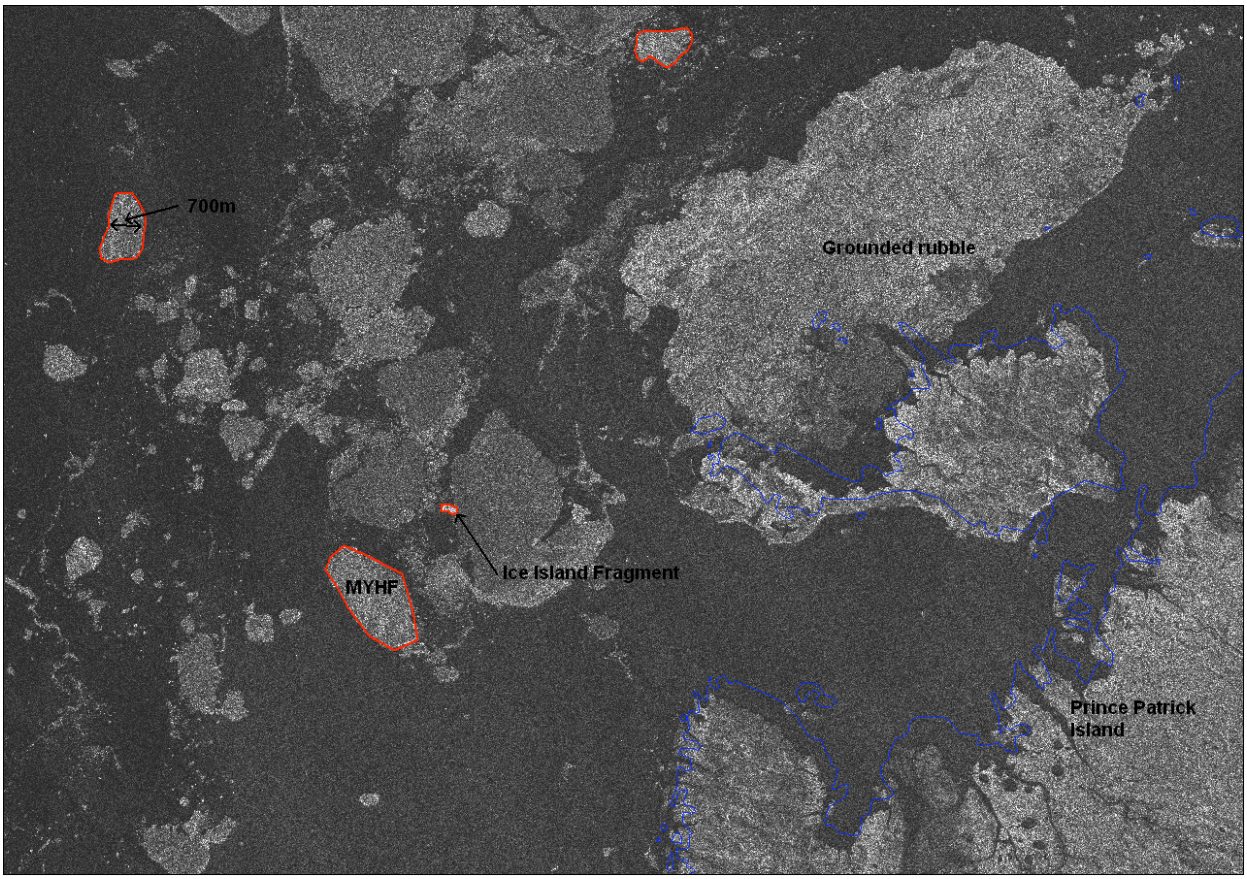

Figure 4-3 Sample of Radarsat 2 Imagery

In the sample image above, three MYHFs and one Ice Island fragment were identified. The area labeled as **Grounded Rubble** was some of the heavily deformed Multi-year ice normally found along the west coast of Prince Patrick Island. Although this area would likely have released MYHFs for a few weeks as it melted and became more buoyant, it was not considered an EIF at the time of this image. Each Radarsat2 image, and a text description, is contained in APPENDIX A – Imagery.

4.1.4 Landsat Data

Landsat data was acquired to cover any Envisat gaps, and to verify targets on the Envisat imagery using a visible-light image as opposed to radar. Although the cost was relatively low, and it was used for verification, the Landsat imagery was not of particularly good

quality. It suffered from an on-board sensor problem where there were bands of missing data consistently running through each image. A sample image is shown in Figure 4-4.

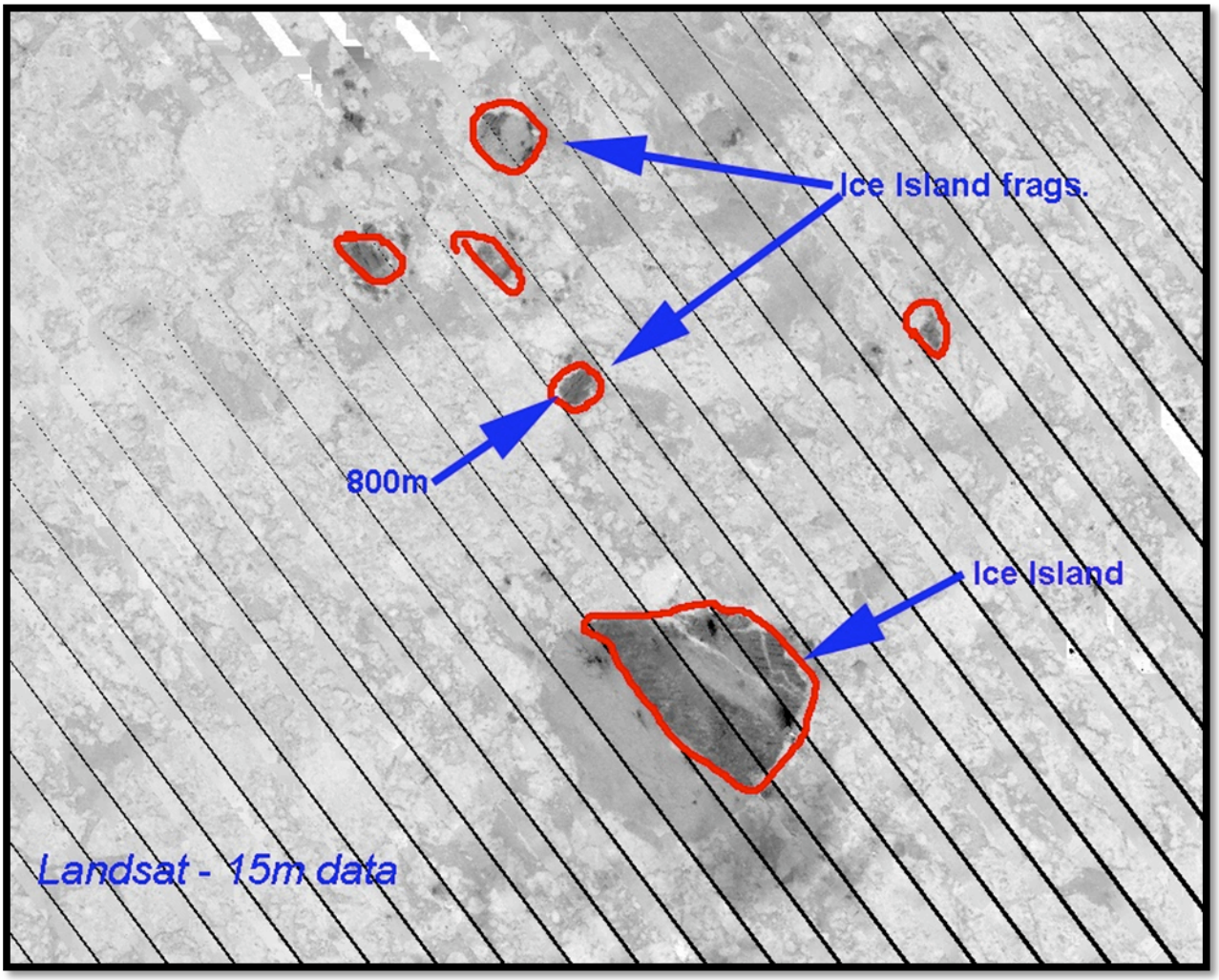

Figure 4-4 Sample of Landsat Imagery, SW of Meighen Island

In Figure 4-4, the bands of missing data are quite obvious. In addition, however, where the black bands narrow towards the top of this image, the imagery provider filled in "other" data so the black lines were not as obvious. Although these "filled in" data caused some complications, this imagery did provide an accurate confirmation of EIF targets. In the above clip, although the radar data depicted the main Ice Island quite clearly, the smaller fragments were far more obvious on this imagery than on the radar imagery. All Landsat images utilized are contained in APPENDIX A.

4.2 EIF Count Methodology

4.2.1 Software Tools

Locating, measuring, and recording of EIFs were accomplished through the use of 3 separate pieces of software. These were:

- **MapInfo** as the GIS program where EIFs were outlined and measured
- **Photoshop CS** where the full resolution 16 bit data was enhanced/manipulated to identify targets so that very subtle signatures could be investigated, and
- **Microsoft Excel** as the spreadsheet where all data were recorded for later statistical analysis

Envisat data formed the "base" on which all EIFs were identified. Although some targets were too small to be confidently identified on the Envisat imagery, when they were identified on other higher resolution imagery they were subsequently added to the Envisat EIF analysis layer. In this way all EIFs ultimately resided on one continuous analysis layer.

4.2.2 Ice Islands and Ice Island Fragments

Identification of ice islands and ice island fragments on radar imagery is accomplished by locating targets that have some or all of the following characteristics:

- Angular shape
- Elongated form
- Linear fractures (resulting long, straight edges indicate a thick ice type)
- Ribbed texture (pattern of undulating ridges and troughs running parallel to the long edge)
- A very strong perimeter radar return from the high freeboard
- Complete lack of ridging in the interior
- Deformation of adjacent Multi-year ice
- A “wake” of Open Water or low concentration due to the much greater draft of IIs vs multi-year ice floes, and
- A light grey tone.

Ice islands (>1km. in any dimension) were relatively easy to identify versus ice island fragments (<1km.). An ice island fragment can, naturally, occur in any size down to its final extinction. Through the use of the Radarsat2 data (8m) verified by the 15m Landsat data, ice island fragments as small as 70m x 35m were identified. Although EIFs of this size are far below what is considered a hazard, particularly when located in high northern latitudes, the “signature” of these targets provided valuable information to the interpreter regarding the sensor’s response to wet shelf ice at a given radar incidence angle. Confident identification of larger more significant EIFs was consequently simplified.

Ice islands were typically relatively easy to identify. The unique “ribbed” texture makes them obvious in most sea ice conditions. As an ice island begins to break-up however, the ribbed texture ultimately disappears. In the normal course of events, an ice island eventually fractures length-wise through two troughs, leaving the one long undulation between them. Numerous Ice Island fragments with a width in the 120m to 150m range were identified. This is to be expected as the typical period of undulation in Shelf ice is approximately 40m, thus the target has 1 trough, 1 undulation, and another trough (3 x 40m = 120m).

4.2.3 Multi Year Hummock Fields

A MYHF is an EIF that is principally associated with extreme on-shore pressure in a multi-year ice environment. This typically causes extreme ridging and total deformation of the ice cover; 10m freeboards in this rubble are not uncommon. The deformation occurs as multiple ridges or hummocks very close together. The features become incorporated into the land fast ice and consolidate over a number of years. Subsequently these floes/areas drift free (typically in summer) when offshore winds carry them off. These features often freeze into larger multi-year floes in the fall, and are then found as separate high-return targets within floes the following year. Identification of MYHFs on radar imagery is accomplished by locating targets that have some or all of the following characteristics:

- High return throughout the feature (no level areas)
- Rounded or jagged shape
- Parallel ridging
- Existing as a separate target (not a ridge)
- Saturated signals in the floe (corner reflectors – standing floes, hummocks)
- No evidence of a drainage pattern
- Ice island or ice island fragment inclusions

The extreme conditions under which MYHFs are created typically deform most multi-year floes. Ice islands and ice island fragments however, are able to withstand these conditions, and occasionally appear as a relatively smoother area within a MYHF. The angular shape and high freeboard of IIs or II fragments distinguish them from the deformed multi-year ice.

MYHFs are distinguished from ridging by their greater degree of consolidation, by their existence as a separate target and by the occurrence of multiple hummocks/ridges rather than a single ridge line. Although a very large multi-year ridge (newly-formed or old) can have dimensions qualifying it as an EIF, ridges are dealt with separately in this report in Chapter 6 on upward-looking sonar profiles. Ridging in multi-year ice along the Arctic Islands is constant throughout the year during periods of on-shore ice drift, and although recently-formed multi-year ridges can be identified on radar, older weathered ridges cannot be reliably detected due to their typically smooth curved surfaces.

In this project the west coast of Prince Patrick Island was imaged at a time when offshore winds were releasing a significant number of MYHFs. Although this area has a history of occasionally remaining fast for several years at a time, in 2008 all coastal ice on the west side of Prince Patrick Island drifted free.

4.3 EIF Count Results and Areal Density

Data from all the imagery was logged in two Excel databases:

1) All EIFs from RDRST2 data and

2) All EIFs from all other sources (Envisat, Landsat, MODIS). For analysis purposes the two databases were ultimately merged, with duplicate targets removed. A total of 200 EIFs were detected in an area of 183,980 sq.km. of radar imagery. In total 235,380 sq.km. of

radar plus visual imagery was searched but no additional features were found in the extra area. Note that search area sizes do not include open water. The resulting breakdown by EIF type is.

- 40 Ice Islands
- 93 Ice Island fragments
- 67 MYHFs

Table 4-1 shows the observed areal densities of the different EIF features (>500 m in equivalent diameter).

Table 4-1 Observed Areal Densities of EIFs >500m in equivalent diameter

EIF Type	Number > 500 m Diam	Area Surveyed km^2	Density in #/km^2
Ice Islands	37	183,980	2.0×10^{-4}
II Fragments	7	"	0.4×10^{-4}
MYHF	55	"	3.0×10^{-4}
Total	99	183,980	5.4×10^{-4}

The spatial distribution of these EIFs is shown in Figures 4-5 and 4-6. Red outline depicts ice islands, pink denotes ice island fragments, and a brown outline signifies a MYHF. The outlines of the EIFs can be seen in larger scale on the individual Envisat and other images shown in Appendix A.

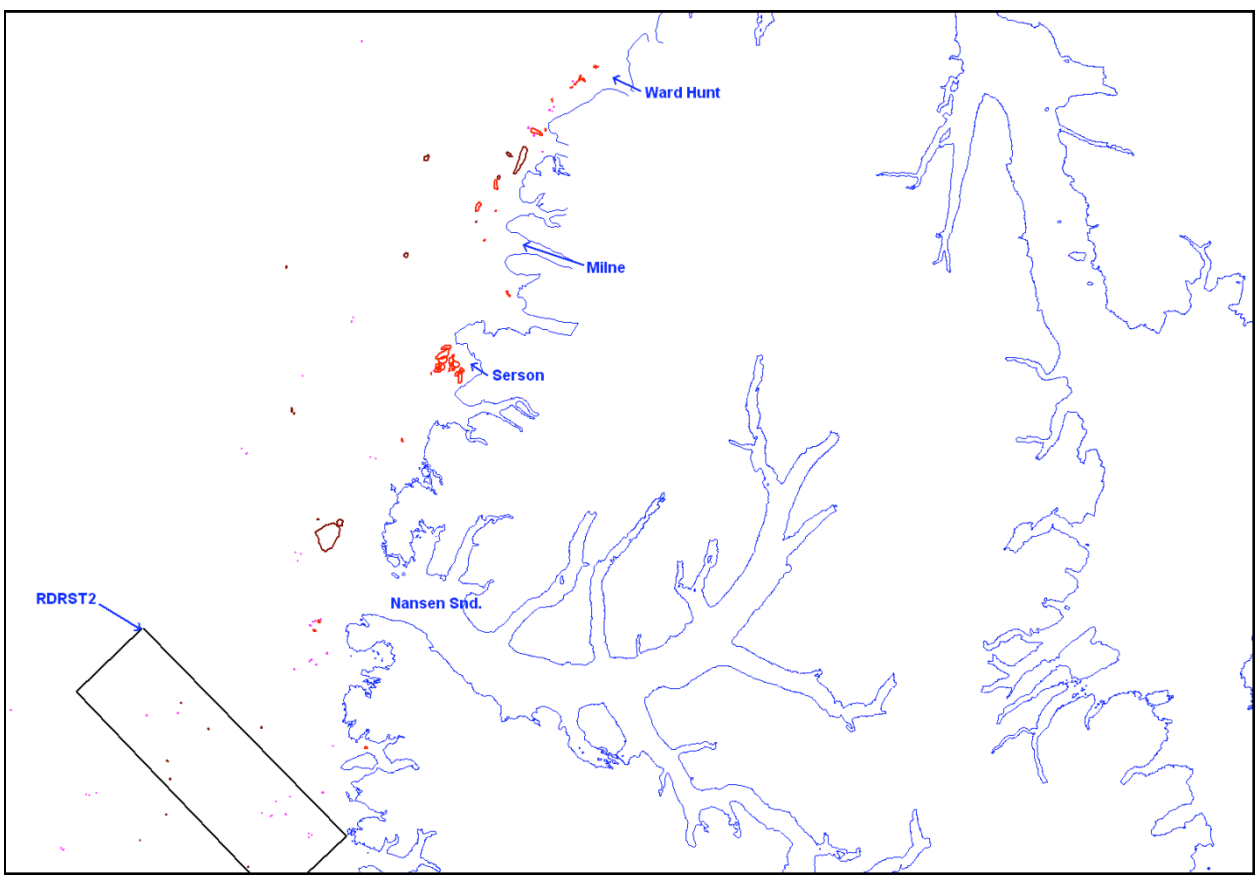

Figure 4-5 EIF Distribution in North Section (II - red, IIF - pink, MYHF - brown)

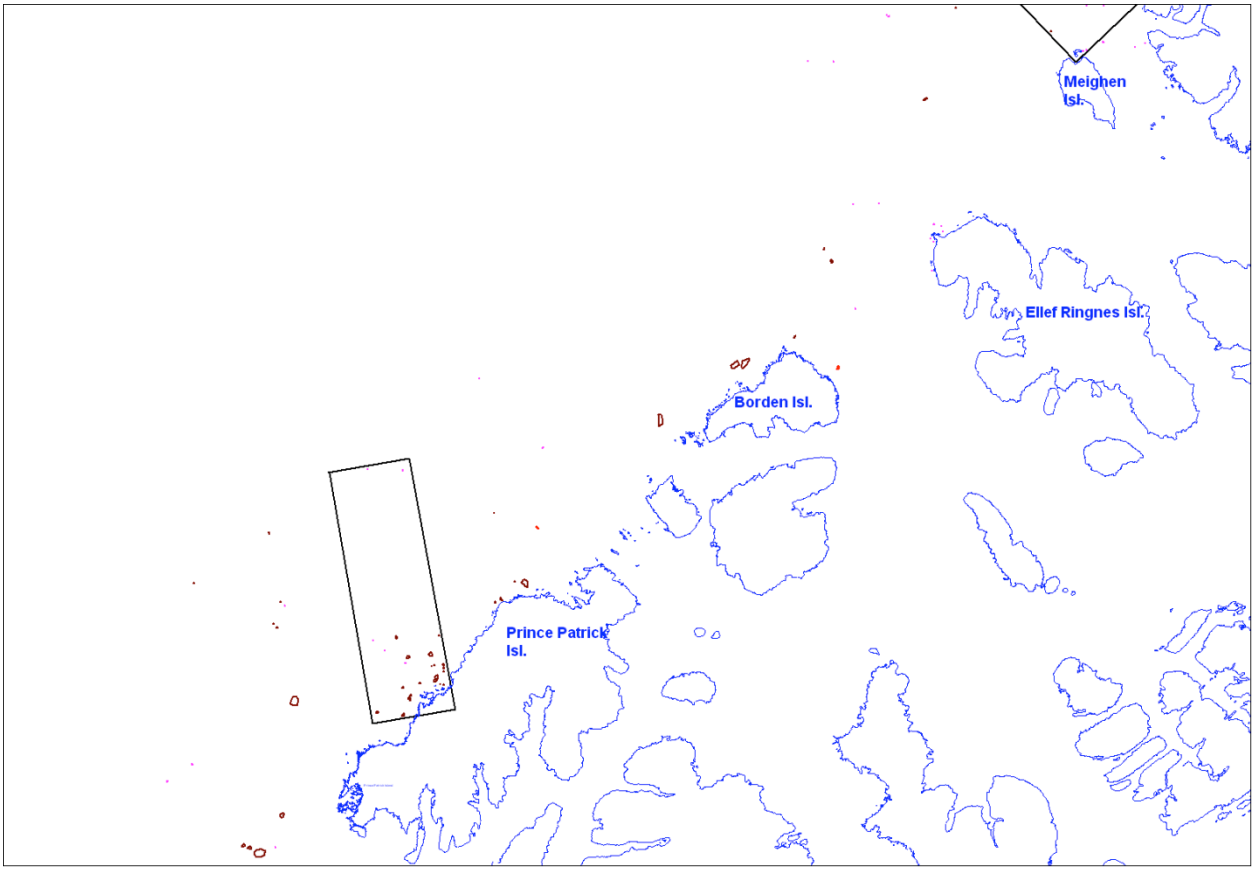

Figure 4-6 EIF Distribution in South Section (II - red, IIF - pink, MYHF - brown)

4.4 EIF Data Base

4.4.1 Data Compilation and Derived Parameters

During the interpretation phase of image analysis, individual EIFs were identified and outlined as polygons whose attributes were stored in different layers in the GIS program. The following set of parameters was recorded in a spreadsheet. (N.B. Re-entrant, marked with * below, is defined as ice shelf ice formed from multi-year sea ice that attaches to the main ice shelf due to onshore pressure and freezing, re-enters the shelf environment and over tens of years attains surface undulations and thickness increases from snow accumulation and bottom accretion).

- Feature ID No.
- General area
- Feature type (Ice Island, Ice Island fragment, MYHF, Re-entrant *)
- Was it contained within a larger floe?
- Satellite image ID (date and exact time)
- Originating ice shelf if known
- Date

- Latitude
- Longitude
- Perimeter length (output from the program)
- Area (output from the program)
- Roughness indication (Low, Medium or High)

In a post-interpretation phase, these dimensions were measured:

- Major axis
- Minor axis
- Diameter

These geometrical parameters were calculated (definitions and formulae in Appendix C):

- Equivalent diameter
- Circularity indicator
- Compactness indicator
- Ellipsoid roundness
- Second moment of area (in m^4)
- Diameter of Gyration.

For the location of the centroid of the EIF, bathymetric charts of the Arctic Ocean were consulted to find:

- Water Depth

In the case of a few of the ice islands it was possible to estimate the average thickness from GPR thickness profiles measured prior to the calving of the I.I. from the Ice Shelf of origin. For future updates to the data base, where more detailed monitoring and tracking might be carried out, columns are included for these parameters:

- Mean and maximum thickness
- Mean and maximum freeboard
- Profile data
- Mass
- Drift Speed
- Drift Direction

Finally, there are some columns for comments and cataloguing information:

- Name of the internal GIS data base
- Comments , and,
- Zone identification used in the analysis.

The Zones are shown in Figure 4-7, where Zone 1 is N of Prince Patrick Island to Borden Island, Zone 2 is from Borden N to Ellef Ringes Island and Zone 3 includes offshore of Ellesmere Island. All EIFs are plotted in Figure 4-7 for reference.

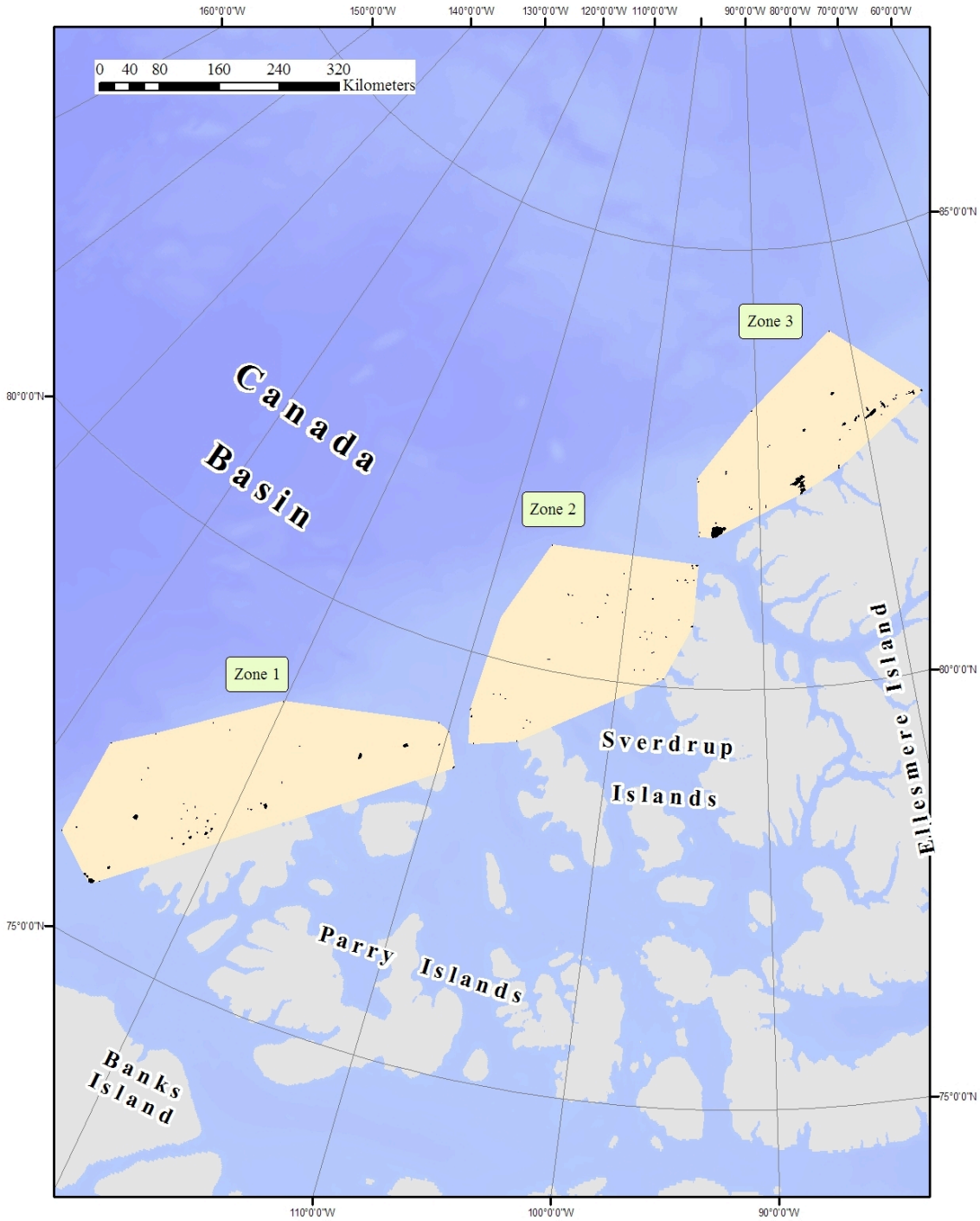

Figure 4-7 Zones Used in the EIF Analysis

4.4.2 Database Description

The EIF database is contained in one Excel file: "EIFs Beaufort Sea Arctic Archipelago 2008", on the accompanying CD. It has 16 worksheets named below in **bold**:

- **Dataset**: shape indicators, latitude, longitude, etc. (see 4.4.1 for complete list)..
- **Coord**: the vertex coordinates (geographic and planar) of the polygons that define the EIFs. For the planar coordinates, the projection employed was the Lambert Conformal Conic (two parallels).
- **Stats**: Summary statistics: mean, percentiles, etc. for all the EIF's, for those with diameters greater than 500 meters, for Ice Islands, Ice Island fragments and MYHF, and for the three zones as well.
- **Chart Data**: the data for the charts (8 charts). Although the units on the Dataset are metres, for clarity we employ kilometres with the charts.
- **Area-zones**: EIF area exceedance probability for all data and 3 zones (log-log)
- **Area-zones>500**: same as above, except using only data where diameter>500m
- **Diam-zones:** EIF diameter exceedance probability for all data and 3 zones (log-log)
- **Diam-zones>500:** same as above, except using only data where diameter>500m
  Area-feat: EIF area exceedance probability for all data and 3 feature types (log-log)
- **Area-feat>500**: same as above, except using only data where diameter>500m
- **Diam-feat: EIF diameter** exceedance probability chart for all data and 3 feature types (log-log)
- **Diam-feat>500:** same as above, except using only data where diameter>500m
- **Equiv_Diam-feat>500:** EIF equivalent diameter exceedance probability for all data where diameter>500m (log-log)
- **Equiv_Diam-feat>500 (II):** EIF equivalent diameter exceedance probability for all Ice Islands where diameter>500m (log-log)
- **Equiv_Diam-feat>500 (IIF):** EIF equivalent diameter exceedance probability for all Ice Island Fragments where diameter>500m (log-log)
- **Equiv_Diam-feat>500 (MYHF):** EIF equivalent diameter exceedance probability for all Multi-Year Hummock Fields where diameter>500m (log-log)

4.5 Statistical Analysis of EIF parameters

4.5.1 Database Subsets Analyzed

If one magnifies Figures 4-5 and 4-6 it is possible to see that most of the Ice Islands and I.I. fragments were located offshore Ellesmere and Axel Heiberg Islands, that the area offshore Prince Patrick Island had mostly MYHFs, and that the area in between (Zone 2) seems to be an even mix of small I.I.s and MYHFs. The main reasons for this kind of division are: (i) 2008 was the summer when major calving took place at the Ellesmere ice shelves and (ii) major break-up of the land fast ice adjacent Prince Patrick Island (one source of MYHFs) also took place. Furthermore the satellite data was acquired within days of these events so it is not surprising that the features were captured near their sources. In future years, as the EIFs drift in the Gyre, the distribution by zone will change. Also, as the ice shelves that are the source of ice islands gradually degrade one would expect to see an increase in total numbers of these features in the coming years until they begin to be

transported out of the Arctic Basin in the Transpolar Drift Stream or until the majority of the remaining floating ice shelf area has calved.

Given this dynamic, key parameters of EIF Area and Diameter were analyzed for subsets of the data broken down into zones and into EIF type. The data was further subdivided into All EIFs and EIFs greater than 500m in diameter. The numbers of EIFs subdivided in this way are presented in Tables 4-2 and 4-3. Statistical distributions according to Zone and EIF type are presented in sub-sections 4.5.2 and 4.5.3 respectively.

Table 4-2 EIFs 2008 Divided by Zone

Zone	Number of EIFs	Number of EIFs of Diam>500m	% of EIFs of Diam>500m	Total Area of EIFs (km2)
1 (Prince Patrick I. to Borden I.)	57	46	80.7	143.6
2 (Ellef Ringnes I. to Axel Heiberg I.)	73	30	41.1	12.9
3 (Ellesmere I)	70	61	87.1	360.7
All	200	137	68.5	517.1

Table 4-2 shows that the major part, 360 sq. km, of the total area of EIFs was in Zone 3, opposite Ellesmere Island.

Table 4-3 EIFs 2008 Divided by Type

EIF Type	Number of EIFs	Number of EIFs of Diam>500m	% of EIFs of Diam>500m	Total Area of EIFs (km2)
MYHFs	67	64	95.5	386.5
Ice Island Fragments	93	33	35.5	7.1
Ice Islands	40	40	100	123.4
All	200	137	68.5	517.1

Table 4-3 shows that MYHFs account for 386 out of 517 sq. km. Note that the two largest MYHFs account for 193 sq.km. (50% of the total for MYHFs), and the three largest account for 221 sq.km.

4.5.2 EIF Statistics By Zone

The Box plots in Figure 4-8 show the main points of the exceedance distributions and allows easy comparison between zones. Zone 3, offshore Ellesmere Island had the largest feature, which happened to be a MYHF. Exceedance plots of Area and Diameter for features greater than 500m diameter are shown in Figures 4-9 and 4-10.

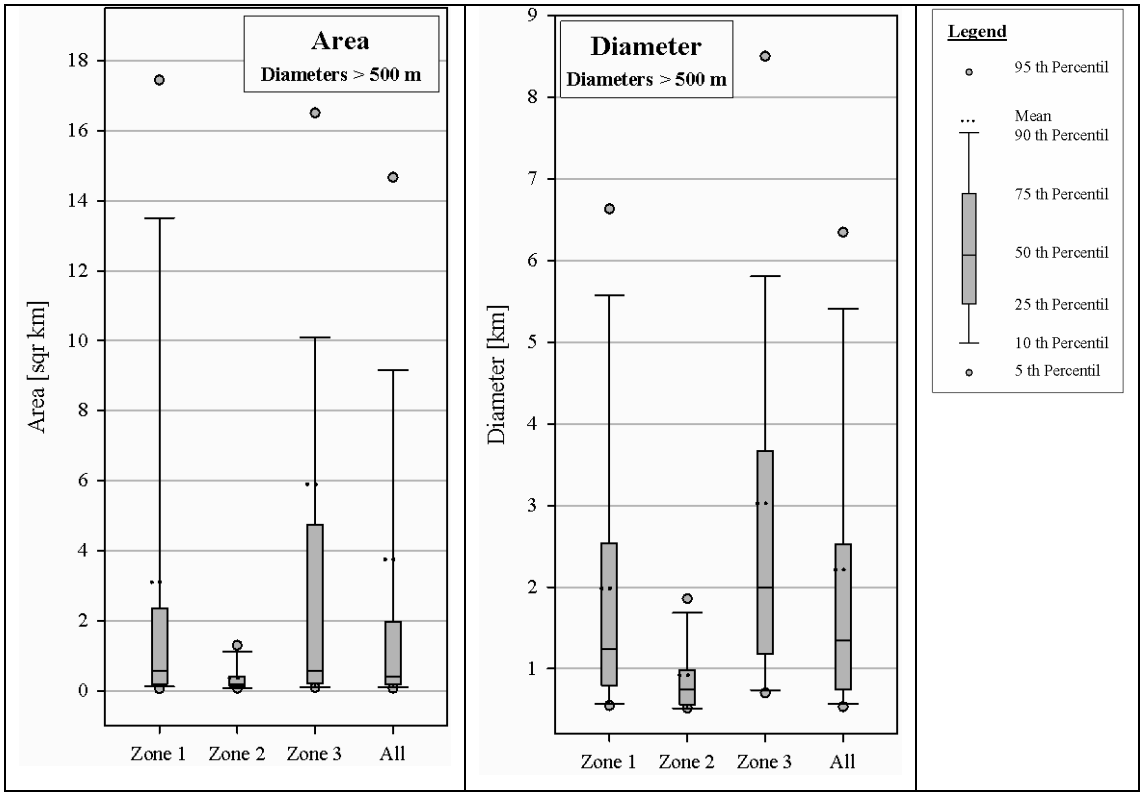

Figure 4-8 Box Plots of EIF Area and Diameter by Zone

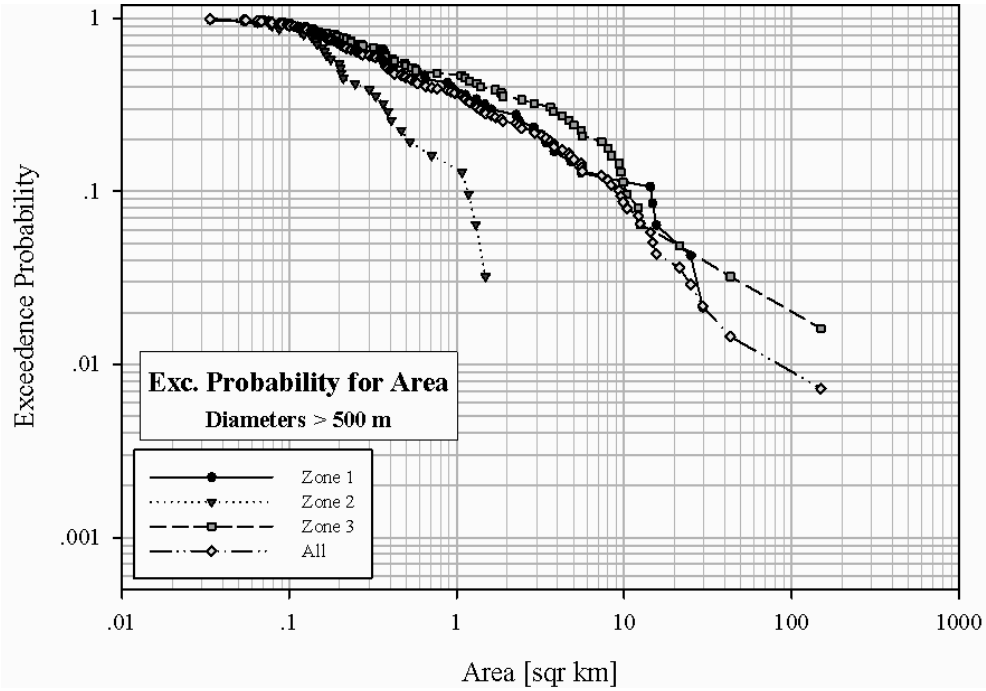

Figure 4-9 Exceedence Probability for Area

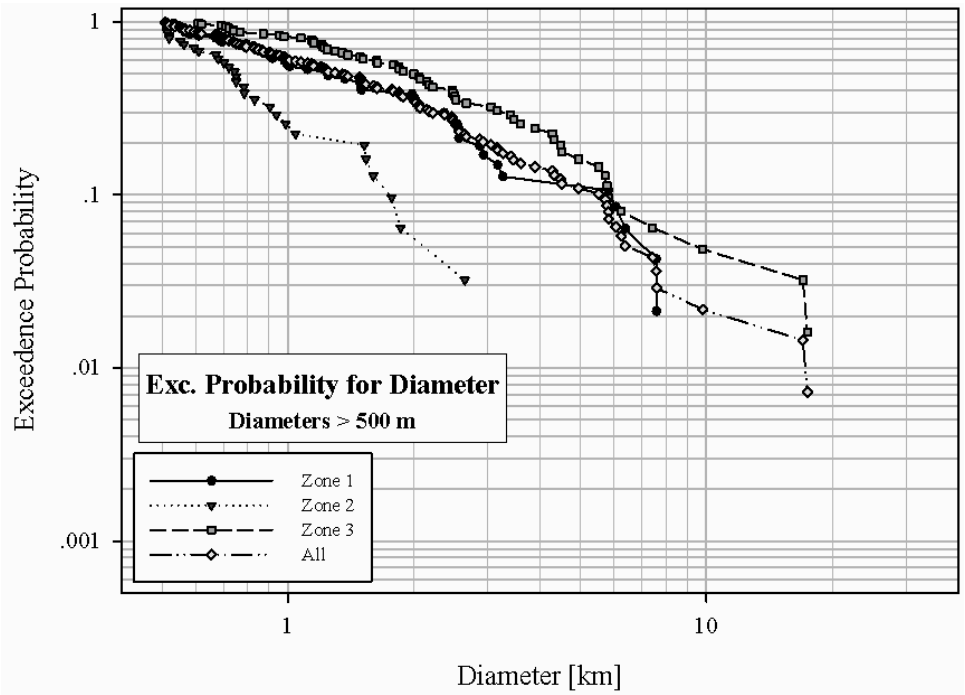

Figure 4-10 Exceedence Probability for Diameter

Figure 4-8 shows that the average area (~5.9 sq.km.) of EIFs in Zone 3, beside Ellesmere I., is larger on average than those in Zone 1 (~3.1 sq.km.), and much larger than those in Zone 2 (0.4 sq.km.). The Zone 3 average is heavily weighted by the 2 largest MYHFs which account for more than half the total area. The median area and diameter are well below the average values in all cases.

4.5.3 EIF Statistics By Type

The Tables 4-4 and 4-5 present the key values for EIFs by Type, both for the total populations and for the populations greater than 500m in diameter. Some of the key numbers are: the largest ice island was 21.4 sq.km. and the mean was 3.2 sq.km. The largest MYHF was 149.8 sq.km, the mean was 5.8 sq.km.

Table 4-4 Basic Parameters for all EIF data by Type

Parameter	All EIFs	Ice Islands	Ice Island Fragments	MYHFs
Sample size	200	40	93	67
Area (sq.km.)				
Max	149.8	21.4	0.4	149.8
Mean	2.6	3.1	0.07	5.8
Diameter (km.)				
Max	17.4	9.8	1.0	17.4
Mean	1.6	2.8	0.43	2.5
Equivalent diameter (km)				
Max	13.8	5.2	0.7	13.8
Mean	1.0	1.6	0.27	1.7

Table 4-5 Basic Parameters for EIFs> 500m in diameter by Type

Parameter	All EIFs	Ice Islands	Ice Island Fragments	MYHFs
Sample size	137	40	33	64
Area (sq.km.)				
Mean	3.8	3.1	0.14	6.0
Diameter (sq.km.)				
Mean	2.2	2.8	0.7	2.6
Equivalent diameter (km)				
Mean	1.4	1.6	0.4	1.8

The Figures that follow indicate the statistics of the EIFs by type for features greater than 500m diameter. Figure 4-11 shows the exceedence probability for area by feature type. Figure 4-12 shows the exceedence probability for diameter.

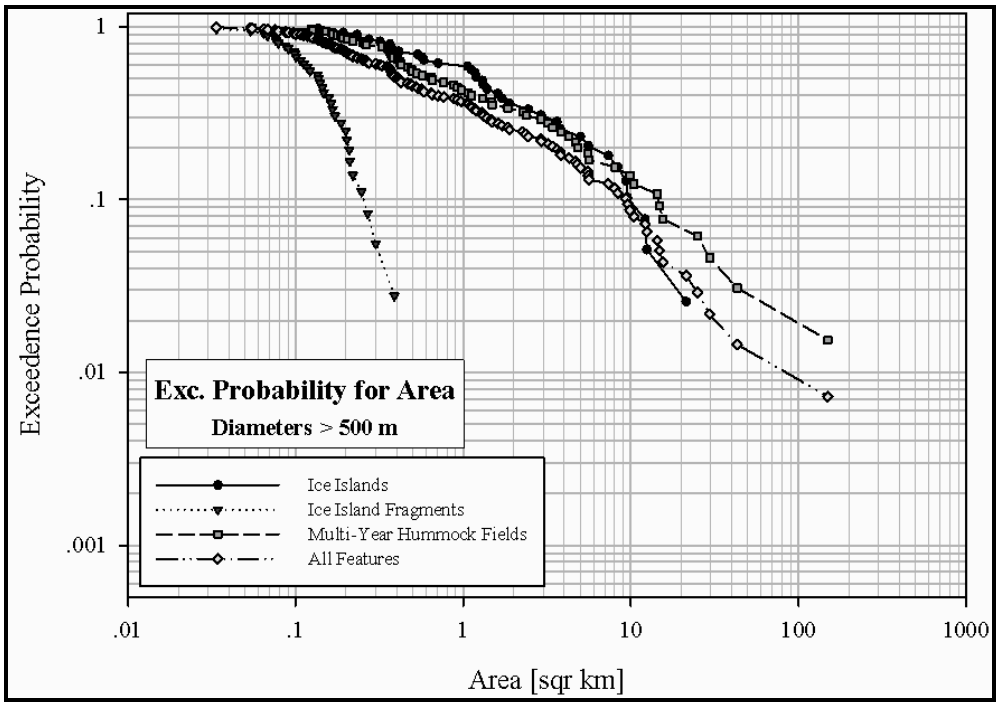

Figure 4-11 Exceedence Probability for Area for features > 500m diam.

.

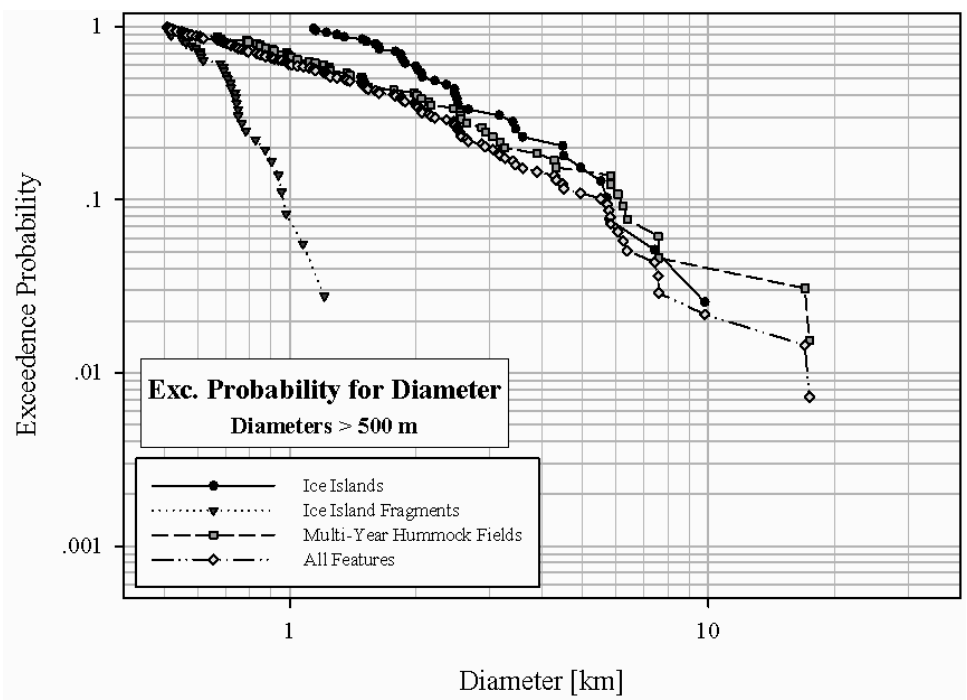

Figure 4-12 Exceedence Probability for Diameter for features > 500m diam.

Figure 4-13 shows the box plot for all features for area and diameter, for features greater than 500m.

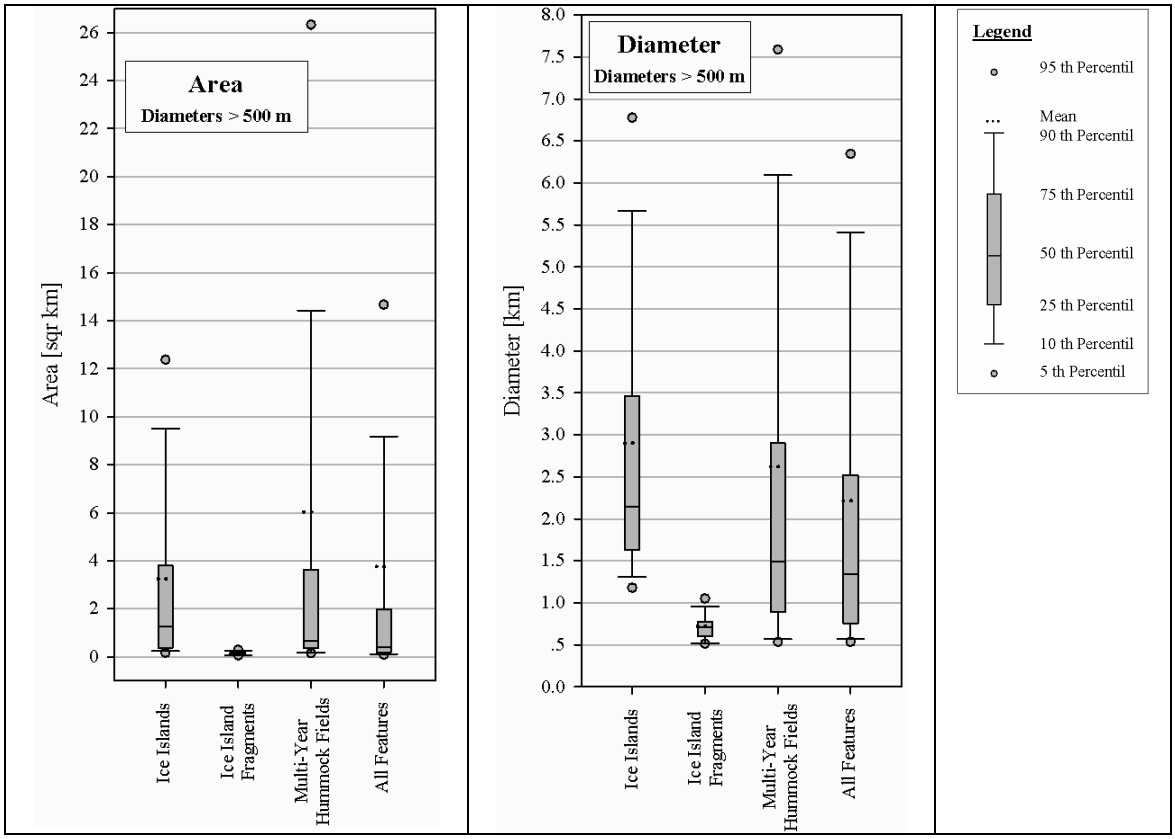

Figure 4-13 Box plots of area by EIF Type for features > 500m diam.

4.5.4 Equivalent Diameter Statistics

For comparison with previous studies it is necessary to use equivalent diameter, defined as the diameter of a circle of equal area to the feature in question. ("Diameter", as it has been used so far in the text, is the longest dimension of the feature). Figures 4-14, 4-15 and 4-16 show the exceedance plots of equivalent diameter for all EIFs, for Ice Islands and for MYHFs, all greater than 500 m in diameter. Key results and listed in Table 4-4.

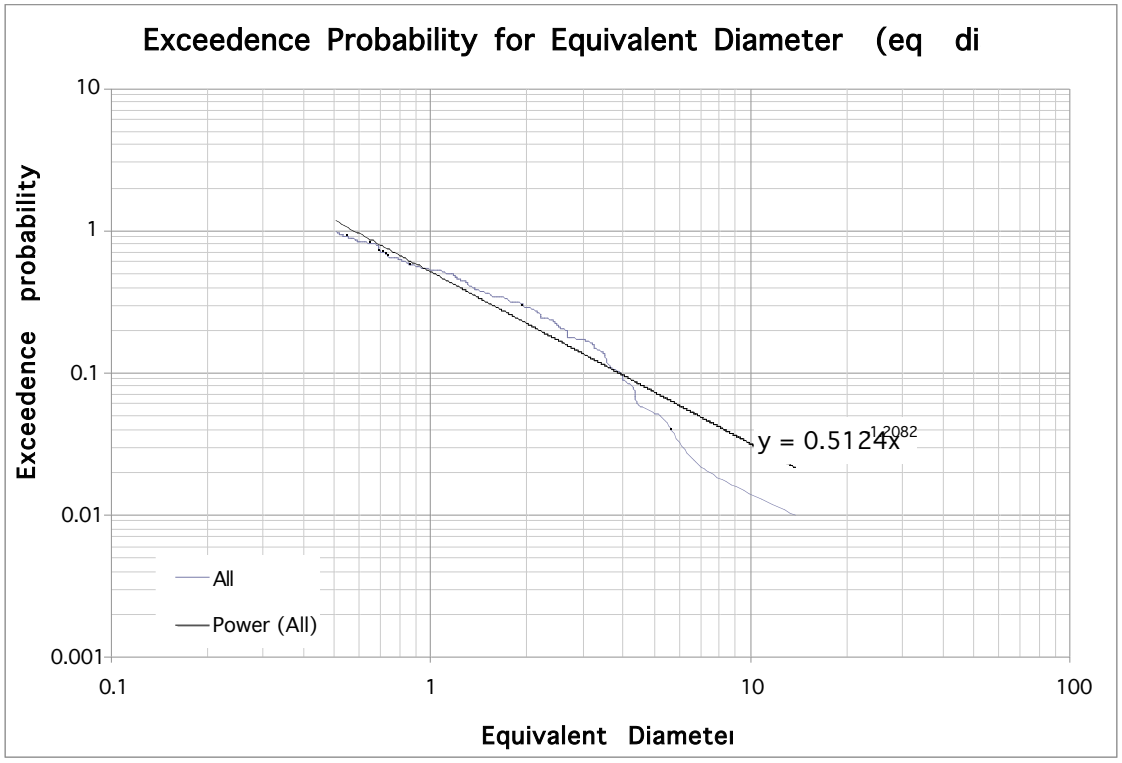

Figure 4-14 Exceedence Plot of Equivalent Diameter All EIFs >500m diameter

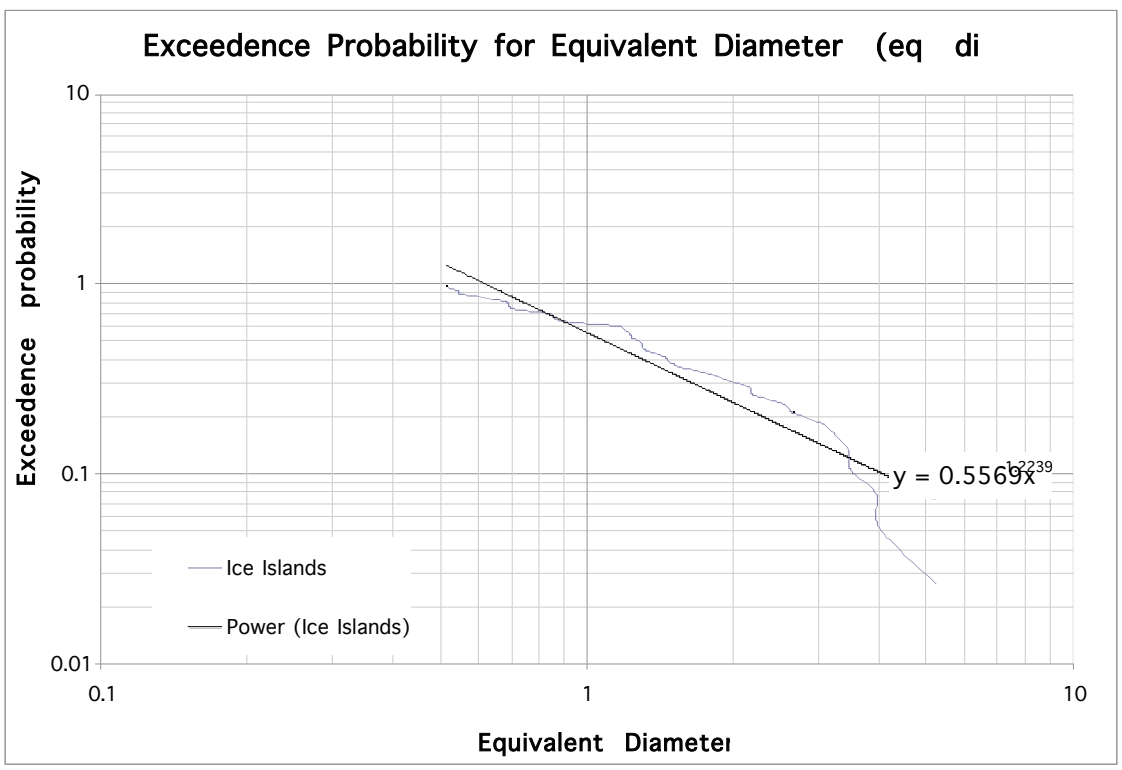

Figure 4-15 Exceedence Plot of Equivalent Diameter for Ice Islands >500m

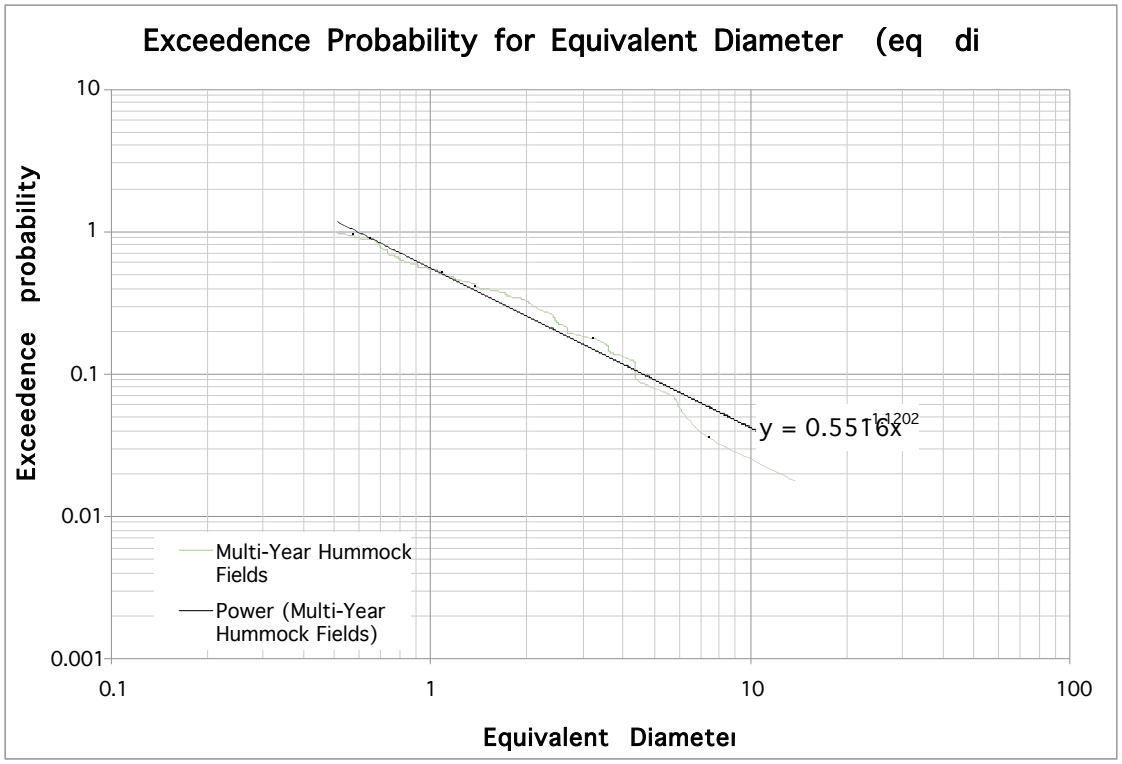

Figure 4-16 Exceedence Plot of Equivalent Diameter Multi-Year Hummock Fields

4.6 Comparison with Previous Surveys

Data bases from previous survey periods are included an Appendix of Pilkington et.al. 1992 (ESRF 115). The first data base covers the years 1946 to1988 and consists primarily of large ice islands. Some of these data were used to develop ice island statistics for the Beaufort Sea EIF in Marcellus et.al. 1982. The second data base resulted from analysis of SAR imagery from 1988-1991 undertaken for ESRF 115 by Pilkington et.al. 1992.. The current data base for 2008 is compared with the previous surveys in terms of populations, areal densities and feature size. This was done for all data, for features whose equivalent diameter was more than 500m and for features greater than 2km in equivalent diameter. Results are shown in Tables 4-6, 4-7 and 4-8.

Table 4-6 compares EIF populations for the three time periods. The survey of 2008 produced 200 EIFs compared with 162 detected from 1988-1991. However, for EIFs of equivalent diameter >500m there were only 99 in 2008 versus 149 two decades earlier. For features larger than 2 km in equivalent diameter, again, there were more in 1988-1991. This suggests that while the number of EIFs has increased, the number that are large enough to be of concern for design may be decreasing.

The relatively few EIFs documented in the period 1946-1988 reflect the lower resolution of the detection tools available at the time, as well as the general interest in very large ice islands that were in circulation at the time. These large ice islands have departed from the Arctic Ocean as discussed by various authors.

Table 4-6 Comparison of EIF Populations

	1946-1988	1988-1991	2008
EIFs - All	42	162	200
All EIFs Equiv Diam >500m	38	149	99
All EIFs Equiv Diam >2km	29	47	29
Ice Islands and Fragments - All	34	41	133
II & IIFs Equiv Diam >500m	30	28	44
II & IIFs Equiv Diam >2km	26	10	11
MYHFs - All	7	86	67
MYHFs Equiv Diam >500m	7	86	55
MYHFs Equiv Diam >2km	2	23	18
Re-Entrant Ice - All	1	35	0
RE Equiv Diam >500m	1	35	0
RE Equiv Diam >2km	1	14	0

Table 4-7 compares the areal density of EIFs for the 2008 and 1988-1991 surveys for EIFs of equivalent diameter greater than 500m and 2km. The area of pack ice surveyed was similar in both cases - close to 180,000 square km.

Table 4-7 Comparison of EIF Areal Densities

	1988-1991		2008	
Area in sq.km.	178,243		183,980	
	population	**density (#/km2)**	**population**	**density (#/km2)**
All EIFs				
All EIFs Equiv Diam >500m	149	8.36E-04	99	5.38E-04
All EIFs Equiv Diam >2km	47	2.64E-04	29	1.58E-04
Ice Islands and Fragments				
II & IIFs Equiv Diam >500m	28	1.57E-04	44	2.39E-04
II & IIFs Equiv Diam >2km	10	5.61E-05	11	5.98E-05
MYHFs				
MYHFs Equiv Diam >500m	86	4.82E-04	55	2.99E-04
MYHFs Equiv Diam >2km	23	1.29E-04	18	9.78E-05
Re-Entrant ice				
RE Equiv Diam >500m	35	1.96E-04	0	
RE Equiv Diam >2km	14	7.854E-05	0	

Considering all EIFs >2km, the areal density decreased over the past 20 years from 2.64 x 10^{-4} to 1.58 x 10^{-4}. However, the areal density of ice islands increased somewhat while that for MYHFs decreased. The increase in ice island areal density is understandable given the dramatic calvings of 2008 The decrease in multi-year hummock field density may mean that fewer are forming, or it may reflect difficulties of image interpretation.

Table 4-8 compares key size parameters and shows that in general the median, mean and maximum size (equivalent diameter) has been steadily decreasing over the decades.

Table 4-8 Comparison of EIF Sizes (Equivalent Diameter > 500m)

	1946-1988	1988-1991	2008
All EIFs			
Median Equiv Diam (km)	4.5	1.4	1.2
Mean Equiv Diam (km)	7.6	1.9	1.8
Max Equiv Diam (km)	22.5	8.1	13.8
Ice Islands and Fragments			
Median Equiv Diam (km)		1.5	1.05
Mean Equiv Diam (km)		2.4	1.5
Max Equiv Diam (km)	22.5	8.1	5.2
MYHFs			
Median Equiv Diam (km)		1.4	1.1
Mean Equiv Diam (km)		1.8	2
Max Equiv Diam (km)		7.4	13.8
Re-Entrant Ice			
Median Equiv Diam (km)		1.6	
Mean Equiv Diam (km)		2	
Max Equiv Diam (km)		5.2	

4.7 Glacial Ice Advance on Ellesmere Island

One of the Envisat images captured the apparent deterioration of a glacier on Ellesmere Island. See Figure 4-17. The glacier appears to be floating for the 15 km length represented by the yellow arrow in the Figure, as indicated by cracks and an irregular edge. Were it not for the protection of the Milne ice shelf, it would probably be a source of icebergs to the Arctic Ocean. The Milne ice shelf is very thick - up to 94 m - and appears to be solidly grounded, so it may provide protection for many years. Never-the-less, this and other glaciers might one day feed icebergs into the Arctic Ocean, and should be monitored with radar imagery from time to time.

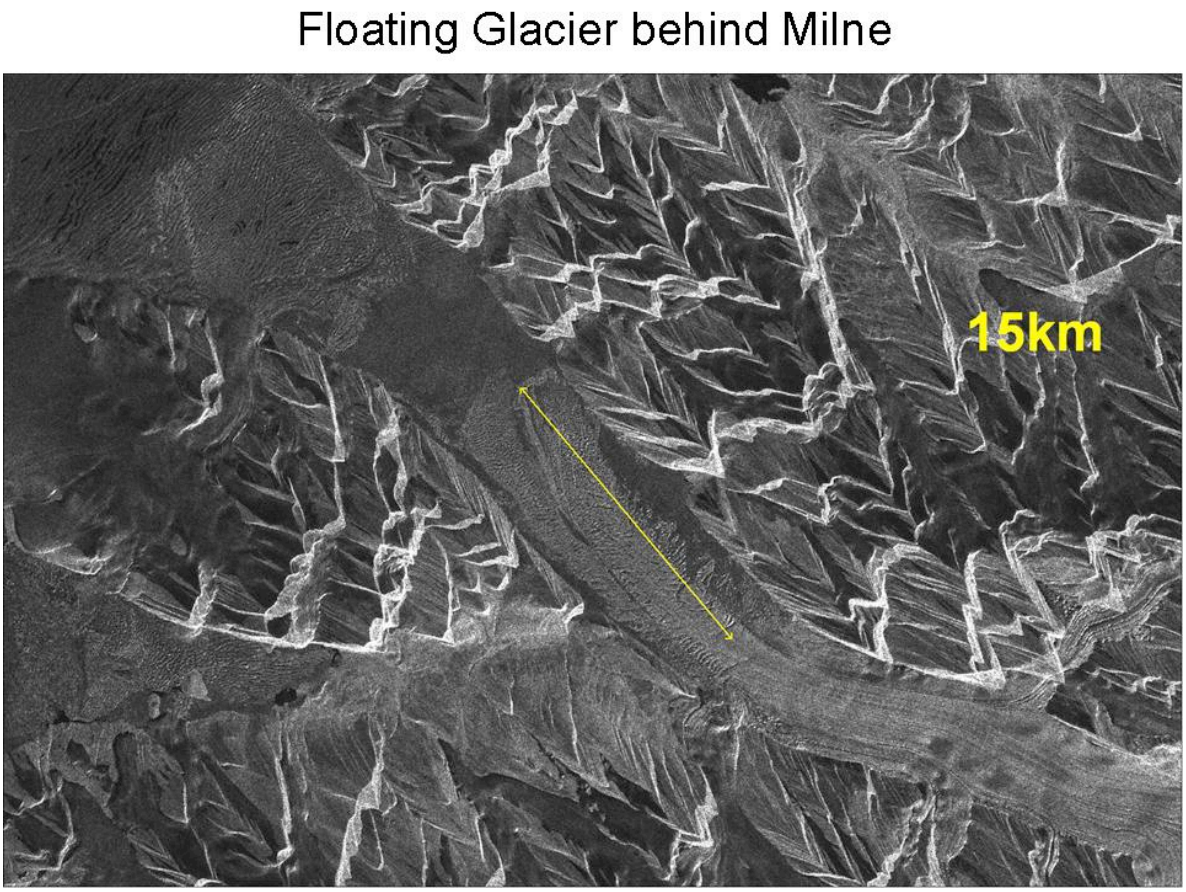

Figure 4-17 Floating Glacier behind the Milne Ice Shelf

5 ICE SHELVES AND MULTI-YEAR LANDFAST SEA ICE

5.1 Introduction

This chapter provides 1) ice thickness measurements from ground penetrating radar (GPR) data for ice shelves and multiyear land fast sea ice (MLSI) and 2) the extent of ice shelves and MLSI along the northern coast of Ellesmere Island using synthetic aperture radar (SAR) remote sensing. It is based on field measurements gathered on the Serson, Peterson and Milne ice shelves in April 2008 by Dr. D. Mueller of Trent University and Dr. L.Copland of the University of Ottawa. The final analysis of the data was conducted as part of the present study. The data may be used with caution to estimate thickness of ice islands and ice island fragments that broke away from the Serson ice shelf in August 2008. which are documented in Chapter 4 and in the EIF data base. The data may also be useful in estimating the thickness of ice islands resulting from future calvings of these ice shelves.

Ice shelves are defined as thick (a priori thickness estimate of > 20 m) floating ice that accreted in situ with or without glacial input. This definition does not include several tidewater glaciers of limited extent whose termini do not coalesce with other floating glacier tongues. The Ellesmere ice shelves are thought to be at least several thousand years old. MLSI is a stable, long-lived ice type that can be considered incipient ice shelf. Much of this ice is several years old, if not decades to (potentially) centuries old. Ice thicknesses are provided for three ice shelves and three regions of MLSI. Ice extents were documented for the entire northern coast of Ellesmere Island (from near Nansen Sound in the west to Cape Sheridan in the East).

5.2 Methods

GPR transects were conducted during the first week of April 2008. A skidoo travelling at a moderate speed (~20 km h^{-1}) towing a GPR (Pulse EKKO, Sensors and Software) recorded radar traces and position (GPS) data every ~3 m. Ice shelves were measured with a 100 MHz antenna and MLSI data were measured using a 250 MHz antenna. The radar data were examined with proprietary software that processed the radar returns and computed the distance to the reflection at the ice/water interface based on an empirically-derived radar velocity of 0.17 m ns^{-1}. The GPR data are often noisy and the algorithm that determines the best reflector (ice depth) may not always 'see' the bottom. This is especially true where the salt content of the ice is high as salt attenuates the radar signal, leading to a 'no return' condition. Thus, despite our best efforts, the thickness of the ice could not always be determined.

To determine ice shelf thickness, the algorithm for detecting the ice bottom was frequently overridden to avoid erroneous data. For MLSI low-quality processed GPR thickness data were removed by thresholding on a quality of detection index. Data were also 3rd quartile filtered, to remove processing artefacts. MLSI transects were accompanied by occasional snow depth measurements and some holes were drilled in the ice to validate the GPR measurements. Ice thickness agreed with GPR measurements within 9 % (Table 5-1). The average observed snow depth for each MLSI transect was subtracted from the GPR data to obtain the ice thickness

Table 5-1 GPR measurements versus direct observations of snow and ice thickness

Survey	Ice and snow thickness (m)		Difference
	GPR	Direct Observation	
Yelverton	2.93	2.85	103%
Taconite	2.29	2.49	92%
Bromley	2.73	2.51	109%
M'Clintock	2.63	2.61	101%

5.3 Ice Shelf Thickness Data

Results for the Milne, Petersen and Serson ice shelf surveys are summarized in Table 5-2. Maps derived from fine beam Radarsat-1 imagery from early February 2008 and thickness profiles are presented in the Figures that follow. The GPR transects are shown with coloured dots, indicating ice thickness.

Table 5-2 Ice Shelf Thickness Data

	Milne	Petersen	Serson
Ice Thickness (m)			
Mean	61.9	16.3	37.9
Standard Deviation	16.5	21.1	9.7
Coefficient of Variation	27%	130%	26%
Maximum	94.4	65.1	63.0
Minimum	2.2	2.7	16.9
1st Quartile	54.0	4.4	31.9
Median	59.4	5.0	33.6
3rd Quartile	77.4	5.7	38.8
Traces recorded	14113	6599	30790
Good observations	8834	1820	1131

Note: Snow depth was not recorded for these transects and therefore ice thickness includes the depth of snow (approx. 50 to 100 cm).

Figure 5-1 shows the GPR transect for the Milne ice shelf. The GPR transect was undertaken on April 4 and 5, 2008. Figure 5-2 shows a histogram of thickness and a thickness profile starting at the red star in Figure 5-1, and proceeding northward.

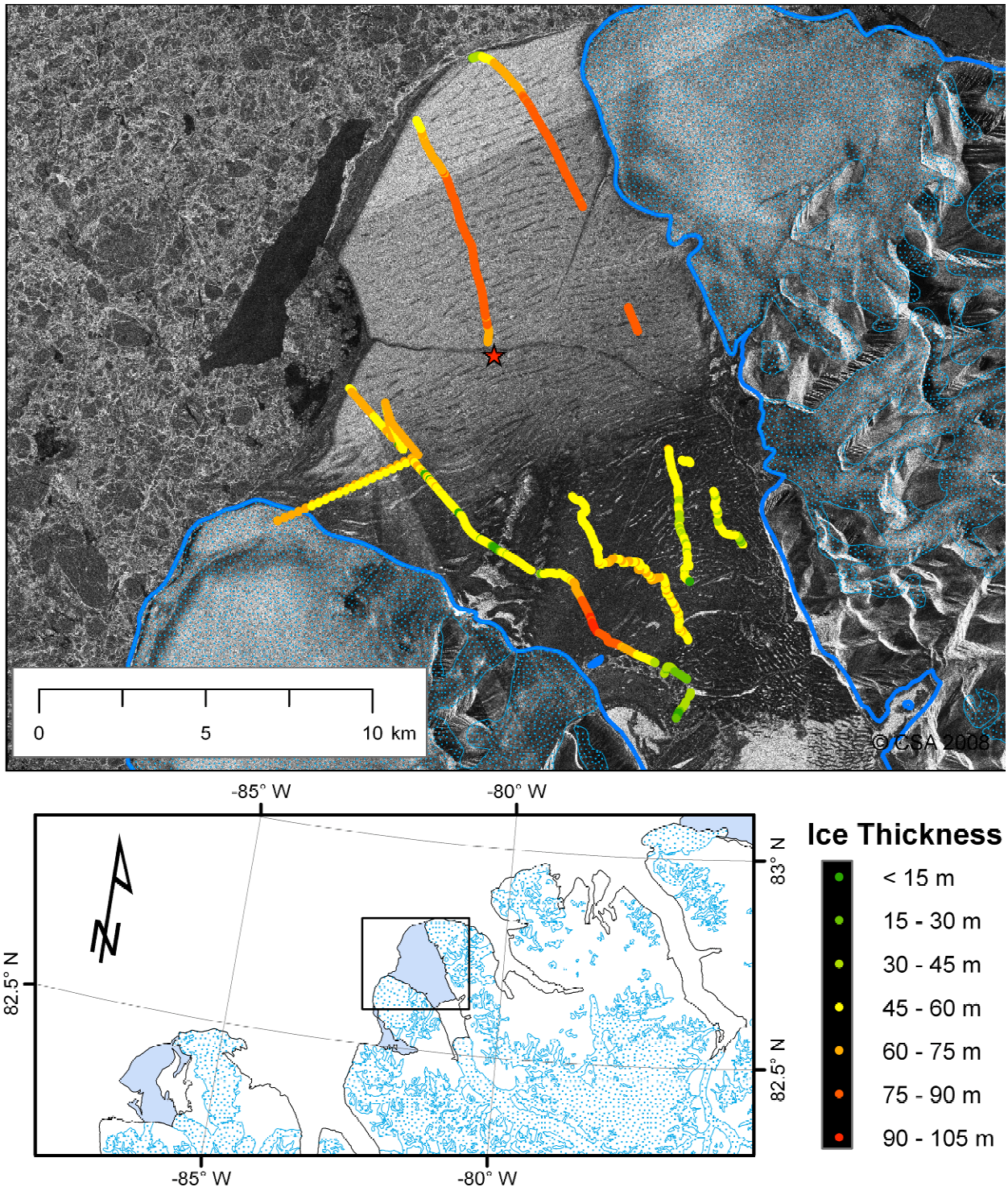

Figure 5-1 Milne Ice Shelf GPR transect and thickness

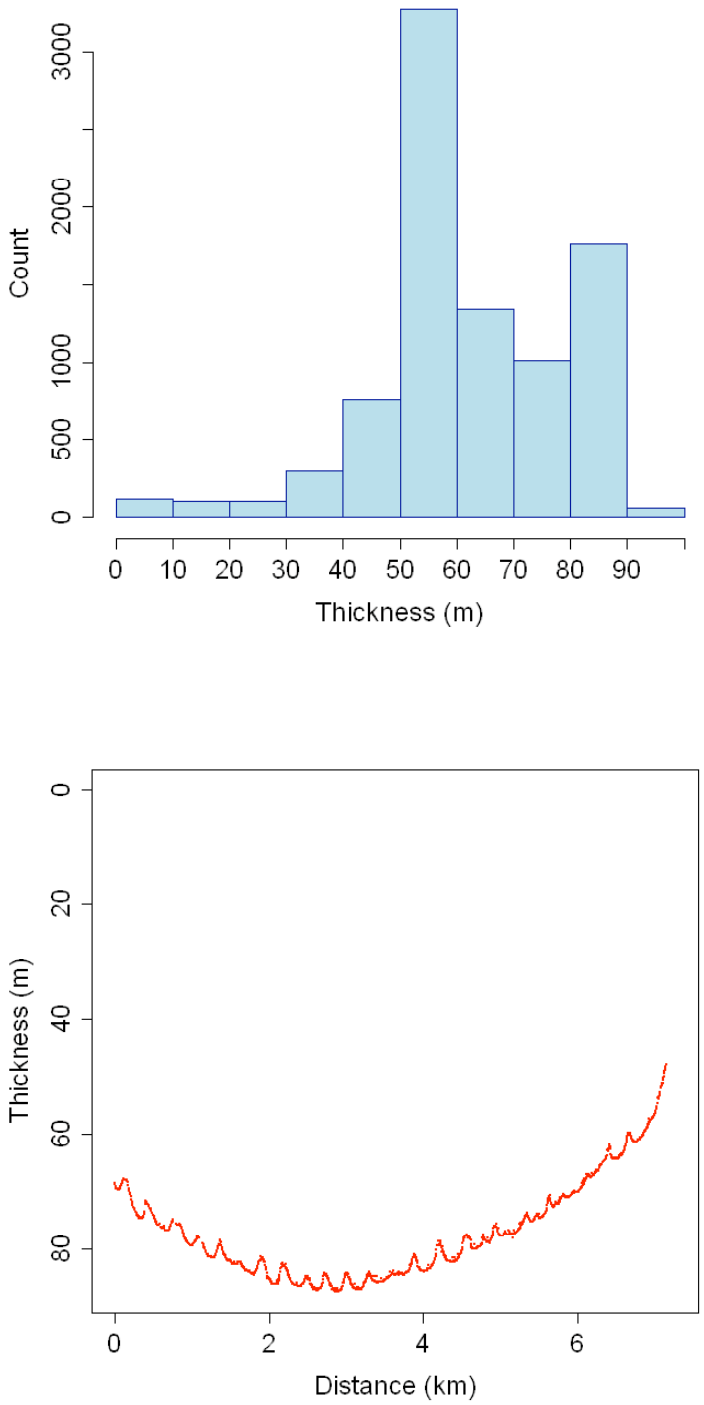

Figure 5-2 Milne Ice Shelf Thickness Histogram and Profile

Figure 5-3 shows the GPR transect of the Petersen ice shelf undertaken on April 6, 2008. The white line indicates where no ice thickness data were recorded.

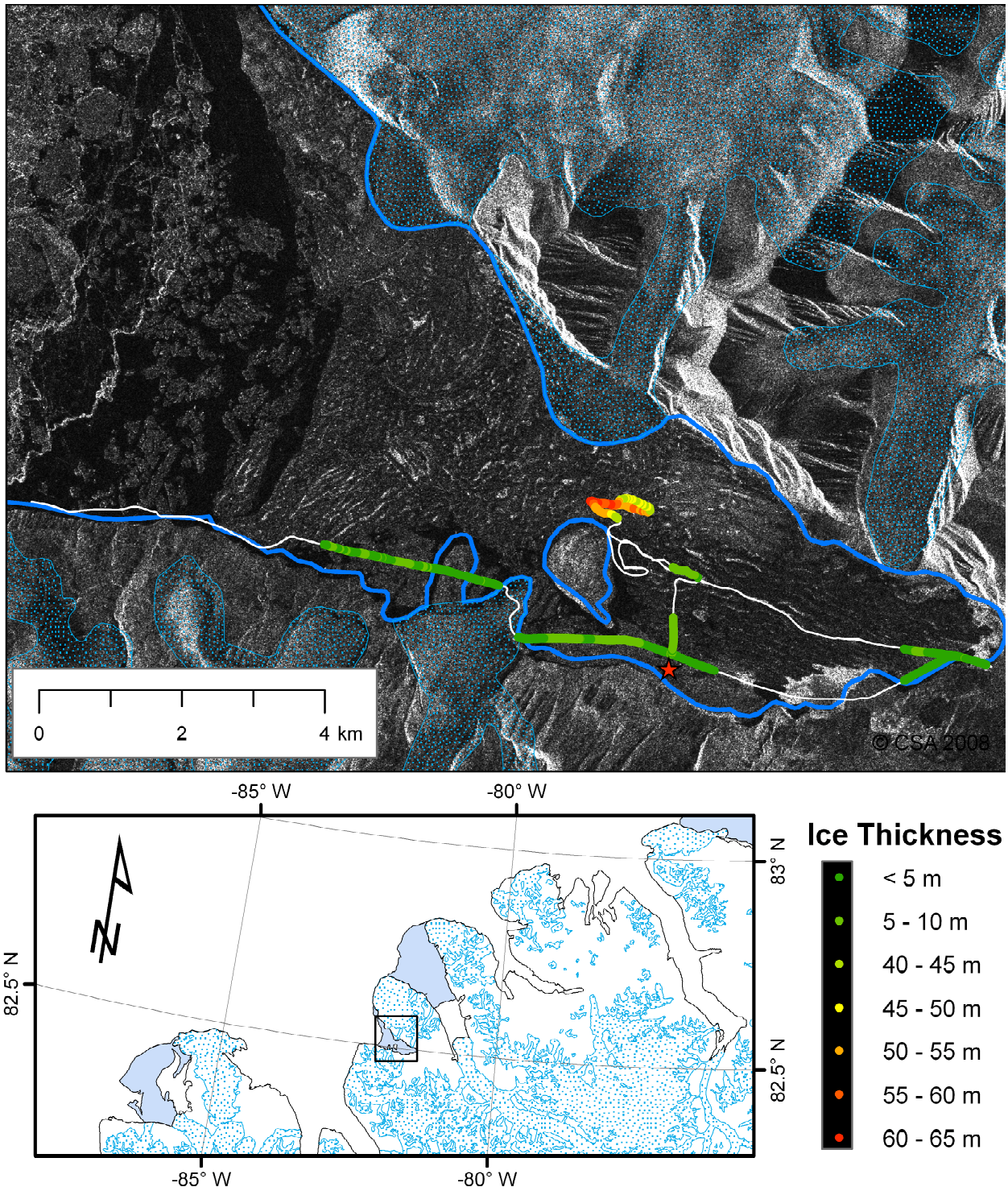

Figure 5-3 Petersen Ice Shelf GPR transect and thickness

Figure 5-4 shows a thickness histogram and profile starting at the red star in Figure 5-3, and proceeding northward to the middle of the ice shelf and then to the eastern edge of the ice shelf.

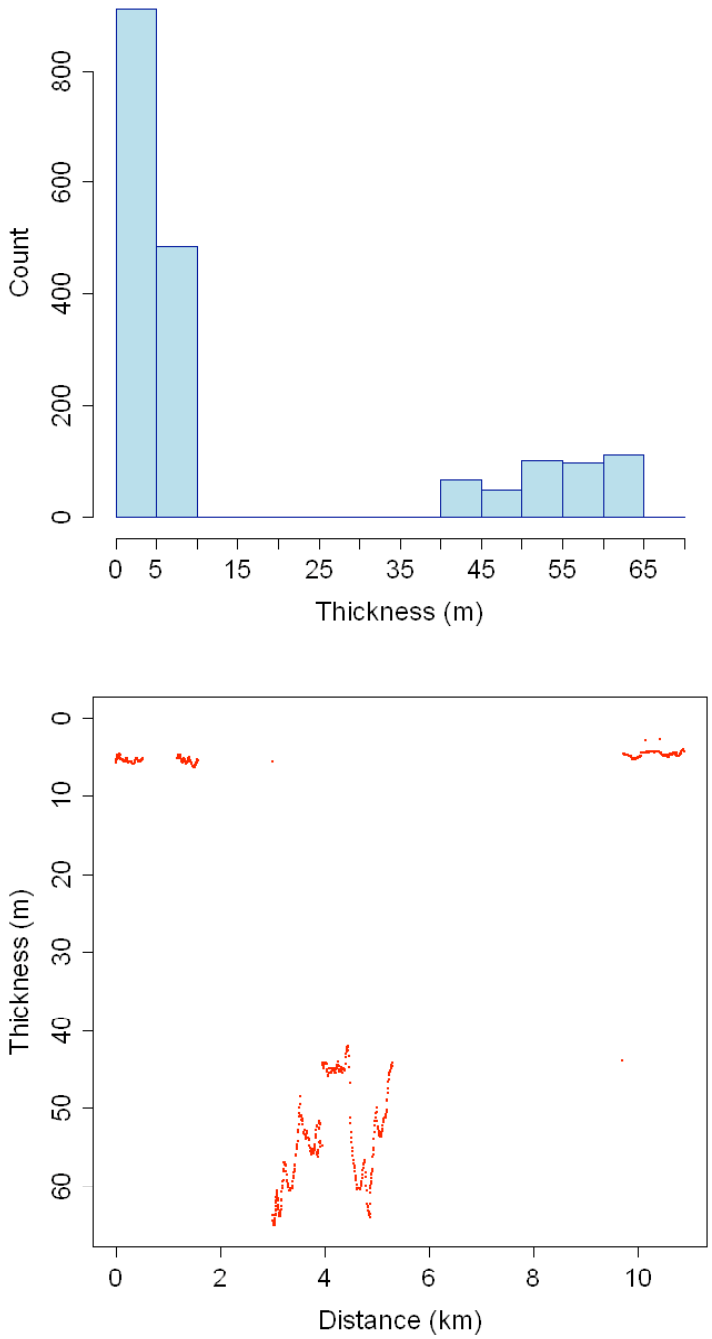

Figure 5-4 Petersen Ice Shelf Thickness Histogram and Profile

Figure 5-5 shows the GPR transect of the Serson ice shelf, undertaken on April 8, 2008. The white line indicates where no ice thickness data were recorded.

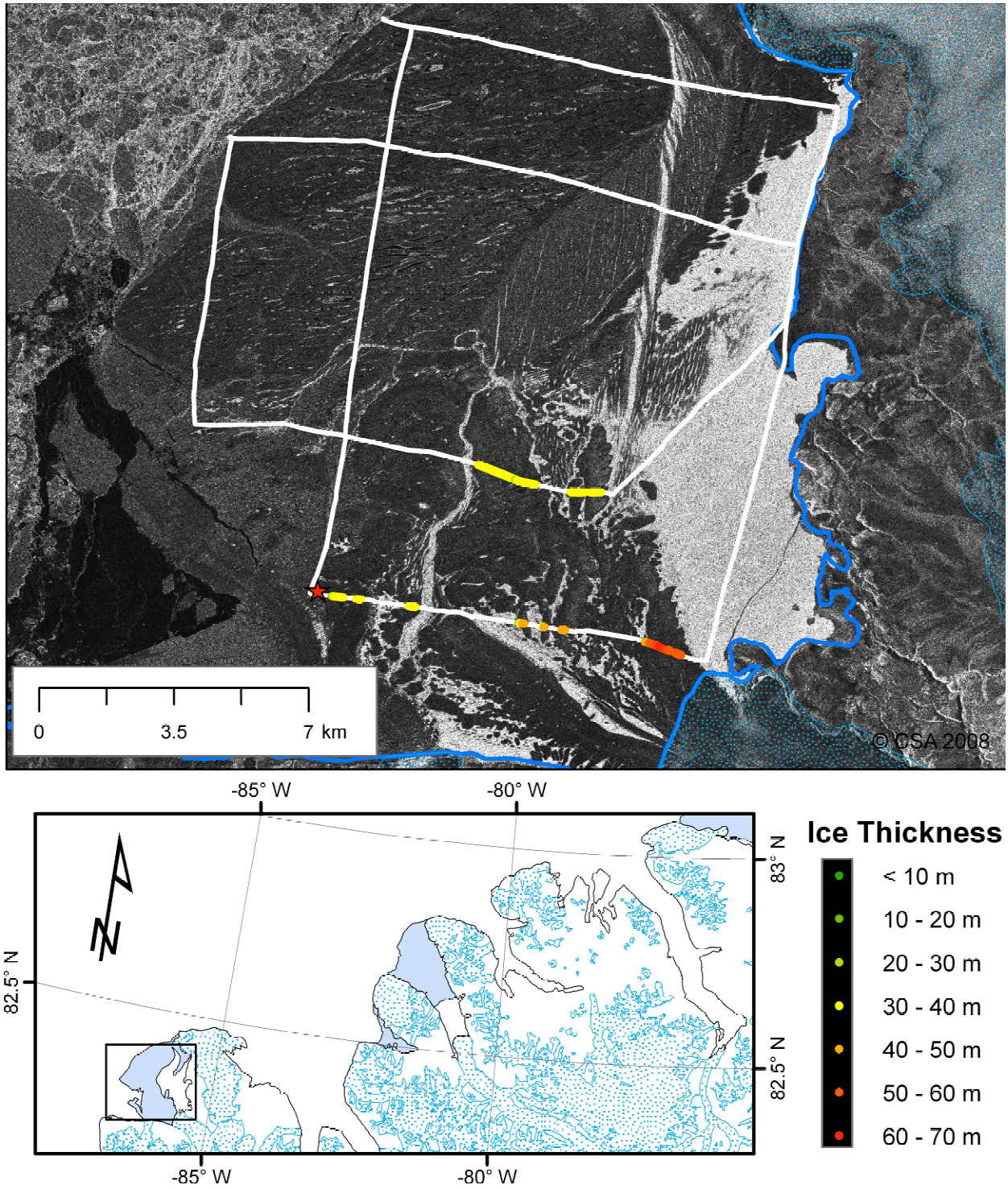

Figure 5-5 Serson ice shelf GPR transect and thickness

Figure 5-6 shows a histogram of thickness and a thickness profile starting at the red star in Figure 5-5, and proceeding east to the eastern edge of the ice shelf.

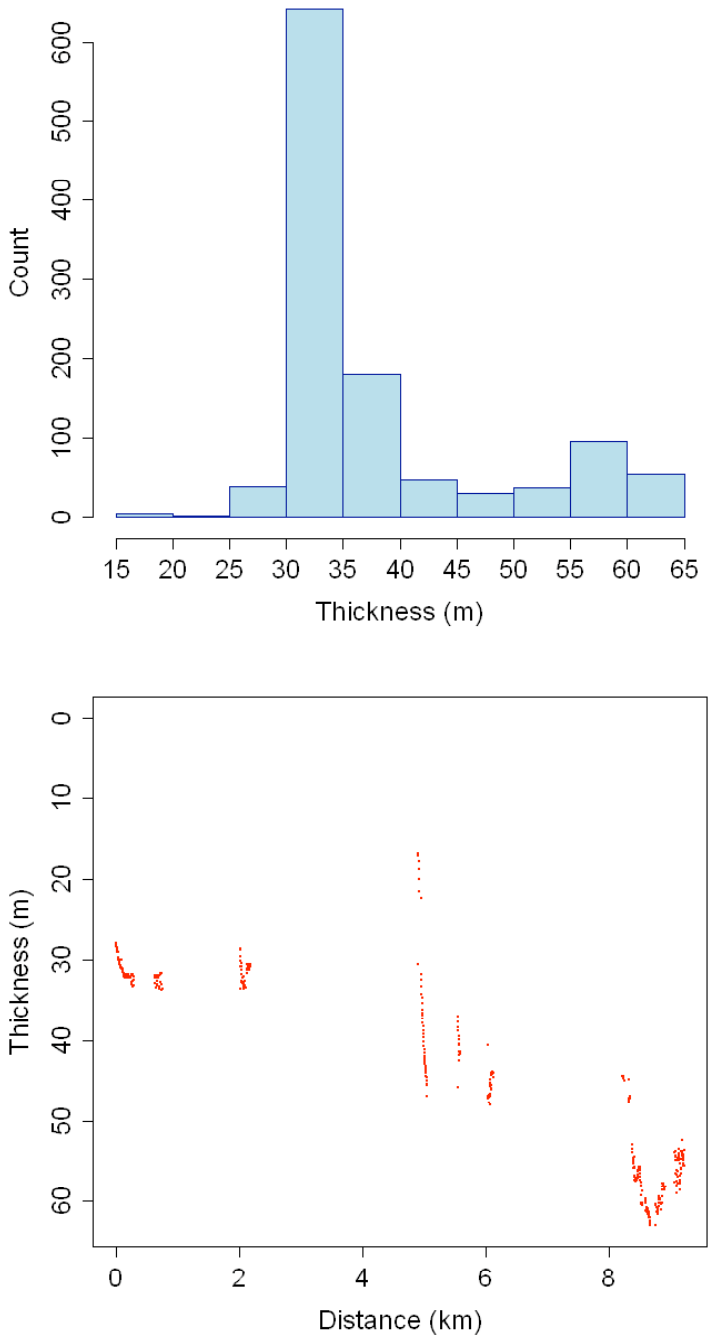

Figure 5-6 Serson Ice Shelf Thickness Histogram and Profile

5.4 Changes in Ice Shelf Extent 1998 - 2008

Table 5-3 summarizes the surfaces areas of the north Ellesmere Island ice shelves over the past decade. Surface areas were derived from Radarsat imagery acquired in January to April of each year listed, with the exception of 2009 which was derived from satellite data acquired in late August 2008 (but represents conditions in the winter of 2009). During the events of August 2008, a total of 227 km2 were calved into the Arctic ocean in the form of ice islands or ice island fragments.

Table 5-3 Ice Shelf Extent 1998-2008

	Ice shelf extent (km^2)						
	Serson	**Petersen**	**Milne**	**Ayles**	**Ward Hunt**	**Markham**	**Total**
1998	204	58	206	61	470	52	1051
2003	204	58	206	61	464	49	1043
2006	204	45	206	0	464	49	969
2008	204	37	206	0	442	49	939
2009	83	37	206	0	386	0	712

Figures 5-7 to 5-11 map the extent of the ice shelves in the years indicated in Table 5-4

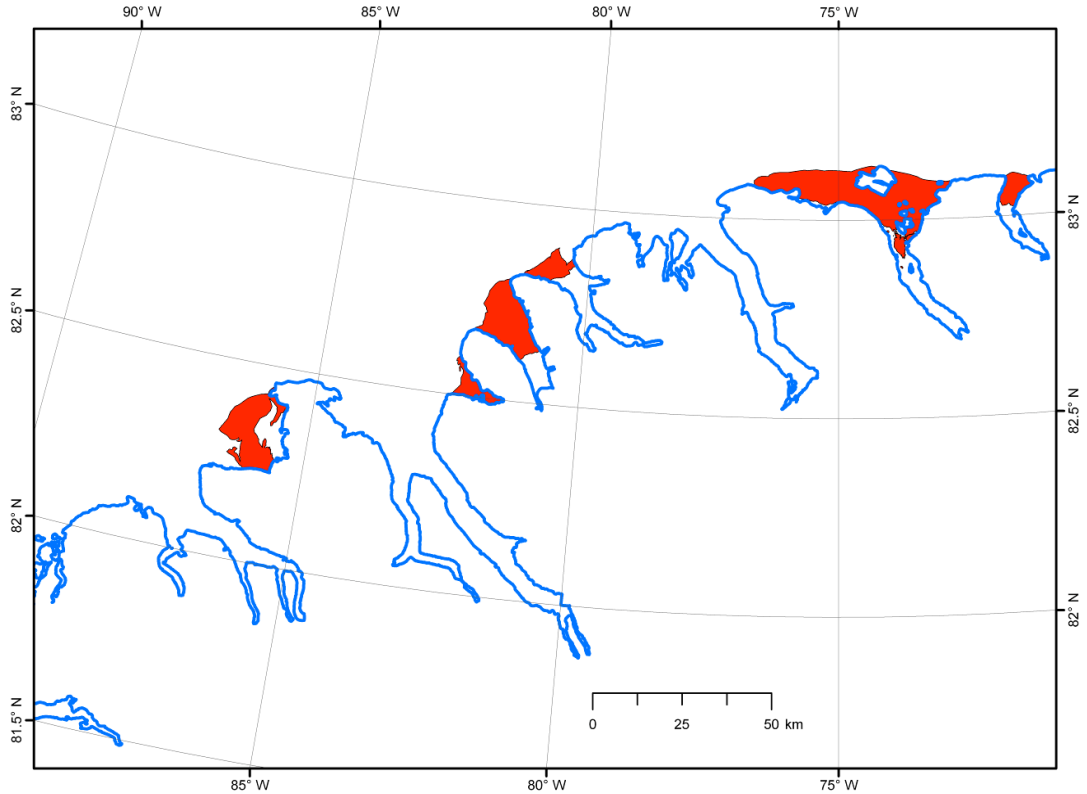

Figure 5-7 Ice shelf extent from Radarsat-1 imagery acquired Jan - April 1998

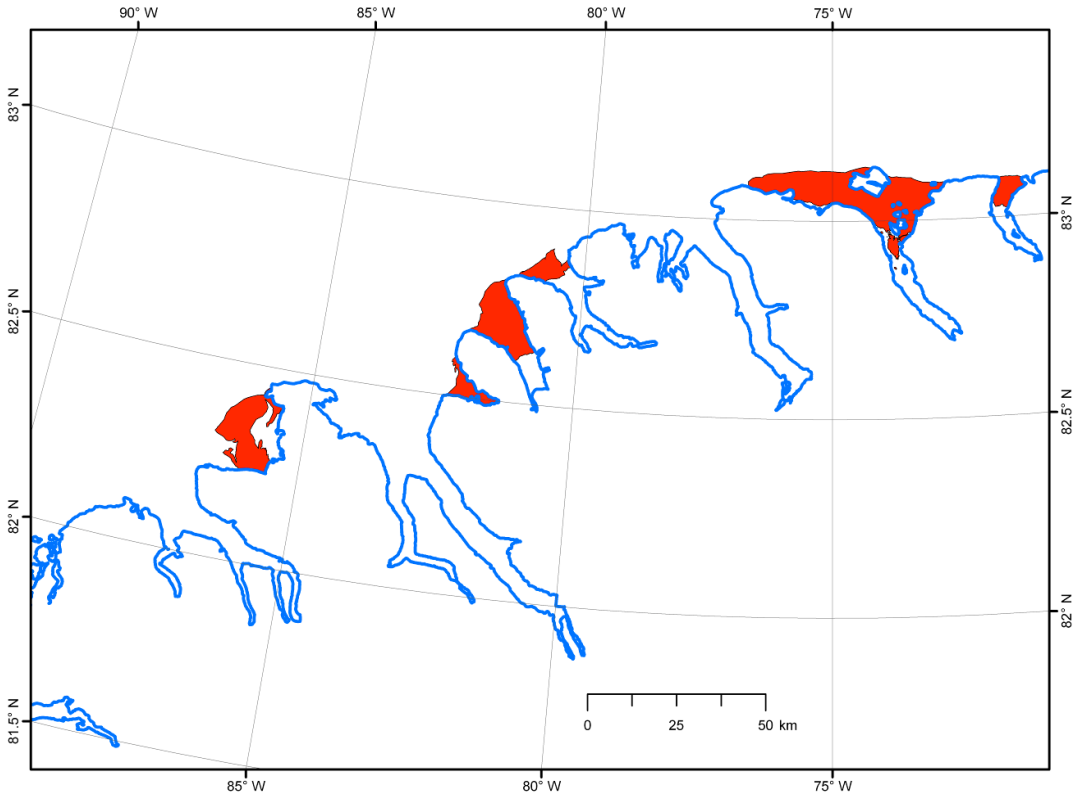

Figure 5-8 Ice shelf extent from Radarsat-1 imagery acquired Jan-Feb 2003

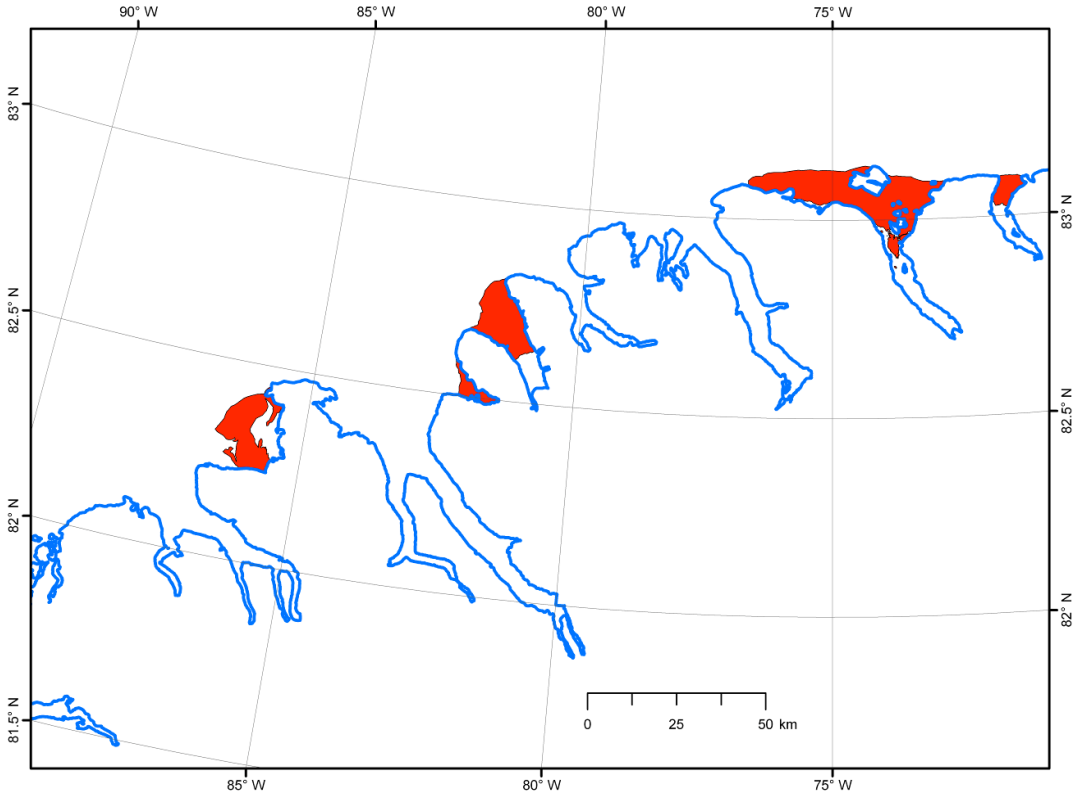

Figure 5-9 Ice shelf extent from Radarsat-1 imagery acquired Jan/April 2006

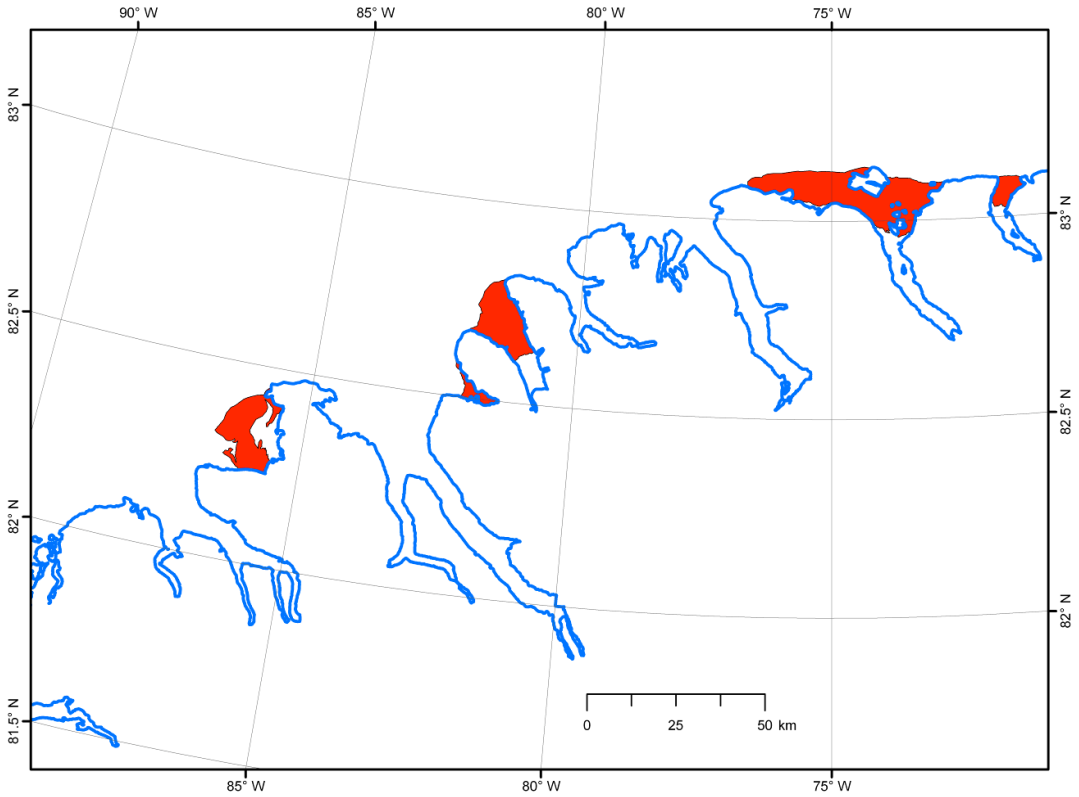

Figure 5-10 Ice shelf extent from Radarsat-1 imagery acquired in February 2008.

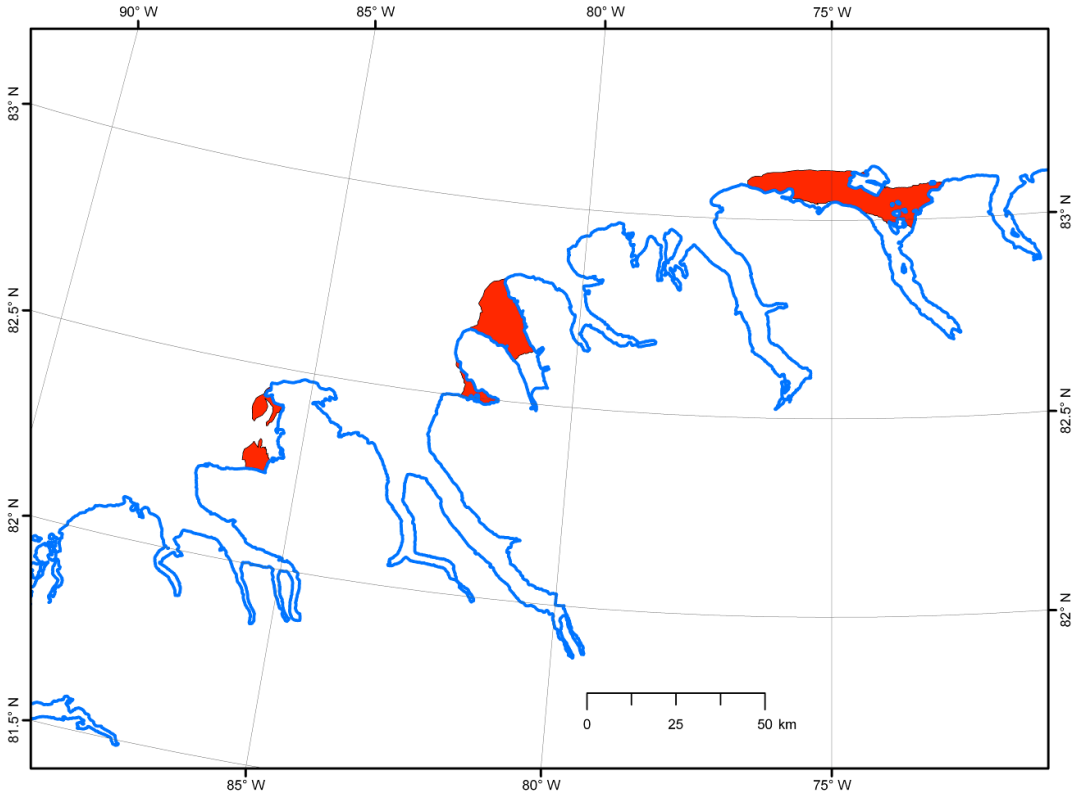

Figure 5-11 Ice shelf extent from MODIS and Formosat-2 imagery late August 2008

5.5 Multi-Year Land Fast Sea Ice Thickness

Results for the Yelverton Bay, Bromley Island, M'Clintok Inlet and Taconite Inlet sea ice surveys are summarized in Table 5-5. Maps derived from fine beam Radarsat-1 imagery from early February 2008 and thickness profiles are presented in the Figures that follow. The GPR transects are shown with coloured dots, indicating ice thickness.

Table 5-4 Multi-Year Land Fast Sea Ice Thickness (MLSI) data

	Yelverton Bay	Bromley Island	M'Clintock Inlet	Taconite Inlet
Ice Thickness (m)				
Mean	3.7	1.9	2.7	1.7
Standard Deviation	2.0	1.1	1.1	0.3
Coefficient of Variation	55%	54%	41%	18%
Maximum	6.7	5.9	5.2	2.1
Minimum	0.0	0.7	0.8	0.9
1st Quartile	1.6	1.3	1.8	1.7
Median	4.2	1.6	2.6	1.8
3rd Quartile	5.7	2.0	3.3	1.9
Traces recorded	18976	19448	14697	982
Good observations	1776	8390	4023	982
Snow Depth (cm)				
Mean	90.2	52.8	69.0	39
Standard Deviation	26.7	8.2	15.8	-
Coefficient of Variation	30%	16%	23%	-
Maximum	138	64	98	-
Minimum	54	39	48	-
1st Quartile	75	52	61.5	-
Median	89	54	67	-
3rd Quartile	105	54	73.5	-
Observations	11	9	7	1

Figure 5-12 shows the Yelverton Bay GPR transect undertaken on April 9, 2008. The large, thick pieces of ice on the top right are former multiyear land fast sea ice from southern Yelverton Bay. This ice broke up in 2005 after 60–70 years of in situ growth. Figure 5-13 shows a histogram of thickness and a thickness profile starting at the red star in Figure 5-12, and proceeding and proceeding in a clockwise direction.

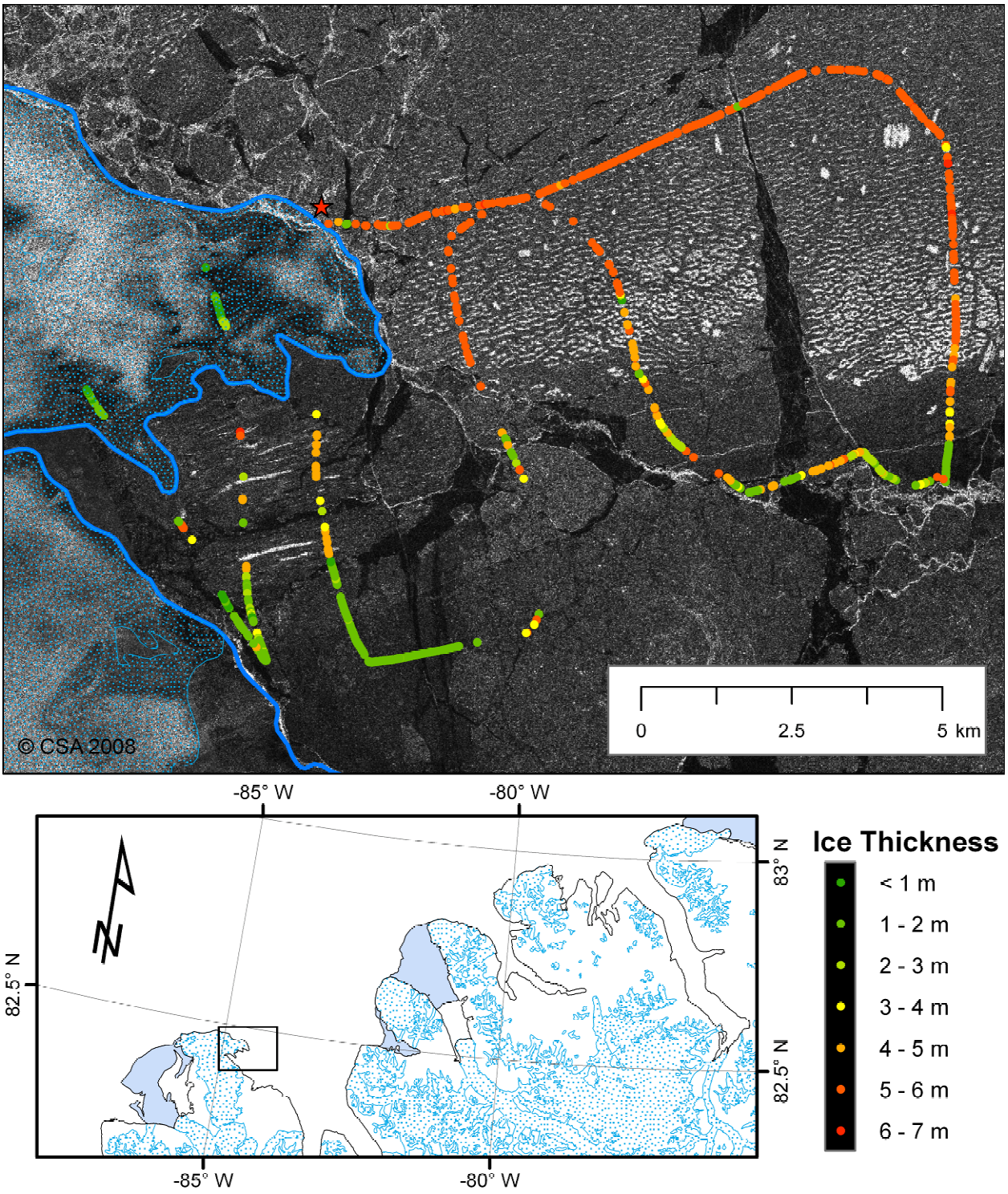

Figure 5-12 Yelverton Bay multi-year sea ice GPR transect and thickness

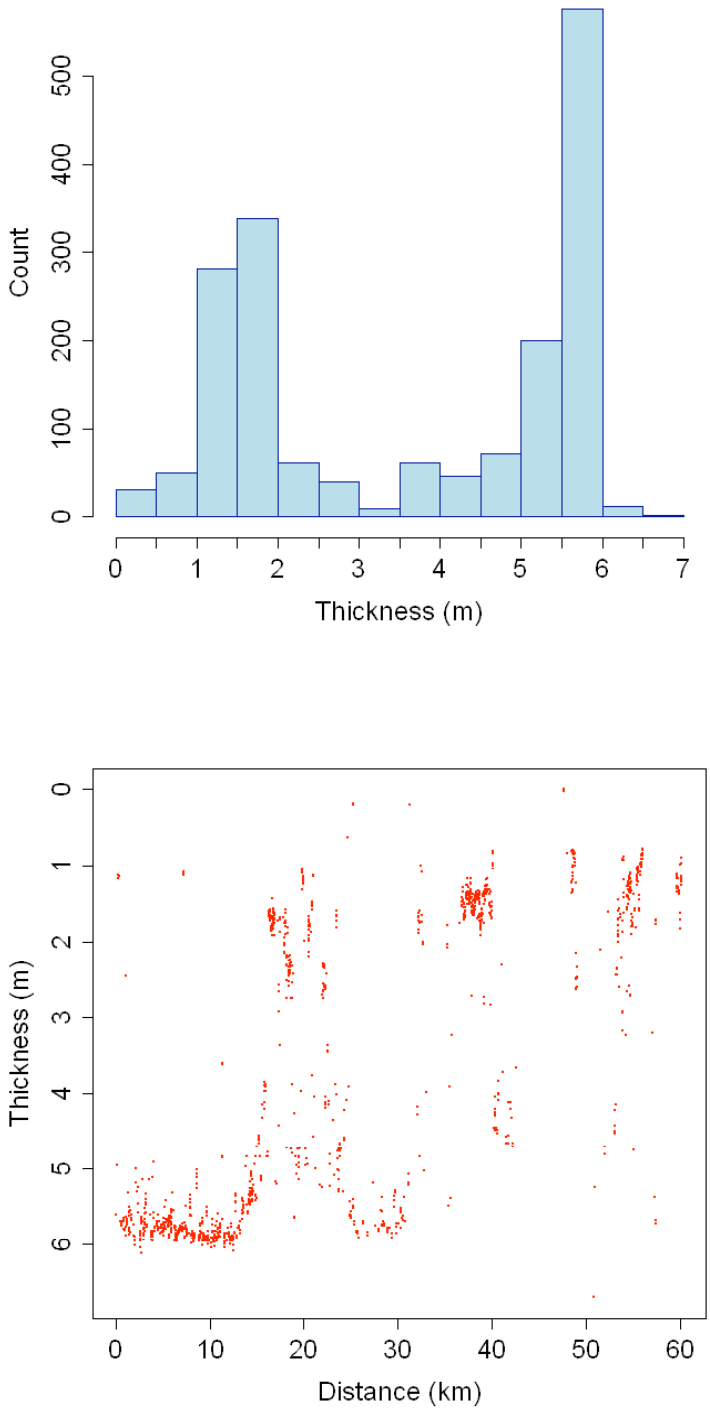

Figure 5-13 Yelverton Bay ice thickness histogram and profile

Figure 5-14 shows the M'Clintock Inlet GPR transect undertaken April 3, 2008. Figure 5-15 shows a histogram of thickness and a thickness profile starting at the red star in Figure 5-14, and proceeding and proceeding in a counter clockwise direction.

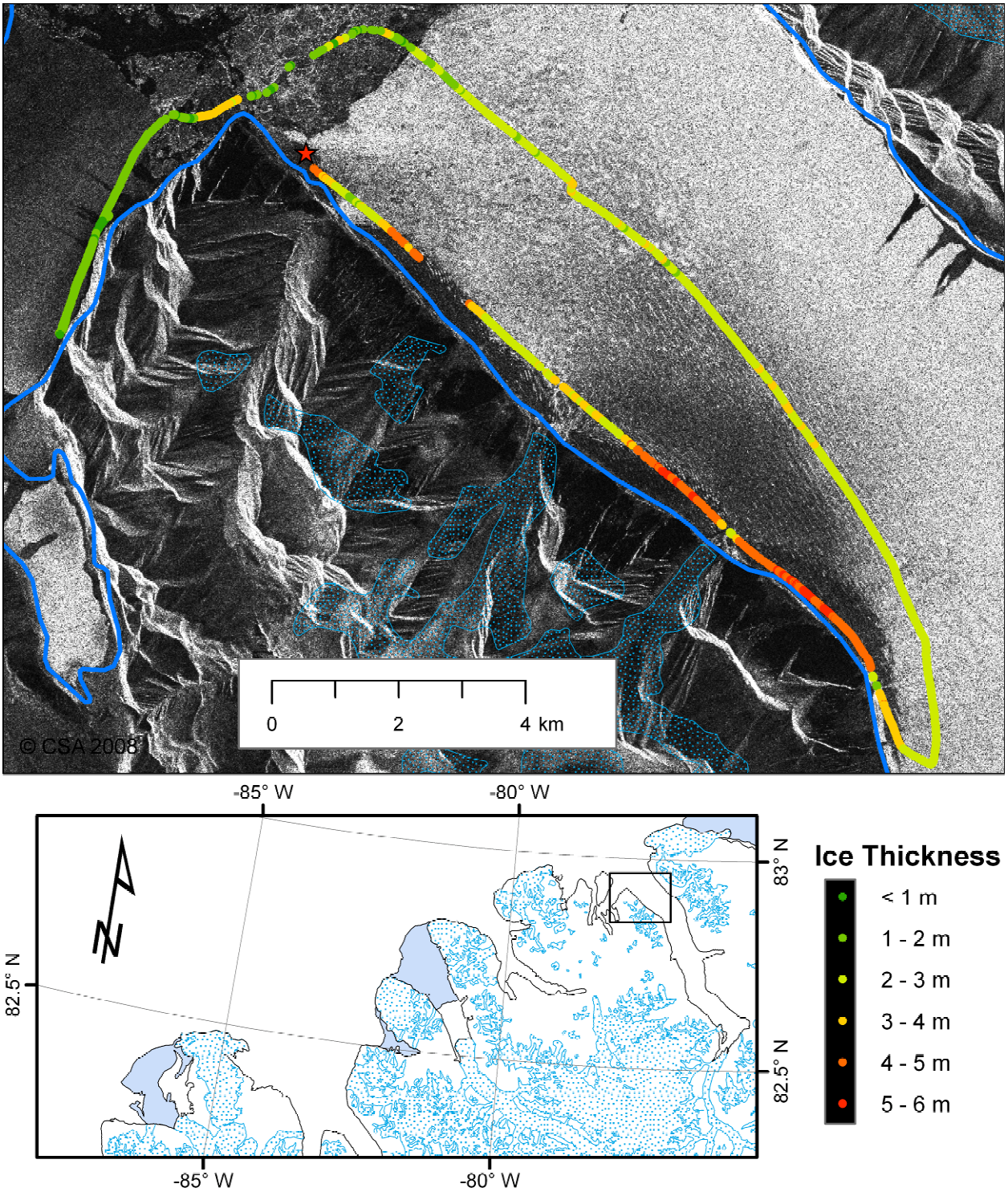

Figure 5-14 M'Clintock Inlet multiyear sea ice GPR transect and thickness

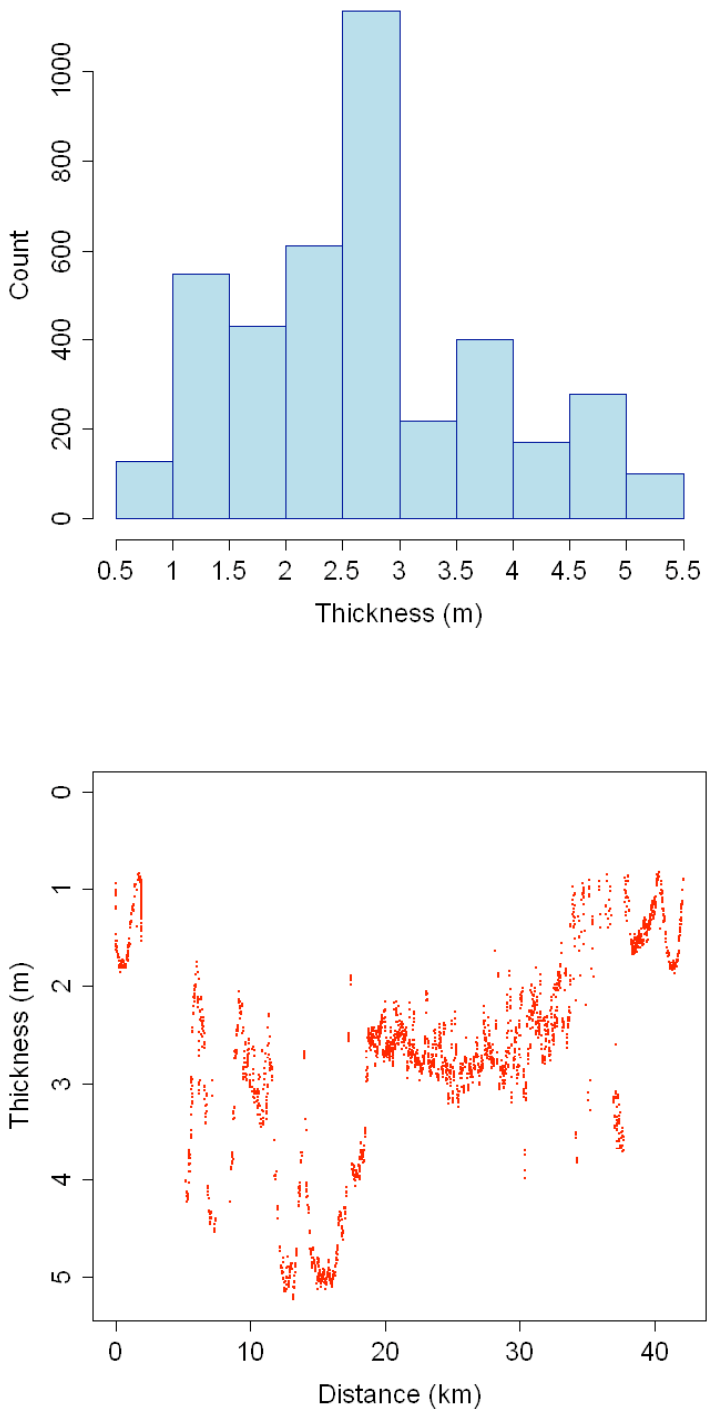

Figure 5-15 M'Clintock Inlet ice thickness histogram and profile

Figure 5-16 shows the Bromley Island, Cape Richards GPR transect undertaken April 3, 2008, and the Taconite Inlet GPR transect undertaken April 2, 2008.

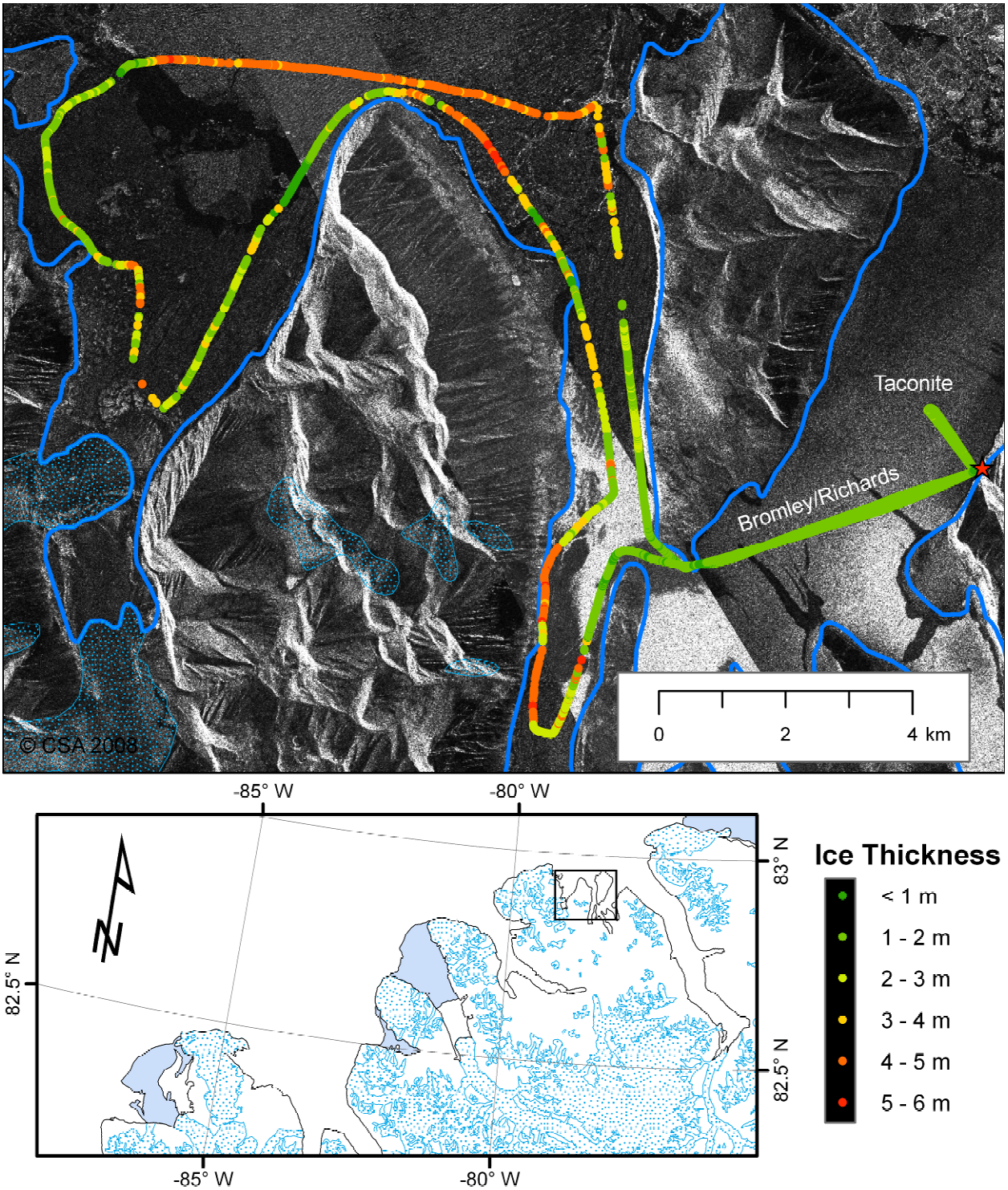

Figure 5-16 Bromley Island, Cape Richards and Taconite Inlet MLSI GPR transect

Figure 5-17 shows a histogram of thickness and a thickness profile for the Bromley Island/Cape Richards transect. It starts at the red star in Figure 5-16, and proceeds in a

counter clockwise direction up the west side of Bromley Island, over to Cape Richards (top left corner) and then following the shore on the return.

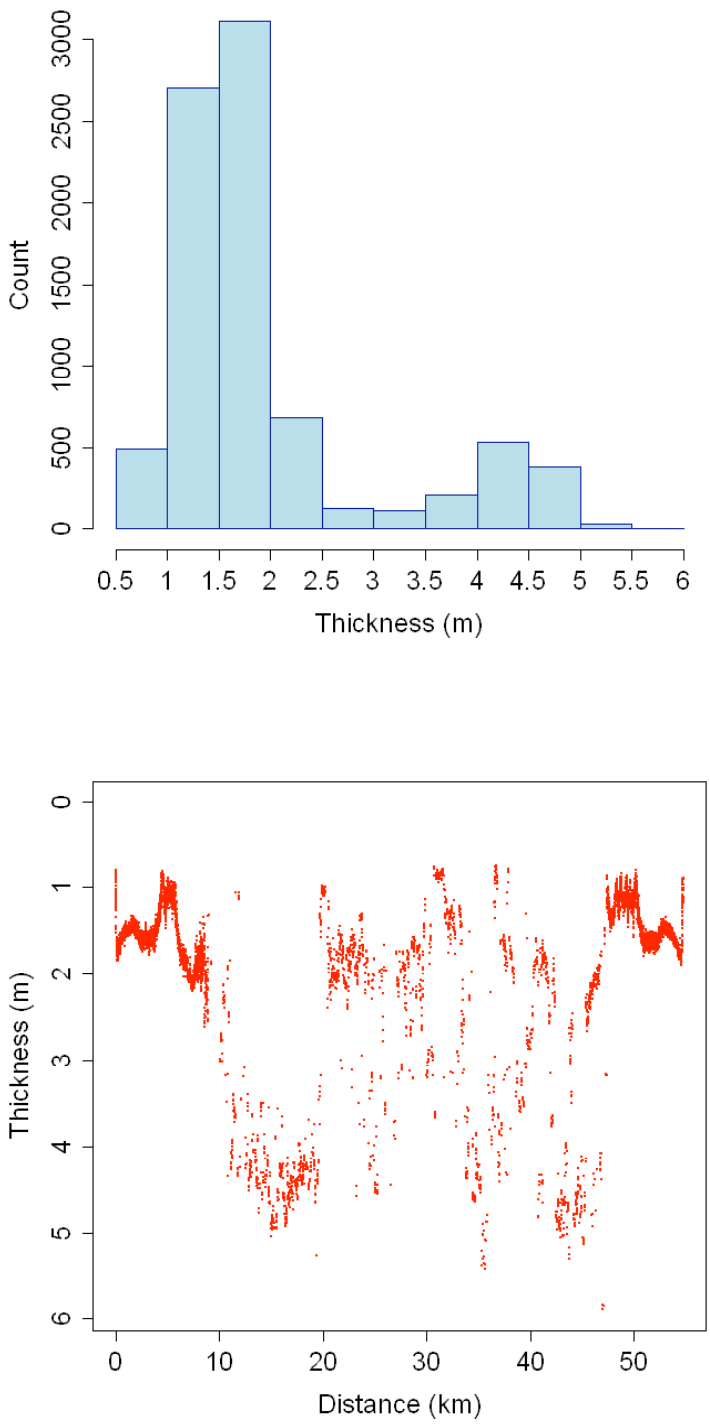

Figure 5-17 Bromley Island, Cape Richards ice thickness histogram and profile

Figure 5-18 shows a histogram of thickness and a thickness profile for the Taconite Inlet transect which started at the red star, proceeded northwest a short distance and returned.

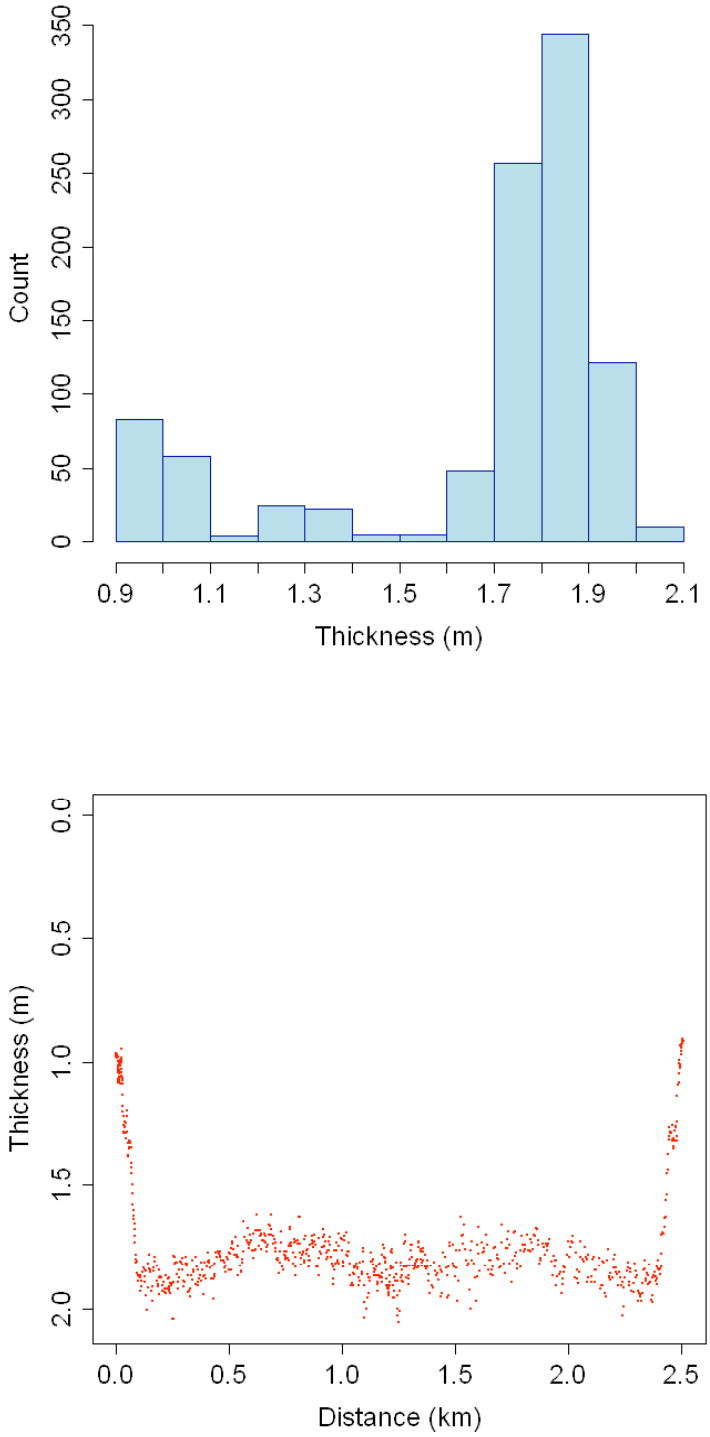

Figure 5-18 Taconite Inlet ice thickness histogram and profile

5.6 Changes to Multi-year Land Fast Sea Ice Extent 1998 - 2008

Table 5-4 summarizes the surface areas of the north Ellesmere Island ice shelves over the past decade. Surface areas were derived from Radarsat imagery acquired in January to March of each year listed. Figures 5-19 and 5-20 map the extent of MLSI for those two years.

Table 5-5 Multi-Year Land Fast Sea Ice Extent 1998-2008

	Multiyear land fast sea ice extent (km^2)		
	Seaward of ice shelves	Landward of ice shelves	Total
1998	3604	513	4117
2006	2499	310	2809

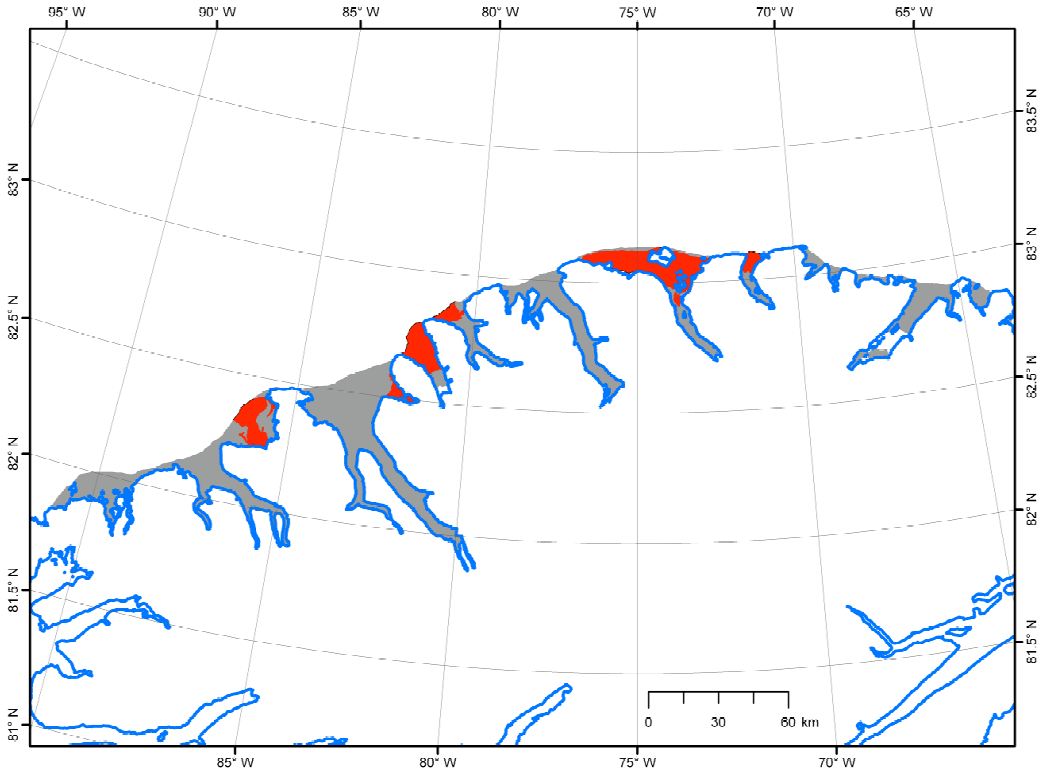

Figure 5-19 Ice shelf (red) and MLSI (grey) extent from Radarsat-1 Jan-April 1998

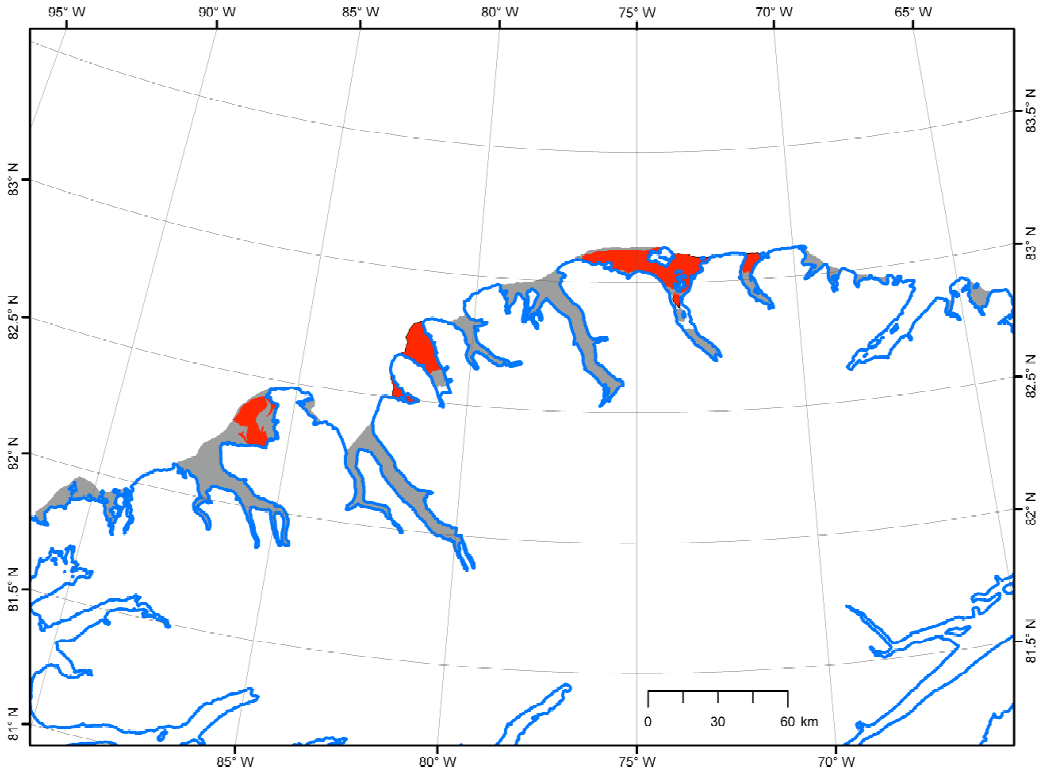

Figure 5-20 Ice shelf (red) and MLSI (grey) extent from Radarsat-1 Jan/April 2006

6 MULTI YEAR FLOE SIZES

6.1 Overview

The purpose of this part of the project was to quantify the statistics of Multi-Year floe sizes for the three areas of potential offshore operations shown in Figure 6-1 and to identify differences. The diameters and areas of MYFs were measured from radar images collected in early June 2008 which were made available by Shell USA for the 3 areas. This time-frame was referred to as late-winter. Exxon-Mobil made available several images from August and September 2008, referred to as early and late summer. This allowed a comparison of floe distributions by area, and by season.

In addition to the above three areas, a floe size analysis was also undertaken for an area to the SW of Prince Patrick Island. Although this area is north of most operational areas, it does represent the "source" of floes for the Southern Beaufort. A single assessment was done on August 1, 2008 Envisat data. One MODIS scene from March 2008 was analyzed to get an idea of mid-winter conditions.

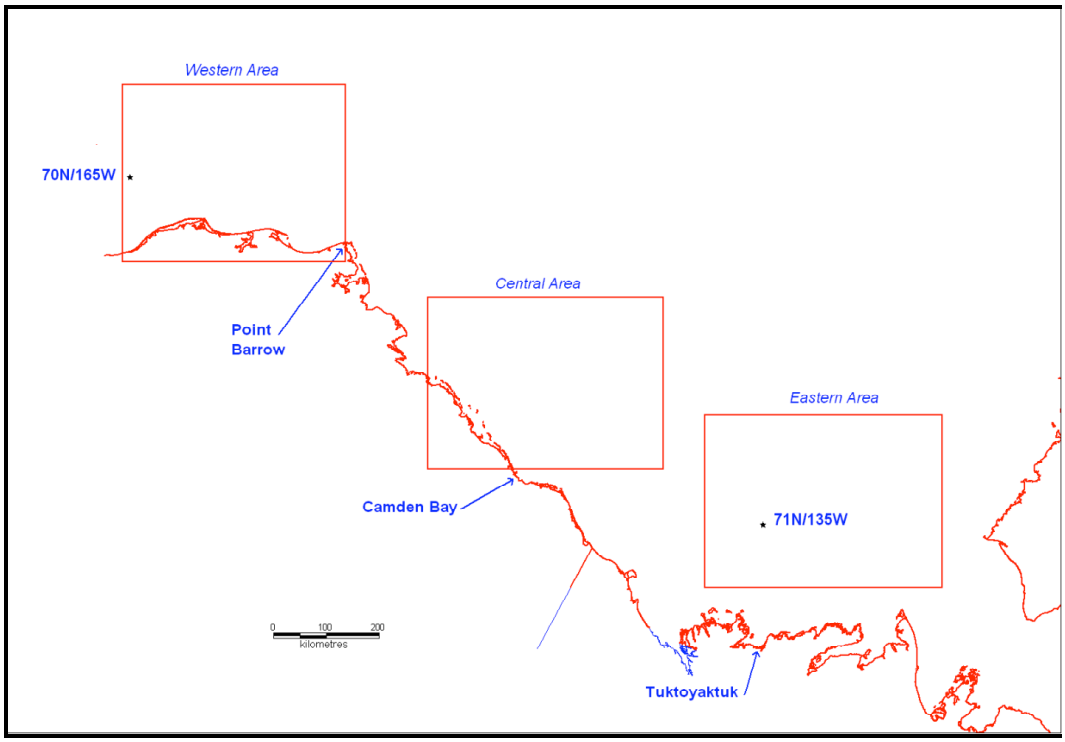

Figure 6-1 Three General Areas for Floe Size Analysis

6.2 Methodology for Analysis and Interpretation

6.2.1 Procedure

Images depicting ice conditions in summer and late winter were analyzed for each areas. Images were geo-referenced and identifiable floes 100m in diameter and larger were outlined on a GIS analysis layer. All floes were treated as ellipses. The major and minor diameters and the diameter (maximum linear dimension) were measured. The GIS program calculated the perimeter and the area. The data were entered into a spreadsheet and additional parameters were calculated as described in section 5.4.

6.2.2 Variations in Image Resolution

The minimum floe size of 100m was attainable with some but not all datasets. Envisat data (30m resolution) and Radarsat2 Wide data (30m resolution) allowed identification of floes down to the minimum; however the Radarsat ScanSAR Wide data (100m resolution) and the MODIS (240m res) were not capable of resolving the minimum floe size. Although floes with a diameter of 2 pixels were occasionally identified, 3 pixels were found to be a more dependable minimum (depending on time of year and ice conditions). Thus, the minimum detectable floe size for the Envisat and Radarsat Wide data was 60-90m, for the Radarsat ScanSAR was 200-300m, and for the MODIS was 480-720m. First-year ice, young ice, extreme ice features (EIFs), open water and floes less than 100m diam were not included in the analysis layer.

6.2.3 Conglomerate and Continuous Floes

Multi-year floes in the Beaufort and Chukchi Seas occur in two principle forms: conglomerate and continuous. Conglomerate M-Y floes contain a number of M-Y floes frozen into a matrix typically made of first-year ice. Percentages of multi-year ice in a conglomerate floe can vary from 10 to 90%. Conglomerate floes are very common in winter, and progressively rarer as melt progresses. Continuous M-Y floes contain only Multi-year ice, and show no evidence of individual pieces in the floe. From a structures perspective, knowing whether a 20km diam floe contains 20% Multi-year or 80% is important because a floe with a higher proportion of first year ice is likely to fail in the thinner areas and with a lower force . For the 3 late winter data sets, a second analysis layer was created that contained only conglomerate floes. In this way it is possible to digitally subtract the Multi-year *inclusions* in a conglomerate floe and analyze them as separate floes.

The 2 layers of floe outlines (continuous and conglomerate) were subsequently exported to the data base spreadsheets. In generating the statistics, the conglomerate floes were left out of the analysis.

6.3 Multi – Year Floe Data Base

6.3.1 Data Sets

The database consists of eight data sets, one for each image. Table 6-1 summarizes the numbers of floes in total and floes with diameters greater than 500 m for all data sets. Data sets 1, 2, 3, and 4 are for the summer (Aug/Sept 2008), set 5 is for mid-winter (March 2008), and sets 6, 7 and 8 are for the late winter (June 2008).

Table 6-1 Data sets developed from analysis of satellite imagery

Dataset	Date	Location	Number of Floes	Number of Floes > 500 m	% of Floes > 500 m
1	2008-09-27	S Canadian Beaufort	1357	130	9.6
2	2008-08-12	S Canadian Beaufort	1506	189	12.5
3	2008-08-02	Chukchi Sea Pt Barrow	202	172	85.1
4	2008-08-01	NE Canadian Beaufort SW Prince Patrick Isl	1735	1155	66.6
5	2008-03-07	Alaskan Beaufort	1101	1101	100.0
6	2008-06-04	Alaskan Beaufort Prudhoe Camden	1005	967	96.2
7	2008-06-09	Chukchi Sea NW Pt Barrow	210	208	99.0
8	2008-06-09	S Canadian Beaufort Herschel Isl	460	440	95.7

6.3.2 Multi-Year Floe Parameters

The data reside in Excel spreadsheet files on the accompanying CD. Files are named by date and location in exactly the same way as in Table 6-1. Recorded parameters were:

- Feature ID No.
- Latitude
- Longitude
- Water depth
- Perimeter length (output from the program)
- Area (output from the program)
- Major axis
- Minor axis
- Diameter (the largest linear dimension)

These geometrical parameters were calculated (see Appendix B for definitions):

- Equivalent diameter
- Circularity indicator
- Compactness indicator
- Ellipsoid roundness
- Second moment of area (in m^4)
- Diameter of Gyration.

A second Worksheet, “Coord” records the lat and long of all the vertices of each M-Y Floe.

6.3.3 Spatial and Temporal Coverage

Figure 6-2 shows the spatial distribution of the data from all the images. In order to assess the overlapping and to delimit the datasets, a convex hull[1] was created for every dataset, as shown in Figure 6-3. The data is further delimited by season in Figures 6-4, 6-5 and 6-6.

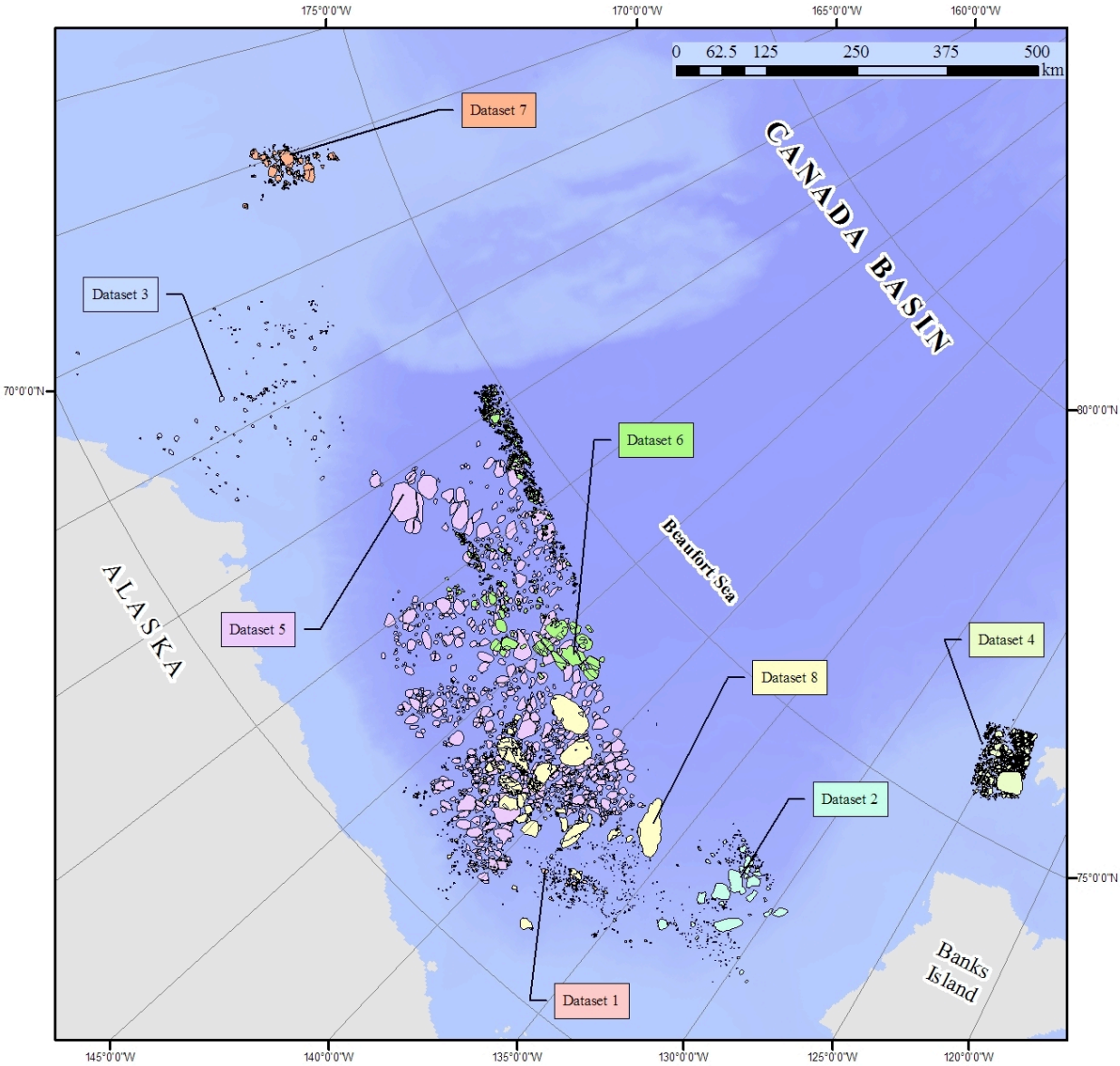

Figure 6-2 Map of All M-Y Floes Analyzed for Chukchi and Beaufort Seas 2008

[1] A convex hull is the smallest convex polygon that contains a set of points.

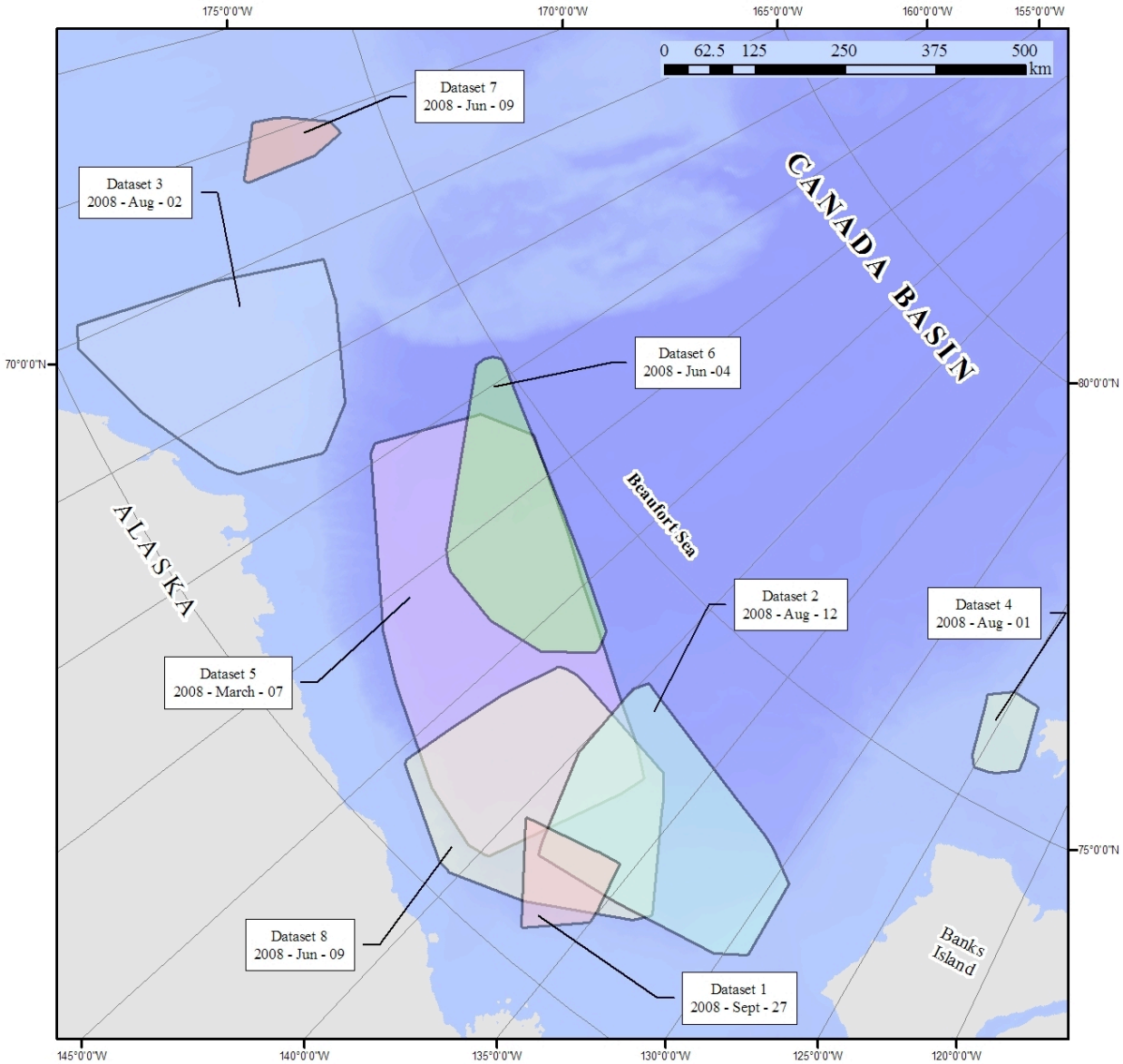

Figure 6-3 Map of Convex Hull Polygons Enclosing M-Y Floe Data Sets

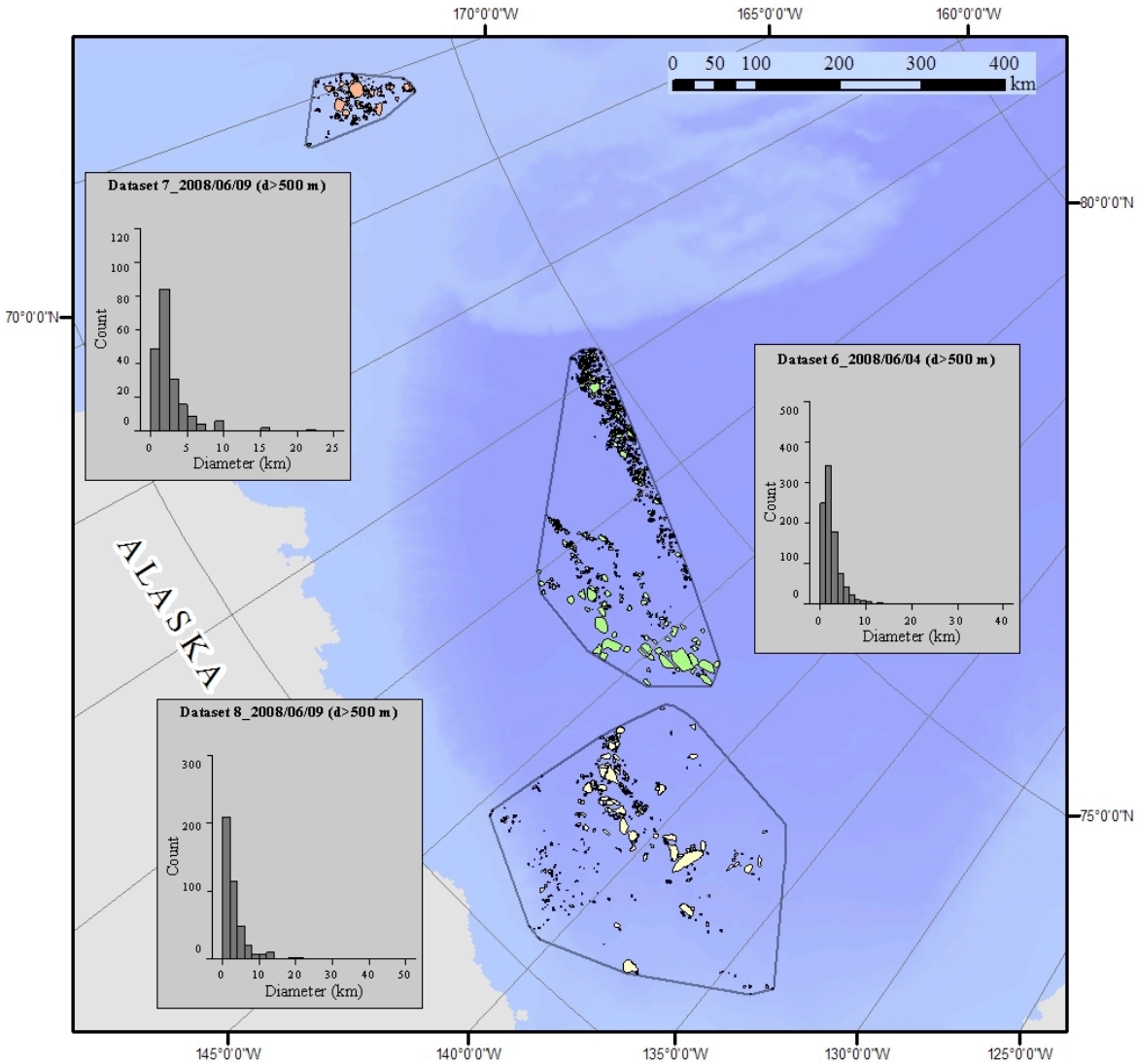

Figure 6-4 Convex Hull Polygons of M-Y Floes for 3 Areas in Late Winter

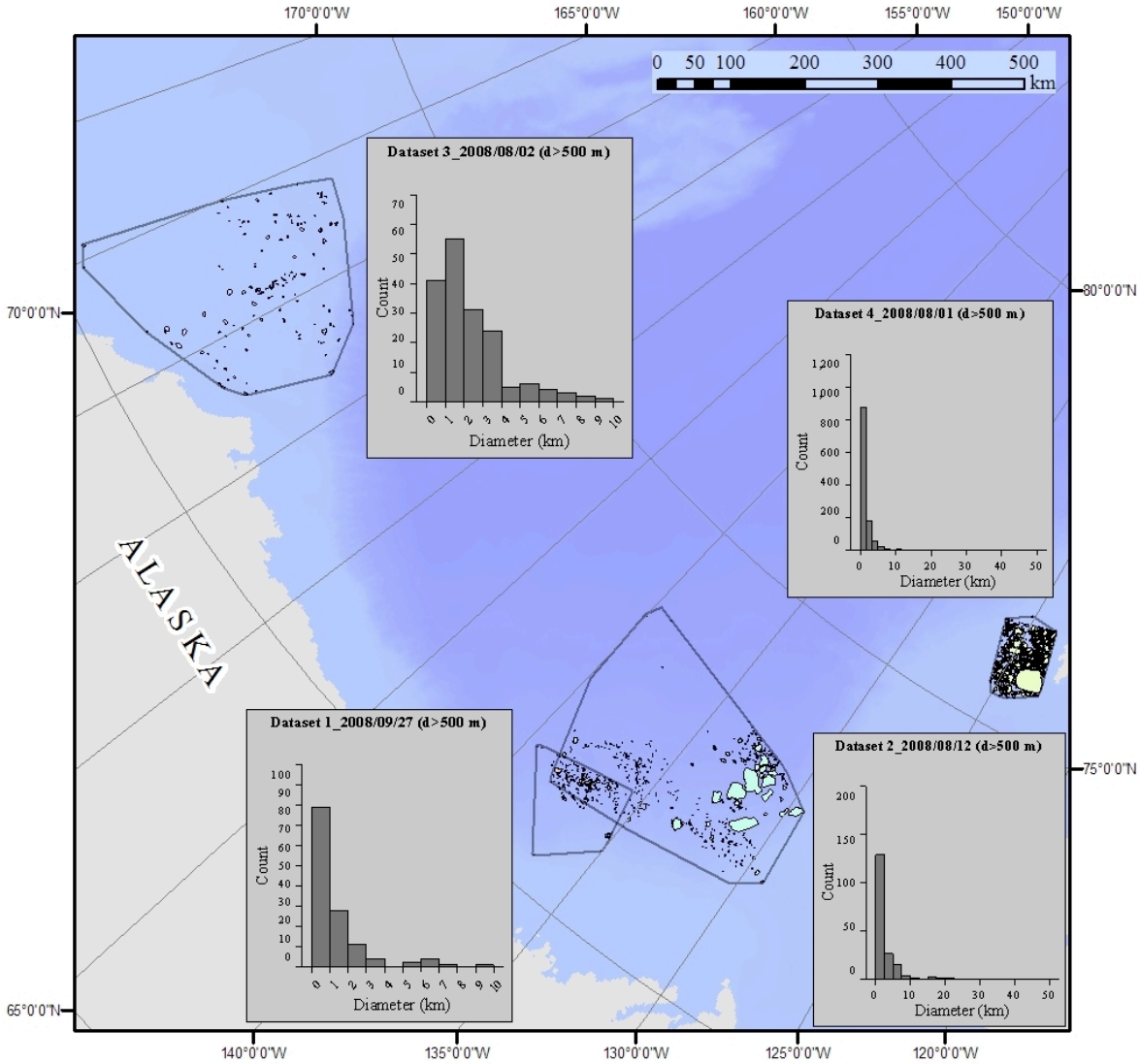

Figure 6-5 Convex Hull Polygons of M-Y Floes for 4 areas in Summer

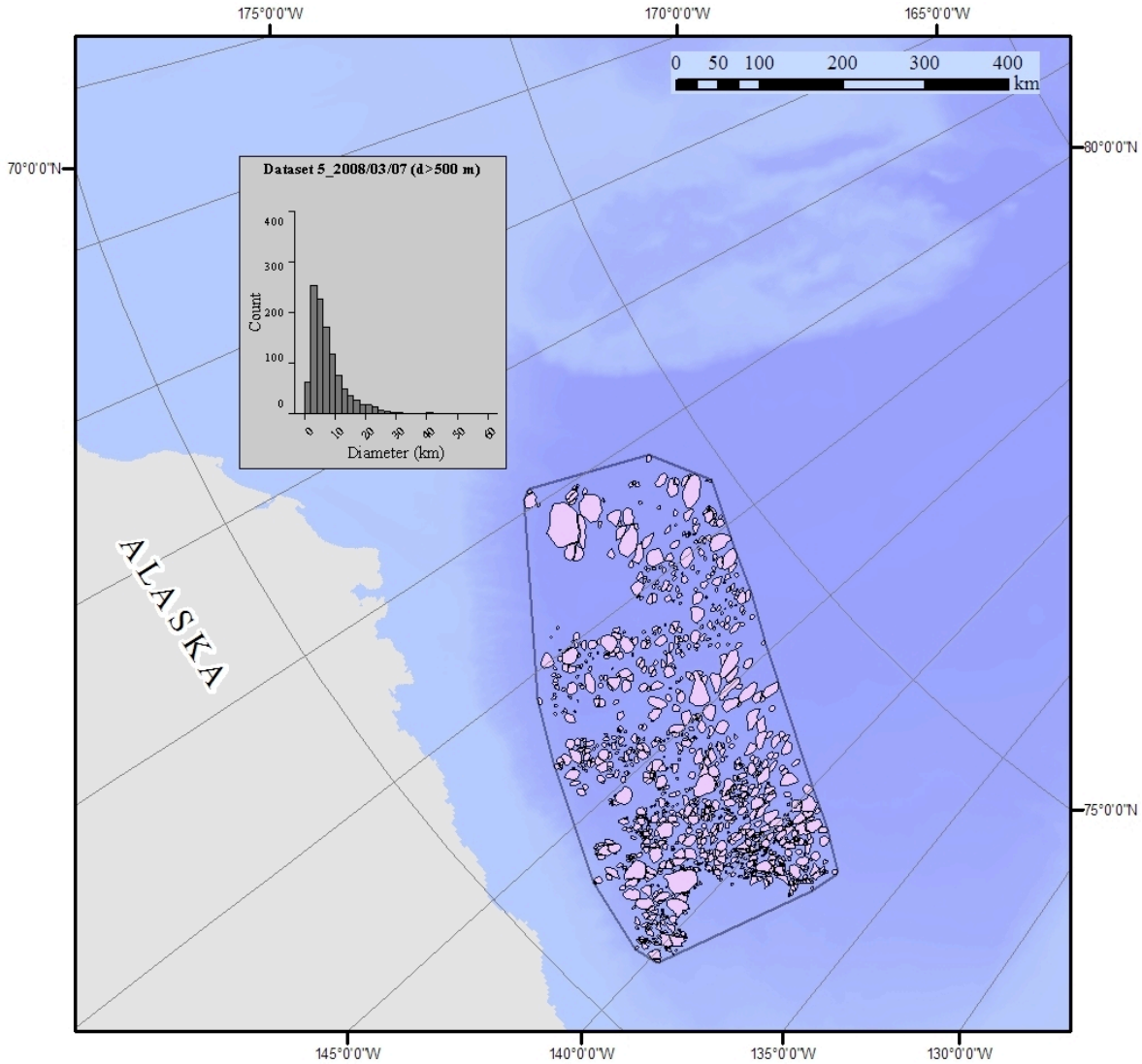

Figure 6-6 Convex Hull Polygon of M-Y Foes in Mid Winter

6.4 Interpretation and Analysis of Multi-Year Floe Size

6.4.1 Late Winter Floe Sizes using RadarSat 2 June 4 & 9, 2008

6.4.1.1 Chukchi Sea/Barrow, June 9, 2008

Figure 6-7 shows the outlines of multi-year floes measured from a Radarsat2 ScanSAR wide image. This image captured an area of predominantly Multi-year ice about 450 km NW of Point Barrow, in the Chukchi Sea. Although no Multi-year ice is shown south of the main patch, this is partially related to the resolution of the imagery. To the south of the main patch of Multi-year ice there were numerous small "bright returns" on the image that were likely Multi-year ice (confirmed on Environment Canada's Ice Charts), however they were below the sensor's resolution to accurately depict them. Through experience in this

project analyzing 100m resolution data, 3 pixels (300m) was about the minimum floe size that could be accurately determined for ice type, and in cases where the ice was wet or under pressure, 6 pixels (600m) was sometimes required for accurate ice typing. As a result, the scattered Multi-year floes (<300m) between Point Barrow and the main patch, although present, could not be identified on this imagery.

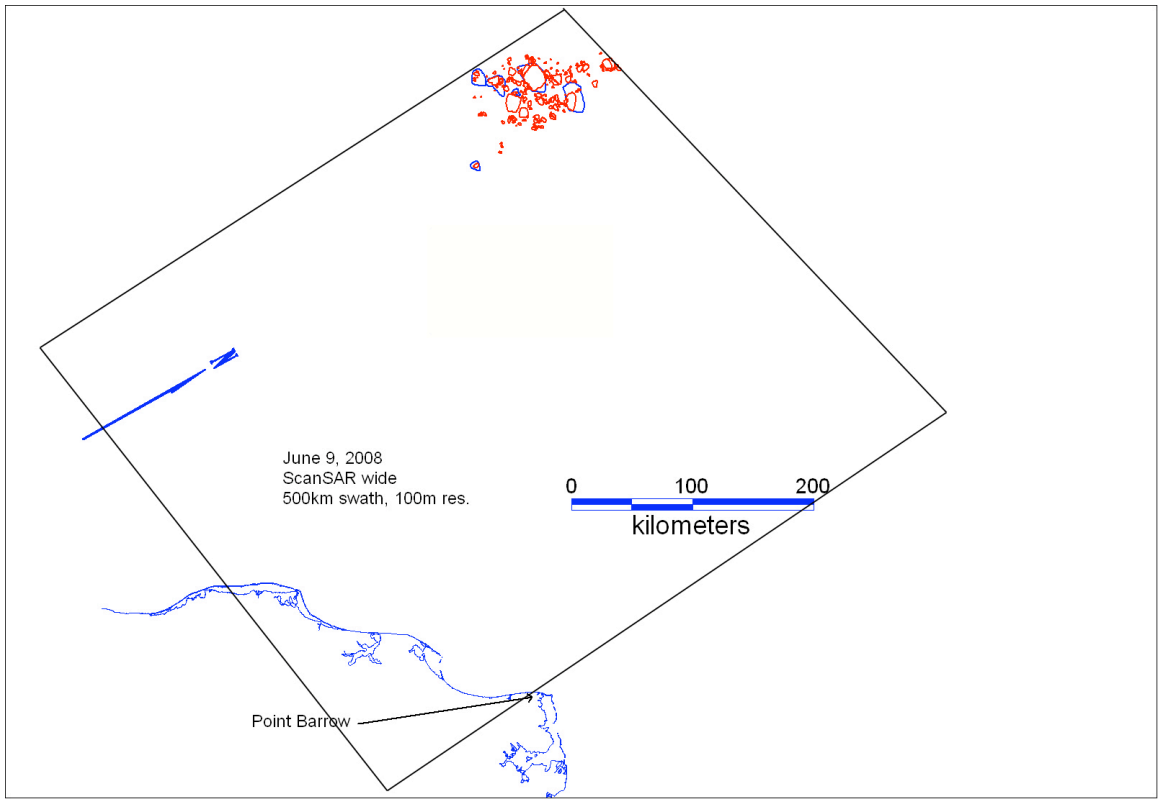

Figure 6-7 M-Y Floes Chukchi Sea June 9, 2008 (Radarsat2 100m res)

Table 6-2 shows the basic statistics for all multi-year floes identified and for the subset of floes that were greater than 500m in diameter. Due to the lower resolution of the image and the stated uncertainties, very few floes of less than 500m diameter were measured. As a result there was very little difference in the statistics for the two datasets. Mean and median diameter were 2.7 and 1.9 km respectively. Mean and median area were 6.6 and 1.6 km^2. Figure 6-8 and 6-9 show the exceedence plots for diameter and area.

Table 6-2 Basic M-Y Floe statistics for late winter Chukchi Sea

Parameter		All Floes	Floes > 500m diameter
Location		Chukchi Sea	
Date		June 9, 2008	
# Floes in sample		204	202
Floe Area (km^2)	- median	1.64	1.65
	- mean	6.56	6.62
	- max	260.24	260.24
Floe diameter (km)	- median	1.89	1.90
	- mean	2.69	2.71
	- max	21.49	21.49

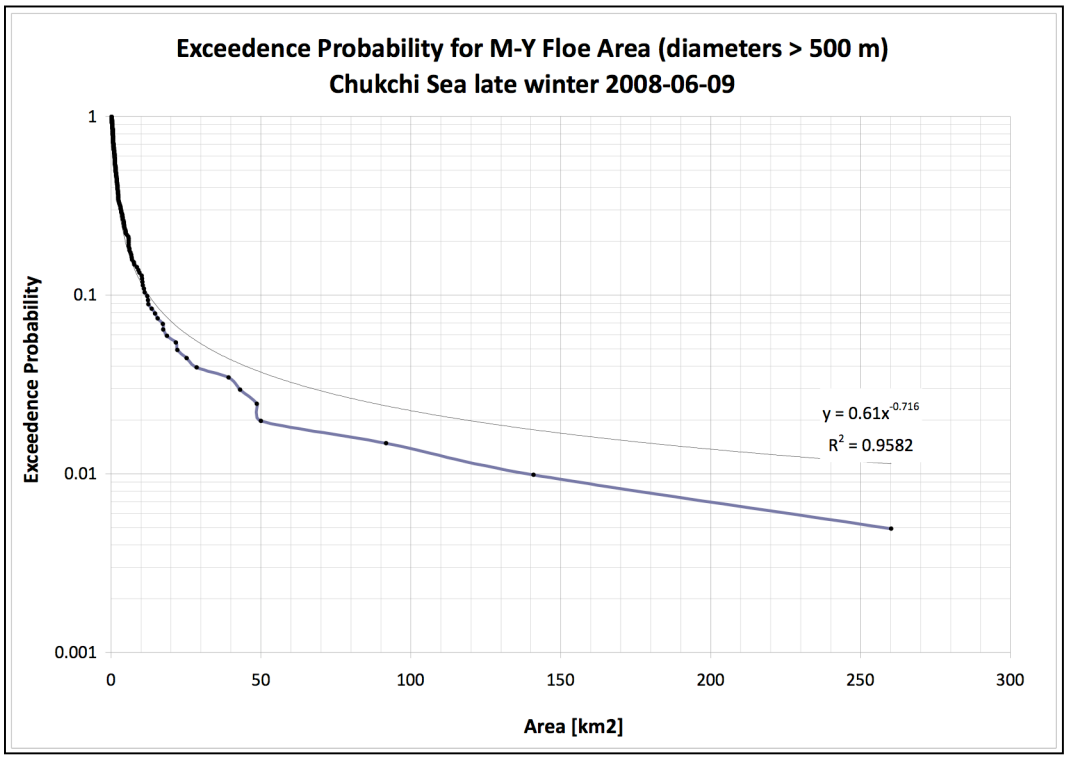

Figure 6-8 Exceedence Probability - multi-year floe area - Chukchi late winter

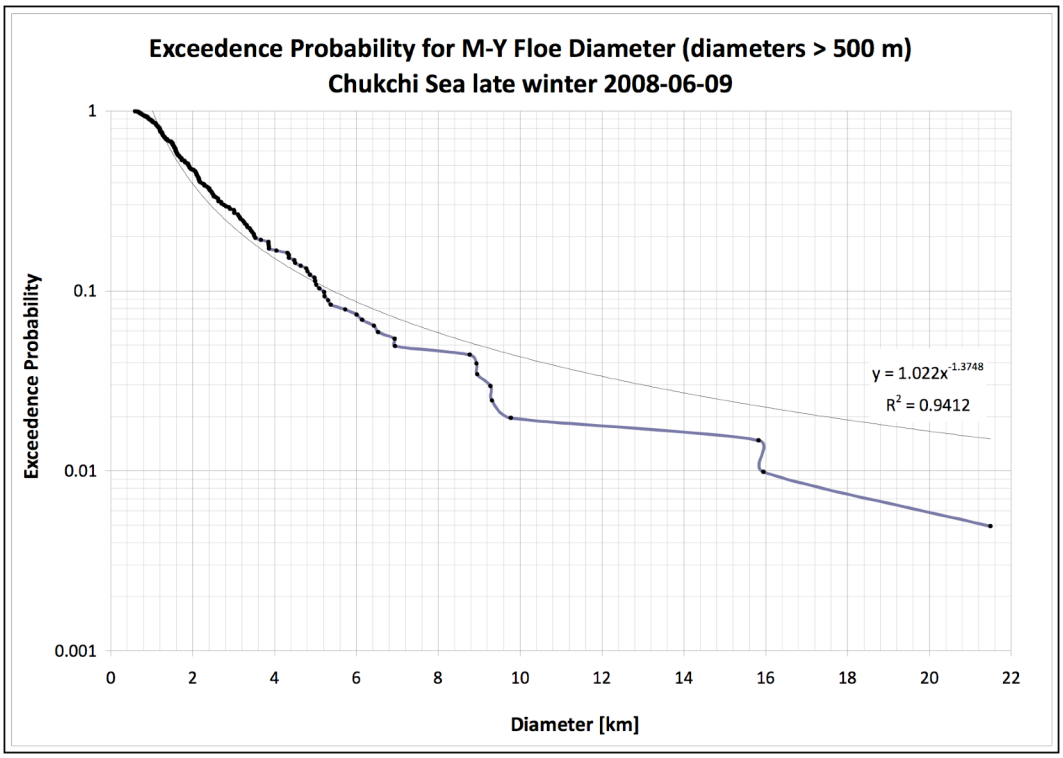

Figure 6-9 Exceedence Probability - multi-year floe diameter - Chukchi late winter

6.4.1.2 Alaskan Beaufort/Camden Bay June 4, 2008

Figure 6-10 shows late winter multi-year floe conditions captured by Radarsat offshore of the Alaskan coast. At the time of this image the Multi-year ice was clearly apparent along the northern edge of the image. In this image the multi-year floes were outlined in red, and conglomerate floes containing Multi-year ice were outlined in blue. In subsequent analysis the percentage of Multi-year in the conglomerate floes was calculated in order to generate accurate floe mass calculations. Table 6-3 shows key statistics for M-Y floes in the image. Figure 6-11 and 6-12 show the exceedence plots.

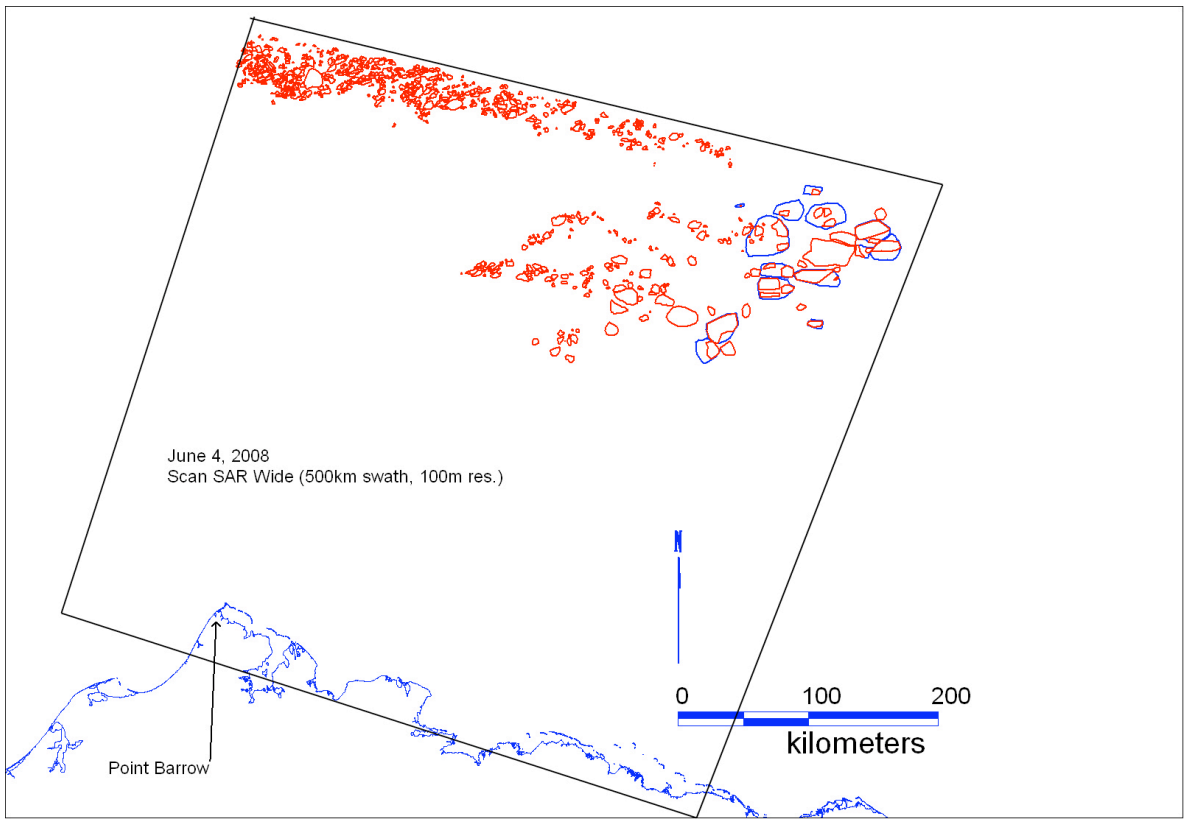

Figure 6-10 M-Y Floes Alaskan Beaufort June 4, 2008. Radarsat2

Table 6-3 Basic M-Y Floe statistics late winter Alaskan Beaufort

Parameter		All Floes	Floes > 500m diameter
Location		Alaskan Beaufort	
Date		June 4, 2008	
# Floes in sample		991	953
Floe Area (km^2)	- median	1.57	1.66
	- mean	5.97	6.20
	- max	469.34	469.34
Floe diameter (km)	- median	1.92	1.98
	- mean	2.67	2.76
	- max	35.15	35.15

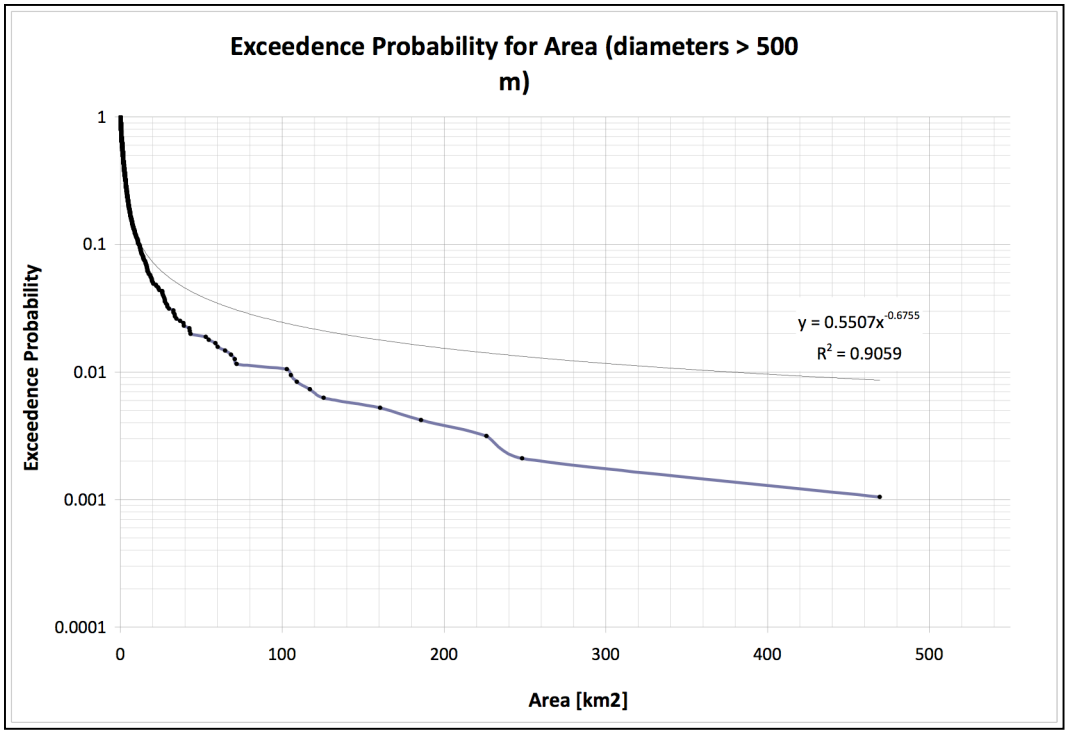

Figure 6-11 Exceedence Probability - M-Y Floe Area - Alaskan Beaufort late winter

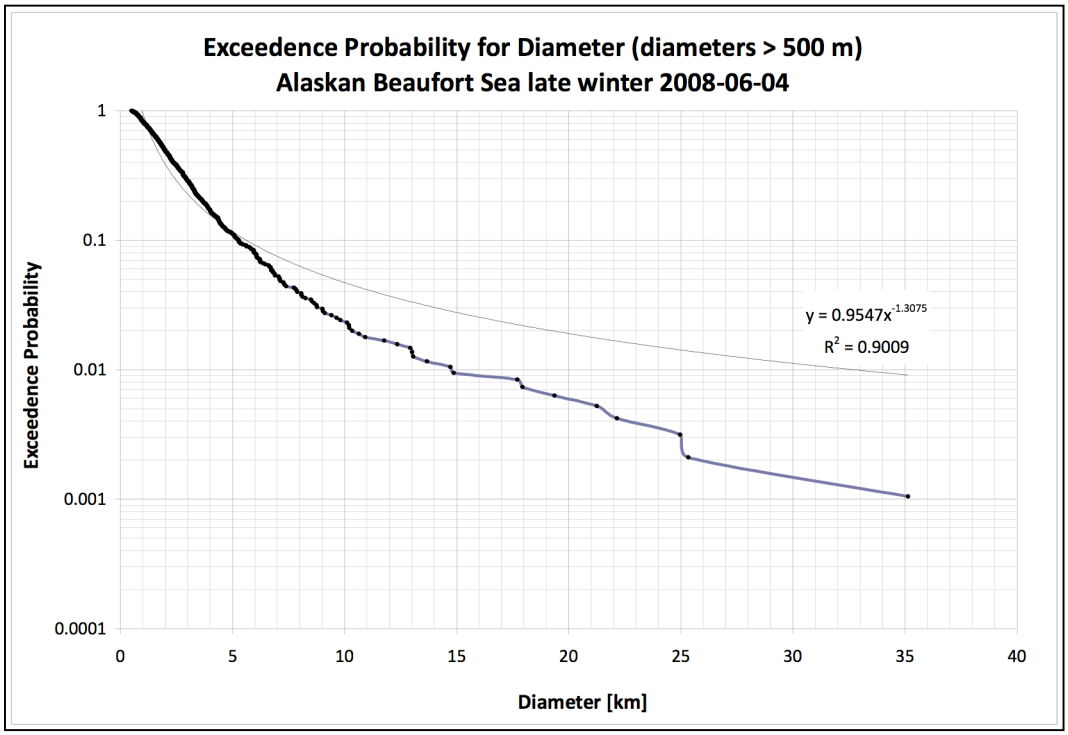

Figure 6-12 Exceedence Probability - M-Y Floe Diam. - Alaskan Beaufort late winter

6.4.1.3 Canadian Beaufort/ Herschel Island, June 9, 2008

Figure 6-13 depicts late winter conditions offshore of Herschel Island from a Radarsat image. The right side of the image was mostly open water, and much of the ice on the left side of the image is actively fracturing and melting out. Although the average size of the multi-year floes is not too large (5 km., circled in red), the remaining conglomerate floes in this image are quite large, averaging 25km. Table 6-4 shows the statistics of the floes noted on the June 9th 2008 Radarsat image, with conglomerate floes excluded. Multi-year floes on the left side of this image were not circled as they had been identified earlier on the overlap portion of the Camden Bay image shown in Figure 6-10. Figures 6-14 and 6-15 show the exceedence plots.

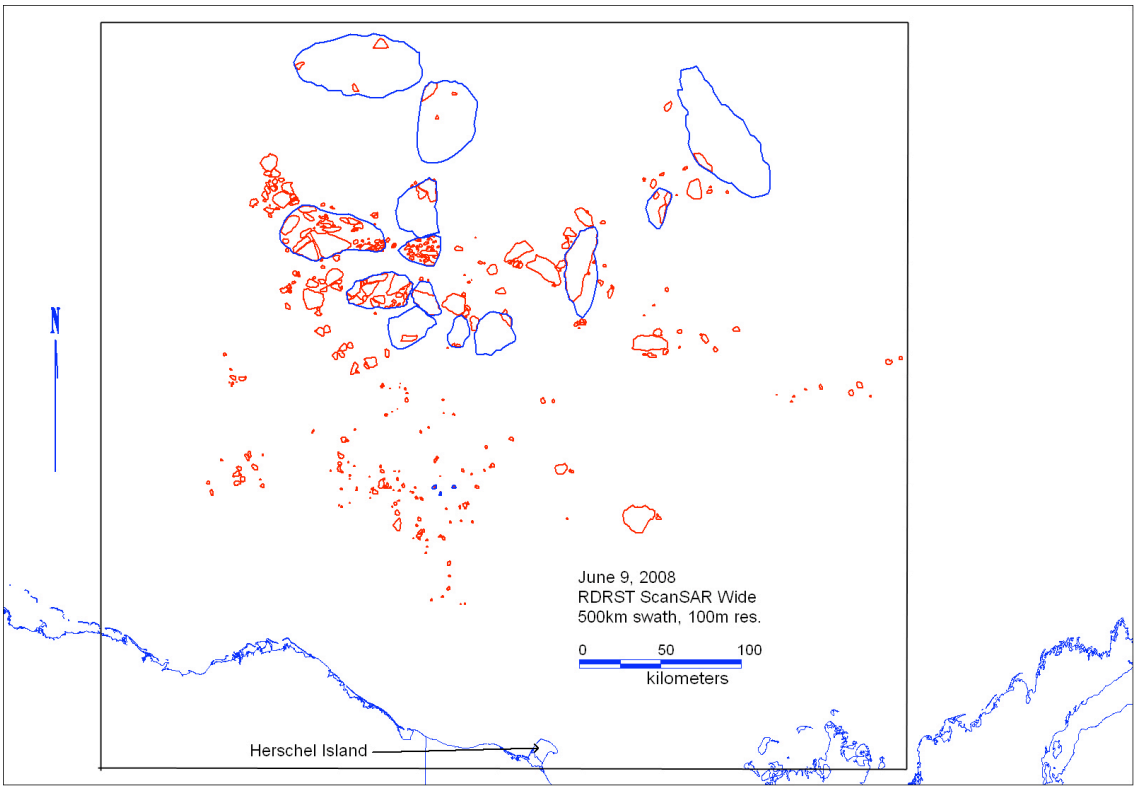

Figure 6-13 M-Y Floes Canadian Beaufort June 9, 2008. Radarsat2

Table 6-4 Basic M-Y Floe statistics for late winter Canadian Beaufort Sea

Parameter	All Floes	Floes > 500m diameter
Location	Canadian Beaufort	
Date	June 9, 2008	
# Floes in sample	444	424
Floe Area (km^2) - median	1.53	1.84
- mean	9.11	9.54
- max	448.64	448.64
Floe diameter (km) - median	1.95	2.07
- mean	3.21	3.35
- max	44.24	44.24

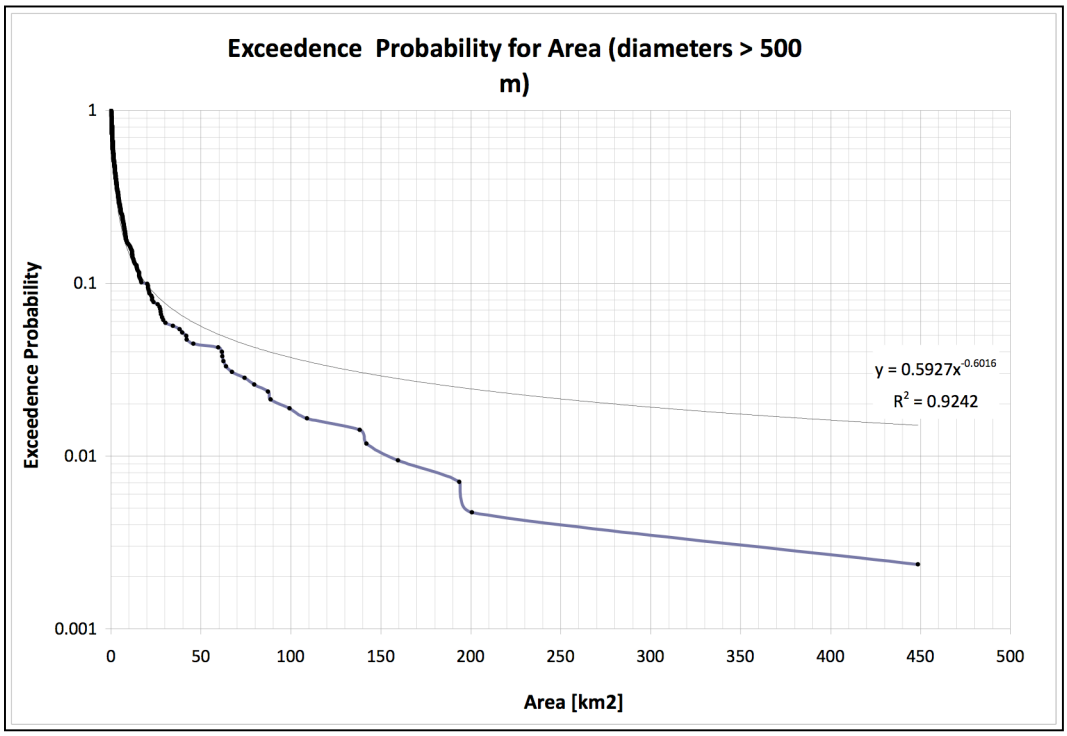

Figure 6-14 Exceedence Probability - M-Y Floe Area - Canadian Beaufort late winter

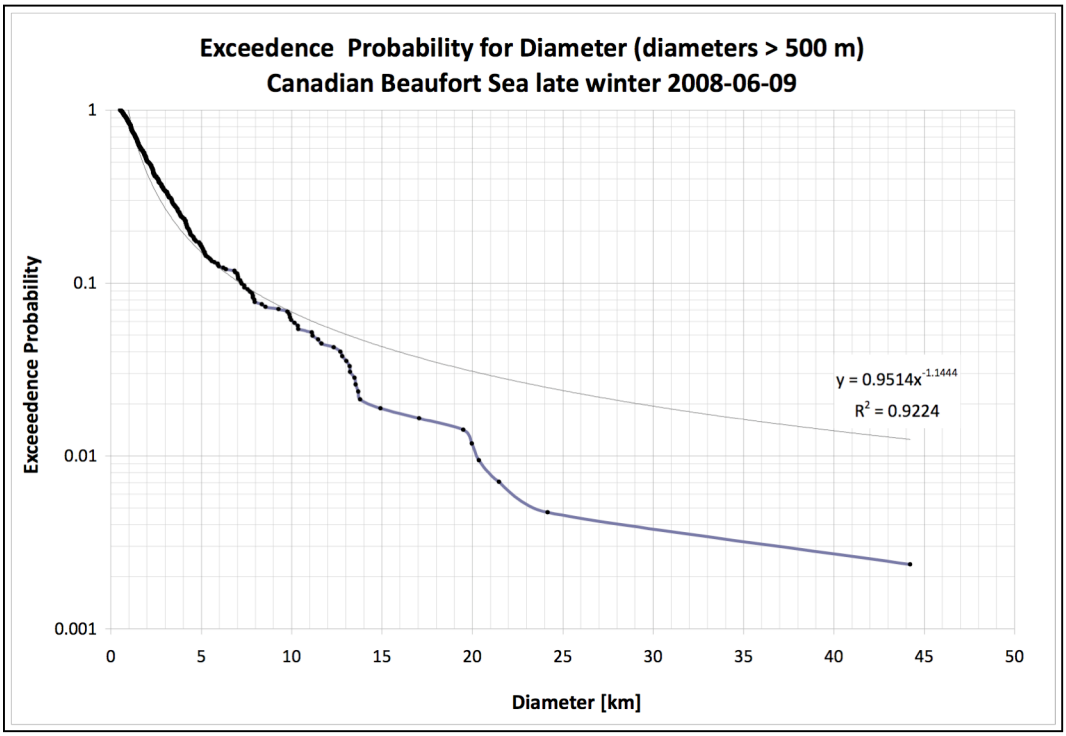

Figure 6-15 Exceedence Probability - M-Y Floe Diam - Canadian Beaufort late winter

6.4.2 Summer Floe Sizes Radarsat 2 Wide Aug – Sept, 2008

6.4.2.1 Chukchi Sea/Barrow, August 2, 2008

This image was a Radarsat2 ScanSAR wide image with 500km swath and 100m resolution. The image captured a time in the ice season when a belt of ice that included significant quantities of multi-year ice extended from the Polar pack across the Chukchi Sea reaching the coast at Point Barrow. The floe outline are shown below in Figure 6-16. Table 6-5 shows the basic statistics for the multi-year floes in this summer Chukchi Sea image. Figures 6-17 and 6-18 show the exceedence plots for diameter and area.

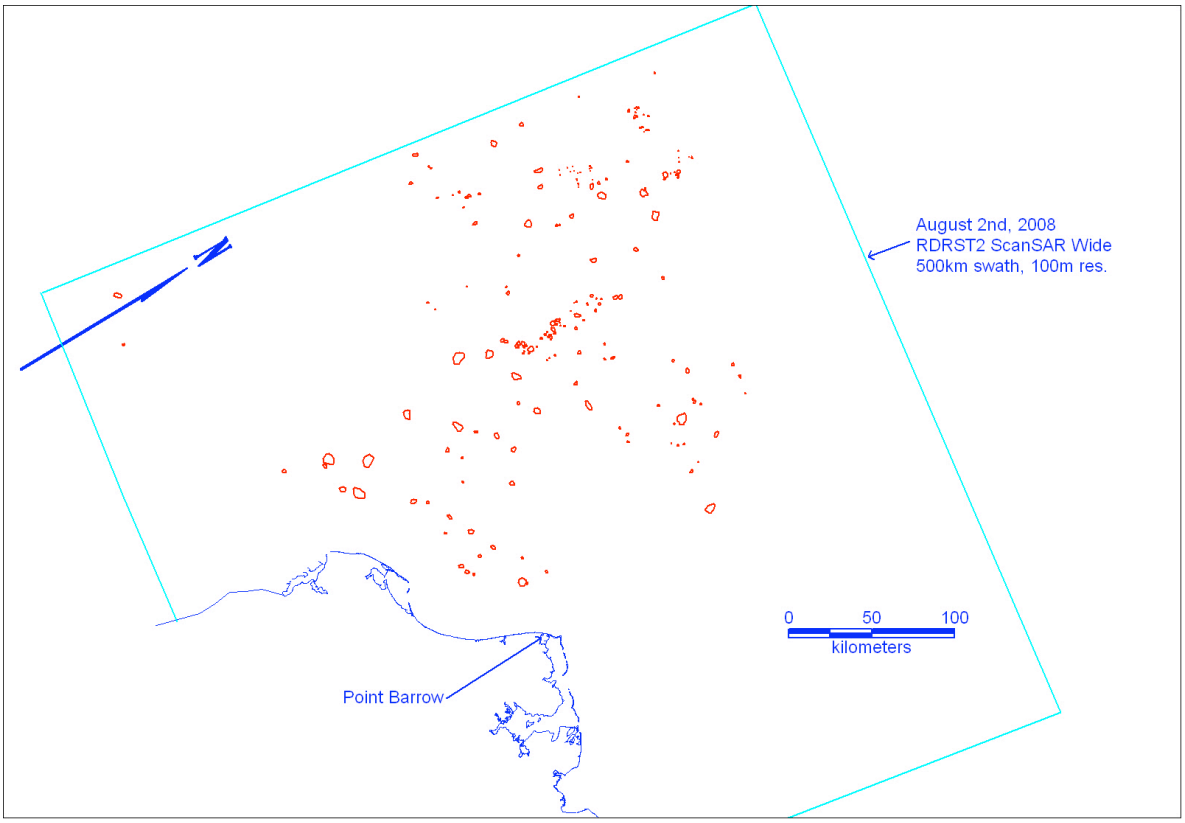

Figure 6-16 M-Y Floes Chukchi Sea August 2nd, 2008 Radarsat2

Table 6-5 Basic M-Y Floe statistics for Summer Chukchi Sea

Parameter	All Floes	Floes > 500m diameter
Location	Chukchi Sea	
Date	August 2, 2008	
# Floes in sample	202	172
Floe Area (km^2) - median	0.97	1.38
- mean	3.25	3.80
- max	34.82	34.82
Floe diameter (km) - median	1.56	1.80
- mean	2.05	2.35
- max	9.22	9.22

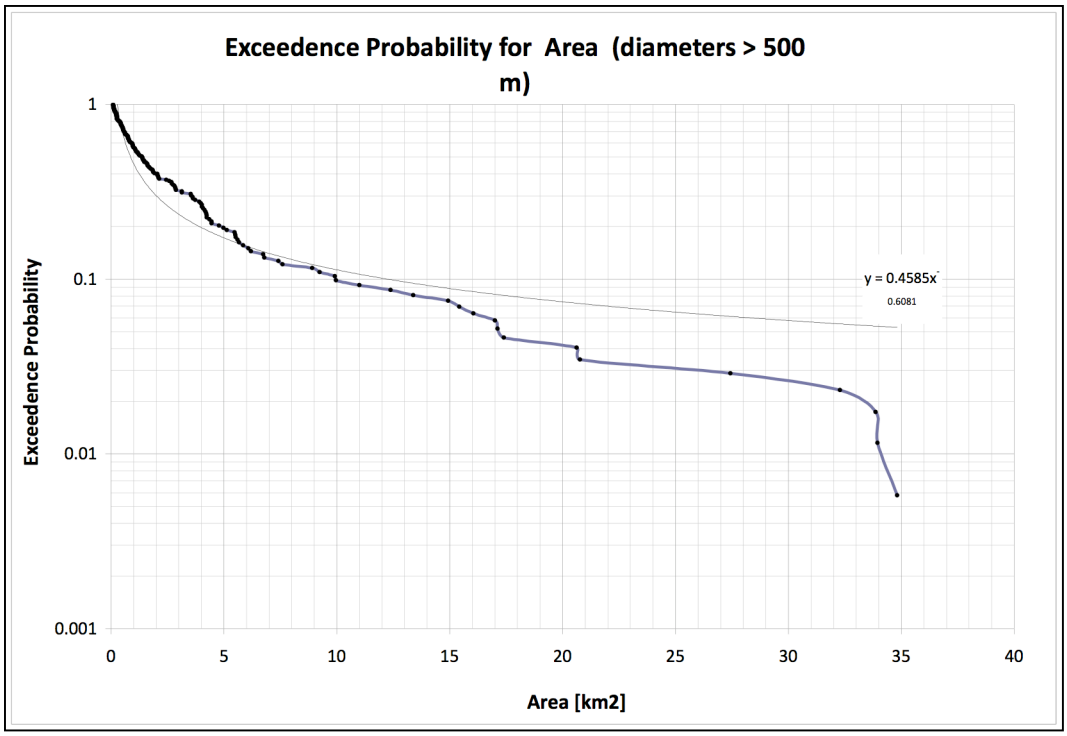

Figure 6-17 Exceedence Probability - M-Y Floe Area - Chukchi summer

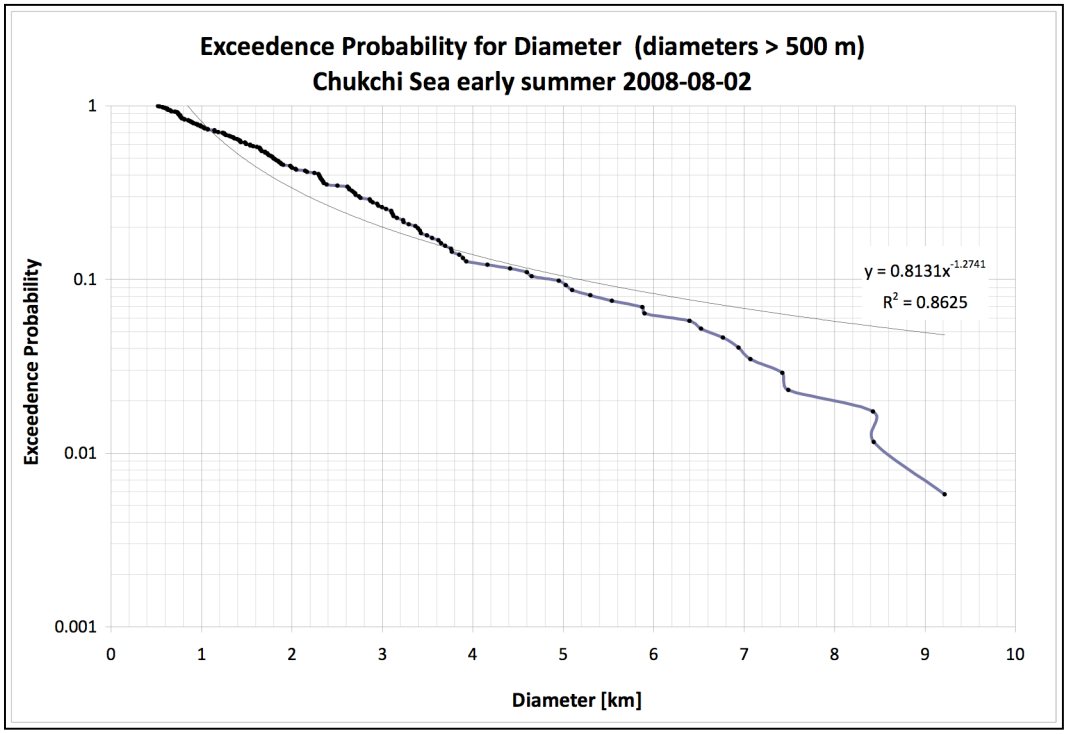

Figure 6-18 Exceedence Probability - M-Y Floe Diameter - Chukchi summer

6.4.2.2 Canadian Beaufort, August 12, 2008

This chart is from a Radarsat2 ScanSAR Wide image – 500km swath, 100m resolution. This image was processed to 50m pixels, and quality was good. A cartoon of the floe polygons obtained from the image is shown below in Figure 6-19. Table 6-6 shows the basic statistics. Figures 6-20 and 6-21 show the exceedence plots for diameter and area.

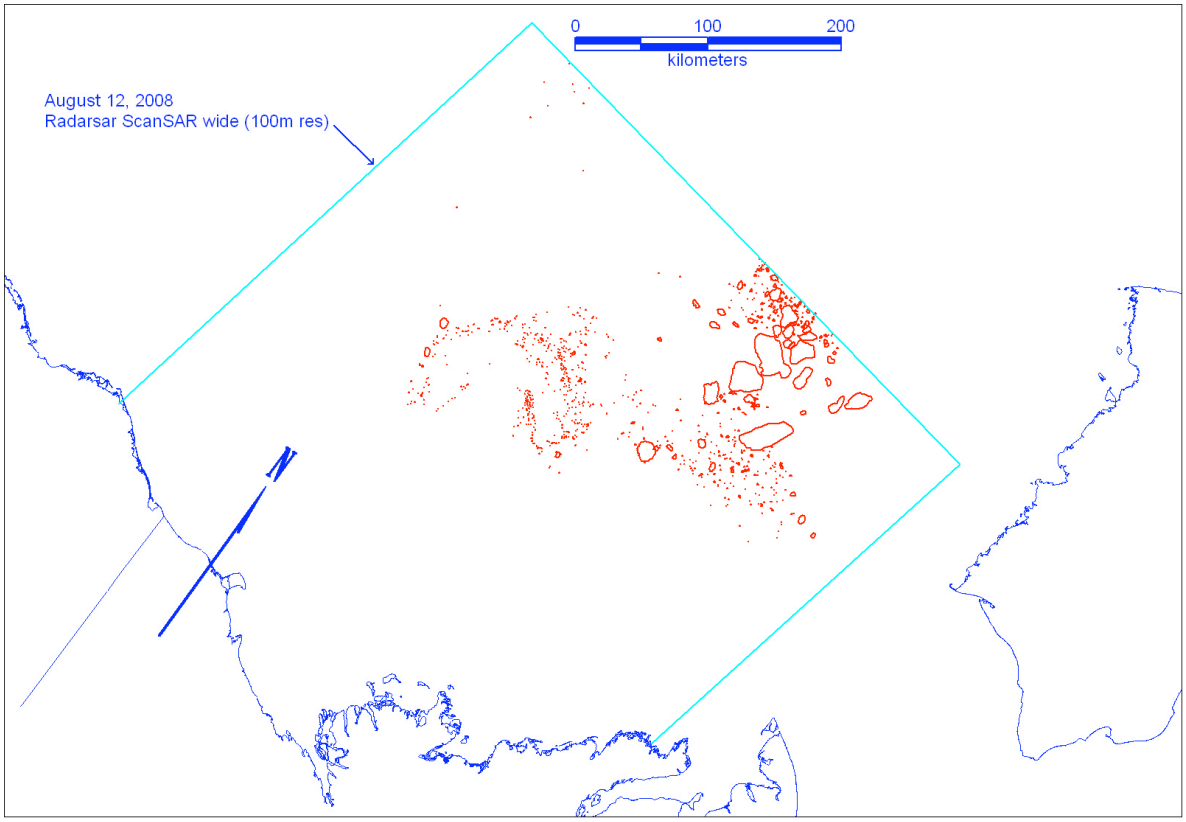

Figure 6-19 M-Y Floes Canadian Beaufort August 12th 2008 Radarsat2

Table 6-6 Basic M-Y Floe statistics for Summer Canadian Beaufort Sea

Parameter	All Floes	Floes > 500m diameter
Location	Canadian Beaufort	
Date	August 12, 2008	
# Floes in sample	1506	189
Floe Area (km^2) - median	0.03	1.21
- mean	2.32	18.22
- max	578.69	578.69
Floe diameter (km) - median	0.24	1.53
- mean	0.64	3.46
- max	41.63	41.63

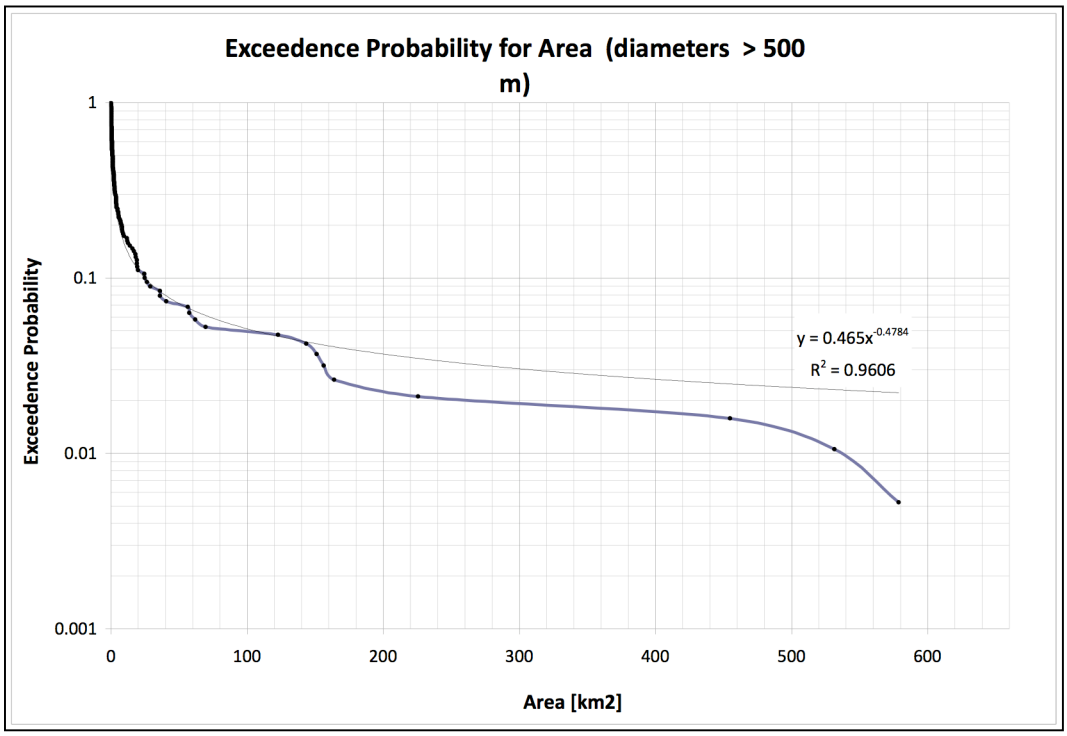

Figure 6-20 Exceedence Probability - M-Y Floe Area - Canadian Beaufort summer

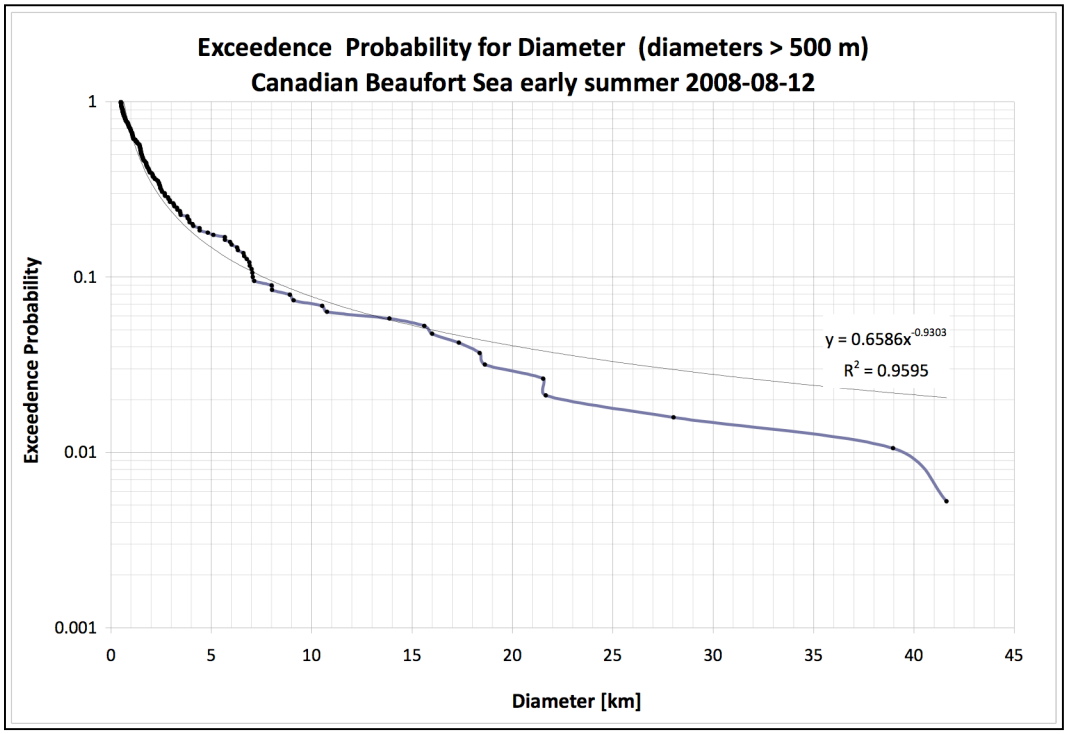

Figure 6-21 Exceedence Probability - M-Y Floe Diam - Canadian Beaufort summer

6.4.2.3 Canadian Beaufort, Sept 27, 2008

Figure 6-22 shows the ice floe polygons obtained from the Radarsat 2 Wide image of September 27th 2008. It had a 150km. swath width and 30m resolution. The image was processed to 12.5m pixels, and this produced a very good quality image. Table 6-7 lists the basic statistics for all floes and for floes > 500m I n diameter. Figure 6-23 and 6-24 show the exceedence plots for diameter and area.

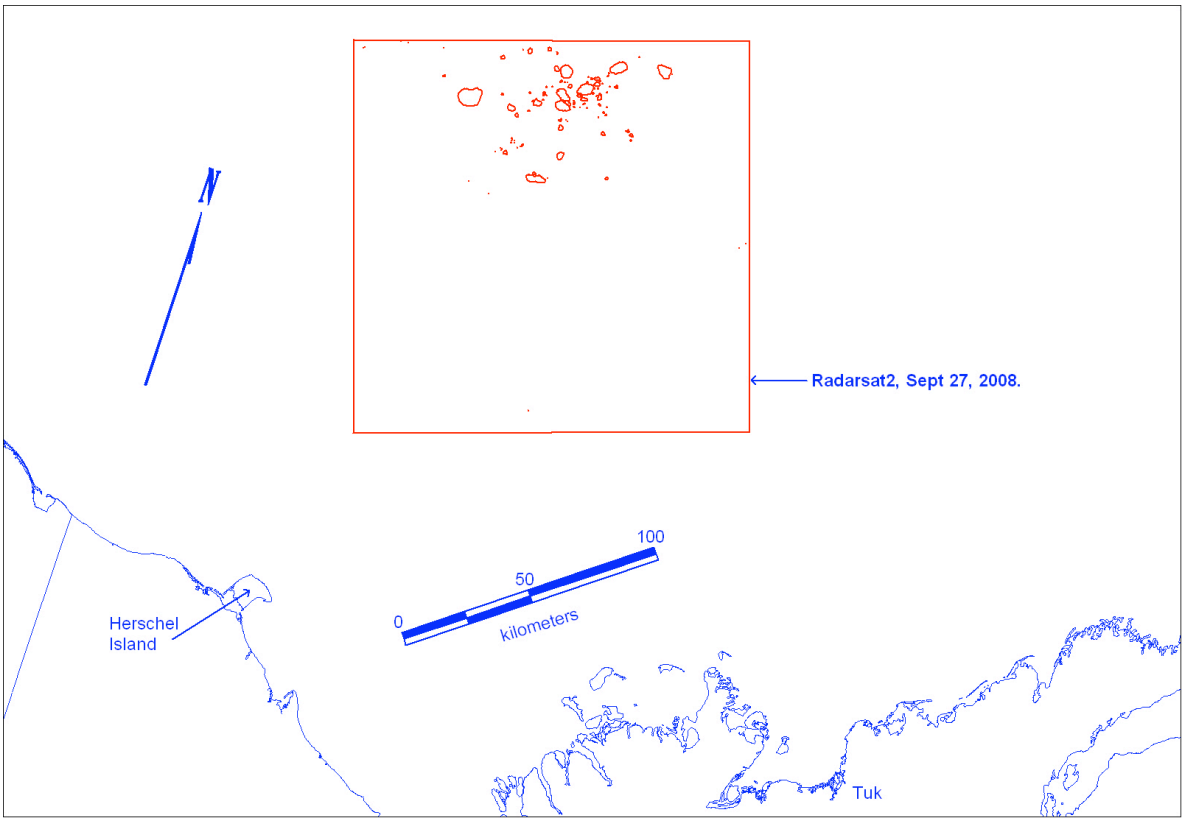

Figure 6-22 M-Y floe sizes Sept 27th, 2008 Canadian Beaufort

Table 6-7 Basic M-Y Floe statistics for late Summer Canadian Beaufort Sea

Parameter	All Floes	Floes > 500m diameter
Location	Canadian Beaufort	
Date	Sept 27, 2008	
# Floes in sample	1357	130
Floe Area (km^2) - median	0.003	0.28
- mean	0.20	2.00
- max	51.14	51.14
Floe diameter (km) - median	0.075	0.83
- mean	0.24	1.44
- max	9.81	9.81

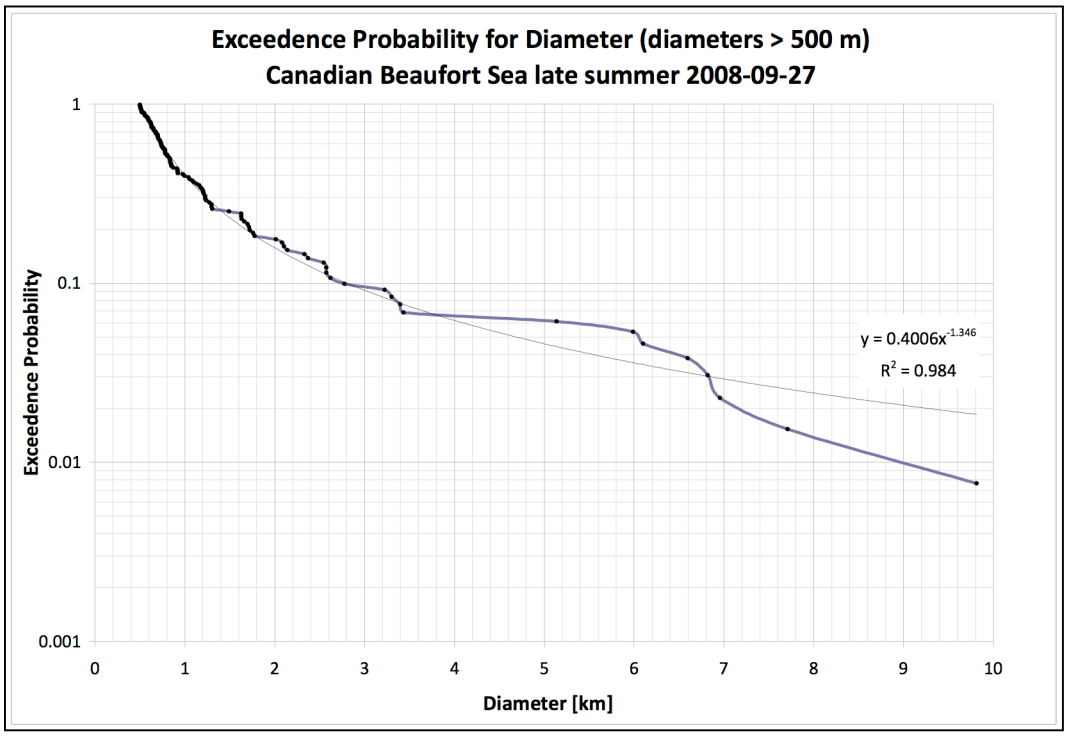

Figure 6-23 Exceedence Probability - M-Y Floe Area - Canadian Beaufort Sept 27

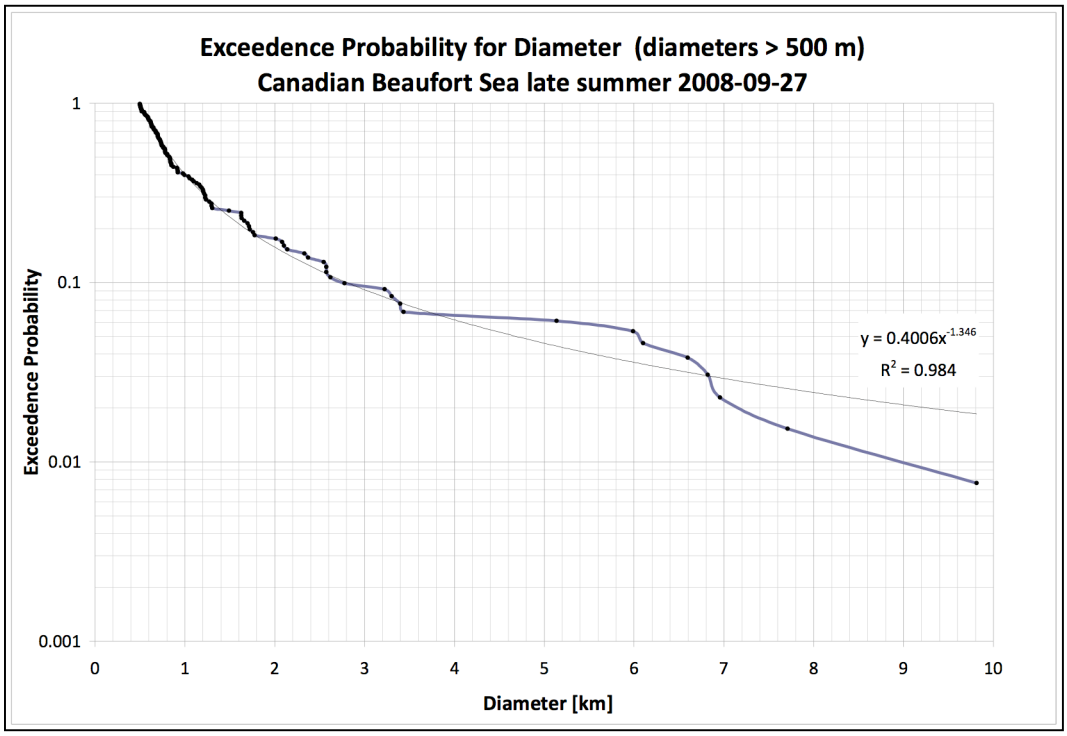

Figure 6-24 Exceedence Probability - M-Y Floe Diam - Canadian Beaufort Sept 27

6.4.3 Summer Floe Sizes High Arctic Envisat August, 2, 2008

A low-resolution JPEG of the Envisat image near Prince Patrick Island is shown in Figure 6-25 below with multi-year floe outlines identified. Almost every floe was multi-year ice. Table 6-8 shows the basic floe statistics for summer off Prince Patrick Island. Figure 6-26 and 6-27 show the exceedence plots for floe diameter and area.

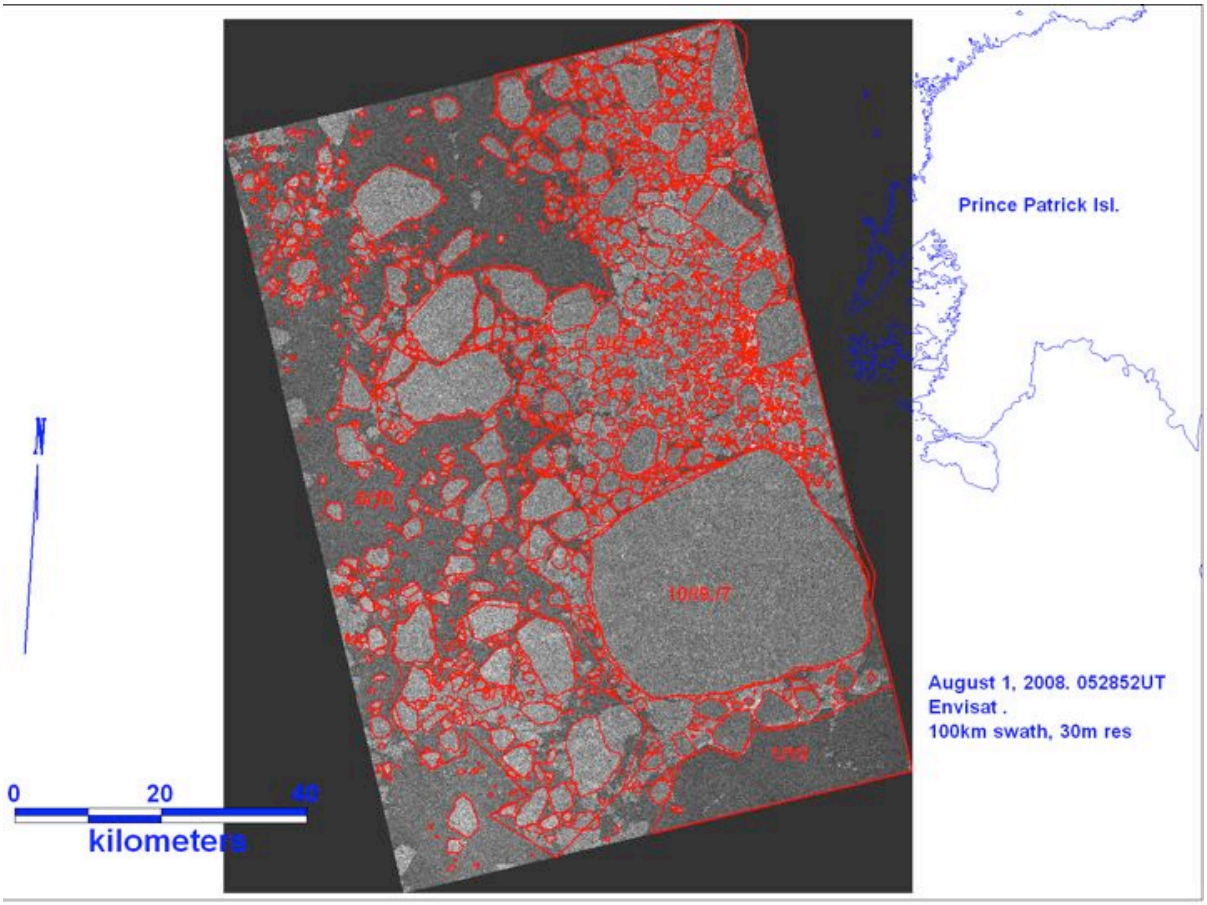

Figure 6-25 M-Y Floes SW Prince Patrick I. Aug 2nd, 2008 Envisat

Table 6-8 Basic M-Y Floe statistics for Summer Prince Patrick I.

Parameter	All Floes	Floes > 500m diameter
Location	Prince Patrick Island	
Date	August 1, 2008	
# Floes in sample	1735	1155
Floe Area (km^2) - median	0.23	0.48
- mean	1.97	2.92
- max	956.23	956.2
Floe diameter (km) - median	0.70	1.00
- mean	1.14	1.53
- max	40.61	40.61

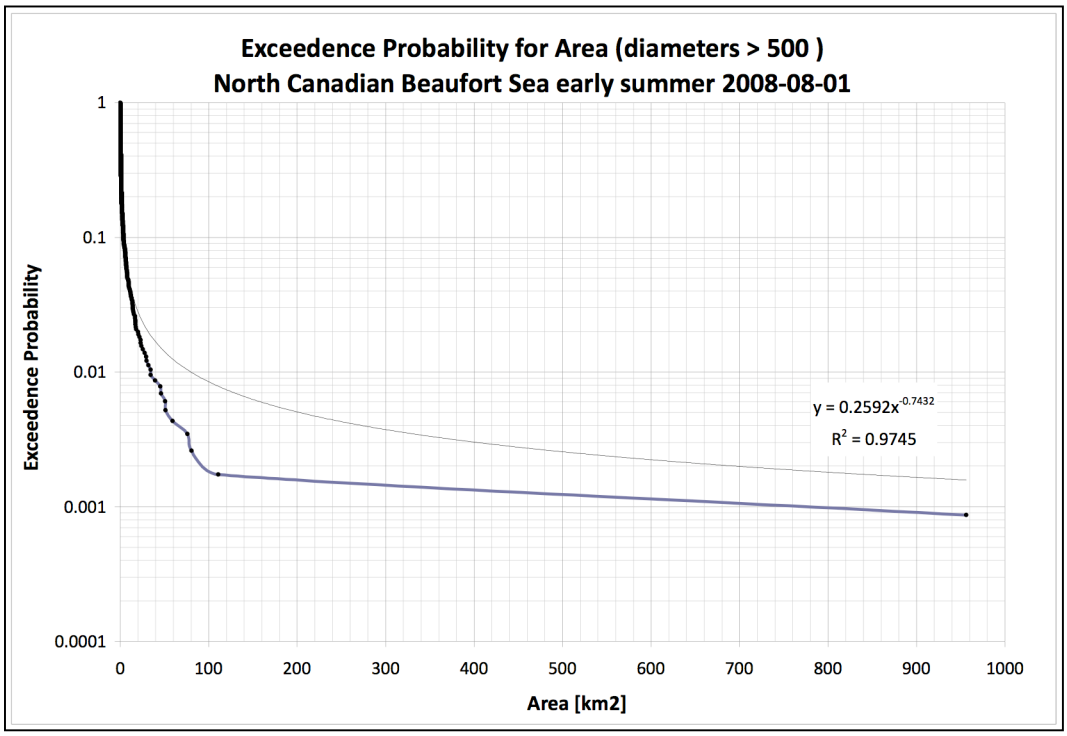

Figure 6-26 Exceedence Probability - M-Y Floe Area - N. Canadian Beaufort summer

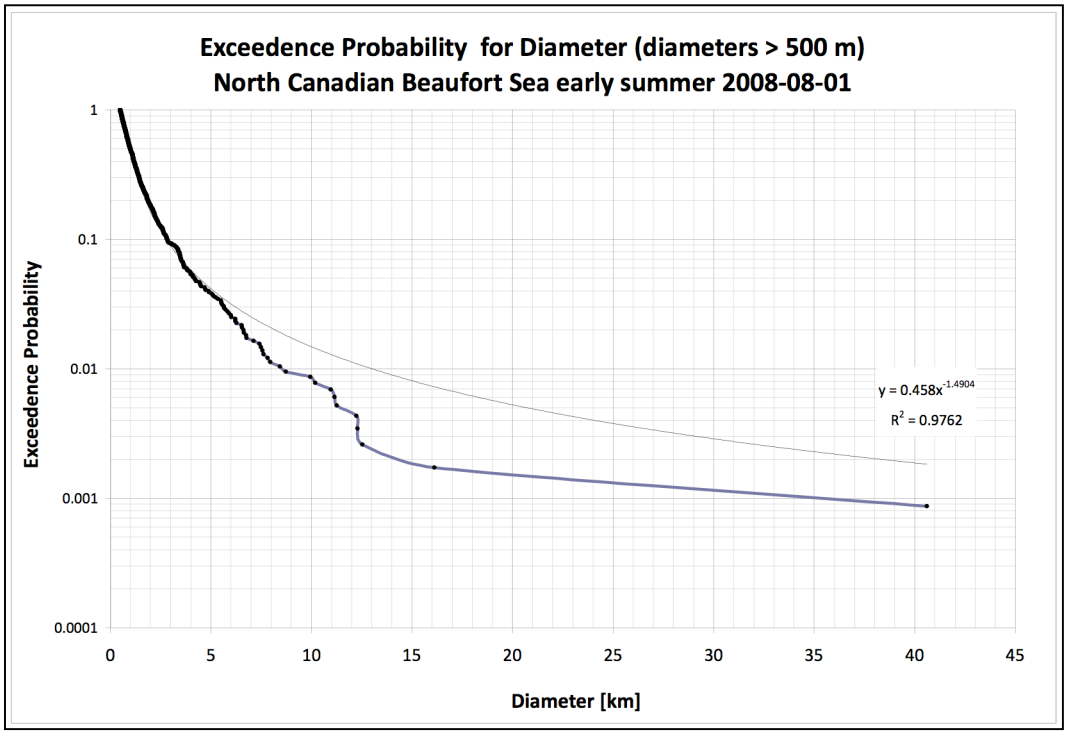

Figure 6-27 Exceedence Probability - M-Y Floe Diam - N.Canadian Beaufort summer

6.4.4 Winter Floe Sizes MODIS March 7, 2008

This image was a Terra MODIS Band 1 image of 2300 km swath and 240m resolution. Although a single frame was able to cover the entire region, the relatively low resolution (and ice fog) made floe perimeter identification difficult. In Figure 6-28 below, the green line shows the edge of the Multi-year ice as shown in the March 3, 2008 Western Arctic Ice Chart produced by the Canadian Ice Service, Ottawa. Floes were large with an average area of 41 km^2 and average diameter of 7.8 km as shown in Table 6-9. Figure 6-29 and Figure 6-30 show the exceedence plots for diameter and area.

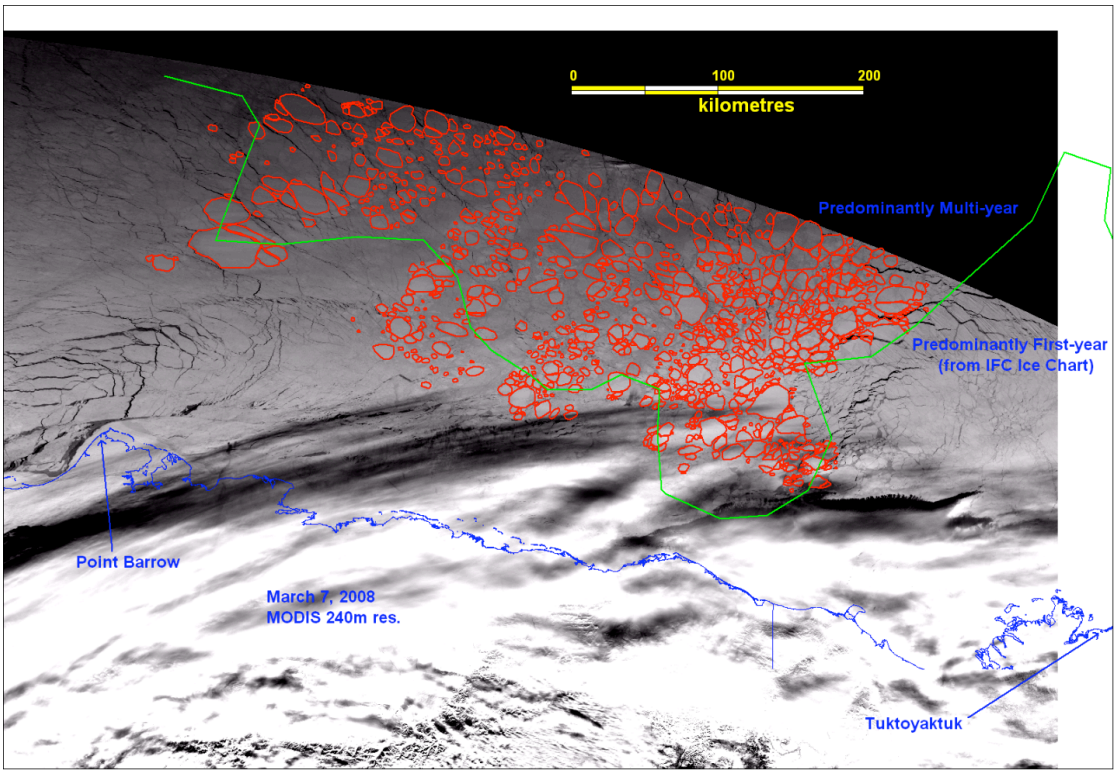

Figure 6-28 March 7, 2008. MODIS 240m resolution

Table 6-9 Basic M-Y Floe statistics for mid-winter Alaskan Beaufort Sea

Parameter	All Floes were > 500m diameter
Location	Alaskan Beaufort
Date	March 7, 2008
# Floes in sample	1101
Floe Area (km^2) - median	15.52
- mean	41.46
- max	1648.14
Floe diameter (km) - median	6.05
- mean	7.80
- max	55.54

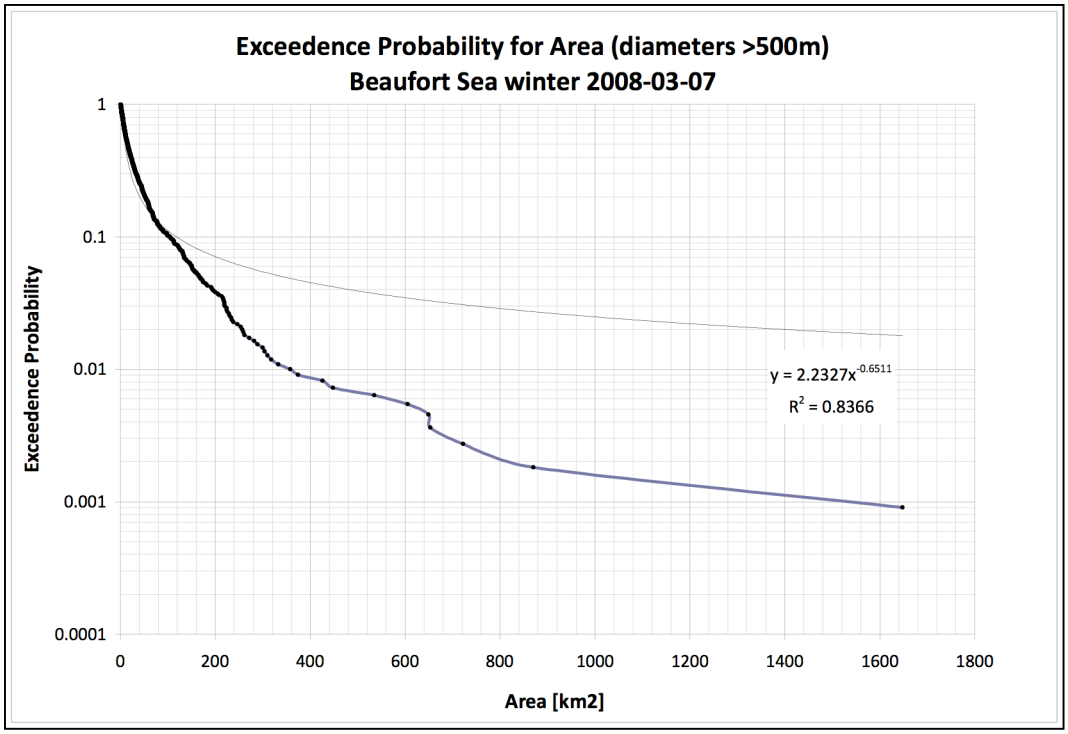

Figure 6-29 Exceedence Probability - M-Y Floe Area - Beaufort winter

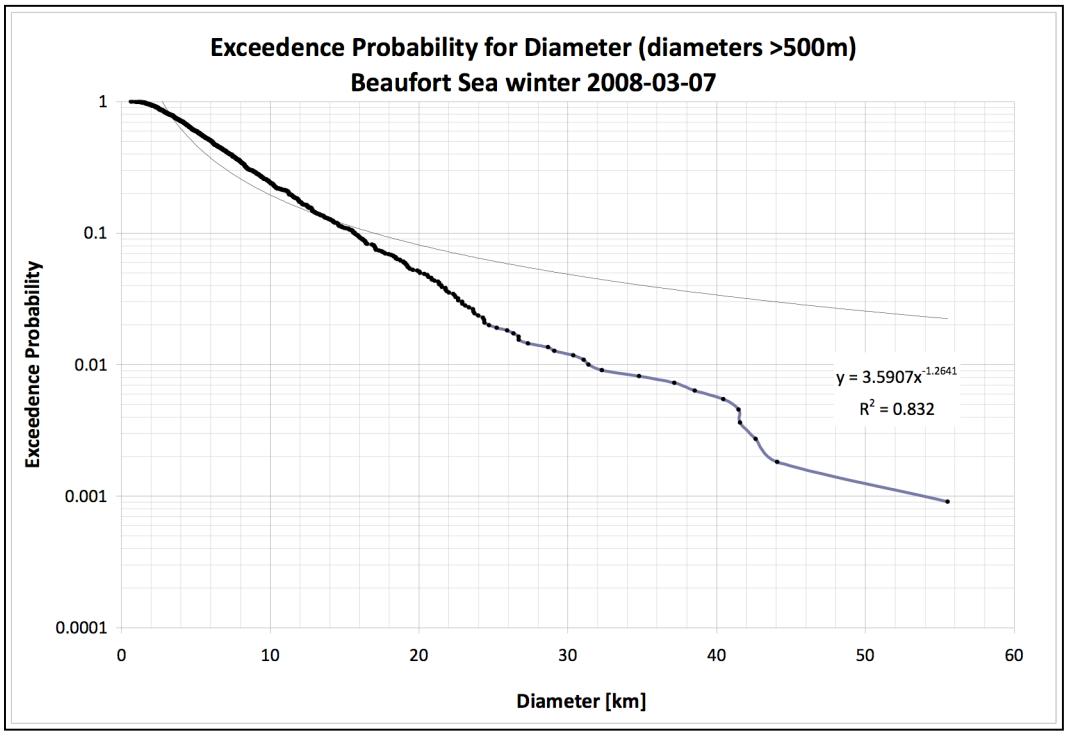

Figure 6-30 Exceedence Probability - M-Y Floe Diameter - Beaufort winter

6.4.5 Statistics of Shape Indicators

Figure 6-31 shows the histograms of the circular-like shape indicators. Of all the indicators, the circularity indicator seems the most reliable as it does not depend on sometimes inconsistent measurements like diameter or axis. Even so, the three indicators confirm that overall, the floes tend to have a circular-like shape, i.e. circularity indicators are near 1.

To assess the circular-like shape trend among the datasets, Figure 6-32 shows box plots for the circularity indicator; notice the existence of extreme lower values in all the datasets.

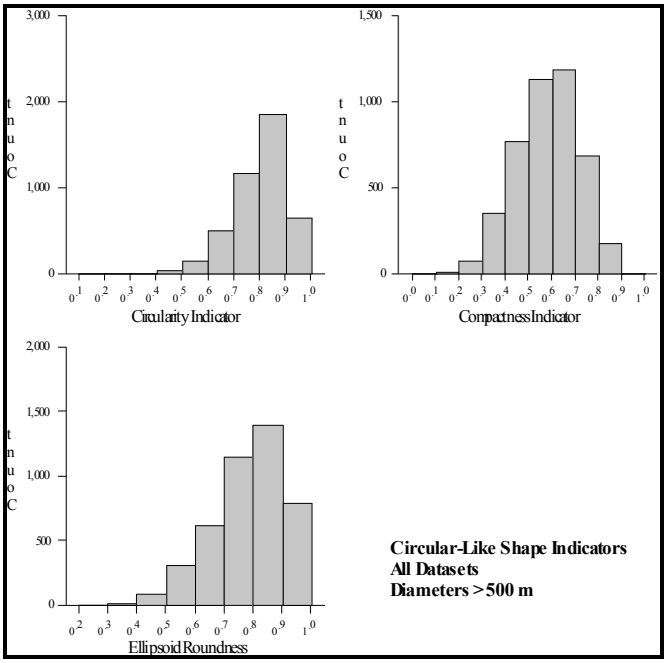

Figure 6-31 Histograms of circularity Indicators for all datasets

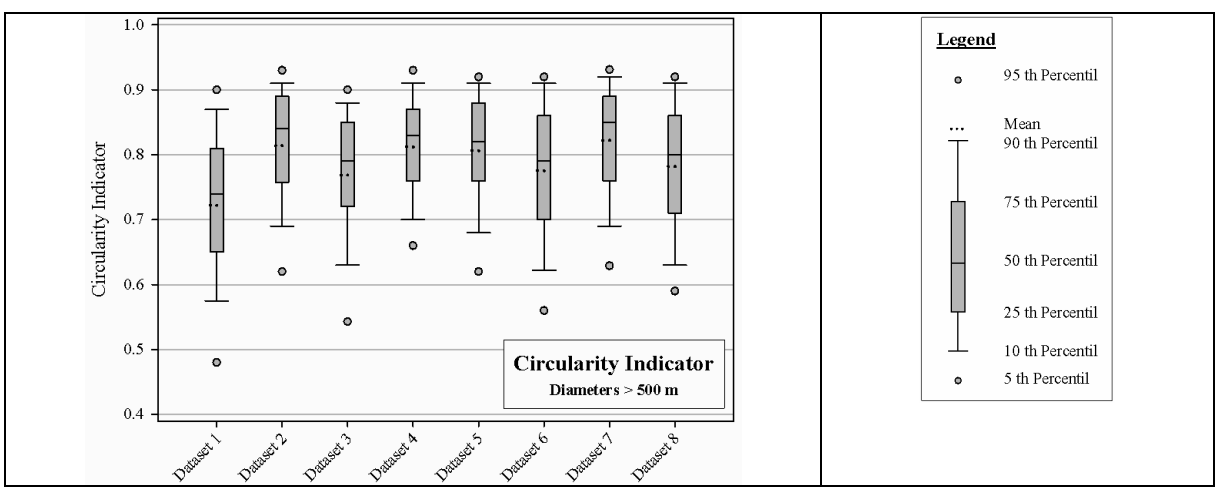

Figure 6-32 Circularity Indicator for the different datasets.

6.5 Discussion of Results

6.5.1 Regional Variations in Late Winter

Statistical distributions in the form of box plots are presented as a means of comparing the multi-year floe sizes for the 3 areas of interest. The data sets include all multi-year floes over 500m in diameter but do not include conglomerate floes. Figure 6-33 shows differences in M-Y floe diameter (longest linear dimension) between regions.

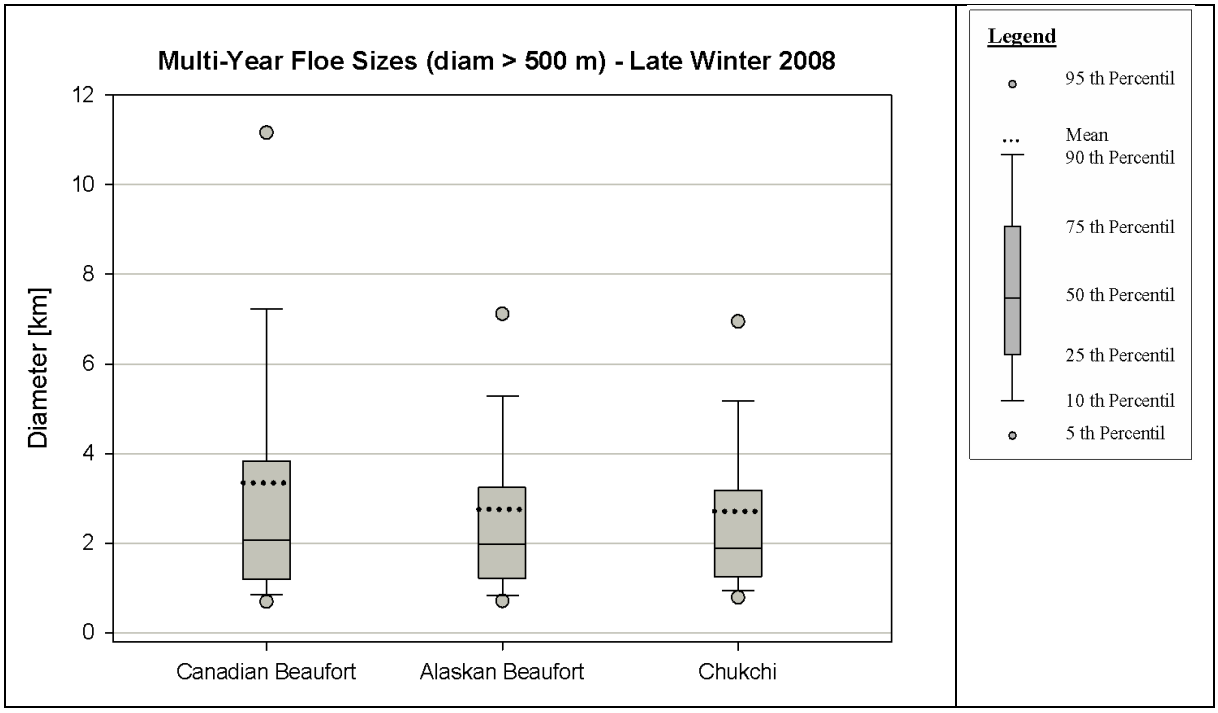

Figure 6-33 M-Y floe diameter (in km.) for three regions in late winter

There is a trend to smaller floe sizes on average from east to west. At the end of winter, just before break-up, the multi-year floes in the Canadian Beaufort Sea were generally larger than those in the Alaskan Beaufort and Chukchi Seas. Statistics of floe sizes for the latter two areas were very similar. For example, the median diameter was 2.1 km in the Canadian Beaufort, 2.0 km in the Alaskan Beaufort and 1.9 km in the Chukchi Sea. The differences between east and west became greater for higher levels of exceedence, e.g. 90% of floes were smaller than 7.2 km in the east compared with 5.1 km in the west. The largest floe in the east was 44.2 km in its longest dimension compared with 21.5 km in the west. The trend was similar for M-Y floe area statistics as shown in Figure 6-34.

The median floe area was 1.8 km^2 in the east vs. 1.6 km^2 in the west. At the 90 percentile level, the floe area was 17.3 km^2 in the east compared with 11.5 km^2 in the west. The largest floe by area was 469 km^2 in the eastern part of Alaskan sector, close to Canadian waters. The largest floe measured in Canadian waters at that time was 449 km^2, compared with 260 km^2 in the Chukchi. A visual appreciation of these trends can be seen in Figure 5-4 which combines the floe outlines for the 3 areas in one map.

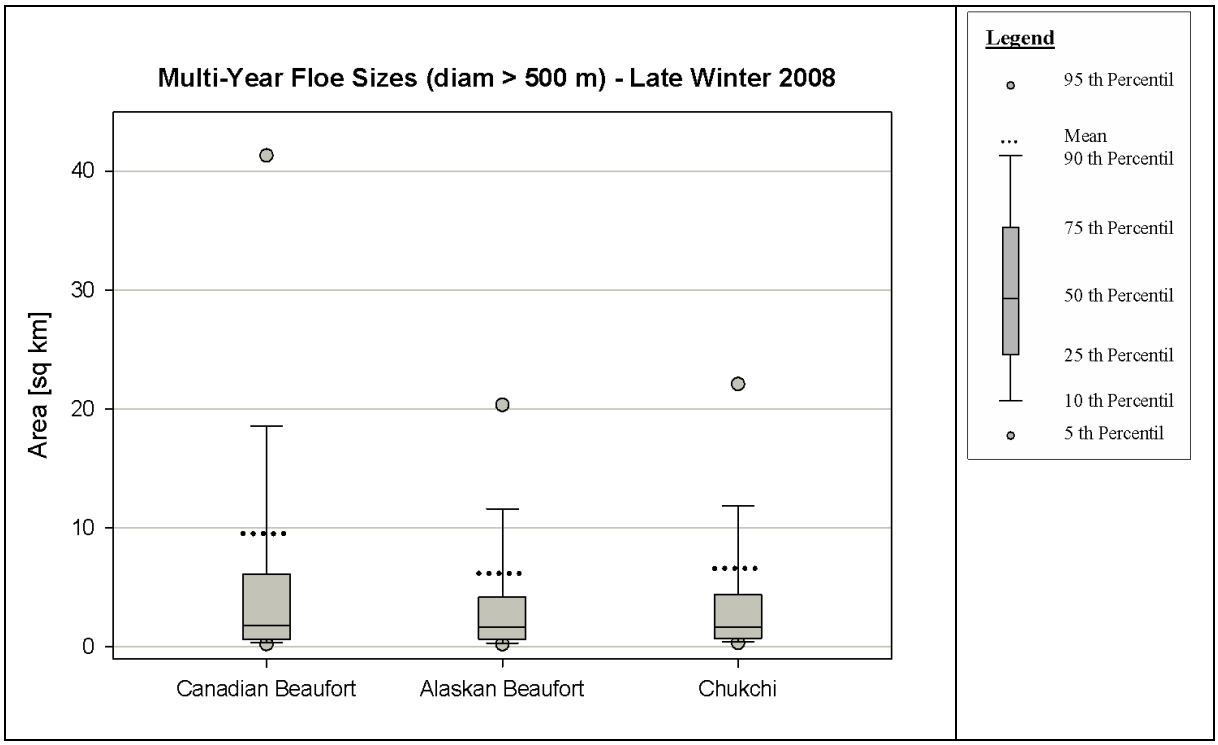

Figure 6-34 M-Y floe area (in sq.km.) for three regions in late winter

The relatively few very large floes in the samples tended to elevate the arithmetic means quite a bit. Mean diameter fell between the median and 75 percentile values. Mean floe diameter was 3.3 km in the east and 2.7 km in the west. For the floe areas, the mean value fell between the 75 and 90 percentile values due to the very large areas of the few largest floes which were well over 100 square km. The mean floe area was 9.5 km^2 in the east versus 6.6 km^2 in the west.

One possible explanation for this trend is that many M-Y floes may be exposed to increased pressure in the passage westward through the Alaskan Beaufort Sea at the northern edge of the shear zone. As the Beaufort Gyre moves the polar pack from east to west, ice floes are drawn from an area of low constriction (Canadian Beaufort) to an area of high constriction (Alaskan Beaufort). This results in the well known and severe shear ridging at the edge of the land-fast ice offshore Alaska. It is also possible that the internal stresses in the drifting ice between the Gyre and the land-fast ice lead to a certain amount of breaking down of the multi-year floes as they pass through this zone. Some floes may be split in two by pressure. Others may have their edges and corners abraded by rotation and translation.

Having passed Point Barrow heading west, these same floes are again located in an area that is relatively less constricted as the Alaskan coastline veers southwest and opens into the southern Chukchi Sea. In this regime, there is little chance of a further increase in internal stresses in the pack ice (and more likely a decrease). There would be no particular reason for floe sizes to continue decreasing, hence the similarity in Multi-year floe sizes in the Chukchi and Alaskan Beaufort.

6.5.2 Regional Variations in Summer

Two Radarsat images (Scansar Wide with 100m resolution) were available to compare east and west floe populations in early August. By this time the Canadian and Alaskan Beaufort Seas were mostly clear of ice but there was an area of 4 tenths ice near the coast on either side of Point Barrow, and patches of 9 tenths ice farther offshore with traces of multi-year in it. The Canadian Beaufort was largely open water but an incursion of deteriorated multi-year ice had advanced south to about 71 degrees North.

A total of 1506 floes were measured in the eastern image and 202 floes in the Chukchi Sea. Considering only those floes greater than 500 m in diameter, the two populations were reduced to 189 for Mackenzie Bay in the Canadian Beaufort and 172 for the north Chukchi, so they are comparable. Figure 6-35 compares the statistics of diameter.

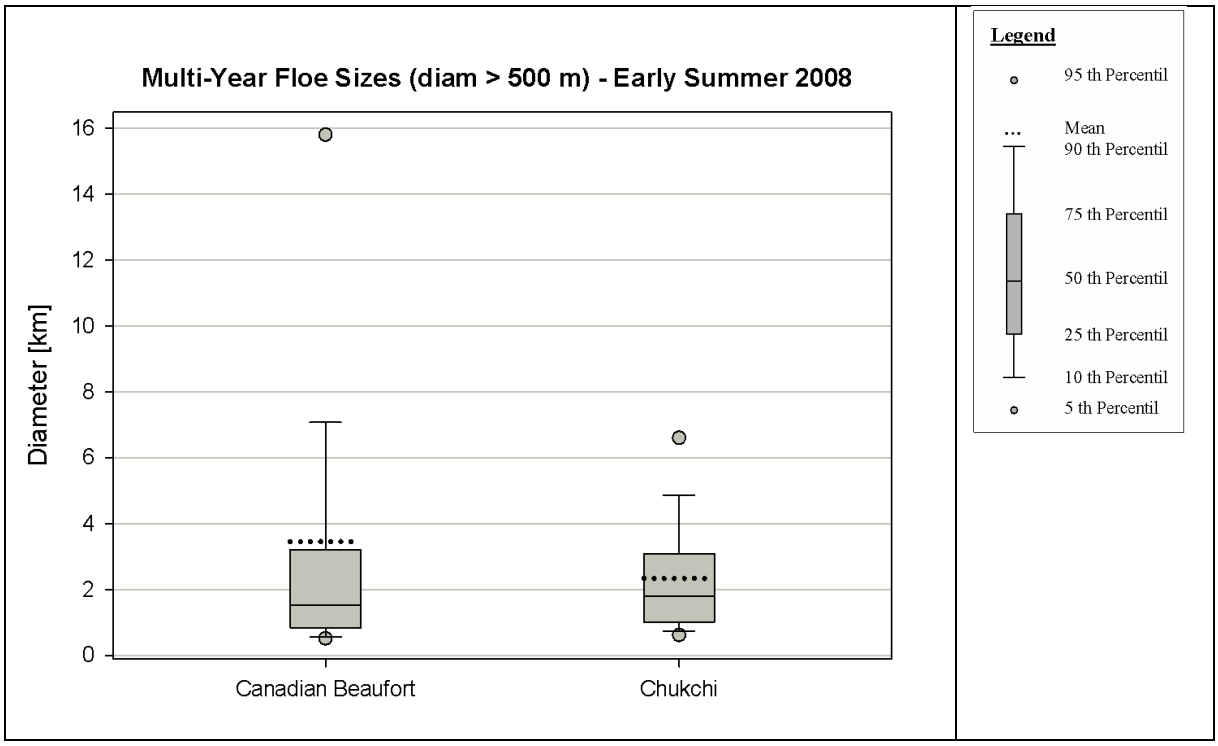

Figure 6-35 M-Y Floe Diameter for two areas in early summer

There were few large floes in the west and many in the east. The largest in the east was 41.6 km in diameter compared with 9.2 km in the west. However, there were more small floes in the east than in the west. The median diameter in the east was 1.5 km while in the west it was 1.8 km. The Chukchi summer M-Y floe population could be characterized as mostly moderate sized floes from 1 to 9 km in diameter, while the Mackenzie Bay population had more floes in the small and the large categories. The greater number of large floes in the east augmented the average diameter to 3.5 km compared with 2.3 km in the west.

The average area of floes in the east was 18.2 km^2 while in the west it was 3.8 km^2. Maximum floe size in the east was 579 km^2 compared with 34.8 km^2 in the Chukchi. This is not surprising since the Canadian Beaufort was being replenished with large M-Y floes from the polar pack. In the part of the Chukchi Sea that was surveyed, there was no such re-supply of M-Y floes and the imagery showed a sparse population of floes that had been deteriorating in open water for some time. Figure 6-36 compares box plot distributions of floe area for the two regions.

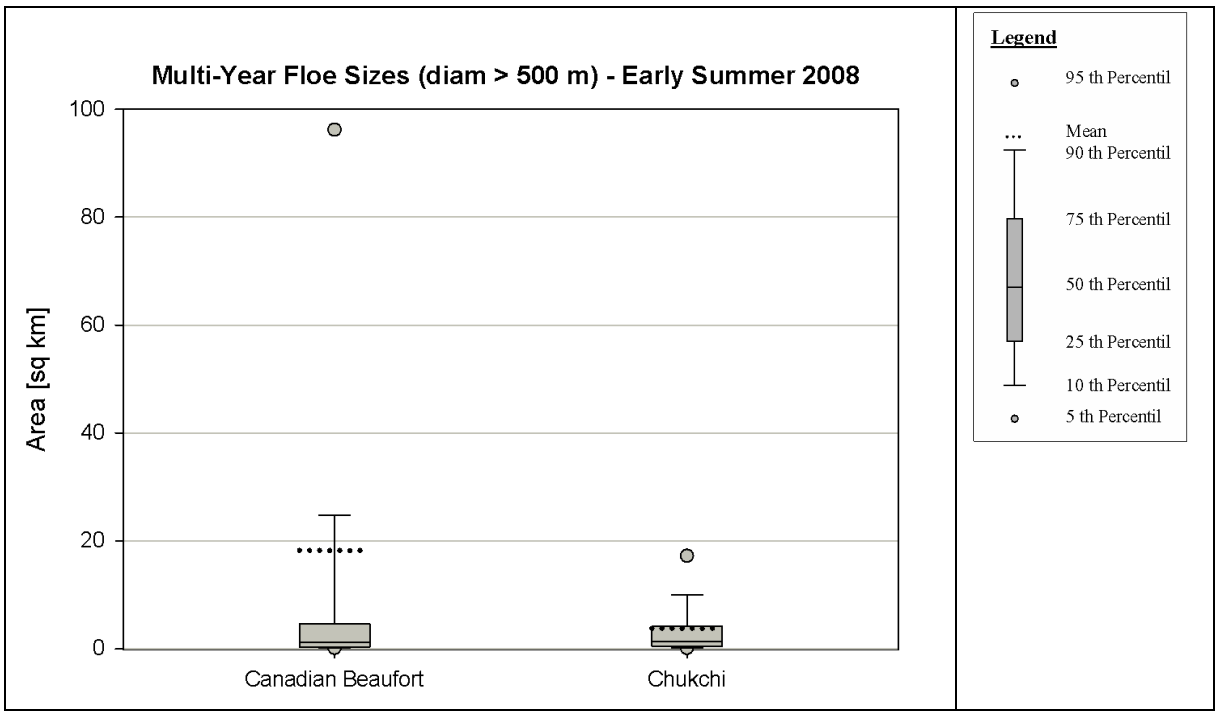

Figure 6-36 M-Y Floe Area for two areas in early summer

The many small floes in the Mackenzie area were the result of deterioration of larger floes due to wave action and melting. It is interesting to note that there were only 30 floes detected in the Chukchi Sea image that were less than 500 m across, while in the Mackenzie area there were 1,317 such floes. This difference can be appreciated in Figures 5-5, 5-16 and 5-19.

6.5.3 Seasonal Variations

The deterioration of M-Y floes in the open water season is well known from experience. When the melt season is underway, poorly consolidated first year ridges will deteriorate, and large conglomerate multi-year floes will break down into progressively smaller floes. As the first-year ice melts out in the summer the multi-year floes become surrounded by open water. Wave action breaks down the floes even more until some melt away completely. The larger multi-year floes will survive until the next winter.

Figure 6-37 compares the floe diameter distributions for mid-winter, late winter, early summer and late summer for the Canadian Beaufort Sea. Progressive deterioration over time is demonstrated by the decreasing values of the diameter at various exceedence levels.

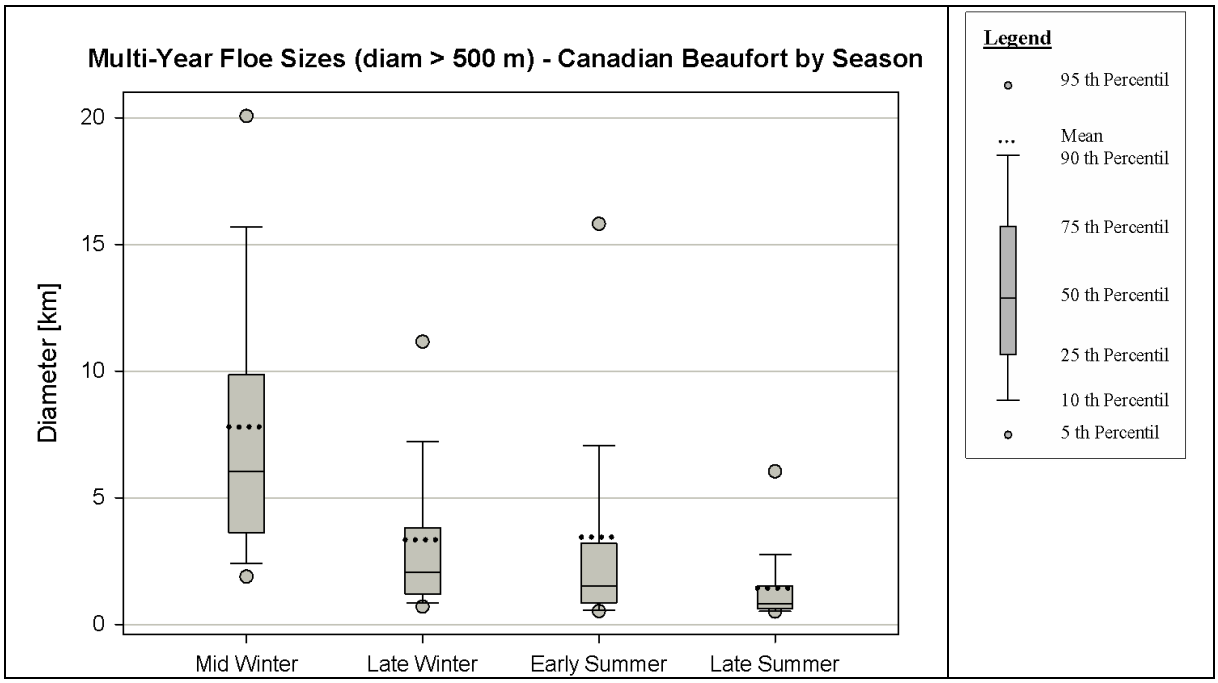

Figure 6-37 M-Y Floe Diameter progression from winter to summer 2008

Multi-year floes in mid-winter reached 55 km in diameter and averaged 7.8 km. The median was 6 km.

During late winter (early June) the average size of M-Y floes along the perimeter of the Beaufort Gyre decreased to 3.4 km with a median of 2 km. However, the largest floes were still more than 40 km across.

In early summer (August) the average floe size was similar to June at 3.5 km. though the median fell to 1.5 km. However some very large floes up to 40 km in diameter persisted in the area.

The Radarsat 2 image from late September captured a multi-year ice incursion in the operational area north of the Mackenzie Delta and did not include the main pack ice edge. As would be expected the M-Y floes in the sample were highly deteriorated with an average diameter of 1.4 km and a median of 800m (for those floes more than 500m in diameter). The largest floes were 8-10 km in the longest dimension. Since the image was a Radarsat-2 Wide image with a 30m resolution, it was possible to detect a large population of very small floes. Considering all floes the average diameter was 240m and the median just 75m.

6.5.4 Comparison with Previous Data

There are two previous studies of M-Y floe size available for comparison with the data from the present study. These are a late-season survey in the Canadian Beaufort Sea by Arsenault (1980) for Dome Petroleum, and a mid-winter survey of the Alaskan Beaufort Sea by Canatec (1990) for Amoco and partners in AOGA study 380.

In September/October 1980 a multi-year ice incursion occurred in the operations areas of the Canadian Beaufort Sea. The ice cover was surveyed by side looking airborne radar, or SLAR, and results were reported by Arsenault, (1980). These results were then used as a basis for design criteria in the Beaufort Sea EIS (1982) and in APOA 205 (1984). The 1980 and 2008 results for September are compared in Table 6-10.

Table 6-10 M-Y Floe Diameter in late September - Comparison 1980 and 2008

Study	Arsenault	Present Study
Year	1980	2008
Date	25-Sept	27-Sept
Sensor	SLAR	Radarsat2 Wide
Resolution	500m	30m
Cut-off Size	500m	500m
Sample Size	566	130
Median diameter (km)	1.5	0.8
Mean diameter (km)	2.1	1.4
99 percentile diameter (km)	9	8
Maximum diameter (km)	26	9.8

The surface area surveyed was similar in both cases. Though the maximum floe detected in 1980 was much larger than in 2008, the rest of the large floes were on the order of 7 to 11 km in diameter – similar to the 9.8 km maximum floe in 2008. The 99% value that would be used for design is remarkably similar in the two cases: 9 km vs 8 km. The smaller median and mean values in the present study could be a result of better resolution of the satellite imagery

In February 1990 the Atmospheric Environment Service of the Canadian government surveyed the Canadian and Alaskan arctic offshore ice conditions using the STAR-2 synthetic aperture radar system. Canatec analyzed and reported on multi-year floe sizes in the Alaskan offshore in AOGA 380 (1990). The present study was based on a MODIS image from offshore Alaska on 7th March 2008 as described in section 5.4.4. Table 6-11 shows the comparison.

Table 6-11 M-Y Floe Diameter in mid-Winter – comparison 1990 and 2008

Study	AOGA 380	Present Study
Year	1990	2008
Date	2-Feb	7-Mar
Sensor	SAR	MODIS
Resolution	25m	250m
Cut-off size	60m	500m
Sample size	~18,000	1101
Median equivalent diameter (km)	0.6	4.4
Mean equivalent diameter (km)	1.2	5.7
99 %ile equivalent diameter (km)	11.4	20.9
Maximum equivalent diameter (km)	39.3	45.8

The equivalent floe diameter was used as a basis of comparison. Maximum floe size was similar in the two samples. The mean, median and 99 percentile equivalent diameter values were considerably smaller in the 1990 study compared with the present study. This is probably a result of the much finer resolution of the SAR imagery compared with MODIS.

7 OLD ICE CONCENTRATION

7.1 Ice Concentration statistics.

Old ice concentration is one of the factor that influences the calculation of impact rate by multi-year floes and ridges in summer and winter. The Canatec ICE2008 database program was utilized to generate contours of old ice (second year and multi-year) in the region from the Chukchi Sea to Northern Banks Island. Contours for each month were first generated and summary statistics for a complete year, a winter period (November to July) and a summer period (August to October) were then created. Figure 7-1 shows the yearly results. Figures 7-2 and 7-3 show the data for winter and summer respectively.

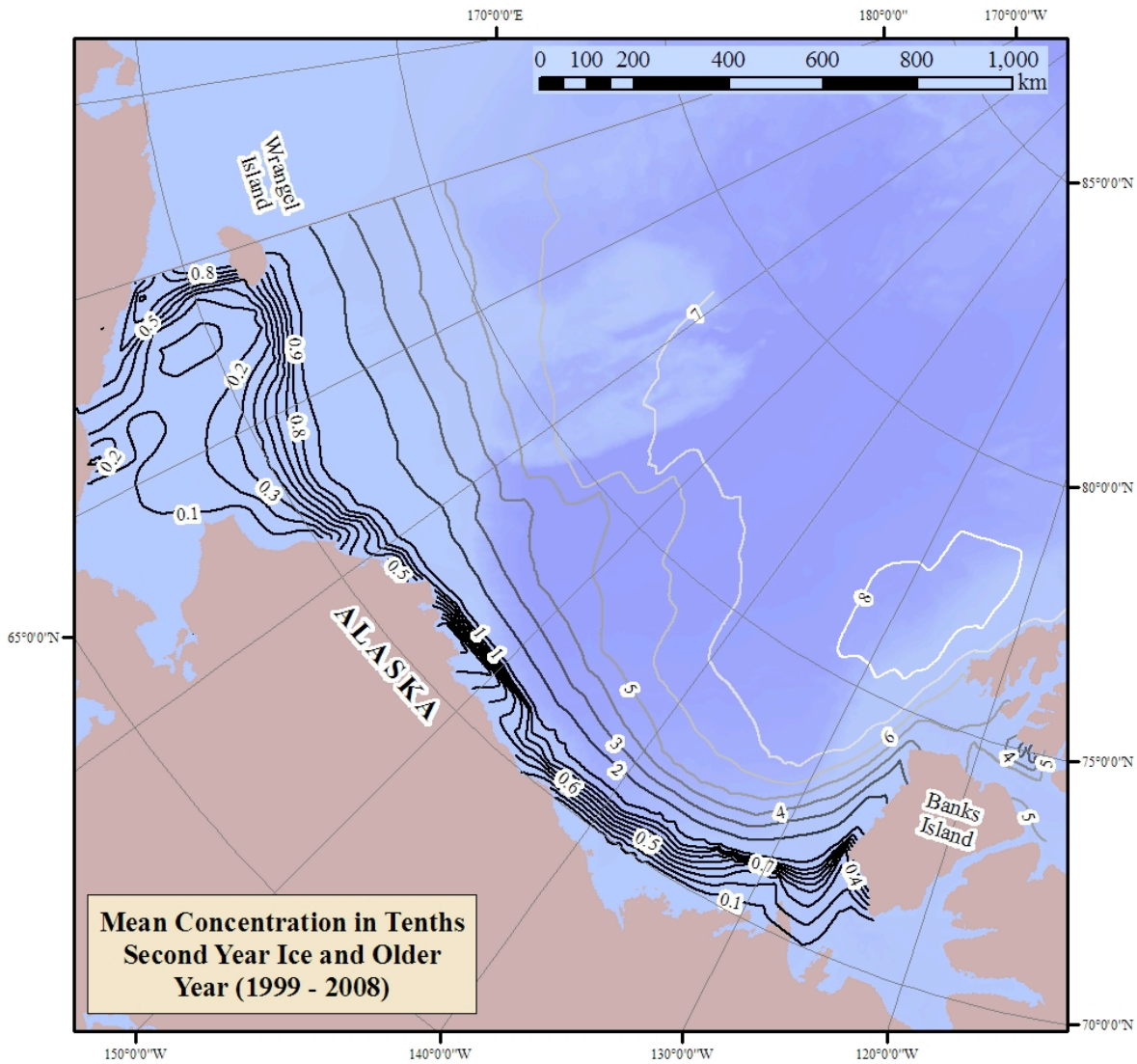

Figure 7-1 Annual Old Ice Concentration Contours from 1999 to 2008

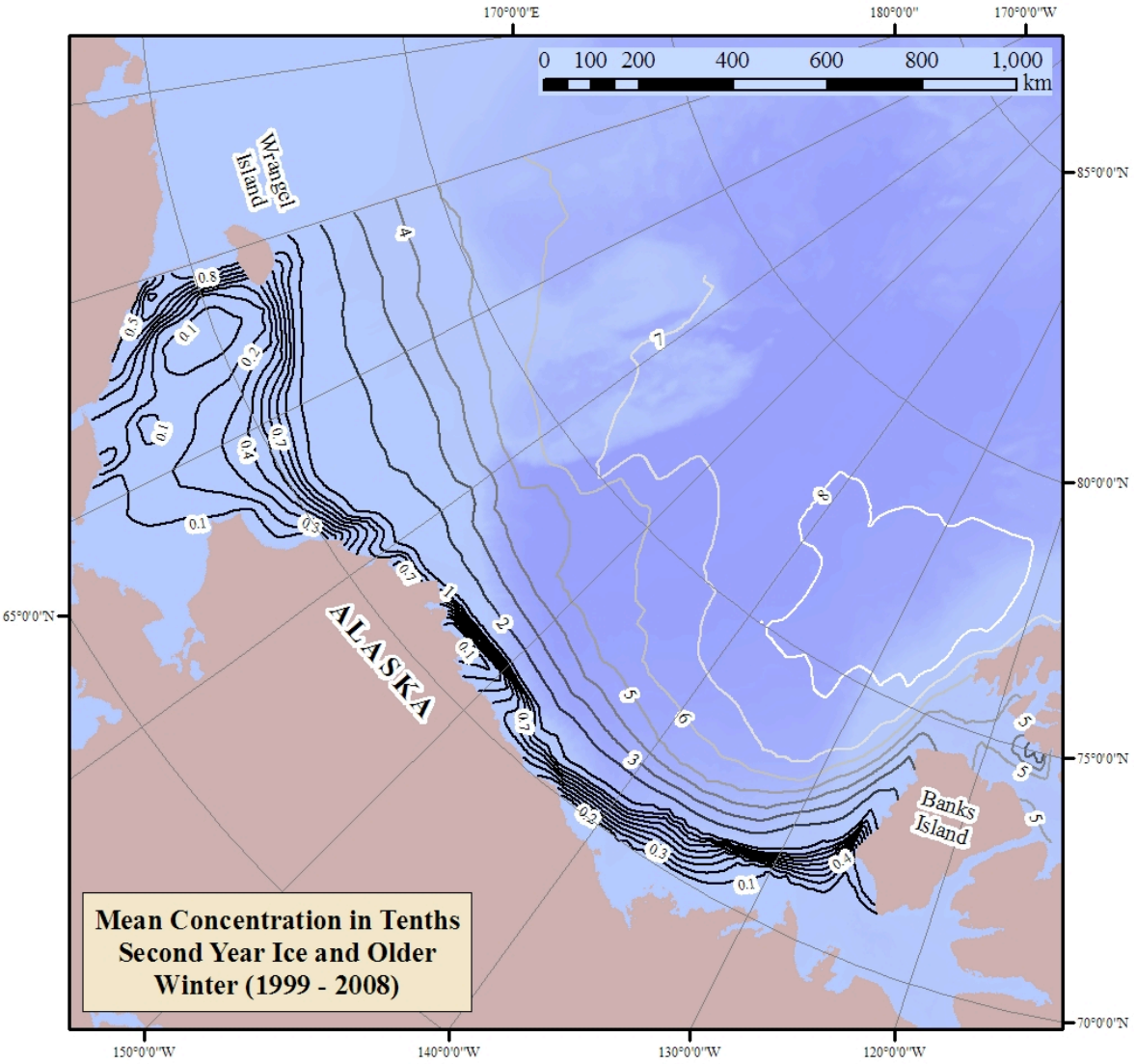

Figure 7-2 Winter Old Ice Concentration Contours from 1999 to 2008

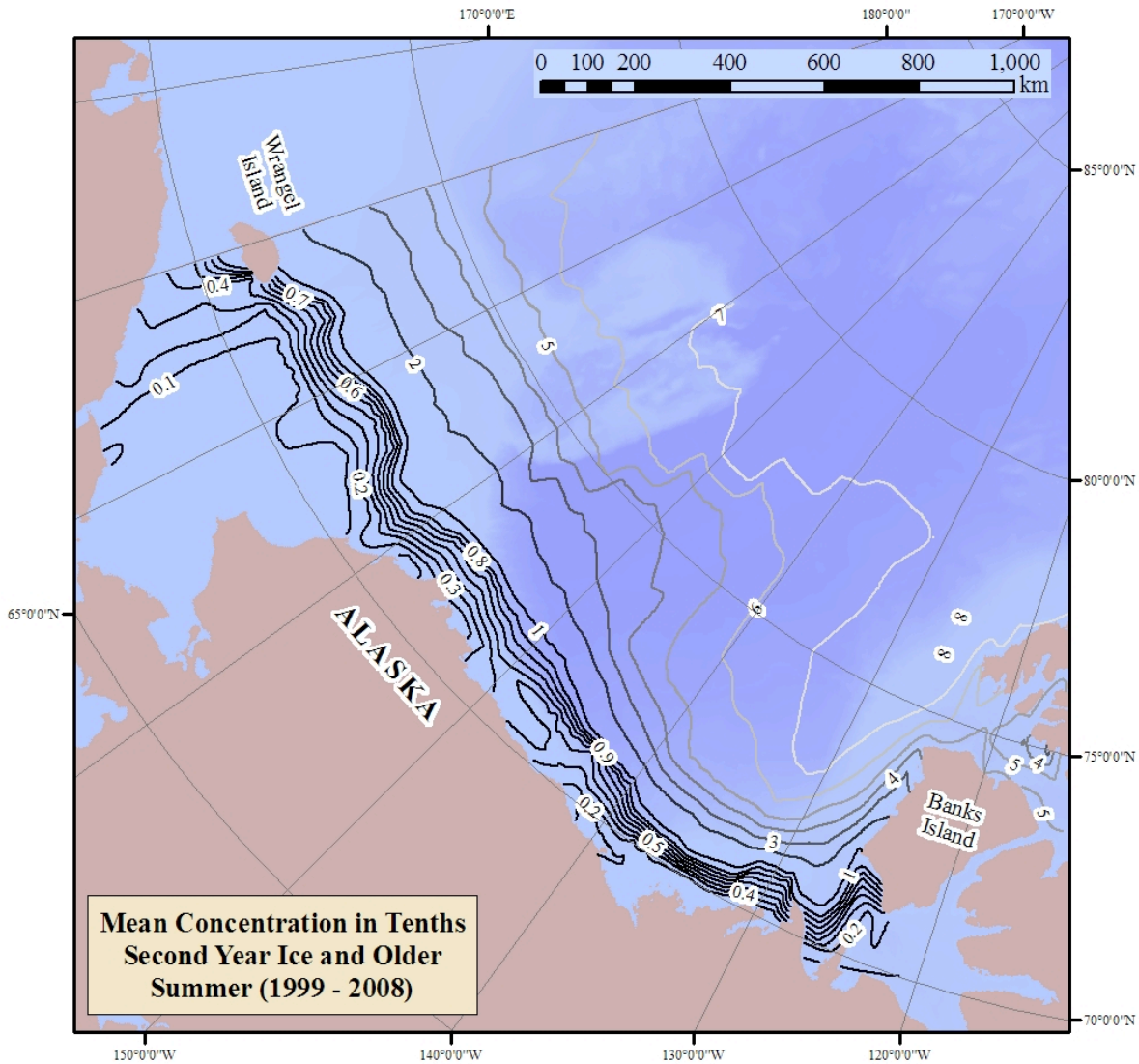

Figure 7-3 Summer Old Ice Concentration Contours from 1999 to 2008.

7.2 Changes in Old Ice Concentration

Figure 7-4 shows a comparison of Ice concentration statistics contours between 1969-79 and 1999-2008 (~30 years apart) for the Canadian Beaufort Sea. The contours have moved NNW approximately 25-50 km at a minimum. The decrease in M-Y ice concentration decreases the probability of impact between an EIF and a fixed structure anywhere in the area compared to previous studies.

Similar comparisons were not made for the Alaskan Beaufort or the Chukchi Seas.

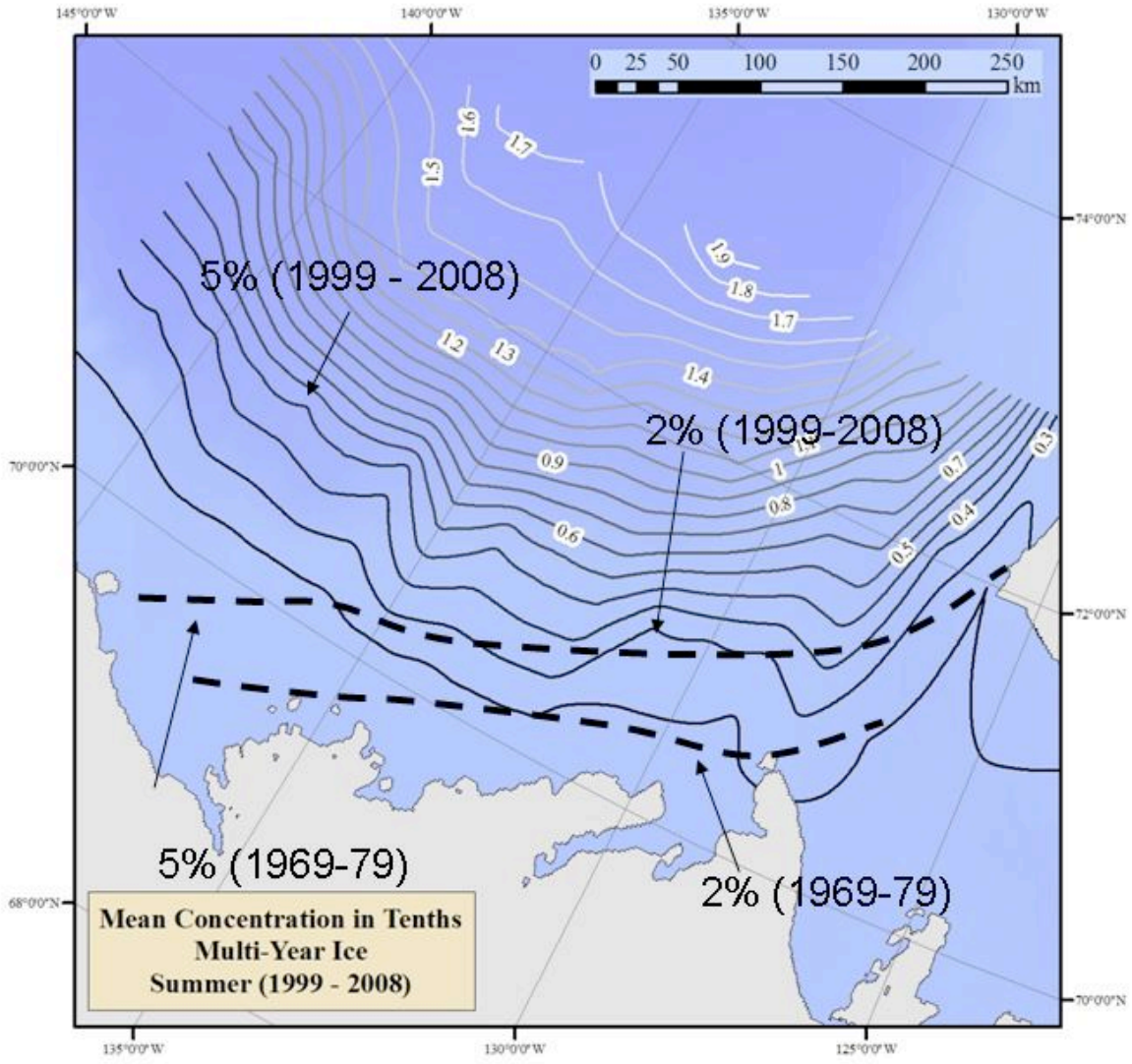

Figure 7-4 Summer Multi-Year Ice Concentration 1970s and 2000s Canadian Beaufort

8 OLD ICE THICKNESS FROM ULS and IPS

8.1 ULS Data Source and Initial Processing

Data from the submarine run referred to as 2000a was obtained from the National and Ice Center (NIC) in Boulder Colorado. The data was obtained between the 10th and 30th of October 2000. Figure 8-1 shows the locations of the 84 segments of data utilized for this work. The primary data provided was length from the start of the segment and draft. The 84 data sets were modified in Excel to include mid-point latitude and longitude of the segment. These were then combined into one large text file and quality checked in MS Access.

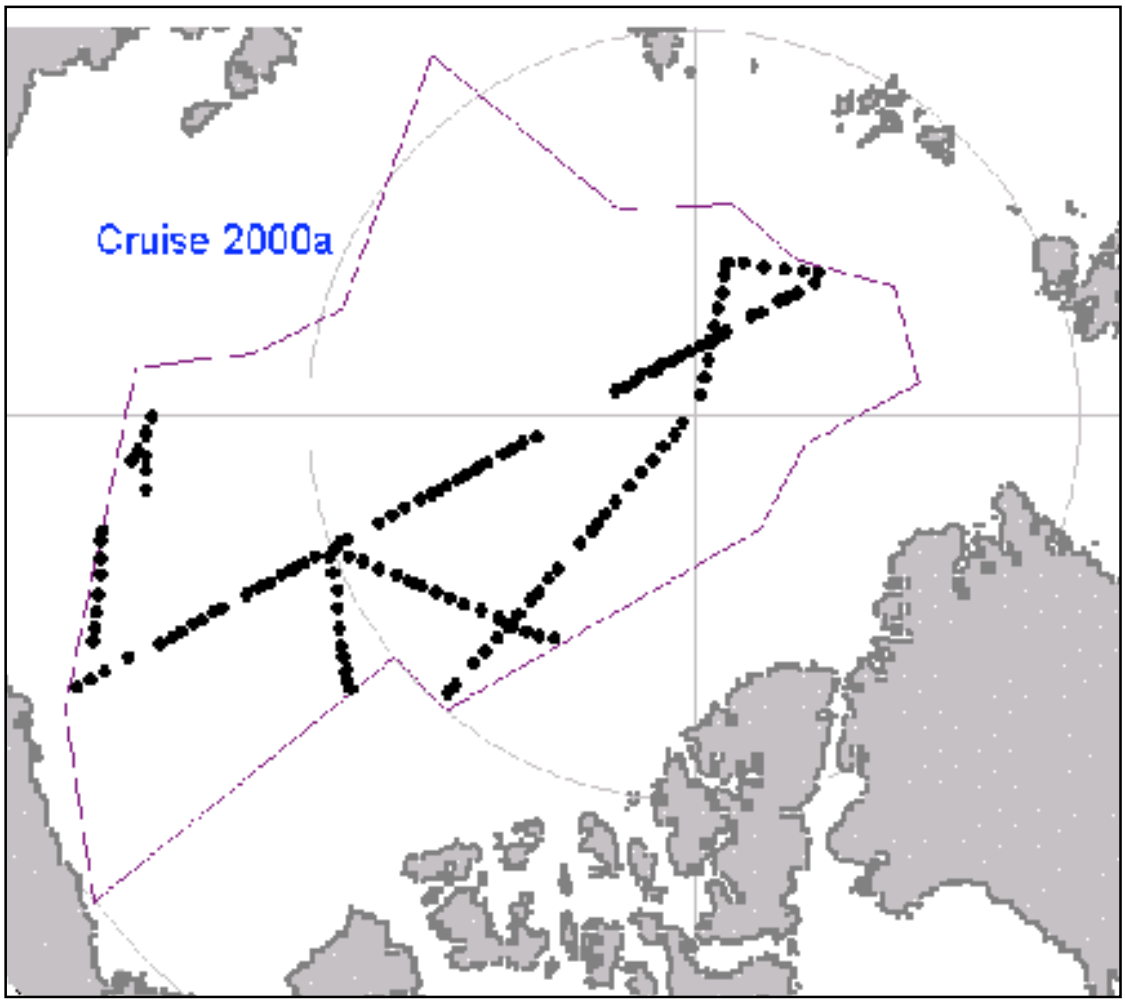

Figure 8-1 Upward looking sonar Submarine Cruise October,2000

8.2 ULS Data Grouping and Gaps in the Data

The 84 data sets were grouped into a continuous text file, which was then separated by querying the Latitude and Longitude in MS Access. Figure 8-2 shows the six areas analyzed.

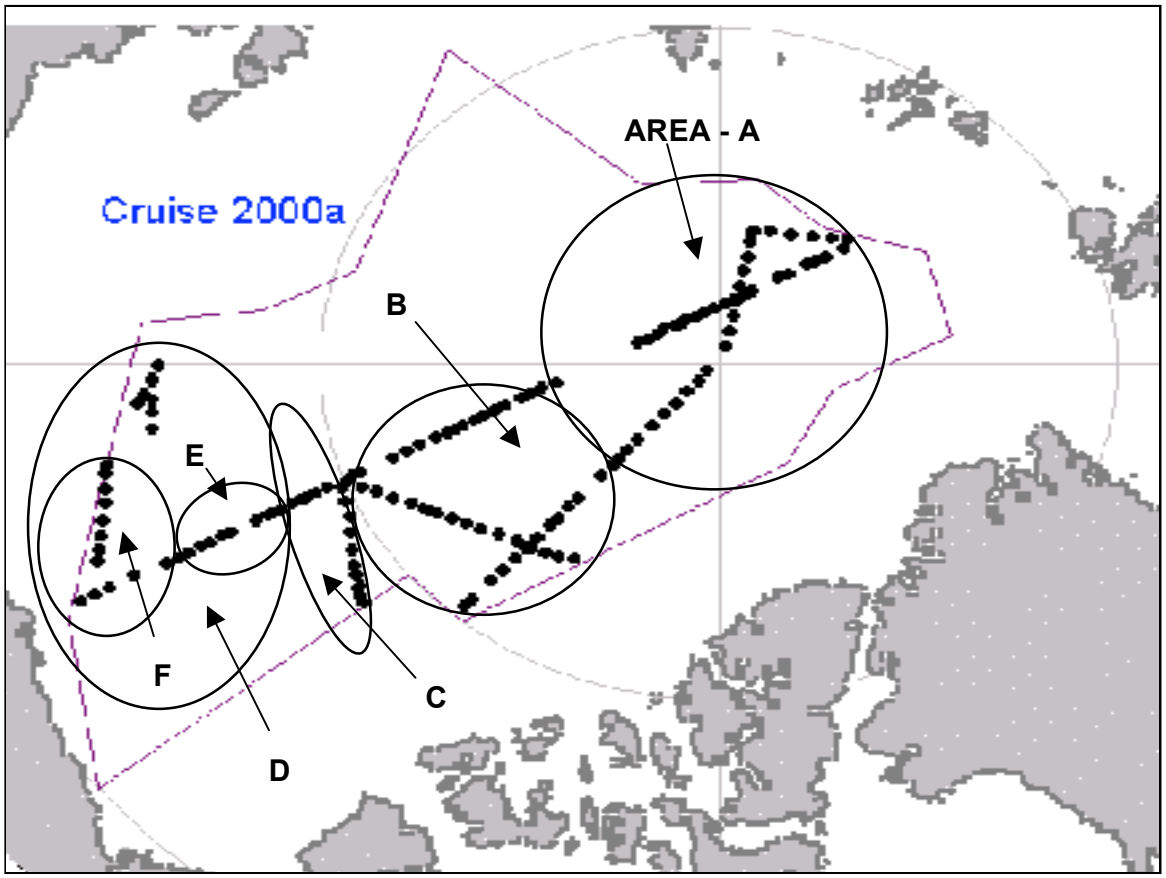

Figure 8-2 Areas Analyzed for the 2000a Submarine Data

After the data were combined for each of the different areas a preliminary analysis for each of the different areas was conducted. Table 7-1 shows some of the data obtained.

Table 8-1 Draft data for Different Areas of the 2000a Submarine Transect

Area	# Drafts	Average Draft	Average Draft>1m	Minimum Draft	Maximum Draft
A	509,386	2.02	2.47	-0.61	23.9
B	559,259	2.33	2.54	-0.39	19.6
C	225,306	1.70	2.22	-0.5	15.3
D	586,529	1. 04	2.26	-1.1	15.3
E	292,713	1.54	2.26	-0.5	15.3
F	93,000	0.34	2.02	-0.39	12.51

Note: The negative Minimum Draft is a good indication of data accuracy.

The dataset was then sorted to identify gaps in the data. The largest gap was over 5 km and all gaps greater than 42m were inspected to determine if terminating the floe at the gap would have any influence on the resulting statistical analysis. Only one gap 154 m wide at 88.25 N and 150.1 E (as shown in Figure 8-3) with width greater than 42 m was left in the dataset.

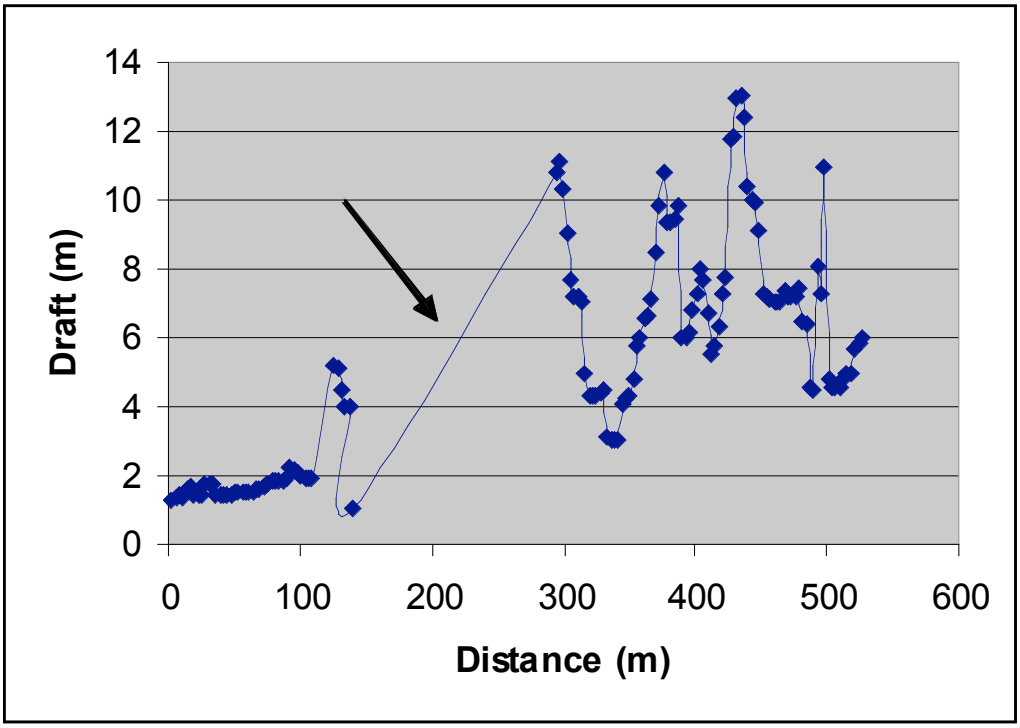

Figure 8-3 Gap in the 2000a Dataset at 88.25 N and 150.1 E

The normal horizontal distance between sonar returns ranged from 0.7 m to .3 m depending on the speed of the submarine. Gaps with drafts greater than 1 m and widths less than 42 m were left in the dataset. One of the deeper draft feature gaps is shown in Figure 8-4.

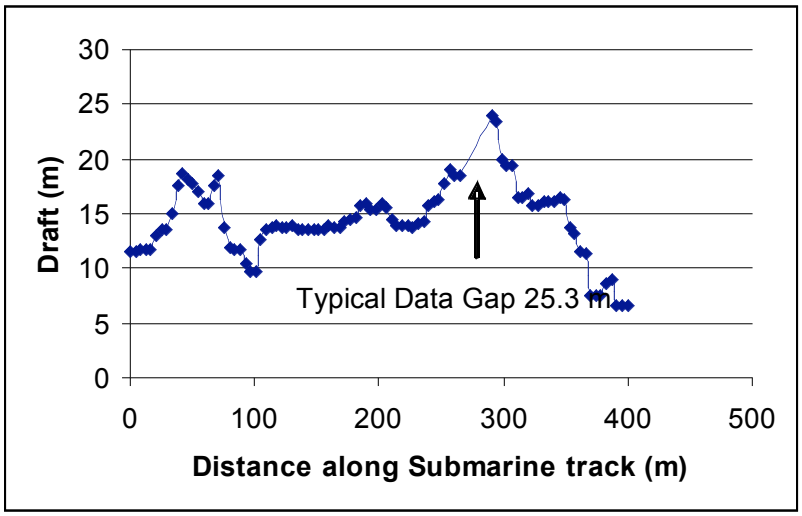

Figure 8-4 Typical Data Gap in the 2000a sonar data.

8.3 ULS Data Analysis and Parameter Definitions

8.3.1 Data Analysis Procedure and Disposition of Data Plots

Routines were created in MATLAB to analyze the different datasets. The data were first read in and an equalized horizontal distance dataset was created for each data file. That is the original data were reformatted into data sets with equal horizontal distances. Plots of the original data and the re-sampled data are provided in the folder on the accompanying hard drive (HD): Upward Looking Sonar Data\2000a Submarine Cruise\ Area… \ All Data Plots and Resampling Plots. The data were then analyzed for floe, thin ice, and ridge statistics and text files were created for all of the statistics. These can be found on the accompanying HD under: Upward Looking Sonar Data\2000a Submarine Cruise\ Area… \Database Text Files. Figure 8-5 shows a typical floe plot contained on the HD. The ridge locations and associated ridge index numbers are provided on the upper chart in this Figure.

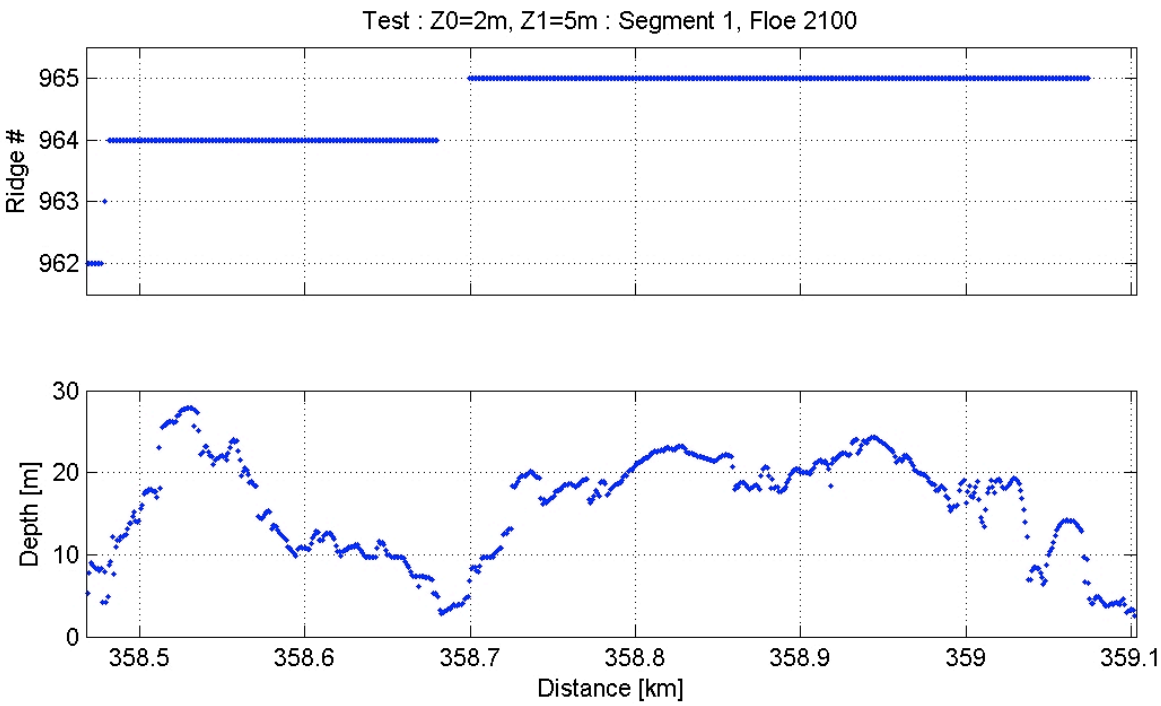

Figure 8-5 A Typical Floe Plot (contained on the HD)

8.3.2 Alternative Ridge and Floe Definitions

Two different analyses of the data are provided on the HD. Firstly the data were analyzed using a 5 m draft cutoff definition for a ridge and a 1 m draft cutoff for a floe. Since the data were collected in October of 2000 it was felt that only analyzing ice that was greater than 1 m would account for old ice that had survived at least one summer season. That is, since the freezing season in the Arctic had just begun in September, the new first year ice would not have reached a thickness of 1 m by late October. The 5 m draft cutoff for ridges is a normal value used by other researchers, e.g. Melling et. al. (1995).

In the first analysis ridges were defined as only ice with draft greater than 5 m. In the second analysis ridges were initially identified as being greater than 5 m and then the

Rayleigh Criterion (50% decrease in draft) was used to define the ridge end point. The start and end points for a Rayleigh ridge were taken back to where the ice leveled out (or increased after decreasing 50%. Figure 8-6 shows a 5 m cutoff ridge and a Rayleigh ridge. Note: that plots of all floes and ridges for both definitions are provided under the different areas on the hard drive.

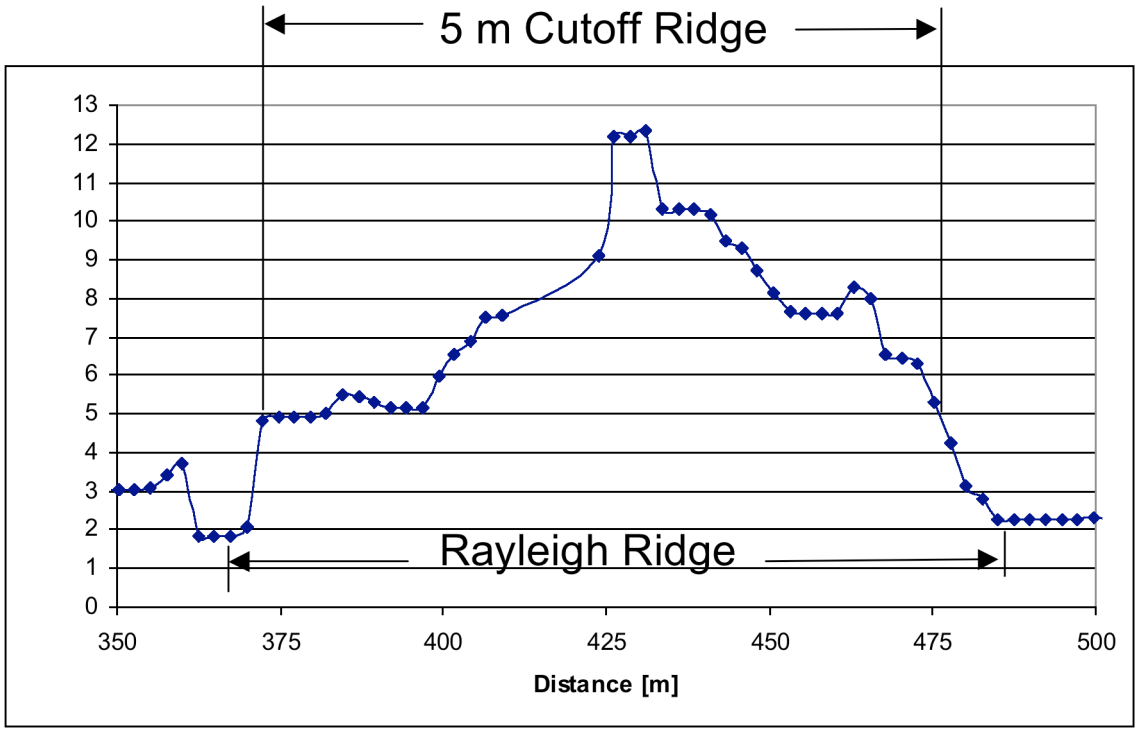

Figure 8-6 Plot of a 5 m Cutoff Ridge and a Rayleigh Ridge

8.3.3 Standard Deviation of 5m Cutoff and Rayleigh Ridges

A comparison of the accuracy of the two different ridge analyses was undertaken. One of the ridge parameters calculated is the standard deviation of ridge draft. This parameter calculates the statistics of how accurate the actual ridge profile at each point along the ridge matches the profile as modeled by a line between the start and end points of the ridge and the Ridge peak. Each ridge gives a single standard deviation. Figure 8-7 shows the analysis for 5 m Cutoff ridges on the top and the analysis for Rayleigh ridges on the bottom. The ridge draft standard deviations have a mean of 0.6 m (and Std. Dev. of 0.57 m) for the Cutoff Analysis and 1.51 m (and Std. Dev. of 0.65 m) for the Rayleigh Analysis. The 5 m Cutoff Analysis models the ridges better (at each point along the ridge) by 0.9 m on average. This is due to the fact that the Rayleigh Ridges in most cases includes ice below 5 m draft. It is noted that the lognormal distribution fits the Rayleigh ridges better at higher standard deviations.

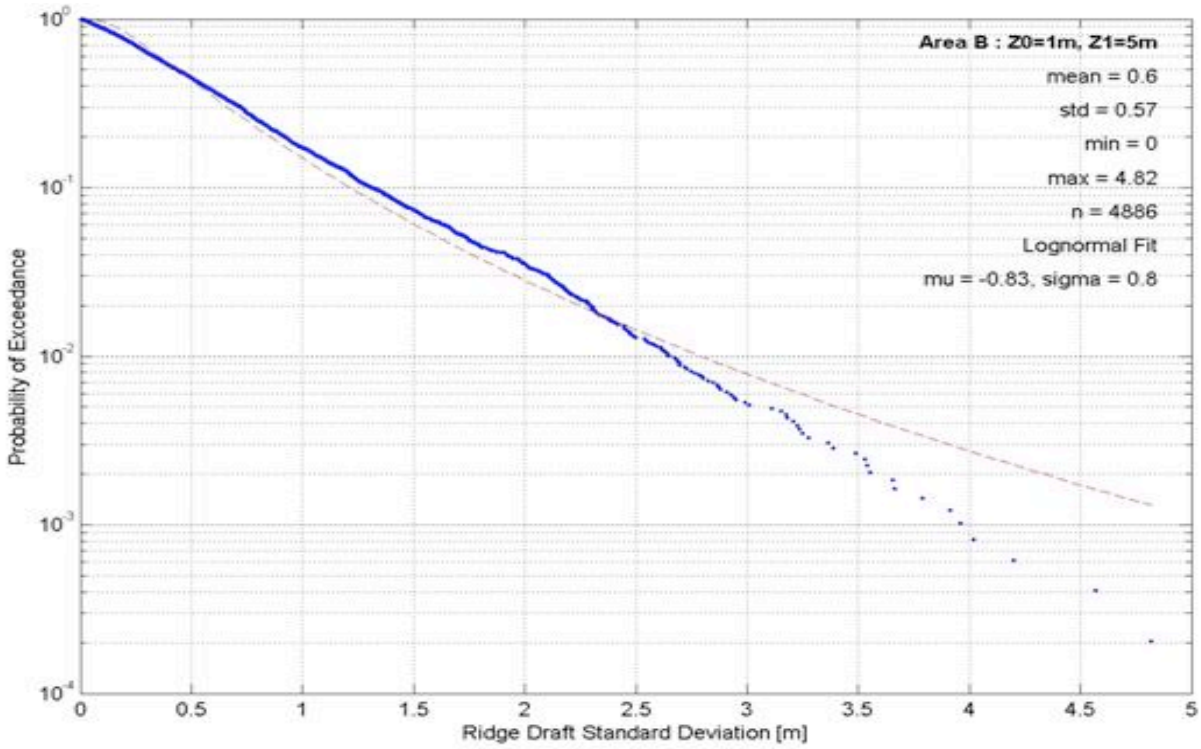

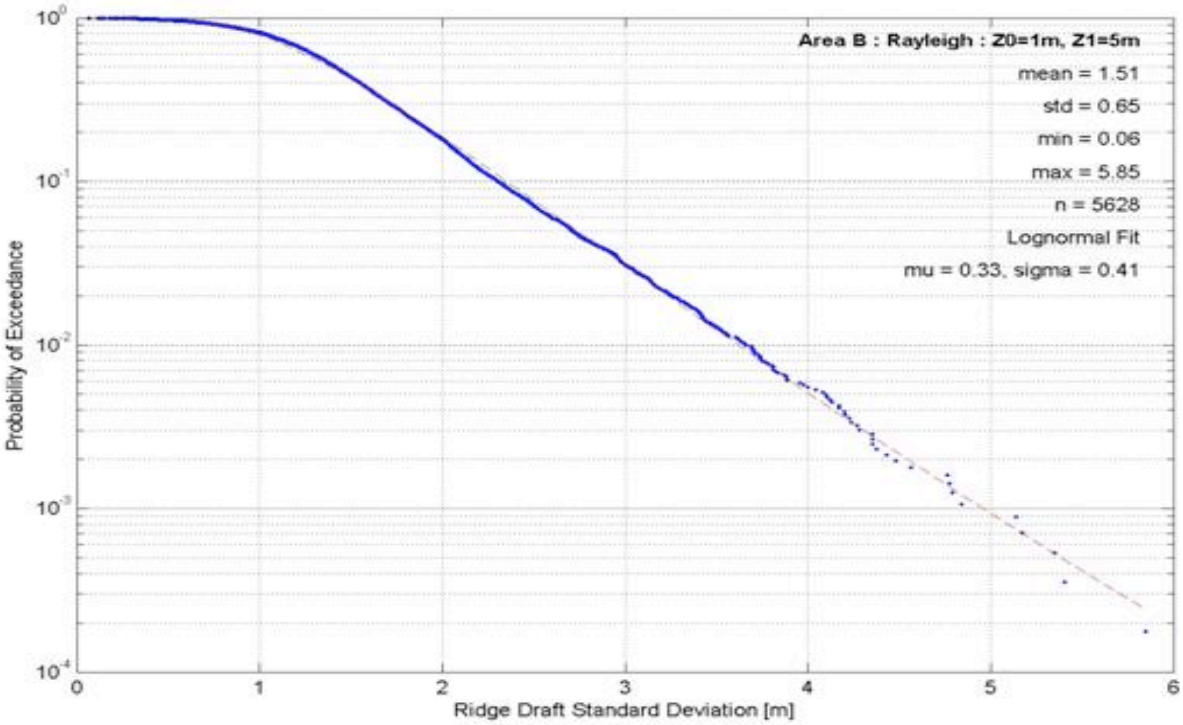

Figure 8-7 Comparison of the Standard Deviation of Ridge Draft for Cutoff (upper graph) and Rayleigh Ridges (lower graph)

8.3.4 Data Base Parameters

The statistical data indicated in Tables below were extracted for all the areas shown in Figure 8-2. Note that the actual information is contained in the txt files under 'Database Text Files' on the HD. The statistics have been created to allow for a comprehensive probabilistic analysis of ice loading on offshore installations and vessels. Figure 8-8 illustrates some of the key parameters used to characterize multi-year floes and ridges.

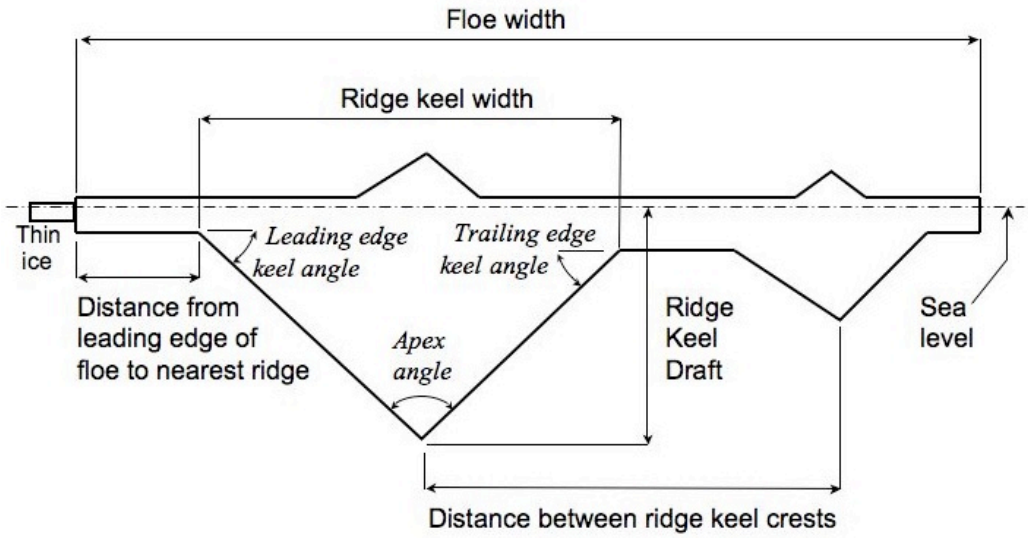

Figure 8-8 Definition sketch of key multi-year floe and ridge parameters

Table 8-2 describes the database of thickness and extent of thin ice regions. Table 8-3 and Table 8-4 list the statistics of parameters relevant to ridges within multi-year floes. Table 8-5 describes the database of multi-year floes, with and without ridges. Table 8-6 lists numbers of floes and ridges found in each Area shown in Figure 8-2

Table 8-2 Thin Ice Statistics contained in the Database files (
(Area _RES_T.txt)

Column	Units	Detail
1		thin ice index
2		data segment containing this thin ice area
3	deg	latitude of thin ice (mid point of segment containing floe)
4	deg	longitude of thin ice (mid point of segment containing floe)
5	m	width of thin ice along track
6	km	along track distance of start of thin ice
7	m	mean thin ice thickness
8	m	standard deviation of thin ice thickness

Table 8-3 Ridge Statistics contained in the Database files
(Area _RES_R.txt and Area _R_RES_R.txt for the Rayleigh Ridges)

Column	Units	Detail
1		ridge index
2	m^2	keel cross section area
3	deg	apex angle
4	m	distance between all ridge crests
5	m	distance from leading edge of floe to leading edge of ridge (even if ridge is not closest one to edge)
6	m	distance from trailing edge of ridge to trailing edge of floe (even if ridge is not closest one to edge)
7	m	distance from start of keel to maximum draft
8	m	distance from end of keel to maximum draft
9		index of floe containing this ridge
10		data segment containing this ridge
11	deg	latitude of ridge (mid point of segment containing floe)
12	deg	longitude of ridge (mid point of segment containing floe)
13		lag 1 correlation for ridge keel draft
14		lag 2 correlation for ridge keel draft
15		lag 3 correlation for ridge keel draft
16		leading edge keel angle from horizontal
17		trailing edge keel angle from horizontal
18	m	along track ridge width
19	km	along track distance of start of ridge
20	m	maximum draft of ridge
21	m	standard deviation of ridge draft

Table 8-4 Extra Ridge Statistics contained in the Database files
(Area _RES_RR.txt and Area _R_RES_RR.txt for Rayleigh Ridges)

Column	Units	Detail
1		extra ridge index
2	deg	latitude of ridge (mid point of segment containing floe)
3	deg	longitude of ridge (mid point of segment containing floe)
4		distance between ridge crests within same floe

Table 8-5 Floe Statistics contained in the Database files
(Area _RES_F.txt)

Column	Units	Detail
1		floe index (floe number)
2	m	distance between leading edge of floe and leading edge of first ridge
3	m	distance between trailing edge of last ridge and trailing edge of floe
4	deg	latitude of floe (mid point of segment containing floe)
5	deg	longitude of floe (mid point of segment containing floe)
6		data segment containing this floe
7	m	along track width of floe - all floes
8	m	along track width of floe with ridges
9	km	along track distance of start of floe - all floes
10	m	mean floe draft, including ridges - all floes
11	m	standard deviation of floe thickness, including ridges - all floes
12	m	mean floe thickness, excluding ridges - all floes
13	m	standard deviation of floe thickness, excluding ridges all floes

Table 8-6 Number of floes and Ridges Found

AREA	# of Floes	# of Rayleigh Ridges	# of 5 m Cutoff Ridges
A	6,459	4,696	4,653
B	4,967	5,630	5,568
C	4,860	1,087	1,078
D	9,993	1,674	1,661
E	6,330	1,328	1,317
F	717	30	30
Totals	33,326	14,445	14,307

8.4 Summary Plots for Area D, Alaskan Beaufort Sea

In total, 26 summary plots were created for each area of the 2000a data for both the 5m Cutoff and Rayleigh analyses. The figures following show the 5 m Cutoff results for Area D - comprising the Alaskan Beaufort and Chukchi Seas. Plots of ridge geometry parameters are presented first, then floe geometry and finally, plots related to thin ice thickness and extent. Figures 8-9 to 8-22 plot exceedance curves of the ridge geometry parameters in Tables 8-3 and 8-4. In most cases the best fit distribution curve is plotted with the data. The parameters are maximum keel draft, keel width, apex angle, keel angle, distance between ridge crests, distance between ridge crests within the same floe, distance

from the floe edge to the start of a ridge, and keel cross-sectional area. Correlations are plotted between keel width, draft and area. A lag analysis was performed to test whether the ice type could be verified as multi-year. Figure 8-9 plots exceedance of ridge keel draft using data only. Figure 8-10 plots the data with the best fit distribution (gamma). (N.B. It is necessary to add 5m to the value on the x-axis of Figure 8-10).

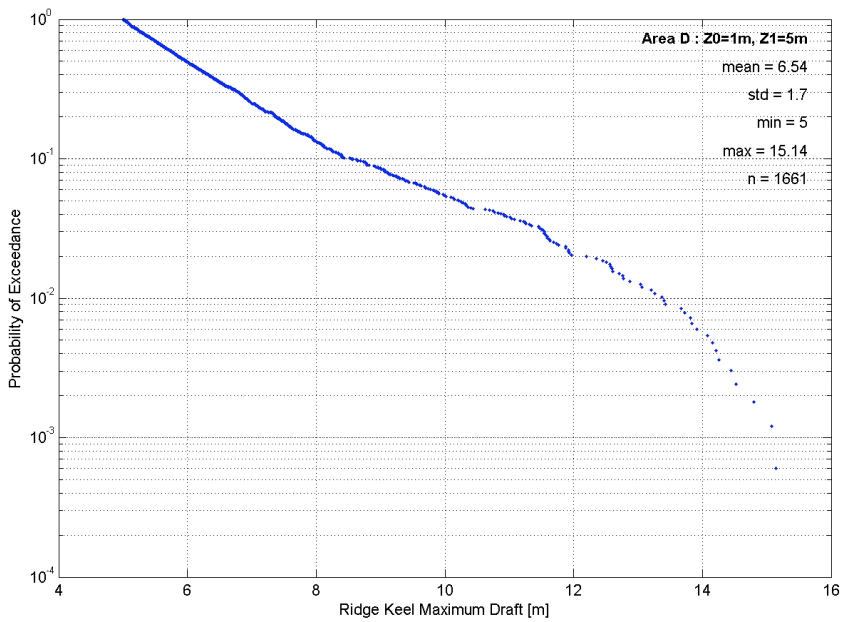

Figure 8-9 Area D Exceedance Plot of Ridge Maximum Draft

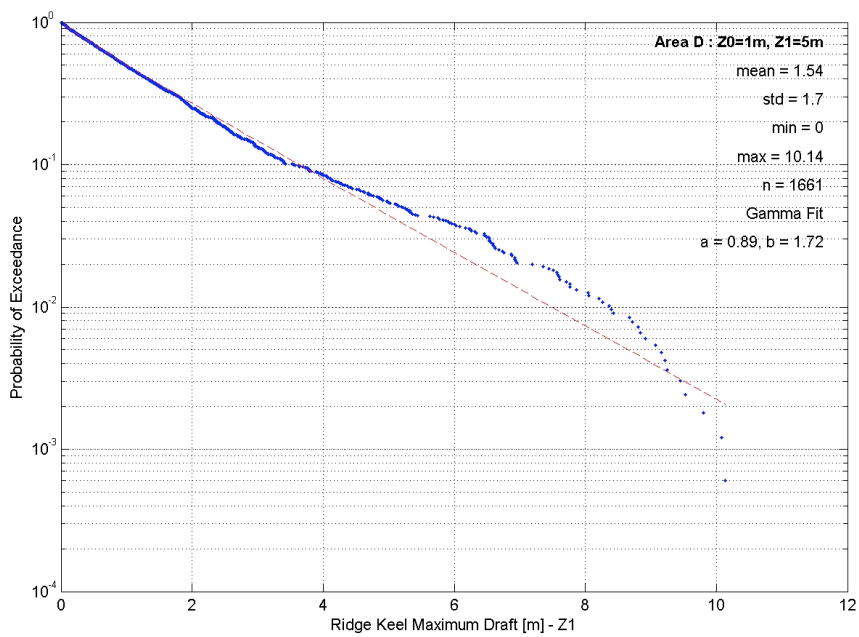

Figure 8-10 Area D Exceedance Plot of Ridge Maximum Draft less 5 m with best Fit

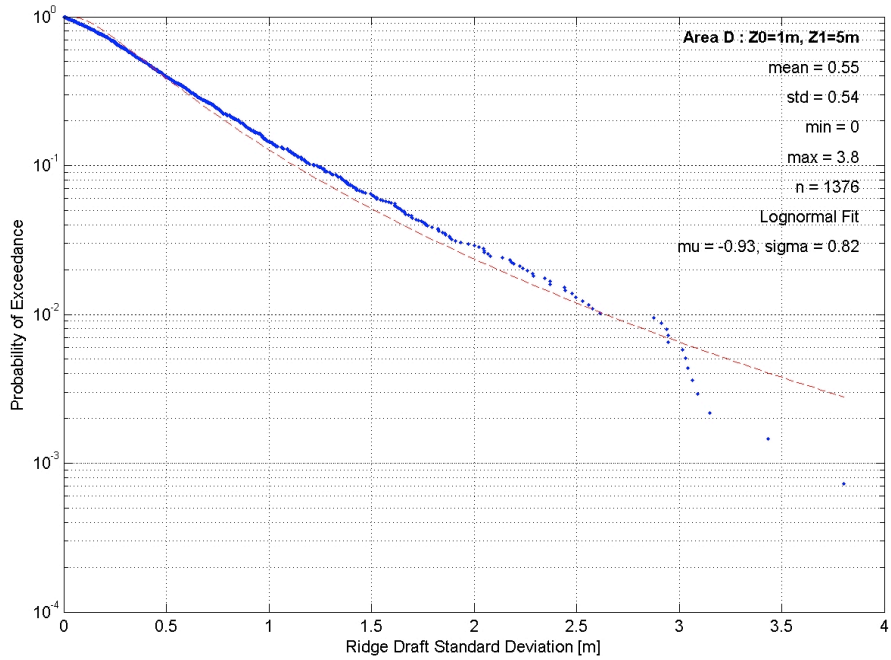

Figure 8-11 Area D Exceedance Plot of Ridge Draft Std. Dev.

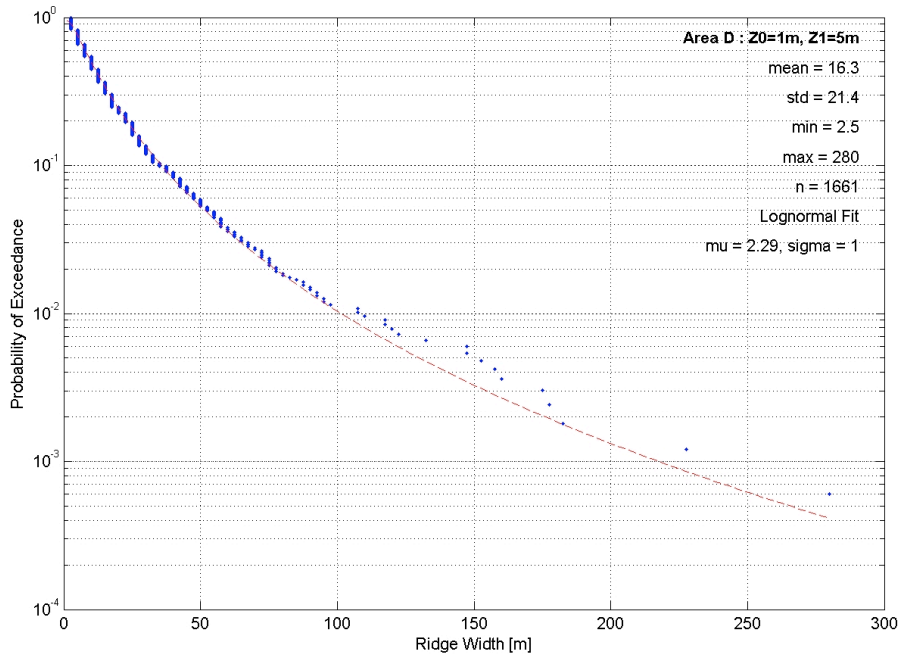

Figure 8-12 Area D Exceedance Plot of Ridge Width

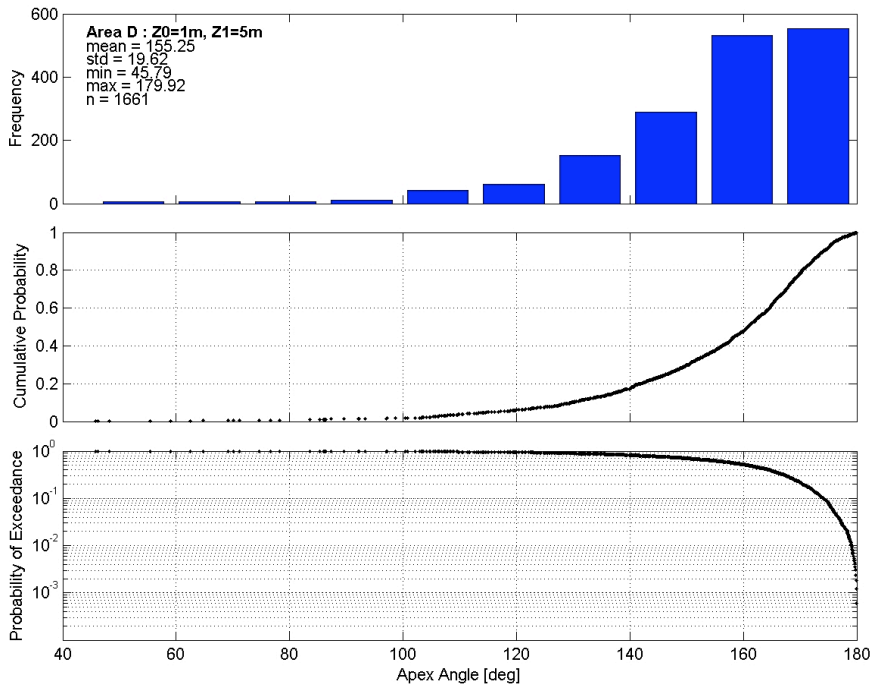

Figure 8-13 Area D Ridge Apex Angle Statistics (mean apex angle of 159 degrees)

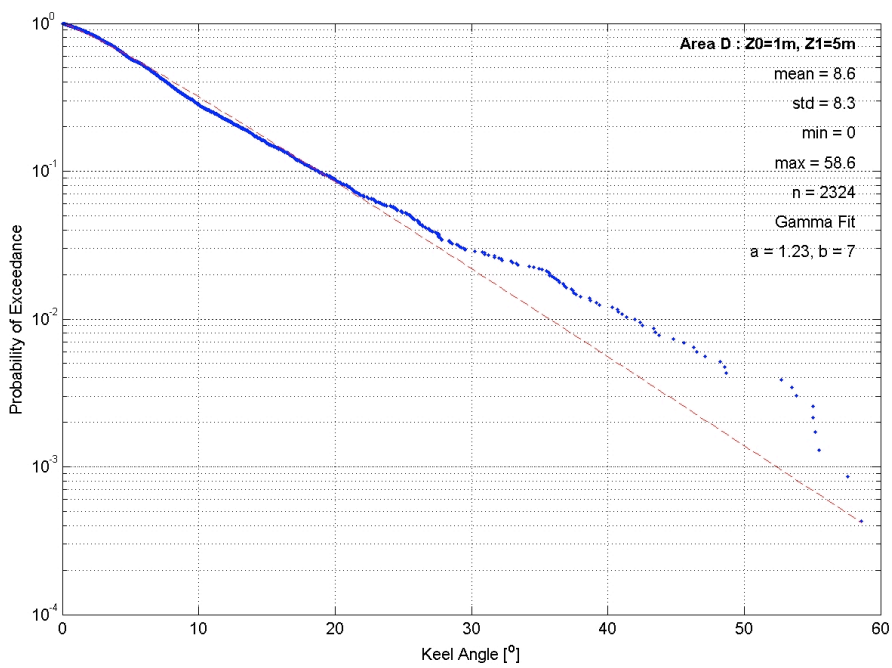

Figure 8-14 Area D Exceedance Plot of Ridge Keel Angle

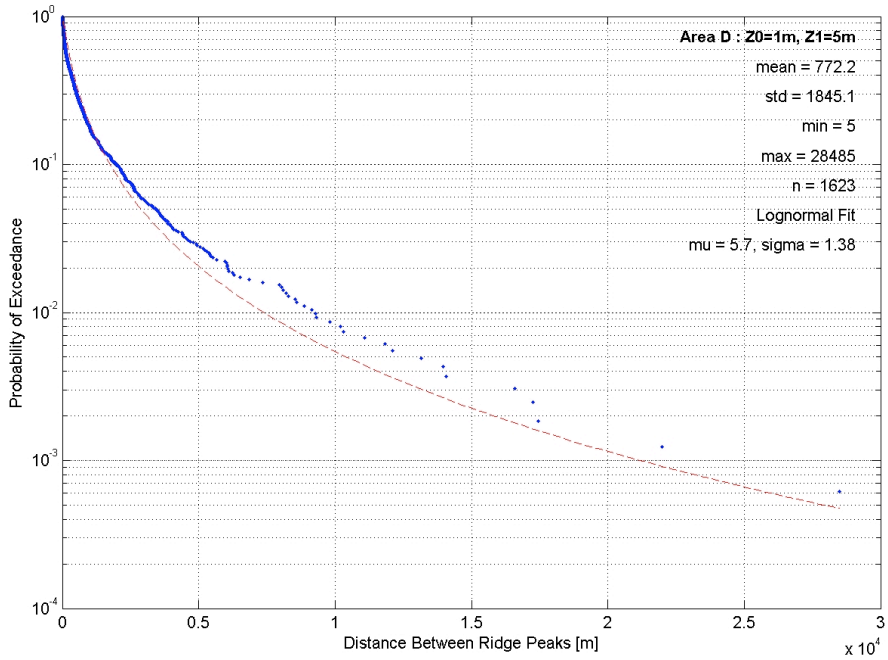

Figure 8-15 Area D Exceedance Plot of Distance (x10⁴ m) between Ridge Crests (a spatial representation of frequency of ridges along a line in an Area including thin ice)

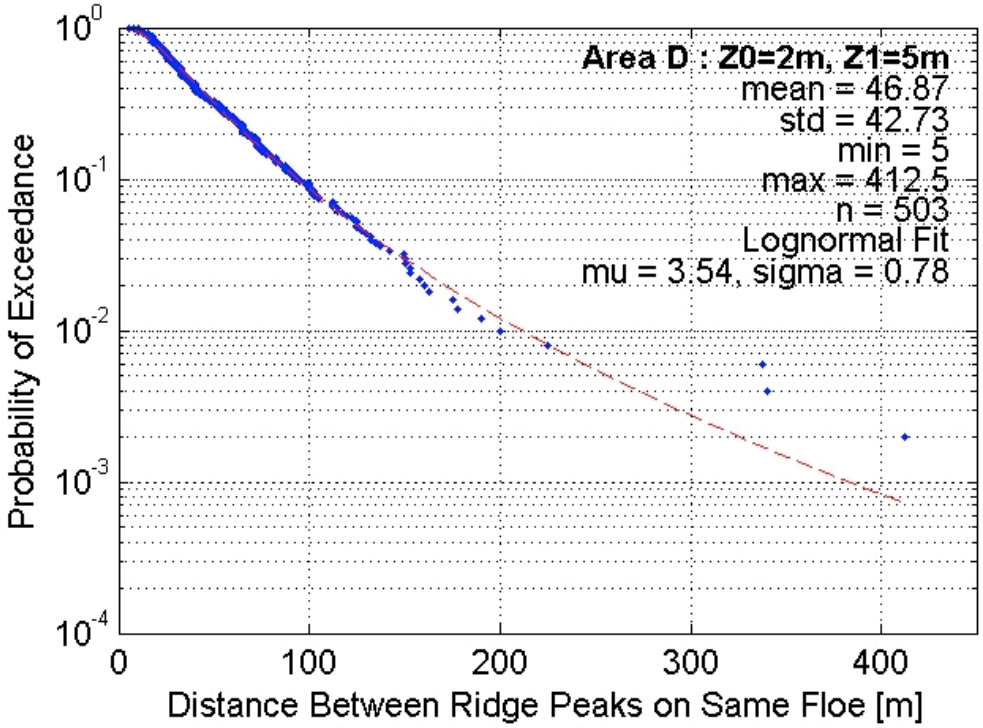

Figure 8-16 Exceedance Plot of Distance between Ridge Peaks on Same Floe

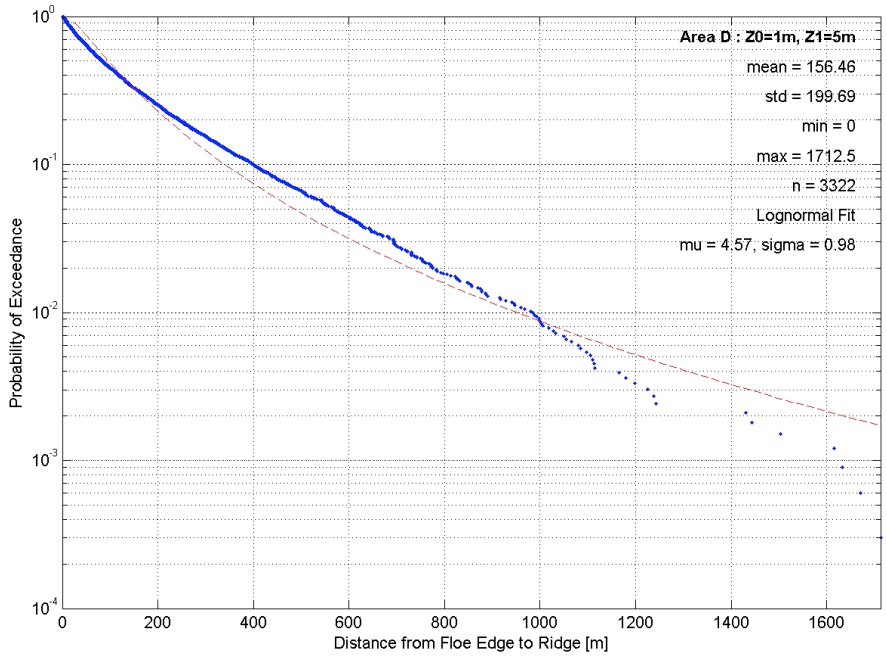

Figure 8-17 Area D Exceedance Plot Distance from Floe Edge to Ridge Starting Point

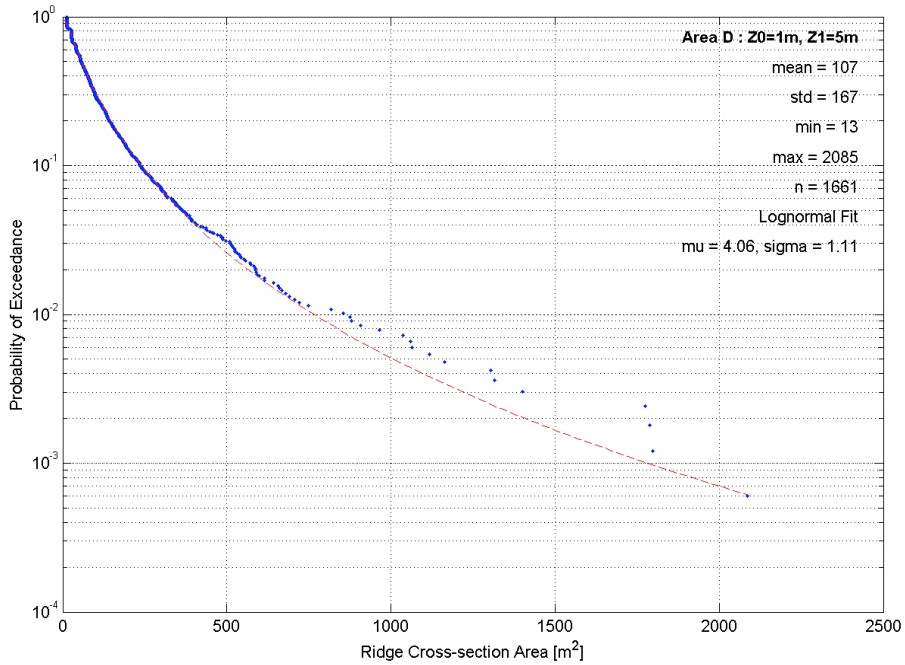

Figure 8-18 Area D Exceedance Plot of Ridge Area

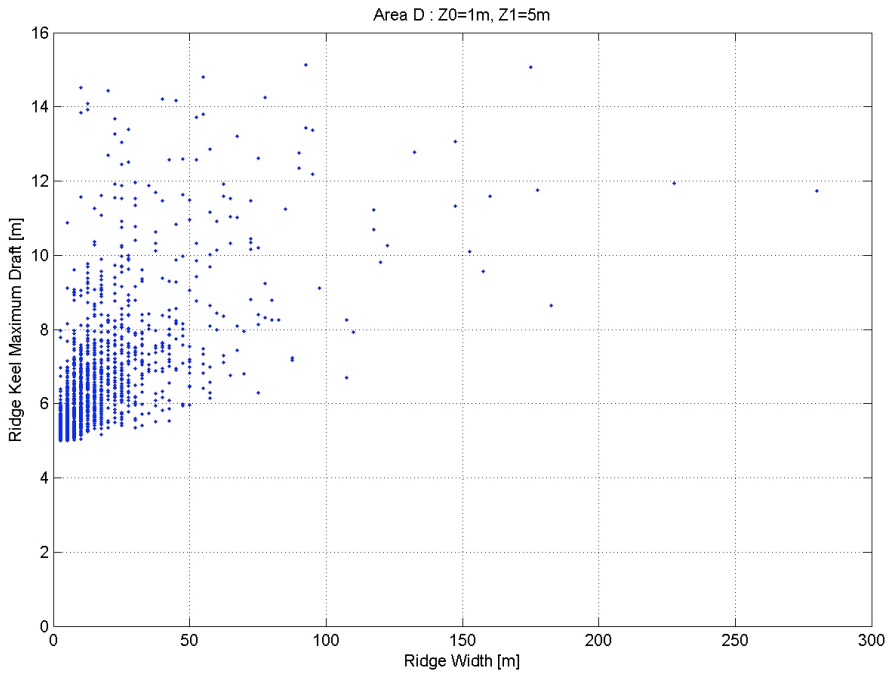

Figure 8-19 Ridge Width vs. Keel Maximum Draft

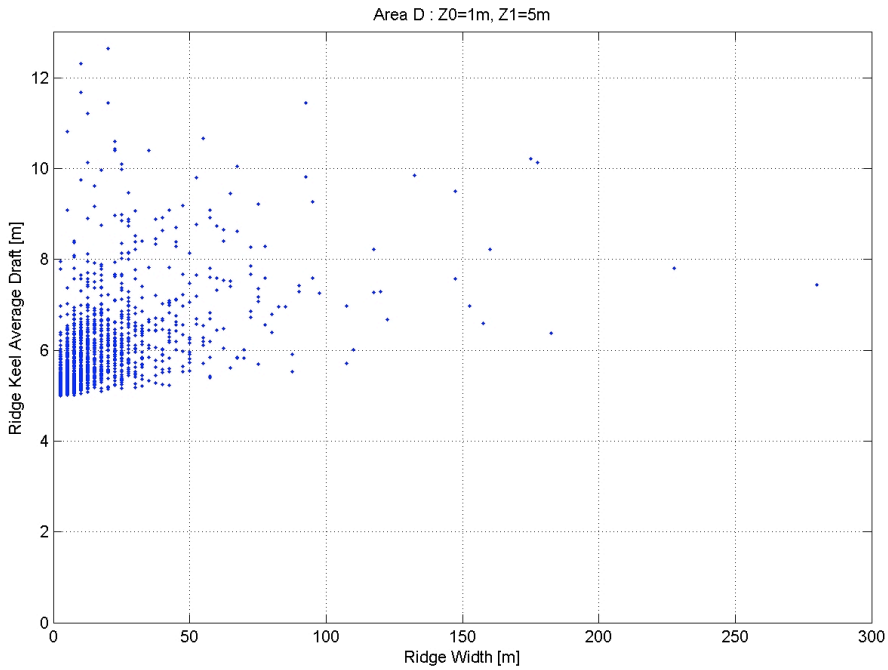

Figure 8-20 Ridge Width vs. Keel Average Draft

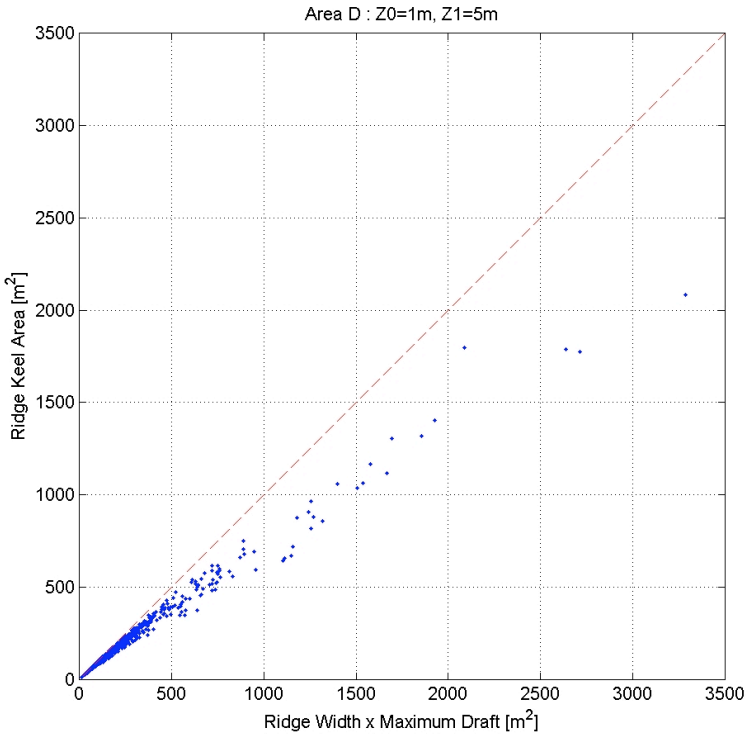

Figure 8-21 Ridge Width x Max. Draft vs. Ridge Area.

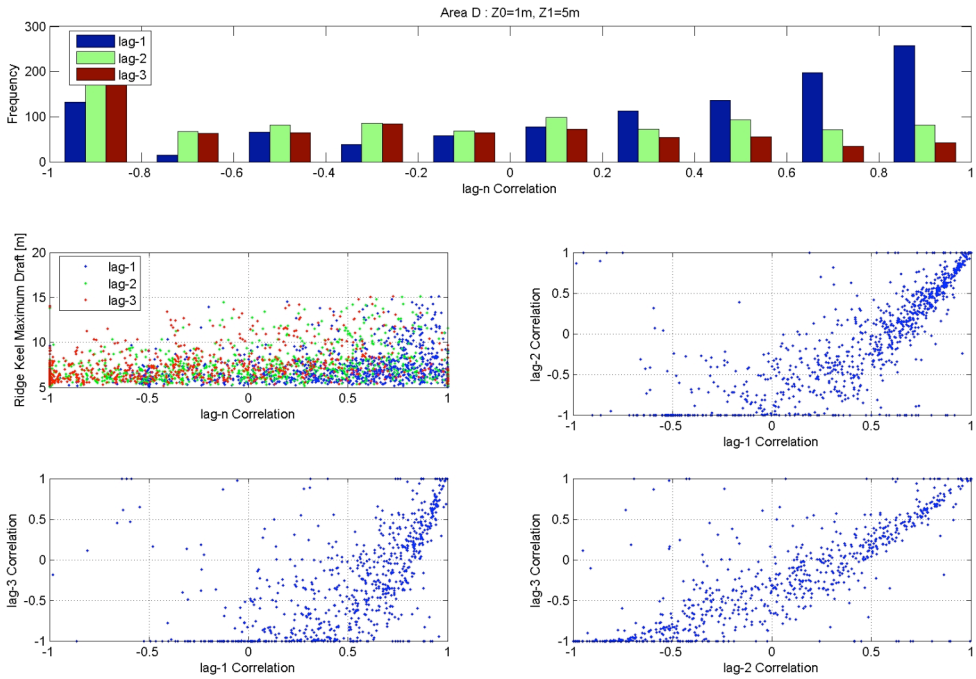

Figure 8-22 Area D Correlation Lag 1, Lag 2, and Lag 3 Analyses

In Figure 8-21, above, data points following the dashed line would indicate rectangular shaped ridges. Data points along a 22.5 degree line to the horizontal (not shown) would indicate ridges which are triangular in shape.

Figure 8-22, above, shows the results of the correlation analyses for a 1, 2, and 3 units shift in the ridge draft data. These data were obtained by taking all draft points in a ridge keel and shifting them one (two, three) distance units and then calculating the correlation coefficient between the original draft data and the shifted data. Coefficients near 1 and -1 show a good match in the two data sets. Coefficients between 0.5 and -0.5 show little correlation between the data sets. The results in the top histogram show that the lag 1 correlation is highest above 0.5 and near -1. It is interesting that the lag 2 and 3 correlations are the highest near -1. The data do not show a significant trend which might have been used to attempt to identify new (rougher) ridges and older (smoother) ridges. Further study with a 3-D data set is recommended.

Figures 8-23 to 8-30 describe the statistics of multi-year floe parameters listed in Table 8-5. These are: mean and standard deviation of floe draft including and not including ridges, width of all floes and width of those floes that had ridges embedded, and distance from the floe edge to the closest ridge. Note that the value of the x-axis must be increased by 1 metre to obtain the actual mean draft of the floe.

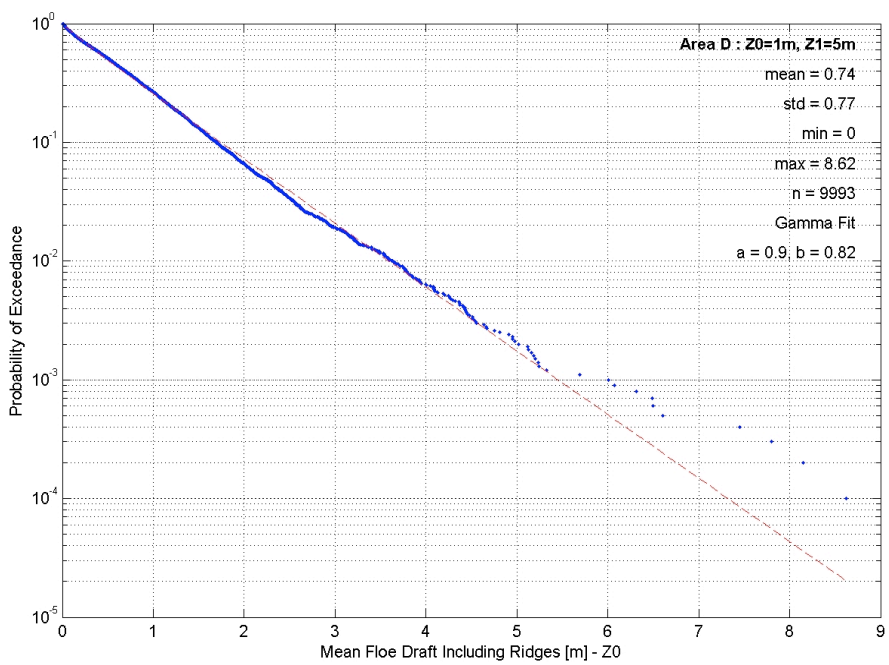

Figure 8-23 Exceedance Plot of Mean Floe Draft Including Ridges less 1 m

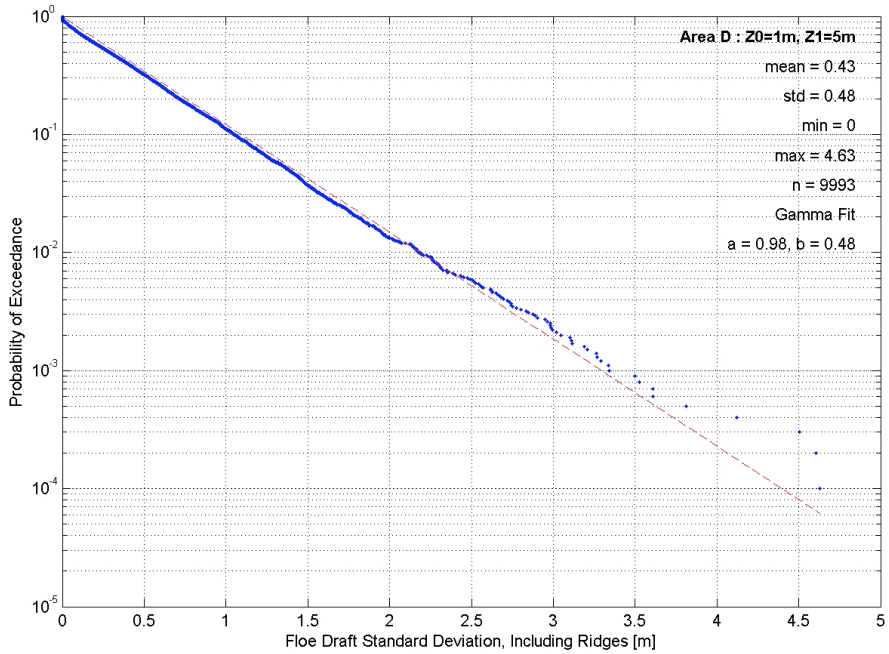

Figure 8-24 Exceedance Plot of Floe Draft Std. Dev including ridges

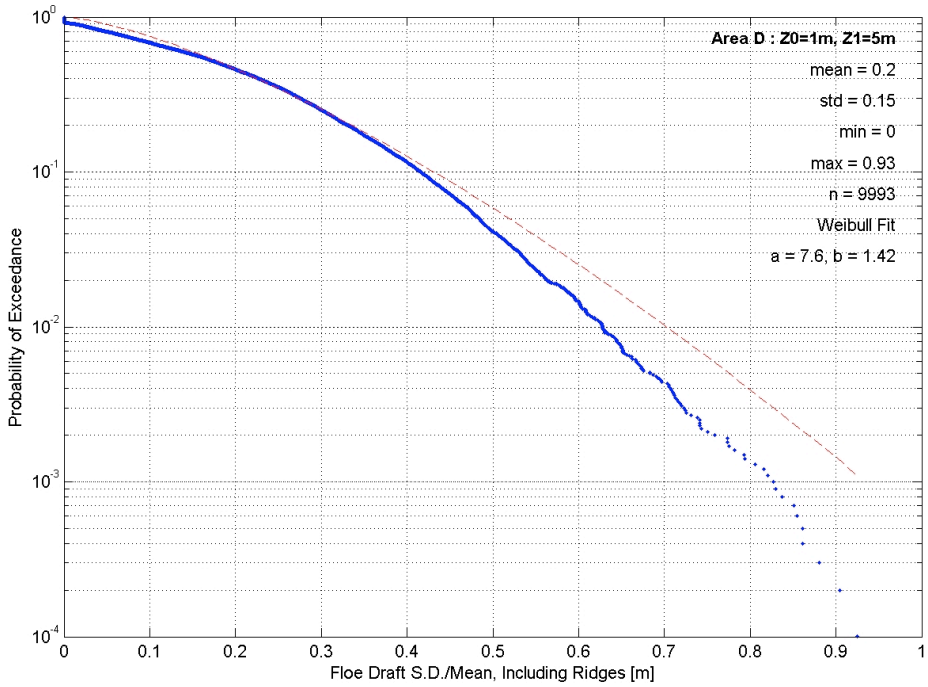

Figure 8-25 Exceedance Plot of Floe Draft Std. Dev./Mean Including Ridges.

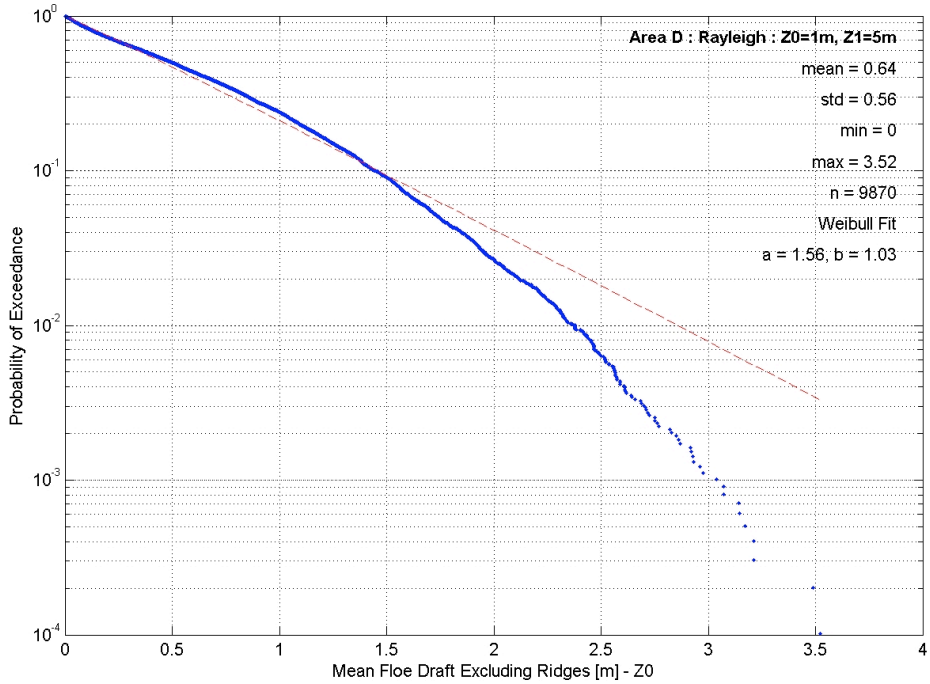

Figure 8-26 Exceedance Plot of Mean Floe Draft Excluding Ridges

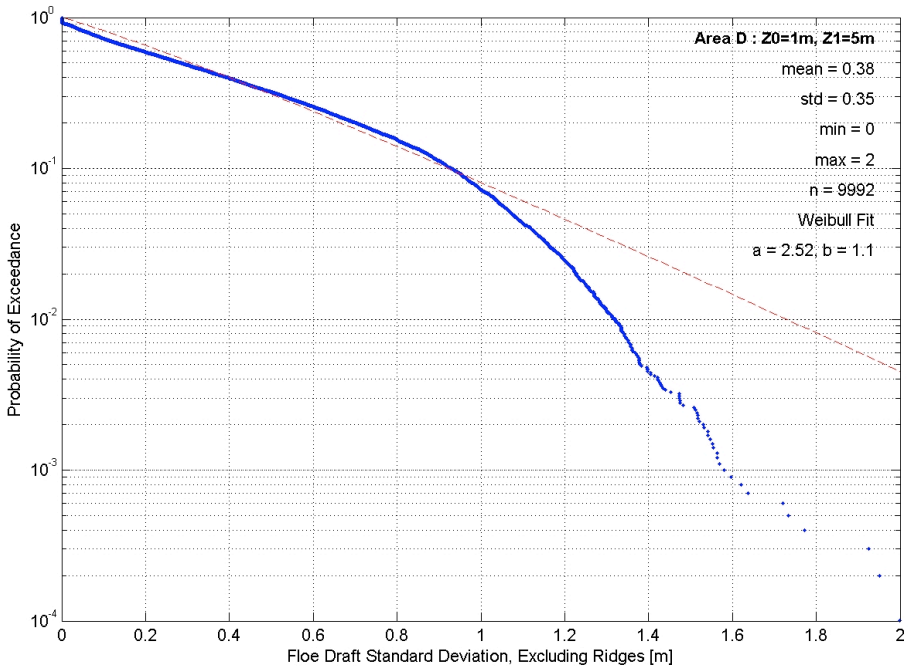

Figure 8-27 Exceedance Plot of Floe Draft Std. Dev. Excluding Ridges

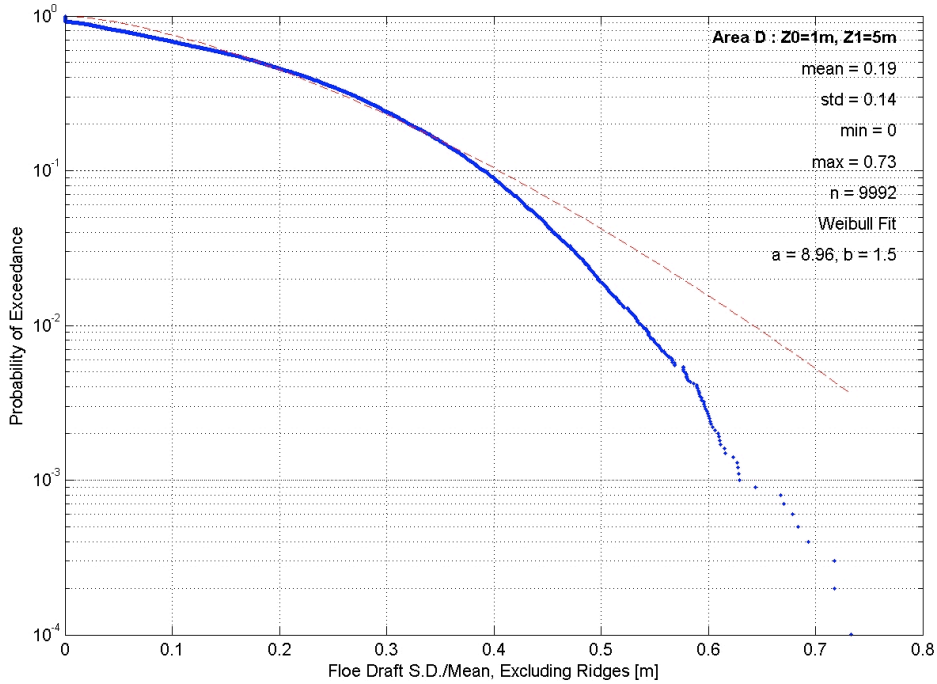

Figure 8-28 Exceedance Plot of Floe Draft Std. Dev./Mean Excluding Ridges

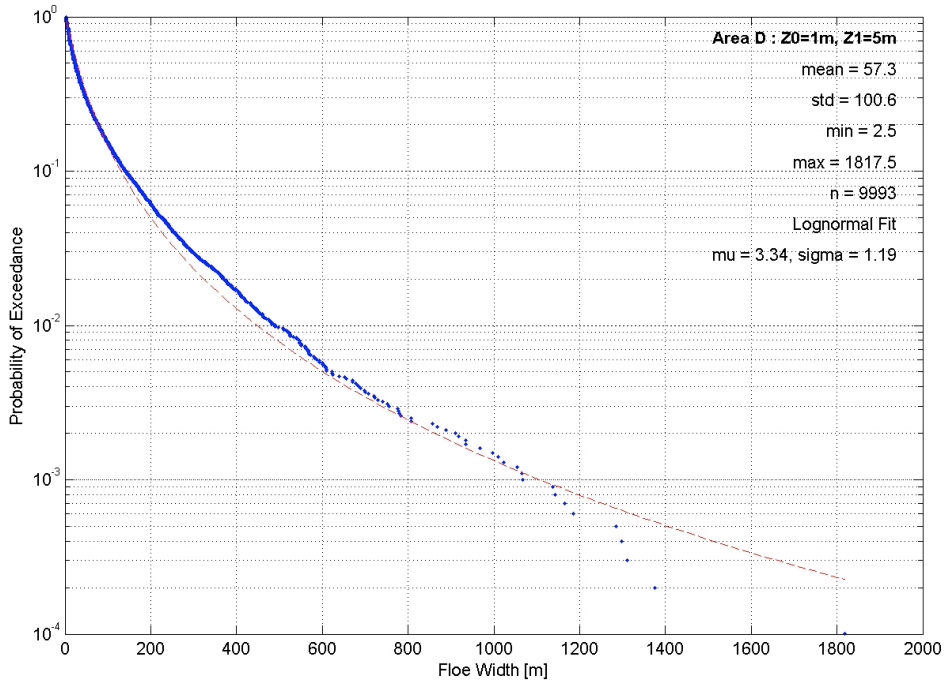

Figure 8-29 Exceedance Plot of Floe Width

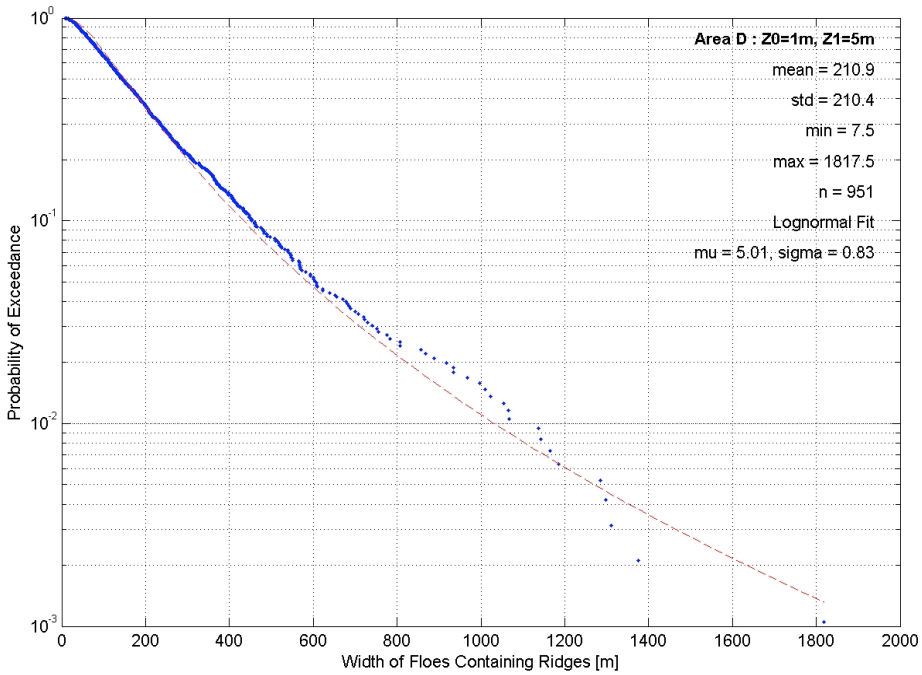

Figure 8-30 Exceedance Plot of Width of Floes Containing Ridges

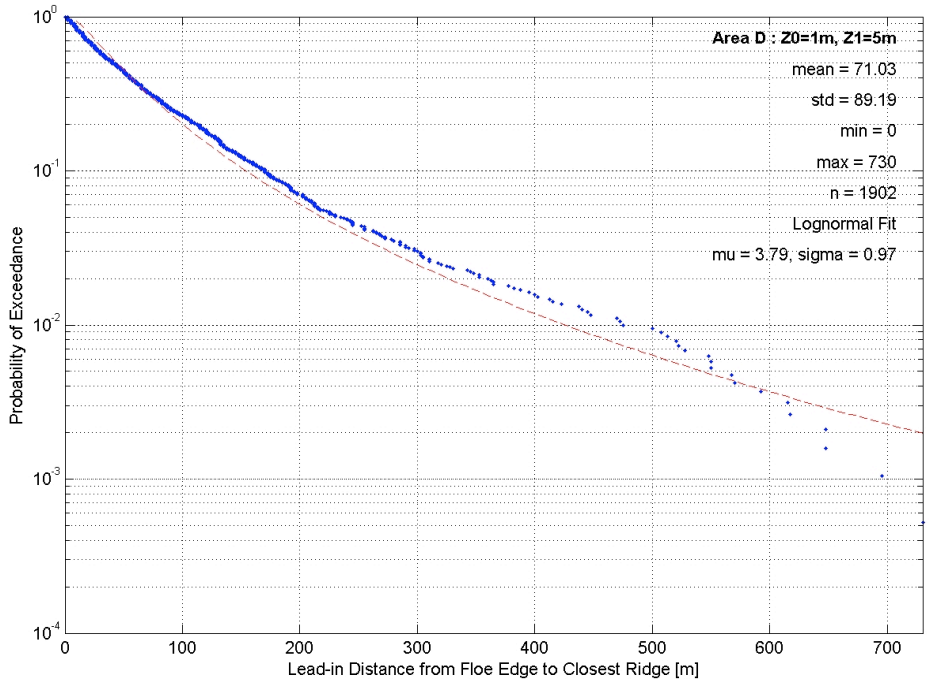

Figure 8-31 Exceedance Plot of Lead in distance from Floe Edge to Closest Ridge

Figures 8-32 to 8-33 describe the statistics of thin ice extent and draft.

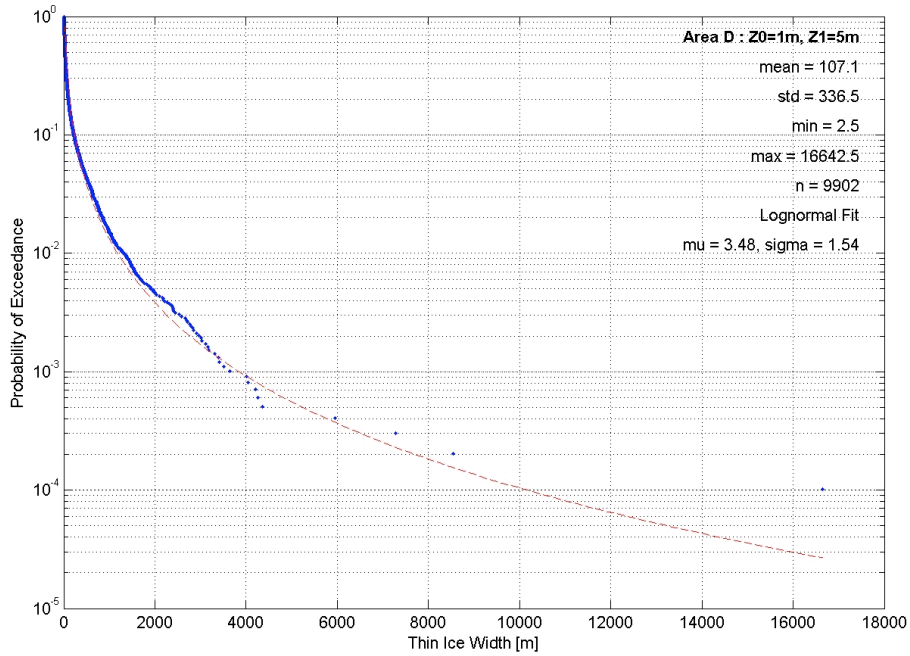

Figure 8-32 Exceedance Plot of Width of Thin Ice Sections

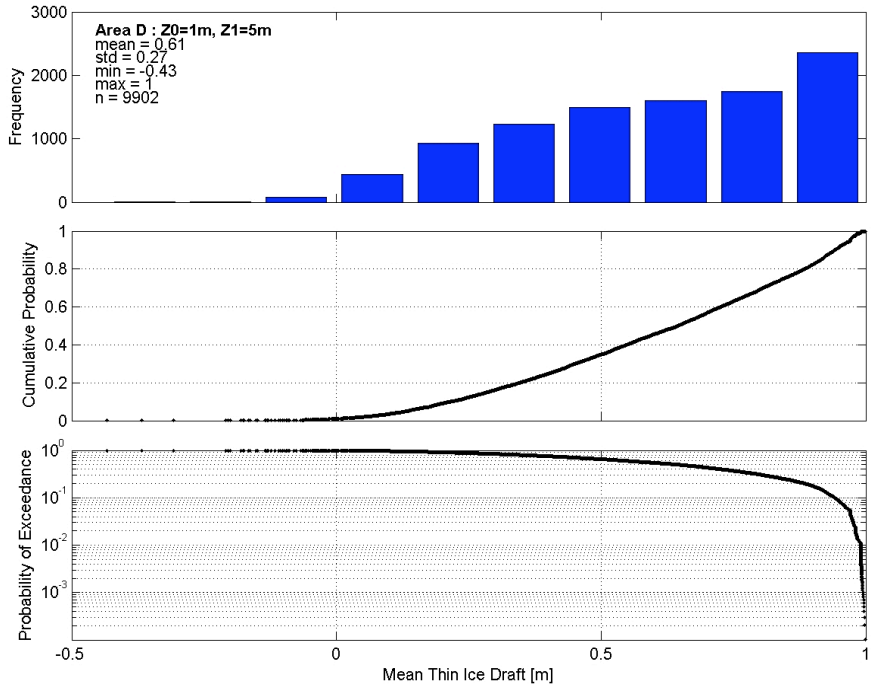

Figure 8-33 Mean Thin Ice Draft Statistics

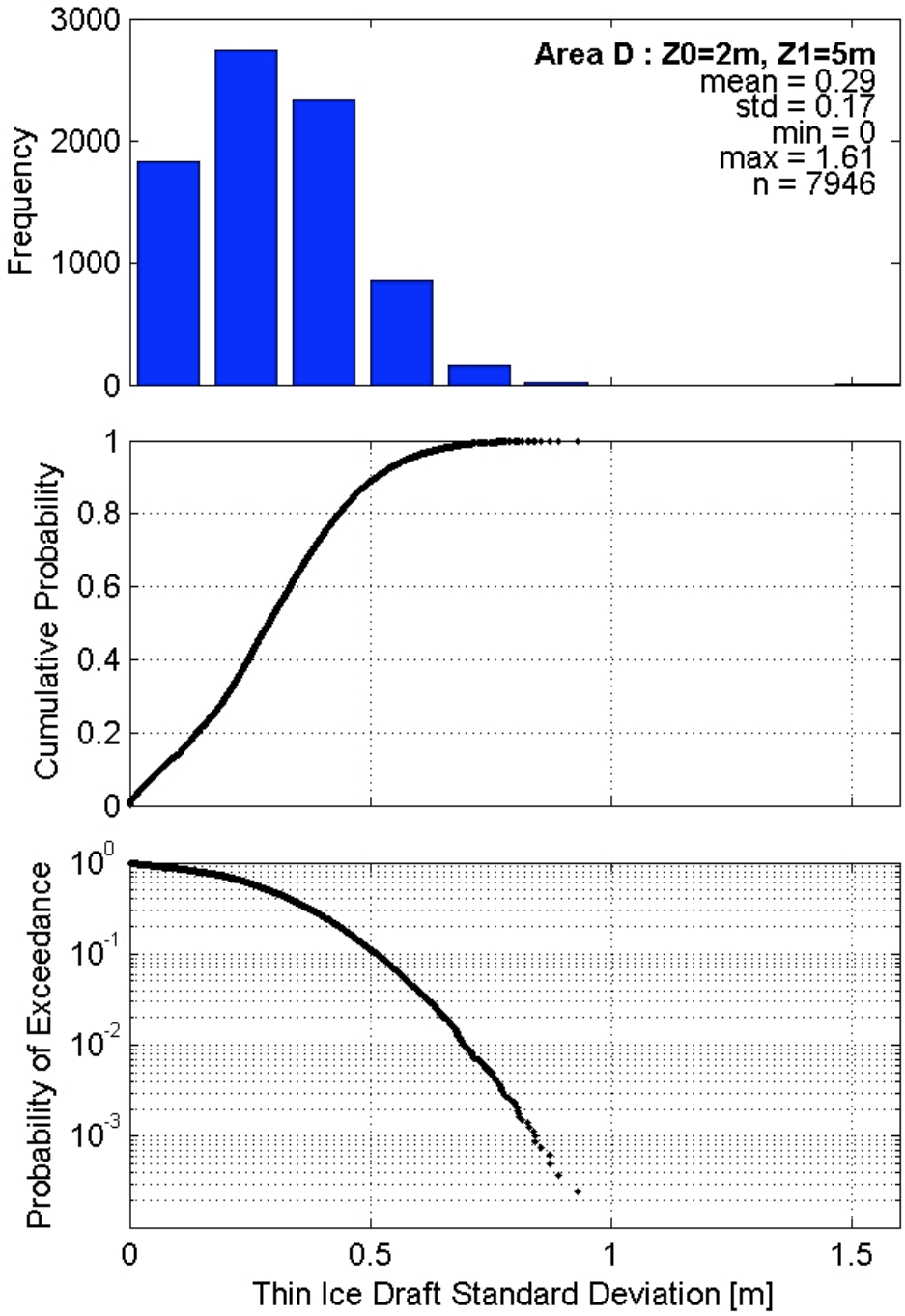

Figure 8-34 Thin Ice Draft Standard Deviation Statistics

For Figures 8-9 to 8-34 the distribution with the best fit was chosen from log-normal, gamma or Weibull. In most cases the fits to the data shown on the Exceedence plots are fairly accurate except for the Weibull fits. For these cases one could use the raw data, in probabilistic analyses, which can be extracted from the database files on the HD.

8.5 Comparison of Ridge Statistics by Area

8.5.1 Keel Maximum Draft and Standard Deviation

Figure 8-35 and Figure 8-36 compare Keel Maximum Draft (less 5m) and standard deviation of keel draft, respectively, for the 6 Areas defined in Figure 6-2. (N.B. It is necessary to add 5m to x-axis value since keels are defined by drafts of 5m and below).

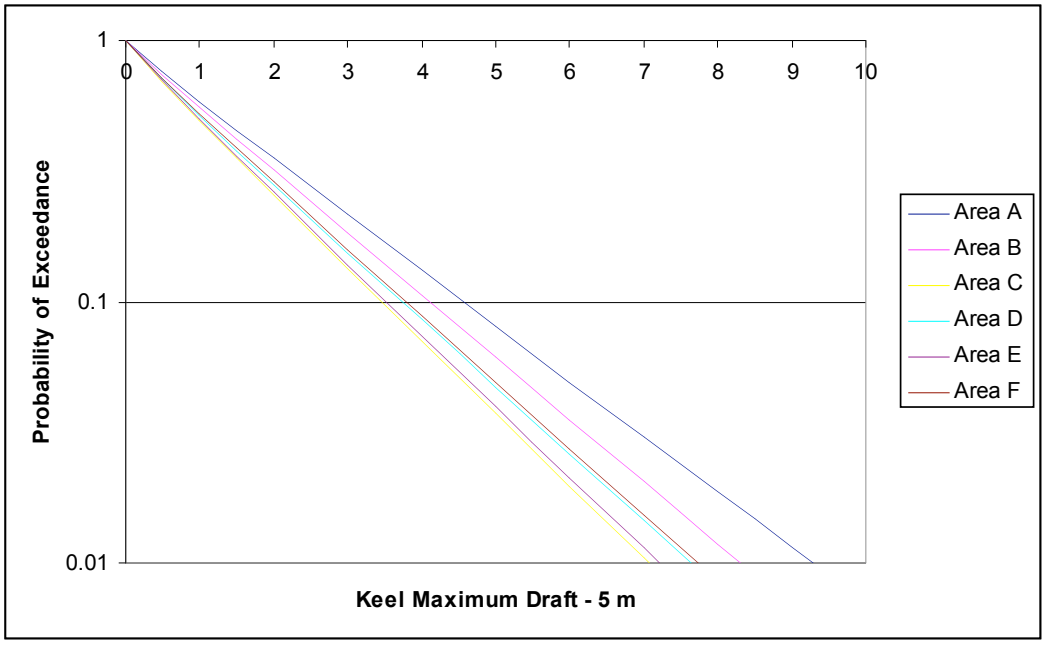

Figure 8-35 Exceedance Plot of Keel Maximum Draft for Different Areas

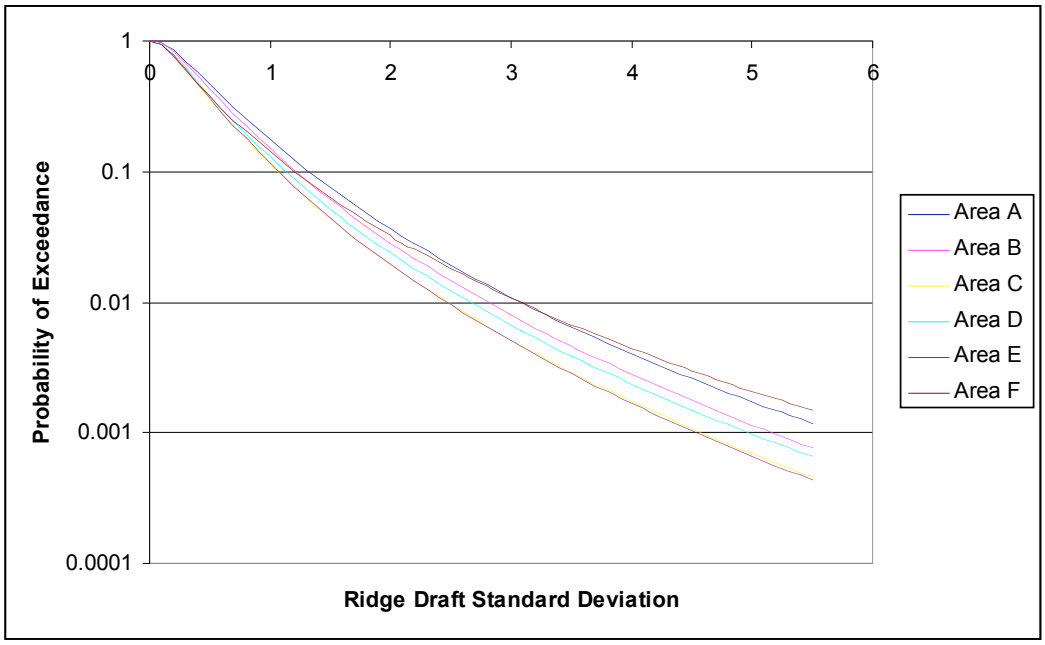

Figure 8-36 Exceedance Plot of Ridge Draft Standard Deviation for Different Areas

At an exceedance level of 10^{-2} Areas C and E give keel drafts of about 12 m. Areas F and D are about 12.6 m, Area B gives 13 m and Area A is about 14 m. This shows that the keel depth is deeper for the Northern areas (A and B), but there seems to be little difference in keel maximum draft for the central and Southern areas. Keel depth standard deviation curves show no significant trends by area.

8.5.2 Ridge Widths

Figure 8-37 shows the exceedance plots of ridge widths for the different areas. Area A has the widest ridges with a width of about 150 m at an exceedance of 10^{-2}. Area F has the narrowest at 60 m and the remaining areas have about 110m width at an exceedance of 10^{-2}.

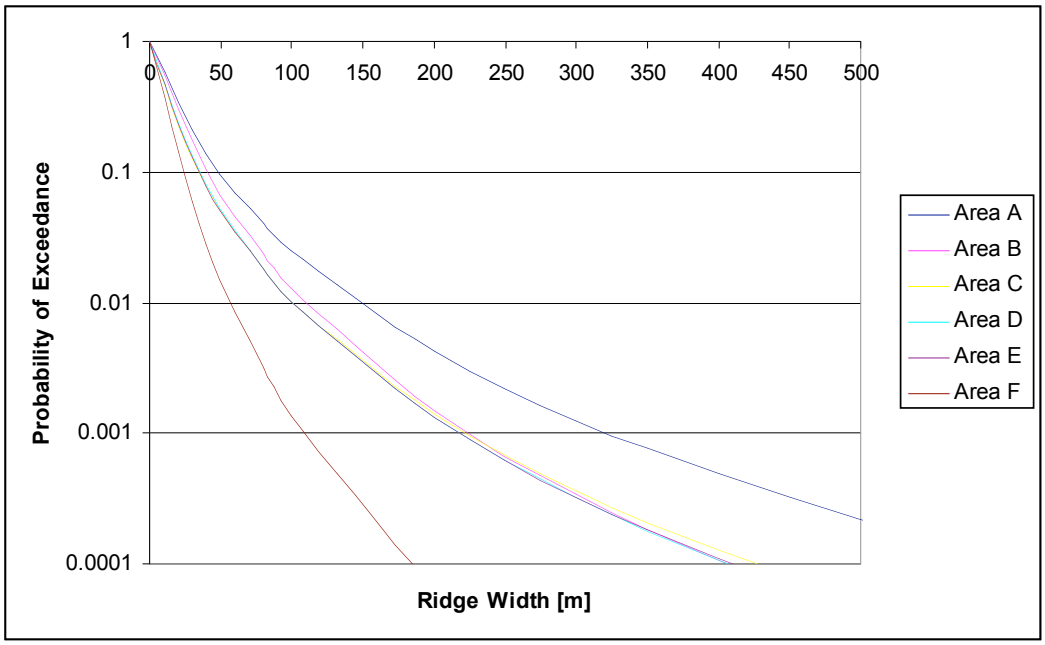

Figure 8-37 Exceedance Plot of Ridge Widths for Different Areas

8.5.3 Mean Floe Draft Excluding Ridges

Figure 8-38 shows the comparison plots of the mean draft of floes excluding ridges. For this plot all floes are included but any ridge sections have been excluded. It is cautioned that the Weibull distribution used for this graph did not fit the raw data well. Nevertheless the Figure shows a decrease in mean draft with a decrease in Latitude as expected.

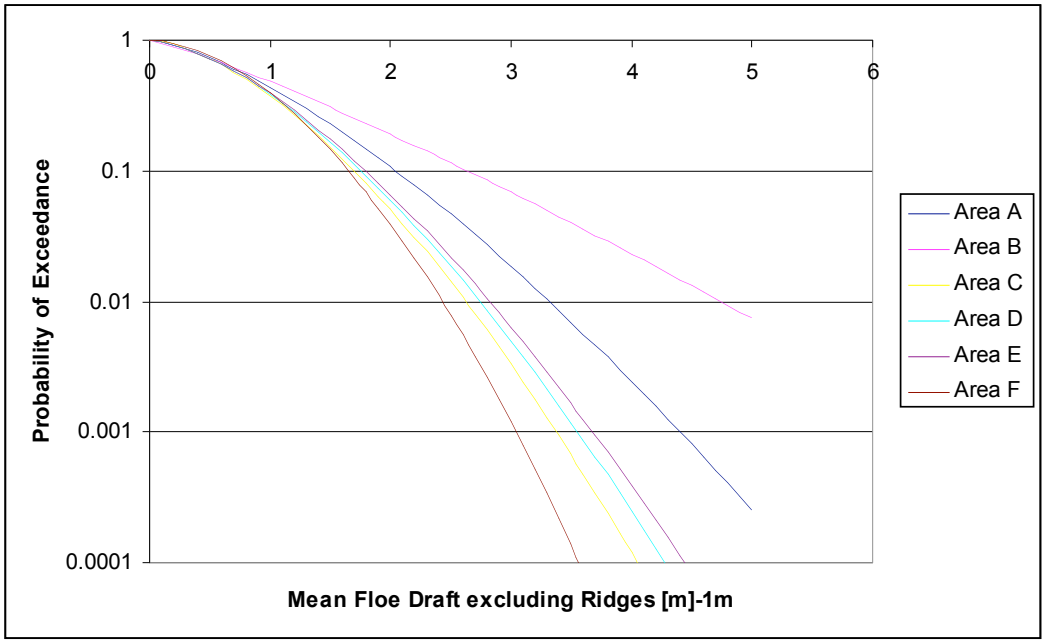

Figure 8-38 Exceedance Plot Mean Floe Draft Excluding Ridges for Different Areas

8.5.4 Spatial Distance between Ridge Keel Peaks

Figure 8-39 shows the plots of the distance (thin ice and floe ice less than 5 m draft) between adjacent ridge keel peaks.

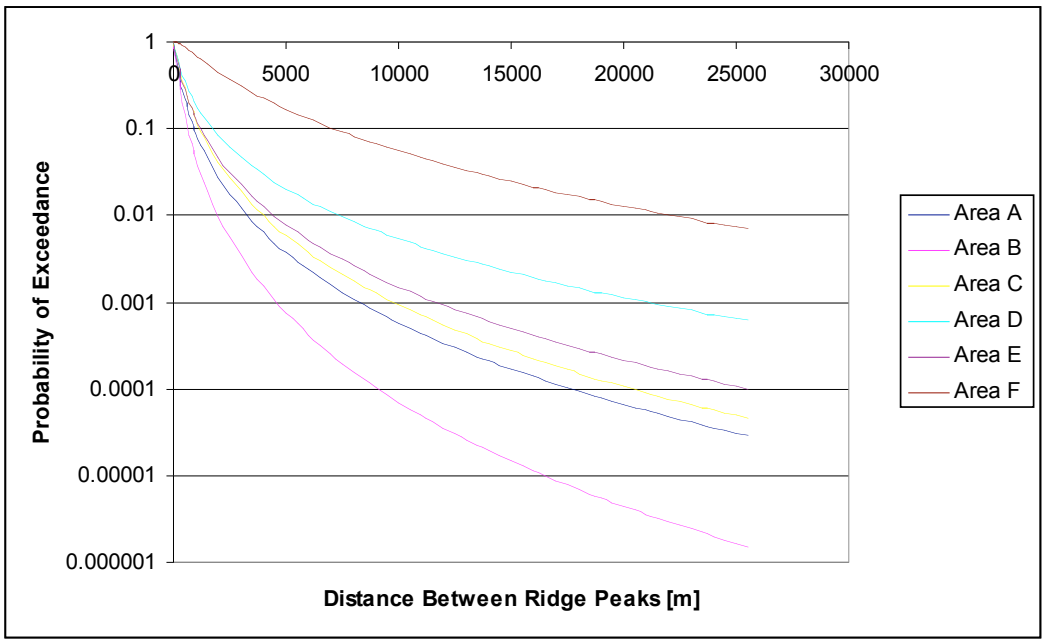

Figure 8-39 Exceedance Plot Distance between Ridge Peaks for Different Areas

Area B has the smallest distances between ridge peaks, followed by Areas A and C. Area D partly includes Areas E and F and curve D lies between curves E and F. Area F has vast areas of thin ice and few (only 30) ridges and only 27 floes,

At an exceedance of 10^{-2} the ridges are spaced about 23 km apart in Area F and about 2 km in Area B.

8.5.5 Width of Floes Containing Ridges.

Figure 8-40 shows the plots of Floe widths for floes containing ridges. This figure indicates that there were very small floes in Area F. From a further inspection of the ridge and floe data for Area F from the HD, it was discovered that the floes are only 10-20 m wider than the ridges.

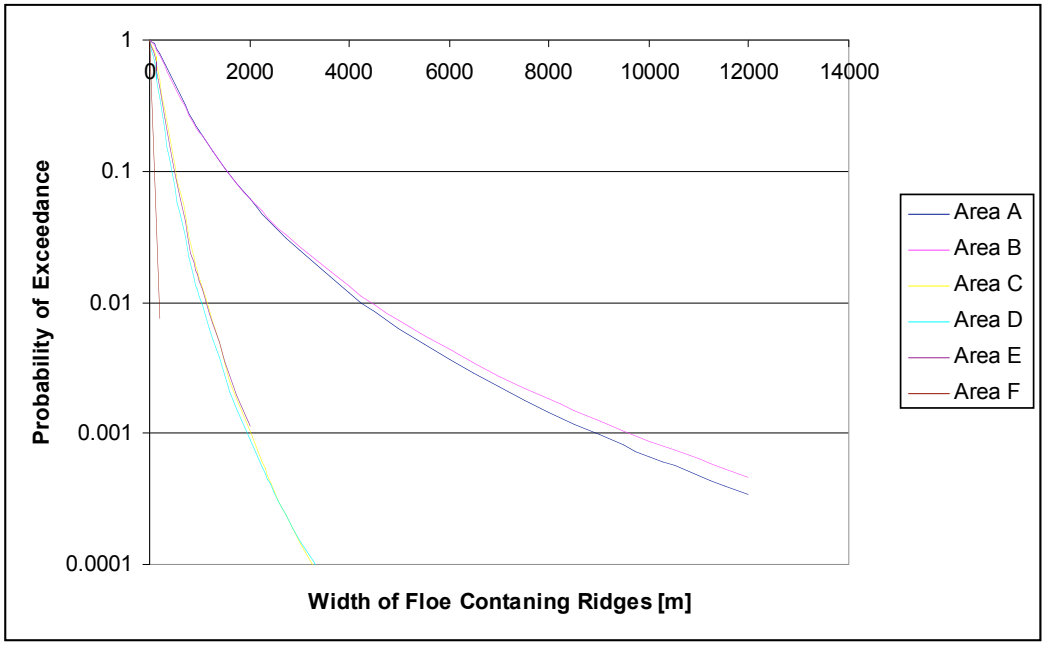

Figure 8-40 Exceedance Plot of Width of Floes Containing Ridges for Different Areas

Figure 8-40 shows an interesting segregation of the Floe width data. Further investigations of Areas A and B were then undertaken with a 2 m cutoff for Floes to see if the results were a result of thicker ice between the floes in the Northern Areas. Figure 8-41 shows the results of this comparison. Indeed the cutoff level significantly affects the floe size decreasing the large floes down to about 1.5 km from about 9.5 km at the10^{-3} exceedence level.

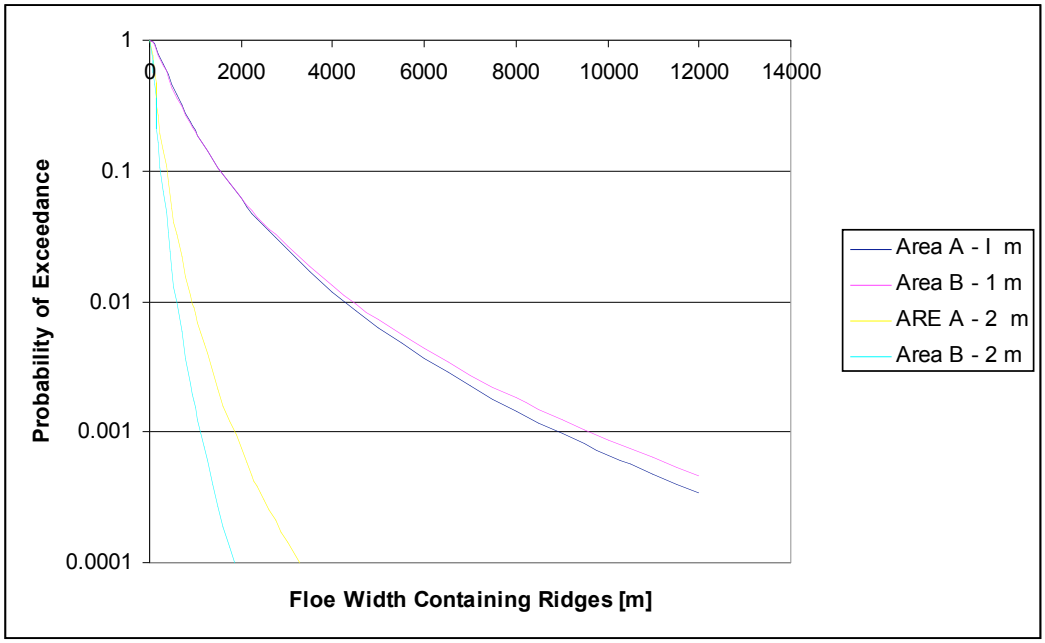

Figure 8-41 Exceedance Plot of Width of Floes Containing Ridges for a 1 m and 2 m Floe Cutoff for Areas A and B

8.5.6 Summary of 2000a Submarine Cruise Data Area Comparison

A main conclusion of the Area comparison is that floe widths decrease considerably along the edge of the pack ice - that is, as one proceeds south. Ridge depths however do not vary that much, but ridge widths decrease from North to South. The results shown in the last figure on the difference in Floe Widths based on different cutoff criteria may have a significant influence on modeling ice structure interactions. Knowing that the large floes contain thinner ice between 1 and 2 m thick definitely affects the loading scenarios. Further analyses of these data can be undertaken in the future, if required.

8.6 IPS Data Analyzed and Selected Results

Data from Stationary Ice Profiling Sonars (IPS) located on the seabed off the coast of Banks Island between 1996 and 2004 were selected to supplement the ice and ridge geometry data provided in Chapter 6. These data may be considered more representative of the old ice that may be present during an old ice invasion into shallow water in the southern Beaufort Sea. The data were provided by Dr. H Melling of IOS (Institute of Ocean Sciences in Sidney B.C. Canada).

Figure 8-42 shows the locations of Sites 5, 6, and 8 which were subjected to the same 5 m Cutoff and Rayleigh ridge analyses presented in Section 8-3. Since the majority of the data sets spanned more than a year a 2 m cutoff floe depth was selected for all analyses. The results of the analyses along with the raw data used for the analyses are provided on the HD accompanying this report. Table 8-7 shows the 10 data sets analyzed, and the dates of IPS operation.

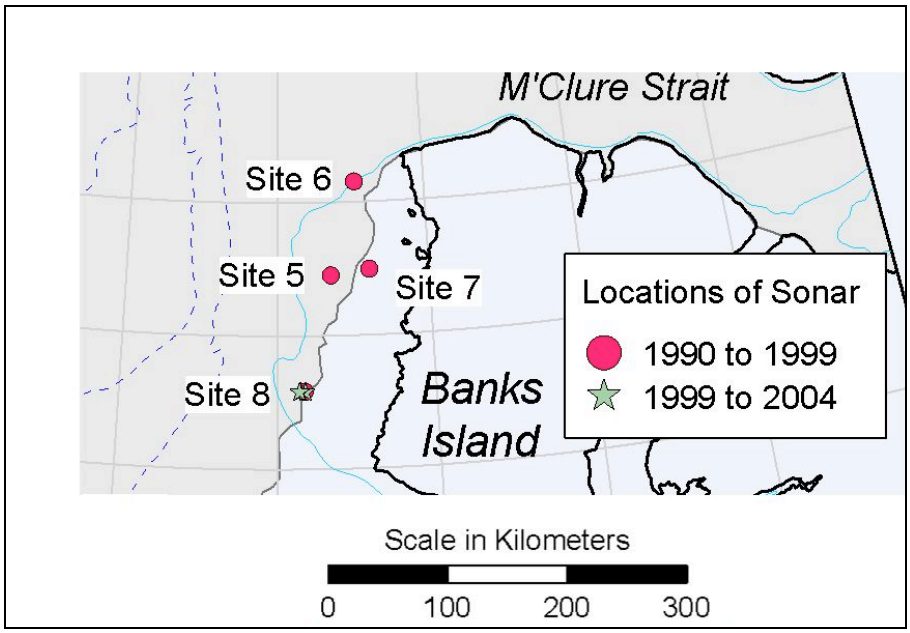

Figure 8-42 Stationary Upward Looking Sonar Data Sites west Banks Island

Table 8-7 IPS Data Analyzed

Site	Start	End	Distance (km)	File Name on Plots in This Study
5	1996/04/14	1997/06/14	2,219.0	PS3-03-A
5	1997/07/30	1998/07/18	1,859.3	Test
6	1997/09/15	1998/05/19	2,744.5	Site 6
8	2003/09/15	2003/09/23	109	Site 8 2003 09 15
8	2003/09/25	2003/10/08	171	Site 8 2003 09 25
8	2003/10/17	2001/01/01	928	Site 8 2003 10 17
8	2004/01/01	2004/05/01	438	Site 8 2004 01 01
8	2004/05/01	2004/09/01	917	Site 8 2004 05 01
8	2004/09/01	2004/09/26	272	Site 8 2004 09 01
8	2004/09/30	2004/11/28	875	Site 8 2004 09 15

The analyses of the IPS Data provided all of the geometric data described in Section 8-3 for the floes, thin ice and ridges. The detailed data is provided on the HD. Only summary data are provided in this Chapter. Table 8-8 shows the numbers of floes and ridges analyzed in the IPS data. Both 5 m Cutoff Ridge and Rayleigh Ridge results are provided on the HD.

Table 8-8 Populations of floes and ridges from the IPS analysis.

Site	Start Date	End Date	# of Floes	# of Ridges	Length of Ice Passing Site [km]
5	1996/04/14	1997/06/14	22172	19523	2219
5	1997/07/30	1998/07/18	10431	4953	1859
6	1997/09/15	1998/05/19	15086	6270	2744
8	2003/09/15	2003/09/23	1340	598	109
8	2003/09/25	2003/10/08	2778	1214	171
8	2003/10/17	2001/01/01	4301	1425	928
8	2004/01/01	2004/05/01	4994	2338	438
8	2004/05/01	2004/09/01	11693	10100	917
8	2004/09/01	2004/09/26	5422	1642	272
8	2004/09/30	2004/11/28	2658	350	815

8.7 Discussion on Ice Types Contained in the IPS Data

Later in this chapter the observation is made that a certain percentage of the observed ridges may have been recently formed and therefore may not act as solid ice during an interaction with an offshore structure. Figure 8-43 and Figure 8-44 show the exceedance plots of all the draft data for the 97/98 data for Site 6 and the 96/97 data from Site 5. The mean ice draft for site 6 as shown on the Figure is 1.05 m. Only 10% of the data has a draft greater than about 2.5 m. For Site 5 the mean draft is 2.79 m and 10% of the drafts are greater than about 5.5 m.

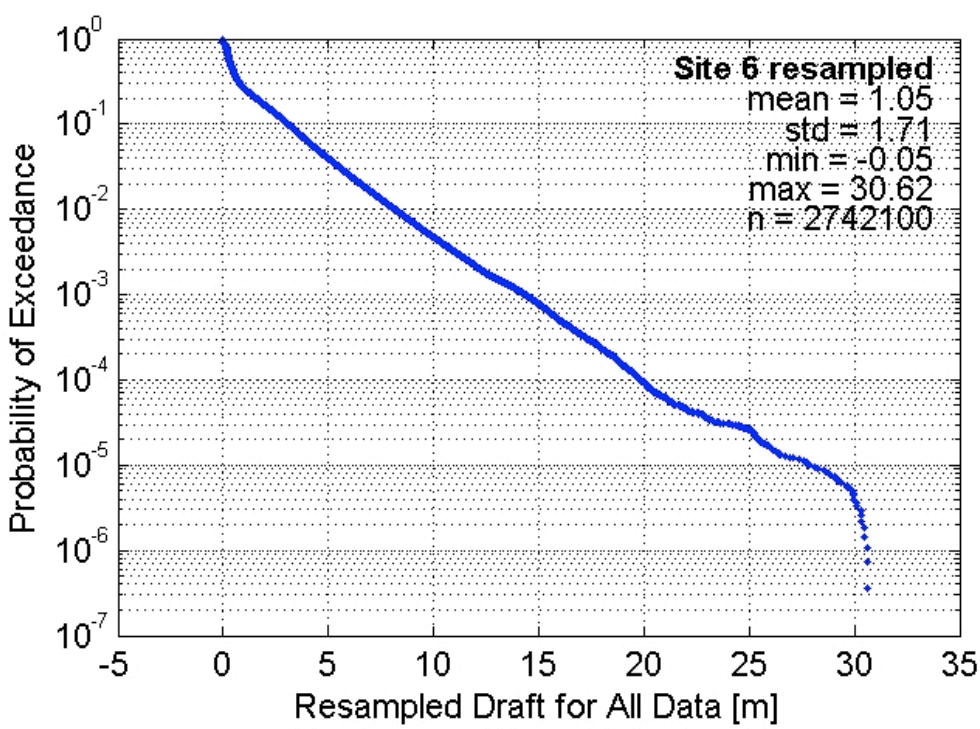

Figure 8-43 All Draft Data at Site 6 NE Coast of Banks Island

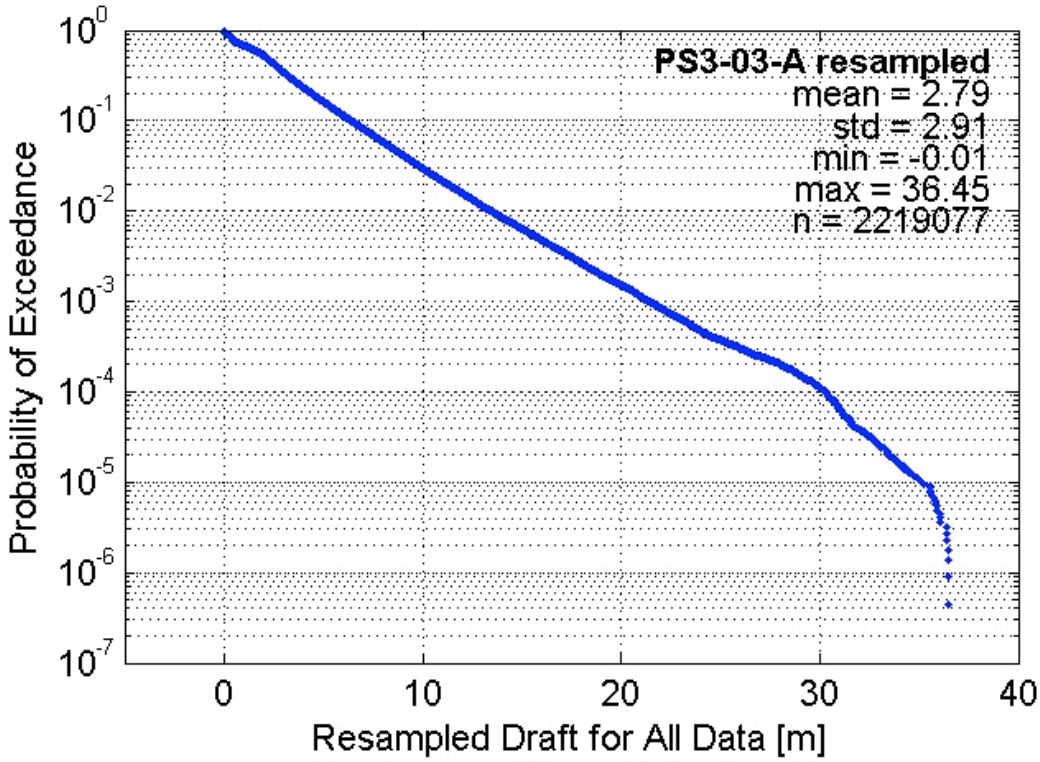

Figure 8-44 All Draft Data at Site 5 West Coast of Banks Island.

Further investigation into the ice types contained in the IPS data was carried out using the Canatec Ice Concentration Statistics Program ICE'06; this program generates a computerized database of sea ice charts and statistics covering the complete Arctic. Tables 8-9 and 8-10 show the results from the ICE'06 Program for Sites 5 and 6 for the times the IPS were deployed.

Table 8-9 Ice Type Concentrations at Site 5 – 96/97

Ice Type	% of Time Ice Type over Site 5
Multi-Year	18.9 %
Second Year	58.3 %
First Year >1.2 m	16.6 %
Open Water or FY< 1.2 m	6.2 %

Table 8-10 Ice Type Concentrations at Site 6 – 97/98

Ice Type	% of Time Ice Type over Site 6
Multi-Year	22.2 %
Second Year	15.7 %
First Year > 1.2m	1.6 %
First Year > 0.7m and < 1.2 m	10.5 %
First Year > 0.3m and < 0.7m	21.1 %
Open Water or FY < 0.3 m	28.9 %

For Site 5 the ice type is second year or greater 77% of the time, compared to about 38% of the time for Site 6. Site 5 therefore had older ice on average.

8.8 Comparison of Submarine and IPS data

Figure 8-45 through Figure 8-48 show selected IPS ice geometry statistics compared to the data from the 2000a Submarine Cruse. In Figure 8-45 the maximum keel draft statistics show that the 1996 to 1998 data at sites 5 and 6 are similar to the most Northerly October 2000 (Area A) data. Figure 8-46 shows that the IPS data has a higher ridge draft standard deviation than most of the submarine data. Since the IPS data has roughly 4 times more data points per kilometer than the submarine data this may be one reason that IPS data has a higher ridge draft standard deviation. Differences in ice dynamics west of Banks Island could be another factor.

IPS Ridge width statistics are similar to the most Northerly submarine Areas as shown in Figure 8-47.

Figure 8-48 shows that the IPS data are also similar to the most northerly submarine data (Areas A and B) when one compares floe sizes containing ridges.

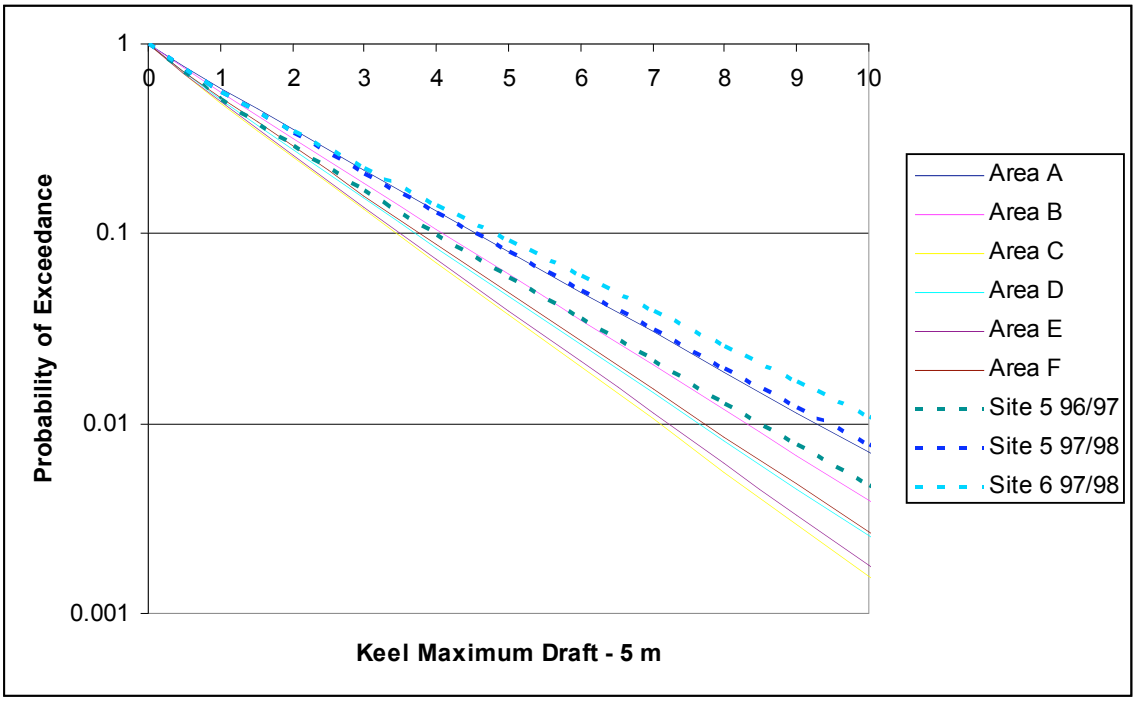

Figure 8-45 Comparison of Maximum Keel Draft Statistics for IPS Sites 5 and 6 and the results of the 2000a Submarine Cruse

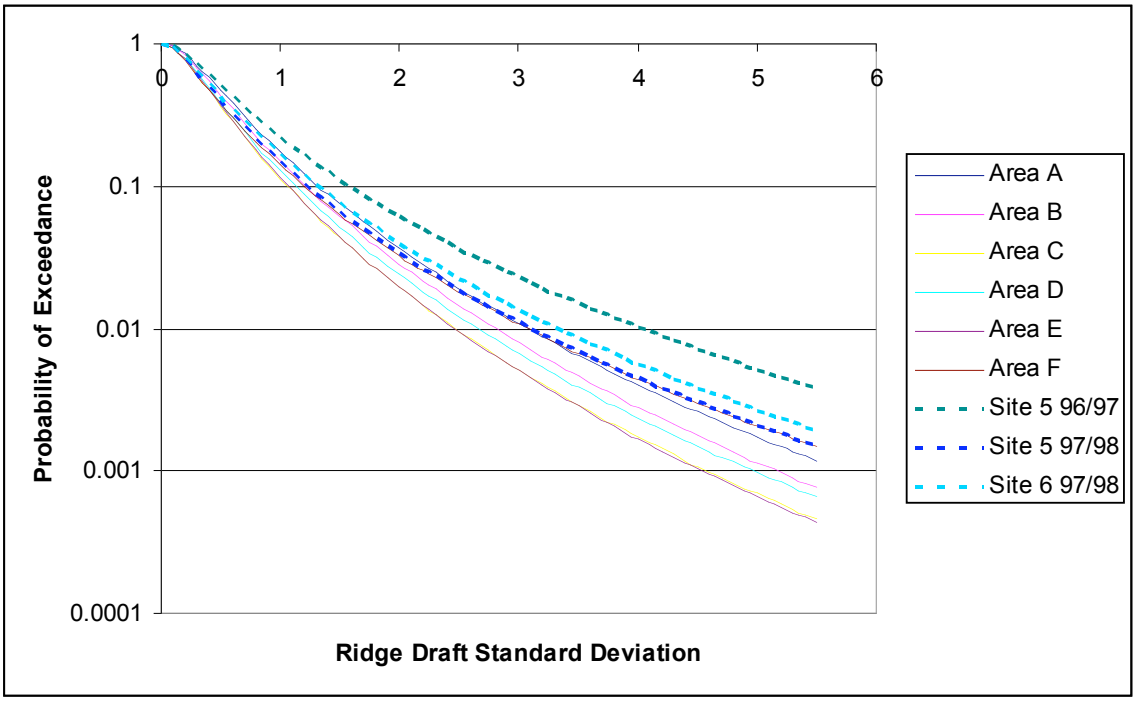

Figure 8-46 Comparison of Ridge Draft Standard Deviation Statistics for IPS Sites 5 and 6 and the results of the 2000a Submarine Cruse

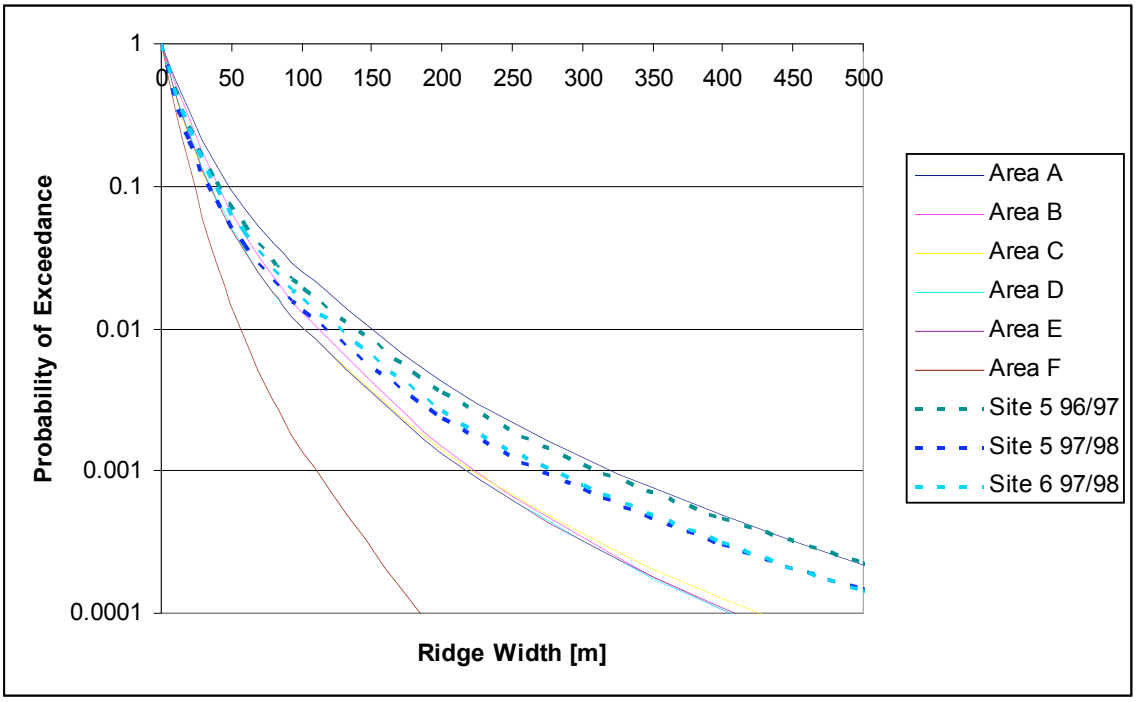

Figure 8-47 Comparison of Ridge Width Statistics for IPS Sites 5 and 6 and the results of the 2000a Submarine Cruse

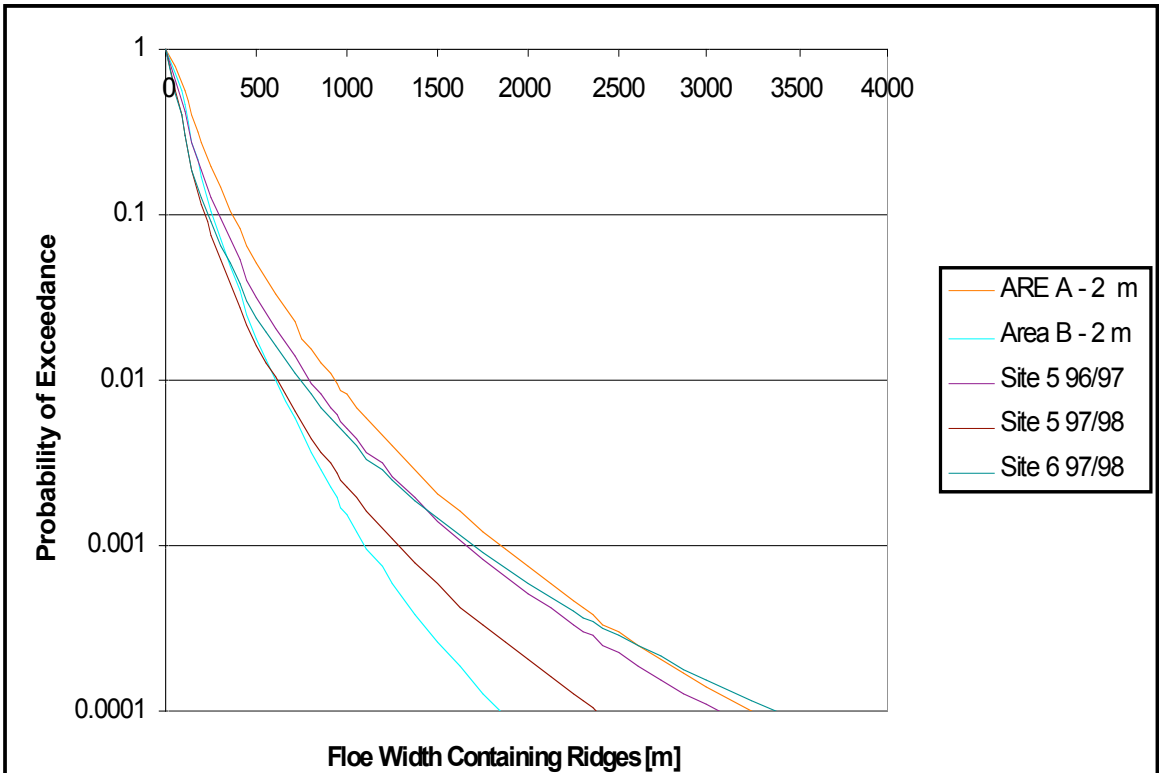

Figure 8-48 Comparison of Floe Width (containing ridges) Statistics for IPS Sites 5 and 6 and the results for Areas A and B of the 2000a Submarine Cruse

8.9 Hummock Fields

8.9.1 Hummock Fields in the ULS Data - Western Arctic Ocean

Previous investigations (De Paoli, Morrison, and Marcellus, 1982) used a definition for MYHF as a contiguous segment of ice with a width greater than 500m with an average depth greater than 10m. indicates the ridge width vs. average thickness for Area D. No ice features in Area D satisfy the preceding criteria for a MYHF. A review of the plots for the other Areas revealed only one ice feature that met or exceeded the above criteria.

Figure 8-49 shows the scatter plot for Area A. One feature has an average thickness of 13 m and is about 1,150 m wide (Figure 8-50). This feature was located at 89.5N and 222E. It is noted that this feature was not found from the Rayleigh analysis.

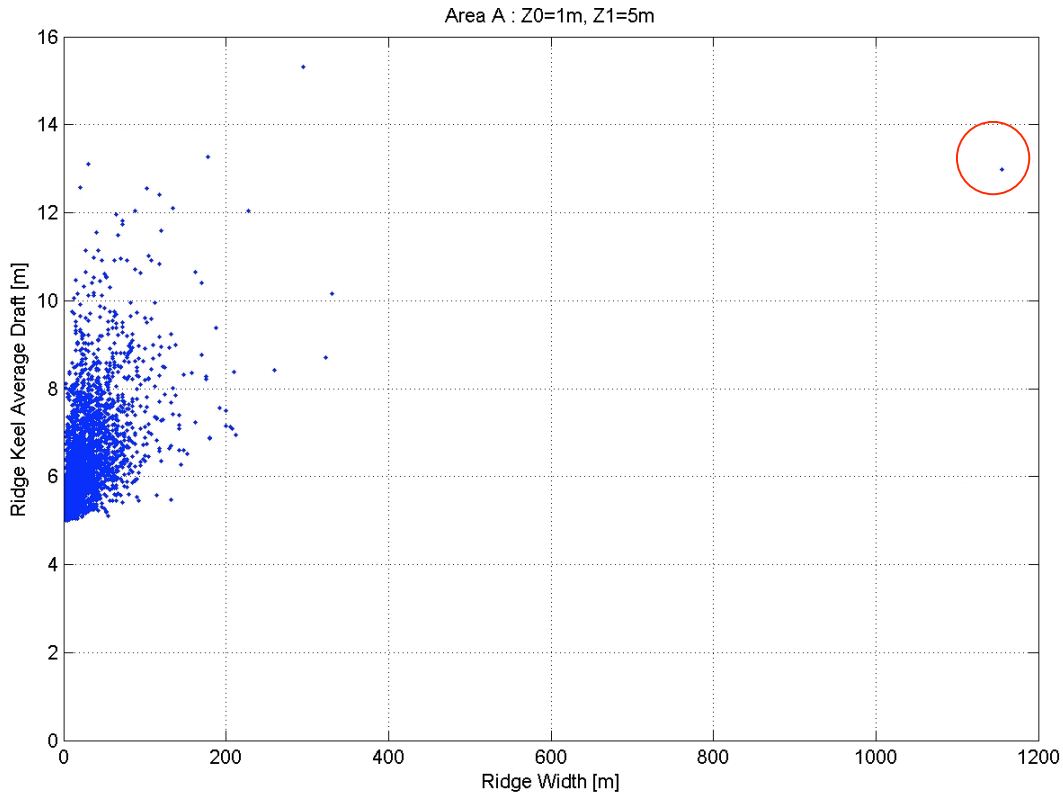

Figure 8-49 Ridge Width vs. Average Thickness from the 5 m Cutoff Ridge Analysis

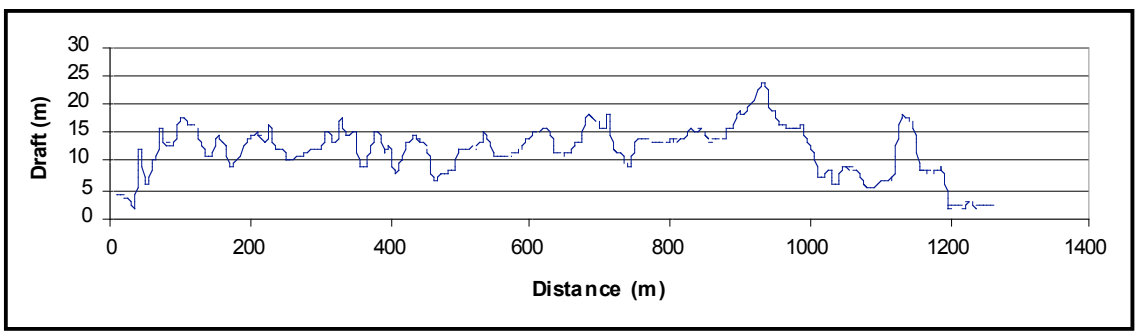

Figure 8-50 Big Hummock Field at 89.5N and 222E.

If this is the only MYHF in the dataset and using the 1 m cutoff definition for floes, then the odds that a floe contains a MYHF is 1 in 33,326 or 0.003%;. (This is not entirely correct since only Floes greater than 500 m wide should be considered.)

In comparison, the Sargo 1960 Cruise (De Paoli, Morrison, and Marcellus, 1982) identified 64 ice features that were greater than 500 m wide with average draft greater than 10m. The average width of these features was 1,600 m and deepest average draft was 17 m. The

location of the Sargo Cruise was however close to the coast of the Queen Elizabeth Islands which experiences higher pack ice pressures, and is known to be a region of MYHFs.

8.9.2 Hummock Fields in the IPS Data West of Banks Island

A review of the IPS data, yielded only two features from the 1996-97 data at Site 5. These features are shown in Figure 8-51 and Figure 8-52. Note that there are more data points in the IPS data sets since the data spacing is around 1 m compared to the Submarine data which was about 4 m.

It is noted that the profiles are quite rough with many smaller ridge peaks on both features.

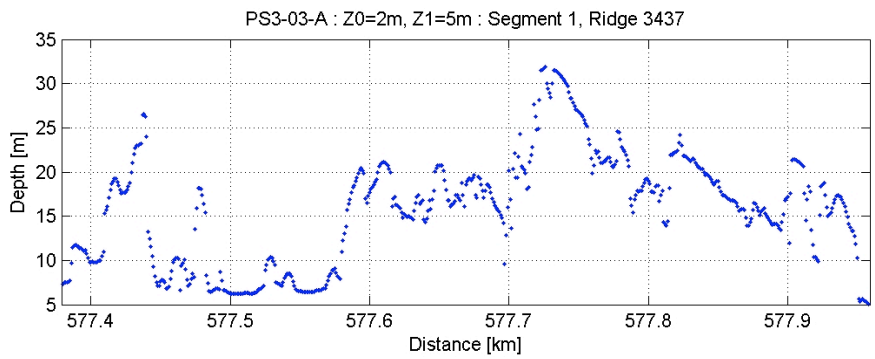

Figure 8-51 Hummock Field found in the 1996-1997 data for Site 5.

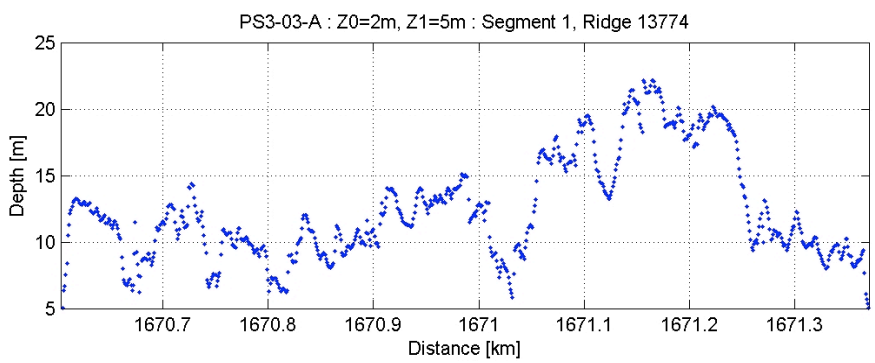

Figure 8-52 Hummock Field found in the 1996-1997 data for Site 5.

8.10 Data on the HD

This analysis has provided a considerable amount of data (16 GB provided on the hard drive for the ULS data, and 15.3 GB for the IPS data analysis). Included are the original data text file, statistical plots for both 5 m Cutoff and Rayleigh Ridges, floe and thin ice statistics, plots of all floes, plots of all ridges (5 m Cutoff only), database text files of all results, which allow further analysis of the data,

It is noted that there has been no mention of MY Ice in this Section. There has been some data provided (lag1, 2, 3 Correlation and Apex Angle) which might lead to a means of identifying MY Ice from the ULS data. However, there have been no identified trends from the current analyses that could be used to distinguish new and old ridges.

8.11 Ridge Count from Satellite Imagery

Following up on the quandary of identifying ice types from ULS data an analysis of 30m Envisat satellite imagery was undertaken to attempt to better understand the data. Image resolution was 30m. Figure 8-53 shows the location of imagery off Ellesmere Island.

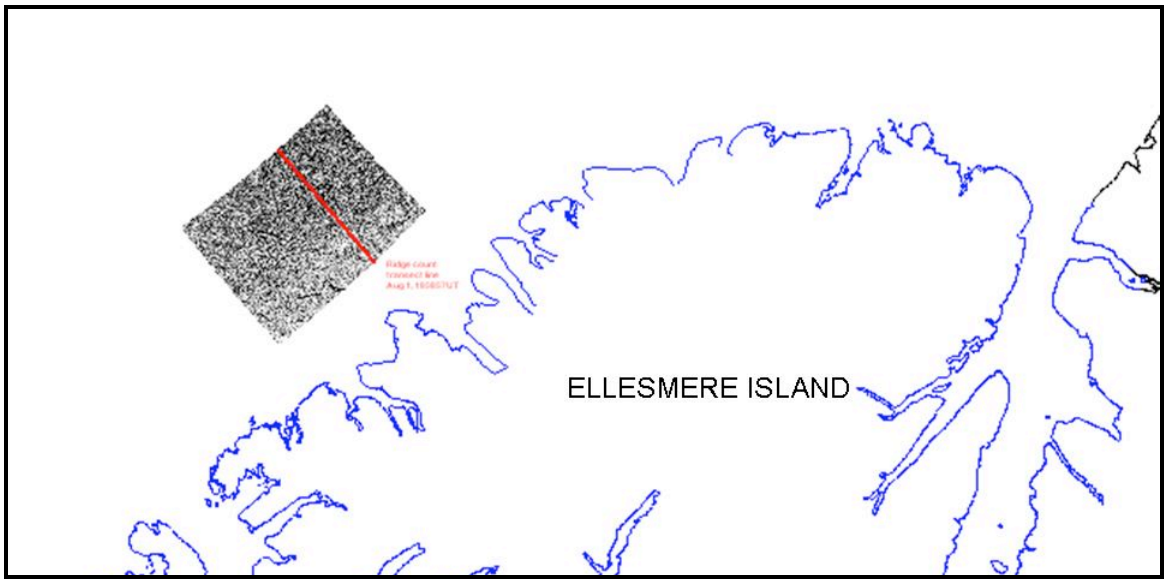

Figure 8-53 Location of Imagery used in the Ridge Count Analysis.

The red line on Figure 8-53 was inspected in detail to determine if ridged areas could be identified. An 83 km line from 28 km offshore to 109 km offshore was inspected for ridged areas.

Ridges crossing the transect line were identified by a red line, older ridged areas with 6 - 8/10 ridging were circled in green; see Figure 8-54 and. Figure 8-55. (Note: that the upper bound of 8/10 could be higher, but due to the resolution of the data, it was uncertain whether the area was ridged or a rubble field). Ridges and ridged ice prevail near shore, whereas offshore (left side of image) ridging and ridged ice decreases significantly.

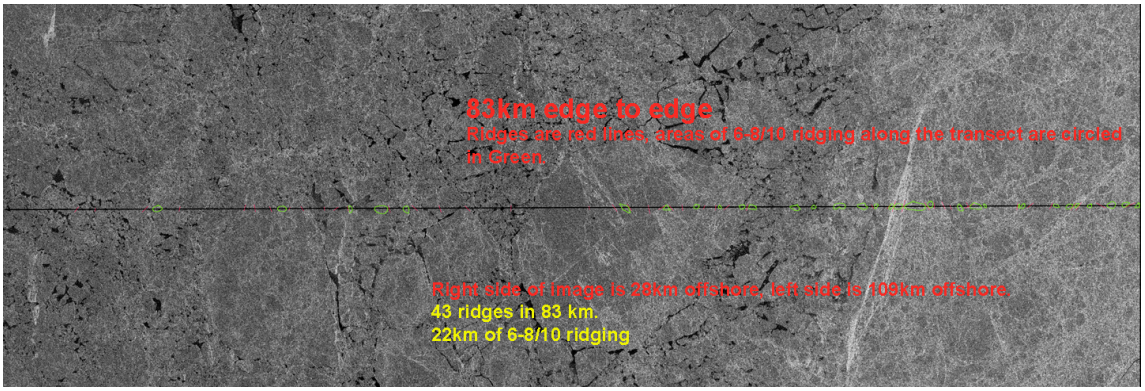

Figure 8-54 Ridges and Ridged Areas Identified on the Envisat Image

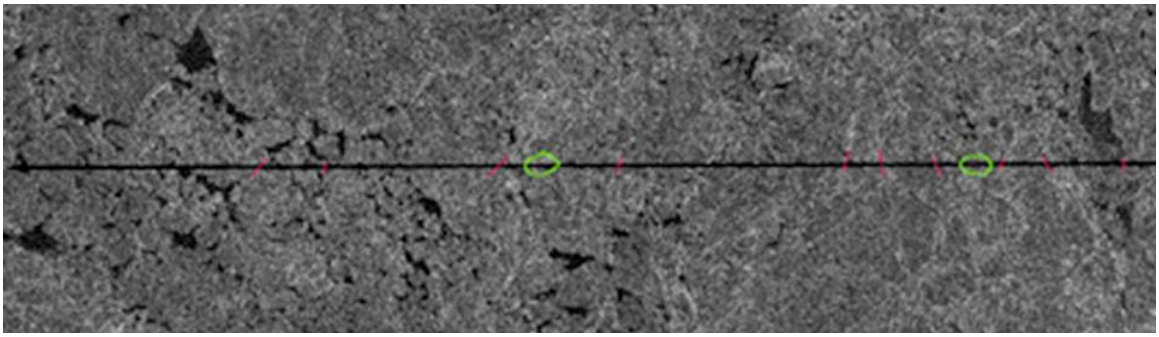

Figure 8-55 Enlargement of the left side of Figure 6.54

The portions of ridged ice were added up, yielding a total of 19 km (of the possible 83km). In addition to the 19 km of 6-8/10 ridged ice, the physical distance covered by each identified ridge also needs to be added to it.

On the image in Figure 8-54, 43 ridges were identified crossing the transect line. The identified ridges averaged 60-90m wide on the ice surface, resulting in 3.2 km of new ridges. This includes only the ridge sails. The total width of keels would have been several times greater than 3.2 km. In the analyst's estimation, the ridges identified were primarily new – formed sometime between the time of the image and the previous few months. No first-year ice was identified anywhere on the image.

Summarizing this assessment there were 19 km of older ridged areas, and 43 ridges measuring 3.2 linear km of recently formed (from MY ice) new ridges in an 83 km line running offshore from Ellesmere Island. Further study using higher resolution satellite imagery such as Quickbird, is recommended.

The key observation here is that the pack ice does contain a large percentage of newly formed ridges composed of blocks of fractured old ice. Such ridges would not exert the same load on an offshore structure as a fully consolidated ridge

9 CORRELATING SURFACE IMAGERY WITH KEEL PROFILES

9.1 Introduction

The IPS data are a very important source of ice information, however, the question has often been raised about the possibility of determining ice type from the IPS profiles. Others (Melling et al, 1998) have tried this in the past with no success. Presumably the reasons are many fold:

- There is generally a mixture of ice
- Multi-year ice is generally surrounded by pressure ridges or ice piles of usually new ice but also from old ice.
- Multi-year ice can be two or more years old, and we do not know exactly how the different ages of ice look on the underside. For a pressure ridge composed of first year ice, the ice blocks in the sail are readily visible, even in September, and they still have their angular form. In the second year, the ice pieces are becoming smoother, and frozen snow and ice fill the spaces within the blocks. By the third year, the individual ice blocks are or are becoming difficult to see. In the high arctic where the water is permanently at the freezing point, it is likely that the keel deteriorates more slowly, whereas in the southern Beaufort Sea where the surface water temperature warms as a result of river influx and sunshine, it is likely that the keel deteriorates more rapidly to form a smooth featureless form. Studies of the keel of a first year ridge in the southern Beaufort Sea indicated that by June, the blocks in the keel were like Swiss cheese, full of large holes that the diver could put his fist into. Very likely these ridges would have melted completely shortly after being investigated.

9.2 Comparison of IPS and Satellite data

In the current analysis, an attempt was made to correlate the ice thickness as indicated by a stationary Ice Profiling Sonar (IPS) on the seabed, with the ice as seen in a satellite image. The satellite image provides a picture of the ice surface. This ice surface moves around as a result of winds and currents, and in particular, it moves around over the IPS and results in the different ice thicknesses seen by the IPS. The ADCP installed alongside the IPS indicates how the ice moves. In principle, if the ice sheet remains intact and simply translates with a trajectory as indicated by the ADCP, then it should be possible to draw the ice movement trajectory onto the satellite image, based on the ADCP data, and compare the IPS data directly with the satellite image – one would hope to see thin ice as indicated by the IPS and corresponding to areas of thin ice in the satellite image. In practice, the ice rotates and converges and diverges, and so attempting to compare IPS data with satellite data may or may not work, depending on the motions of the ice sheet. At least we would expect the method to work for a few hours to maybe two days on either side of the date and time of the satellite overpass.

In this project, we use the IPS and ADCP data obtained by IOS and Synthetic Aperture Radar images from the ERS-2 (European Remote Sensing satellite). Data from Melling's

Site 5 at Latitude 73° 27.133' and Longitude 126° 36.051' was used. These instruments were located in 108m of water just off the north west coast of Banks Island.

Figure 9-1 shows an overlay of IPS data onto the ERS-2 image of 30 August 1996. The Canadian Ice Charts indicated that the ice over the site at the time was 9+/10 concentration with 8/10 old ice, 1/10 Medium First year and <1/0 Nilas.

The ice movement data as indicated by the ADCP for two days before and after the date and time of the satellite image were reversed and expressed in nautical miles north-south and east-west relative to the date and time of the satellite image. These data were then converted to latitude and longitude using the location of the IPS/ADCP instruments as the zero point. The color of the ADCP track was changed according to the ice thickness as indicated by the IPS, and the resulting track was overlain onto the satellite image, as shown in the Figure.

Figure 9-1 shows the satellite image, the ice thickness coded ice track, and two graphs indicating ice thickness. The CIS ice chart interpretation agrees with the ice conditions as indicated by the satellite image, and the thickness of the ice as indicated by the IPS; about 2m and thicker. As we do not know the actual thickness of the ice as indicated by the satellite image, the only regions that we can actually correlate are regions of very thin ice or open water as indicated by IPS and the black inter floe regions on the image. These show little or no correlation on a one to one basis between IPS and the satellite image. The cross on the IPS line indicates where the IPS was located at the date and time of the image (the satellite over pass); a close correlation of ice thickness and satellite image would be expected at this location. The IPS data indicate a region of thin ice at or near this spot, but no corresponding region can be seen in the satellite image. The large ice thickness graph in Figure 9-1 indicates a lead comprising very thin ice or open water. No corresponding feature can be seen in the image. This would suggest that the ice sheet contained leads, and these subsequently closed prior to the time of the satellite overpass.

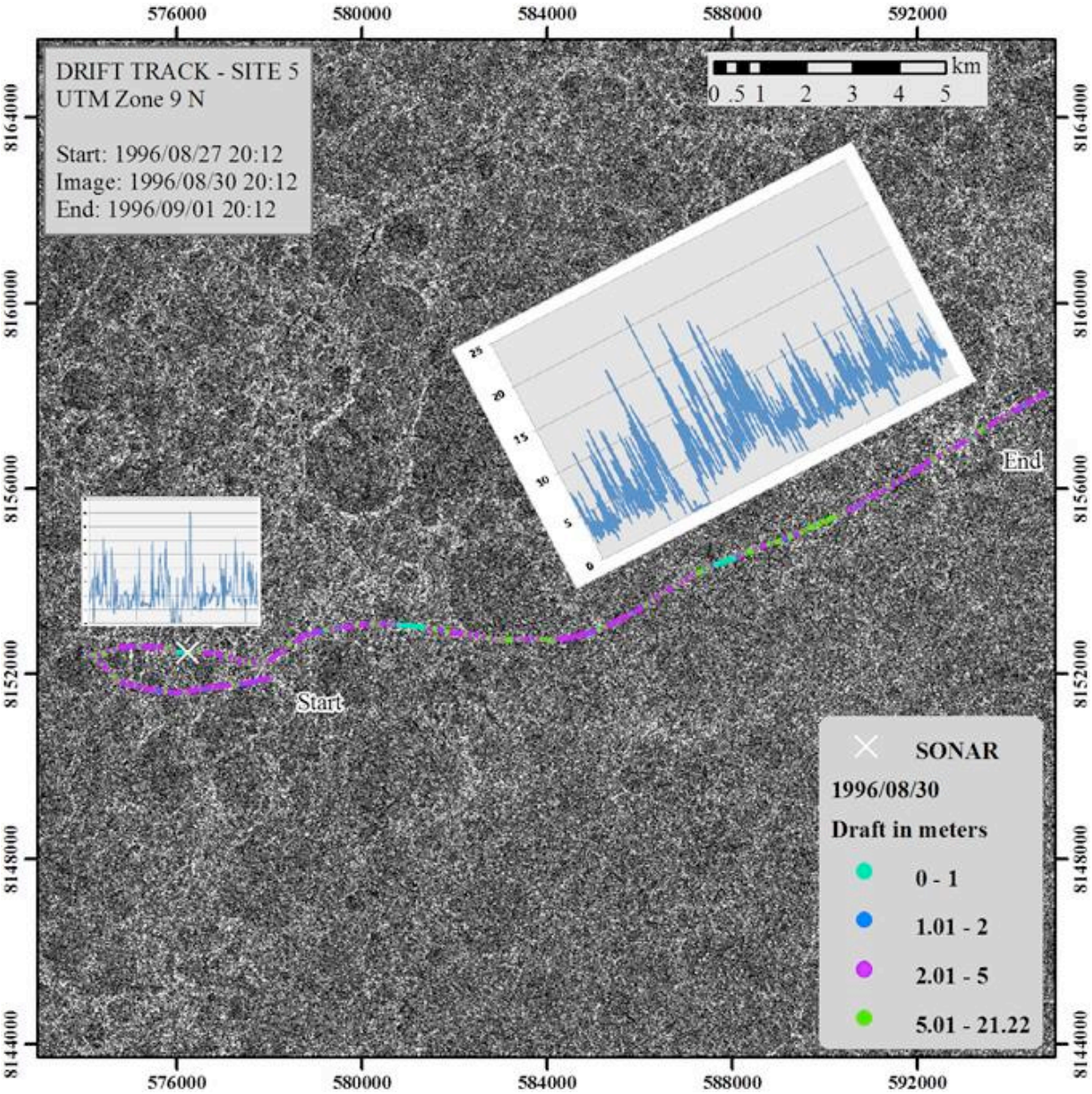

Figure 9-1 Overlay of IPS data on ERS-2 SAR image for 1996/08/30

Figure 9-2 shows the overlay of IPS data onto ERS-2 SAR for 18 September 1996. The ice is composed of old ice floes as indicated by their smooth roundish shape, interspersed with rubble composed of new or old ice. The CIS Ice Chart for 19th September indicated 9+/10 total concentration with 9/10 old ice and 1/10 Thick First year ice, which generally agrees with the image. The IPS data indicate an ice thickness of 2 to 5m, which, in September, would be second-year or old ice, again reasonable. However, when we try to find a correlation on a one to one basis for features that we can specifically see, such as thin ice or open water, we do not see a particularly good correlation, clearly because the ice rotates, diverges and converges as it moves. Looking at the loop near the location of the IPS, as

indicated by the white cross, the large floes to the west of the cross are 2 to 5m thick, which is reasonable, but there appears to be a similar old floe along the track just east of the cross and it is indicated as only 0 to 1m thick. The small polynya due south of the cross is indicated correctly as 0 – 1 m as is an area to the north east of this, although the region appears to have closed up somewhat. As one moves away from the location of the IPS (the cross), the correlation deteriorates to the point where there is no correlation. The IPS indicates a region of thin ice or open water, which is not evident on the satellite image. This region was scanned by the IPS before the date and time of the satellite image, so clearly the ice converged after this particular point passed over the IPS. Note that this lead or polynya was about 2.5km wide at the time it passed over the IPS then closed – the small polynya just south of the region might be the remnants of this polynya.

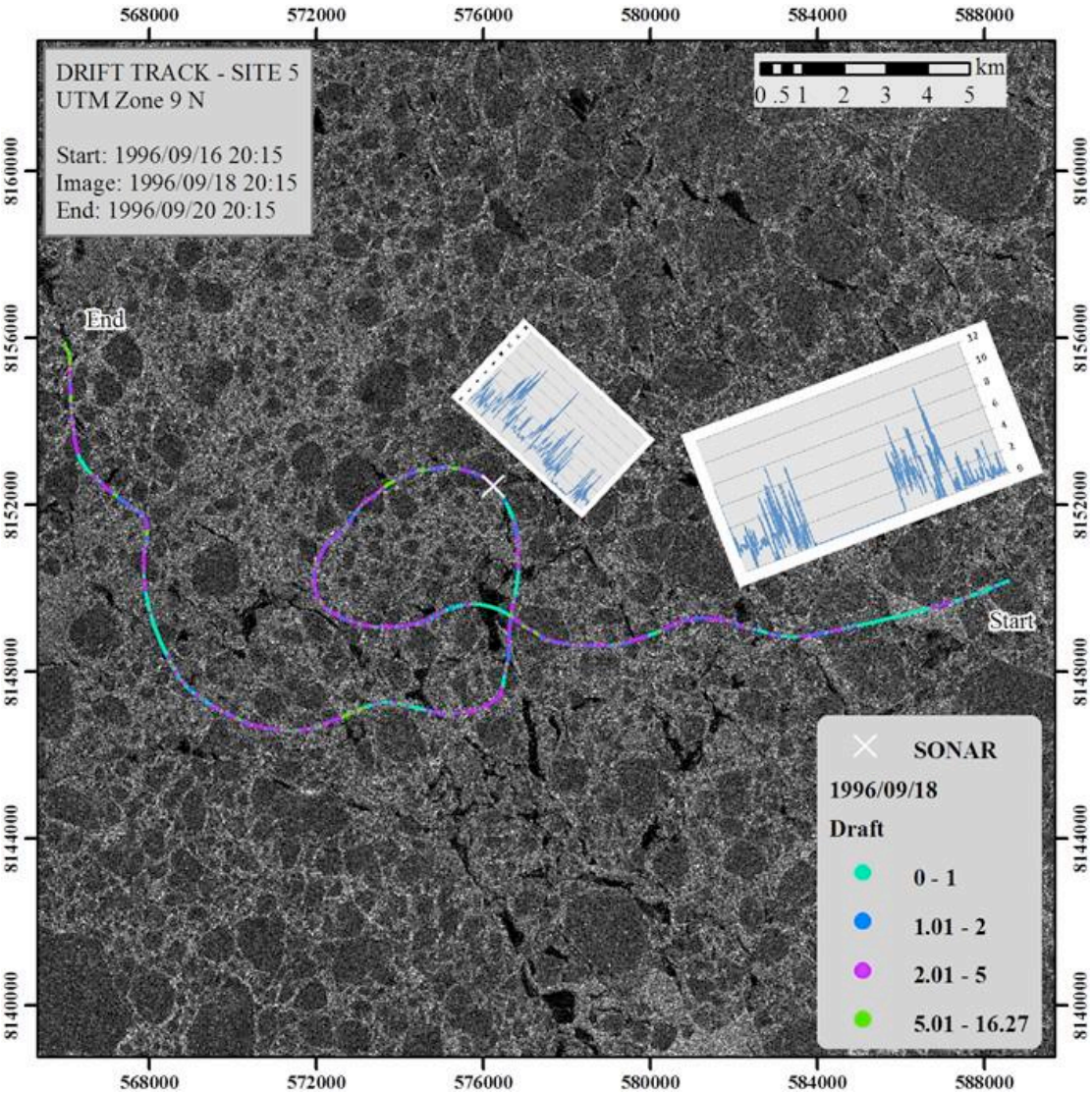

Figure 9-2 Overlay of IPS data on ERS-2 SAR image for 1996/09/18

Figure 9-3 shows the ERS-2 satellite image for 26th October 1996. The CIS Ice Chart for 29th October indicates 9+/10 total concentration of ice, with 9/10 multiyear ice and 1/10 old ice. The satellite image indicates that the ice sheet was 9/10 old and multi-year and 1/10 new ice, suggesting that the ice converged between the 26th and 29th Oct. The IPS indicates ice that is 2 to 5m thick (purple) which agrees with the designation of old ice at this time of year. On a one to one basis, there is good correlation between IPS data and satellite image for the region of thin ice at the centre of the graph, although the region in the satellite image is wider than that in the IPS data. Moving to the right beyond the graph the IPS indicates thin ice (blue-green) and this does not appear to agree with the satellite image. This poorer correlation is expected as one moves away from the IPS and the date and time of the satellite image.

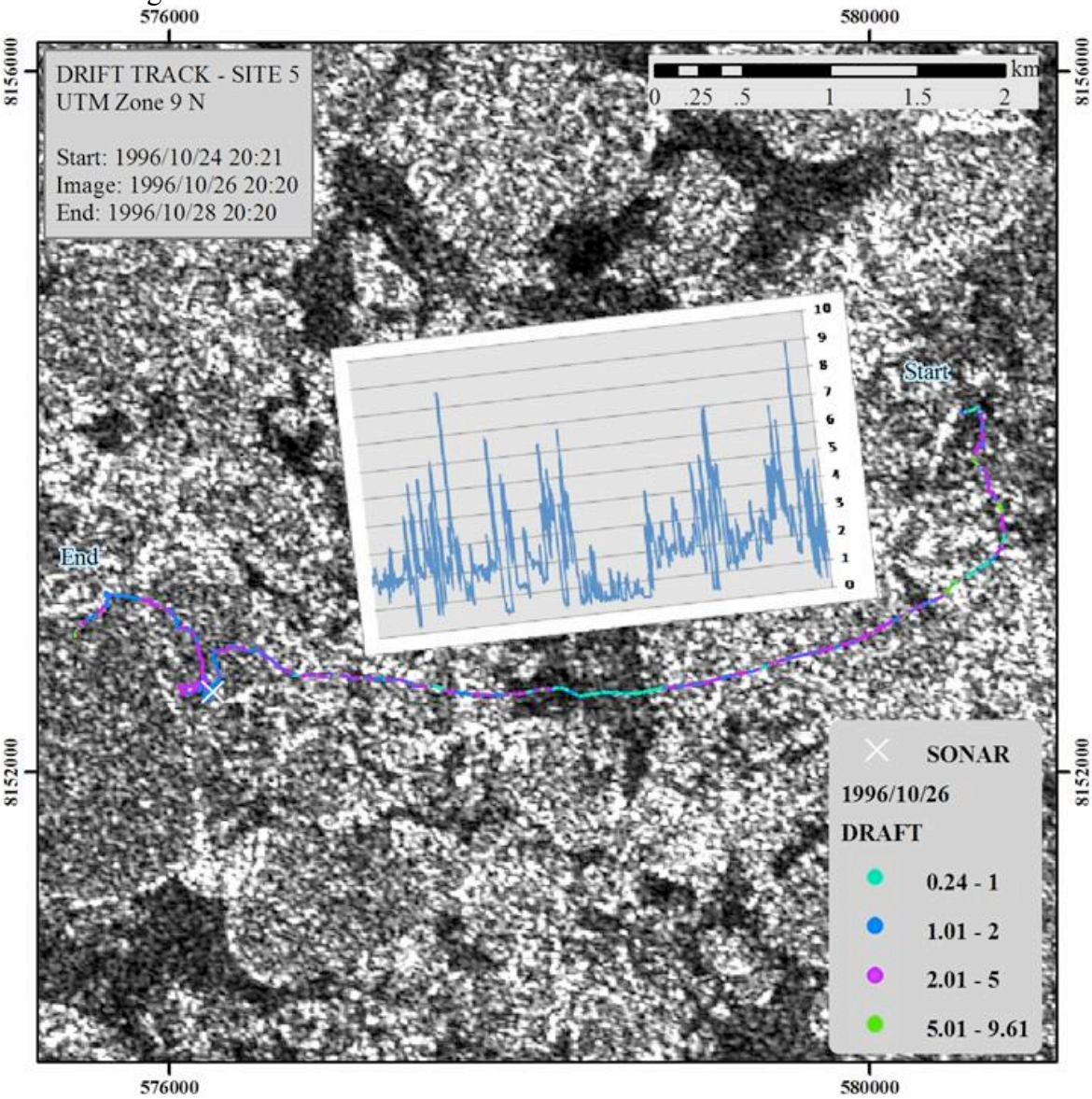

Figure 9-3 Overlay of IPS data on ERS-2 SAR image for 1996/10/24

Figure 9-4 shows the overlay of IPS data onto the ERS-2 image for 11th November 1996. The CIS ice chart for 12th November indicates 9+/10 concentration with 9/10 multiyear and 1/10 old or second year ice. The satellite image indicates 9+/10 total concentration with about 8/10 old or multiyear ice and 2/10 first year ice. The IPS indicates ice greater than 2m thick (old or Multiyear) and ice about 1m thick (medium first year ice); hence there is generally good agreement. The IPS indicates several probable first year ridges 12 to 16m deep - note how spiky the ridges are. There is a good correlation in this case. One can see several cases where the IPS indicates thin ice and these correlate with polynyas between floes, particularly close to the location of the IPS (A) and even at some distance away (B). At Region C, the IPS track is slightly displaced relative to the polynya, but this point is over a day from the time of the satellite over pass, and one would expect the ice to have diverged, converged or rotated over this period.

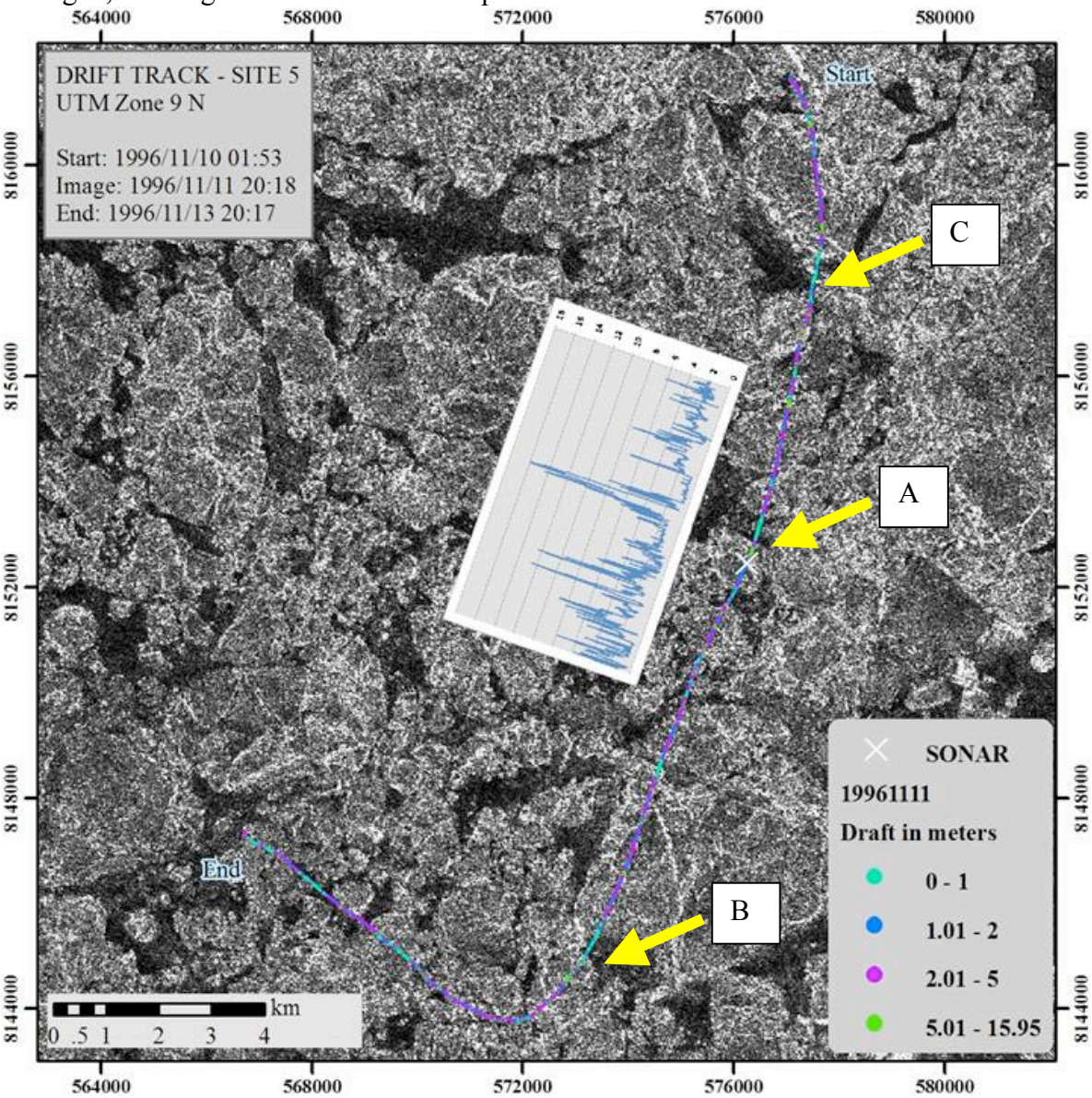

Figure 9-4 Overlay of IPS data on Radarsat image for 1996/11/10

9.3 Detailed Look at IPS Data

As indicated above, it is known that the ice surface is a mixture of level first year ice, second ice and multiyear ice and first and old ice ridges. A region of predominantly first year ice, such as the land fast ice and seasonal pack in the Beaufort Sea, the ice is very level, interspersed with first year ridges that are very spiky. Such areas are clearly evident in the IPS data at almost any horizontal scale. Figure 9-5 shows an example of 0.7m thick first year ice with a 6m pressure ridge. Note the smooth first year ice and the spiky pressure ridge, which is almost 6m deep.

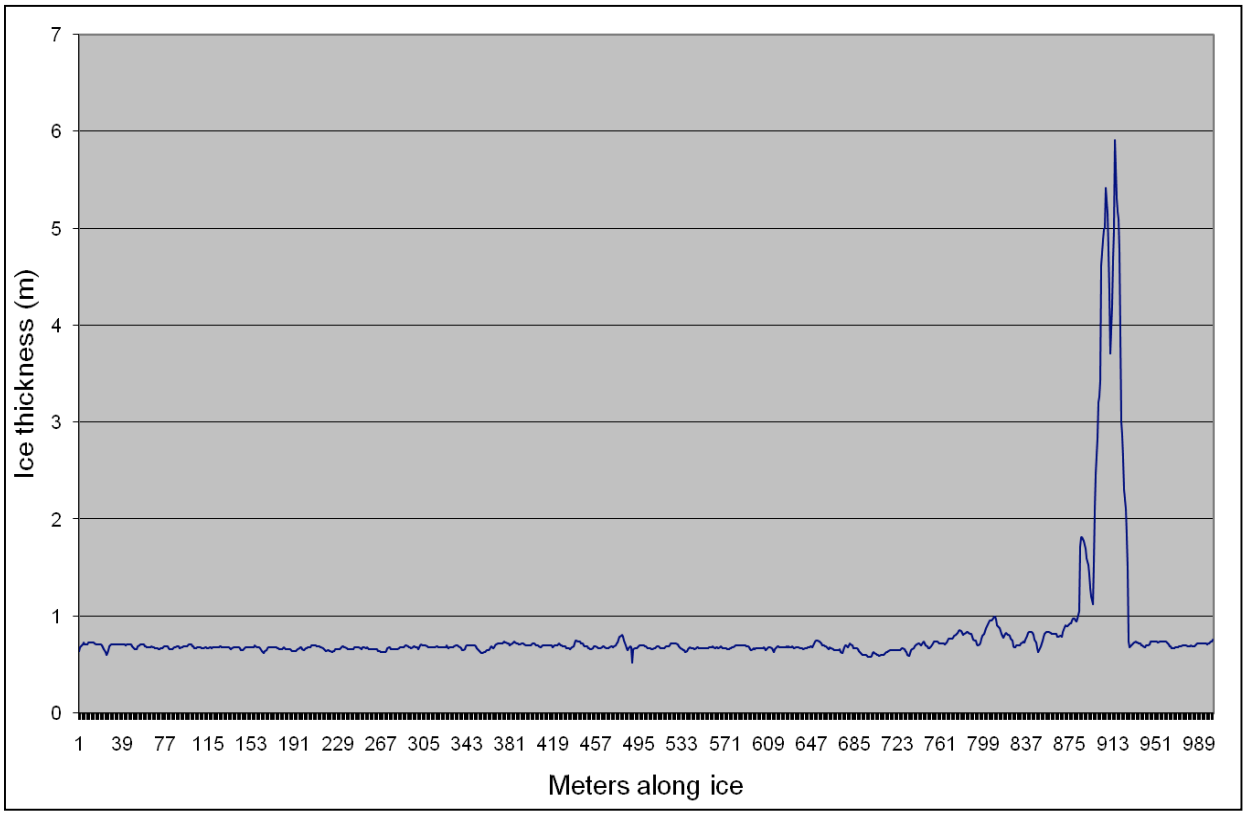

Figure 9-5 Example of first year ice in IPS data

Figure 9-6 shows an example of level first year ice, ridges and old ice, as interpreted by "what one would expect". By stretching out the chart, it is possible to see the old ice greater than 2m, 0.5m thick level first year ice, and a series of ridges that could be either first or old ice. A region is identified as second year ice but it appears that there are a number of new ridges within this ice, as indicated by their spiky features. It is noted that the smooth ice, which is believed to be old ice, is generally smaller than what is believed to be new ice ridges; this is to be expected as old ice generally derives from ridges.

Note that new ridges could be either comprised of first year ice or old ice. A ridge in a region of first year ice would most likely to be comprised of first year ice. Ridges within regions of second or multiyear ice could be either comprised of first or old ice. However, offshore, where this IPS is located, the ridges are most likely formed from new ice - for example from a refrozen first year lead, as the pack ice pressures are unlikely to be enough to destroy thick old ice. Ridges near shore could be either first or old ice, as the presence of land can amplify pack ice pressures and fail even thick old ice, particularly in the late summer when the ice is weaker.

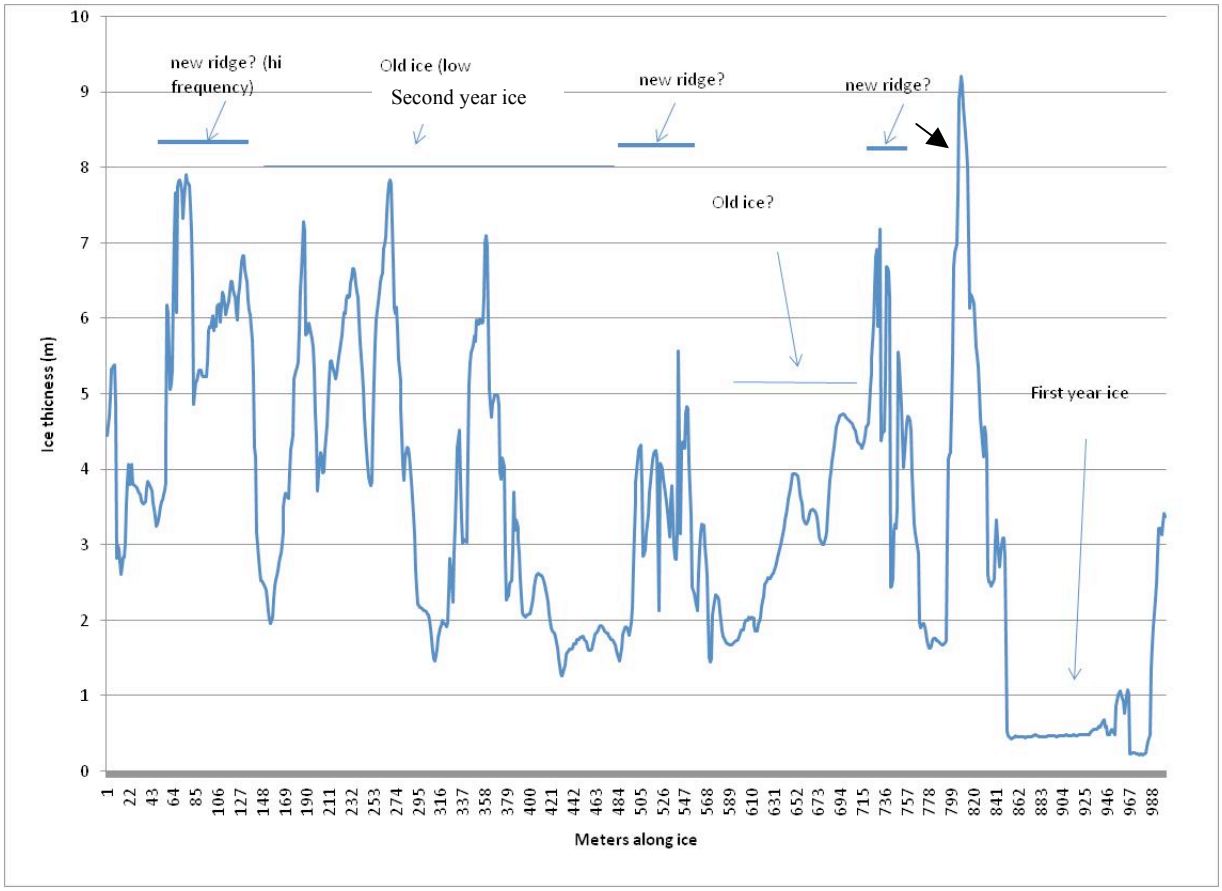

Figure 9-6 Example of old and first year ice in the IPS data (author interpretation)

Figure 9-7 shows mainly what is believed to be second or third year ice. The base ice thickness is about 1.7m thick, and the ridged ice is not as spiky as one would expect from first year ridges, but spikier than one would expect from old ice. There is clearly a first year ridge at 840m. Again the first year ridge is larger than the (what is believed to be) second year ice, as one would expect, as the second year ice derives from first year ice and deteriorated first year ridges.

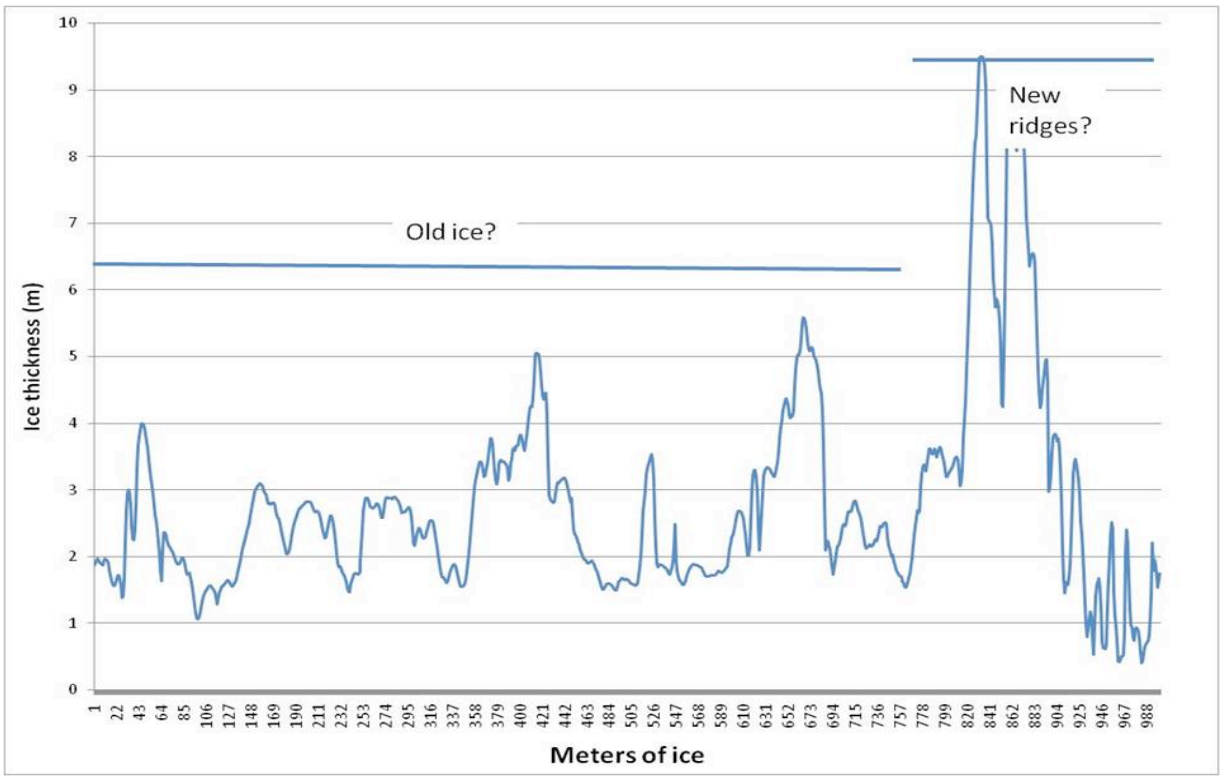

Figure 9-7 Example of mainly second year ice in IPS data

9.4 Conclusions

The comparison of IPS and ERS-2 radar satellite data indicates:

1. In general, the ice types as indicated by the CIS ice chart, satellite image, and IPS data agree. However, as one does not know the thickness of ice in a satellite image, it is difficult to say how well the satellite image agrees with the IPS data in general.
2. If one tries to correlate specific features in the IPS and satellite image, such as thin ice or open water – features that one can see in the data, then the correlation is generally not good. Clearly the ice converges, diverges, and rotates as it moves. Expecting a good correlation in such a comparison would require the ice sheet to simply translate.
3. In one case in November when there was clearly new ice forming between the floes, a reasonable correlation is noted between IPS and radar image for both the general ice type and the occurrence of thin ice or open water. There are several cases in which regions of thin ice in the IPS data overlay regions of thin ice in the satellite image, particularly close to the IPS location. There is one case in which it would appear that thin ice in the IPS is close to but not overlapping a region of thin ice in the image, clearly because the ice has deformed as well as translated as indicated by the ADCP.

4. A detailed look at sections of IPS data indicates what is believed to be first year, second year and old ice. Level first year ice is easy to detect by its thickness (less than 2m) and very level appearance. First year ridges can be identified by the very spiky appearance, and they are likely thicker than other ice. Second year ice is greater than about 1.7m and not as spiky as first year ridges, but smoother than old ridges. Old ridges are very smooth.
5. Ideally one would like to be able to sort out the different ice types by means of some electronic filter that would pick out the different ice types. Clearly one problem is that the sections of different ice types are too short. This requires further review by an expert on filtering. If one could filter the data, then it might be possible to identify regions of old ice and so obtain the thickness of just the old ice. As indicated, pressure ridges are the deepest ice features, and it is likely that the thickness of old ice determined from IPS or submarine data has been greatly over estimated as it is impossible to separate the old ice from the ridges.

10 ICE VELOCITY FROM MOORED ADCP – CANADIAN BEAUFORT SEA

10.1 Data Source

Ice profiling sonars (IPS) and doppler sonars (ADCP) were deployed at 11 locations on the seabed of the Canadian Beaufort Sea over the period 1990-2004 by the Institute of Ocean Sciences (IOS). See Figure 10-1. Data for this project were obtained from Dr. H. Melling of IOS. They are available from the following source:

"Melling, H. and D.A. Riedel. 2008. Ice Draft and Ice Velocity Data in the Beaufort Sea, 1990-2003. Boulder, Colorado USA: National Snow and Ice Data Center. Digital media." URL http://www.nsidc.org/data/g02177.html

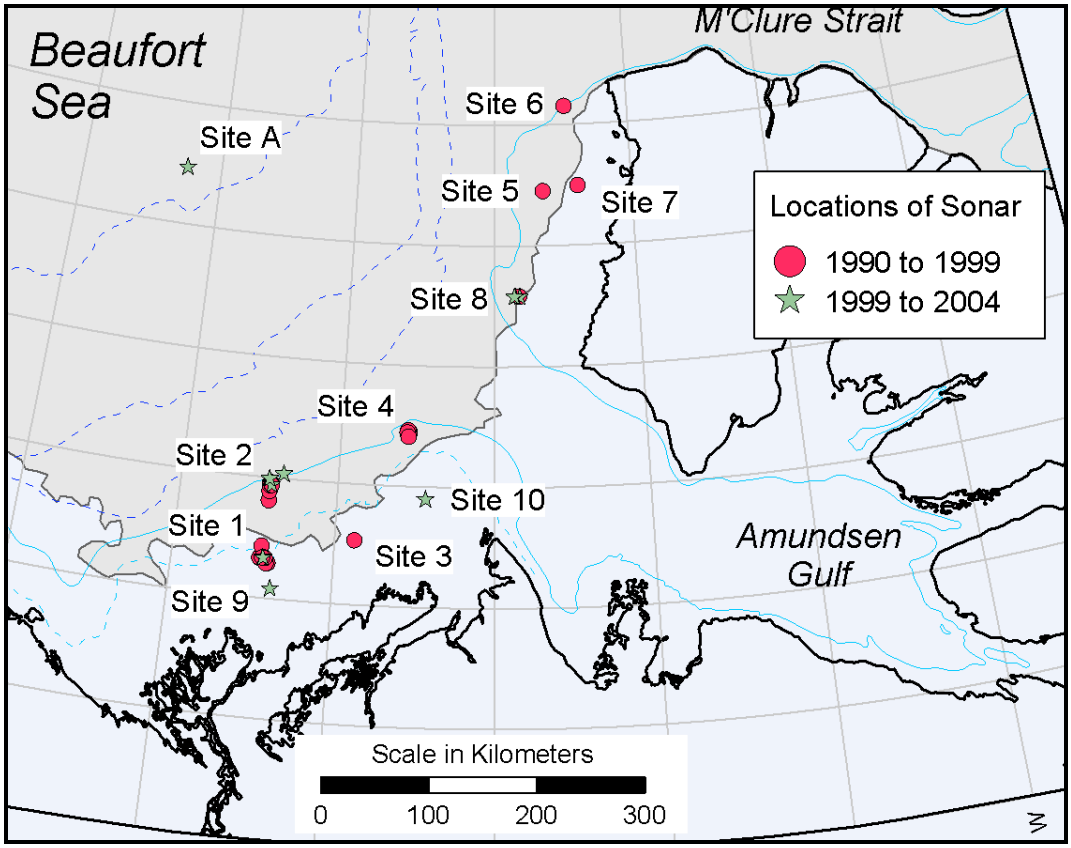

Figure 10-1 Map of IPS/ADCP Deployment Locations by IOS

Ice movement at all sites is influenced by the Beaufort Gyre. From previous analyses of drift buoy data (e.g. as in Figure 2-3) it is known that Sites 1 to 4, which lie in the area of historical offshore operations, are in a different ice drift regime from Sites 5 to 8. Ice drift in these two areas is therefore treated separately in Sections 10.2 and 10.3.

10.2 Ice Velocity Statistics – Southern Canadian Beaufort Sea

10.2.1 Data Description

For the present study, the 13-year data set from Site 1 in Figure 10-1 was taken to represent the ice drift in the common operating areas. Table 10-1 from Melling's report "Mooring Site History", shows the years, locations, and sample intervals for the IPS that he installed.

Table 10-1 Summary of IPS Deployment Locations

Year	Latitude	Longitude	Sample Interval [min]
1990	70.30500	133.61033	31.6
1990	70.34717	133.73267	30
1992	70.33032	133.82777	40
1993	70.29220	133.61258	40
1994	70.28962	133.65660	30
1995	70.42885	133.79468	30
1996	70.33620	133.70573	15
1997	70.33375	133.69698	15
1998	70.33418	133.75130	30
1999	70.33445	133.74827	15
2000	70.33458	133.74847	15
2001	70.33160	133.73720	30
2002	70.33287	133.74017	30
2003	70.33288	133.74105	30

Break-up and Freeze-up times (Table 10-2) were determined using the Canatec ICE'06 Program. Here we define summer as "loose pack" in which there is little ice-ice interaction and winter as when we have significant ice-ice interaction. "Breakup" was defined as the date when the total ice concentration dropped from greater than 5/10 to 5/10 or less and "freeze-up" when the ice concentration rose to 8/10 or more (usually from a significantly lower ice concentration.

Table 10-2 Break-up and freeze-up dates at the IPS Locations

Year	Break-up	Freeze-up	Year	Break-up	Freeze-up
1990	June 21	October 11	**1997**	June 7	October 11
1991	June 7	October 4	**1998**	May 31	October 21
1992	July 12	October 4	**1999**	May 31	October 11
1993	June 7	November 1	**2000**	August 9	October 4
1994	August 2	October 18	**2001**	August 2	October 18
1995	May 3	October 21	**2002**	July 12	October 4
1996	June 21	September 27	**2003**	June 20	October 11

The total number of IPS records is 229,844 and of these, 69,219 were classified as "bad data"[2]. Table 10.3 summarizes the number the records for winter and summer.

[2] Data with temporary ambiguity in the validity of echo ranges (Melling, H. and D.A. Riedel)

Table 10-3 Number of Records for Summer and Winter

	Total number of records	Number of "Bad Data" records	Effective number of records	Effective number of records (%)
All	229,844	69,219	160,625	69.9
Summer	64,168	59,057	5,111	8.0
Winter	165,676	10,162	155,514	93.9

Besides the considerable number of bad data records, for the most part in summer, there are also time gaps in the data (Table 10-4) due to periods of open water, when there were no ice targets. As expected, these gaps occur mainly in summer, but can occur at other times of the year, as indicated in the table below.

Table 10-4 Gaps in the IPS Data

Gaps
March 12 1991 to April 25 1992
August 9 1992 to September 25 1992
April 17 1993 to April 26 1993
September 19 2001 to September 25 2001
September 10 2002 to September 14 2002

10.2.2 Ice Velocity Analysis Site 1 – All Years

10.2.2.1 Drift Speed Distribution Site 1 – All Years

Figure 10-2 shows the speed frequency distributions. Figures 10-3 to 10-5 show the speed exceedance probability charts for all data, for all winters and for all summers, respectively. Note that the term Year in the Figures refers to all of the data for a complete year.

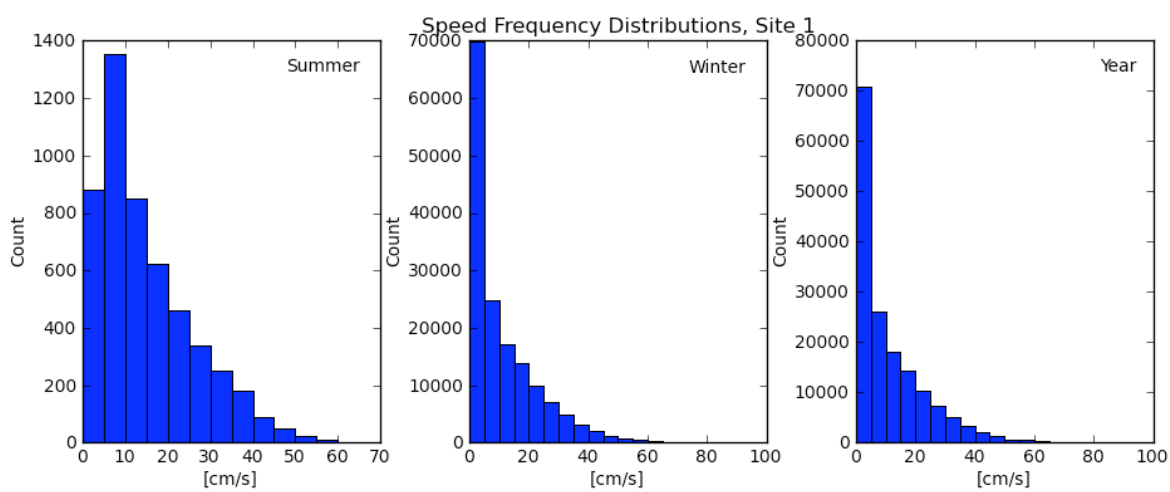

Figure 10-2 Frequency histograms for Ice Speed for all years at Site 1

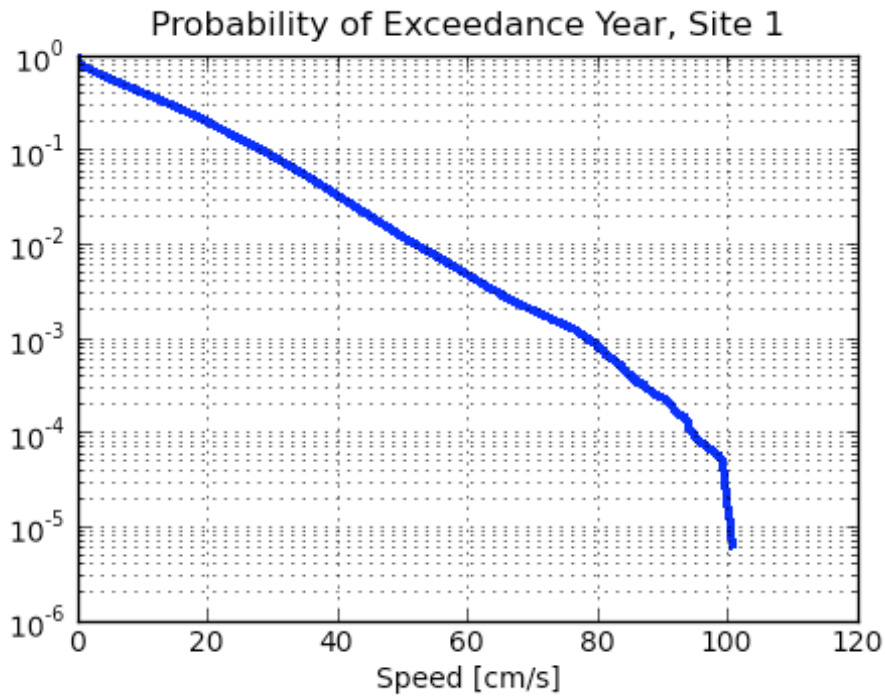

Figure 10-3 Exceedance Probability for Ice Speed at Site 1 - Annual

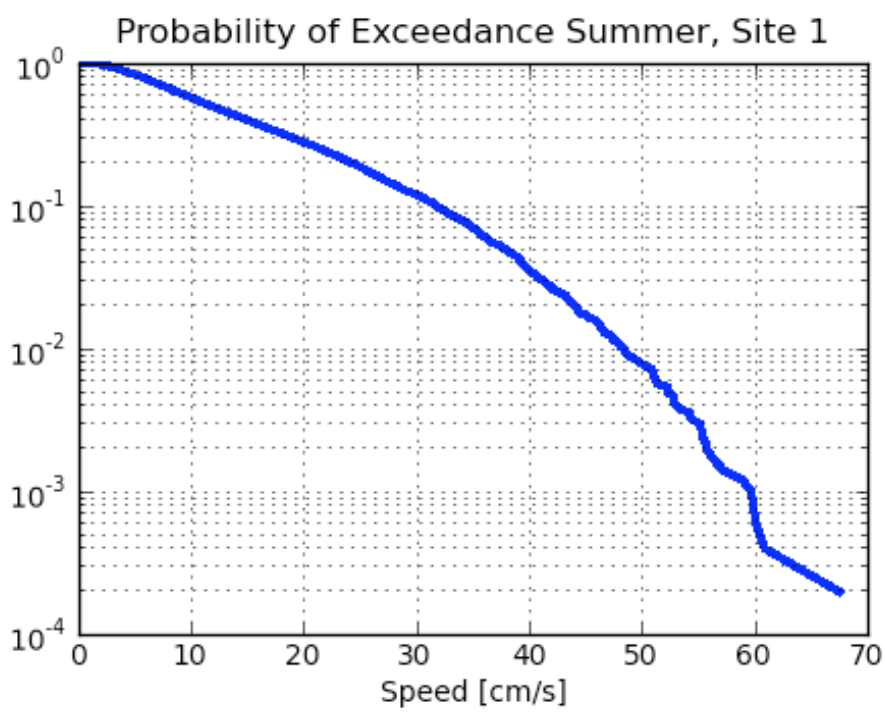

Figure 10-4 Exceedance Probability for Ice Speed at Site 1 - Summer

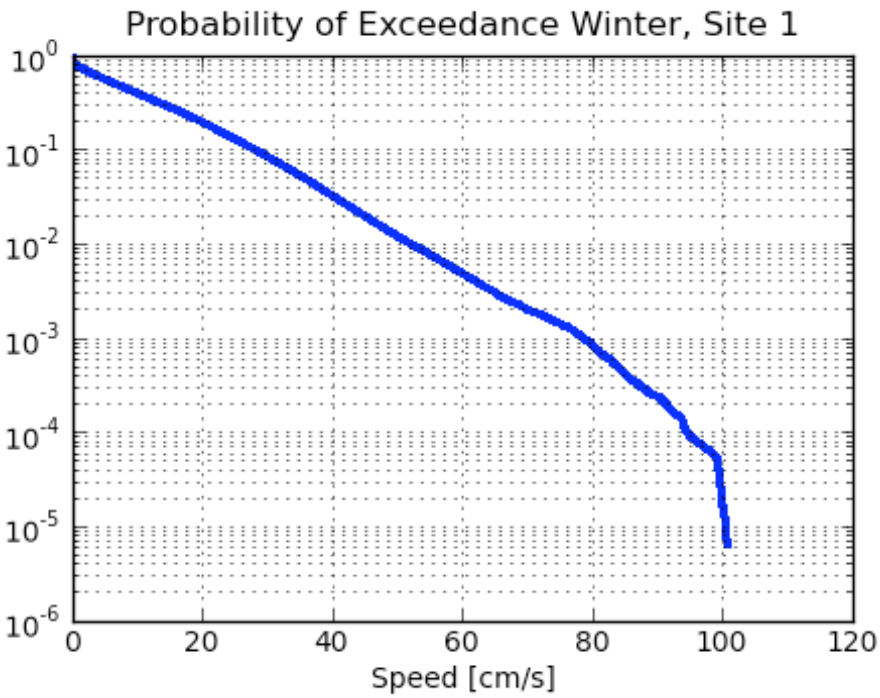

Figure 10-5 Exceedance Probability for Ice Speed at Site 1 - Winter

10.2.2.2 Summary of Drift Speed Statistics Site 1 – All Years

Table 10-5 presents ice speed statistics. Figure 10-6 shows a Box Plot as a visual guide for the percentiles.

- As expected mean and median speeds are higher in summer, as the ice floes are free drifting. Mean was 10.7 cm/s for winter and 15 cm/s for summer.
- 80 % of the speeds are in the range 0 - 28 cm/s in winter and 3.6 - 31.7 cm/s in summer.
- The maximum measured ice drift speed of 100.7 cm/s was observed in winter. Summer maximum was 67.5 cm/s

10.2.2.3 Drift Direction Site 1 – All Years

A suitable method to graphically describe the ice drift (speed-direction-frequency) is the drift-rose, analogous to the wind rose. Following the oceanographic convention, the ice direction is the direction towards which it is drifting. In order to better illustrate the lower speeds in the dataset, a scatter plot is provided beside the drift rose in Figure 10-7 The predominant winter drift directions were to the W, WNW and WSW. The extreme values tend to occur in the westerly directions or in the ESE'ly direction. Summer drift directions were more somewhat evenly distributed than in the winter but there was a tendency to greater frequency of movement in the WNW and ESE directions.

Table 10-5 Ice Speed Statistics for Site 1

	YEAR	WINTER	SUMMER
N of Cases	160625	155514	5111
Minimum	0	0	0.2
Maximum	100.7	100.7	67.5
Arithmetic Mean	10.8	10.7	15.0
Standard Deviation	12.314	12.326	11.183
Coefficient of Variation	113.9%	115.5%	74.8%
Pct 1	0	0	1.2
Pct 5	0	0	2.5
Pct 10	0	0	3.6
Pct 20	0.5	0.3	5.6
Pct 25 (Lower Quartile)	1	0.8	6.3
Pct 30	1.8	1.7	7.3
Pct 40	3.9	3.7	9.2
Pct 50 (Median)	6.6	6.3	11.5
Pct 60	9.9	9.6	14.8
Pct 70	14.2	14	18.9
Pct 75 (Upper Quartile)	16.7	16.6	21.3
Pct 80	19.6	19.4	24.1
Pct 90	28.1	28	31.7
Pct 95	35.6	35.5	37.7
Pct 99	51.7	51.9	48.178

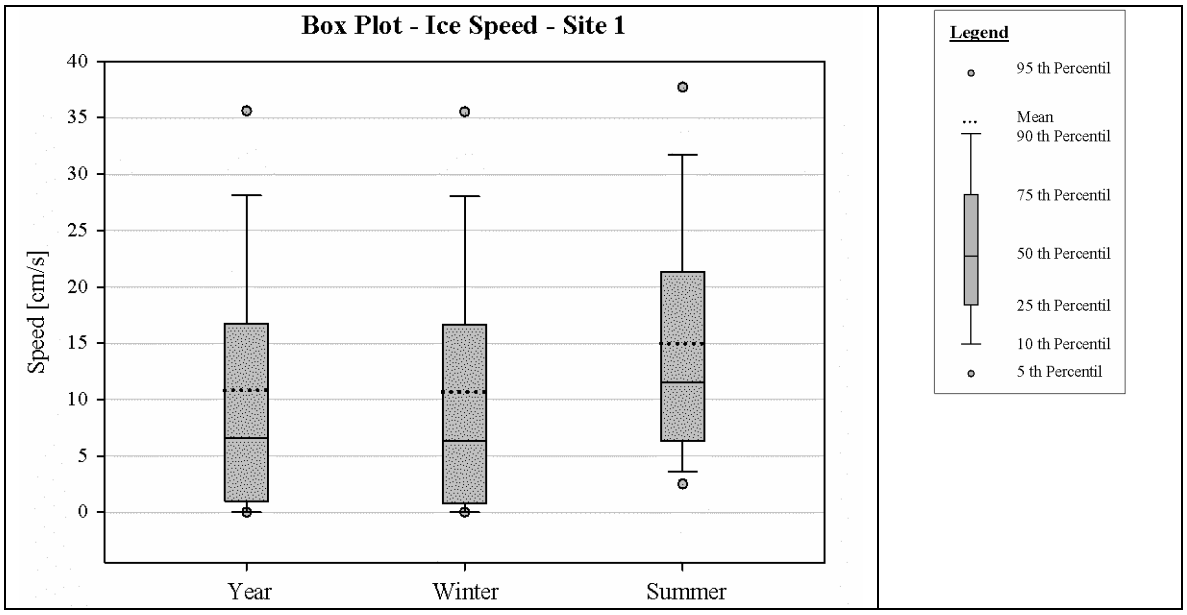

Figure 10-6 Box Plot of Ice Speed Statistics for Site 1: Annual, Winter, Summer

.

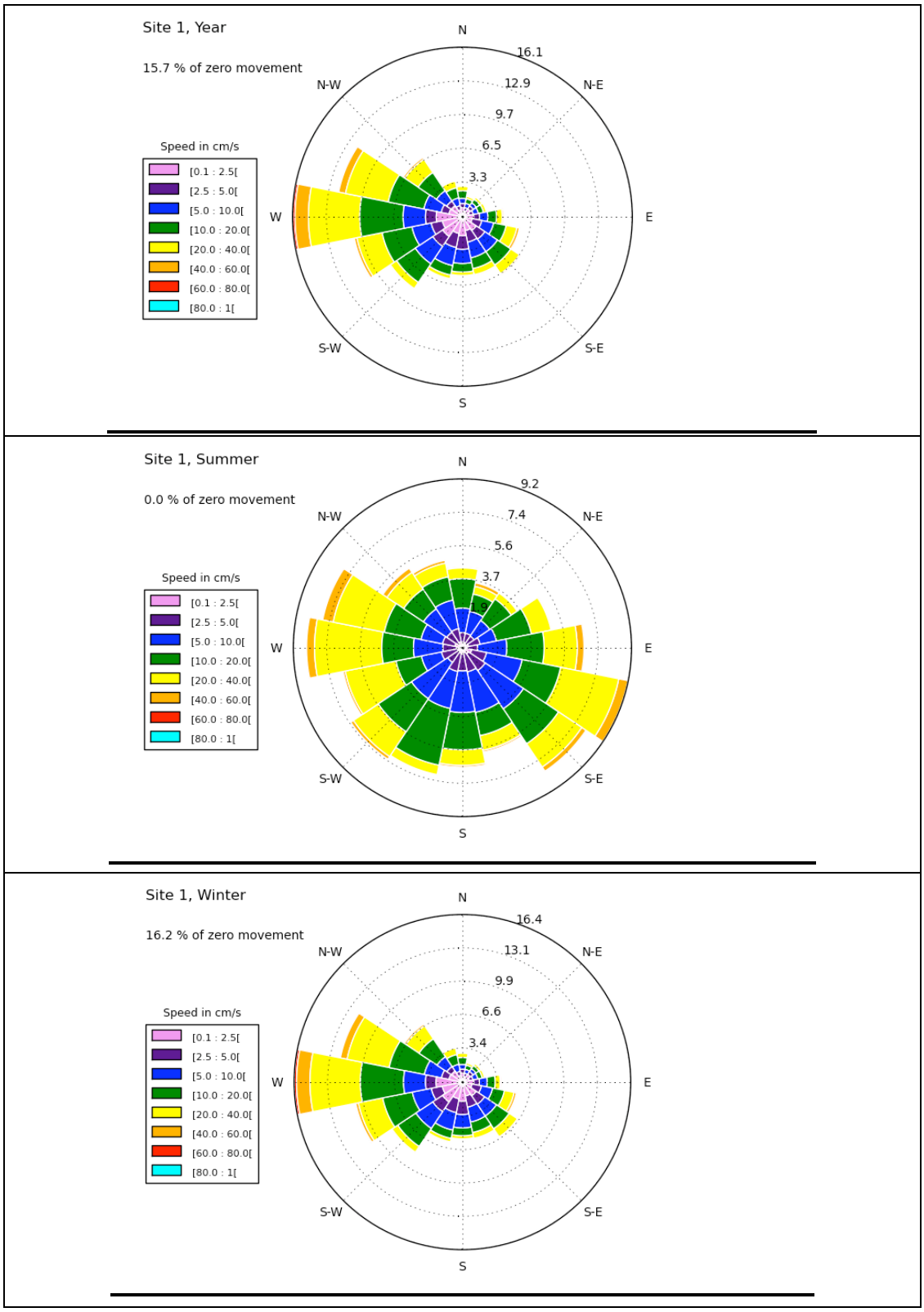

Figure 10-7 Ice Drift Roses and Scatter Plots for Site 1: Annual, Summer, Winter

Although we cannot represent zero speed values in the wind rose or the scatter plot, it is important to keep in mind that a significant percentage of the records contain zero values. More precisely, 15.7% of the records in all years are zero and 16.2 % in winter. For the times when there are data in summer, there are no zero ice drift speeds; thus whenever there is ice in summer, it is moving.

10.2.3 Ice Velocity Analysis for Calendar Year 2002

10.2.3.1 Drift Speed Distribution for Site 1 – Year 2002

Ice drift was analyzed for the year 2002, which is the most recent full year of data. It is interesting to note that this one-year data set did not capture such extreme speeds as the 13-year data set. Figure 10-8 shows the speed histograms for winter, summer and the whole year. Figures 10-9, 10-10 and 10-11 show the exceedance plots.

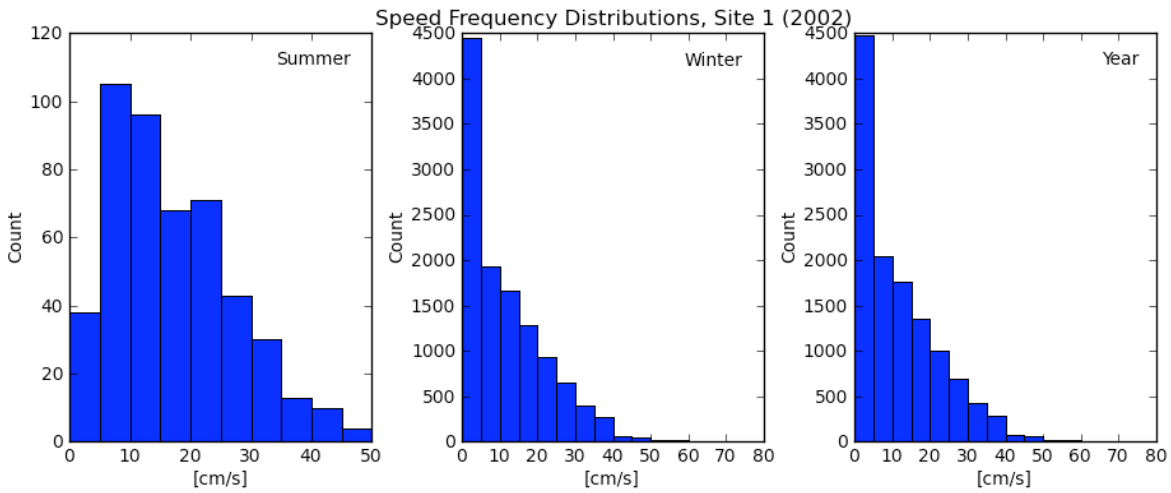

Figure 10-8 Frequency histograms for Ice Speed for 2002 at Site 1

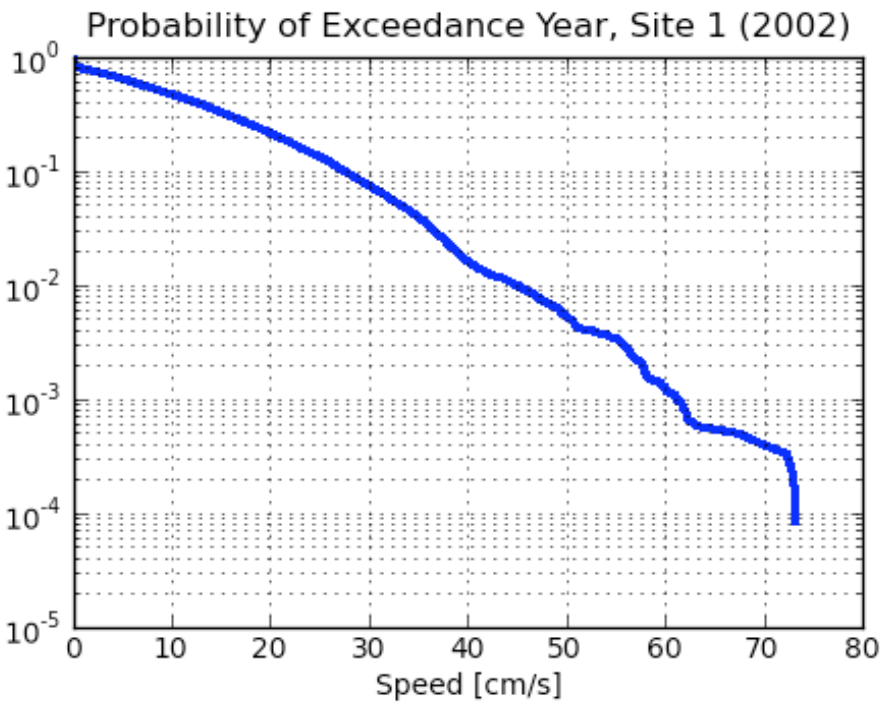

Figure 10-9 Exceedance probability for ice speed 2002 at Site 1 - annual

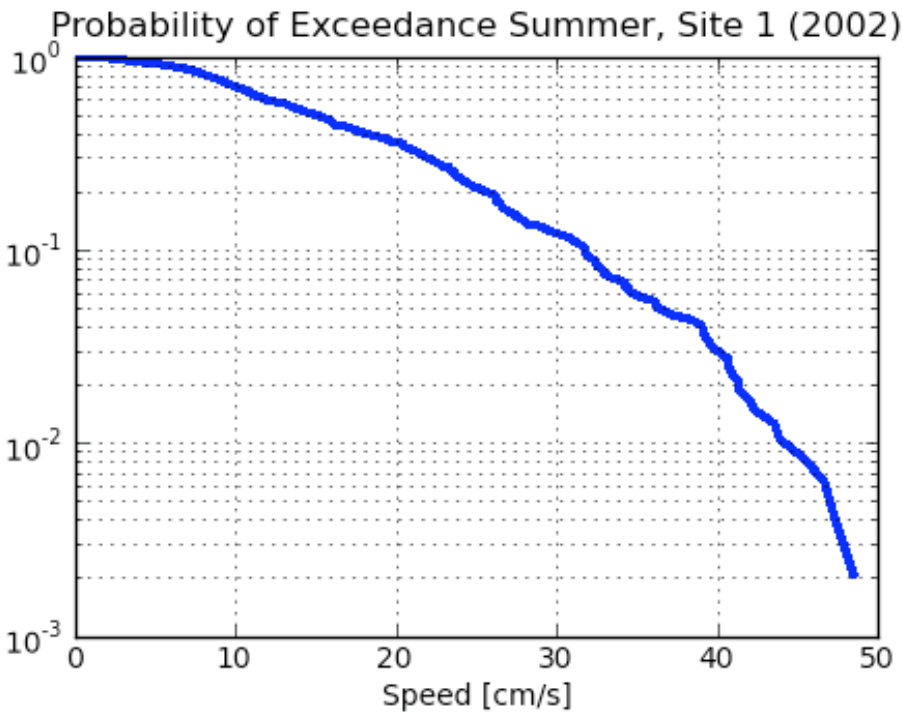

Figure 10-10 Exceedance probability for ice speed 2002 at Site 1 - summer

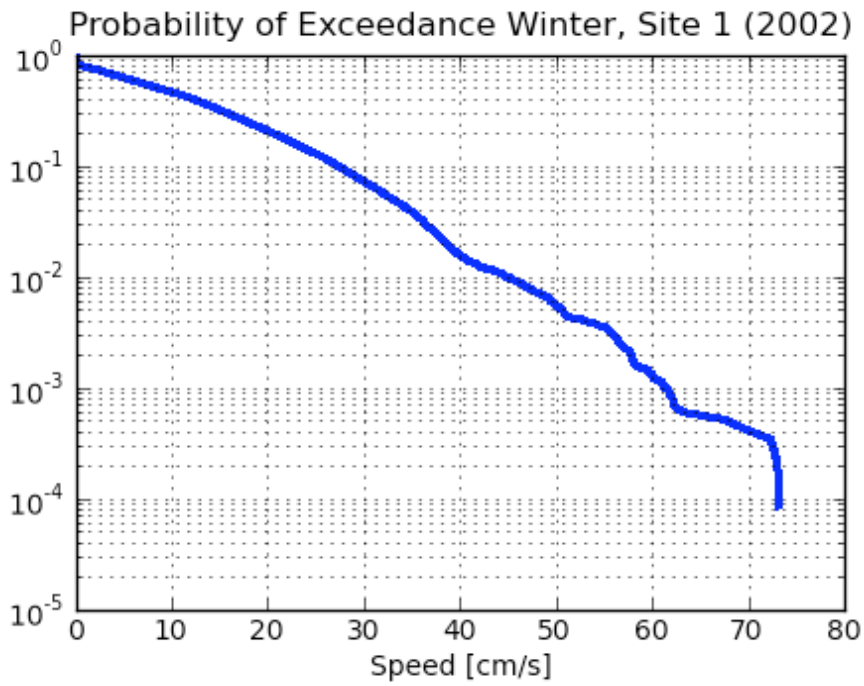

Figure 10-11 Exceedance probability for ice speed 2002 at Site 1 - winter

10.2.3.2 Summary of Drift Speed Statistics for Site 1 – Year 2002

Figure 10-12 shows the box plots and Table 10-6 shows the statistics. Compared with the 13-year database, the mean ice drift speed is slightly higher in both winter and summer, being 11.3 cm/s and 17.8 cm/s respectively. The maximum speed of 73.2 cm/s occurred in winter.

10.2.3.3 Drift Direction for Site 1- Year 2002

Ice Drift roses and scatter plots of speed vs direction for the year, winter and summer appear in Figure 10-13. The winter ice drift directions are predominantly to the west as was the case for the 13-year data set. Summer drift directions in 2002 were almost exclusively to the E and ESE compared with the long-term trend of W, ESE and SW drift. The maximum speed of 73.2 cm/s was towards the WNW.

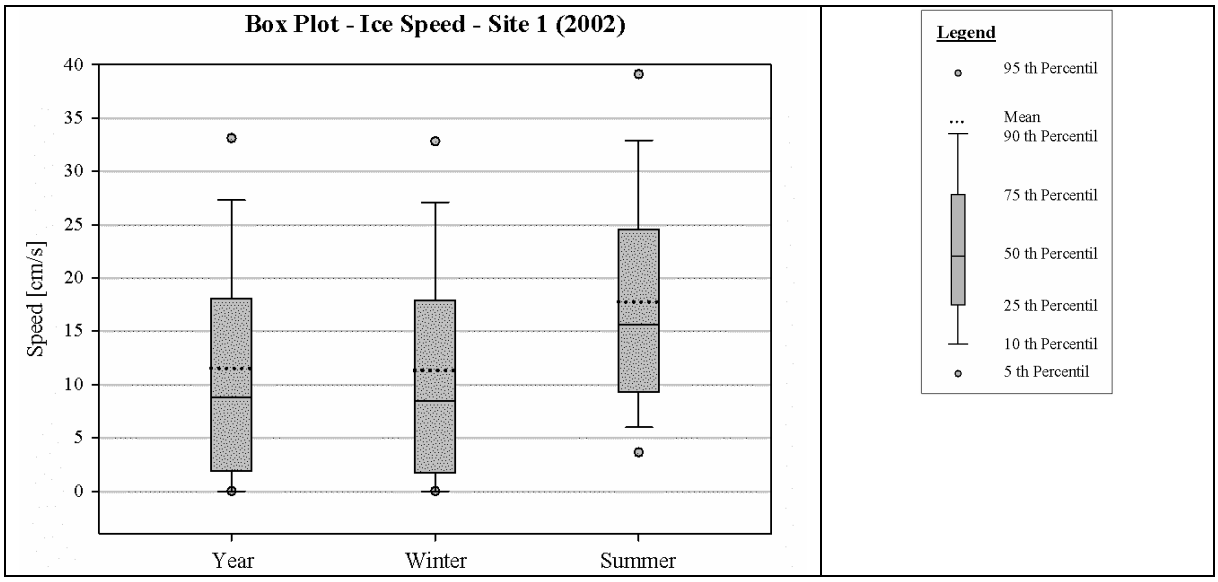

Figure 10-12 Box plot of drift speed statistics for Site 1 2002

Table 10-6 Summary Drift Speed Statistics for Site 1 2002

	YEAR	WINTER	SUMMER
N of Cases	12250	11886	364
Minimum	0	0	1.2
Maximum	73.2	73.2	48.5
Arithmetic Mean	11.5	11.3	17.8
Standard Deviation	11.121	11.0841	10.501
Coefficient of Variation	96.5 %	97.8 %	59.2 %
Pct 1	0	0	1.542
Pct 5	0	0	3.64
Pct 10	0	0	5.99
Pct 20	0.5	0.3	8.43
Pct 25 (Lower Quartile)	1.9	1.7	9.35
Pct 30	3.3	3	10.47
Pct 40	5.9	5.6	12.32
Pct 50 (Median)	8.8	8.5	15.6
Pct 60	12.3	12.1	19.49
Pct 70	15.9	15.6	23.4
Pct 75 (Upper Quartile)	18.1	17.9	24.55
Pct 80	20.6	20.33	26.44
Pct 90	27.3	27.1	32.91
Pct 95	33.1	32.8	39.1
Pct 99	44.6	44.6	45.19

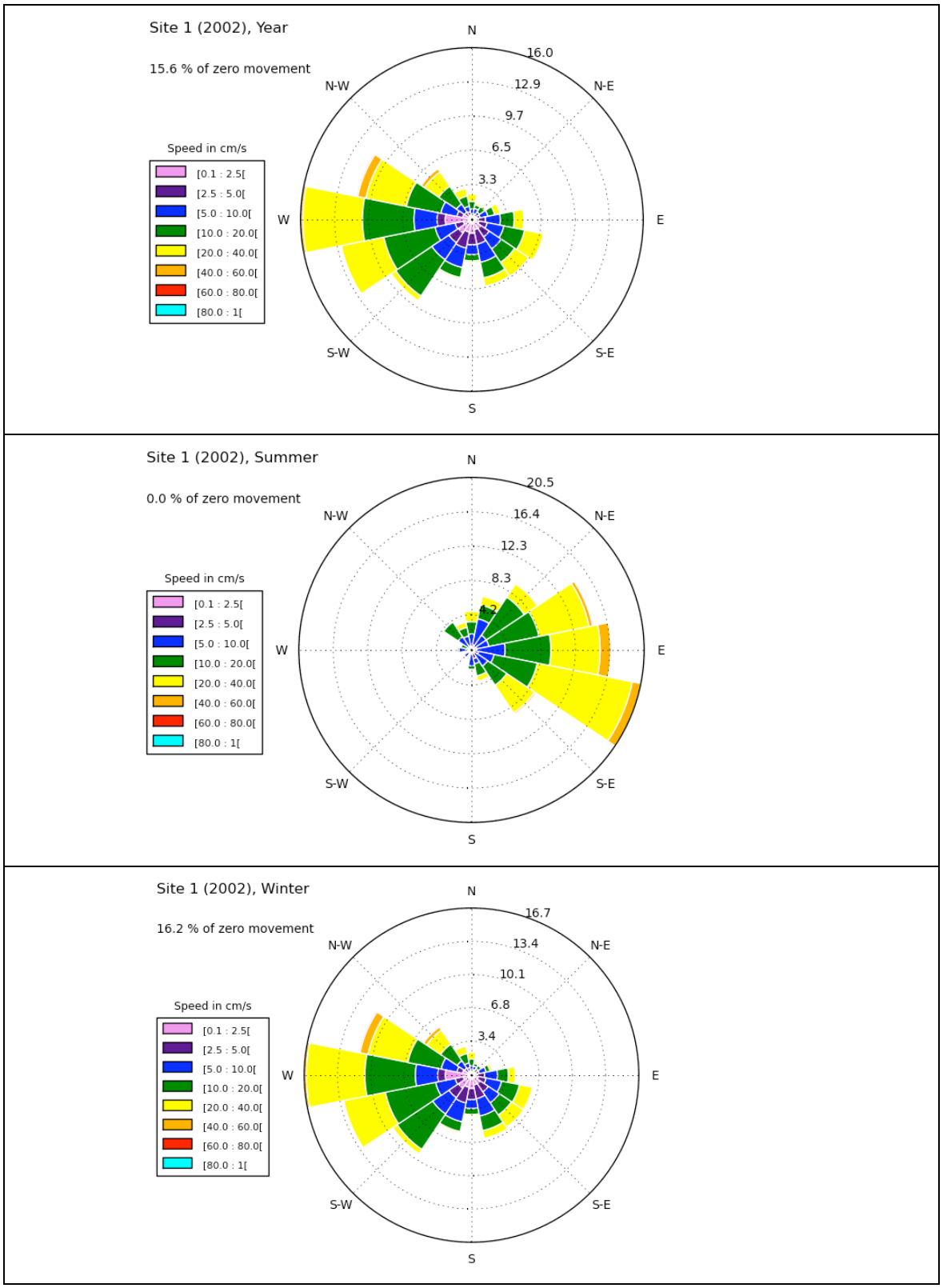

Figure 10-13 Ice Drift Roses and scatter plots for Site 1 - 2002

10.3 Ice Velocity Statistics - North-East Canadian Beaufort

10.3.1 Data Description

ADCP data were analyzed for Site 5 located off the west coast of Banks Island (Figure 10-14). Located at 70.4522 N 126.6009 W, Site 5 was instrumented for 2 almost full years (1996/04/14 – 1997/06/14 and 1997/07/30 – 1998/02/22). The sampling interval was 30 minutes. Break-up and Freeze-up dates were delimited with the ICE 06 program and appear in Table 10-7. Table 10-8 summarizes the workable number the records.

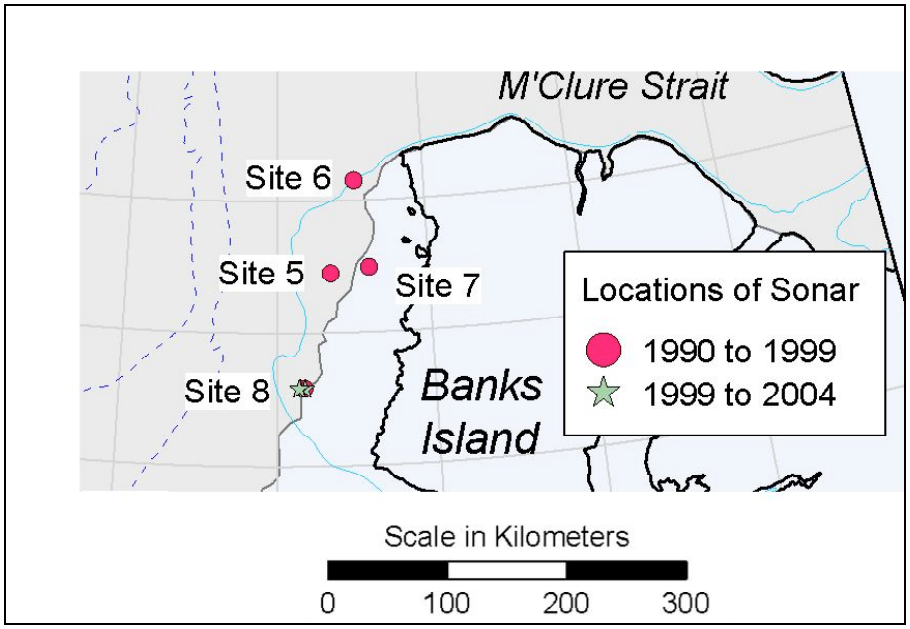

Figure 10-14 IPS/ADCP Locations West of Banks Island NE Canadian Beaufort

Table 10-7 Break-up and Freeze-up Dates at Site 5 1996 - 1998

Year	Break-up	Freeze-up
1996	No break-up	
1997	June 14	October 4
1998	May 17	November 8

Table 10-8 Total and useful number of records for Site 5

	Total number of records	Number of "Bad Data" records	Effective number of records	Effective number of records [%]
All	32564	3763	28801	88.4
Summer	5424	3054	2370	43.7
Winter	27140	709	26431	97.4

10.3.2 Ice Velocity Analysis for Site 5 – 1996-1998

10.3.2.1 Drift Speed Distribution for Site 5

Ice drift was analyzed for the entire span of data. Figure 10-15 shows the speed histograms for winter, summer and the whole year. Figures 10-16, 10-17 and 10-18 show the exceedance plots for the total time, for the winter records and the summer records.

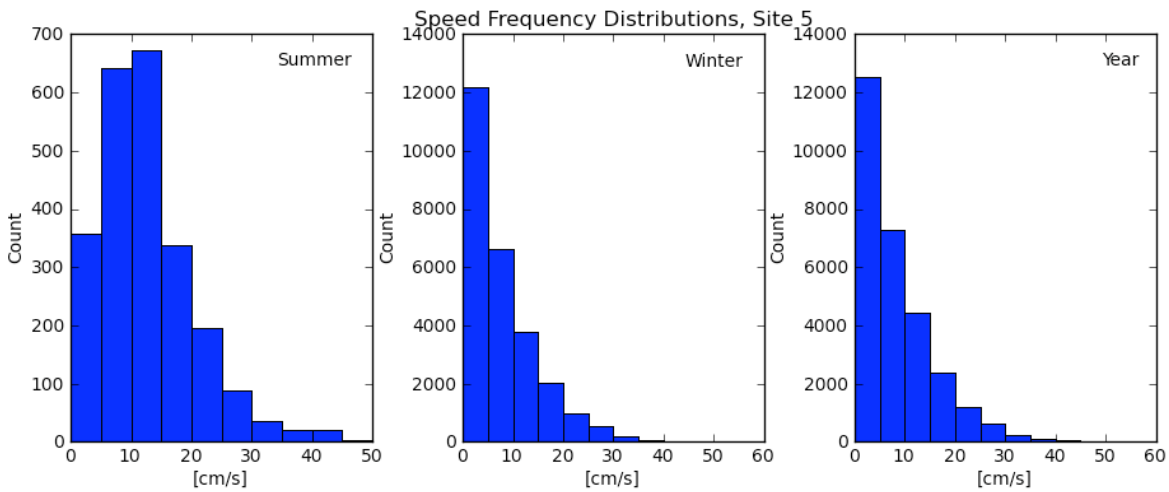

Figure 10-15 Frequency histograms of Ice Speed at Site 5 1996-1998

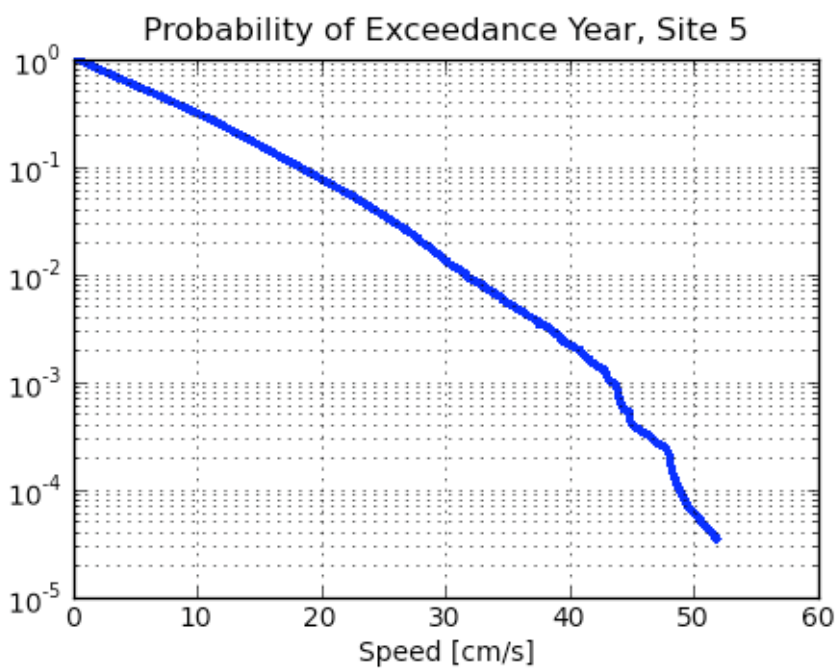

Figure 10-16 Exceedance probability of speed at Site 5 – All data

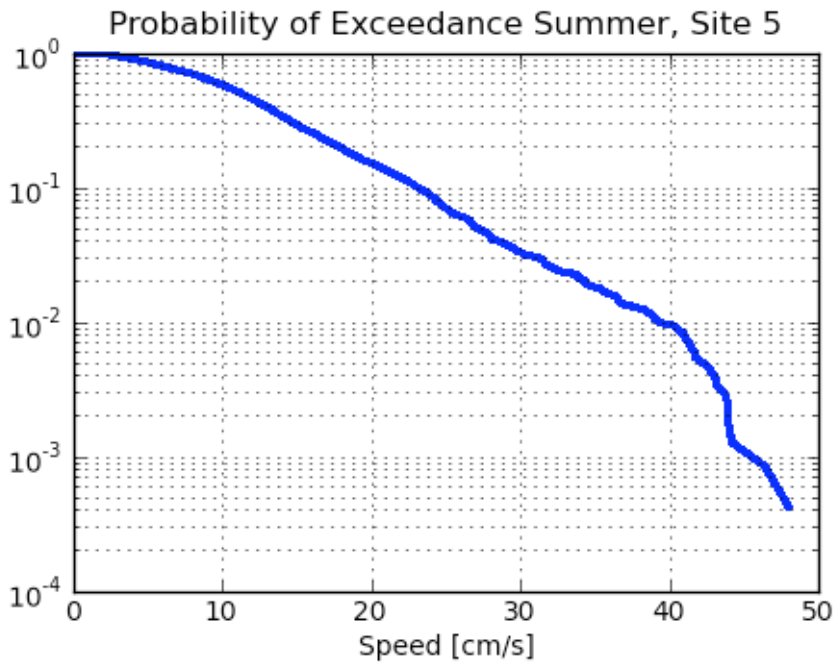

Figure 10-17 Exceedance probability of speed at Site 5 - Winter

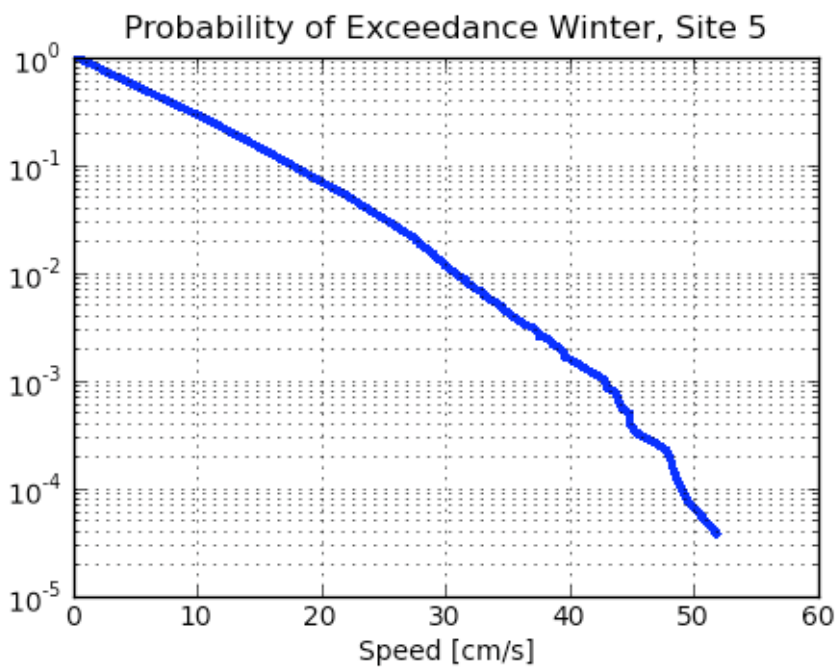

Figure 10-18 Exceedance probability of Speed at Site 5 – Summer

10.3.2.2 Summary of Drift Speed Statistics – Site 5

Figure 10-19 shows the box plots and Table 10-9 shows the statistics. Mean speed slows to 7.5 cm/s in winter from 12.5 cm/s in summer. Maximum speed was 51.8 cm/s in winter.

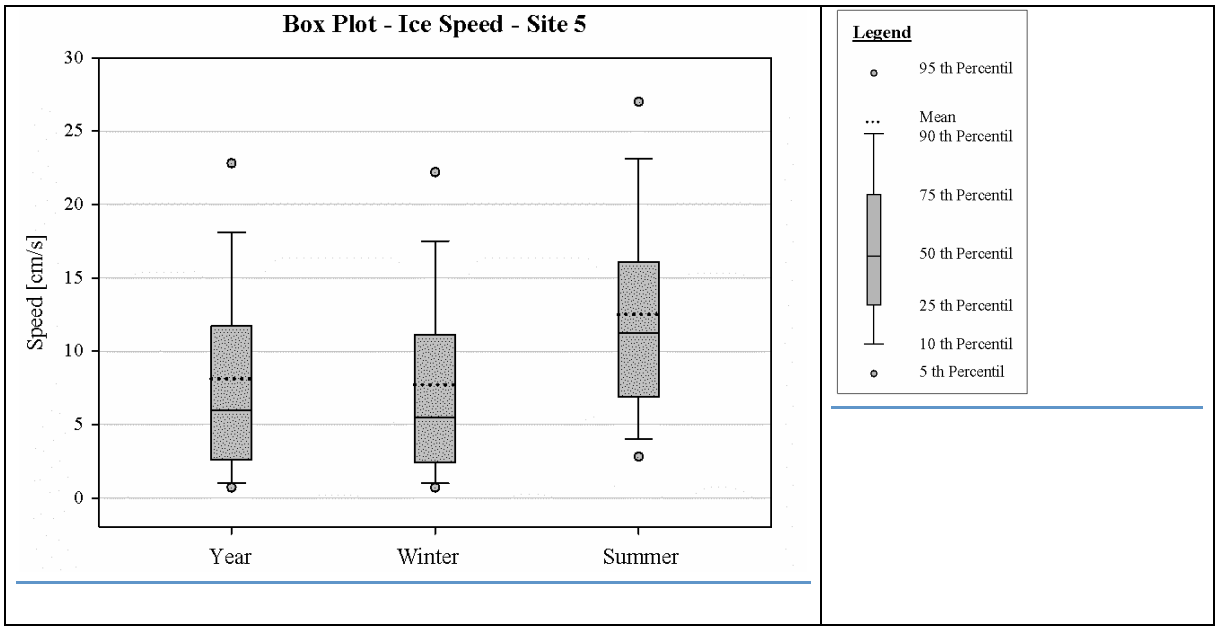

Figure 10-19 Box Plot of Drift speed statistics for Site 5

Table 10-9 Summary of drift speed statistics for Site 5

	YEAR	WINTER	SUMMER
N of Cases	28801	26431	3103
Minimum	0	0	0
Maximum	51.8	51.8	48
Arithmetic Mean	8.1	7.7	11.0
Standard Deviation	7.211	7.028	7.686
Coefficient of Variation	88.9%	91.1%	69.9%
Pct 1	0.2	0.2	0.9
Pct 5	0.7	0.7	2
Pct 10	1	1	2.9
Pct 20	2	1.9	4.4
Pct 25 (Lower Quartile)	2.6	2.4	5.1
Pct 30	3.1	2.9	5.9
Pct 40	4.5	4.1	7.7
Pct 50 (Median)	6	5.5	9.5
Pct 60	7.9	7.3	11.4
Pct 70	10.3	9.6	13.4
Pct 75 (Upper Quartile)	11.7	11.1	14.575
Pct 80	13.4	12.7	16.3
Pct 90	18.1	17.5	21.6
Pct 95	22.8	22.2	25.8
Pct 99	31.6	30.6	36.947

10.3.2.3 Drift Direction for Site 5

Ice Drift roses for the year, winter and summer appear in Figure 10-20. Ice drift is predominantly to directions in the SW quadrant. The trend is more pronounced in summer. In winter there can be more movement to the northerly directions than in summer.

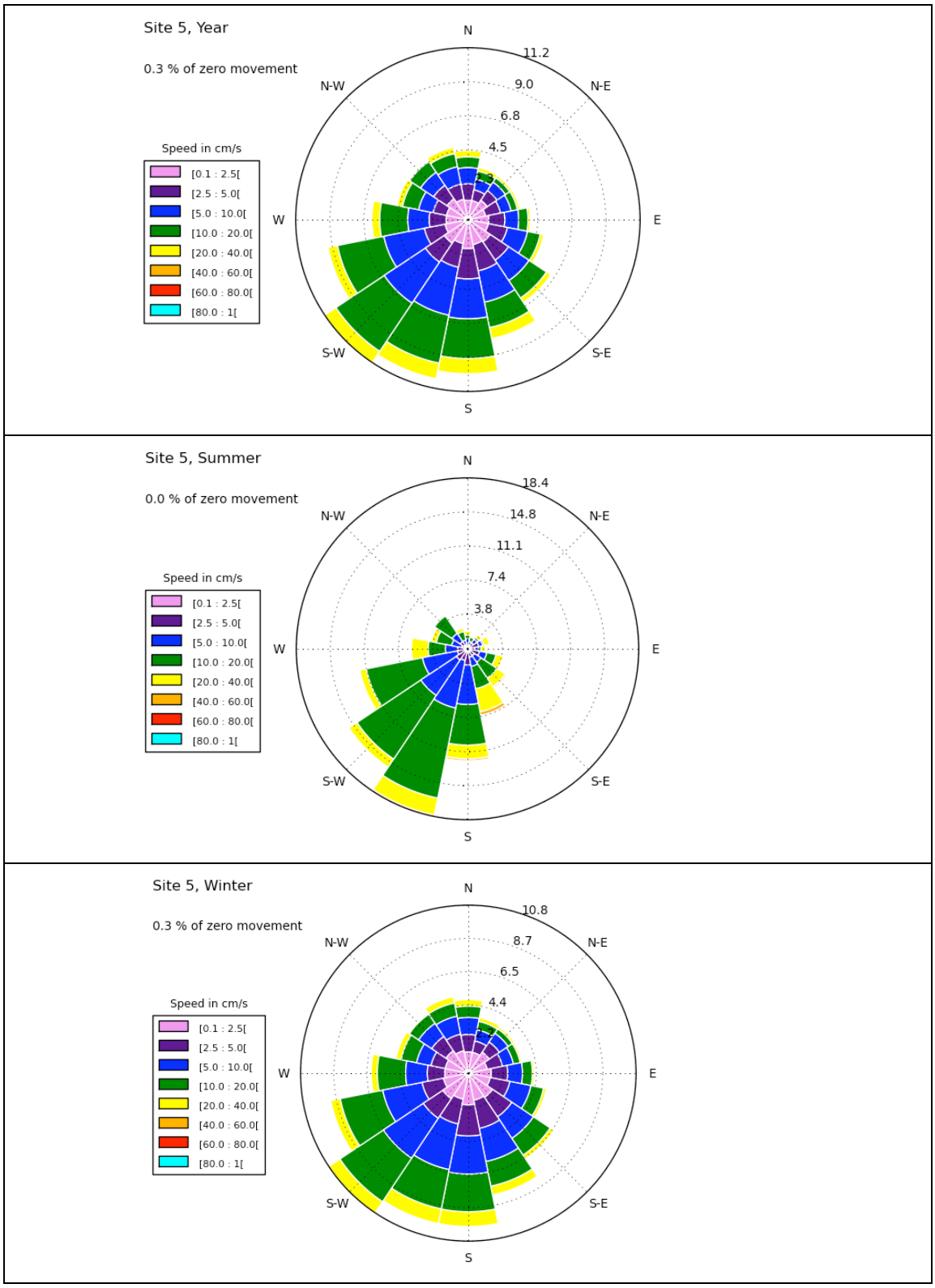

Figure 10-20 Ice Drift Roses and Scatter Plots of ice drift at Site 5

11 ICE VELOCITY FROM DRIFT BUOY DATA – CHUKCHI AND ALASKAN BEAUFORT SEAS

11.1 Data Source

The International Arctic Buoy Program has collected a considerable amount of data on the drift patterns in the Arctic Basin. They also give daily drift buoy positions and publish these on the website. Figure 11.1 shows buoy drift for the 60-day period ending April 23, 2009. Figure 11.2 shows a scatter plot of buoy tracks in the Arctic basin from 1999 to 2008. See http://iabp.apl.washington.edu/research_seaiceageextent.html.

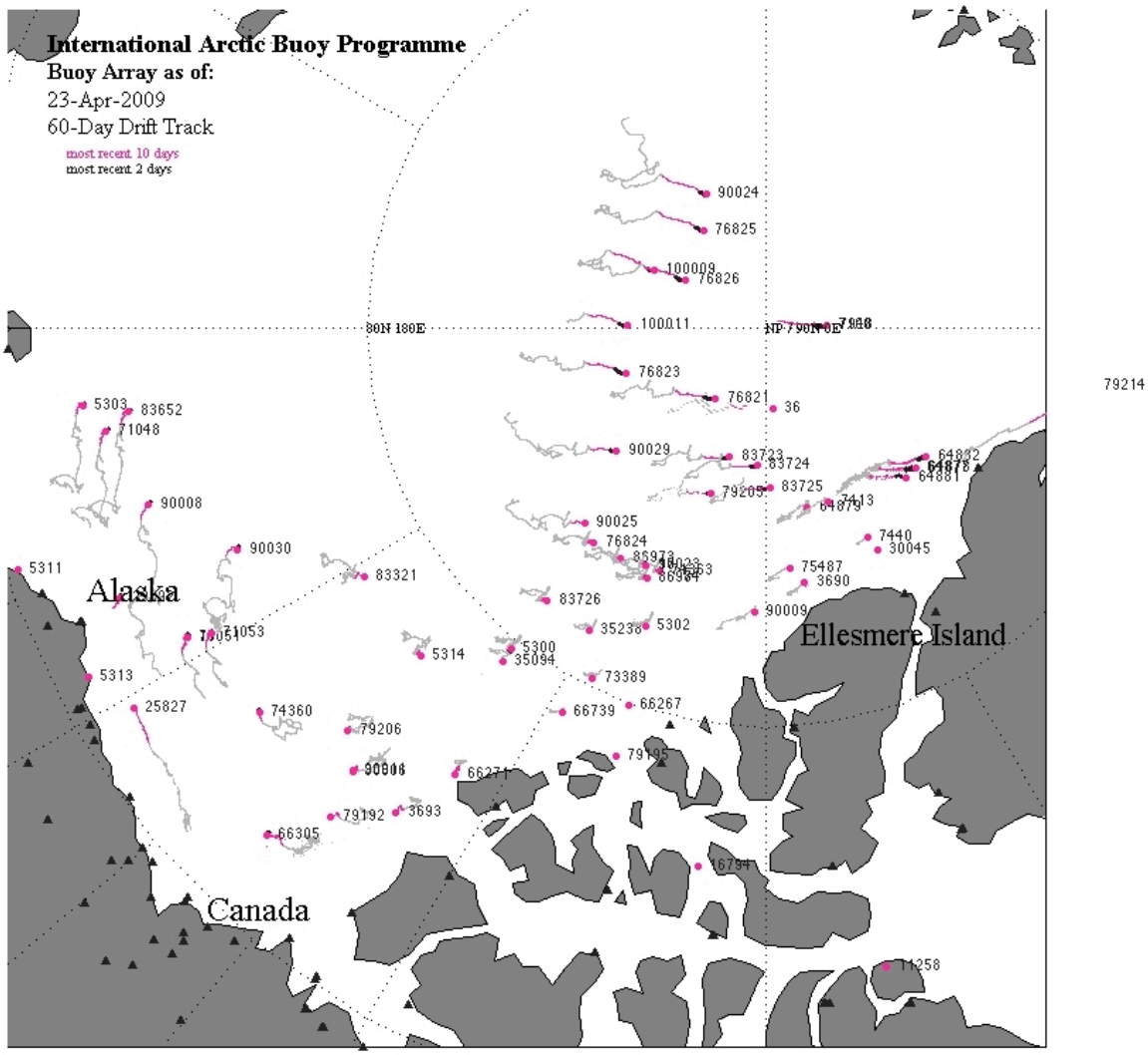

Figure 11-1 Ice Drift over a 60 day period to April 23, 2009 from IABP website

Unfortunately very few buoys traversed the lease areas of the Chukchi and Alaskan Beaufort.

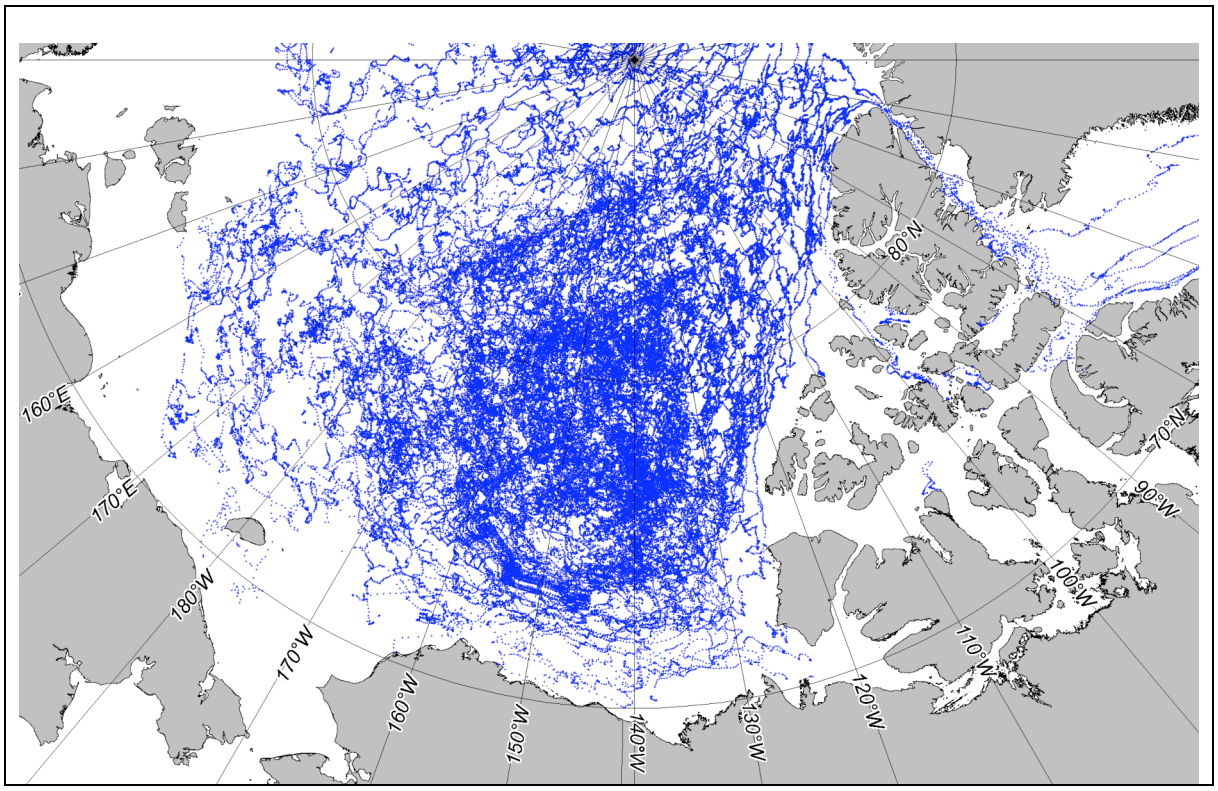

Figure 11-2 Arctic Buoy Drift Tracks 1999-2008 (left image)

In the absence of other public domain data for the Alaskan Beaufort and Chukchi Seas, the records were investigated as far back as 1987. Ice movement data was generated from IABP tracks that passed through the areas of interest. Average speed and direction were calculated for each 12-hour interval and the statistics generated. Table 11-1 lists the buoy track data that was available at the time of writing for the two areas. Six of the ten buoys traversed both Seas. In these cases the drift track data east of Point Barrow was used for Alaskan Beaufort statistics and the rest was considered to be in the Chukchi Sea.

Table 11-1 IABP Buoys traversing Alaskan Beaufort and Chukchi Sea Lease Areas

Buoy #	Alaskan Beaufort			Chukchi Sea		
	Start	End	Number of days	Start	End	Number of days
19577	4-Dec-1998	17-Feb-1999	75	-	-	
9115	15-Oct-2001	21-Dec-2001	67	22-Dec-2001	6-Feb-2002	46
7432	19-Nov-1987	10-Jan-1988	52	11-Jan-1988	23-Jul-1988	194
7431	-	-		21-Nov-1987	15-Aug-1988	268
7430	19-Nov-1987	9-Dec-1987	20	10-Dec-1987	15-May-1988	157
7103	9-Nov-1991	14-Jan-1992	66	15-Jan-1992	11-Jun-1992	148
7102	-	-		16-Jan-1992	30-Jun-1992	166
5311	4-Sep-2008	18-Sep-2008	14	19-Sep-2008	8-Oct-2008	19
5303	21-Sep-2008	7-Nov-2008	47	8-Nov-2008	29-Nov-2008	21
3160	29-Apr-1987	27-May-1987	28	-	-	

11.2 Alaskan Beaufort Sea Drift Buoy Data

Figure 11.3 shows the tracks for the Alaskan Beaufort. The data sets were divided into summer (July - September) and winter (October - June). Data for all buoys was combined. Before the end of winter most of the buoys had drifted into the Chukchi Sea. The winter data for the Alaskan Beaufort mostly represents the early winter period until February. Figure 11-4 and Figure 11-5 present the histograms and exceedance plots for drift speed for summer and winter. Table 11-2 present the statistics for summer, winter and for all data.

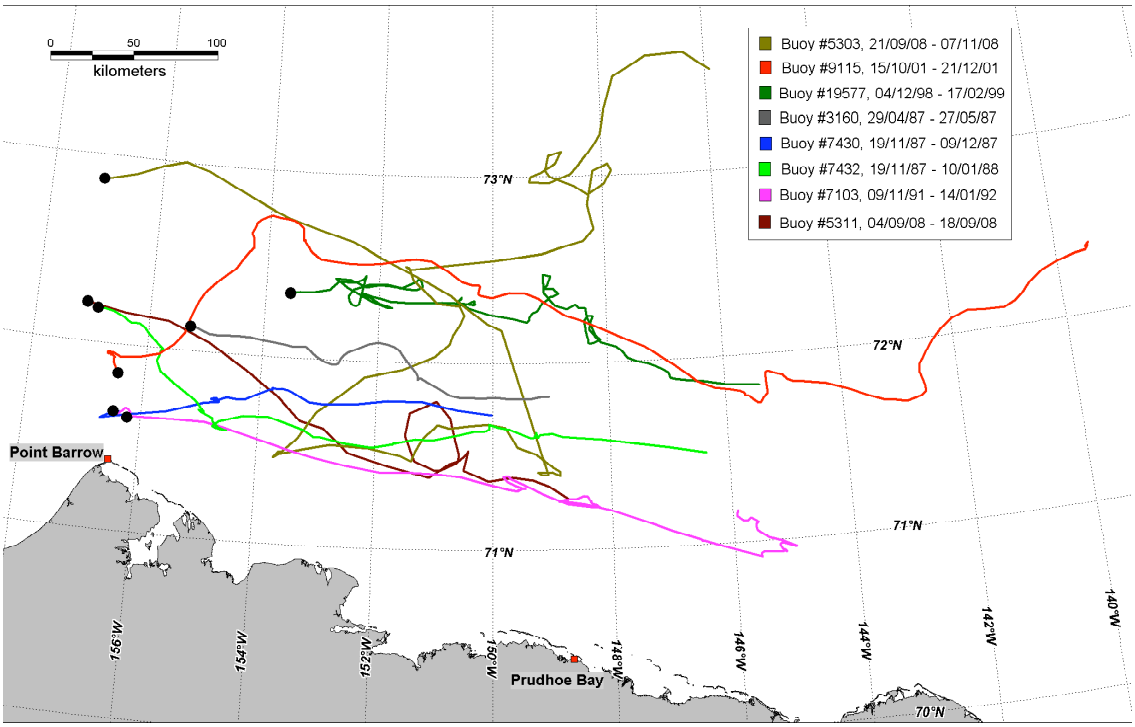

Figure 11-3 IABP Drift Tracks in Alaskan Beaufort Sea 1987-2008

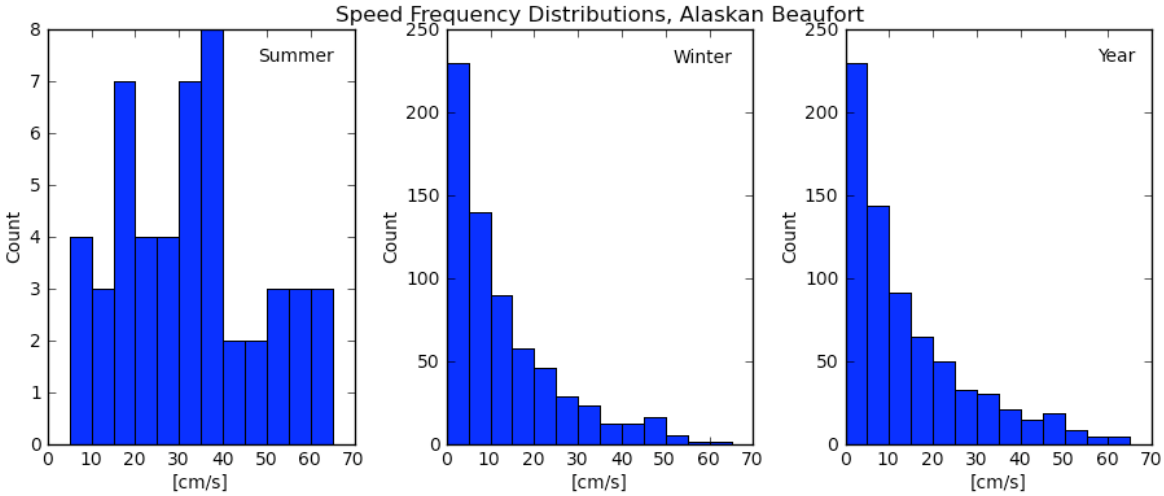

Figure 11-4 Speed histograms for summer and winter – Alaskan Beaufort Sea

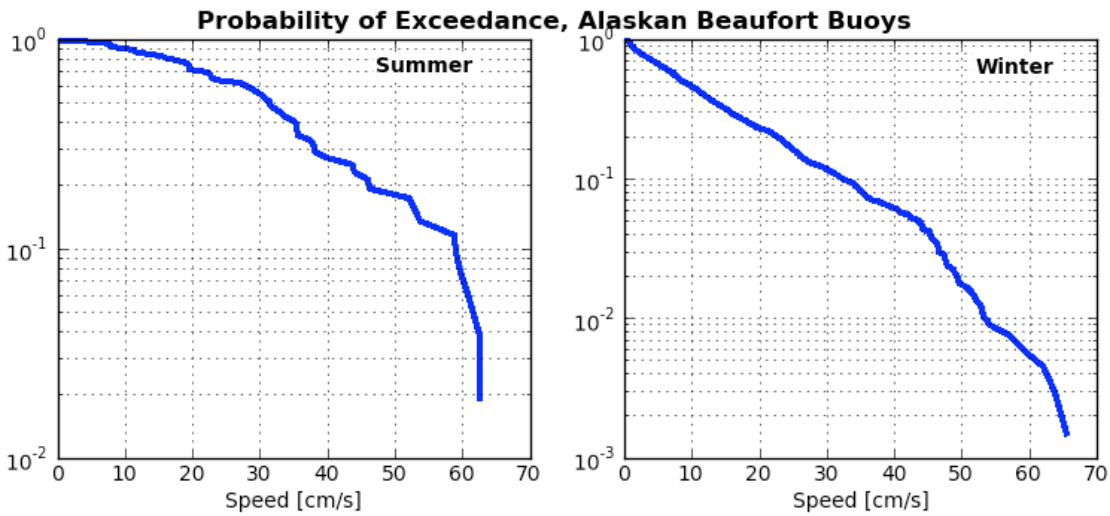

Figure 11-5 Exceedance Plots for summer and winter – Alaskan Beaufort Sea

Table 11-2 Speed Statistics for IABP Buoys - Alaskan Beaufort 1987-2008

	SUMMER	WINTER	YEAR
N of Cases	50	671	721
Minimum	6.4	0.1	0.1
Maximum	62.6	65.5	65.5
Arithmetic Mean	32.4	13	14.3
Standard Deviation	15.79	12.98	14.08
Coefficient of Variation	48.80%	100.10%	98.40%
Pct 1	7.08	0.22	0.24
Pct 5	8.3	0.66	0.66
Pct 10	11.5	1.03	1.14
Pct 20	18.64	2.2	2.37
Pct 25 (Lower Quartile)	19.48	3.09	3.46
Pct 30	22.53	4.05	4.48
Pct 40	28.44	6.3	7.08
Pct 50 (Median)	31.47	8.48	9.56
Pct 60	35.26	11.76	12.82
Pct 70	38.07	15.59	17.61
Pct 75 (Upper Quartile)	42.81	18.35	21.18
Pct 80	46.11	22.51	24.64
Pct 90	58.81	32.12	35.28
Pct 95	60.41	42.94	45.51
Pct 99	62.59	53.01	59.03

Figure 11-6 presents drift roses for summer, winter and all data.

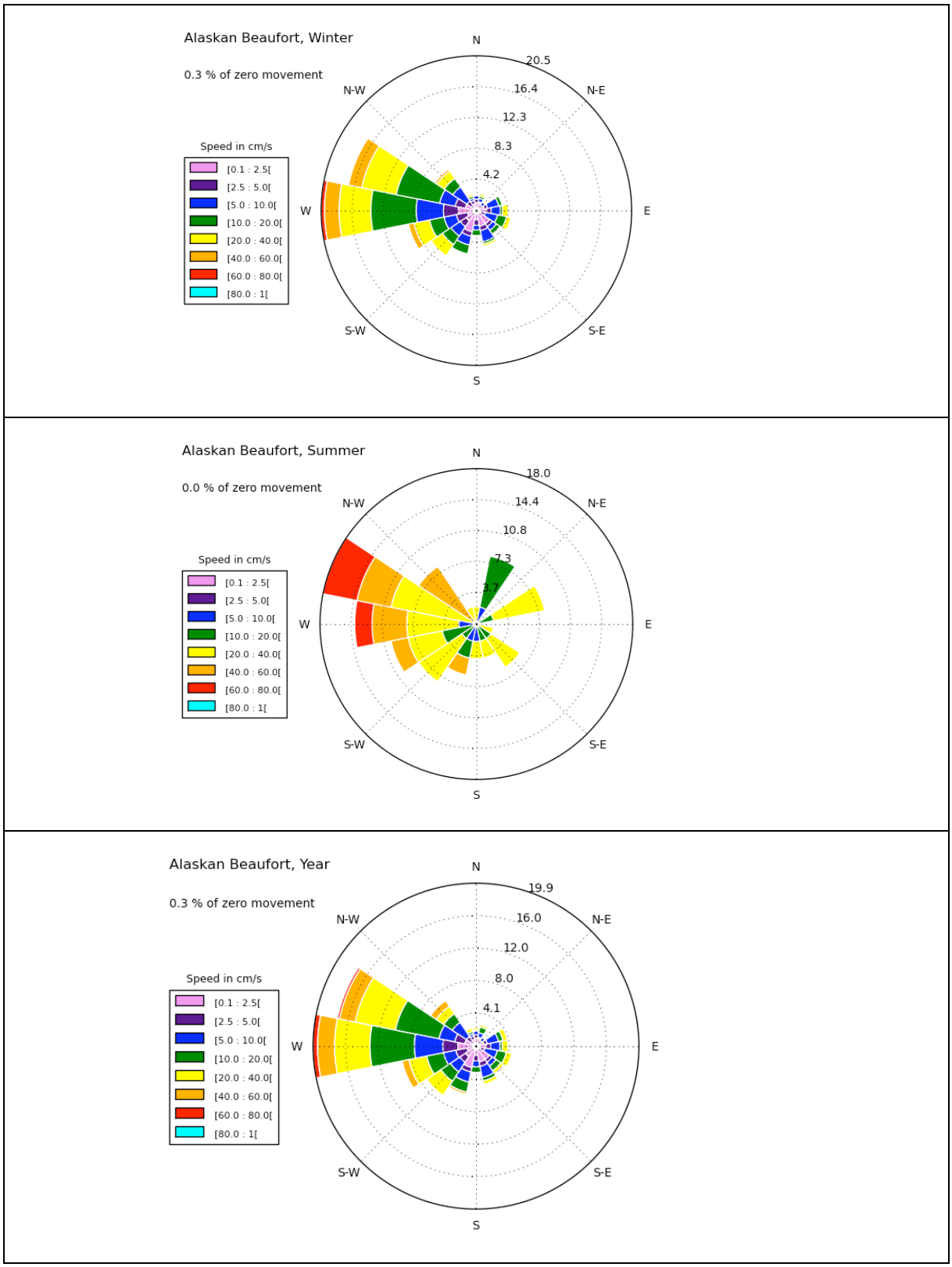

Figure 11-6 Drift Roses for IABP Buoys – Alaskan Beaufort Sea 1987-2008

In winter, the maximum speed was 65.5 cm/s, the mean was 13 cm/s and drift direction was predominantly W and WNW. The relatively high average winter speed, as compared to ADCP results for the Canadian Beaufort, is due to the fact that most of the buoy data is from the freeze-up and early winter period when speeds are generally higher than later in the winter.

In the summer of 2008 maximum drift was 62.6 cm/s and the mean was 32.4 cm/s. For the buoy near shore, drift direction was predominantly to the WNW parallel to the coast. Farther offshore the drift was predominantly to the SW and NE.

Summer data was very sparse consisting of 10 days for buoy #5303 and 16 days for buoy #5311 in late September of 2008. The starting date for winter was defined as 1st October.

11.3 Chukchi Sea Drift Buoy Data

Figure 11-7 shows the tracks for the Chukchi Sea. Most of the tracks cover the mid–to-late winter period. Drift is more omni-directional than in the Alaskan Beaufort. Figure 11-8 and 11-9 show the speed histograms and exceedance plots for summer and winter. Table 11-3 presents the statistics. Figure 11-10 presents drift roses for summer, winter and all data.

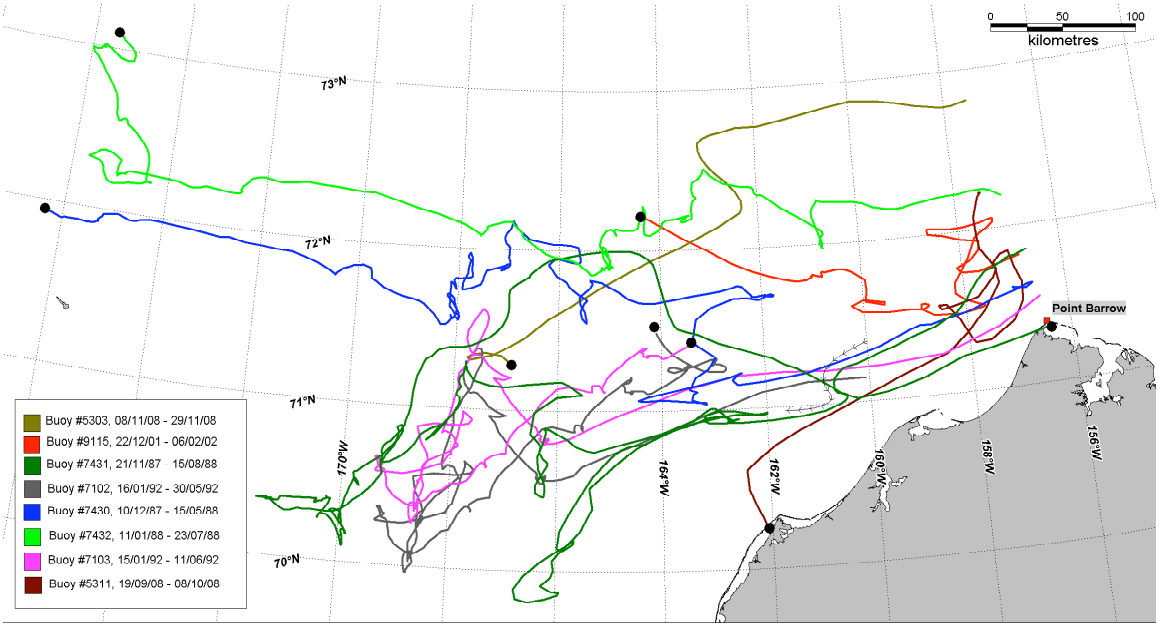

Figure 11-7 IABP Drift Tracks in the Chukchi Sea 1987 - 2008

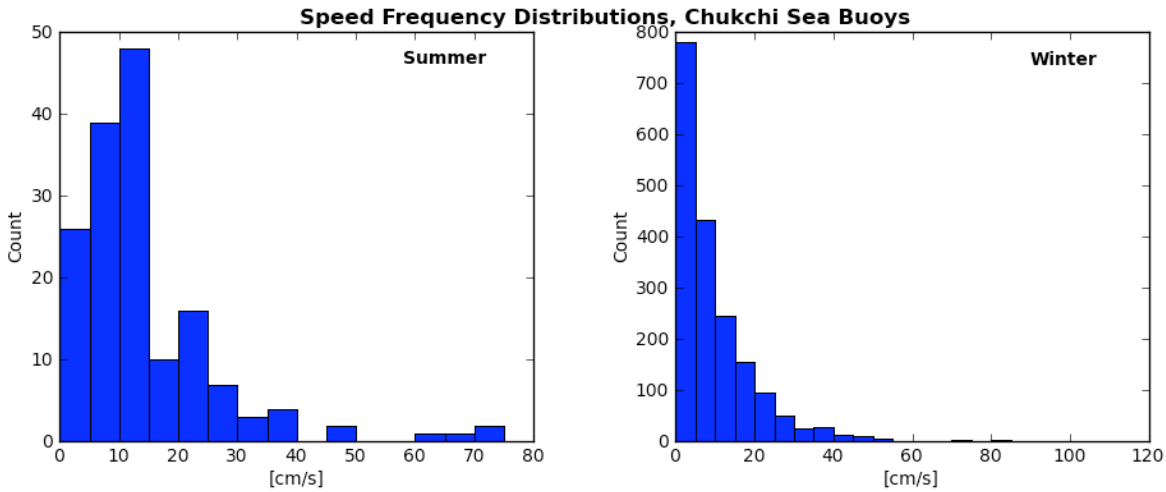

Figure 11-8 Drift Speed histograms for summer and winter - Chukchi Sea

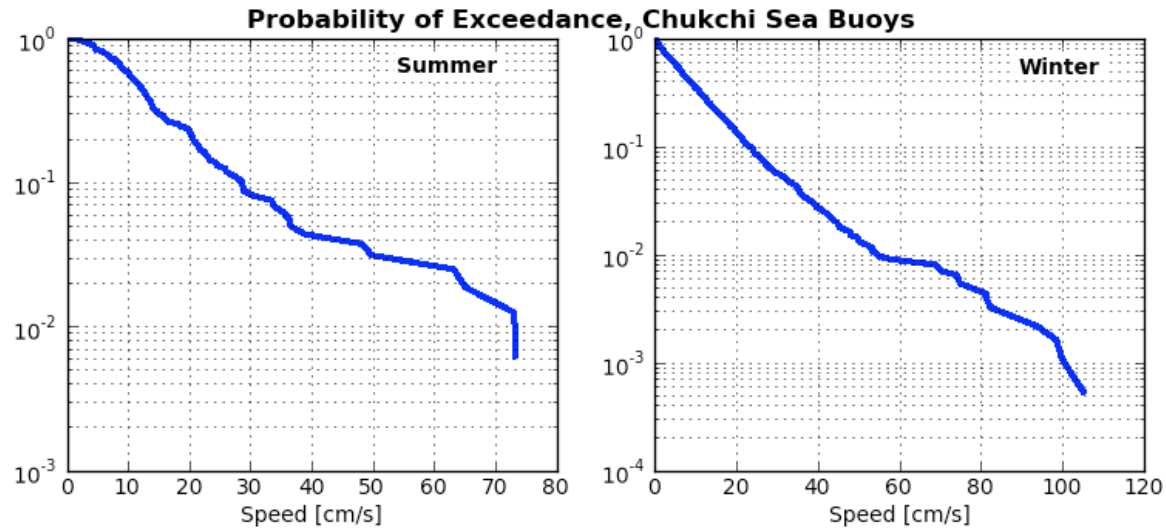

Figure 11-9 Drift Speed exceedance plots for summer and winter - Chukchi Sea

In winter, the maximum speed was 105 cm/s, the mean was 10 cm/s and drift direction was omni-directional with some tendency to predominance in the SW quadrant.

In the summer of 2008 maximum drift was 73.4 cm/s and the mean was 14.6 cm/s. Drift was predominantly to the NW and NE sectors. However, it is not possible to make reliable conclusions about summer drift speed and direction due to the small data set.

The authors were unable to extend this analysis of drift speeds any further in the areas of interest due to a lack of data in the public domain

Table 11-3 Speed Statistics for IABP Buoys - Chukchi Sea 1987 - 2008

	SUMMER	WINTER	YEAR
N of Cases	159	1867	2026
Minimum	1.6	0	0
Maximum	73.4	105.1	105.1
Arithmetic Mean	14.6	10	10.4
Standard Deviation	12.49	11.8	11.92
Coefficient of Variation	85.7	117.4	114.6
Pct 1	1.7	0.17	0.17
Pct 5	3.31	0.43	0.49
Pct 10	4.25	0.79	0.87
Pct 20	6.09	1.74	1.87
Pct 25 (Lower Quartile)	6.89	2.32	2.51
Pct 30	7.96	2.94	3.24
Pct 40	9.45	4.6	5.05
Pct 50 (Median)	11.51	6.42	6.77
Pct 60	13.03	8.52	9.11
Pct 70	14.88	11.63	12.02
Pct 75 (Upper Quartile)	18.16	13.41	13.83
Pct 80	20.56	16.02	16.35
Pct 90	28.13	23.12	23.59
Pct 95	36.33	32.19	32.61
Pct 99	68.46	53.78	56.44

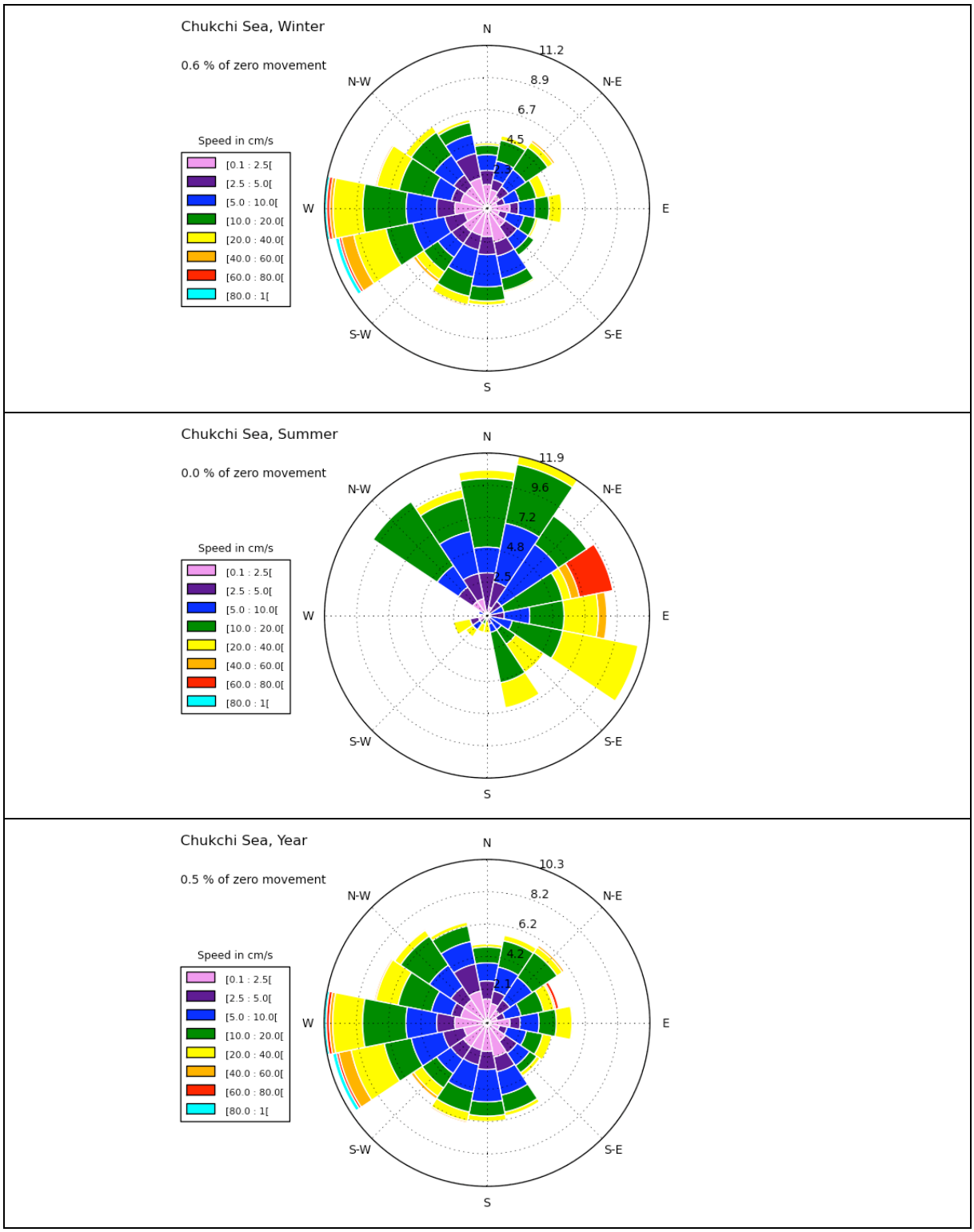

Figure 11-10 Drift Roses for IABP Buoys – Chukchi Sea 1987 - 2008

12 CONCLUSIONS AND RECOMMENDATIONS

12.1 Overview

This study documents the recent statistics of key extreme ice feature parameters relevant to the design of structures for the Chukchi and Beaufort Seas. It was initiated in order to determine if the changes observed in the Arctic ice regime since the early 1990s would result in changes to ice design criteria compared with previous studies.

Ice parameters examined were those that would normally enter into calculations of impact probability of an ice feature with a structure in the lease areas of interest, or into calculations of ice forces for various ice-structure interaction scenarios:

- population, areal density and size distribution of Extreme Ice Features (EIFs) which include multi-year hummock fields and ice islands calved from ice shelves,
- thickness of ice shelves as an estimate of the thickness of certain existing ice islands and those yet to be formed in future calving events,
- thickness of large areas of multi-year land fast sea ice (MLSI),
- population, concentration and size distribution of multi-year floes,
- thickness and geometry of multi-year ridges and floes,
- speed and direction of ice drift.

Recent data and analyses of these parameters are discussed in the following sections.

12.2 Literature Review

Relatively little attention was given to extreme ice features and multi-year ice for application to the offshore industry since the 1993 study (Pilkington et al.(1993)) . The focus of Arctic research has largely shifted to climate change over the past 2 decades.

Never-the-less large volumes of data were gathered by government research agencies and the military from sonar and ice drift buoy deployments in the areas of interest and in the Arctic pack ice in general. In particular, recent sonar data from submarine transects under the polar pack, and from multiple deployments of Ice Profiling Sonar devices were accessed to analyze ice keel geometry and ice drift. Ice drift data from the International Arctic Buoy Program was also accessed and analyzed.

Improvements in satellite surveillance technology have resulted in more and better coverage of ice conditions in the polar pack and changes in the ice shelves. The increase in calving of ice islands from the ice shelves since 2000 spurred interest from academia and government agencies to monitor the fate of several ice islands by radar satellite, and to investigate ice shelf stability and thickness in the field, albeit at a small scale and with limited budget. Some of that data, which previously had not been processed, was analyzed as part of this project. It is recommended that the tracking of new ice islands and the measurement of ice shelf and ice island thickness be continued.

Some recent research has shown an acceleration of calving from glaciers and ice shelves of northern Greenland. It is currently not well understood if there is a risk that some of the

features produced from Greenland can drift into the Beaufort Gyre and eventually into the Southern Beaufort and Chukchi Seas. It is recommended that a detailed review of the Arctic Buoy Program data be undertaken to determine if there is a risk of old ice from Greenland entering the Gyre. If a risk is apparent then it is recommended that radar satellite monitoring of the north Greenland ice shelves be implemented to determine the drift tracks of the ice features generated from Northern Greenland.

The use of sonar to investigate the underside of multi-year floes and ridges has been attempted in various field studies, most recently using 3-D sonar from a camp on the ice surface and from a submarine deployment. It is recommended that more of this kind of work be undertaken to understand the characteristics of multi-year keels and that the analysis of the most recent submarine data (2007) be undertaken.

12.3 Satellite Data Acquisition

New satellite imagery was acquired to assess the populations and sizes of EIFs in the High Arctic updrift of the lease areas. A combination of 30m resolution Envisat and 8m resolution Radarsat was found to be a cost effective way to cover a large area where EIFs are created.

The imagery was acquired on July 31st - August 1st 2008, less than a week after a major calving event at Ward Hunt and Serson ice shelves. A few days later the Markham Ice shelf came adrift from its inlet and broke up completely.

A total area of 183,980 sq. km. of radar imagery was obtained over the EIF area of interest. Additional areal coverage was made up by MODIS and Landsat imagery.

For the Multi-Year Floe size survey, Radarsat imagery was provided by two of the JIP sponsors. This allowed the measurement of M-Y floe sizes in each of the 3 areas of interest for summer and winter.

It is recommended that for future surveys, other high-precision optical satellite sensors be investigated to complement radar imagery.

12.4 Extreme Ice Features EIFs

12.4.1 General

Analysis of the radar imagery yielded a total of 200 EIFs including 40 Ice Islands, 93 Ice Island fragments and 67 Multi-year Hummock Fields. All EIFs were located and measured in GIS program layers and subsequently analyzed by area and by type.

The areal density of all the EIFs was 5.4 x 10^{-4} per km^2 (200 features over 183,980 km^2). This compares with the previous estimate of 6.4 x 10^{-4} per km^2 for the period 1988-1991.

It is recommended that the same area be re-surveyed at regular intervals to monitor the drift and spatial densities of EIFs and to capture future calving events.

Tracking of a number of ice islands via satellite reporting buoys, is also recommended.

12.4.2 Ice Islands and Ice Island Fragment Occurrence

Most of the ice islands and ice island fragments were located offshore Ellesmere Island since they had recently calved there. The total measured area of all ice islands and

fragments was 123 sq.km. Subsequent calvings brought the total area of ice shelf lost in the summer of 2008 to 227 sq.km. The calculated areal density of ice islands and ice island fragments (2.4 x 10^{-4} per km^2) might therefore be considerably higher.

The largest ice island measured 9.8 km in its longest dimension (diameter) and 21.4 sq.km. in area. The equivalent diameter was 5.2 km. Mean ice island diameter was 2.8 km and mean area was 3.2 sq. km. The mean of the equivalent diameter was 1.6 km. Considering only the ice islands greater than 500 m in length, the mean of the equivalent diameter was 1.5 km. For ice island fragments the mean of the equivalent diameter was 0.56 km.

Comparing with previous data, the largest ice island detected has decreased in equivalent diameter from 26 km in 1980 to 6.8 km in 1991 to 5.2 km in 2008. There is a similar trend in the median equivalent diameter which has reduced from 4.5 km in 1980 to 3 km in 1991 to 1.2 km in 2008. This trend is partly due to the decreasing area of ice shelf available for calving. The more that calves off the more difficult it is to calve large pieces since what remains is more protected by headlands and may be more solidly grounded. The trend could also be a result of increasing precision of the sensors, and the fact that the very large ice islands first detected in the post -war years have left the Arctic Basin via the trans polar drift stream or via the channels between the Canadian Arctic islands.

12.4.3 Multi-Year Hummock Field Occurrence

Most of the MYHFs occurred offshore Prince Patrick and Borden Islands. It appeared that parts of the land fast ice there were still breaking up at the time of the survey, so it is possible that other MYHFs are now adrift. The calculated areal density of MYHFs was 3.5 x 10^{-4} per km^2 (67 features over 183,980 km^2).

The largest MYHF was 17.4 km in its longest dimension (with equivalent diameter of 13.8 km) and 149.8 sq.km. in area. Mean MYHF diameter was 2.5 km and area was 5.8 sq.km. Mean equivalent diameter was 1.7 km. Considering only the MYHFs greater than 500 m in length, the mean of the equivalent diameter was 2.0 km

The size (in equivalent diameter) of the largest MYHF detected has increased over the years from 3 km in 1980 to 5.6 km in 1991 to 13.8 km in 2008. Conversely, the median diameter has decreased from 4.5 km to 3 km to 1.2 km for the same years. This could be a result of increasing precision in the sensors used and of software improvements that allow image enhancement.

12.5 Thickness of Ice Shelves and Multi-Year Land Fast Sea Ice (MLSI)

Recent (April 2008) GPR data of the thickness of 3 ice shelves and 4 areas of land fast sea ice on Ellesmere Island was analyzed. The Milne ice shelf is the thickest with mean and maximum of 61.9m and 94.4m.

The Serson ice shelf broke up in the summer of 2008. The GPR measurements from April 2008 showed a mean thickness of 37.9m and maximum of 63.0m. Unfortunately large sections of the measured transects resulted in no data. However, from the outline of the shelf after its collapse it would appear that the sections 30-40m thick calved off and the thicker sections of 40-60m remained in place. It would appear that 17 of the ice islands

identified from the Envisat imagery had the Serson ice shelf as their source and it would be reasonable to assign an average thickness of 35m to these EIFs.

The Petersen ice shelf had zones 45m to 65m thick in the middle and 6 m thick at its edges.

The MLSI in Yelverton Bay broke up sometime between 1998 and 2006. However, some large floes formed from the break-up have remained in the vicinity. One large floe about 5.8m thick and more than 10km long was surveyed. There was also a large expanse of MLSI about 10km long and 4 to 5m thick between Bromley Island and Cape Richards. These measurements are less than the extreme MLSI feature (called a re-entrant) of thickness 10m and dimensions 7km x 3.6 km identified in 1987 by Jeffries and Sackinger.

12.6 Multi-Year Floe Size and Concentration

Satellite images of multi-year floes at the edge of the polar pack ice near the lease areas of the Beaufort and Chukchi Seas were obtained from two of the project sponsors. There were 3 images from late winter (early June), and 3 from the summer (August and September). In addition one Envisat from Prince Patrick Island in summer, and one MODIS from the Alaskan Beaufort in mid-winter were analyzed. Floe sizes were analyzed and compared by region and by season.

There is a trend to smaller multi-year floe sizes in the winter from East to West by all measures of floe size: median, mean 99th percentile or maximum. In late winter (early June) the median floe diameter was 2.1 km in the Canadian Beaufort, 2.0 km in the Alaskan Beaufort and 1.9 km in the Chukchi Sea. Mean diameter was 3.3 km in the east versus 2.7 km in the west. Maximums were 44 km in the east and 21 km in the west. One possible reason for this trend is the nature of the Alaskan coastal area as a zone of shear between the coast and the moving pack ice. As the Beaufort Gyre carries the pack ice generally west from Canadian waters, multi-year floes are exposed to increased internal pressure in the ice as they pass by Alaska. Splitting and abrasion may occur to break down some of the floes and decrease the average size.

No such trend can be noted in summer (August). Median floe size in the east was smaller than in the west: 1.5 km compared to 1.8 km. Yet the larger floes were bigger in the east. The greater number of large floes in the east augmented the average floe diameter to 3.5 km compared with 2.3 km in the Chukchi Sea. In the Canadian Beaufort summer many large floes continue to enter the lease areas from the polar pack to the north. At the same time, warmer water and wave action deteriorate most of the floes to produce many small floes and a small median value.
The time variation in floe size was documented for the Canadian Beaufort Sea. Floes in mid-winter are mostly conglomerate and large : 7.8 km in mean diameter. This decreases to 3.4 km in late winter and early summer, and to 1.4 km in late September.

Comparing floe sizes (>500m diameter) for multi-year incursions in 1980 and 2008 the distributions are similar. Mean diameter was 1.2 km in 1980 and 1.4 km in 2008. At the 1% level diameter was 8.1 km in 2008 and 6 km in 1980.

Multi-year ice concentration contours were produced for the lease areas of interest. The concentration contours decrease rapidly from the shelf edge south to shallow water. In the Canadian Beaufort lease areas summer concentration has decreased in the past 30 years.

For example at a point north of Tuktoyaktuk and about 70.5 degrees latitude the average summer concentration of multi-year ice has decreased from 5% to 2%.

It is recommended that the approach of multi-year ice near to the lease areas be monitored in the coming years, imaged and analyzed if possible.

12.7 Old Ice Thickness from Submarine ULS Data

Upward looking sonar records from the 2000a submarine cruise from near Point Barrow to the North Pole were analyzed. The transect was divided into 6 Areas. For each ice floe or ridge a set of geometrical parameters was calculated. This geometric data for each Area was analyzed statistically. Highlights are presented below. The numbers quoted refer to the exceedance level of 10^{-2} or 1%.

The keel depth is 14m for areas close to the North Pole. Closer to Barrow it is 12m.

Ridge widths are widest near the Pole: 150m. In most other areas it is 110m.

For old ice floes, there is a decrease in mean draft with a decrease in latitude.

Spacing between adjacent ridge keel peaks is closest near the Pole. It is 2km at the 1% level.

Floe widths (with ridges) decrease from North to South. Near the Pole the 1% floe width is 4 km compared to less than 1 km over the continental shelf north of Barrow. Floes without ridges are very much smaller.

Comparison of the mean floe draft (containing ridges) data between the February 1960 Sargo and the August 1962 SeaDragon submarine ULS data from (De Paoli, Morrison, and Marcellus, 1982), and that for Area B of the 2000a submarine data gave an average thinning of the ice floes of 1.4 m at the 10^{-2} probability level, and 4 m at the 10^{-3} level.

One MYHF was detected that fit the standard definition of a continuous segment of ice with a width greater than 500 m and an average depth greater than 10m. This feature was 1150m wide with an average thickness of 13m.

From this analysis it is not possible to determine if all the ridges were solid multi-year ice. Some ridges could be formed from multi-year ice but could be new. A test using an Envisat image offshore Ellesmere Island found that along an 83 km transect, 43 ridges were new and had formed from multi-year ice. This demonstrates that the multi-year pack ice does contain a significant percentage of newly formed ridges.

Further study using higher resolution satellite imagery is recommended.

12.8 Old Ice Thickness from IPS Data West of Banks Island

For the exceedance level of 10^{-2} or 1% ice ridge keel depths and widths are similar to the area near the North Pole, i.e. about 14 m and 130m respectively.

This multi-year ice will continue to invade the lease areas from time to time, winter and summer but in lower concentration on average than in the past.

Two MYHFs were detected in the 1997 data from Site 5. One was 550m long with an average thickness of about 15m and a maximum keel depth of 32m. The other was 750m long with an average thickness of about 12m and a maximum keel depth of 22m.

From the ULS and IPS data analysis it was observed that the triangular model of a ridge keel could be improved upon, and it is recommended that this improvement be conducted for ridge structure interaction modeling purposes.

12.9 Correlation of Satellite Images of Surface with Keel Profiles

Radar images were obtained from the Autumn of 1996 to correlate with sonar profiles of ice keels at times when the ice type was known to be mostly (90%) multi-year. A representation of the ice drift track with ice thickness was plotted on to each image of the surface. Results were a mix of good and poor correlation between the features on the surface and the bottom profile. Detailed examination of certain keel profiles gave some indications as to the difference in signals between first year, second year and multi-year ridge keels, but nothing definitive.

It is recommended that opportunities to obtain and analyze simultaneous radar imagery and multi-beam sonar of the ice under-surface be pursued, and comprehensive analyses done.

12.10 Ice Drift in the Southern Canadian Beaufort Sea

Ice drift speed and direction data from ADCP instruments deployed alongside IPS installations in the Canadian Beaufort Sea were analyzed.

A detailed statistical analysis was conducted of 13 years of ADCP data from 1990 to 2003 at Site 1, near 70.5^{o} N 135° W in the Canadian Beaufort Sea.

Mean winter speed was 10.7 cm/sec. Mean summer speed was 15 cm/sec. At the 1% exceedance level, drift speed is 48.2 cm/sec in summer and 51.9 cm/sec in winter. The maximum speed of 100.7 cm/sec (almost 2 knots) occurred in the winter.

Ice drift can be in any direction but is predominantly to the West in winter. In summer it is more evenly distributed with a greater tendency to drift towards the WNW and ESE.

There is a significant difference between the ADCP data and older data derived from RAMS and Argos buoy drift. The average winter drift speed is shown to be twice as much as previously considered: 10.7 cm/sec vs 5.1 cm/sec in the 1982 EIS report. Perhaps this is an indication of more dynamic conditions in winter generally. The summer average speed is similar: 15 cm/sec from the ADCP data 1990-2003 compared with 17.7 cm/sec from radar tracking on drill ships in the early 1980s.

12.11 Ice Drift in the Chukchi and Alaskan Beaufort Seas

Since there was no ADCP ice drift data in the public domain for the Alaskan Beaufort and Chukchi Seas, the analysis was derived from drift buoy tracks. A limited amount of 12-hourly velocity data was available from the International Arctic Buoy Program for the period 1987-2008.

For the Chukchi Sea the mean speed was 14.6 cm/sec in Summer and 10 cm/sec in winter - remarkably similar to the results for the Canadian Beaufort. At the 1% exceedance level the summer speed was 68.5 cm/sec, and the winter speed was 53.8 cm/sec. The maximum speed of 105.1 cm/sec occurred in winter.

Data for the Alaskan Beaufort were sparse - particularly in summer. Mean speed in winter was 13 cm/sec - higher than elsewhere since the only data available was for early winter.

The winter maximum was 65.5 cm/sec. It is possible that the maximum speeds are underestimated due to the long data interval of 12 hours.

Further buoy tracks through the region should be analyzed when available to increase the data base. It is recommended that a public agency deploy ADCPs in the lease areas so that high resolution, short time scale data can be compiled.

12.12 Implications for EIF Impact Probability

The satellite coverage in the summer of 2008 captured a significant release of ice islands due in part to the release of pack ice pressure and the creation of open water directly in front of the ice shelves. This new population will tend to increase the probability of sightings in the lease areas over the next few years, but eventually these will leave the Arctic Ocean via Fram Strait or the channels of the Arctic Islands.

Meanwhile, it will become progressively more difficult for large numbers of ice islands to form because it is the more protected expanses of ice shelf that remain. The decreasing size of ice islands noted in historical comparisons, and the decreasing numbers on average of features greater than 500 m in diameter will tend to reduce the risk of impact with a structure. The numbers of ice islands noted in 2008 should not be used as an annual norm. Such large scale calving events have not been observed to occur every year.

In addition, it is known that many of the ice islands formed are on the order of 30-40 metres thick (e.g. those from the Ward Hunt and Serson ice shelves). Their draft will prevent them from entering lease areas shallower than this.

On the other hand the population of multi-year hummock fields does not appear to be decreasing with time. More needs to be understood about the formation and frequency of these extreme features. However, since they probably travel as part of the polar pack, and since the average concentration of old ice in the lease areas appears to be decreasing, the risk of impact may also be reduced.

A factor that will tend to increase the risk of impact is the ice velocity. Winter drift speed in the lease areas of the Canadian Beaufort is significantly higher than previously estimated. This more dynamic ice regime would tend to cause more ice features to pass an area in proportion to the speed.

It as not the purpose of this project to estimate impact probabilities, however the data analysis provided will allow for improved estimates for site specific applications This is the next step and is recommended.

13 REFERENCES

Abrahamsen, E., Osterhus, S. and Gammelsrod, T., 2006, "Ice draft and current measurements from the north-western Barents Sea, 1993–96," *Polar Research,* Vol. 25, No. 1, pp. 25–37.

Amundrud, T., Melling, H. and Ingram, G., 2004, "Geometrical constraints on the evolution of ridged sea ice," *J Geophysical Research*, Vol. 109, C06005.

Arsenault, L.D., 1981, "SLAR Qualitative Evaluation and Multi-year Foe Size Distribution"

Belchansky, G., Douglas, D. and Platonov, N., 2005, "Spatial and temporal variations in the age structure of Arctic sea ice," *Geophysical Research Letters*, Vol. 32, L18504.

Bowen, R. and Topham, D., 1996, "A study of the morphology of a discontinuous section of a first year arctic pressure ridge," *Cold Regions Science and Technology*, Vol. 24, pp. 83-100.

Braun, C., 2006, *Sensitivity of the Hazen Plateau and north coast, Ellesmere Island, Nunavut, Canada to Climate Change.* Unpublished PhD thesis. Amherst: U of Massachussetts.

Copland, L., Mueller, D. and Weir, L., 2007, "Rapid loss of the Ayles Ice Shelf, Ellesmere Island, Canada," *Geophysical Research Letters*, Vol. 34, L21501.

Darby, A. and Bischof, J., 2004, "A Holocene record of changing Arctic Ocean ice drift analogous to the effects of the Arctic Oscillation," *Paleoceanography*, Vol. 19, p. 1027.

Davis, N. and Wadhams, P., 1995, "A statistical analysis of Arctic pressure ridge morphology," *J Geophysical Research*, Vol. 100, No. C6, pp. 10,915-10,925.

De Paoli, S., Morrison, T., and Marcellus, R. "Analysis of Interaction Probabilities Between Large Ice Features and Offshore Structures in the Canadian Beaufort Sea", made public by Dome Petroleum Ltd. For the Beaufort Sea Environmental Impact Statement, November, 1982.

Dowdeswell, J., Gorman, M., Glazovsky, A. and Macheret, Y., 1994, "Evidence for floating ice shelves in Franz Josef Land, Russian high Arctic," *Arctic and Alpine Research* 26 (1): 86-92.

Dumas, J., Flato, G. and Weaver, A., 2003, "The impact of varying atmospheric forcing on the thickness of arctic multi-year sea ice," *Geophysical Research Letters*, Vol 30, No. 18, 1918.

Fissel, D., Marko, J. and Melling, H., 2008, "Advances in Marine Ice Profiling for Oil and Gas Applications", *ICETECH08*, Banff Alberta, July 20-23.

Flato, G. and Brown, R., 1996, "Variability and climate sensitivity of land fast Arctic sea ice," *J Geophysical Research*, Vol. 101, No. C10, pp. 12,767-25,777.

Fukamachi, Y., Mizuta, G., Ohshima, K., Toyota, T., Kimura, N. and Wakatsuchi, M., 2006, "Sea ice thickness in the southwestern Sea of Okhotsk revealed by a moored ice-profiling sonar," *J Geophysical Research*, Vol. 111, C09018.

Galley, R., Key, E., Barber, D., Hwang, B. And Ehn, J., 2008, "Spatial and temporal variability of sea ice in the southern Beaufort Sea and Amundsen Gulf: 1980-2004," *J Geophysical Research*, Vol. 113, C05S95.

Haas, C., 2004, "Late-summer sea ice thickness variability in the Arctic Transpolar Drift 1991 - 2001 derived from ground-based electromagnetic sounding, *Geophysical Research Letters*, Vol. 31, L09402.

Hienonen, J., 2004, *Constitutive Modelling of Ice Rubble in First-Year Ridge Keel*. Unpublished PhD thesis. Espoo, Finland: Helsinki U of Technology.

Hopkins, M., 1998, "Four stages of pressure ridging," *J Geophysical Research*, Vol. 103, No. C10, pp.21,883– 21,891.

Howell, S. and Yackel, J., 2004, "A vessel transit assessment of sea ice variability in the Western Arctic, 1969–2002: implications for ship navigation," *Canadian J of Remote Sensing*, Vol. 30, No. 2, pp. 205-215.

Hoyland, K., 2007, "Morphology and small-scale strength of ridges in the North-western Barents Sea," *Cold Regions Science and Technology*, Vol. 48, pp. 169-187.

Falkingham, J., Chagnon, R. and McCourt, S., 2002, "Trends in Sea Ice in the Canadian Arctic," *Proceedings, 16th IAHR Symposium,* Dunedin, New Zealand, 2-6 December.

Jeffers, S., Agnew, T., Alt, B., De Abreu, R. and McCourt, S., 2001, "Investigating the anomalous sea ice conditions in the Canadian High Arctic (Queen Elizabeth Islands) during the summer of 1998," *Annals of Glaciology*, Vol. 33, pp. 507-612.

Jeffries, M. 1992, "Arctic ice shelves and ice islands: Origin, growth and disintegration, physical characteristics, structural-stratigraphic variability, and dynamics," *Rev. Geophys*., 30, 245 – 267.

Jeffries, M. and Sackinger, W., 1990, "Near-real-time, synthetic aperture radar detection of a calving event at the Milne Ice Shelf, NWT, and the contribution of offshore winds," in *Ice Technology for Polar Operation: Proceedings of the Second International Conference on Ice Technology*, edited by T. Murthy et al., pp. 321– 331, Comput. Mech. Publ., Southampton, U.K.

Johannessen, K., Gudmestad, O., and Loset, S., 2001, "Drift of Sea Ice Ridges in the Pechora Sea," *J of Navigation*, Vol. 54.

Johnston, M., 2004, *Properties of Second-year and Multi-year Ice during Freeze-up*. Technical Report CHC-TR-024. Ottawa: National Research Council.

Kharitonov, V., 2007, "Internal structure of ice ridges and stamukhas based on thermal drilling data," *Cold Regions Science and Technology*, Vol. 52, pp. 302-35.

Kitagawa, H., 2001, "The History of Applied Ice Research in Japan," *POAC Proceedings*, Ottawa, August 12-17.

Koerner, R. and Lundgaard, L., 1995, "Glaciers and Global Warming" Géographie physique et Quaternaire, vol. 49, n° 3, p. 429-434.

Konig, C., 2007, *Arctic Landfast Sea Ice*. Unpublished PhD Thesis. New York: New York U.

Kovacs, A., 1972, "On pressured sea ice," in, T. Karlsson (ed.), *Sea Ice.* Reykjavik: National Research Council Iceland.

Kwok, R., 2005, "Near zero replenishment of the Arctic multi-year sea ice cover at the end of 2005 summer," *Geophysical Research Letters*, Vol. 34, L05501.

Li, F., 1991, *Simulation of the Recurrence Probability of Ice Islands in the Arctic Ocean*. Unpublished PhD thesis. Fairbanks: U Alaska at Fairbanks.

Lipscomb, W., 1998, *Modelling the Thickness Distribution of Arctic Sea Ice*. Unpublished PhD Thesis. Seattle: U Washington.

Lu, M.,1992, *Massive ice interactions with offshore structures*. Unpublished PhD thesis. Fairbanks: U Alaska at Fairbanks.

Lukovich, J. and Barber, D., 2006, "Atmospheric controls on sea ice motion in the southern Beaufort Sea," *J Geophysical Research*, Vol. 111, D18103.

Mahoney, A., 2006, *Alaska Landfast Sea Ice Dynamics*. Unpublished PhD thesis. Fairbanks: U Alaska at Fairbanks.

McLaren, A., Wadhams, P. and Weintraub, R., 1984, "The Sea Ice Topography of M'Clure Strait in Winter and Summer of 1960 from Submarine Profiles," *Arctic*, Vol. 37, No. 2, pp. 110-120.

Melling, H., Johnson, P.H., and Riedel, D.A., "Measurements of the Underside of Sea Ice by Moored Subsea Sonar", Journal of Atmospheric and Oceanic Technology, Vol 12, No. 3, June 1995.

Melling, H., 1998, "Detection of features in first-year pack ice by synthetic aperture radar (SAR)," *International J of Remote Sensing*, Vol. 19, No. 6, pp.1223-1249.

Melling, H. and Riedel, D., 2005, "Trends in the draft and extent of seasonal pack ice, Canadian Beaufort Sea," *Geophysical Research Letters*, Vol. 32, L24501.

Melling, H., and Riedel, D.A. "Draft and Movement of Pack Ice in the Beaufort Sea: A Time-Series Presentation April 1990 – August 1999, Science Branch - Pacific Region Institute of Ocean Sciences, P.O. Box 6000, Sidney, BC Canada V8L 4B2, , Canadian Technical Report of Hydrography and Ocean Sciences 238, Updated in 2004.

Marcellus,R.W., and T.B.Morrison, 1982, "Ice Design Statistics for the Canadian Beaufort Sea", a report prepared for the partners in the Beaufort Sea Environmental Impact Statement

Mueller, D., Copland, L. and Jeffries, M., *News Release: Scientists Report Massive Ice Shelf Loss during Summer of 2008*. Peterborough: Trent U. http://www.people.trentu.ca/~dmueller/iceshelfloss2008/

Mueller, D. and Jeffries, M., 2003, "Break-up of the largest Arctic ice shelf and associated loss of an epishelf lake," *Geophysical Research Letters*, Vol 30, No. 20, p.2031.

Narod, B., Clarke, G. and Prager, B., 1987, "Airborne UHF radar sounding of glaciers and ice shelves, northern Ellesmere Island, Arctic Canada," *Canadian J of Earth Sciences*, Vol. 25, pp.95-105.

Pfirman, S., Haxby, W., Colony, R. and Rigor, I., 2004, "Variability in Arctic sea ice drift," *Geophysical Research Letters*, Vol. 31, L16402.

Pilkington, R., Hill, C., Metge, M. and McGonigal, D., 1992, *Beaufort Sea Ice Design Criteria*, Environmental Studies Research Funds Report 115. Calgary: National Energy Board.

Rigor, I., Wallace, J. and Colony, R., 2002, "Response of sea ice to the Arctic Oscillation," *J. Climatology*, 15, 2648 – 2663.

Rigor, I. And Wallace, J., 2004, "Variations in the age of Arctic sea-ice and summer sea-ice extent," *Geophysical Research Letters*, Vol. 31, L09401.

Rothrock, D., Yu, Y and Maykut, G., 1999, "Thinning of the Arctic Sea-Ice Cover," *Geophysical Research Letters*, Vol. 26, No. 23, pp. 3469-3472.

Rothrock, D., Zhang, J. and Yu, Y., 2003, "The arctic ice thickness anomaly of the 1990s: A consistent view from observations and models," *J Geophysical Research*, Vol. 108, No. C3.

Sackinger, W., Jeffries, M., Li, F. and Lu, M., 1991, *Ice Island Creation, Drift, Recurrences, Mechanical Properties and Interconnections with Arctic Offshore Oil Production Structures*, Final Report, the Geophysical Institute. Fairbanks: U Alaska Fairbanks.

Shafrova, S. and Hoyland, K., 2007, "Morphology and 2D spatial strength distribution in two Arctic first-year sea ice ridges," *Cold Regions Science and Technology*, Vol. 51, pp. 38-55.

Shirasawa, K., Lepparanta, M., Saloranta, T., Kawamura, T., Polomoshnov, A. and Surkkov, G., 2005, "The thickness of coastal fast ice in the Sea of Okhotsk," *Cold Regions Science and Technology*, Vol. 42, pp. 25-40.

Shy, T., *What Causes North Pole Ice Thickness to Change?* Unpublished PhD thesis. Urbana-Champain: U Illinois.

Smith, O. and Lee, W., 2001, "Risk Analysis Features of the Alaska Sea Ice Atlas," proceedings of the *16th conference on Port and Ocean Engineering under Arctic Conditions*, POAC'01, Ottawa.

Sugden, D., 1982, *Arctic and Antarctic - A modern geographical synthesis.* Blackwell: Oxford.

Symon, C., Lelani, A. and Heal, B. (eds.), 2005, *Arctic Climate Impact Assessment*. Cambridge: Cambridge U Press.

Timco, G., 1996, "NRC Centre of Ice/Structure Interaction: Archiving Beaufort Sea Data," presented at *IAHR Ice Symposium*, Beijing.

Timco, G., Gorman, B., Falkingham, J. and O'Connell, B., 2005, *Scoping Study: Ice Information Requirements for Marine Transportation of Natural Gas from the High Arctic*. Technical Report CHC-TR-029. Ottawa: National Research Council of Canada.

Timco, G. and Burden, R., 1997, "An analysis of the shapes of sea ice ridges," *Cold Regions Science and Technology*, 25, 65– 77.

Tivy, A., Howell, S., Alt, B., Yackel, J. and Carrieres, T., in preparation, "Trends and variability in summer sea ice cover in Canada's Arctic and sub-Arctic regions."

Tucker, W., Weatherly, J, Eppler, D., Farmer, L, and Bentley, D., 2001, "Evidence for rapid thinning of sea ice in the western arctic ocean at the end of the 1980s," *Geophysical Research Letters*, 28: 2851-2854.

U of C Library, 1999, *Cataloguing of Northern Petroleum Industry Reports into the Arctic Institute Collection of the University of Calgary Library*. PERD/CHC Report 35-55. Calgary: University of Calgary Library.

Vincent, W., Gibson, J. and Jeffries, M., 2001, "Ice-shelf collapse, climate change, and habitat loss in the Canadian high Arctic," *Polar Record*, Vol. 37, No. 201, pp. 133-142.

Vinje, T., Nordlund, N. and Kvambekk, A., 1998, "Monitoring ice thickness in Fram Strait," *J Geophysical Research*, Vol. 103, No. C5, pp. 10,437-10,449.

Wadhams, P., Wilkinson, J. and McPhail, S., 2006, " A new view of the underside of Arctic sea ice," *Geophysical Research Letters*, Vol. 33, L04501.

Wadhams, P., 1997, "Ice thickness in the Arctic Ocean: the statistical reliability of experimental data," *J Geophysical Research,* Vol. 102, No. 27, pp. 27,951-27,959.

Wadhams, Peter, "Arctic Sea Ice Changes Under Global Warming", ICETECH 2008, Banff, Canada, July, 2008.

Wadhams, P., Wilkinson, J. and Doble, M., 2008, "Three-Dimensional Mapping of the Sea ice Underside from AUVs and Applications to the Offshore Industry," Paper No. ICETECH08-141-R1, presented at ICETECH08 conference, Banff, Canada, July 20-23.

Wright,B., J.Hnatiuk and A.Kovaks, 1981, Multi-year pressure ridges in the Canadian Beaufort Sea. Coastal Engineering, 5.: 125-145.

Williamson, S., Sharp, M., Dowdeswell, J. and Benham, T., 2008, "Iceberg calving rates from northern Ellesmere Island ice caps, Canadian Arctic, 1999-2003," *J Glaciology*, Vol. 54, No. 186.

14 APPENDIX A - SATELLITE IMAGERY AND EIF ANALYSIS

14.1 A-1 Radarsat 2 Data

Radarsat 2 data was collected in two areas – 4 images NW from the west coast of Prince Patrick Island, and 4 images NW from Meighen Island. Each image, and a brief description of each are shown below.

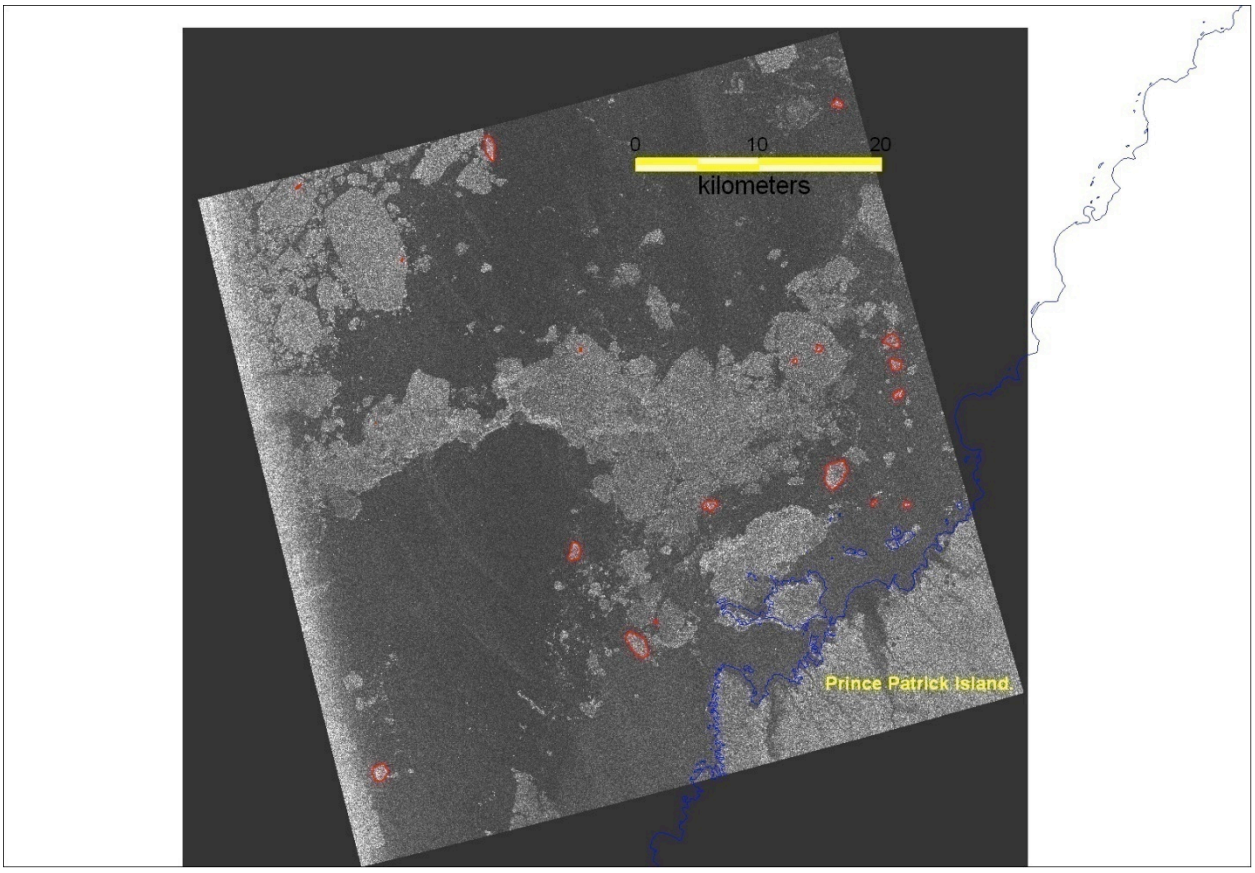

Figure 14-1 Radarsat 2 August 2, 2008 50km swath, 8m resolution. – PPI 1

This image depicts ice conditions from the Prince Patrick Island coast out to the NW. At the time of this image an off-shore wind was moving the rubbled ice off of the coast. The red-circled EIFs in this scene were mostly MYHFs, although three Ice Island fragments were also located. In the center portion of the image an area of rubble remains grounded against the outlaying island.

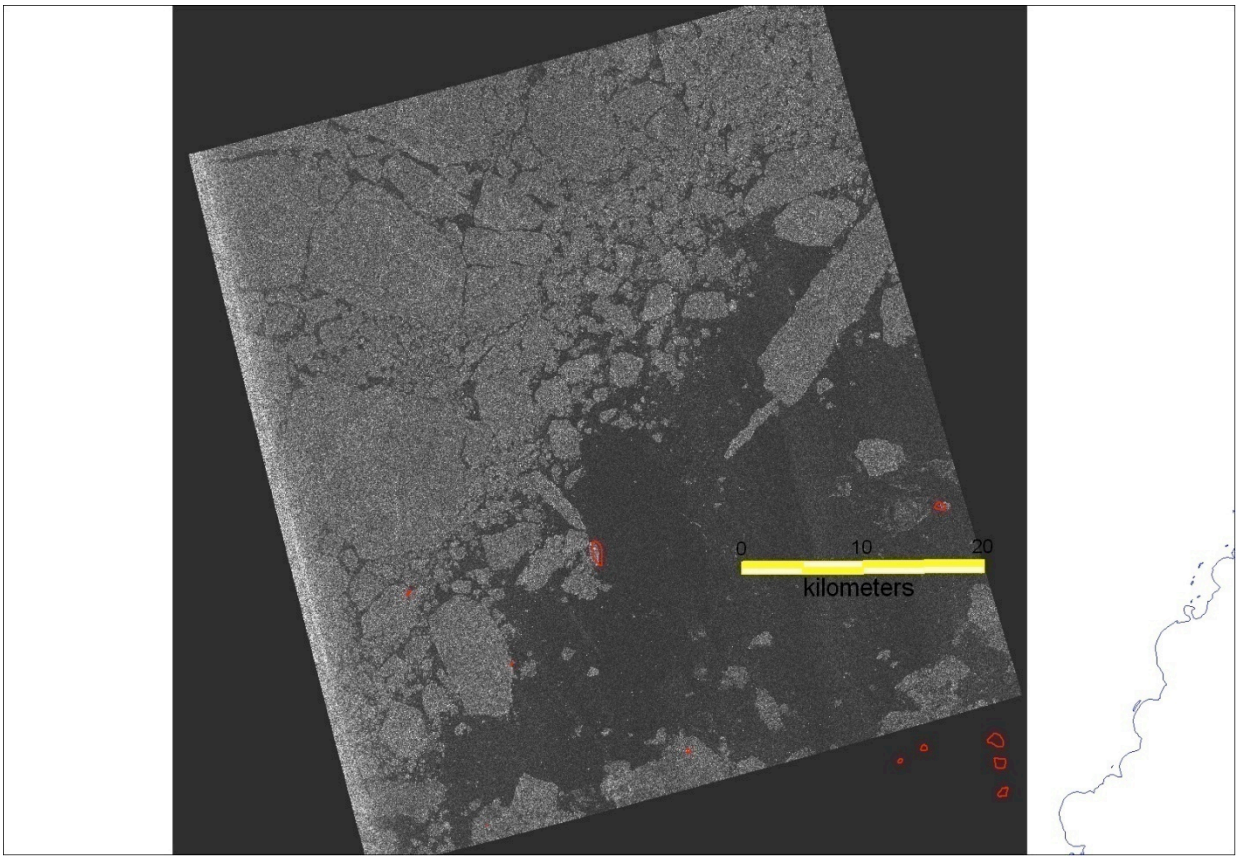

Figure 14-2 Radarsat 2 August 2, 2008 50km swath, 8m resolution. – PPI 2

This image is the next one north from the PPI coast, and the upper portion shows compact ice conditions where the off-shore wind is compressing the ice against the Polar Pack. Considerably fewer MYHFs were identified, and only one Ice Island fragment.

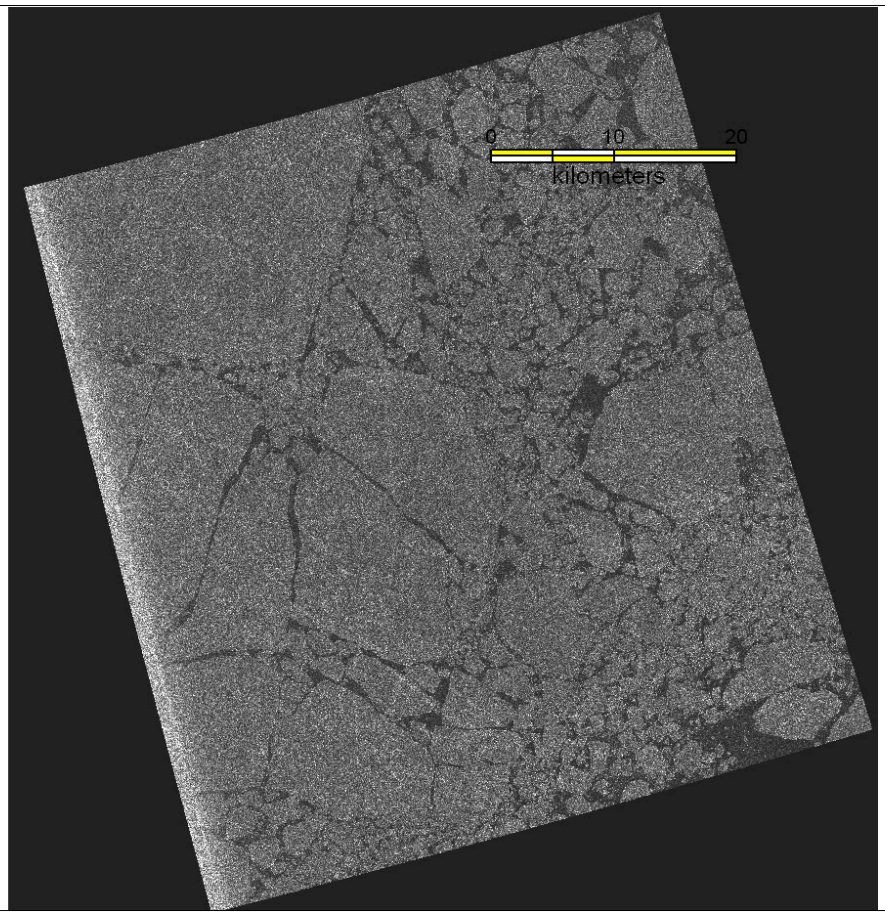

Figure 14-3 Radarsat 2 August 2, 2008 50km swath, 8m resolution. – PPI 3

This is the third image off-shore from PPI, and no MYHFs or Ice Island fragments were identified. This area is now 9/10 coverage of Multi-year ice, and compression from the off-shore winds are breaking up some of the floes.

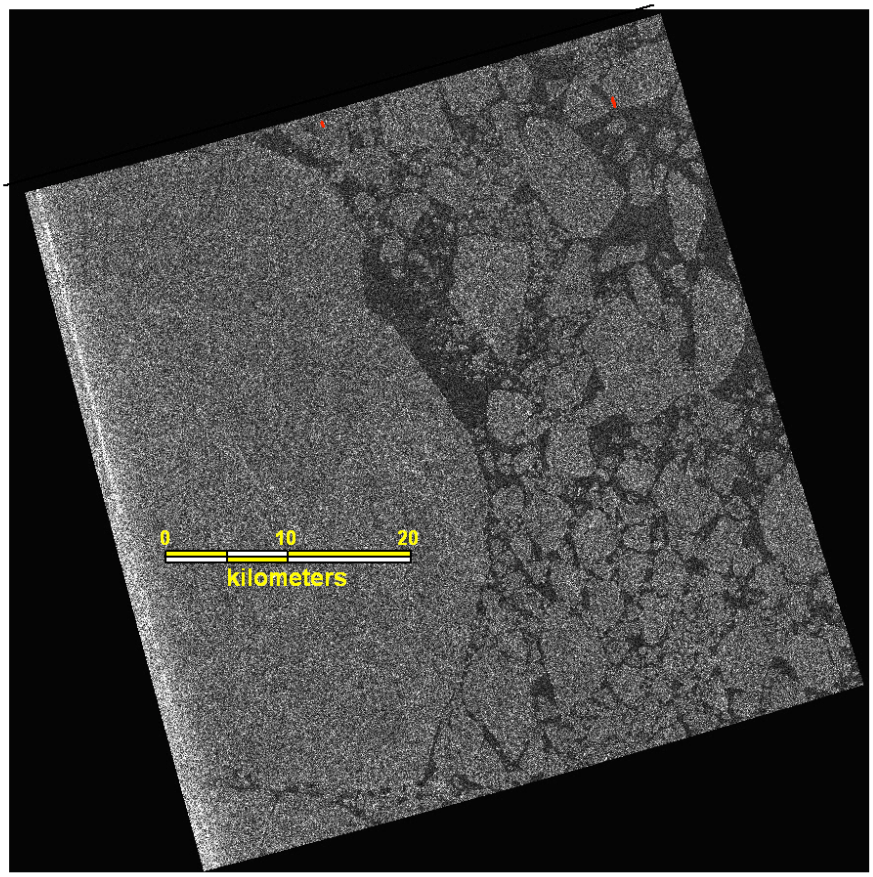

Figure 14-4 Radarsat 2 August 2, 2008 50km swath, 8m resolution. – PPI 4

This is the fourth image in this area, and is the furthest off-shore. A giant multi-year floe dominates the left side of the image, with more broken-up floes on the right side. Two ice island fragments were identified, but no MYHFs were located in this image.

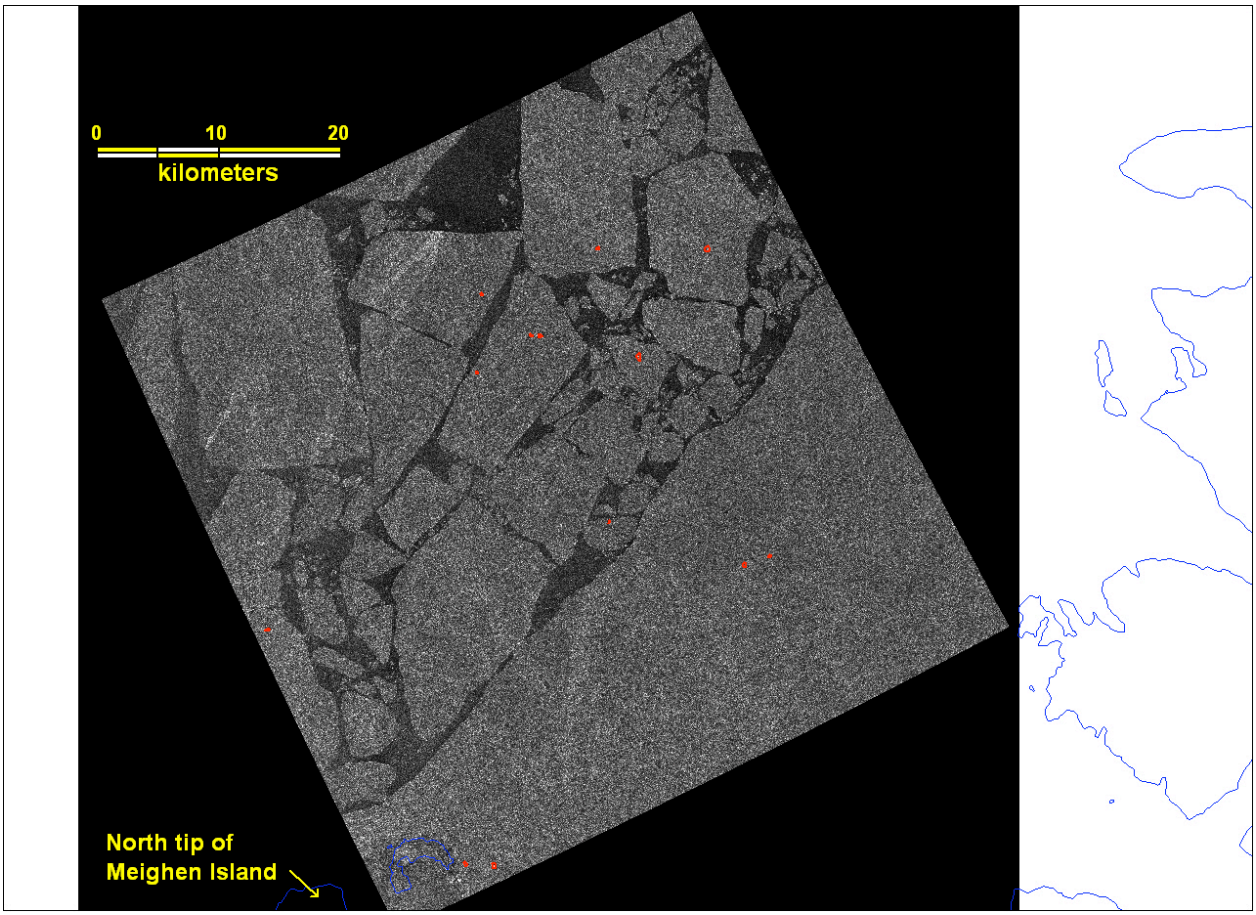

Figure 14-5 Radarsat 2 July 30, 2008 50km swath, 8m resolution. – Meighen #1

This image is the first in the swath that runs NW from Meighen Island. The area in the lower portion of the image is fast ice, with the northern portion being mobile. Numerous Ice Island fragments were identified, but very few MYHFs. Winds were not particularly offshore at the time of this image, and the mobile ice appears to be generally drifting SW, parallel to the coast.

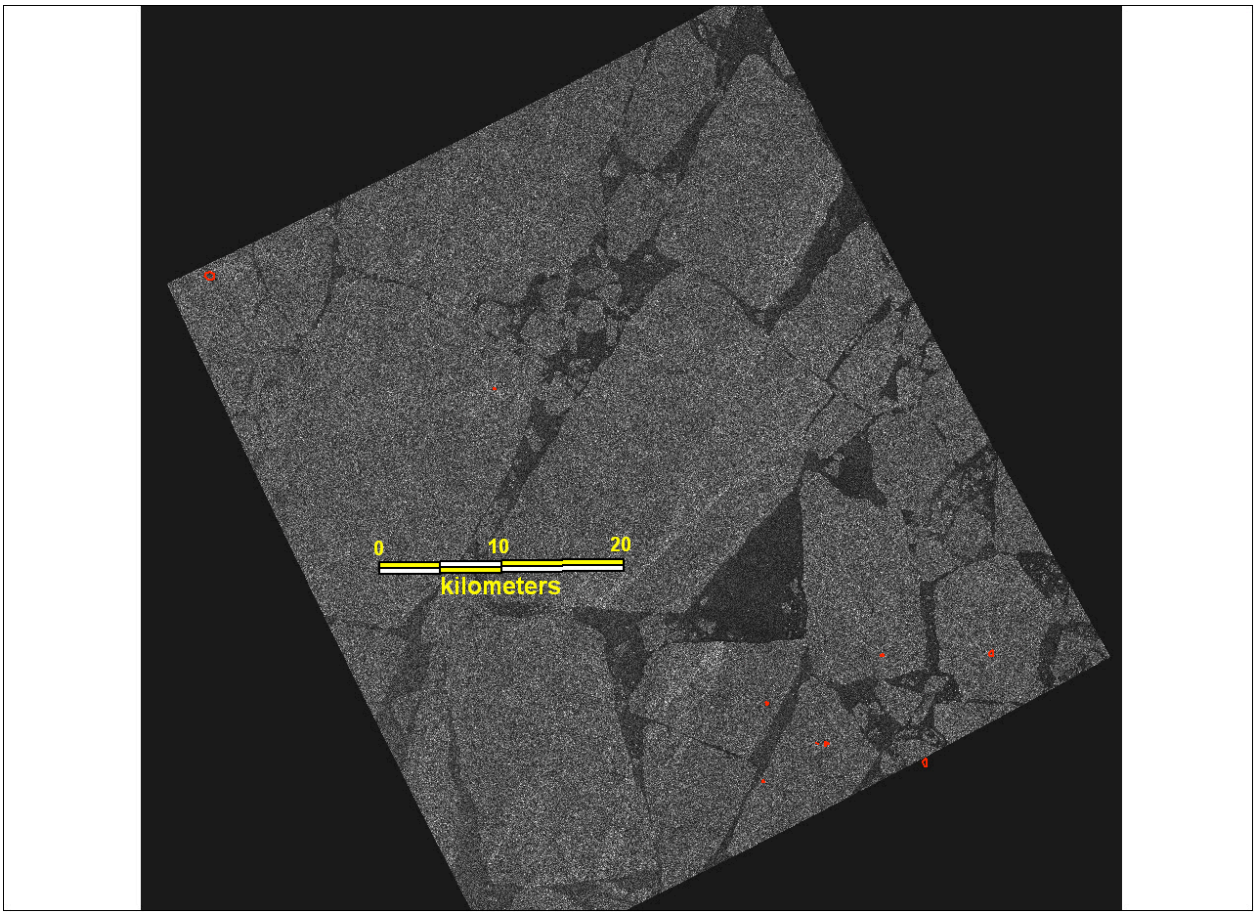

Figure 14-6 Radarsat 2 July 30, 2008 50km swath, 8m resolution. – Meighen #2

This is the second image off-shore, and contains no fast ice. Considerably fewer EIFs were located on this image, with several Ice Island fragments along the southern portion, but only one II fragment and one MYHF located in the north ½ of the image. The scene is dominated by giant floes of Multi-year ice.

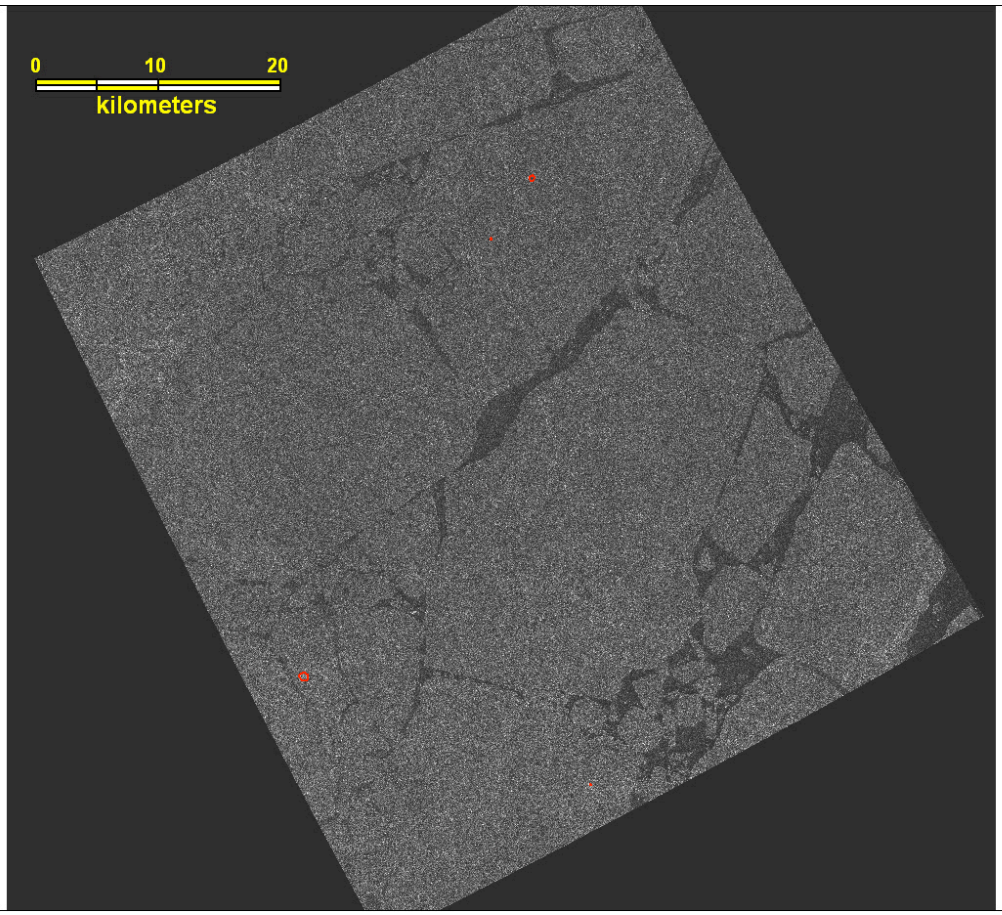

Figure 14-7 Radarsat 2 July 30, 2008 50km swath, 8m resolution. – Meighen #3

This image is well off-shore, and a few giant floes of Multi-year ice dominate the scene. Two multi-year hummock fields and two Ice Island fragment were the only EIFs identified in this off-shore scene.

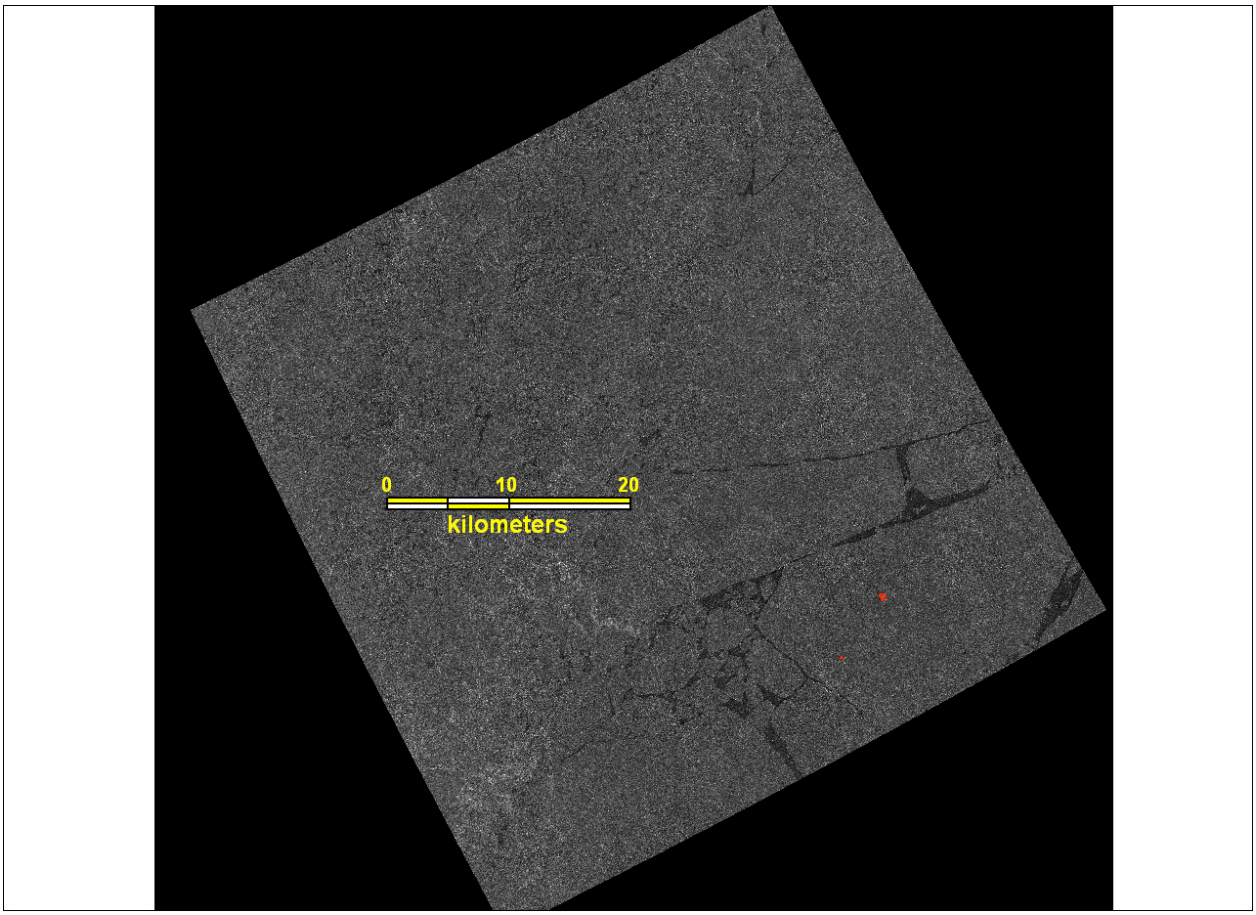

Figure 14-8 Radarsat 2 July 30, 2008 50km swath, 8m resolution. – Meighen #4

This image is the furthest off-shore, and therefore the furthest into the Polar Pack. Conditions were 9+/10 concentration, with some compression evident. No EIFs were identified in the northern portion of this image.

14.2 A-2 Landsat Data

Landsat data was acquired to use in verifying targets identified on radar imagery. Although the Landsat provided valuable information, it was somewhat degraded due to an on-board problem with the spacecraft; the scene had a continuous pattern of narrow bands of missing data. These bands of missing data were filled in by the data provider with "other" data. The manufactured data used to fill in the missing bands did complicate the use of the data, but made for a less distracting image than the original which showed all missing data as solid black areas.

The Landsat images used in this project are shown below, with a brief description of each.

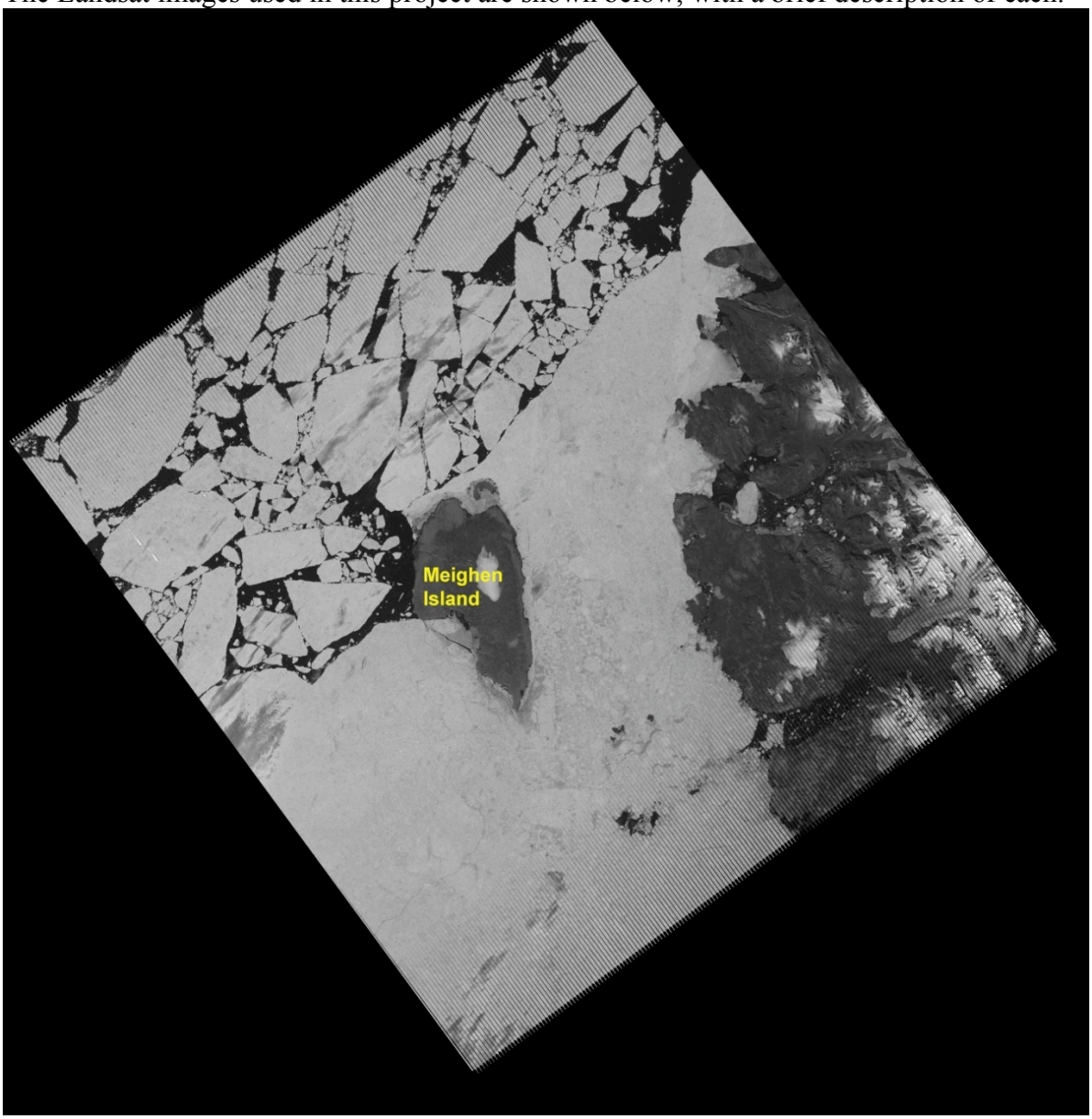

Figure 14-9 LANDSAT July 29, 2008 100km swath, 30m resolution. Meighen I.

The Meighen Island Landsat image was used to verify targets on the Envisat and Radarsat images. Shown below is a zoomed-in view of an Ice Island that was located about 30 n.mi. SE of Meighen Island.

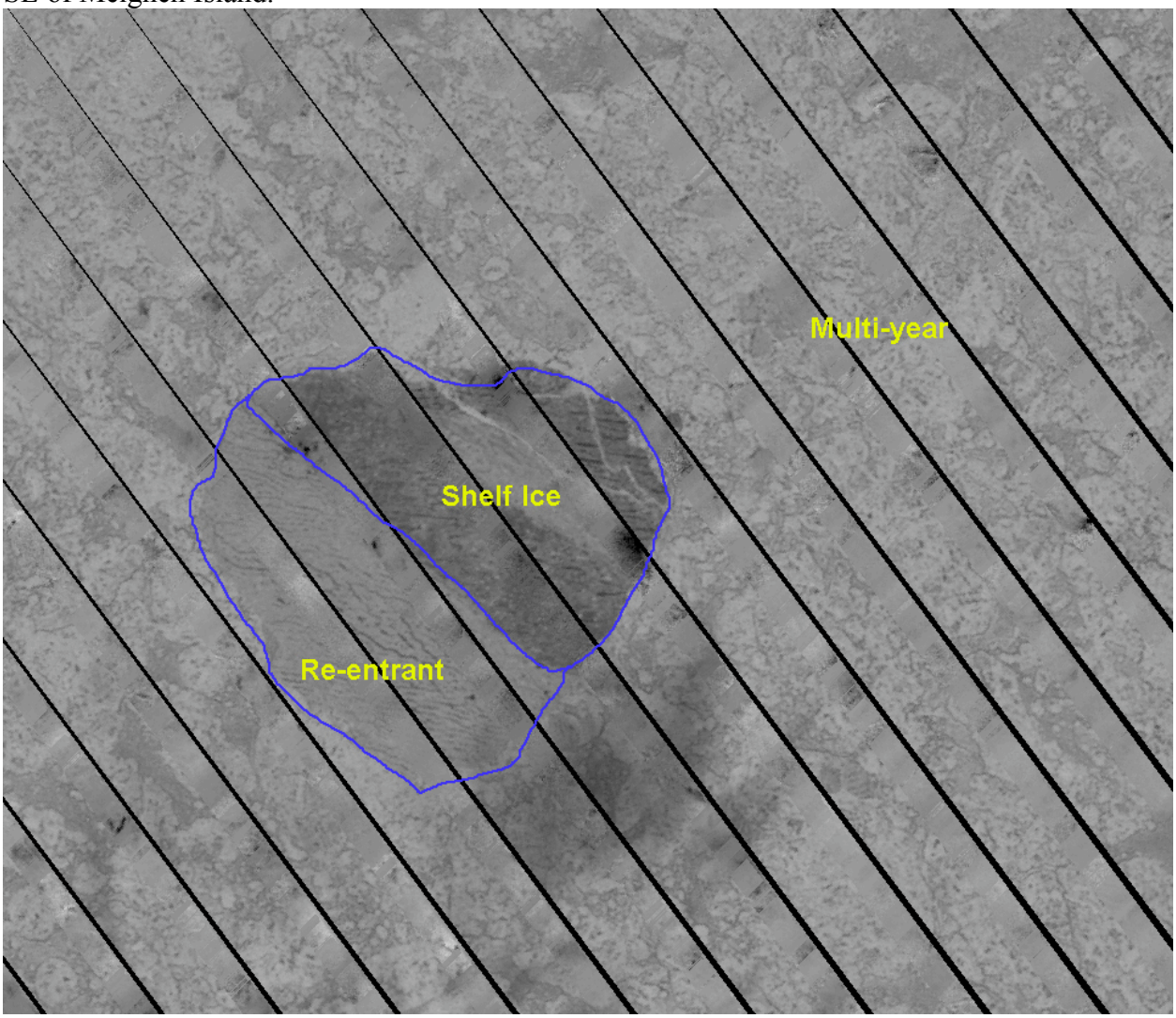

This area is depicted with 15m resolution Landsat, and very high detail is available. Note how the unique surface tone of the Ice Island, and its attached re-entrant, can be clearly identified in this image. The subtle surface differences between the re-entrant and the Shelf ice were not apparent on the radar imagery. More so than in the lower resolution Landsat, the missing (and other) data filled in on this image are a complicating factor that lowered the utility of this imagery.

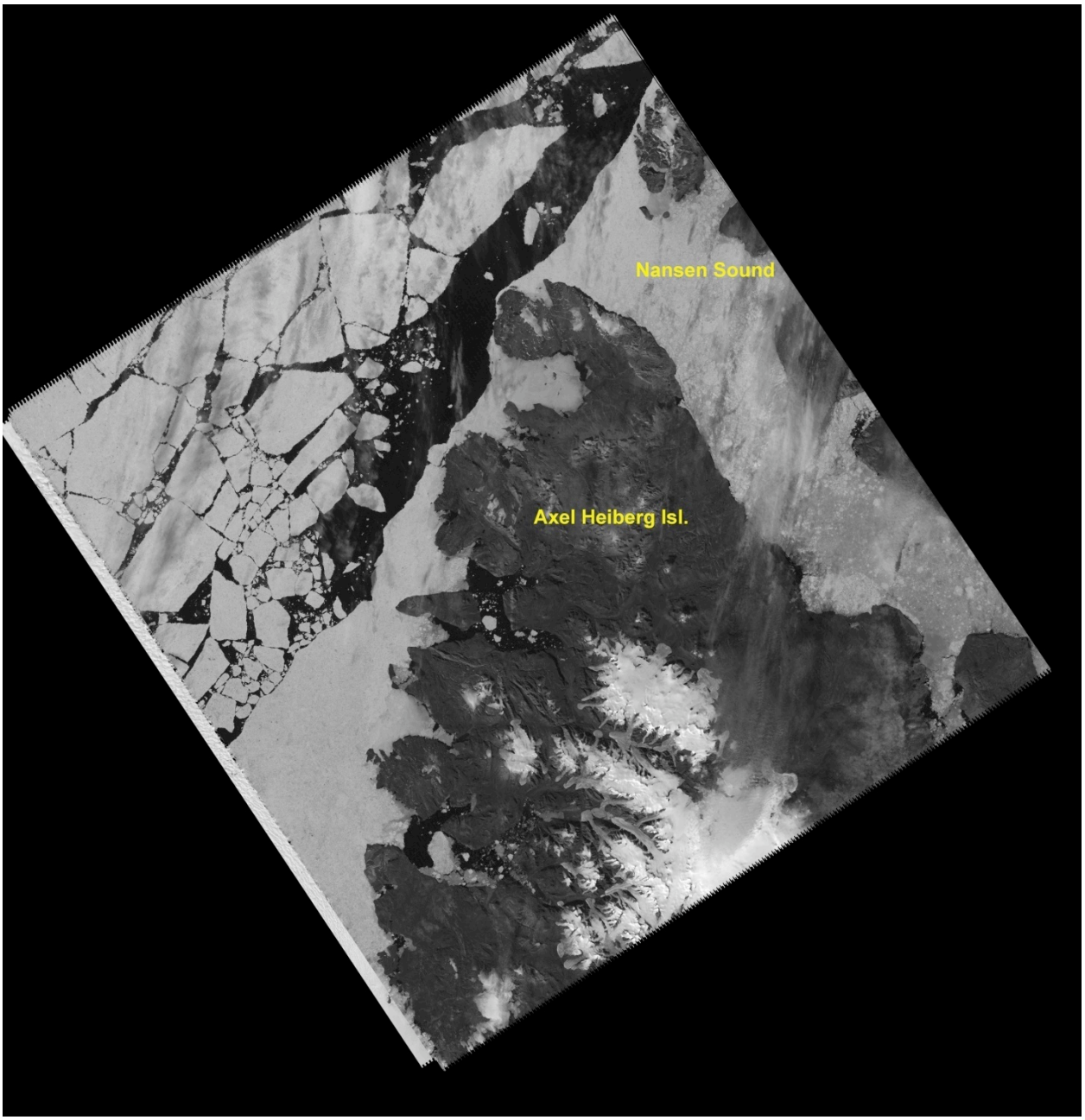

Figure 14-10 LANDSAT July 29, 2008 100km swath, 30m resolution. Axel Heiberg Island

This Landsat image contains significant areas of fast ice, as well as mobile ice off-shore. An off-shore ice drift was occurring at the time of this image, and Open Water is present along the fast ice edge.

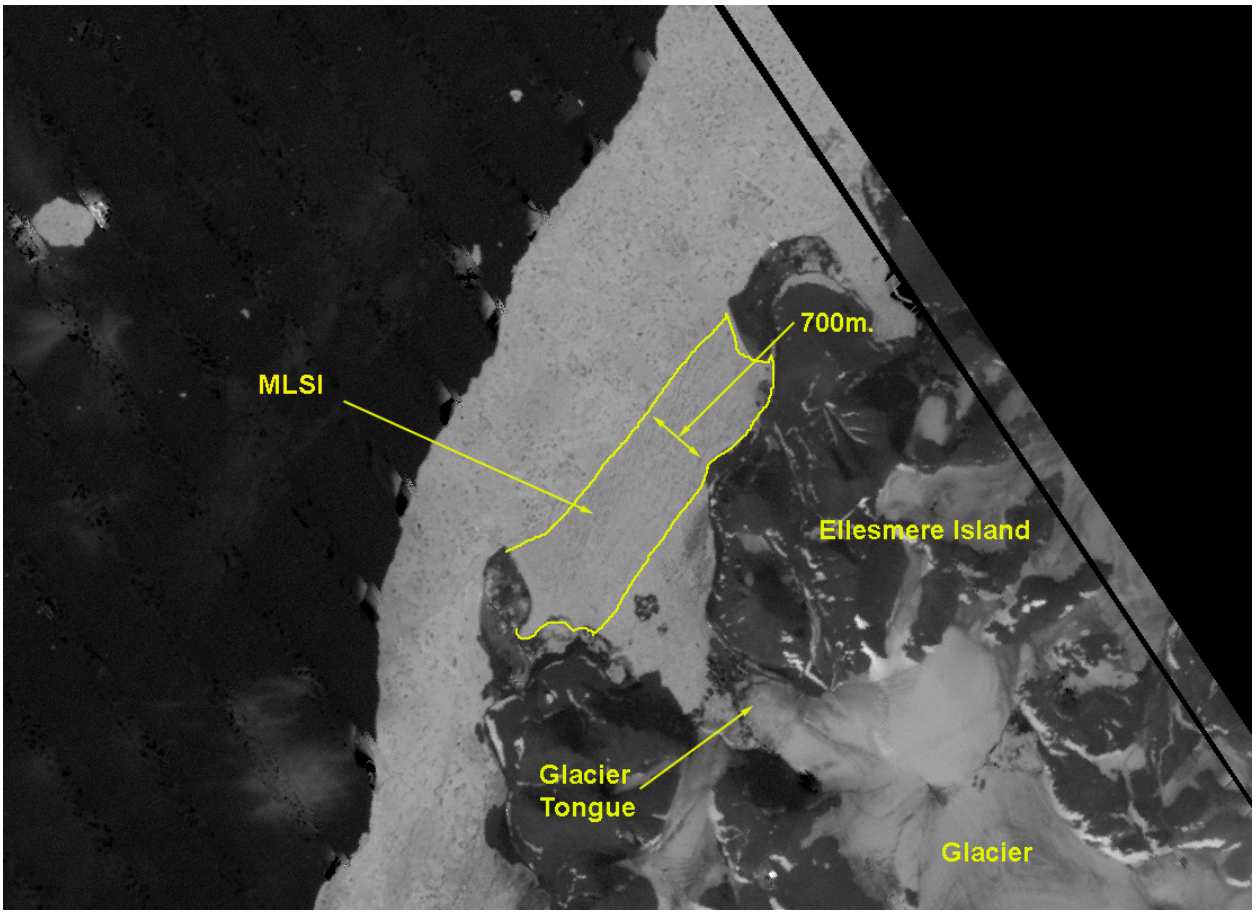

Figure 14-11 LANDSAT – July 27, 2008 12.5m resolution

This clip of the high-resolution Landsat (digitally processed to 12.5m res.) from just north of Nansen Sound shows a small area of Multi-year Land fast Sea ice (MLSI). Although the MLSI does show features that are similar to shelf ice undulations, they do not run continuously. These *Shelf ice-like* features are very weathered ridges from on-shore pressure and the resulting ridging thus runs parallel to the coast – a similar orientation to Shelf ice, but vastly different formation history.

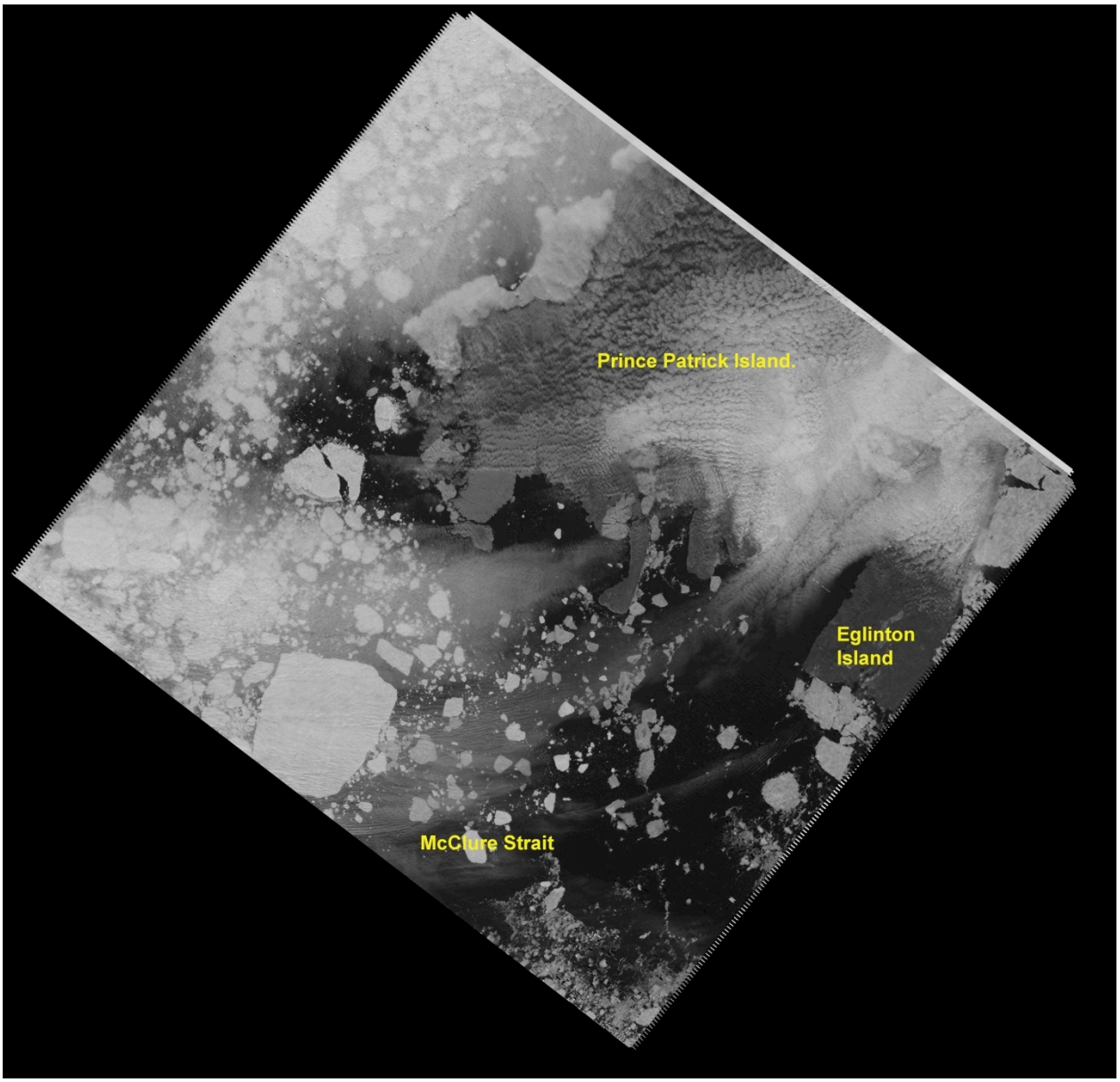

Figure 14-12 LANDSA July 27, 2008 100km swath, 30m resolution. Prince Patrick Island

This image of the southern portion of Prince Patrick Island depicts the low concentrations typical of this area, at this time of year. Although there was an off-shore drift at the time of this image, some of the rubble along the west coast of Prince Patrick Island was still in place. By July 30 most of it was gone, and by August 2nd this entire coast was clear.

14.3 A-3 MODIS Data

MODIS imagery was acquired at the time of the radar imaging as a low-cost addition to the database for use in assessing overall conditions in the area-of-interest. Due to the very large footprint of MODIS (2300km swath) one image covered the majority of the area. The first image is the full area, and the second is an example of the full-zoom color imagery.

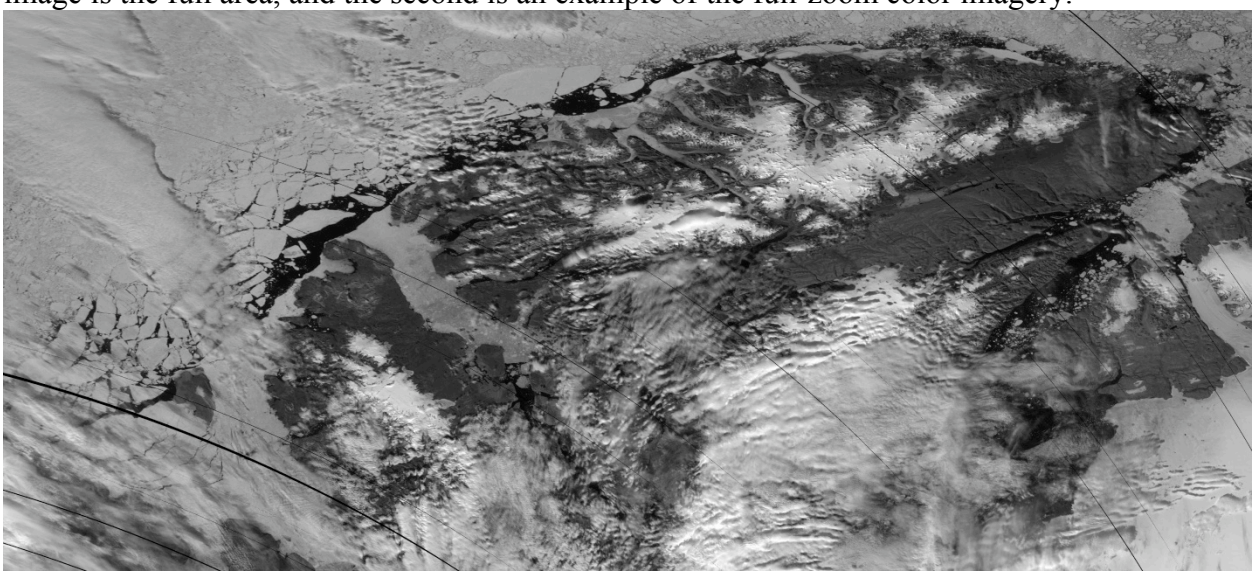

Figure 14-13 Aug. 1, 2008. MODIS of Ellesmere Island at 240m Resolution

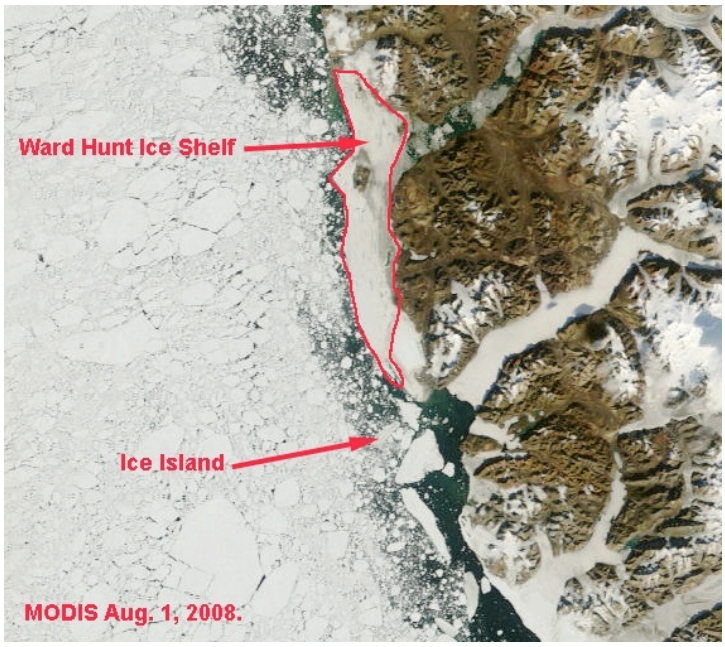

This full-resolution depiction of the area in color provided a very clear view of the area at the time of the radar imaging.

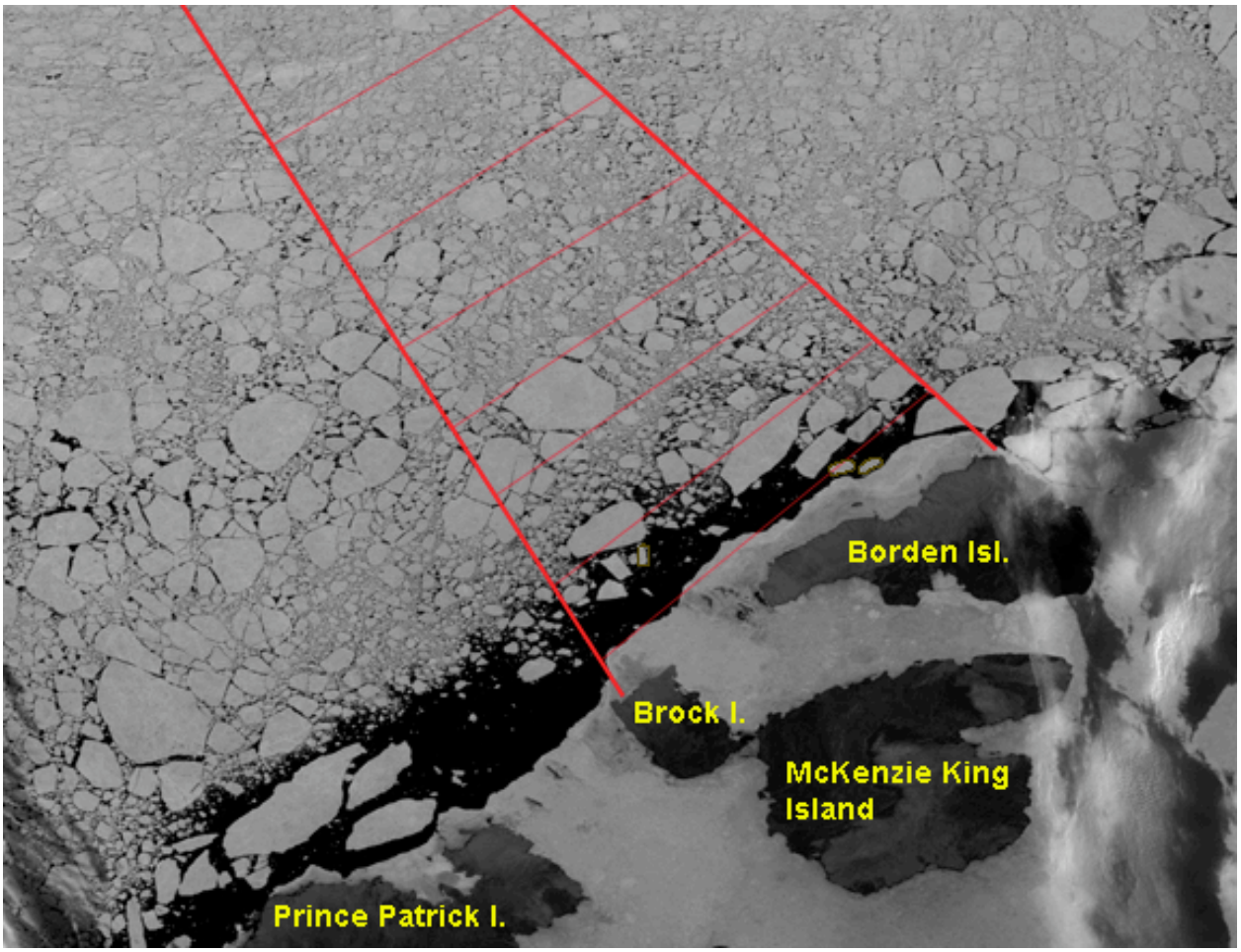

Figure 14-14 Aug 1, 2008 MODIS Pack Ice off Borden Island

The MODIS image above shows the coastal area where this imagery was used to fill in a small gap in the Envisat coverage – Envisat gap is cross-hatched in red. Three MYHFs were identified along the fast ice edge.

14.4 A-4 Envisat Imagery

Envisat imagery was the *backbone* of this project, with the entire area covered at full resolution (30m). The area of this study contained highly mobile ice throughout, and the angular shape of EIFs made them relatively easy to detect amongst the well-rounded floes of multi-year ice typical of this region.
All Envisat images analyzed for this project follow below, with a brief description of each.

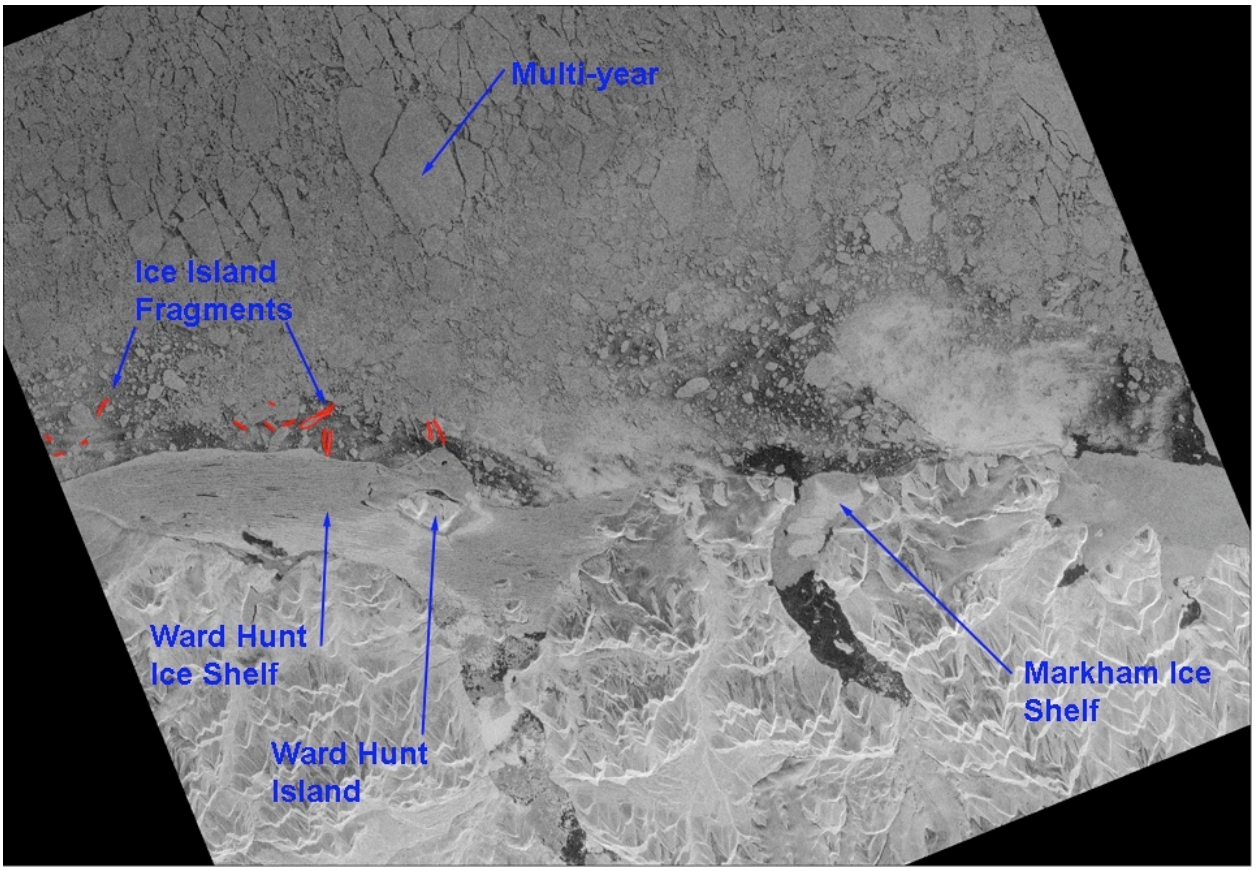

Figure 14-15 (1 of 22) Envisat July 31, 2000 100km swath, 30m res. (Ward Hunt Island)

This image from northern Ellesmere Island includes the Markham and Ward Hunt Ice Shelves. Significant fracturing occurred a few days earlier, and many Ice Islands and Ice Island fragments continue to drift along the coast. Slightly off-shore winds have produced an area of lower concentration along the coast, facilitating calving.

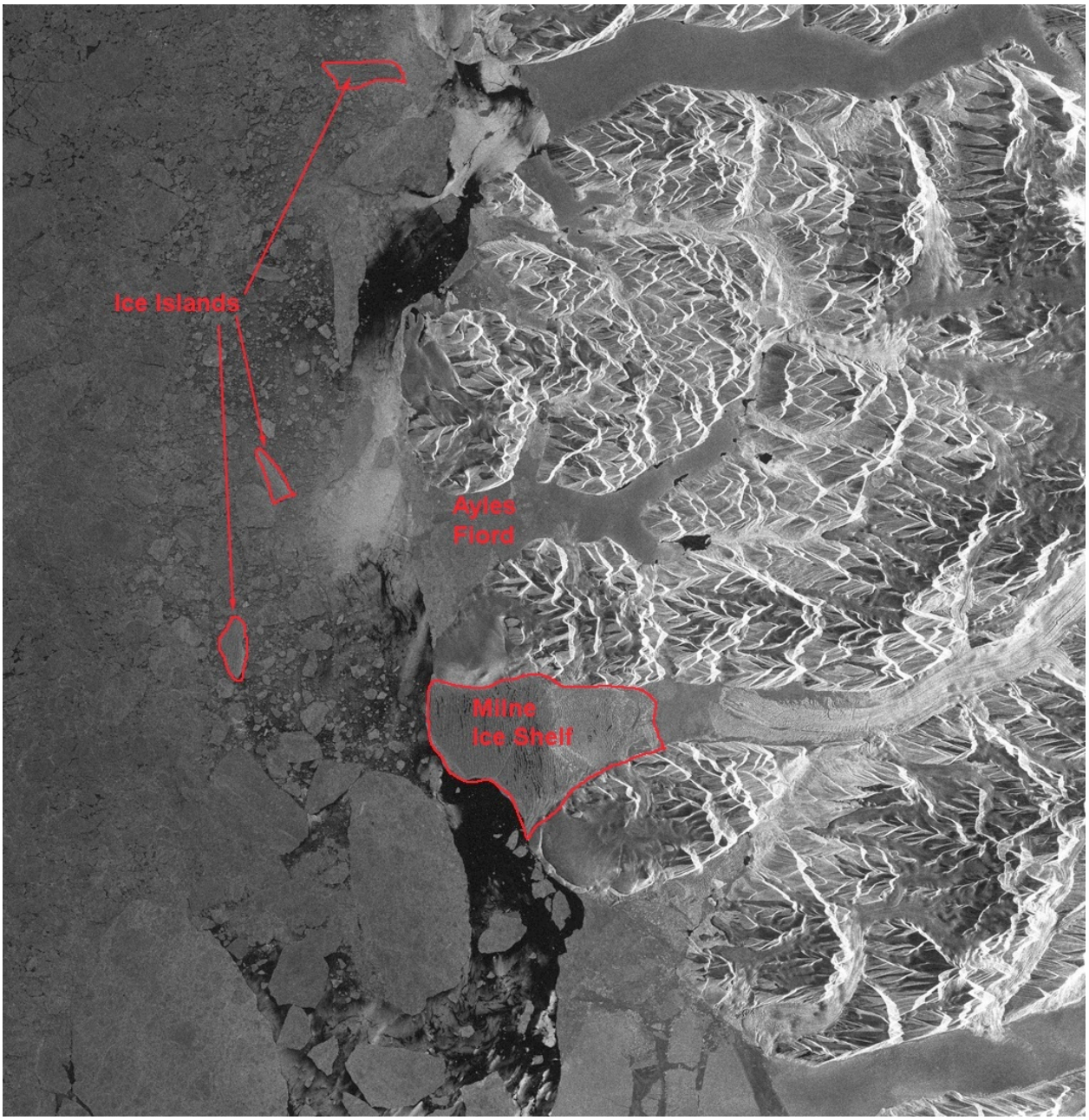

Figure 14-16 (2 of 22) Envisat August 1, 2008 100km swath, 30m res (Ayles-Milne Shelves)

This image is the next one below Ward Hunt, and three of the large Ice Islands that calved from Ward Hunt are identified in this scene. Although Ayles Fiord is clear of Shelf ice (calved out in 2005) the Milne Ice Shelf remains in place, and is identified here. The Peterson Ice shelf is in the inlet just below the Milne Ice Shelf in this scene.

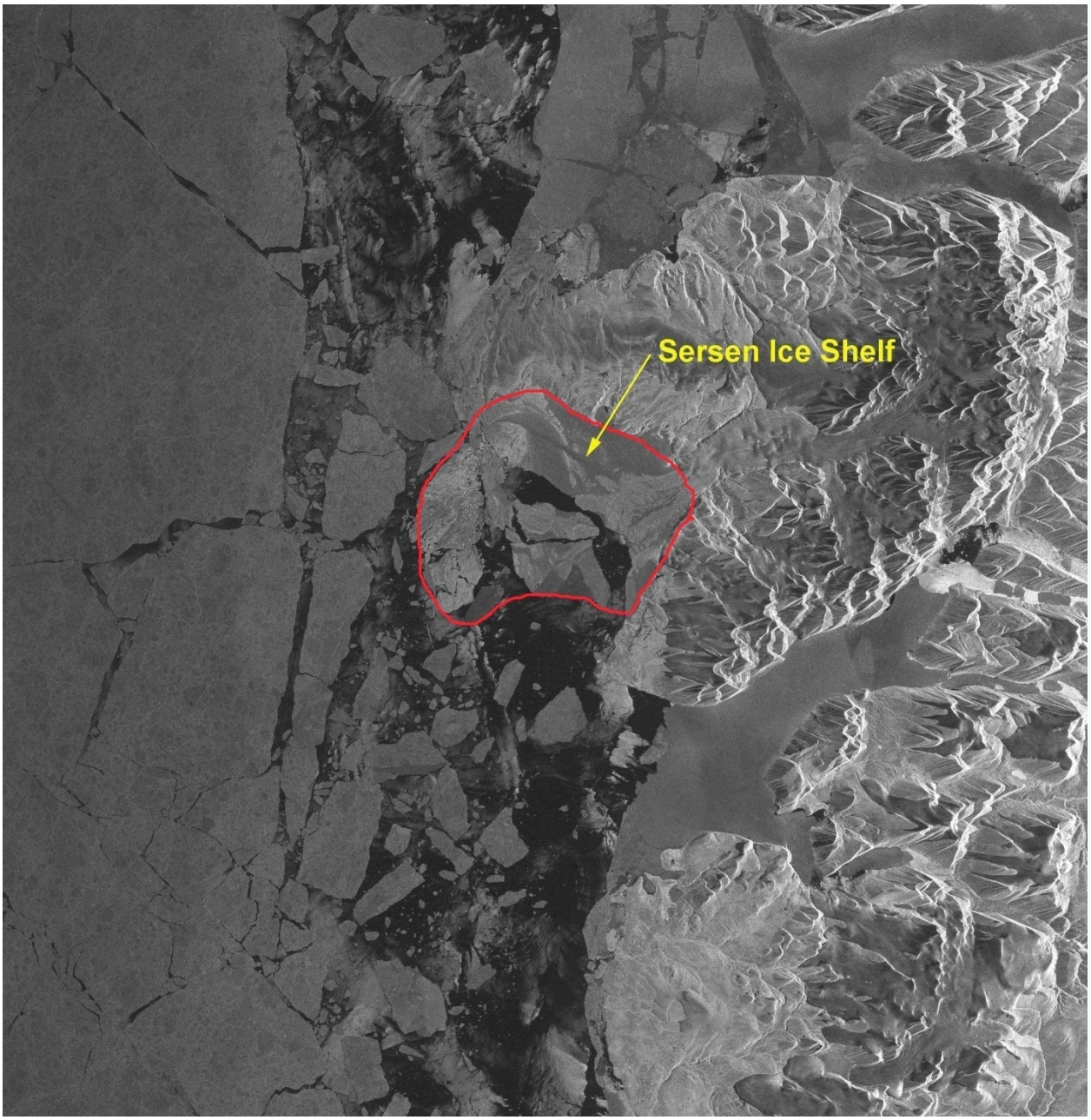

Figure 14-17 (3 of 22) Envisat August 1, 2008 100km swath, 30m res (Petersen - Serson Shelves)

This image includes the Serson Ice Shelf, which is breaking up and drifting out at the time of this image. The upper portion of the Shelf area shows a conglomerate structure indicating that it fractured and partially cleared last year.

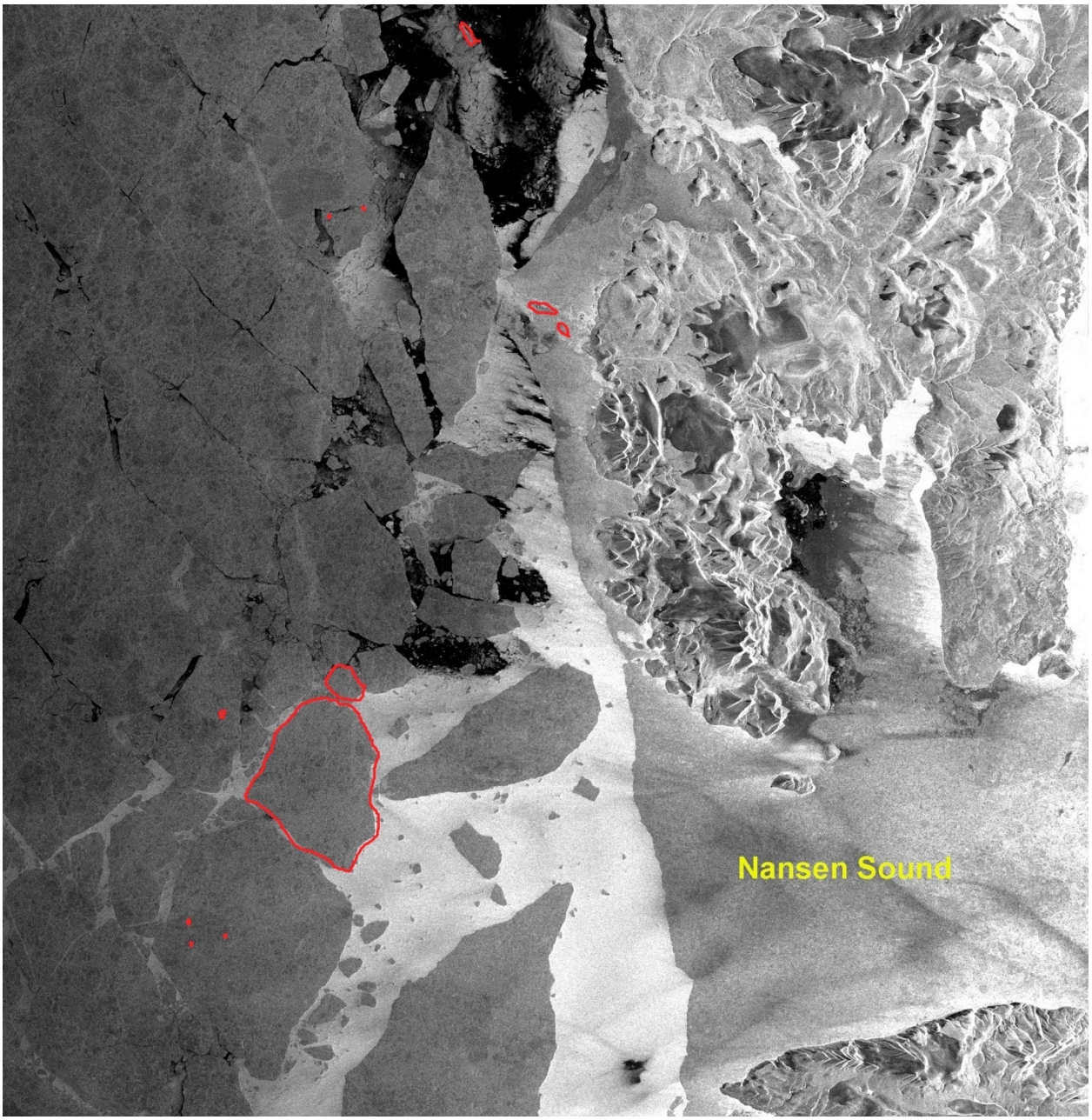

Figure 14-18 (4 of 22) Envisat August 1, 2008 100km swath, 30m res (Nansen Sound and North)

This image of Nansen Sound and north contains large areas of fast ice, several ice island fragments, and two large MYHFs. The conglomerate structure of Multi-year in this area is clear in this image.

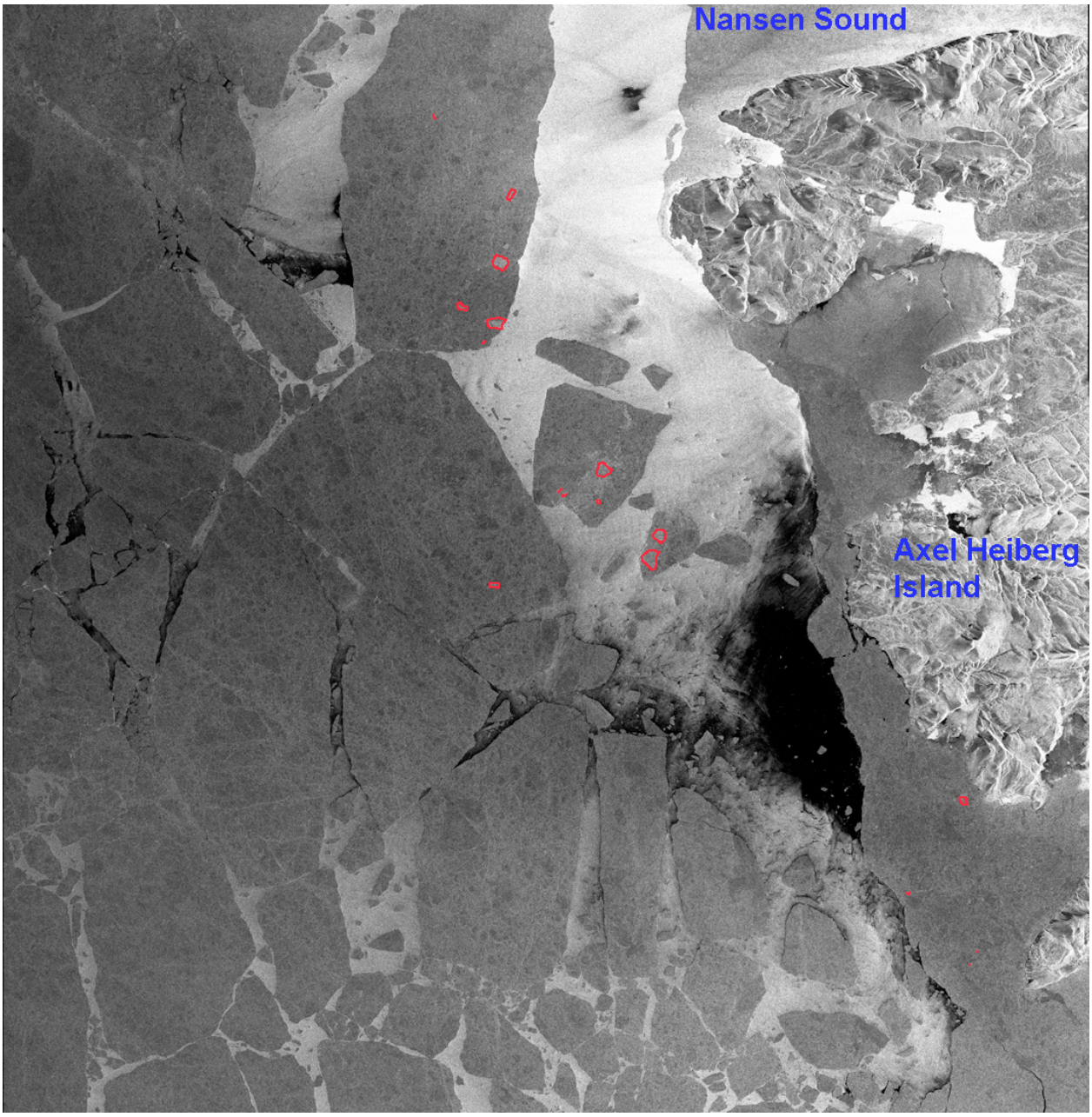

Figure 14-19 (5 of 22) Envisat – August 1, 2008 100km swath, 30m res (Nansen Sound and South)

This image is south of all Ice Shelves, and several Ice Island fragments were identified (circled in red). The fast ice was breaking up and drifting off-shore at the time of this image. Although there were numerous rough multi-year floes in this scene, no well-defined MYHFs were identified.

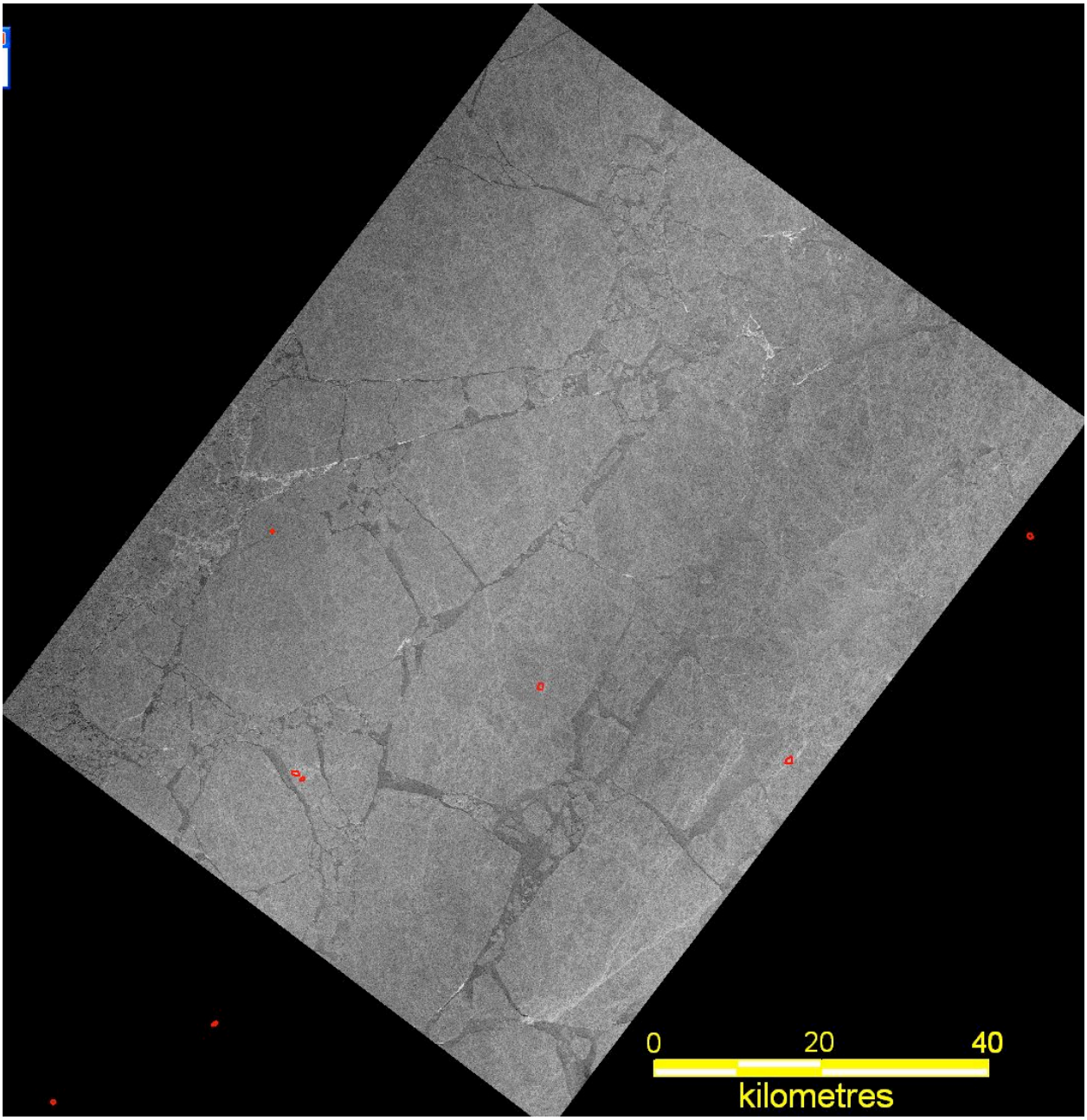

Figure 14-20 (6 of 22) Envisat August 1, 2008 100km swath, 30m res (Offshore Axel Heiberg Island)

This image starts at 35 km offshore, and extends out into the Arctic Ocean. Several Ice Island fragments were identified in this scene dominated by giant floes of Multi-year ice.

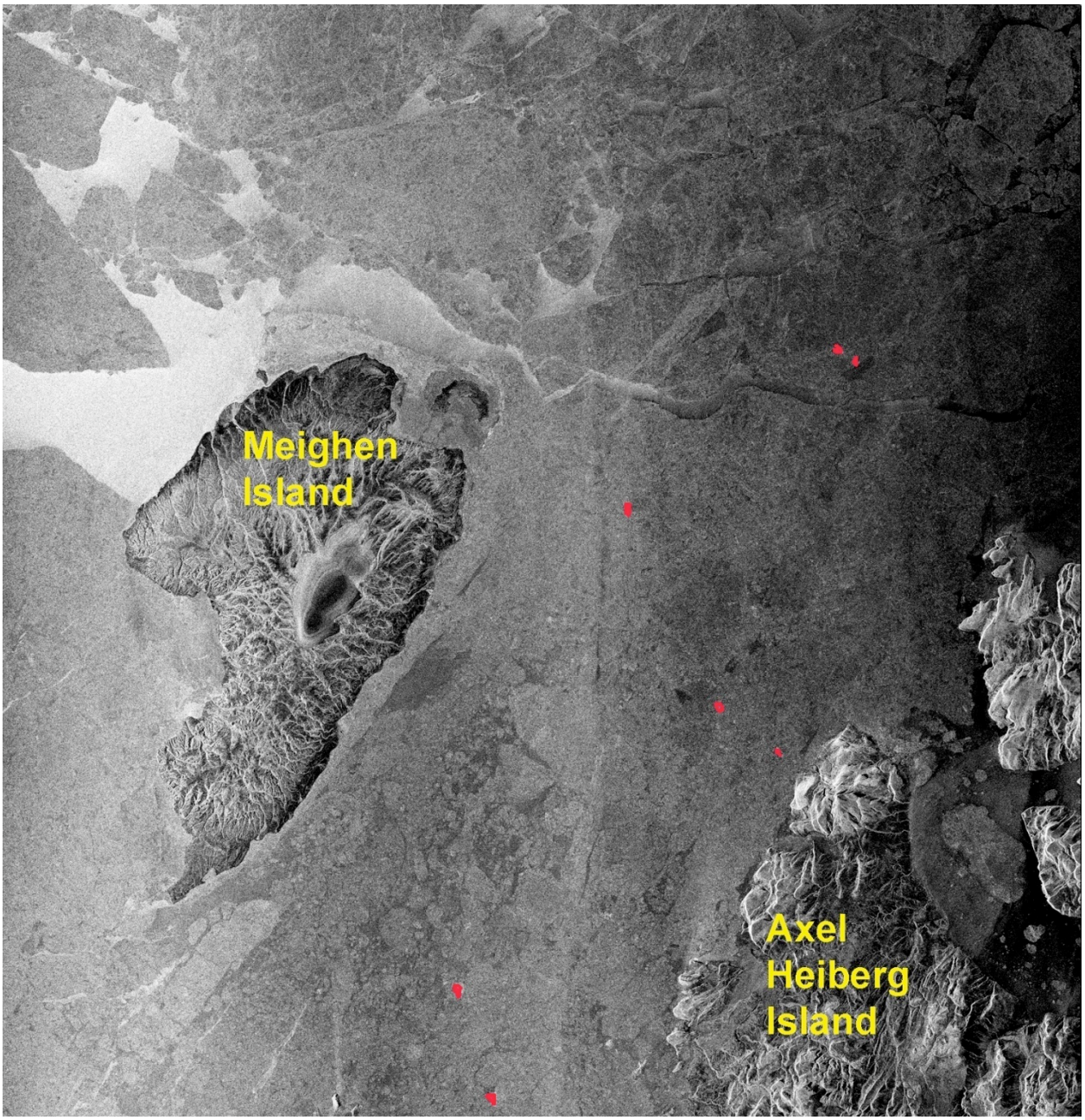

Figure 14-21 (7 of 22) Envisat August 1, 2008 100km swath, 30m res (Meighen Island)

This image contains fast ice in the lower ½. Several ice island fragments were identified. Fracturing of the fast ice was actively occurring at the time of this image.

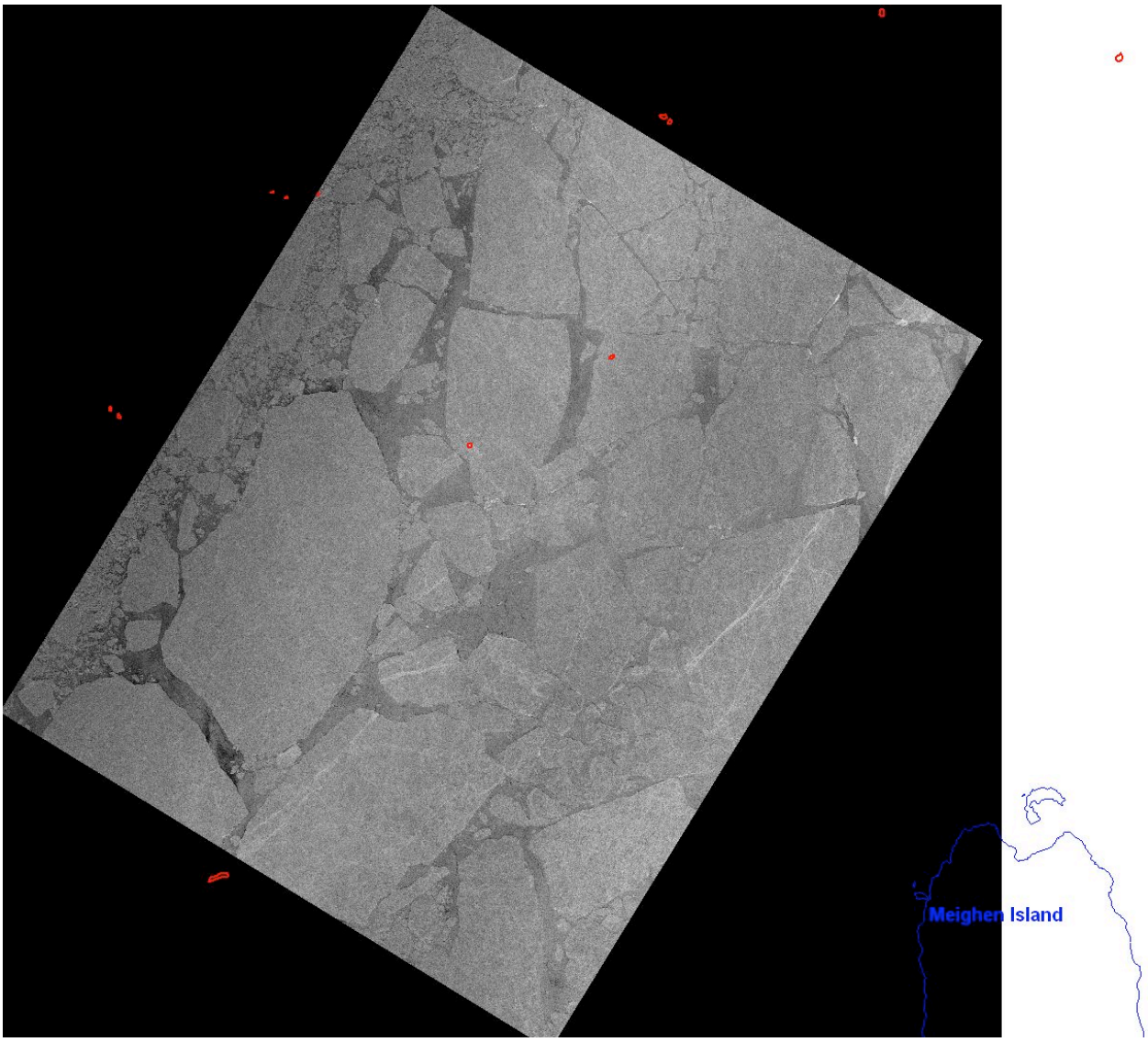

Figure 14-22 (8 of 22) Envisat August 1, 2008 100km swath, 30m res. (NW of Meighen Island)

This image offshore of Meighen Island shows 9/10 concentration, and a few new ridges are apparent on some of the multi-year floes. Two ice island fragments were identified.

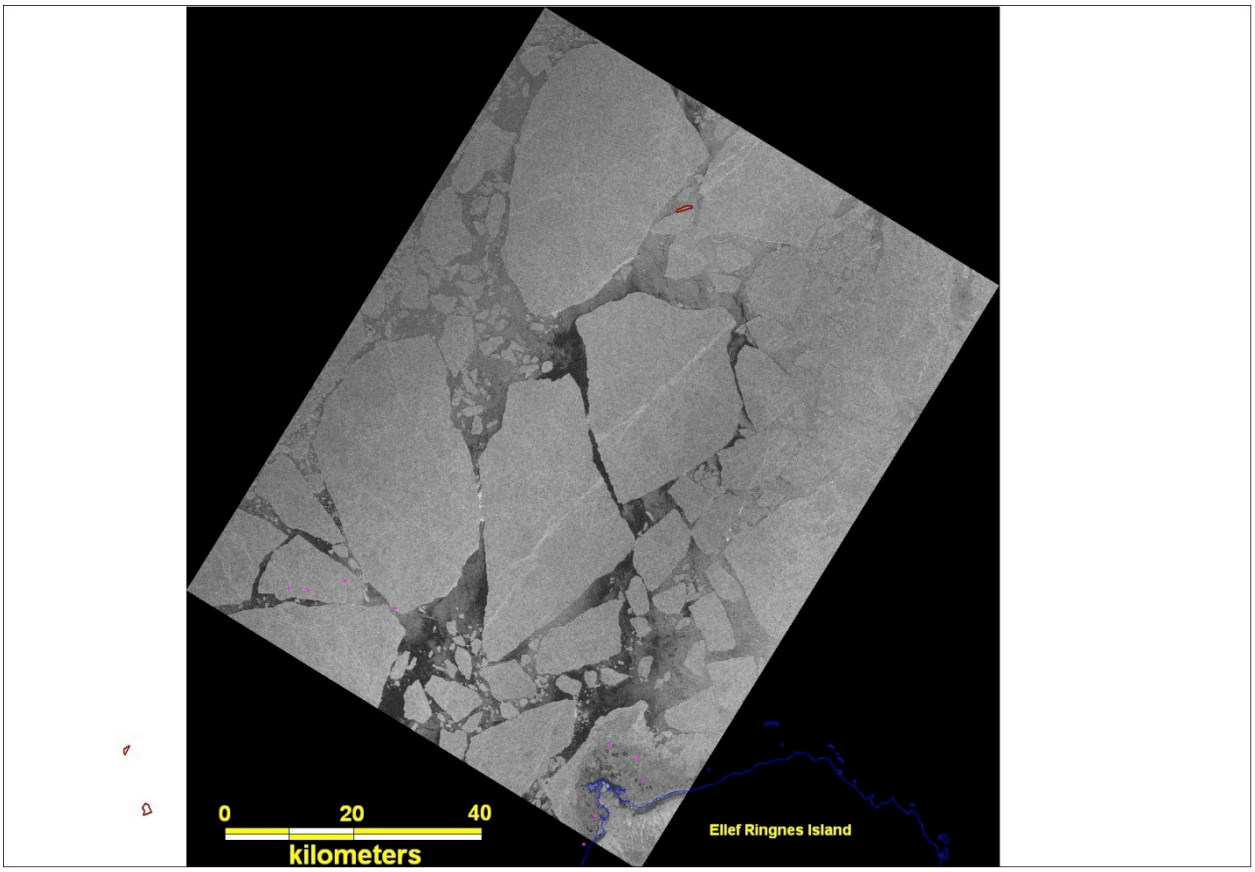

Figure 14-23 (9 of 22) Envisat August 1, 2008 100km swath, 30m res. (NW of Ellef Ringnes Island)

This image NW of Ellef Ringnes Island shows a few Ice Island fragments along the coast of the island, and one Ice Island about 80km offshore. The ice was moving off-shore in this image, but a recent ridge line through 2 floes indicates this area was under pressure earlier in the season.

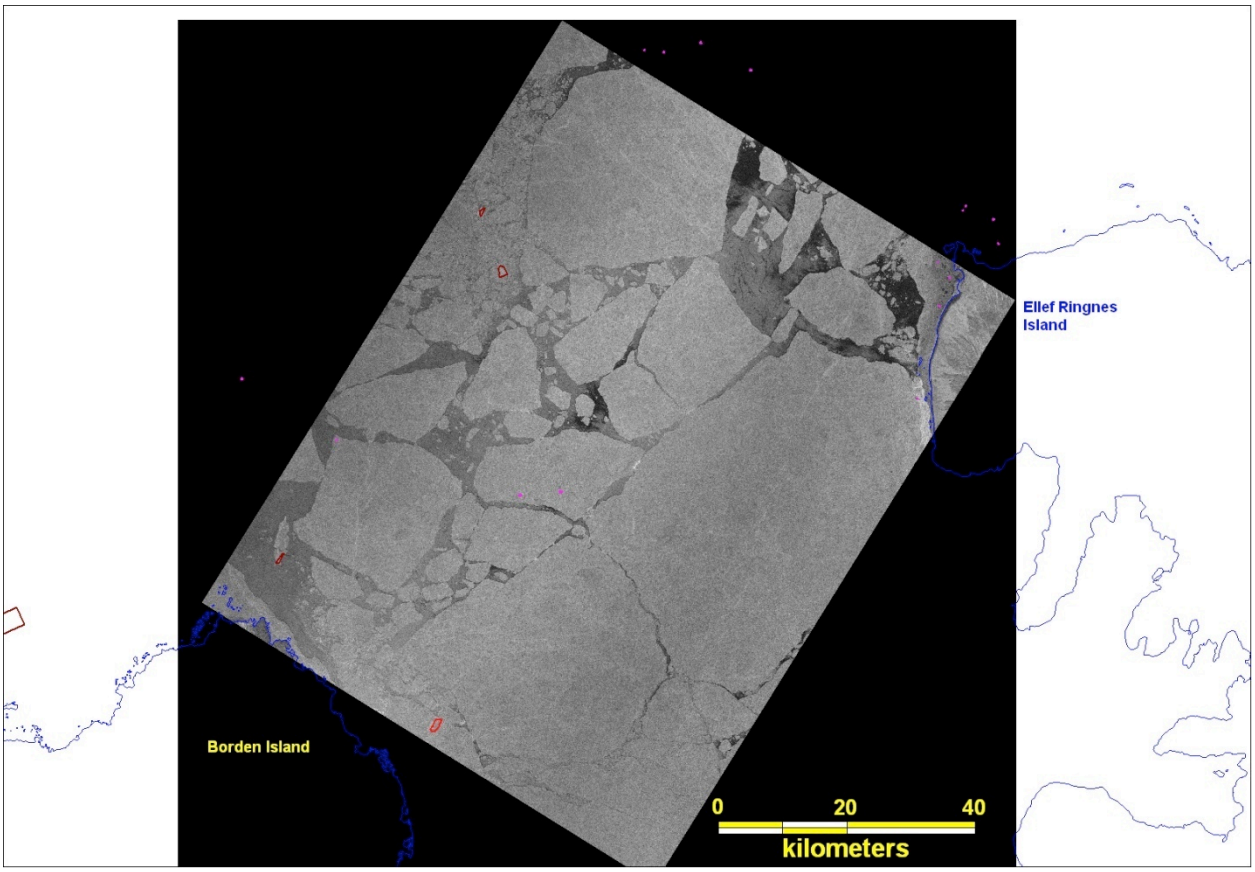

Figure 14-24 (10 of 22) Envisat August 1, 2008 100km swath, 30m res. (Borden Island)

This image between Borden Island and Ellef Ringnes Island shows the fast ice fracturing and clearing. A small ice island (likely grounded) was identified off the Borden coast. Three MYHFs were identified offshore.

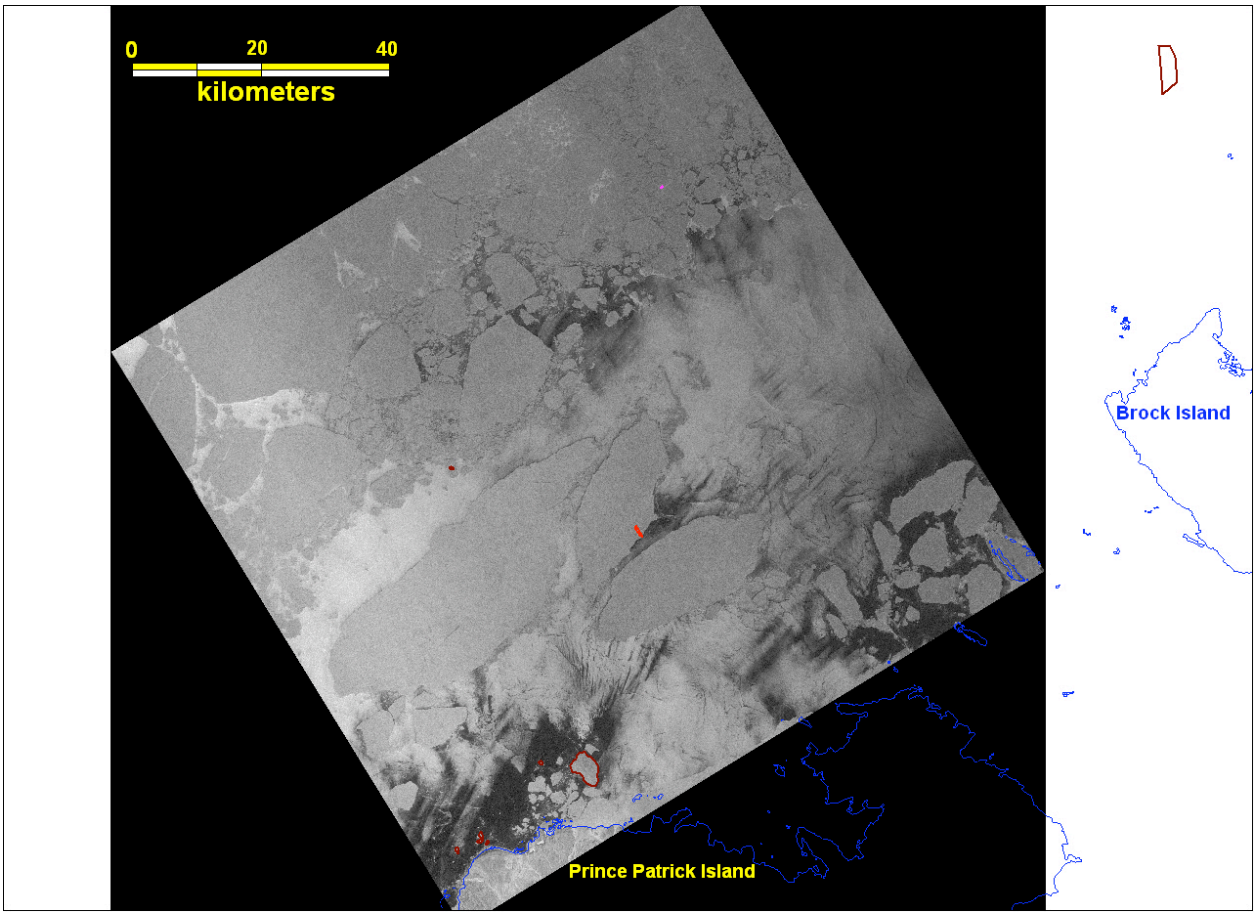

Figure 14-25 (11 of 22) Envisat August 1, 2008 100km swath, 30m res. (NW of Prince Patrick Island)

This image from the NW coast of PPI includes a few MYHFs (circled in brown) that are drifting off of the coast at the time of this image. A small ice island (red) is frozen into a vast multi-year floe offshore. Variable winds produced a lot of random sea-returns in this radar image.

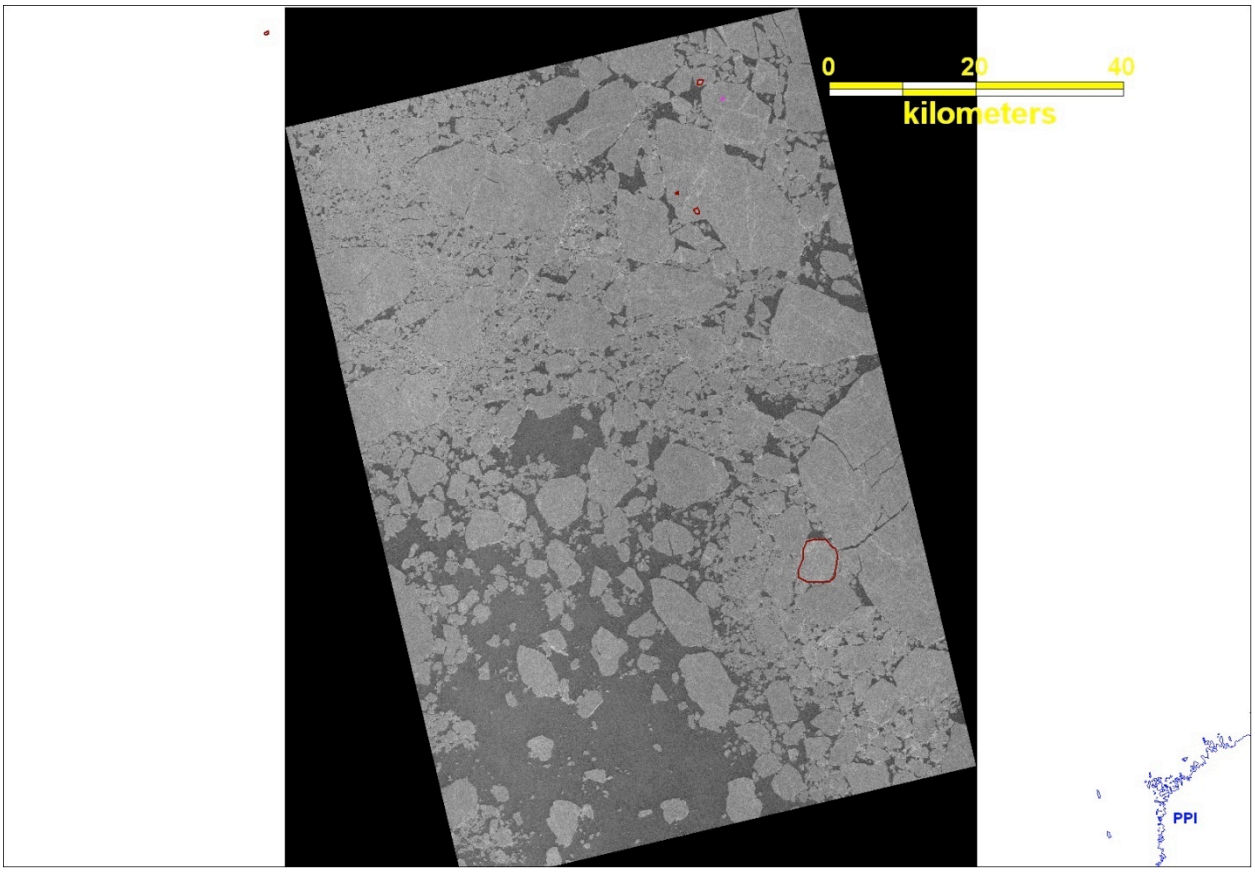

Figure 14-26 (12 of 22) Envisat August 1, 2008 100km swath, 30m res. (WSW of Prince Patrick Island)

This image shows multi-year floes breaking up, and 4 MYHFs from further north. An Ice Island fragment (pink) was located further offshore.

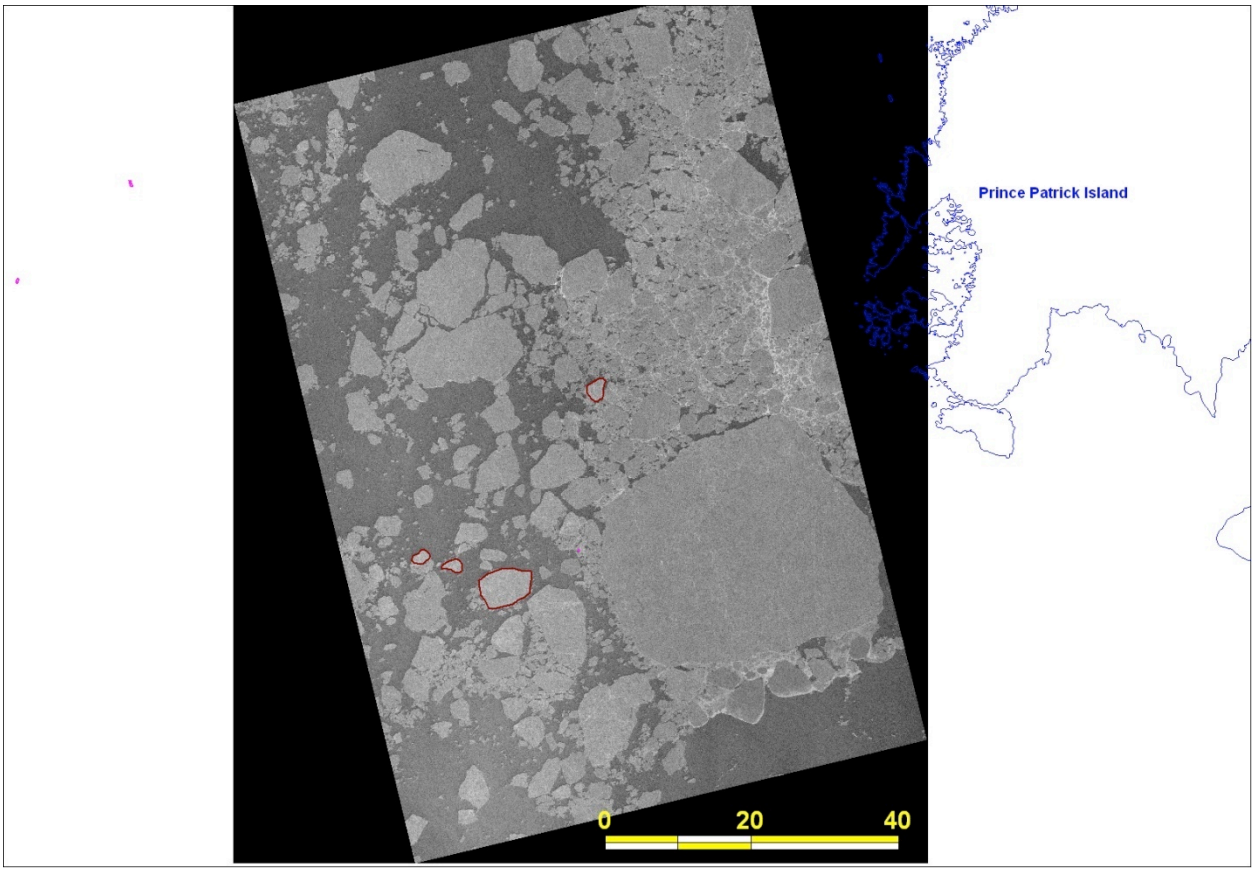

Figure 14-27 (13 of 22) Envisat August 1, 2008 100km swath, 30m res. (SSW of Prince Patrick Island)

This scene contains a giant floe of Multi-year, as well as smaller rougher floes that have come south along the PPI coast. Four MYHFs were identified in this scene. These floes are total rubble fields formed in the pressure along the PPI coast. One small Ice Island fragment (200m x 90m) was also identified.

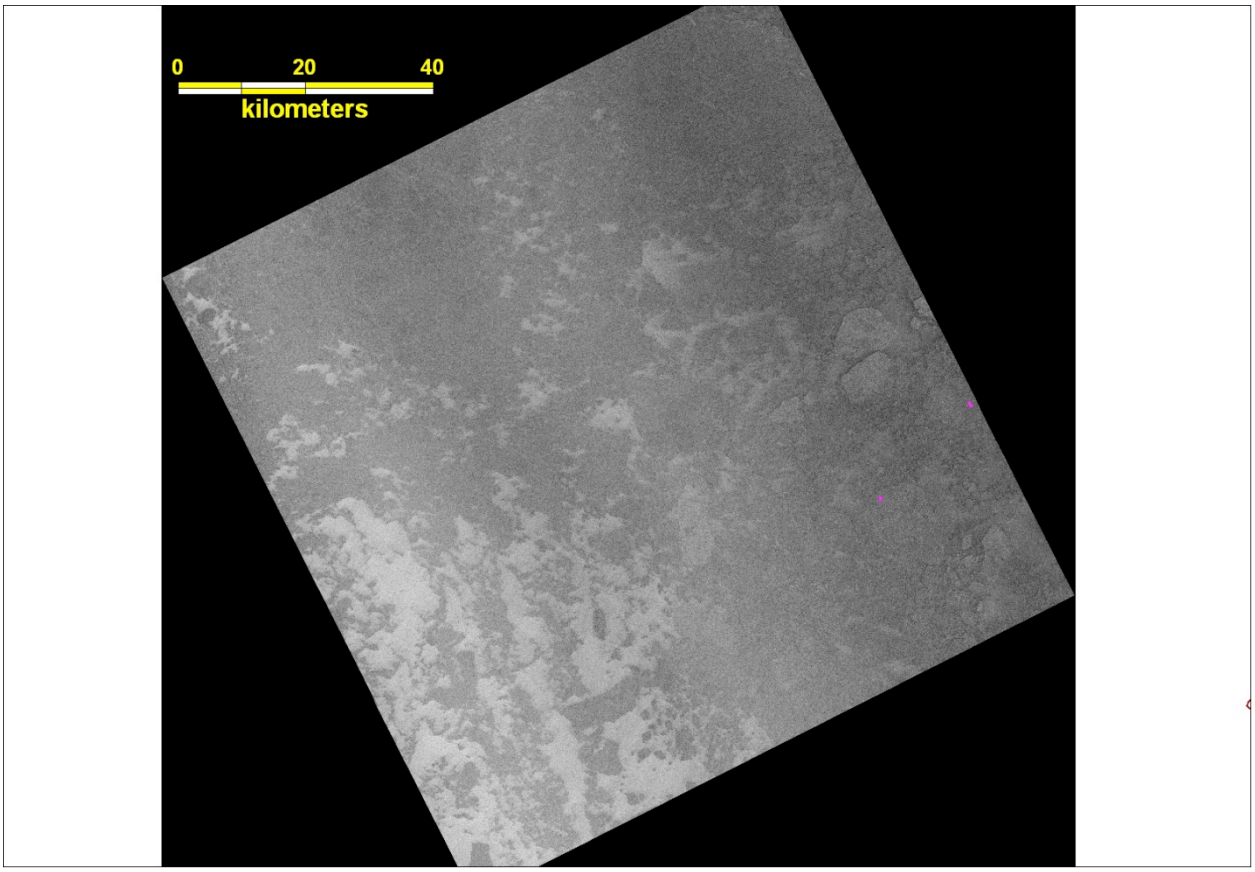

Figure 14-28 (14 of 22) Envisat August 1, 2008 100km swath, 30m res. (W of Prince Patrick Island)

The scene of offshore conditions contains deteriorating ice in rough water in the lower left corner of the image. Distinct rough multi-year floes are present on the right side, as well as 2 Ice Island fragments.

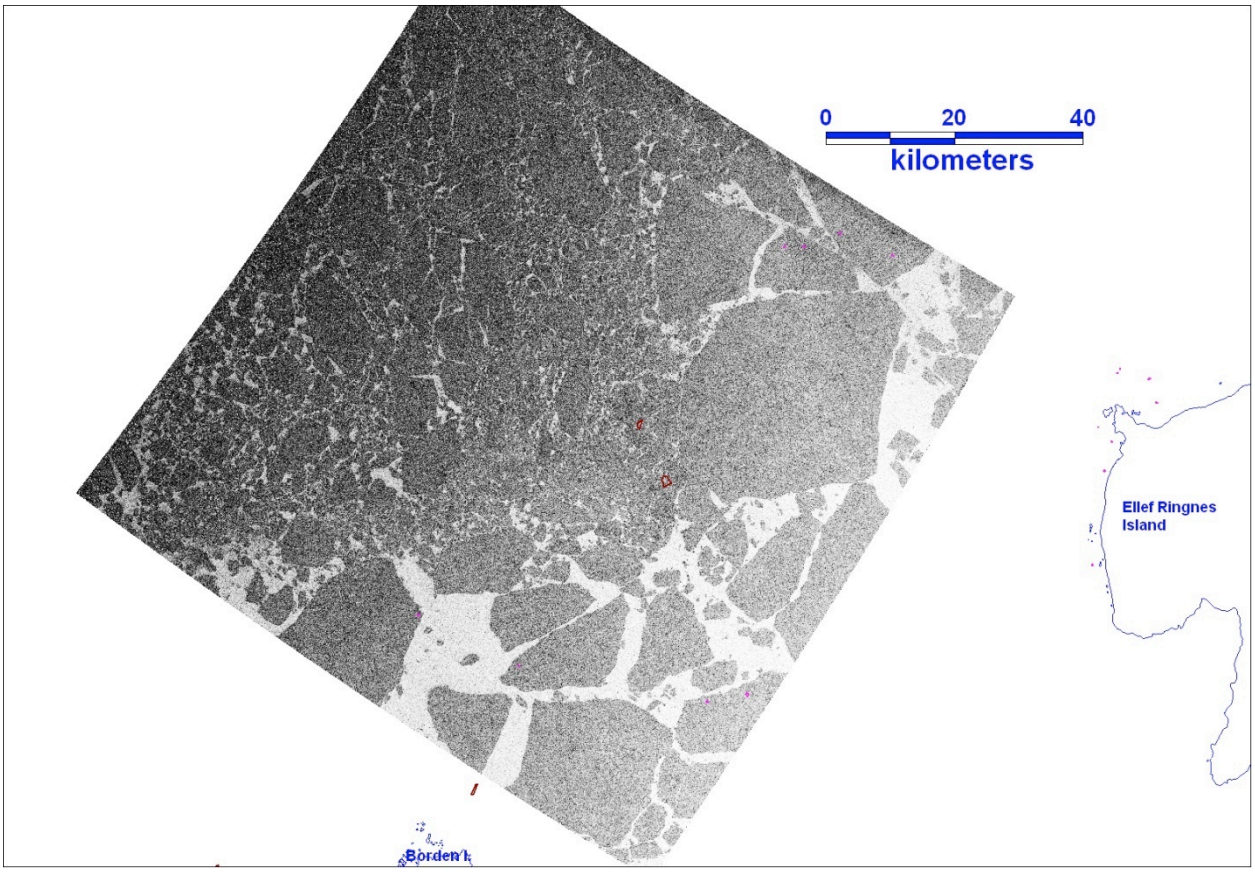

Figure 14-29 (15 of 22) Envisat July 31, 2008 100km swath, 30m res. (W of Ellef Ringnes Island)

This offshore scene shows large floes drifting off-shore, and smaller floes further offshore as compact conditions break up the floes. Six ice island fragments and 2 MYHFs were identified in this scene.

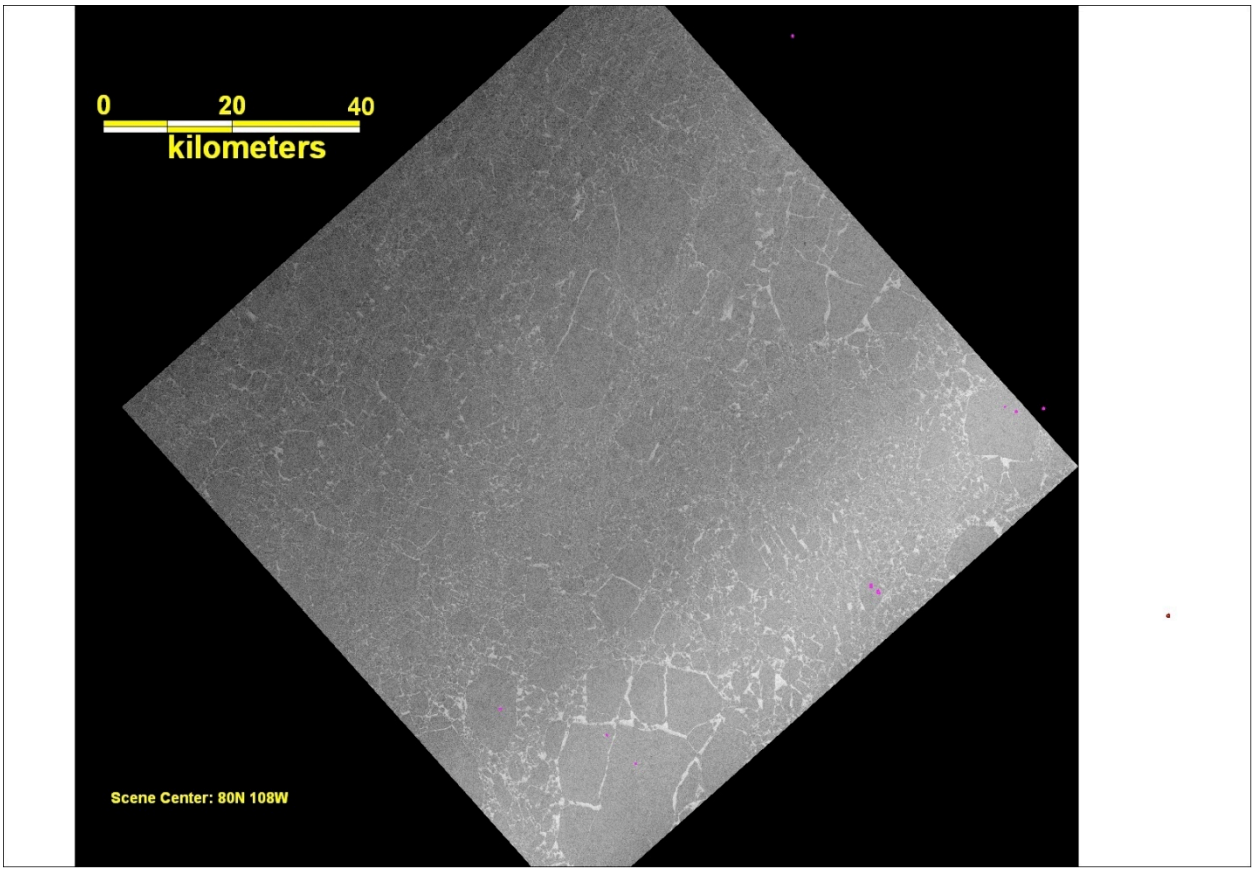

Figure 14-30 (16 of 22) Envisat July 31, 2008 100km swath, 30m res. (100kms W of Meighen Island)

This scene in the Arctic Ocean contains 9+/10 concentration of Multi-year ice in giant floes. Six Ice Island fragments were identified in this image.

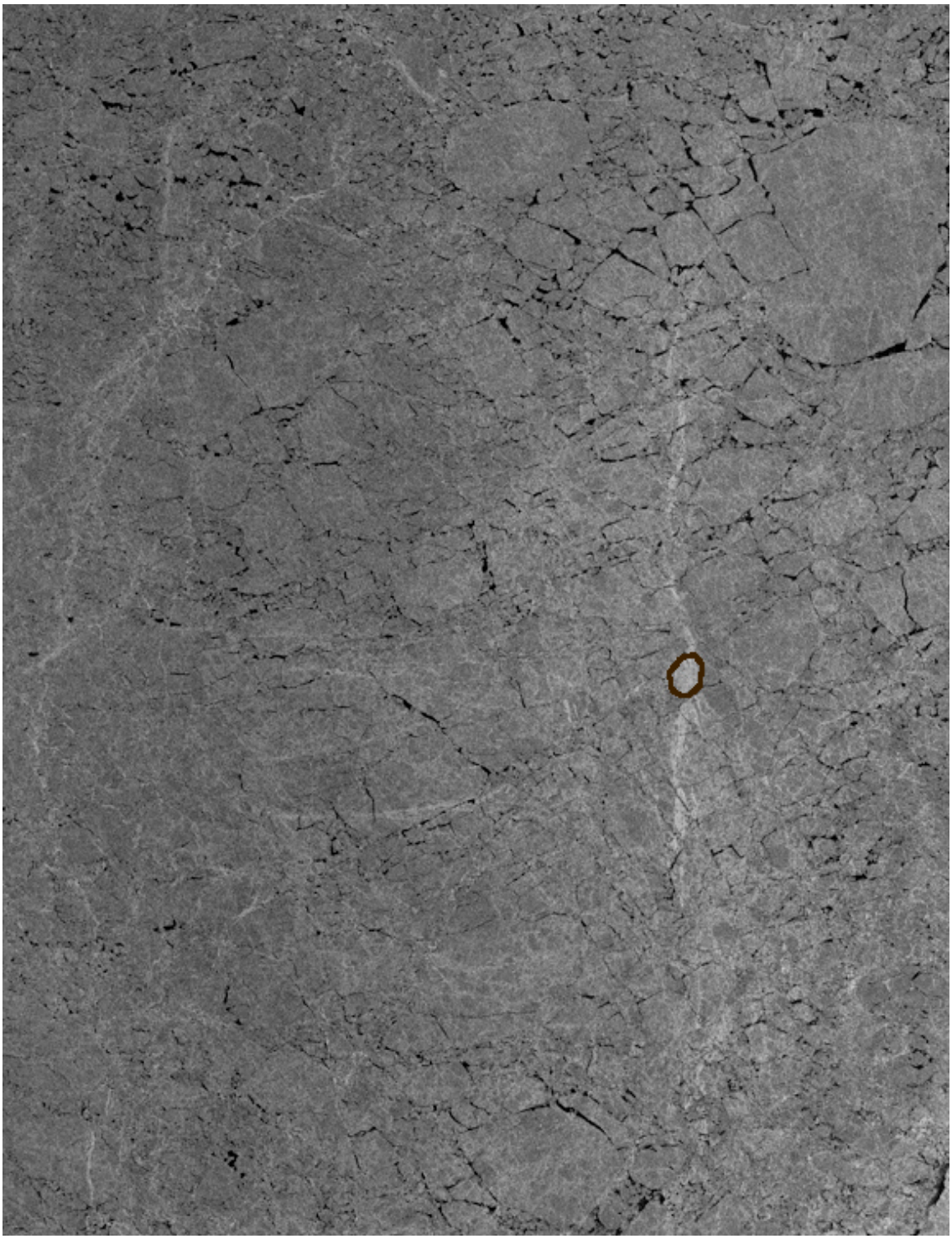

Figure 14-31 (17 of 22) Envisat Aug 1, 2008 100km swath, 30m res. (Arctic Ocean 83N 83W)

This scene from 35km north of Ellesmere Island shows no Ice Islands, and one MYHF where shearing and pressure has created an individual rubble floe.

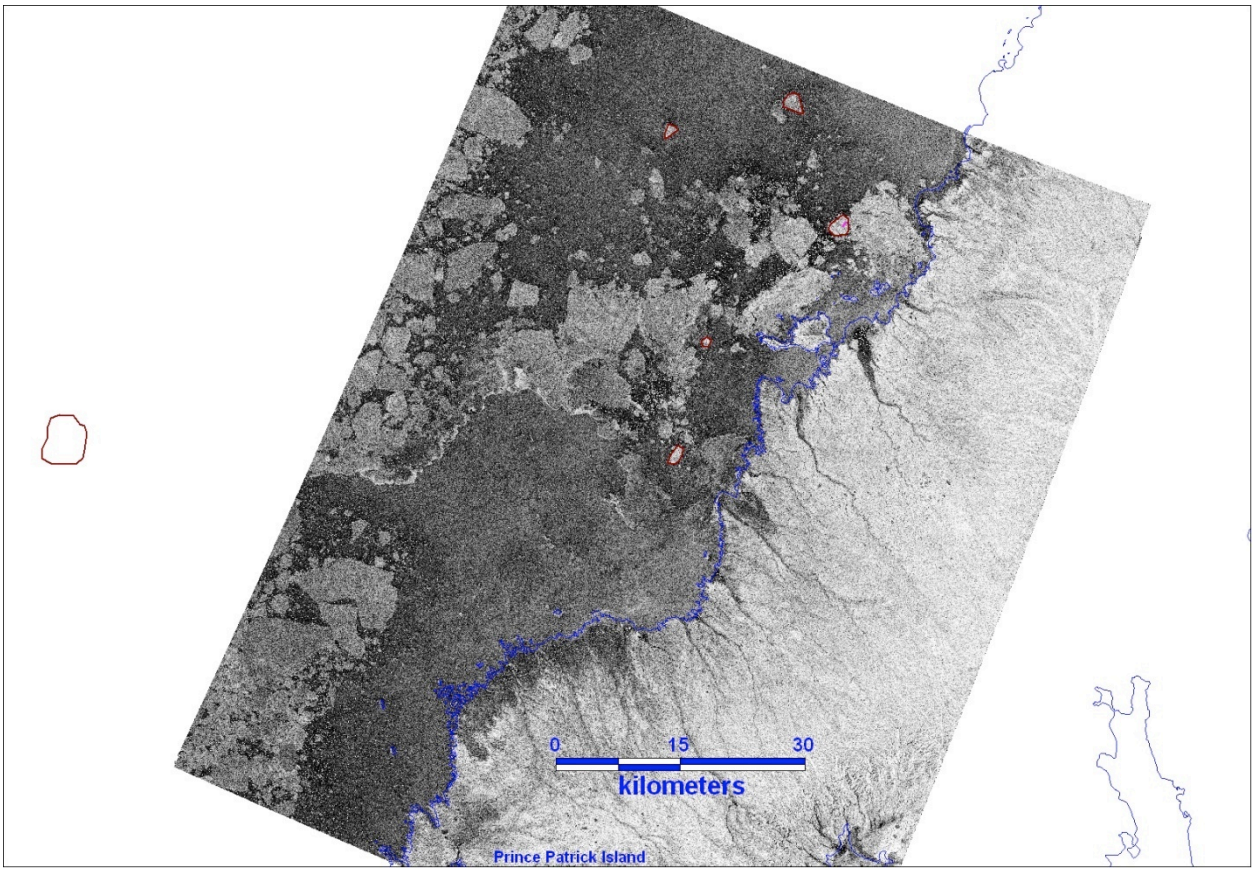

Figure 14-32 (18 of 22) Envisat Jul 31, 2008 100km swath, 30m res. (W Coast Prince Patrick Isl.)

This image of the west coast of PPI captures the last of the fast ice that is drifting away from shore. Open water is present along most of the coast. Five MYHFs and one Ice Island fragment were identified in this scene.

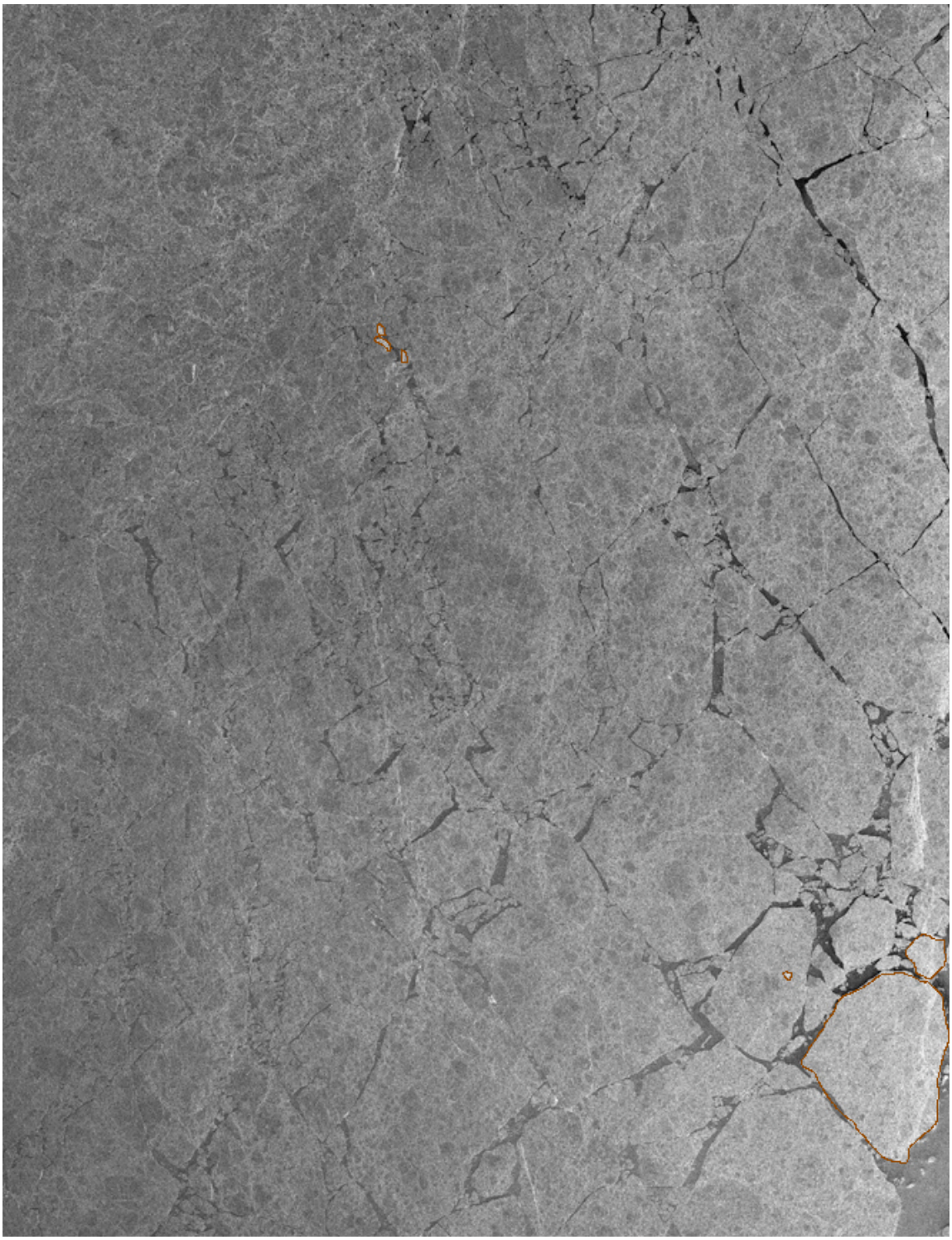

Figure 14-33 (19 of 22) Envisat Aug 1, 2008 100km swath, 30m res. (Along Ellesmere Island coast)

The right side of this scene is 25km off shore of Ellesmere Island, near Nansen Sound. Giant floes of multi-year, and a few MYHFs are present in this scene. The ice is much rougher on the right side of the image (near shore) than on the left side.

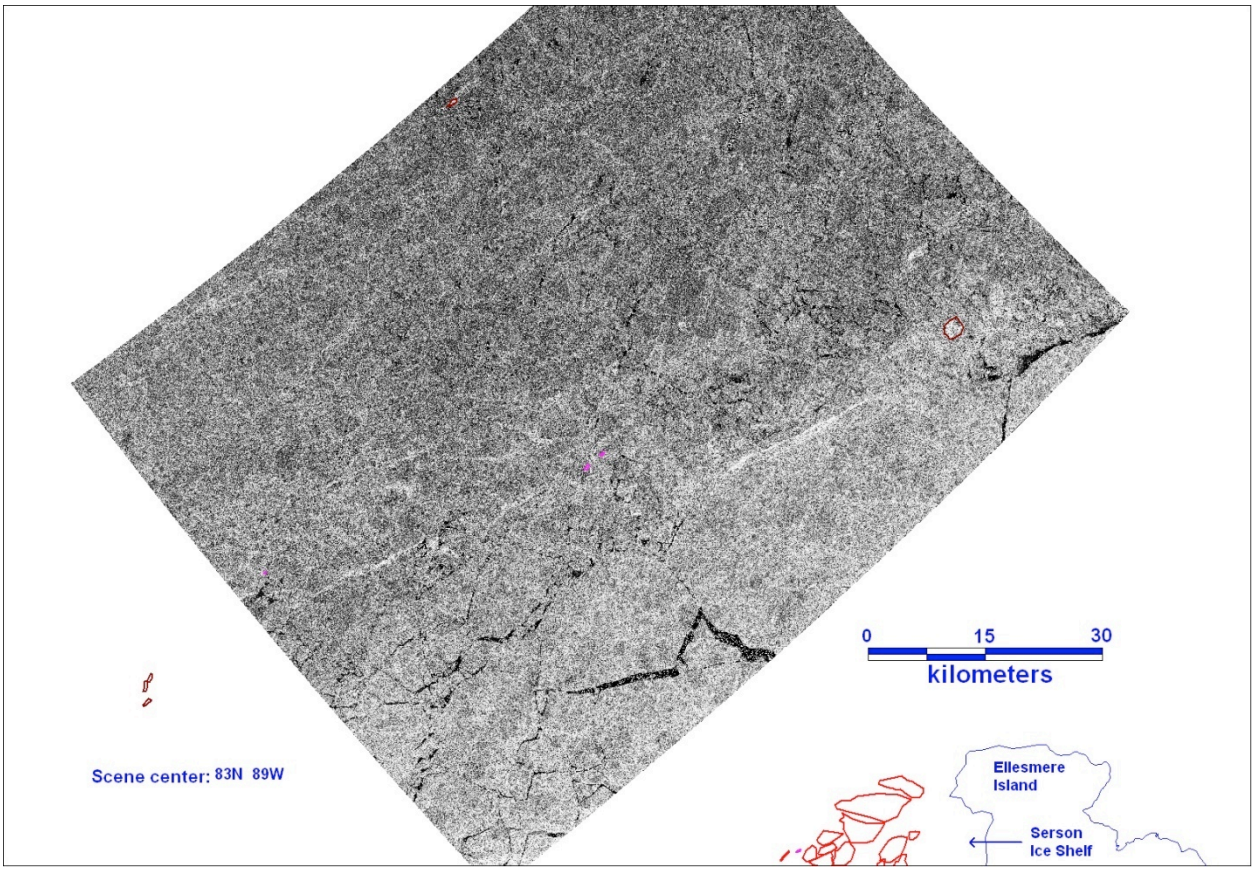

Figure 14-34 (20 of 22) Envisat Aug 1, 2008 100km swath, 30m res. (Along Ellesmere Island coast)

This scene starts about 25km offshore, and covers out into the Arctic Ocean. Although the right side of the image (nearest the coast) is roughest and has the brightest tone, only two MYHFs and two Ice Island fragments were identified on this image. Conditions are 9-9+/10 throughout.

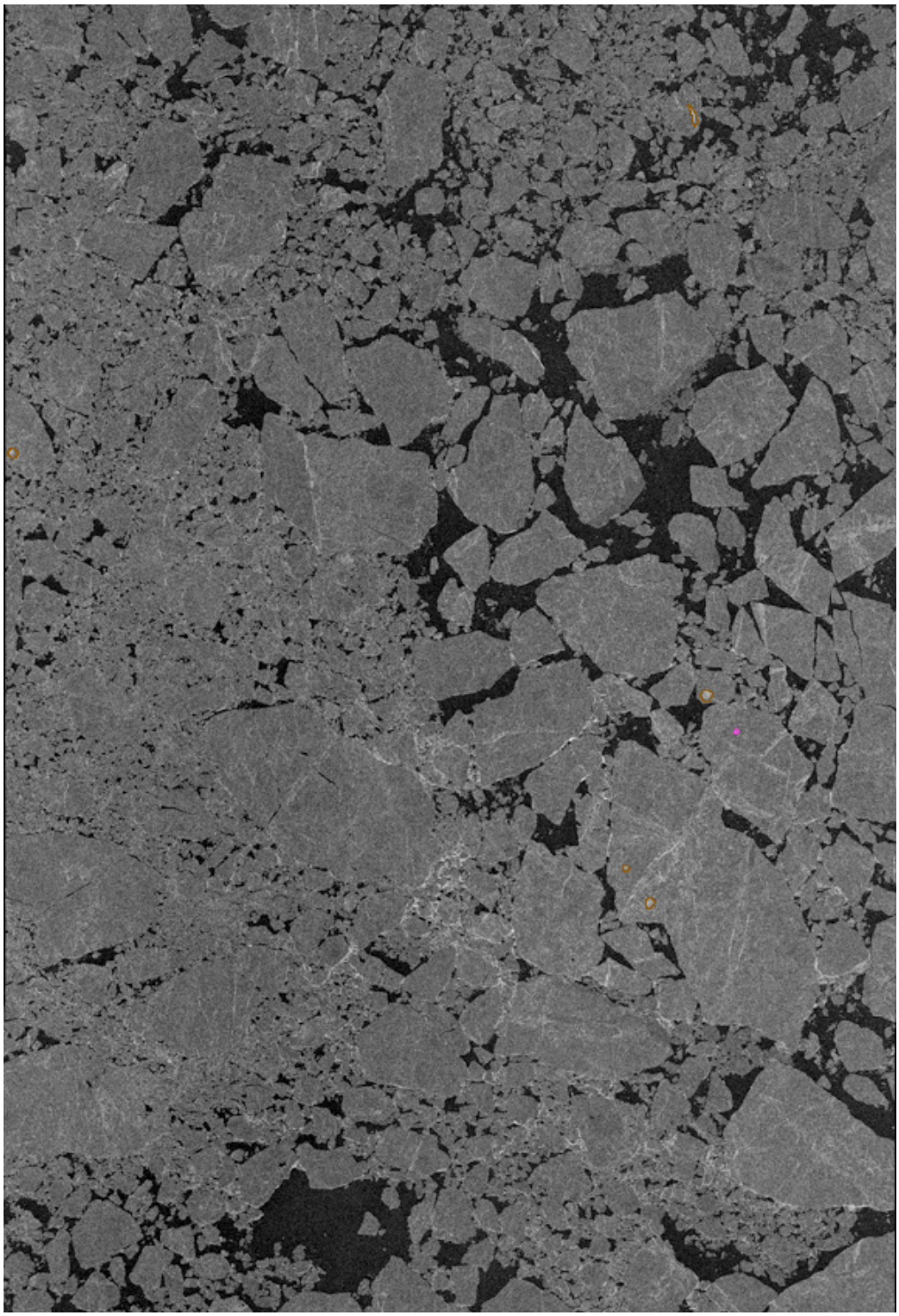

Figure 14-35 (21 of 22) Envisat Aug 1, 2008 100km swath, 30m res. (100km W of Prince Patrick Island – Arctic Ocean)

This scene is well offshore, and the ice is spread out. Five MYHFs and one Ice Island fragment were identified in this scene.

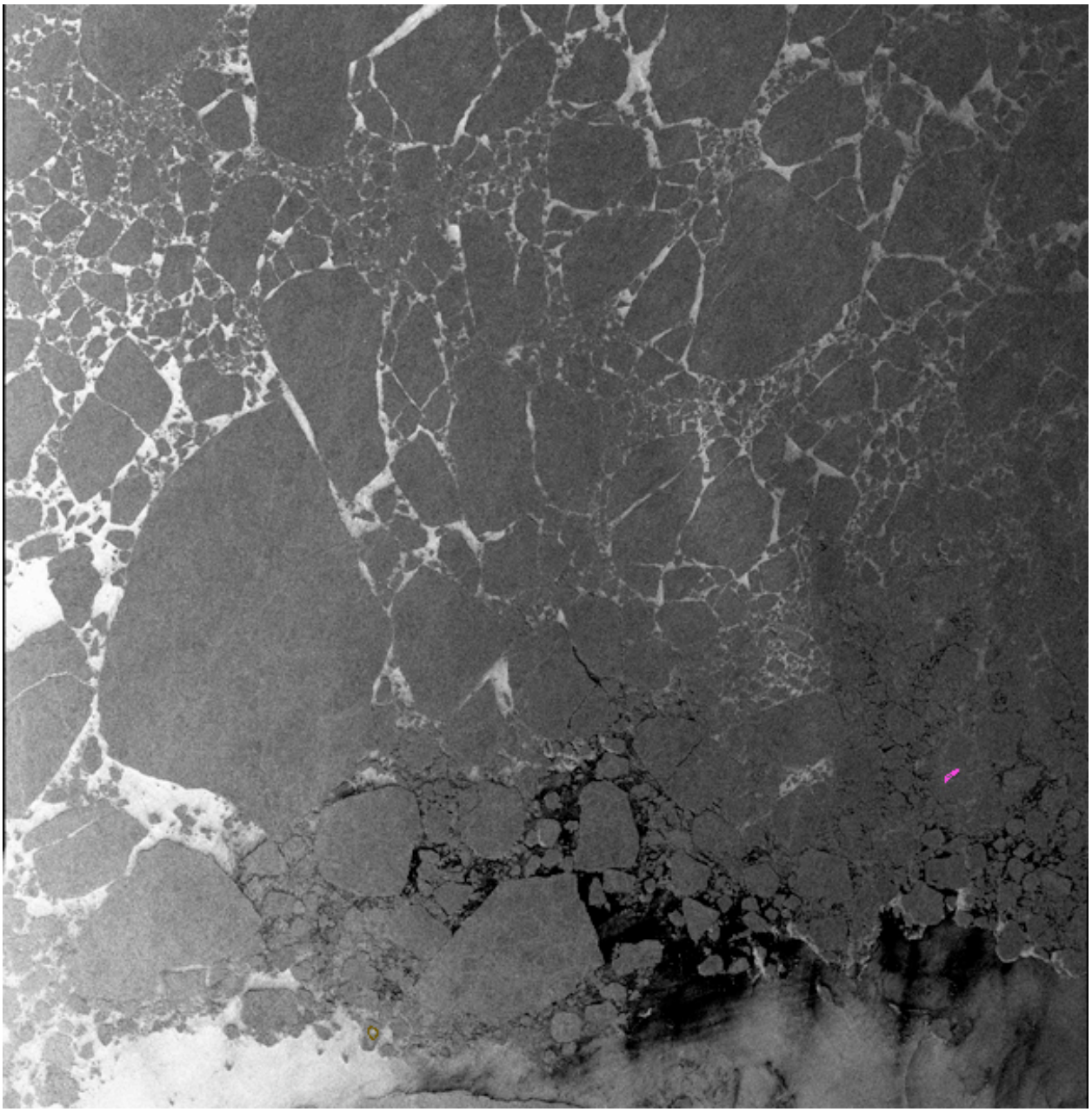

Figure 14-36 (22 of 22) Envisat Aug 1, 2008 100km swath, 30m res. (50km W of Brock Island)

This scene starts 50 km. offshore, and extends seaward. Open water is present along the south edge of the image. One ice island fragment and one MYHF were identified in this scene.

15 APPENDIX B Calculated Parameters for EIF and M–Y Floe Data Bases

Floe Geometrical Properties

For this study, five geometrical properties: perimeter, area, major axis, minor axis and diameter are calculated. In addition, the equivalent diameter, and three circular-like shape indicators were also calculated.

Except for the perimeter and area, which were obtained through the GIS program, MapInfo, and are "spherical", all the parameters were calculated from a map projection. Instead of one projection covering all the datasets, every dataset is projected using the oblique stereographic projection with the central meridian and origin latitude situated near the middle of the respective dataset. The description of the properties and indicators are as follows:

Perimeter and Area

As mentioned, these measurements are obtained through the GIS software. The difference between these values and those obtained from the map projection is not significant, i.e. for the largest polygon on dataset 1, around 7,151 km^2, the difference between areas is about 0.04 %.

Major and Minor Axis

These are axes of symmetry; they divide the floe in two equal parts. The major and minor axes passes through the geometric center and are perpendicular, they follow the angles of the principal axes of the floe (the principal axes yields the maximum and minimum second moments of area).

Diameter

It is a straight line connecting the two furthest-apart points in a floe, in short, it is the diameter of the circumscribed circle. Then, the diameter may or may not pass through the geometric center and will be always equal or greater than the major axis. Figure 15-1 illustrates the axis and diameter for floe #468 (Dataset 1).

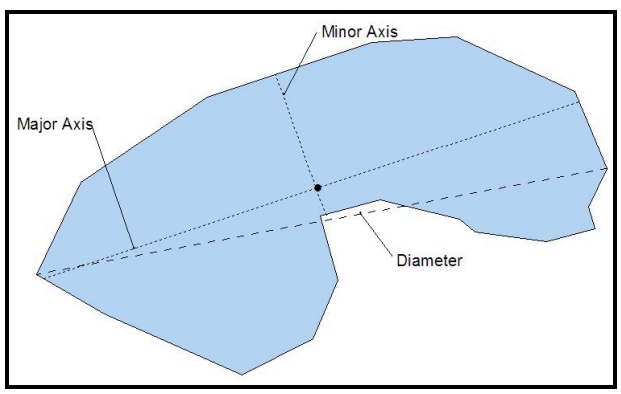

Figure 15-1 Example of Major and Minor Axes and Diameter

Equivalent Diameter

The equivalent diameter is defined as $2*\sqrt{\frac{area}{\pi}}$

Circularity Indicator

The circularity indicator is defined as $\frac{4*\pi*area}{perimeter^2}$, and it goes from zero for a line and one for a circle.

Compactness Indicator

Defined as $\frac{area}{\pi*\left(\frac{diameter}{2}\right)^2}$, and it goes from zero for a line and one for a circle

Ellipsoid Roundness

Defined as $1-\frac{\text{major axis} - \text{minor axis}}{\text{major axis} + \text{minor axis}}$, the range is 0 to 1 for a circular shape.

Notice that an ellipsoid roundness equal to one does not mean that the floe is a circle. A good example is shown on Figure 15-2 (floe # 236, dataset 1).

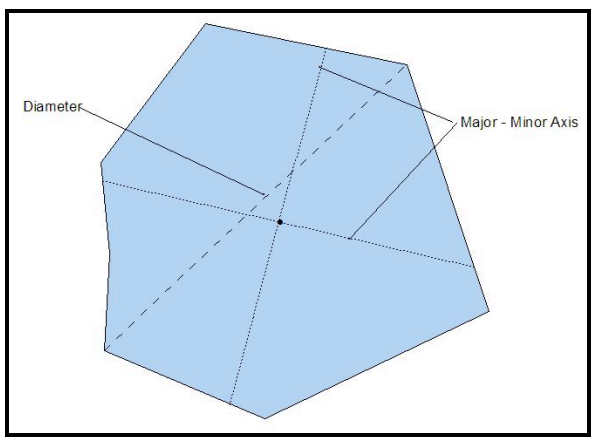

Figure 15-2 Example of shape with Ellipsoid Roundness of nearly 1